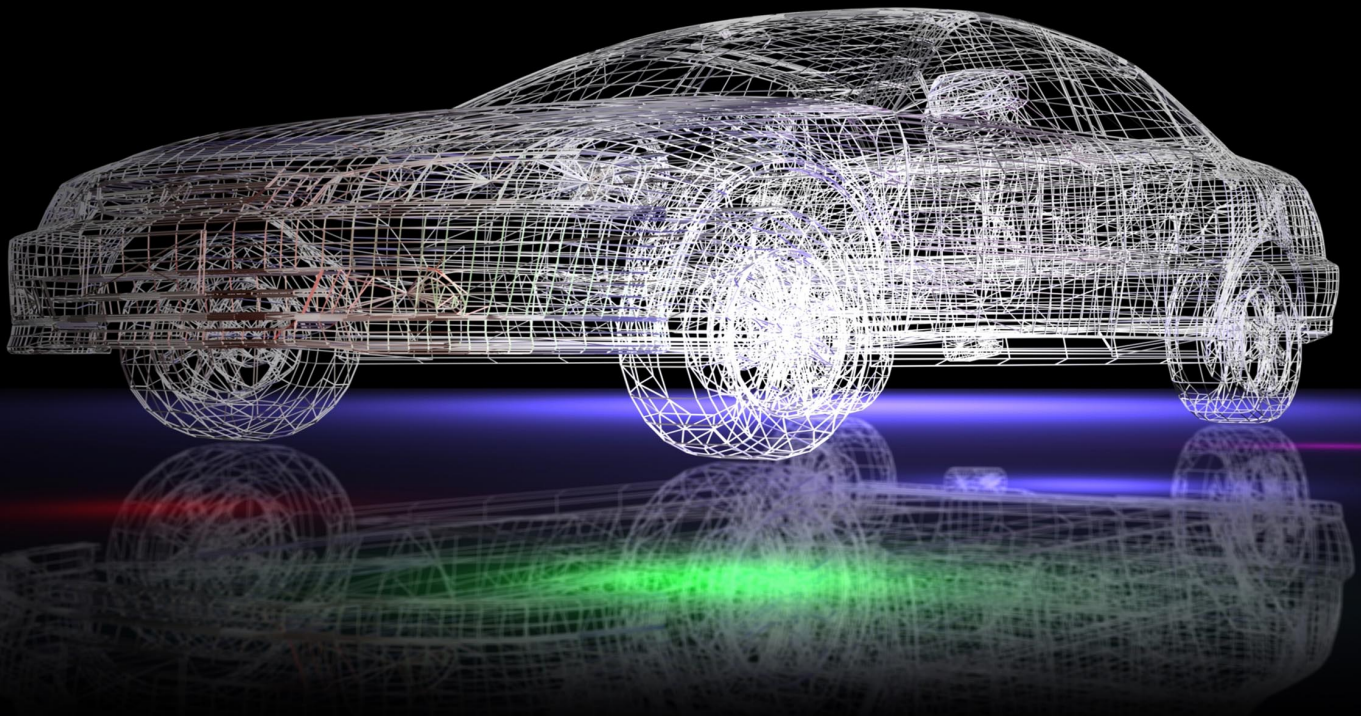


BENCH MARK

Automotive issue . . .

- IMPROVING PRODUCT DEVELOPMENT WITH CAE
- SIMULATING THE WIESEL
- MODELLING CONDENSATION IN AUTOMOTIVE HEADLAMPS
- PREDICTING FUEL CONSUMPTION AND THERMAL COMFORT
- FATIGUE IN ALUMINIUM HONEYCOMB-CORE PLATES
- ABSORBING RAIL IMPACT ASSESSING THE DEFECT TOLERANCE OF RAIL VEHICLE IMPACT ENERGY ABSORBERS AND MORE.....

THE INTERNATIONAL MAGAZINE FOR ENGINEERING DESIGNERS & ANALYSTS FROM **NAFEMS**



Special Edition:
Engineering Analysis &
Simulation in the
Automotive Industry



from your editor

David Quinn
david.quinn@nafems.org
@benchtweet

Automotive manufacturers and suppliers are constantly challenged with delivering innovative, safe and dependable vehicles to market as efficiently as possible. As a result, engineering teams must discover, evaluate, and successfully implement leading-edge technology and methods to produce reliable, effective results. This special edition of Benchmark will address these issues, and more, by bringing together a series of past articles that are strongly relevant to simulation in the automotive industry.

As part of our annual industry series, we are hosting an automotive event which will look specifically at the challenges that the industry currently faces, and will also explore how simulation and analysis can help meet the industry's goals in a cost-effective and efficient manner. Within this special edition of Benchmark, you will find articles on many topics related to the automotive industry, all of which give a best-in-class perspective on a range of issues that are prevalent to all involved.

NAFEMS is the only independent, international association dedicated to engineering analysis and simulation. Our range of best-practise guides, benchmarks, "how to" publications, as well as seminars, courses, e-learning and conferences, allow us to bring industries together to share and exchange experience and knowledge in order to drive the technology forward. Our members come from every industry around the world, giving a truly global perspective to our activities and allowing our community to benefit from the wealth of its own experience. You can find out more about NAFEMS and our activities, as well as details on our industry and technology specific events, by visiting nafems.org

in this issue...

- 6 Improving Product Development with CAE
- 11 Simulating The Wiesel
- 17 Modelling Condensation in Automotive Headlamp
- 22 Predicting Fuel Consumption and Thermal Comfort
- 28 Fatigue in Aluminium Honeycomb-Core Plates
- 35 Absorbing Rail Impact Assessing the Defect Tolerance of Rail Vehicle Impact Energy Absorber
- 41 Ford Motor Company Accelerates Design for Manufacturability of Conical Joints
- 45 Joint Durability on the Rails
- 50 Engineering Design Optimisation
- 55 Prediction of Headlamps' Light Beam Deviation Angle by Thermomechanical Simulation
- 60 Understanding the Effects of Nonlinear Preloads on Engine System Dynamic Response
- 64 Reverse Engineering Made Simple
- 69 Composite Process Simulation - Digitally Reinforcing High-Rate Composite Manufacture
- 74 Addressing Automotive Engineering Challenges in Composite Development by Simulation
- 81 A Practical and Reliable Solution for the Damage Analysis of Composite Structures, with Applications to Automotive
- 86 An Investigation of London Skyscraper's Unexpected Scorching Effect
- 94 Characterization and Model Validation of Laminate Failure and Partial Damage in Industrial Applications
- 111 HPC - The Genesis of SDM

in this issue...

- 114 Assuring Confidence in Simulation Results through Simulation Data Management
- 118 Forming Complex Shaped Components Using High Strength Aluminium Alloys
- 122 Simulation in the Die Casting Manufacturing Process
- 126 Virtual Engineering to Ensure Excellent Customer Experiences for Life
- 129 Multi-Objective Design Optimization of an Inverter for Electric Vehicles
- 137 Multi-objective Adjoint Optimization of Intake Port Designs
- 143 SIMCenter - Advancing the State of CAE in the Transportation
- 147 Multiphysics Analysis of Lithium Ion Battery
- 151 Aero-Vibro-Acoustics for Wind Noise Applications
- 156 Using Artificial Intelligence to Analyze Crash Simulations
- 160 Virtual and Augmented Reality
- 166 Interactive Modelling and Simulation for Virtual Engineering Design and Analysis
- 171 Real-time Mechanism and System Simulation Supporting Human-in-the-loop Simulators
- 175 Simulation Data Management - The Next Challenges
- 178 The Future of Working in F1
- 181 Simulation Limited: How Sensor Simulation for Self-driving Vehicles is Limited by Game Engine Based Simulators

- 184 Event Review “New Methods in CFD – Alternatives to Finite Volumes”
- 191 Validation of Electromagnetics Simulations for Vehicle-to-Everything Applications using Measured Results
- 196 From Simulation to Reality - The Bloodhound Land Speed Record Car
- 206 Human Inspired Generative Design
- 210 Ahead of the Curve - Classifying Guardrail System Radar Signatures using High Fidelity Physics Simulation for 77 GHz Automotive Radar
- 219 Shift towards Electric Vehicle - What does it mean for Simulation?
- 224 Effective and Efficient Simulation for AD and ADAS Systems
- 226 Simulation in the Automotive Industry - Creating the Next Generation Vehicle
- 237 Raptor Titanium - Sharpening their Claws through Reverse Engineering
- 243 Surrogate Model Based Safety Performance Assessment of Integrated Vehicle Safety Systems - Connecting and Accelerating Simulation Domains
- 248 Graph and Heuristic-based Topology Optimisation of Crash-Loaded Structures - A Successful Example of Joint Pre-Competitive Industrial Research
- 255 Integration of Driving Physical Properties into the Development of a Virtual Test Field for Highly Automated Vehicle Systems

Improving Product Development with CAE

How Simulation expertise from the Automotive Industry could benefit other industries.

Dr. Bijan Khatib-Shahidi, Principal Consultant, Engineering Products, Inc., gives a personal opinion based on his vast experience in CAE in the automotive industry, gained over 20 years at major manufacturers..

I have mentioned in a previous article in another publication that despite the recent downturn in consumer demand, and the serious economic challenges across industry worldwide, one can observe that today's modern automobiles have benefited from the extensive use of CAE to make them quiet, durable, comfortable, stable and safe. The design and release engineers, who are responsible for signing-off on the adequacy of the component, part or system that they send to manufacturing for production, have particularly benefited from modern FEA and CFD software and analysis. Their colleagues in the CAE organizations conduct the analysis to better the design for the consumers and the public in general. I also need to mention that in some smaller organizations, the role of the design and CAE engineer is the same, and the same engineer does both the analysis, design and release. However, that does not take anything away from the discussion on the benefits that CAE provides.

In my recent role as a Vehicle CAE Manager at a major automotive OEM, I experienced and watched the growth of FEA and CFD, in both capability and utilization, on engineering applications and design.

Using FEA and CFD, our team was able to create full-vehicle model representations of cars and trucks that included many parts. We swapped different size tires, suspensions, multiple powertrains, and chassis systems to represent a variety of vehicle configurations. We could represent these models as if they were real prototypes; they included acoustic representations to measure noise predictions inside and outside of the cars. We added sub-system representations of multiple engine/ transmissions, axles and drivelines, different trim levels such as inclusion or exclusion of sun or moon roofs, and excited them

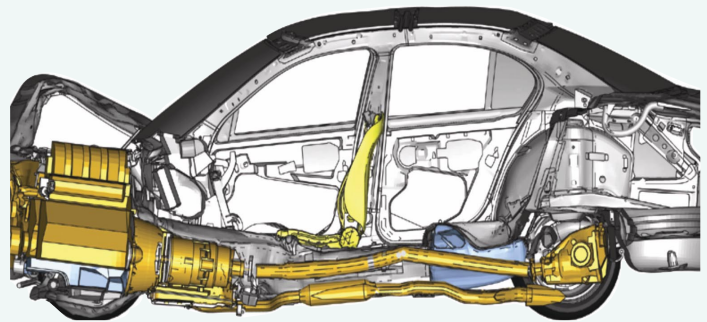


Figure 1

with various load conditions such as road profiles, wind loads (winter and summer modelling, and different yaw angles), engine loads, driveline imperfection scenarios, and so on. New capabilities, such as the one from ABAQUS software, allowed rolling tire capabilities and sub-structuring, as well as the ability to switch from implicit to explicit analysis and vice versa to mimic road NVH and durability analysis.

I need to reiterate that these models enabled our designers and development engineers to identify, early in the design phase, any necessary 'fixes' which were required in order to achieve consumer and regulatory targets and also to avoid heavy back breaking vehicle recalls.



Figure 2

This avoided (for the most part) the building of physical prototyping, which were then only used for validation and comparison. Such CAE simulations also enabled the teams to provide scientific cost forecasts, which otherwise would only have been a good guess on the designer's part, used to report to the senior management before they agreed to sign off on any production go-ahead.

There is huge competition amongst the 100+ car industries across the globe, which is due in no small part to the convergence of design and styling, engineering content, and the never ending demand from the costumers to have 'more and ever more' included in the cars they purchase. Because of this, the companies face major economic pressures on a daily basis. In order for them to stay afloat, these manufacturing companies are more focused than ever on improving engineering efficiency, lowering development costs, and accelerating product innovation faster than the competition next door.

I have seen FEA / CFD and other simulation solutions playing an increasingly prominent role in helping every industry to design better, optimize more often, and modify a product a little and reuse the existing design in a different platform (with the new morphing technologies) to cut costs and to become as competitive as possible. There is no other way. The convergences in the economic conditions have made this problem universal, making it more difficult to build distinctive products. This situation is no longer unique to the automotive industry. Any industry that is in the business of manufacturing can benefit from CAE. Nowadays, every country is building cars, airplanes, washing machines and food processors, so it is necessary to be design distinctive, efficient, and fast to market. CAE tools can play a prominent role in achieving most of these goals.

Nonlinear FEA gets Results Ever Closer to Reality
Advances in commercial FEA technology are enabling engineers to get closer than ever to simulating realistic behaviour through the inclusion of nonlinear effects in processes such as rolling tires, and in materials such as rubber, plastics, and exotic metals and composites. These materials are utilized in design along with standard metals such as steel or aluminium. The nonlinear FEA capabilities dramatically improve the accuracy of FEA results when they are compared to linear simulations, and for instance in noise and vibration (N&V) stress and /or durability, thermal comfort and safety and crash and blast models. Head-on and offset car impact are all represented as detailed models to fulfil the safety and regulatory missions with the simulation.

For example, consider the complex non-linear crash analysis computations done by BMW. The crash management system is well designed and maintained during the crash scenario, including the crumple zone areas in the front and rear, as demonstrated in Figures 1 and 2 (Courtesy of BMW).

Inclusion of various non-linearities such as composite material behaviour and the loads in the simulation



Figure 3

models make the results come closer than ever to the physical reality.

Figure 3 represents the non-linear crash simulation that is done on a composite structural member subjected to offset axial crushing.

The complex composite analysis results have been compared to the test set up in the lab with great accuracy. The rail crush example (Figure 3) is run in CZone for Abaqus which is an add-on product to Abaqus/Explicit (courtesy of Engenuity, Ltd.).

Modelling conditions such as variability on what percentage of welds could be missing in the manufacturing process during the build process are important. Adding the stochastic and probability modelling on top of the aforementioned non-linearity makes the analysis more valuable than ever. Hardware Powers Increasingly Sophisticated Software
The computer hardware on which advanced analyses, such as full crash analysis and NVH, thermal comfort, CFD, safety or blast analysis, are run has also come a long way in recent years—and will become even more

powerful in the future. An additional benefit of less expensive, parallel and faster computing is that the design of experiments (DOE), optimization, stochastic and probability analysis can now become a natural extension of the engineer's analysis and modelling process.

In addition to the computing power, the capabilities available to the CAE engineer have increased in the last few years in tandem with the improvements in the parallelization of algorithms in FEA, CFD and multiphysics software, in combination with other enhancements, such as accurate sub-structuring that allows the models to get even larger in size and content. These refinements are allowing engineers to build ever more realistic FEA/CFD models with increasingly finer and finer meshes.

One other noteworthy remark is that not only have software and hardware come a long way from its power of representation in Multi-Physics, it is also getting simpler to use. A case in point is the utilization of pre-processors such as Hypermesh (From Altair Engineering), ANSA (from Beta CAE), ABAQUS CAE (From Simulia) and the Mesh Wrapping capability in the STARCCM+ (CD-Adapco) to create complex models quickly, and even to get them to communicate and pass results between different software packages. All in all, it is allowing the engineer to learn and adapt quickly to changing economic conditions. I remember the first safety model I built had about 10K elements to represent a C/D size sedan in the late eighties. That safety model, although helpful in designing the trigger mechanisms for better crash repeatability and axial load management, missed the crush distance by quite a lot when the model's crush distance was compared to its physical prototype counterpart. That was due to the limitation of the computing power that existed within the CRAY XMP, one of the most powerful computers that existed at the time. We could only get qualitative results to fine tune a model and help with the component detail design to strategically place the front rail trigger mechanisms and optimise the crush absorption. However, we could not sign off on a design with such crash models or even totally eliminate a prototype. Today, because computers are so much more powerful and available, one can do wonders with non-linear analysis even on household computers.

Crash models with 2 million elements or more are common nowadays.

The crash and safety engineers at Toyota have reported that they have created models reaching over 14 million elements, with elements as small as 1-2 mm in size. These types of models include so much detail that they can then be utilized to decide, for example, where the

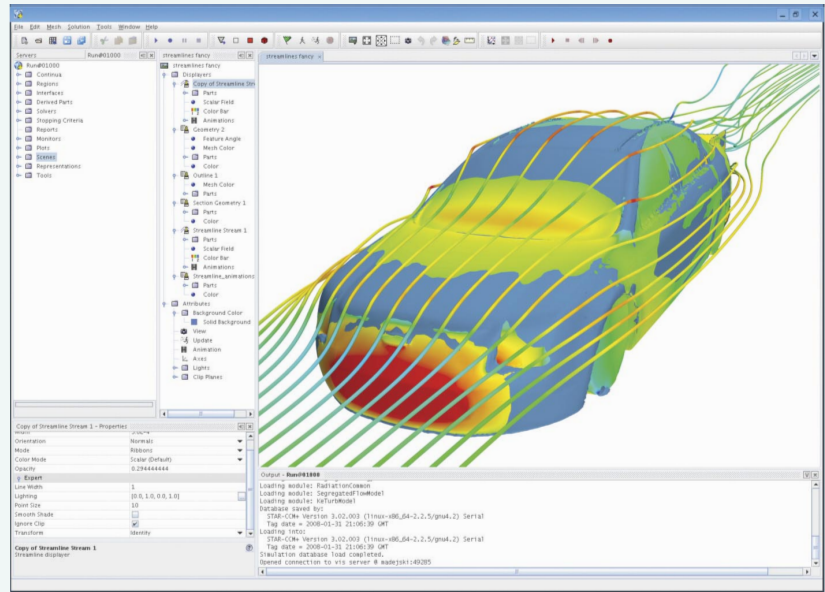


Figure 4

location is for airbag sensors and what amount of deceleration should trigger them.

CAE models provide a great deal of detailed information which in turn improves the quality of designs, ensuring better results decade after decade. This results in a general reduction in the need for expensive physical prototypes, which cost hundreds of thousands of dollars and are destroyed in fraction of a second.

The NVH linear models of the 1990's era only ever had around 100K linear representations with a number of super element structures to predict noise levels at the 80-100 Hz frequency coverage. These models are now represented by over 2 million elements in a single shot, including rolling tires and the frequency coverage of 300-450 Hz, thanks in part to software such as sub-structuring and AMLS (Automated Multi-Level Substructuring), as well as the availability of inexpensive powerful computers available to the greater public. These types of models can help designers and engineers to place Quiet Steel, multi-layer laminates in strategic locations, in the cars and trucks to quiet down the noisy panels. The models can also help in the realization of the type of trim materials, such as carpet and plastics, which can be used. This trim modelling capability was not possible or readily available in the 1980s and early 1990s.

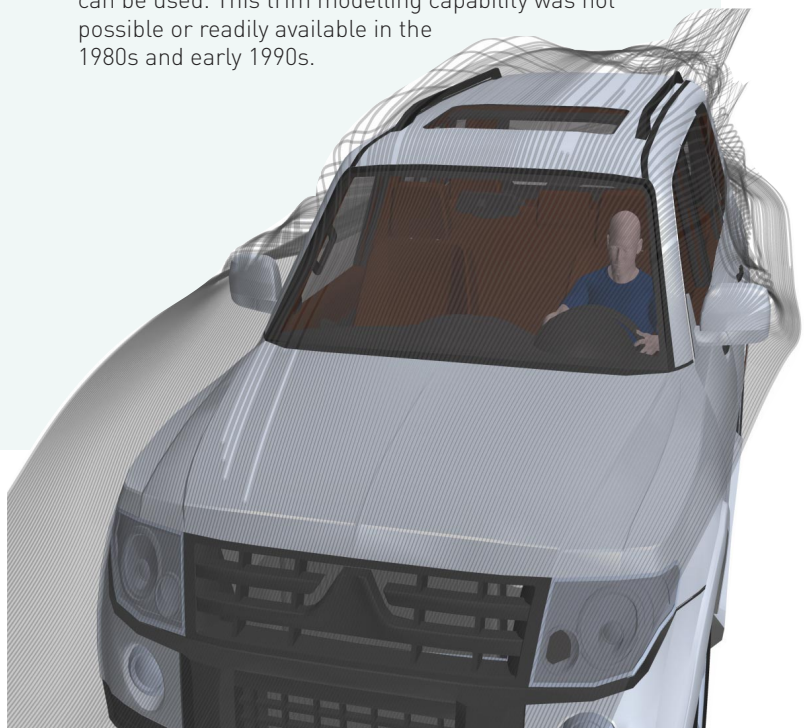


Figure 5

On the CFD front

In previous times some of our CFD engineers would take approximately 2-3 weeks to create 2.5 million finite volume cells in my aerodynamics section, which would take a few days to run on multiple CPUs. The results would vary by about 0.020 when we compared the Coefficient of Drag prediction to the wind tunnel tests. A higher number of cells would provide a better prediction, but it would take even longer for the analysis to complete. For this reason, engineers often preferred to go to the wind tunnel for quicker results as well as a more accurate representation.

These days, it is extremely easy to create CFD models. I recently created an external aero model of a full vehicle representation with the inclusion of the occupants, including the windows open condition, with about 30 million cells. This took only about 3 hours to complete, and a few hours later (in the same day I might add) I would get the results back with accurate aero predictions, and certainly within the variability range of a shape and content. Utilizing the CCM+ for model creation is very easy; all one needs is CAD data that is fairly air and water tight. CCM+ is also forgiving if there are few holes which it can repair after one takes it to its pre-processing mode. Once in there, you can fill the unwanted holes and move on to wrap the surface, and then with a few clicks you can create an 'automated' volume mesh. It is relatively straightforward, and as such the learning curve is very fast even for first time CCM+ users, although obviously it helps if one has some background in the theory and its application utilization.

I could not show my analysis results and pictures for confidentiality reasons, but instead I have included some publicly released pictures from CD-Adapco, Figures 4, 5 and 6 are examples of what one can do with their software and even in some more advanced applications, one can transfer results such as the pressure fluctuations to a structural software, such as Simulia's ABAQUS, NASTRAN or acoustic software such as ACTRAN, for further analysis, such as noise predictions inside the cabin of a car due to structural vibrations from that of the dynamic fluid pressure induced upon it.

Blast and Explosion

Another extension of the CAE capabilities is in the area of safety design for blast and explosion mitigation. This is a technology that combines the Lagrangian Mesh that is traditionally used for typical crash modelling and analysis with that of the Eulerian mesh that is used to represent the blast of explosives that travels through the air or ground, and delivers a supersonic shock to the vehicle in question. The aim is to design a vehicle which is safe under the blast explosion through analysis and modelling. In some sense, one can think of it as the FSI (Fluid / Solid Interaction) of the air blast and that of the vehicle that gets the shock through the fluid. Once again, this type of analysis requires a

great deal of computer horsepower since the models can contain very large amounts of nodes and elements.

This type of analysis can become even more complex when one adds erosion, regularization and complex tri-axiality failure criteria on elements that erode or blast away, which could easily bring models upward of 15 million elements for blast type applications.

As an example we can take a look at the analysis below that was done by Altair Engineering's Mr. Jean-Pierre Bobineau using the Altair Suite of software, to demonstrate the capability of the non-linear RADIOSS that is readily utilized in the crash and safety departments in the automotive industry for blast and mitigation applications (Figures 7-10, courtesy of Altair Engineering).

Automotive Simulation Advances Benefit Other Industries
The automotive industry is certainly one of the major staging grounds for large-scale FEA / CFD in terms of degrees of freedom. The use of vehicle Durability, NVH and safety analyses have grown tenfold in the last decade, with enabling tools such as sub-structuring on calculating modal presentation. There are also several attempts going on to use MDO (multi-disciplinary optimization) analysis among these attributes.

We have come to the realization that the knowledge and experience gained in the automotive industry can become quite beneficial in other industries as well. The CAE engineers in the automotive industry have been eager to share their results and spread the success and the news of these capabilities at regional and world seminars and conferences. So the "lessons learned" in automotive simulation capability are feeding directly into heavy vehicle, military, defence, off-road, mining, aerospace and shipbuilding engineering. Newer industries, such as life sciences, are learning that the design challenges they face in Noise & Vibration control of devices and machinery, such as the breathing apparatus design that needs to be "whisper quiet" during the patient's utilization, can also benefit from the CFD and NVH know-how that automotive CAE engineers can provide. We are also likely to see increased knowledge transfer to medical, pharmaceutical, and other industries.

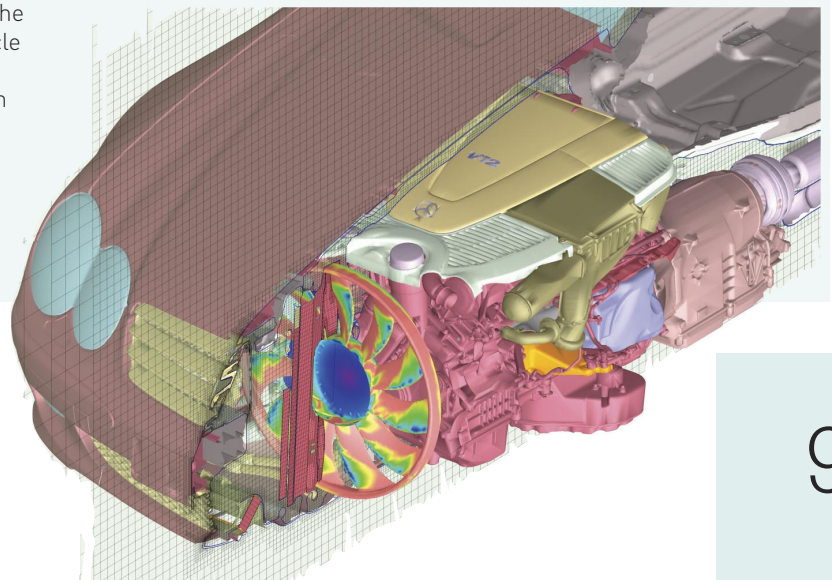


Figure 6

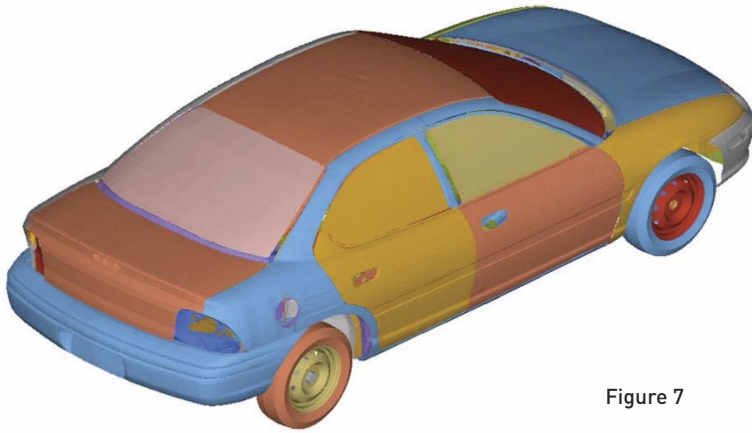


Figure 7

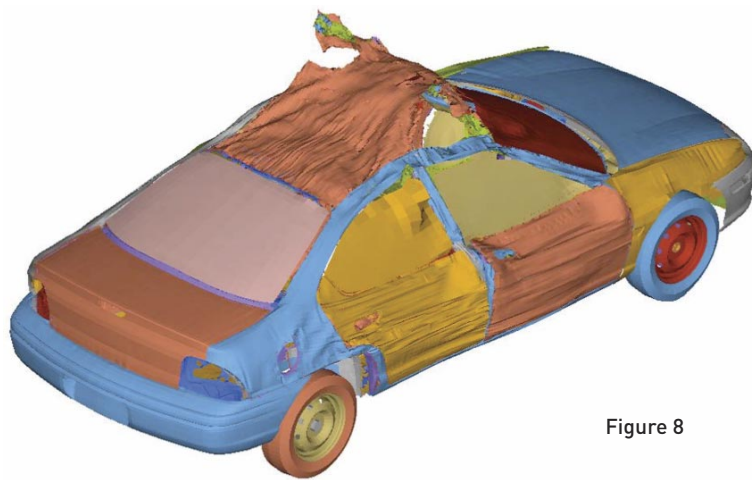


Figure 8

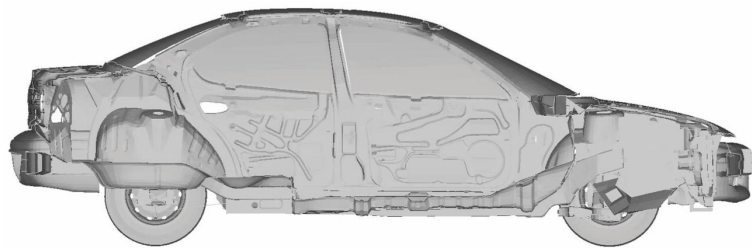


Figure 9

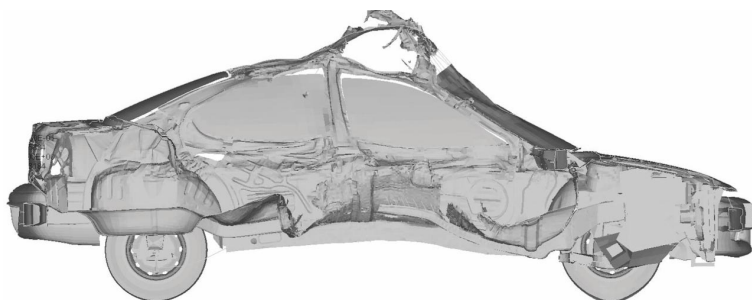


Figure 10

A Look Ahead

I see two new frontiers. First, the explicit FEA methods that have become part of crash/safety and blast & penetration simulations in recent decades will be increasingly applied to noise and vibration applications, and obviously in blast and mitigation. This will result in an increased demand for even faster computing hardware and better integration of implicit and explicit FEA techniques to help design the lighter-weight, efficient, yet comfortable vehicles of tomorrow. Software that communicates and transfers implicit and explicit data seamlessly is well-positioned for such challenges.

I also see that it is necessary to better integrate FEA and CFD, whether this is used to couple wind loads to vehicle structure, take thermal fluid and map it to the structural surface, or to help the engineers predict the fuel sloshing noise under braking and acceleration in automobiles.

Once again, the software that has this capability, or even unified software that offers both FEA and CFD, is in a better marketing position than those who do not have such capabilities built-in.

Secondly, the advent of isogeometric analysis. A technique using NURBS and T-Splines as a basis for construction of element shape functions is currently being championed by Prof. Tom Hughes at the University of Texas at Austin. It is a new way of thinking about how finite elements will be created or modified in the future, or at least as an element selection option. This is a tremendous way to seek better accuracy to compute stresses, velocities, pressures and buckling loads. This technique even has promise in automotive applications to overcome the limitations of modal contents in N&V analysis as well as perhaps more accurate computations gained in the Fluid Dynamics.

In summary, those companies willing and able to continue investing more in realistic simulation technology and appropriate staff will certainly benefit as they develop the next generation of 'green' products. The engineers who excel in using Advanced CAE simulation technology and apply it to products will be in high demand, not only in the automotive industry but as innovation leaders who will be able to apply their knowledge about the benefits of FEA / CFD applications across many other industries as well.

Simulating The Wiesel

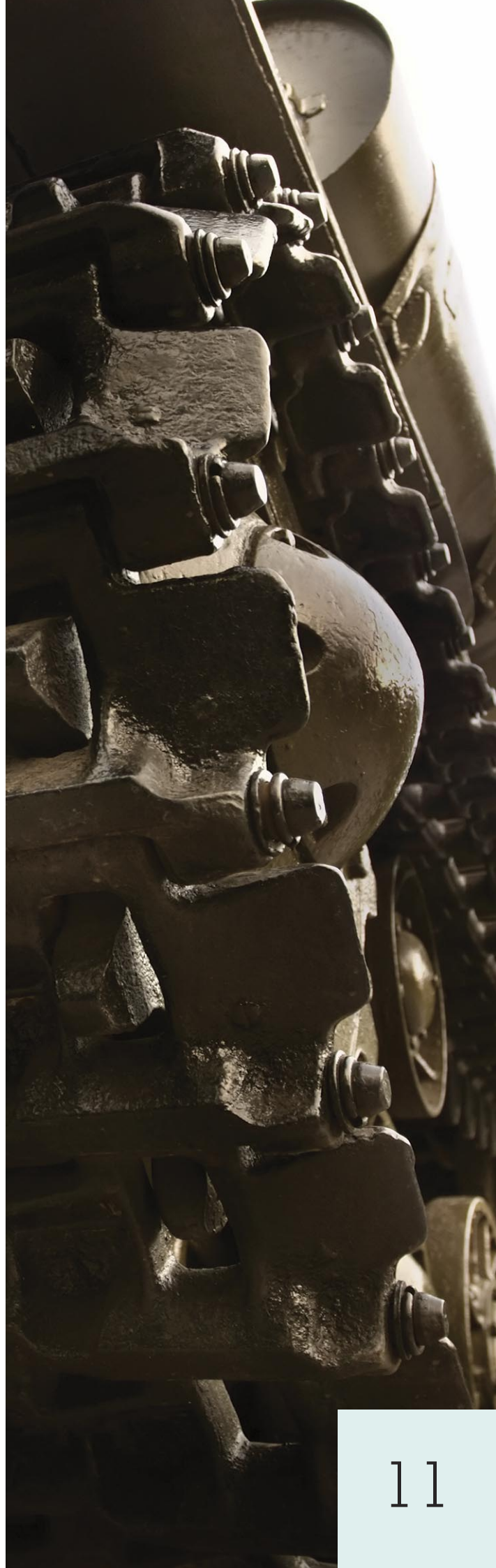
Real-Time and MBS/FEM Model for Simulating
a Tracked Vehicle on Deformable Soils

Bastian Fuhr, Martin Meywerk,
Thomas Fortmüller & Stephan Baß
Helmut-Schmidt-University – Hamburg, Germany.

Simulation is just one way in which to gain insight into the behaviour of a moving vehicle, specifically in this case, a tracked military tank (the German-built "Wiesel II") on deformable soils. Many publications cover this topic, but most of the simulations described therein cannot be run in real-time, i.e. the response time is much longer than the time period which should be simulated. The ability to run a simulation in real-time is essential for driving simulators. This article describes an approach for the real-time simulation of the tank.

Vertical oscillations in tracked vehicles can lead to discomfort, illness or to the increase of injuries when transporting injured people. In order to investigate the mainly vertical oscillation, especially with regard to the effects on the human beings, driving simulators are a useful option. The main components of a driving simulator are the moveable cabin with viewing and sound system in which the driver or an occupant is sitting, and the real-time computer with the MBS software (Figure 1). The motion of the cabin is calculated by the real-time computer and then transferred to the motion system, which moves the cabin with the driver. The ability of the real-time computer to calculate the correct movement of the vehicle instantaneously is essential for driving simulation. Therefore, special dynamic software is necessary. There are some commercial MBS software packages available, but the combination of MBS, tracked vehicle, deformable soil and rough uneven terrain is not considered in these packages.

The interaction between vehicles and deformable soils is described in references 1-6, especially the interaction between tracked vehicles and deformable soils which is analysed by Garber and Wong [4], where an analytical solution is given. The pressure distribution between tires or tracks and deformable soils is described by Bekker [1,2]. The shear stress between track and soil is described by Janosi and Hanamoto [7].



In the real-time approach presented here, the ordinary differential equation of the catenary as suggested by Garber and Wong [4] is used in a discrete form for the description of the geometry of the track between two road wheels. The pressure-sinkage equation of Bekker [1] is used for the pressure distribution, and shear stress is calculated by using the approach of Janosi and Hanamoto [7].

The elevation profile of the terrain and the soil properties, i.e. mainly the Bekker values and the values for shear stress calculation [7], are stored in lookup tables in MATLAB/Simulink. Therefore, arbitrary functions of the elevation and the values can be used in the calculation. It is possible to implement the change of these values due to the passing of a vehicle or a road wheel in order to take multi pass effects into account. Elastic spring back of the soil after its plastic deformation is not considered.

The simulated vehicle is a 'Wiesel II', the tank used by German armed forces. Several velocities and angles are compared to a dynamic experiment where the tracked vehicle drove on an asphalt street with obstacles. The same experiment was also simulated in a detailed MBS/FEM model. The aim of this model is to verify the correct behaviour of the real-time model, because comparison between experiment and model is difficult. Furthermore, different manoeuvres on some deformable soils were simulated with the detailed MBS/FEM model.

Coupled MBS/FEM model

In order to compare the results of the real-time model with the results of a tracked vehicle driving on deformable soils, a detailed model of the 'Wiesel II' tank was created (see Figure 2). The Wiesel II is one of the smaller German armed forces tanks. It has a length of 3.8m and weighs around 4.1t. The main components of the model are: the body of the tank (rigid body), torsion bar suspension for the road wheels, road wheels, driving sprockets, return rollers, dampers, track tensioner and two tracks, each consisting of 60 rigid bodies connected to each other on both sides with bars.

The main body has six degrees of freedom. Inertia properties such as mass, centre of gravity and moments

of inertia are the same as in the real-time model, and close to the real vehicle.

Both driving sprockets, at the left and right front of the vehicle, have one rotational degree of freedom about the horizontal axis, with respect to the main body. A constant angular velocity is applied to the driving sprockets. The engine and gearbox are not implemented in the model. A driving sprocket is depicted in Figure 3, and consists of three different parts. The teeth shown in the figure are necessary for the transmission of forces between driving sprocket and track; the details of force transmission are explained below. Figure 3 also shows four nodes (left of the driving sprocket) that are essential to define the rotation axis of the driving sprocket.

Unlike the rest of the vehicle's wheels, the two rear road wheels are not attached to the main body by regular torsion bar suspension, but by a more complex track tensioner. The wheels have a rotational degree of freedom with respect to the track tensioner (defined by the lower nodes in Figure 4). The track tensioners themselves have one translational (defined by nodes in the thin and big cylinders) and one rotational degree of freedom with regard to the main body. The two-stage tension spring acts in parallel with the translation joint.

Both springs are responsible for the tension forces in the tracks, and are represented as the lean and bulky cylinders in Figure 4. The spring characteristic of the track tensioner is approximated by two linear functions (see Figure 5). In the zero position, the track tensioner is pre-stressed by 4.41 kN.

The remaining eight road wheels are attached to the main body by torsion bar suspension elements. This means that their centres of gravity have one degree of freedom, as they are moving in a circle. The circle is determined by the rigid arms at the ends of the torsion bars (Figure 6). The torsion bars also have a rotational degree of freedom at the upper end as well.

The spring rate of the torsion bar suspension is equal at all four road wheels. What is different are the preload torques, which decrease from the front to the fourth

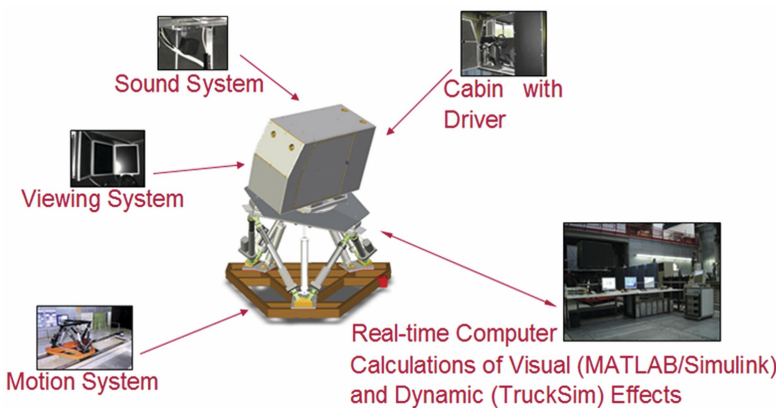


Figure 1: Main components of a driving simulator

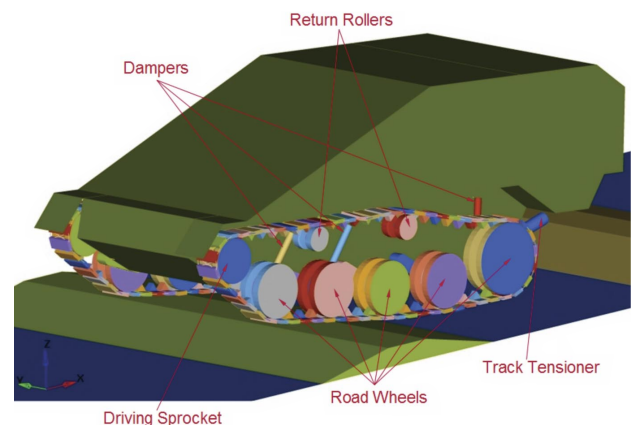


Figure 2: Detailed MBS/FEM model of the tracked vehicle

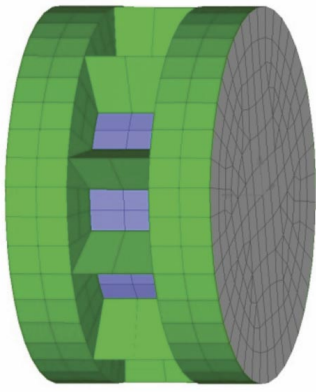


Figure 3: Simplified geometry of the driving sprockets

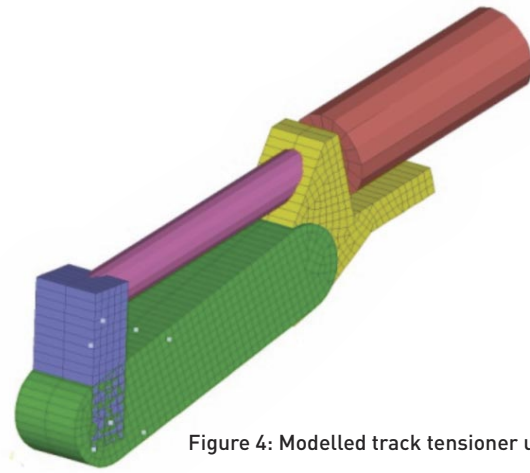


Figure 4: Modelled track tensioner unit

wheel. The preload of the first wheel is about 1600 Nm, and around 900 Nm at the fourth wheel. Furthermore, the stop angles are different and are also bigger at the first wheel than at the fourth. Despite the degree of freedom of the centres of the road wheels, they do have a translational degree of freedom (on a circle). The smaller return rollers of each track have a rotational degree of freedom with respect to the main body (see Figure 7). All wheels are generated from the same original model by scaling it in the x- and y- directions.

Each of the two tracks is represented by 60 links. The track links are defined as rigid bodies which are connected by four bars. To make the contact algorithm more efficient, every track link consists of two different "Part Identification numbers" PID (see Figure 8).

The bars are introduced for modelling the rotational degree freedom of the linked plates. That means that the revolute joints are approximated. Due to the high bar stiffness, this approximation ensures the flexibility of the bearings, which can be found for example in rubber bearings (in this application, the track links are connected by using so called 'bars' (special FE elements). These elements are very stiff but they can rotate around the point where they are placed. This approximation allows that the bearing (the point where the ends of the bars are placed) is flexible. And this behaviour is identical to the behaviour of a rubber bearing / rubber mounting). Modelling in this way has the advantage that no closed chain in the sense of multi-body dynamics has to be introduced. The beams are modelled using Finite Elements.

The interaction between the tracks on the one side and the wheels (driving sprockets, road and return wheels) on the other side is modelled by penalty contact forces. The geometry of the above mentioned rigid parts is described by segments. The penalty contact algorithm calculates the distances between nodes of the segments of one part and the segments of the other part. If this distance is lower than the contact thickness, a penalty force is applied to the penetrating node, as well as to the nodes of the segment considering the equilibrium of moments (see Figure 9).

There are two key parameters for describing deformable soils. The soil compression shows the interrelation of the pressure p and the sinkage z , and is determined by many experimental indentation tests. During the test series, the diameter of the plate has to be modified.

The other important parameter is the shear strength τ . This value is dependent on the pressure p and it is significant in identifying the maximum power transmission on deformable soils. Therefore several tests are essential with varying pressure.

The deformation of the soil is described by an elasto-plastic material law similar to Drucker-Prager-Cap. One characteristic of this law is how the linear dependency of von Mises yield stress σ_y depends linearly on the hydrostatic pressure p_{hyd} (see Figure 10). The second characteristic is the volumetric plastic behaviour which occurs for the hydrostatic stress distribution. Therefore, plastic deformation takes place under two conditions: either when the second invariant of the deviatoric stress

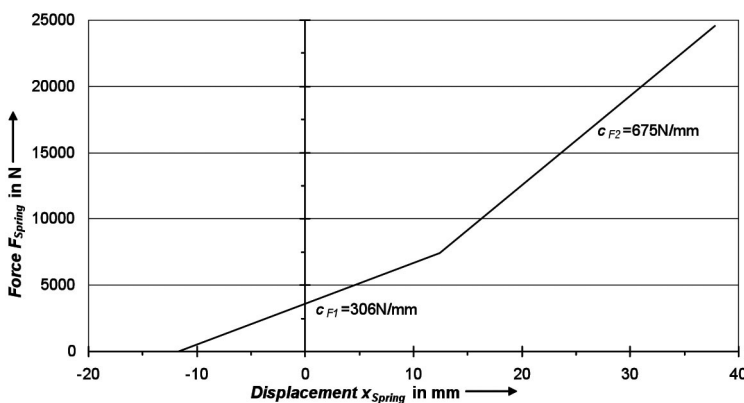


Figure 5: Spring characteristics of the track tensioner

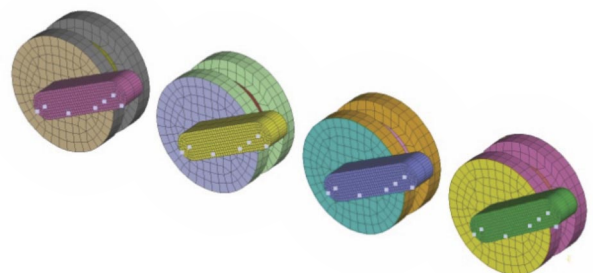


Figure 6: Rigid arms of torsion bar suspension for the road wheels

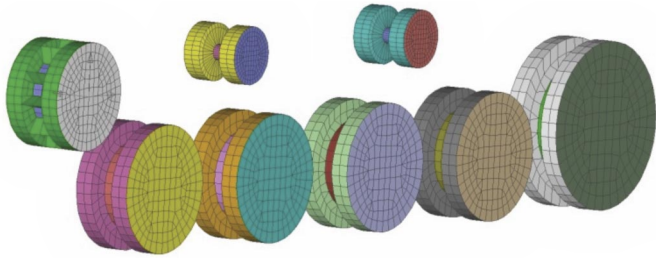


Figure 7: Wheels of the left track device

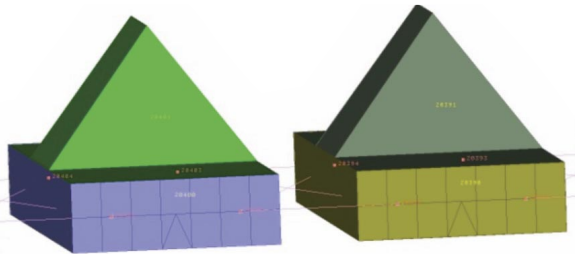


Figure 8: Four very stiff bars as track links

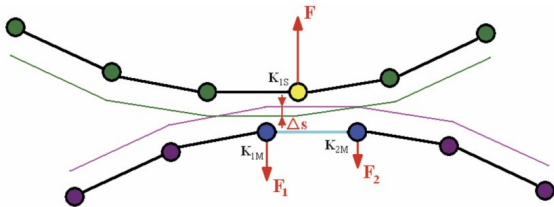


Figure 9: Penalty contact algorithm in the MBS/FEM model

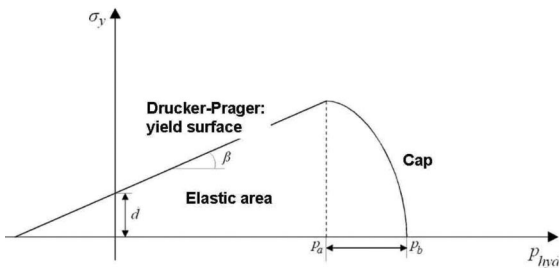


Figure 10: Yield surface of Drucker-Prager-Cap material law (parameter erläutern)



Figure 14: Vehicle on a rigid street with an obstacle

tensor exceeds the von-Mises yield stress or when the hydrostatic pressure exceeds the volumetric pressure curve. Yielding under hydrostatic pressure means a kind of 'cap' in the deviatoric yield curve. This cap will be pushed to higher values if the soil is deformed plastically by hydrostatic pressure, resulting in a kind of soil hardening. This hardening is necessary for the description of multi-pass effects.

Real-time Model

The real-time model of the tracked vehicle can be divided into two parts: the MBS part contains the chassis, the torsion bar suspension, the dampers and the wheels (driving sprockets and road wheels). Since the track is supposed to form a straight line between the driving sprockets and the last road wheels, the return rollers can be neglected. This MBS part is modeled in TRUCKSim, a commercial MBS software package capable of real-time simulation. The second part of the model contains the track and the deformable soil. This part is implemented in MATLAB/Simulink.

Further detail on the real-time model can be downloaded in PDF format from www.nafems.org/realtime

Results

In this section some results of the models are discussed. First of all the models are compared to experimental results, where the vehicle drives with a slightly increasing speed on a rigid street with seven obstacles. Figure 14 shows the vehicle with one of these obstacles.

One difficulty in comparing the models and the experiment is with the translational velocity in the global coordinate system. In the experiment, the velocity fluctuates intensively while the mean velocity is increasing (see Figure 15). The increasing velocity has a significant effect on all dynamic quantities and makes it harder to compare the MBS/FEM model with the vehicle.

The reasons for the fluctuations are the obstacles. While the vehicle has to "climb" them, the velocity decreases, and because of the limited motor torque, downhill velocity increases. The suspensions of the torsion bars have a hand in there too. In the MBS/FEM model, the angular velocity is prescribed to the driving sprockets. Therefore the fluctuations are smaller than in the experiment. But nevertheless the fluctuations are

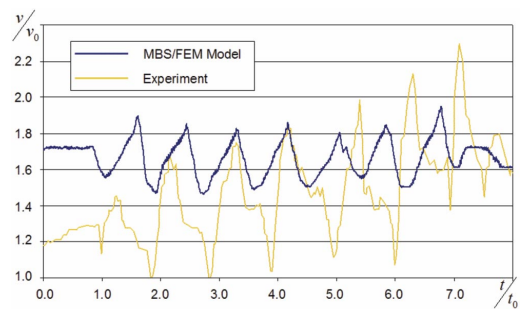


Figure 15: Velocity of the vehicle in the experiment and of the MBS/FEM model.

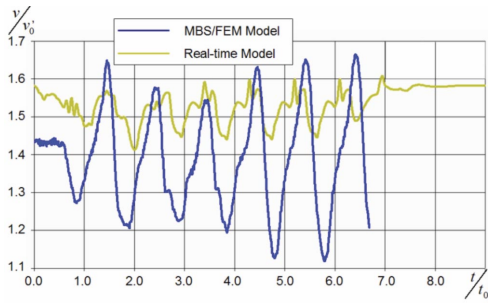


Figure 16: Velocity of the real-time model and of the MBS/FEM model

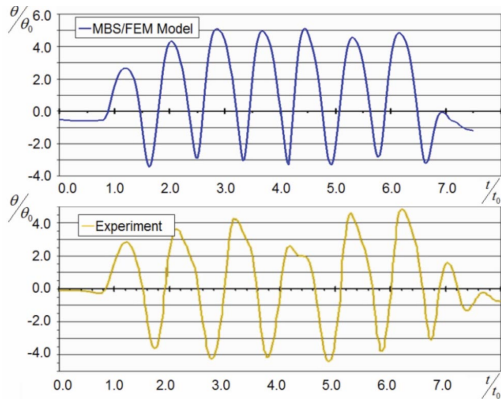


Figure 17: Comparison of the pitch angle between experiment and MBS/FEM model

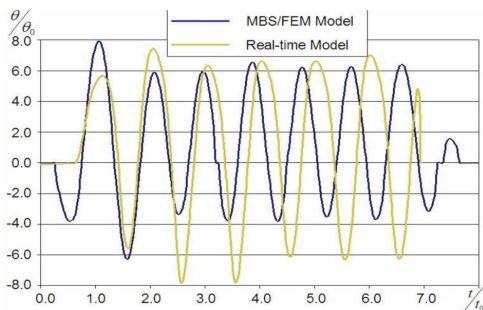


Figure 18: Comparison of the pitch angle between MBS/FEM model and real-time model

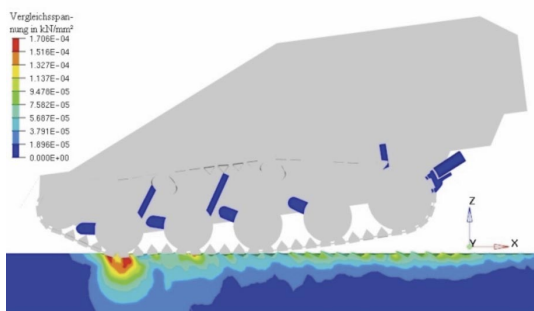


Figure 19: Hydrostatic pressure distribution in the MBS/FEM model

obvious. Prescribing angular velocities equates to an motor torque, and therefore the fluctuations in the MBS/FEM model are smaller than in the experiment. During the whole test drive the mean velocity in the simulation is almost similar to the velocity in the experiment.

Another reason for the lack of comparability of the translational velocity is that the velocity in the experiment is measured by using the angular velocity of the driving sprockets. In the simulations the measured velocity is the effective velocity of the centre of gravity in the global coordinate system.

The comparison of the velocity between the real-time model and the MBS/FEM model is shown in Figure 16. The velocity of the real-time model is controlled by an algorithm, and the engine characteristic map is used. The velocity fluctuates less than in the MBS/FEM simulation because some dynamic aspects are neglected to enable real-time simulation. It is not possible to couple a control algorithm with the MBS/FEM model just like that. Therefore the comparison between MBS/FEM and the real-time model is restricted. Notice that the mean velocity is different than it was when comparing the vehicle with the MBS/FEM model.

Figure 17 shows the pitch angle of the test vehicle and the MBS/FEM model. The similarities are quite good. Differences are due to the deviation of the velocity, because a higher velocity in the simulation leads to a longer jump over the obstacle. Consequently, the tank touches down on the ramp of the following obstacle, and this reduces the negative pitch angle and enlarges the positive pitch angle. When the velocity is alike in test and simulation, the pitch angles are almost similar (compare pitch angle at obstacles 5 and 6 in the test with obstacles 6 and 7 in the simulation).

In Figure 18 the pitch angle of the real-time model is compared with the MBS/FEM model. Both curves correlate strongly. The differences in the amplitudes are caused by the dynamic aspects that have been neglected.

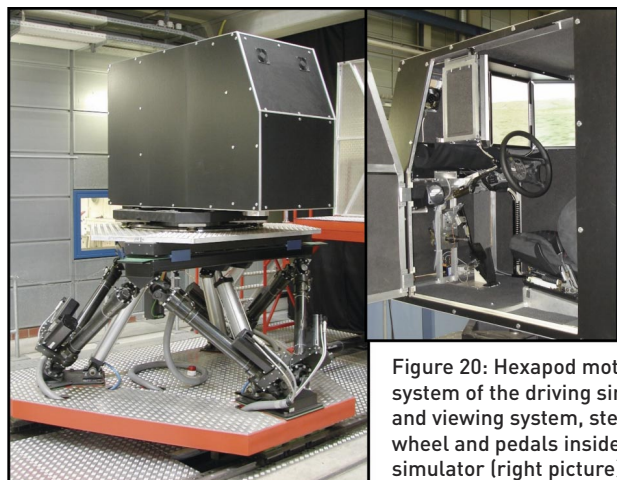


Figure 20: Hexapod motion system of the driving simulator and viewing system, steering wheel and pedals inside the simulator (right picture)

Several other comparisons have been done, especially those between the test vehicle and the MBS/FEM model on several soft soils to use the MBS/FEM model for referencing the real-time model. The results are also quite good. This is not surprising, as driving on the rigid pavement with obstacles is a greater challenge for the real-time model than driving on soft soil. In Figure 19 an example of the hydrostatic pressure distribution for a braking manoeuvre for the MBS/FEM model is shown.

Summary

The aim of this research was to determine the impact of an active suspension and damping system in a tracked vehicle. In this case the tank Wiesel II of the German armed forces was chosen and a real-time model was built up to implement it in the driving simulator MARS of the Institute of Automotive and Power Train Engineering at Helmut-Schmidt-University in Hamburg (see Figure 20).

Several studies have been done with a subject driving the vehicle on a virtual terrain in a simulator cabin, where the soil profile evoked vibrations inside the cabin. The driving simulator was used to investigate active and passive damping devices. In this investigation, the subject should judge the differences between passive and active damping and suspension systems.

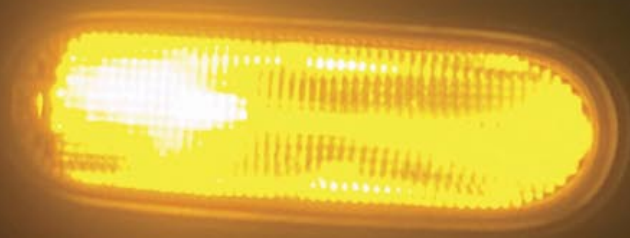
For verifying the real-time model, an MBS/FEM model is essential. Therefore the MBS/FEM model itself is compared to a real vehicle driving over several obstacles

on asphalt. Furthermore, several manoeuvres of the MBS/FEM model on different deformable soils were simulated and analysed. The results are necessary to have a comparison for the real-time model and making the virtual ride in a simulator as realistic as possible.

The different types of simulation were made either with PAM-CRASH or with MATLAB/Simulink and TruckSim.

References

- [1] Bekker, MG. Theory of land locomotion, Ann Arbor: The University of Michigan Press; 1956.
- [2] Bekker MG. Introduction to terrain vehicle system, Ann Arbor: The University of Michigan Press; 1969.
- [3] Wong JY. Terramechanics and off-road vehicles. Amsterdam: Elsevier; 1989.
- [4] Garber M, Wong JY. Prediction of ground pressure distribution under tracked vehicles- Part I. An Analytical method for predicting ground pressure distribution. J Terramech 1981; 18(1):1-23.
- [5] Garber M, Wong JY. Prediction of ground pressure distribution under tracked vehicles- Part II. Effects of design parameters of tracksuspension system on ground pressure distribution. J Terramech 1981; 18(2); 71-79.
- [6] Park WY e.a. Prediction of tractive performance of flexible tracked vehicle, J Terramech 2008;45 (1-2); 13-23.
- [7] Janosi Z., Hanamoto B. The analytical determination of drawbar pull as slip for tracked vehicles in deformable soils. In: Proceedings of the 1st International conference on the mechanics of soil-vehicle systems. Torino, Italy; 1961.



Modelling Condensation in Automotive Headlamps

Jacopo Alaimo & Sergio Zattoni, Automotive Lighting Italia, Italy

Alberto Deponi, Fabio Damiani, Luca Brugali, & Lorenzo Bucchieri EnginSoft, Italy

The environment inside an automotive headlamp has high thermal and low mass exchanges with the external environment, causing condensation on the lens. An acceptable headlamp design can only be produced if this condensation can be disposed of in a fixed time under severe thermal conditions.

Experimental studies are performed in climatic chambers under highly controlled conditions, whilst long transient numerical simulations are performed on large meshes in order to capture the relevant physics of the problem. This article outlines a new numerical method which has been used in order to study the problem, and the results obtained when applied to real-world designs.

Until a few years ago, lenses were typically designed using glass and covered by an optical prism to obtain the correct light distribution (see Figure 1). The increased sophistication of molding capabilities has now led to the mass production of large transparent plastic lenses. Curved shapes and transparent surfaces have opened a new world for style solutions, but a transparent lens lets the eye see all the way inside the headlamps. Today the observer has a free view of the inside of the headlamp, highlighting even the slightest optical fault, any thermal damage of the inner components and the possible presence of water droplets. The presence of condensation inside the headlamp is perceived by the customer as a lack of quality and reliability.

The most common solution for decreasing condensation quantity and disposal time is represented by the optimization of inner air flows and of temperature distribution on the main lens. Typically, at least two vent holes are present on the headlamp housing; in order to optimize their efficiency, it is important to find their optimal number and locations by performing numerical and physical tests during the pre-industrialization phase. Until today the solution to condensation formation has always been sought by trial and error. This leads to a great increase in time and costs. The use of appropriate numerical methods and test rooms therefore becomes a strategic tool for decreasing production time and cost and, in the near future, for optimizing headlamp design with respect to condensation formation and disposal.

From a fluid-dynamic point of view, an automotive headlamp can be considered as a cavity with low massflow interaction but high thermal interaction with the external environment. One wall of the cavity, the lens, is transparent while the others are opaque. Inside the headlamp, there are one or more lamps and a number of components: reflectors, screens, caps, connectors,

pipettes, etc. These components are used for the functionality of the headlamp but also play a fundamental role in the thermo-fluid-dynamic behavior of the fluid inside the headlamp which is a mixture of air and water vapour.

The headlamp can undergo the phenomena of heating and cooling because of internal and external heat sources. The external heat sources or sinks are represented by the external environment temperature or by the heat coming from the engine. The internal heat source is represented by the switched-on lamp, which heats up the surrounding fluid and emits radiation. Since the fluid inside the headlamp is composed of a mixture of air and water vapour, it changes density because of thermal evolution. Density differences are the cause of internal convective motions which are always laminar. Since temperature is, in the final analysis, the cause of the motion of the internal fluid, it is important to precisely and accurately characterize all of the components of the headlamp. They are to be characterized both from a thermal and an optical point of view in order to model temperature, heat transfer to surrounding fluid, radiation absorption, emission and reflection. In addition, the assembly of all components limits the space where fluid can flow, hence determining the motion field inside the headlamp.

All components should be modelled with a geometrical detail which is adequate for the level of accuracy needed for the fluid-dynamic results. On the other hand, great geometric detail leads to a large mesh and, consequently, large computational costs. A trade-off between geometric detail and computational cost needs to be achieved. In addition to this, temperature evolution of the headlamp may cause water phase changes; in particular it may cause water condensation and evaporation on the lens which is a main issue for headlamp producers and the target of the present work.

The problem to be studied is a typical multi-phase problem in which it is important to properly describe the phase change between liquid water and water vapour. In this problem it is imperative to capture the natural convection velocity field due to the different density of fluid masses inside the headlamp. For this reason it is important to account for gravity and buoyancy effects in the fluid. Since the motion field is driven by natural convection, the flow is laminar and no turbulence model is used. Another important phenomenon to be modelled is the heat transfer between walls and fluid, between different fluid masses and, particularly, the latent heat absorbed by water evaporation and released by vapour condensation. Finally, when a switched on lamp is considered, thermal radiation is to be accounted for.



Figure 1: Comparison Between an Old Fashioned Glass Headlamp (top) and a New Transparent Plastic Headlamp (bottom)

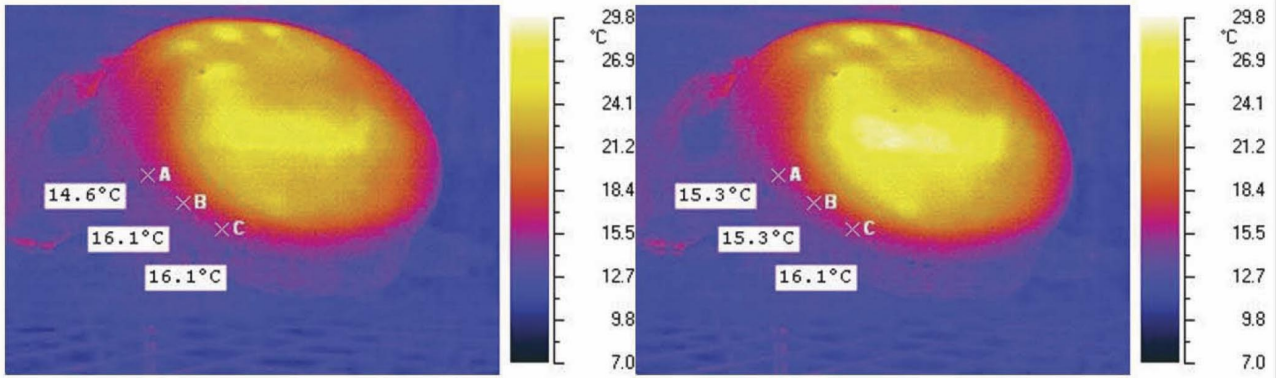


Figure 2: Thermal Maps on the Lens at Two Different Times

Experimental Studies

ALIT Condensation Test Room

ALIT (Automotive Lighting Italia) Condensation Test Room is a metal room with a volume of about 30m³. Glass windows allow the technicians to follow the ongoing tests. By using dedicated hardware, it is possible to control all the main variables related to the condensate disposal process such as:

- Heat Transfer Coefficient (HTC) on headlamp boundary walls;
- Internal and external air relative humidity (RH);
- Internal and external air temperature;
- Pressure and air flow fields in the proximity of ventilation pipettes;
- Mission profile reproduction accounting for engine induced temperature and wind speed;
- Interaction between headlamp-engine assembly.

The ALIT condensation test room is projected to control all the main factors involved in the HTC distribution. It is possible to control external air RH and temperature; moreover, an air speed of up to 80Km/h can be produced along the longitudinal car axis. Inside the room, an engine box mock-up reproduces the effects of the average temperature produced by the engine. Since the HTC is influenced by aerodynamic effects too, the engine box mock-up reproduces the car shape. At present the

effects not reproducible are represented by pressure and air flow fields inside the engine box. Indeed, geometric and thermodynamic effects of the engine are still too complex to be reproduced. Nevertheless, a good approximation is obtained by using an average temperature inside the engine box mock-up.

Measurement devices

A major problem related to the condensation issue is represented by the difficulty of an objective condensation tracking. Indeed large variations in condensation layer thickness as well as in water droplets diameters may occur, and this has a direct influence on the human eye perception. The use of a standard photographic camera with flash usually highlights even the smallest traces of condensation which may not be visible by human eye. At the same time, it is not possible to measure a continuous distribution of the dew point. Several temperature and humidity probes are present inside ALIT condensation test room, these are located in the free-area zone and inside the engine box mock-up. Moreover, it is possible to place thermal couples and moisture meters inside the headlamp in order to get data. Finally, the temperature distribution on the lens is tracked by means of an infrared camera. Combining these data together with photos and videos of condensation distribution it is possible to track the dew point line. At present it is not possible to measure condensation thickness.

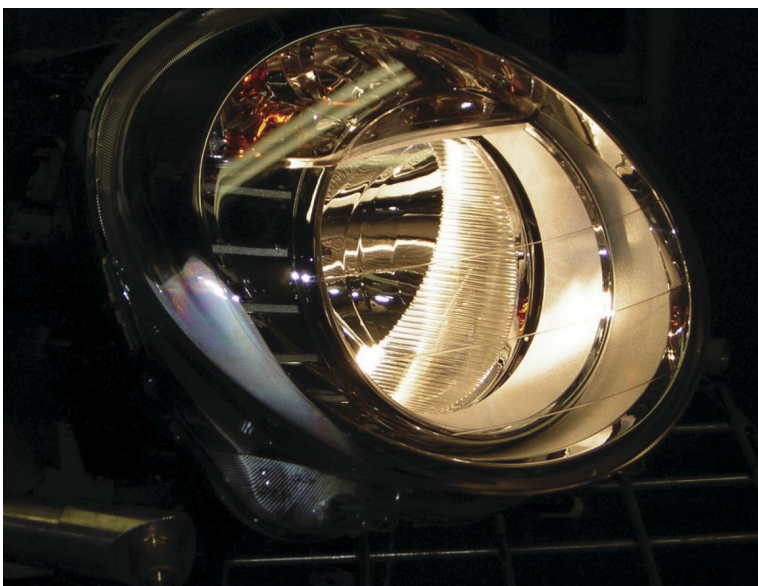


Figure 3: Condensate on a prototype specifically designed for enhancing condensation

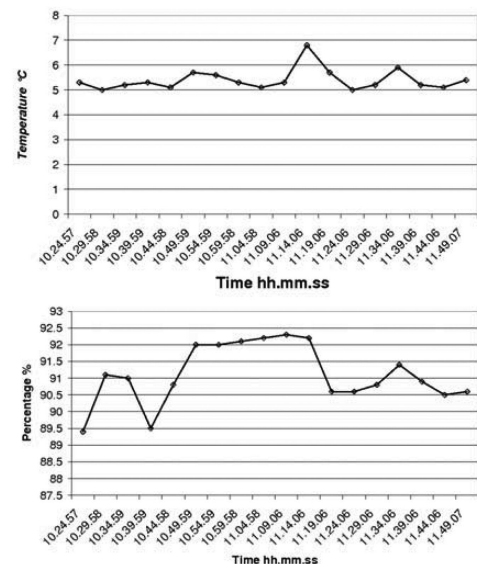


Figure 4: Temperature and Relative Humidity Graphs in ALIT Condensation Test Room

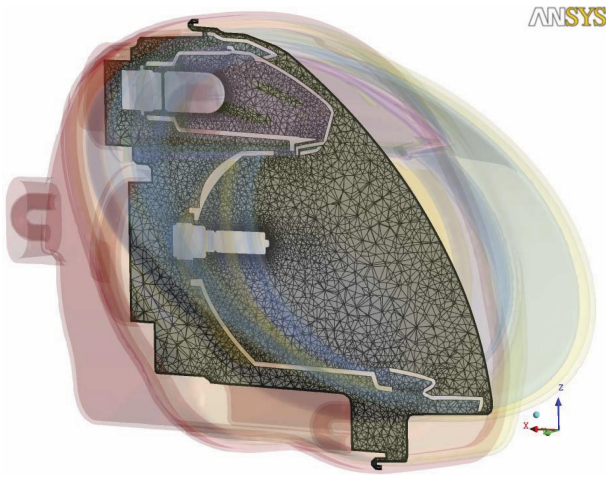


Figure 5: A Typical Tetra-Mesh Optimized for Thermal and Condense Simulations.

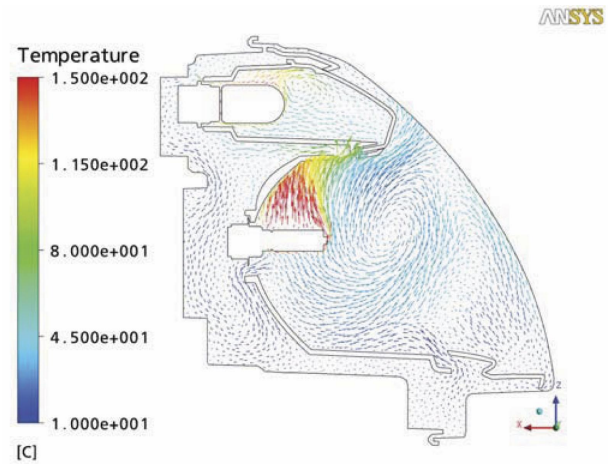


Figure 6: Velocity Vectors on a Vertical Plane Passing Through the Lamps (note that vectors are colored with temperature distribution)

Test Results

The outputs of the condensation test are:

- thermal maps and videos shot using infra-red camera (Figure 2);
- condensation images and videos shot using photographic camera with flash (Figure 3);
- temperature and relative humidity graphs measured by the thermal couples and moisture meters placed inside the headlamp, inside the engine box mock-up and in the external environment (Figure 4).

From Figure 3 it can be noticed that condensation tends to accumulate on the outer side of the headlamp (left side in the figure) which is the coldest part of the lens, as shown by Figure 2.

Numerical Simulations

The Numerical Method

When a switched-on lamp is to be modelled, a radiation model has to be used in order to compute the source term for the energy equation and the radiative heat flux at walls. In this case, the Discrete Transfer model is used for the directional approximation and the Grey model is used for the spectral approximation. The Gray model assumes that all radiation quantities are nearly uniform throughout the spectrum, consequently the radiation intensity is the same for all frequencies. The Discrete Transfer model assumes that the scattering is isotropic. The switched-on lamps are modelled by imposing the temperature data coming from experimental measurements. In the evaporation/condensation model considered, the liquid phase is not modelled directly. Instead, the evaporation/condensation processes occurring on the lens are modelled by means of suitable mass and heat sources for the continuity and thermal equations. The mass source term applied to the conservation law for water vapour mass in the gas is:

$$S_M = \dot{m}A = \frac{\pi L \mu Sh (e - m_f)}{A_l} A.$$

Here m is the water mass per unit area transferred between liquid and gas, A is the area of the element face where evaporation and condensation processes occur, A_l is the total area of the surface where evaporation and condensation processes occur, L is the typical length scale of the process, μ is the diffusivity of water vapour in the air, considered equal to the air dynamic diffusivity, e is the water mass fraction at equilibrium, m_f is the water mass fraction and Sh is the Sherwood number. The air volume fraction is the complement to unity of the computed vapour volume fraction. The energy source due to phase change applied to the conservation law for internal energy is:

$$S_E = -\dot{m}C_p,$$

where C_p is the water latent heat for vaporization/condensation. Mass and energy sources are applied only at surfaces where evaporation/condensation processes occur. In the framework of this evaporation/condensation model, it is possible to define the water mass per unit area lying on the lens as:

$$m_w(\mathbf{x}, t) = m_w(\mathbf{x}, 0) - \int_0^t S_M(\mathbf{x}, \tau) d\tau.$$

Here, the space and time dependency of the water mass per unit area is explicit. This variable allows for precise tracking of the amount of condensation lying on the lens. Moreover, in the case of evaporation, the local mass source has to be null where local water mass per unit area is null; this is achieved by a local control of the mass source term. Mass and energy sources are implemented in ANSYS CFX by means of properly defined functions and variables using the CEL language. The analyses were run using an upwind advection scheme and the first order backward Euler transient scheme. The time step and the convergence criteria were chosen in order to minimize the computational time without compromising result quality and method robustness.

The Computational Mesh

Solid and fluid domains were discretized using a tetra-prism mesh. In particular, prism layers were used inside

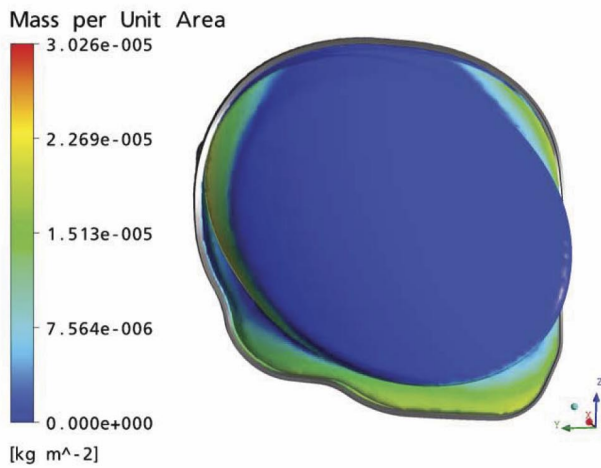


Figure 7: Qualitative Comparison Between Numerical and Experimental Results

each of the solid domains and outside of the rear body, the lens and the lamps. A total of about 1.750.000 elements were used to discretize the entire headlamp. (Figure 5)

Initial and Boundary Conditions

At the start the lamps are switched off, the temperature is 6°C and the relative humidity is 95%. At the beginning of the simulation, the lamps are switched on. After 20 minutes rain starts. After 40 minutes rain stops and a wind of 30 km/h starts blowing until the end of the simulation at 60 s. These conditions are simulated by varying external temperature and relative humidity together with HTC on the lens. The initial and boundary conditions used in the simulation are summarized in Table 1.

Results

The simulation was run on 32 parallel CPUs with OS Linux CENTOS. The computational time was roughly 12 days. In Figure 6 velocity vectors on a vertical plane passing through the lamps is presented; note that vectors are colored with temperature distribution. The strong buoyancy effect caused by the switched on lamps can be appreciated.

Conclusions

Because of difficulties in measuring condensation mass on the lens, at present, only a qualitative comparison can be made; in Figure 7 such a comparison is presented. It can be noticed that the two results are in good agreement highlighting a region of condensation accumulation in the outer side of the headlamp. It has to be highlighted that some sensitivity analyses showed a strong dependency on initial and boundary conditions demonstrating the complexity of the phenomenon under study and the need of strongly controlled experimental conditions. Due to the complexity of the problem, and the

fact that numerical simulations are to be performed over long time period and on large meshes, high computational power is needed. Nevertheless, numerical simulations are able to give detailed information on the thermo-fluid-dynamics of the headlamp, taking into account the condensation/evaporation phenomena that may occur on the lens. Moreover, by superimposing numerical results and condensation images taken from the experimental tests, it is possible to correlate results and to get important information about the condensation issue in terms of distribution and thickness of the water layer. The combined use of numerical and experimental studies is a powerful tool for optimizing headlamp design and obtaining high performance headlamps.

References

- ANSYS CFX-Solver Modelling Guide.
- ANSYS CFX-Solver Theory Guide.
- Perry, R.H. and Green, D.W. (Editors) (1997). Perry's Chemical Engineers' Handbook, 7th Edition, McGrawhill.
- Kreith, F. and Bohn, M.S. (2001). Principles of Heat Transfer, Thomson Learning.
- Chenavier, C. (2001) Thermal Simulation in Lighting Systems - 5 Days / 5 Degrees. PAL Symposium Darmstadt, 2001.
- Preihs, E. (2006). Analytic Solution and Measurements of Condensation inside a Headlamp, COMSOL Conference 2006.
- Nolte, S. and Maschkio, T. (2007). Development of a Software Tool for the Simulation of Formation and Clearance of Condensation in Vehicle Headlamps, LLAB.
- Schmidt, T. (2008). Nanotechnologies surface modifications for anti-fog applications in automotive lighting and sensor serial production, SAE 2008

Conditioning – 1 step	Temperature = 6°C Relative Humidity= 95%
Conditioning – 2 step	Uniform distribution on the lamps and radiation model External relative humidity = 95% HTC on the lens = 10 W/m ² K
Condense development (20')	Uniform distribution on the lamps and radiation model External relative humidity = 100% HTC on the lens = 500 W/m ² K
Condense disposal (40')	Uniform distribution on the lamps and radiation model External relative humidity = 95% Variable HTC on the lens

Table 1: Initial and Boundary Conditions

Predicting Fuel Consumption and Thermal Comfort

In this article, Dr. Stefan Staudacher of TWT GmbH Science & Innovation and Dr. Michael Weinrich of Daimler AG, discuss a heterogeneous co-simulation environment which aims to balance the need for reduced fuel consumption with increased passenger comfort requirements.

CD



MENU

TP

FM

AM

AS



0 1 2 3 4



One of the main tasks in the development process of a modern vehicle is achieving good fuel efficiency. On the one hand, this is driven by the shortage of fossil oil, which leads to increased fuel cost. On the other hand, legislature is enforcing ambitious goals to reduce CO2 emissions.

During the last decade, the efficiency of internal combustion engines has increased substantially. As engines become more efficient, auxiliary power consumption shifted into focus. This is especially true for tasks such as ensuring passenger climate comfort, as they heavily rely on engine waste heat, which decreased with increasing engine efficiency. To close the gap between availability and demand, a variety of different measures was introduced – all of them utilizing different sources of energy. The reduction of fuel consumption and the improvement of the interior comfort is one resulting example of conflicting goals for modern consumption-optimized vehicles. Considering the complex warm-up process, one key development challenge is to arrange the heat flux and fluid flow within a vehicle in such a manner, that the requirements of fuel economy, exhaust quality, and heating comfort are met.

As the goals appear at least partially contradictory, it is necessary to develop a strategy on how to temporally distribute the available heat flux to the different fluids and components. With a proper strategy and the efficient use of all available heat sources in the vehicle, the fuel consumption could be reduced particularly during the warm-up process.

In this article, we will present a transient model called “VehEMent” (VEHicleEnergymanagEMENT), which incorporates the main energy fluxes within a vehicle. The model is able to describe transient operating conditions, e.g. speed and load changes, driving cycles (NEDC), and the warm-up process. VehEMent offers the opportunity to

optimize the heating strategy and to quantify the additional fuel consumption due to passenger climate comfort needs. It is very important for the development of cars to have a model which represents a whole vehicle with all heat sources, heat sinks and all mechanical and electric auxiliaries. Using such a model, different investigations are possible in an early stage of the development process.

As the model includes submodels from multiple physical domains (and departments) it can serve as an example for a heterogeneous co-simulation environment.

VehEMent (VEHicleEnergymanagEMENT)

The simulation tool VehEMent, which was developed by Daimler AG, is in daily use to testify and rate different components and energy management measures in a vehicle context. This is necessary in order to see the effects of the interaction of different measures. Nowadays, there are several measures integrated in the vehicle which react depending on different driving states and the status of others measures. For example, the opening and closing of the shutter is dependent on the state of the air conditioning and coolant temperature. Another usage of this tool is the description of vehicles in the digital prototype process at early development stages. For that purpose, a whole vehicle is virtually built up with all necessary components, such as engine, cabin, coolant circuit etc. (Figure 2) [2, 3].

To achieve maximum reliability for each submodel, the parts are provided and verified by the different departments and merged together in a Matlab/Simulink simulation environment. In order to have maximum performance in simulation time, the model is built in 1D, which represents all the existing parts with adequate accuracy. In this process some transformation from 3D to 1D has to be done in a preprocessing step. This is done for the flow through the radiator and engine

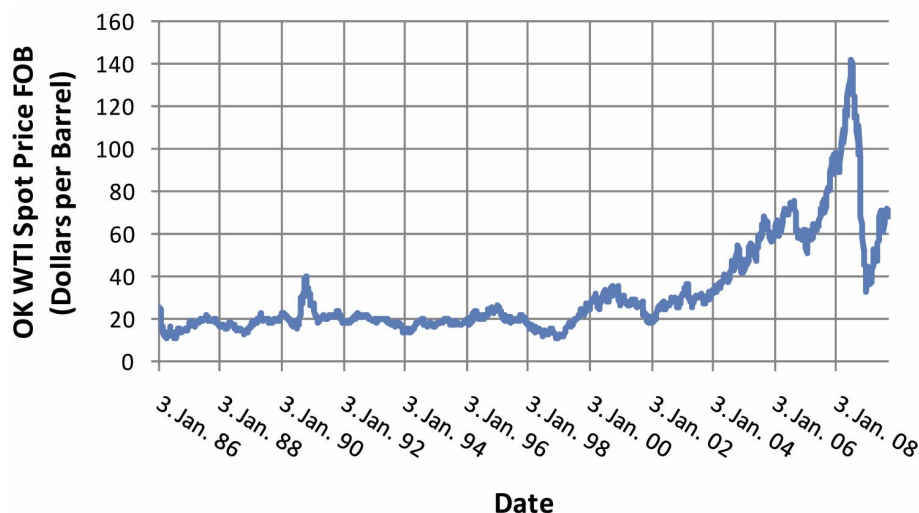


Figure 1: Development of the oil price from 1996 to 2009 [1]

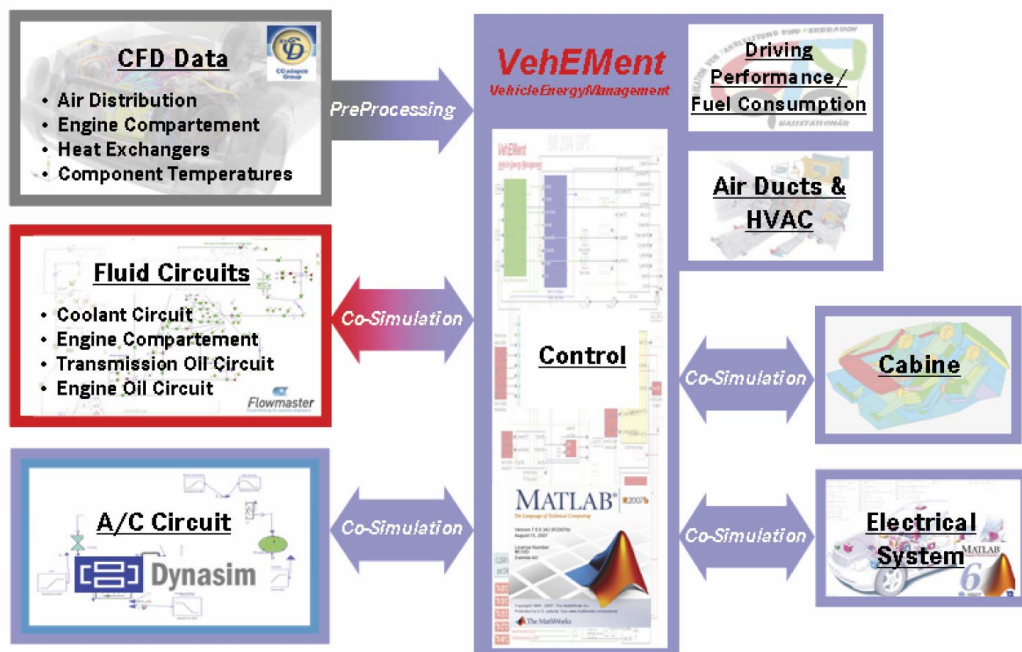


Figure 3: Submodels in VehEMent

compartment. The cabin, the air ducts and the air distribution itself also result from a 3D representation.

Due to the modular composition of VehEMent it is easy to expand or to replace the submodels with modified or new ones. Typically, the departments use different simulation tools to gain maximum benefit for their own stand alone simulation model. The provision of submodels by different departments is without doubt advantageous; however, the necessity is given to couple different simulation tools. In consequence, this leads to a co-simulation for the whole vehicle model in VehEMent.

VehEMent itself combines different modeling environments: The main part is modeled in Matlab/Simulink and represents the vehicle control system with all open and closed loops for the integrated components. By running a Matlab script, all the necessary parameters are set in the corresponding Simulink model. This dataset includes parameters, e.g. vehicle mass, engine data, gearbox data. Investigations could be made for different driving cycles or stationary points, which are also set into this main model. Another important value is the fuel consumption for those measures and cycles, which is also calculated in the main model. For the representation of transient warm-ups, it is necessary to describe the engine and gearbox friction depending on the corresponding oil temperature. In order to realize this dependency a simple representation of the engine with a thermal network, including a coolant and oil circuit, is built. For the simulation of the fluid circuits, another simulation tool (Flowmaster/GT) is used, which is coupled by co-simulation. The AC-Circuit is modeled in Dymola and integrated into VehEMent by coupling another Matlab instance to the main model. Almost the same is realized

for the electrical system which also runs in an additional Matlab instance.

VehEMent has no driver model, which actuates the gas pedal in order to obtain the desired operating point. Instead of calculating the necessary driving power in forward direction (from the engine to wheel), the power is calculated in backward direction. This means that as a first step the power needed at the wheel is calculated. As a second step, following the drivetrain backwards and taking into account all appearing efficiencies, the required engine operating point is calculated. For each component the losses are calculated depending on operating point and temperature. To describe the auxiliaries, i.e. air conditioning and generator etc., an additional load is added to the actual engine load. The fuel consumption is calculated in the driving performance block in which the driving parameters are also provided. By contrast, the engine itself with the heat rejection is modeled in another block. This model block provides the heat flux from the combustion chamber to the walls and from that point to oil and coolant. A simple thermal network represents the engine with its heat capacities. In order to be able to simulate a transient warm-up, all closed loop control parameters must be set. Those parameters are depending on different engine parameters, i.e. the control of the water pump or thermostat.

One result of the simulation could be the thermal comfort for the cabin temperature during a warm-up. Therefore the vehicle starts at an ambient temperature of -20°C at a constant speed of 50km/h and is running for 30min . For comparison, different additional external heater could be investigated.

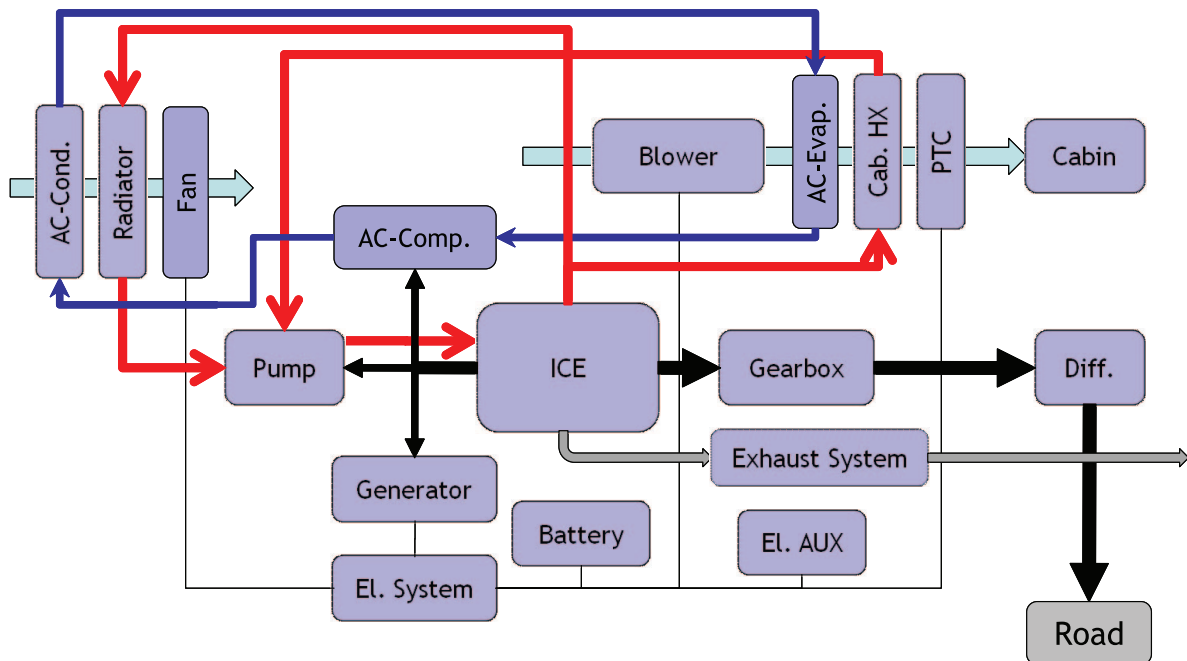


Figure 2: Main physical domains represented by VehEMent

Model Structure and Co-Simulation

As stated previously, VehEMent is a heterogeneous co-simulation environment. A large portion of the model as well as most of the data infrastructure is handled via Matlab/Simulink. Simulink itself plays the role of the master, as far as model initialization is concerned. Other modules are based on other proprietary tools, such as Flowmaster or Dymola/Modelica.

As a full vehicle model VehEMent is steadily growing: Additional functionality is continuously added to the main model. The main reason for choosing a co-simulation approach is that the desired submodel functionality was already present and validated within a different model environment. Instead of rebuilding and maybe simplifying the model in Simulink it is mostly easier to include the already available model and worry about the coupling (error prevention and direct model usage). As a prerequisite, it is necessary to keep submodels modular. Each submodel must be self-sufficient as far as models and parameters are concerned. Only general parameters such as environment conditions are specified on a global basis.

As a side effect, this approach opens the opportunity to vary each submodel's level of detail. For example, it may be desirable to employ a rather coarse model for most of the vehicle in order to save computational time and have a rather complex submodel for a certain subsystem. This setup allows for comparative studies with rapid turnaround times. Again, the prerequisite is that the interfaces between coarse and fine regions of the model are well defined and fixed and the (sub-)models and their (sub-)configuration is modular [4].

In general, using the co-simulation approach will reduce development time at an expense of computational time, as in most cases rather detailed models from other departments are integrated. Another benefit is the exploitation of the higher level of detail of the included models.

VehEMent relies on three different coupling schemes. In the following, we will refer to them as "Embedded models", "Bilateral Coupling" and "Middleware". Embedded models are submodules, which are integrated in the main model. They can be either Simulink blocks or S-functions. They share the solver and solver settings (e.g. time step) with the main model. Coupling is straight forward, the blocks are included in the main model and the submodel's parametric data has to be provided at runtime. It is not necessary to provide means to start a second process to handle the submodel and of course no additional communication delay is introduced as both models share the same process. However, this coupling is not suitable for most applications, either, as the submodel is based on third party software which cannot be included in Simulink, or, as different submodels require different solvers/solver settings, which prevents direct inclusion.

Bilateral Coupling is employed in most cases by third party software vendors, in order to provide their users with means to couple their software with Simulink. Examples are Flowmaster or GT. They operate as follows: A certain Simulink block provided by the software vendor is included in the main model. This block operates as a sink for signals to the submodel and source for signals from the submodel. The submodel to be coupled is equipped with inverse functionality. At model start-up the

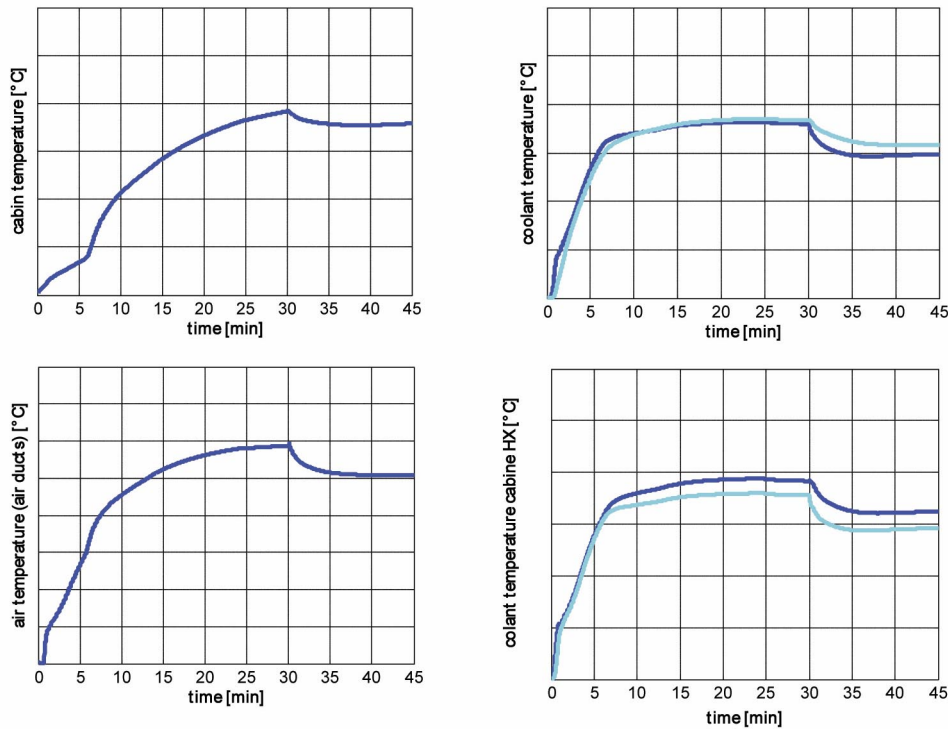


Figure 4: Results of a warm-up simulation

Simulink block initializes the external submodel solver process via callbacks. Communication is realized via ports. Depending on the software vendor's implementation both processes must be running on the same machine or can be distributed over the network. The exact details of the communication, such as submodel initialization and termination, parallel or sequential execution order, communication delays et cetera are highly dependent on the vendors interface implementation. Bilateral couplings allow users to choose each (sub-)models solver and solver settings according to the models needs, i.e. a model of the electrical system can be run with a small and fixed time step, coupling can be done on a coarser basis, while the main model employs a variable step solver.

Some interfaces run out of the box, others may require a huge effort to achieve a stable operation. Besides the aforementioned, there are two additional drawbacks: The amount of work necessary to maintain the interfaces should not be underestimated. This is especially true, if there are multiple bilateral interfaces within one model. If two submodels need to communicate with each other, this can be done only via Simulink. This again introduces additional communication delay, as communication has to be done via Simulink. This in turn may require a reduction of the time step in order to fulfill stability criteria.

We refer to the third coupling scheme as coupling via 'middleware'. This setup relies on an additional server process, which is responsible for data transfer between

clients. With this setup an arbitrary number of clients can be merged together. Each client is using its own solver and settings, resulting in good standalone computational performance. The server is responsible for the transfer of the requested signals from client to client. Some servers are able to sample signals, i.e. different submodels can communicate on different time steps and the server is taking care of interpolation [5]. Well known middleware is e.g. TISC or EXITE [6]. Larger models only require the attention for one coupling infrastructure instead of multiple interfaces in the case of bilateral coupling.

Using Bilateral Coupling or Middleware allows the exploitation of parallelism, i.e. calculation of submodels can be done simultaneously. This can significantly speed up the simulation if the underlying hardware features multiple cores. The other side of the coin is that parallelism may require a shorter time step, in order to maintain stability, due to coupling. Two rather mundane and obvious shortfalls of the co-simulation approach are the requirement for licenses for third party tools and a high knowledge of IT skills.

Outlook – Modelisar

The introduction of standards for co-simulation interfaces will be set with the results of the research project Modelisar in the near future. Different industrial and research partners from five European countries are working together on the development of an open and standardized interface. The project has started in July 2008 and will end in June 2011. The purpose of Modelisar

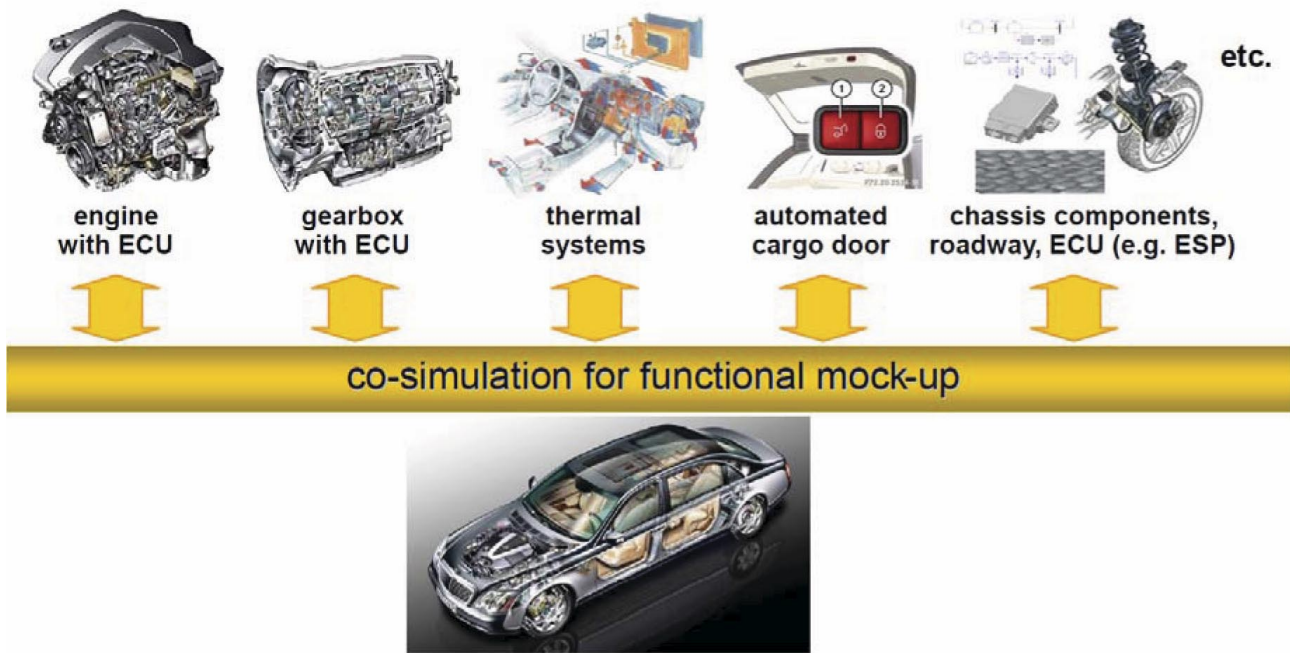


Figure 5: Technical simulation models and embedded software [7]

is to introduce functional mock-up (FMU), a next generation of methods, standards and tools to support collaborative model-based design, simulation and test of systems and embedded software [7].

The coupling of different systems with the functional mock-up interface (FMI) is graphically described in Figure 5. Different simulation tools can be coupled to co-simulation using different solvers. A model can also be integrated into the existing simulation environment using one solver. With this functionality, different complex systems in different simulation environments can be coupled to an integrated simulation by using just one type of interface.

References

- [1] N.N.: "Energy Information Administration (EIA) - Official Energy Statistics from the U.S. Government", <http://tonto.eia.doe.gov/dnav/pet/hist/rwtcM.htm>
- [2] Flögel, H.; Kauf, F. et al.: „Wärme- und Energiemanagement Gesamtfahrzeug Simulationstool Vehement“, Wärmemanagement des Kraftfahrzeugs II; Expert Verlag; 2000
- [3] Duhme, M.; Flögel, H.: „Parameterstudie im thermischen Übertragungspfad Motor – Kabine“, Wärmemanagement des Kraftfahrzeugs III; Expert Verlag; 2002
- [4] Lindemann, M, Wolter, T.-M., et. al.: „Konfiguration von Hybridantriebssträngen mittels Simulation“, ATZ 5/09, 2009
- [5] Puntigam, W., Balic, J. Almbauer, R., Hager, J.: "Transient Co-Simulation of Comprehensive Vehicle Models by Time Dependent Coupling", SAE Technical Paper 2006-01-1604
- [6] Wilhelm Tegethoff, Claudenê Correia, Roland Kossel, Michael Bodmann, Nicholas Lemke, Jürgen Köhler: „Co-Simulation und Sprach-Standardisierung am Beispiel des Wärmemanagements“, Tagungsbeitrag in Wärmemanagement des Kraftfahrzeuges V, Haus der Technik Fachbuch 68, Expert Verlag, 2006, S. 231-242
- [7] http://www.itea2.org/public/project_leaflets/MODELISAR_profile_oct-08.pdf

Fatigue in Aluminium Honeycomb-core Plates

Laurent Wahl, Arno Zürbes, Stefan Maas and Danièle Waldmann, from the University of Luxembourg, investigate the fatigue properties of the honeycomb ‘core’ of aluminium ‘sandwich panels’, as used throughout the aerospace and automotive industries.

Honeycomb composite lightweight structures made of aluminium or aramid fibres are used in airplanes, railway carriages and automobiles. These structures are subjected to dynamic loading but hardly any fatigue properties of the honeycomb core exist in current literature (A summary of the state of the art: [1]).

The lightweight panels which were investigated are made of a honeycomb core of aluminium, which is connected by an adhesive layer with two outer sheets of aluminium (Figure 1).

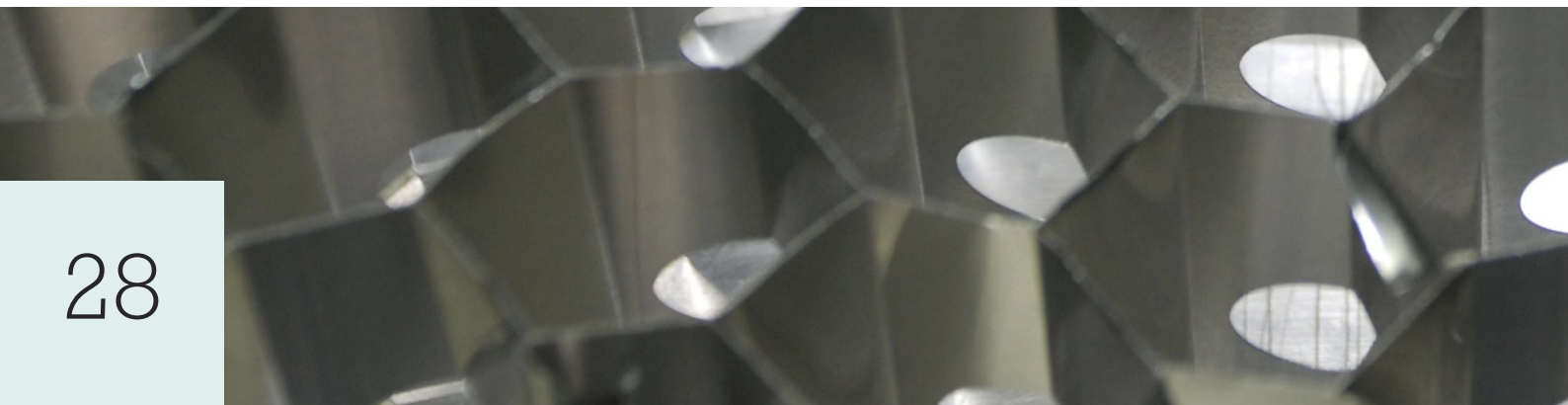
During this project, fatigue tests with failures of the core structure were conducted in parallel with Finite Element calculations. An analytical model was created, which explains the experimental results.

Since the behaviour of the panels is orthotropic, the panels react differently depending on the direction of the loading. For this reason, it is necessary to distinguish between the three directions of symmetry, which are called L, W and T direction (Figure 2).

The walls of the honeycomb cells have different wall thicknesses. This is due to the manufacturing process, where the foils are partly glued together. The glued walls with double thickness are called ribbons (Figure 2). The dimensions of the examined panels are shown in Table 1.

Material	Aluminium
Panel dimensions	138mm x 76mm x 10mm
Face sheet thickness	0.6mm
Honeycomb foil thickness	0.08mm
Cell size	6.4mm
Support distance of the 3-point bending test	102mm

Table 1: Material and dimensions of examined Panels



Failure Modes of Honeycomb core Sandwich Panels

In a 3-point bending test, sandwich structures are mainly subjected to three types of stress:

- Tension / Compression in the cover sheets due to bending
- Shear stress in the core
- Compressive stress in the core in proximity of the load application

Each stress type must be examined in order to figure out which is the critical one.

The bending stress leads to cracks in the face sheets, which was examined in a former project [3].

The core of the sandwich panels usually fails due to shear or compressive stress (Figure 3). The type of stress which prevails, depending of the geometry and the load application, is responsible for the core failure.

The distribution of the stresses in Figure 3 was simulated in ANSYS by moving the load horizontally. The shear stress is maximal somewhere between the two points of the force application. The compression stress in the core has a maximum just below the middle load. Core indentation is occurring, when the compression stress surpasses the buckling strength of the honeycomb core. In this case, the structure fails locally due to buckling of the core (Figure 3).

Materials

The sandwich structure consists of three different materials:

- Glue
- Aluminium alloy AlMg3 H44 (AW 5754) for the face sheets
- Aluminium alloy AlMn1Cu H19 (AW3003) for the honeycomb structure

Test Methodology

Dynamic 3-point bending tests were performed in order to provoke core failure. The test setup is powered by a hydraulic cylinder from Instron Structural Testing Systems (IST). The hydraulic cylinder can be excited displacement or force controlled.

In order to provoke the two failure types of Figure 3, the load was applied in two different ways:

- Steel roll with a small diameter (25mm), which implies a high contact pressure and the component fails by core indentation (Figure 5a)
- Elastomeric roll (Vulkollan 80 Shore A) with a big diameter (76mm), which implies a low contact pressure so that the core fails due to the shear forces (Figure 5b)

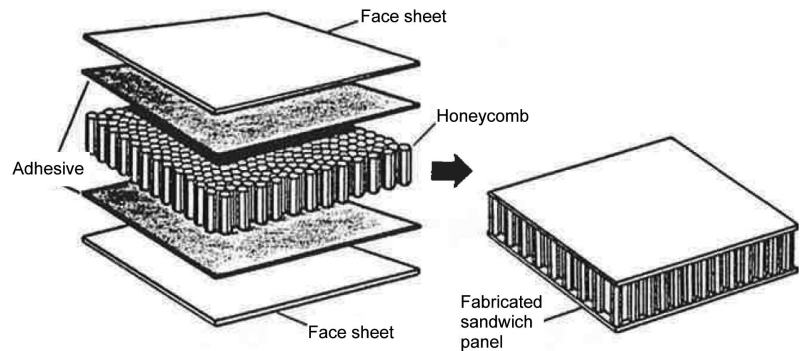


Figure 1: Sandwich structure with honeycomb core [2]

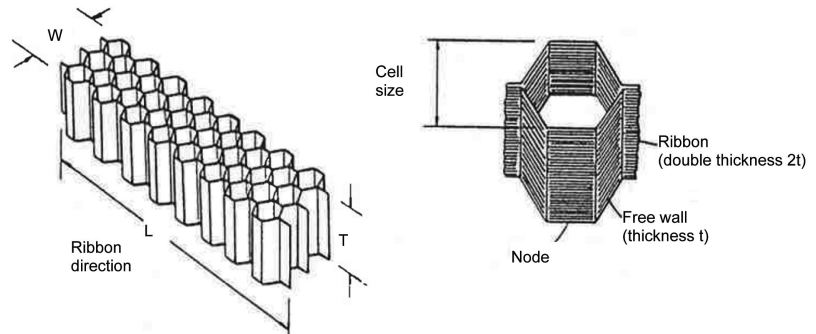


Figure 2: L, W and T directions [2]
(Ribbon has double thickness, due to the manufacturing process)

Fatigue Test Results

Dynamic tests were carried out to study the fatigue properties of the structure. The samples were loaded in a three-point bending test with a sinusoidal load with constant amplitude at a power ratio of $R=10$. The excitation was force controlled.

The soft load application (Figure 5b) leads to shear failure in the honeycomb core. Cracks are initiated in the interior of the honeycomb core, which grow predominantly in the diagonal direction of the cells (Figure 6). These cracks are not exactly under the load, but some cells away from it. Here the shear stress is maximal, as shown in Figure 3.

If a hard load application is chosen (Figure 5a), the specimens fail due to the pressure load induced by the load (core indentation). In the damage pattern of Figure 7, it can be seen, that the cracks are exactly under the load application. The W-specimen shows horizontal and diagonal cracks in the cell walls. The L specimen shows only horizontal cracks.

The tests showed that first cracks occurred after less than 10% of the total life period of the specimen. The buckling process creates locally high stresses and cracks, which are not imperatively leading to the total direct failure of the structure.

In Figure 8, the fatigue diagrams of L and W-samples with identical dimensions are shown. In the ordinate of the fatigue diagram the force amplitude is displayed and not the stress amplitude at the location of the crack initiation. These two values are related, but the relationship is not

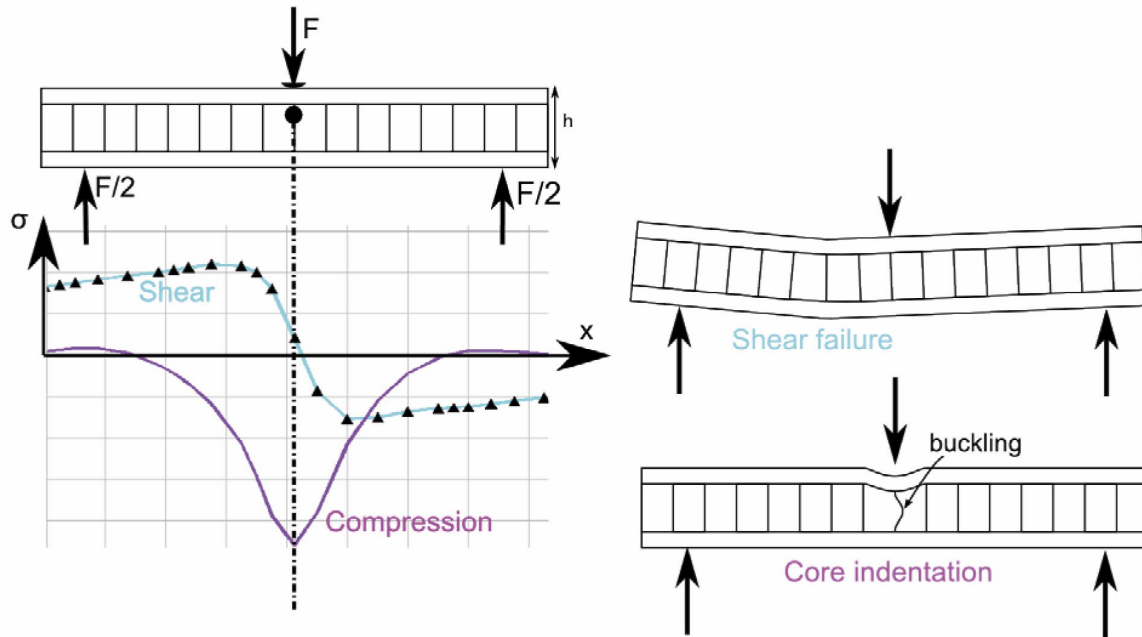


Figure 3: Stress distribution and failure modes of the honeycomb core

necessarily linear. The number of cycles on the abscissa corresponds to the number of cycles to complete failure of the part and not until the first crack. These boundary conditions imply that the diagrams are not conventional SN-diagrams. The experimental results, however, lie well along a straight line.

The curves of the specimens which fail due to buckling (core indentation), are flat, compared to the shear failure curves. This flat curve is due to the high nonlinear stress increase during buckling.

Simulations

A model of the sandwich structure was created using ANSYS. The structure is modelled with shell281 elements, which have 8 nodes with 6 degrees of freedom each. Shell281 elements are also suitable for large deformations and plastic behaviour. The roll for the load application is modelled with solid95 elements, volume elements with 20 nodes with 3 degrees of freedom each. The contact condition between the roll and the sample is modelled with the elements conta174 and targe170. These elements have 8 nodes and are placed on the surface of the shell elements. Contact occurs when the surface of a conta174 element penetrates one of the targe170 elements.

To make the simulation as realistic as possible, several imperfections are introduced (Figure 9):

- Roll not centred (load inserted on ribbon or next to ribbon) ($\epsilon \leq 1\text{mm}$)
- Roll rotated around the x-axis, so that the device won't be loaded evenly ($\epsilon \leq 0.2^\circ$)
- Roll rotated around the z-axis ($\epsilon \leq 0.5^\circ$)
- Cells are not regular hexagons (all the coordinates are moved by a small random value) ($\epsilon \leq 0.3\text{mm}$)
- Cells not planar (Small forces ($F_i \leq 0.5\text{N}$) are inserted into the simulation, which dent the walls)

The simulations showed that a rotation of the roll around the x-axis (ϵ) has a big influence. A horizontal displacement of the roll (ϵ) can move the force application from a ribbon to a free wall, which also has an influence on the results. All other imperfections are quite insignificant.

The failure of the glue is not the main subject of this article, but it should still be modelled in order to examine the influence of the glue to the buckling load. The adhesive layer covers the honeycomb core and stabilizes it. This overlap is simulated by expanding the shell model of the honeycomb core with two layers of constant thickness, which have the properties of the adhesive (Figure 10). The simulations showed that the influence of the glue to the buckling load is less than 10%.

Core indentation (Buckling of the core)

The experiments have shown that the samples, loaded

	Young's modulus	Tensile yield strength	Tensile ultimate strength	Ultimate strain
AlMg3 H44	69'000 MPa	200 MPa	270 MPa	5%
AlMn1Cu H19	69'000 MPa	190 MPa	265 MPa	2,5%
Glue ST 1035	1'900 MPa		50 MPa	

Table 2: Mechanical properties of the materials used in the Sandwich panels

1 Test Methodology

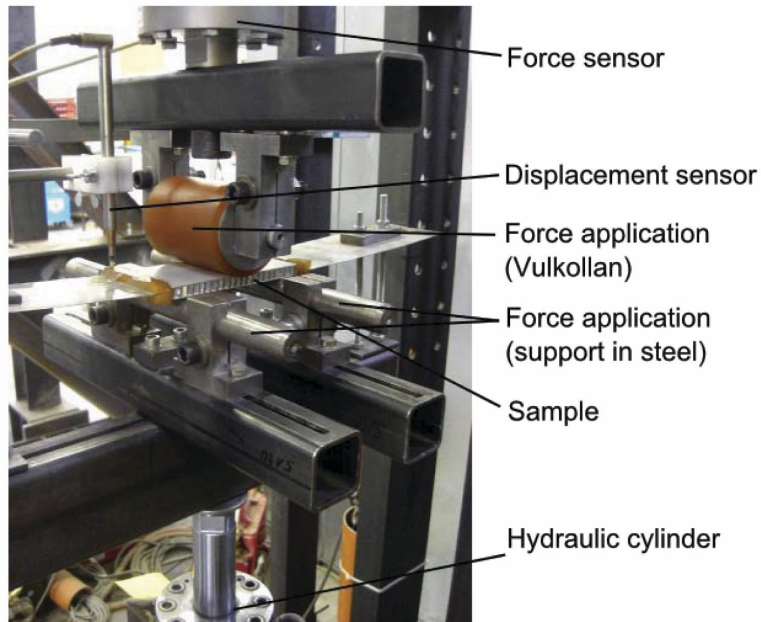


Figure 4: Three-point bending setup used for fatigue testing

with the hard roll, failed in the mode of core indentation. Physically, core indentation of honeycomb panels means that the cell walls are buckling (but usually they can still carry loads). The buckling process induces bending stresses in the cell walls, including high tensile stresses. These tensile stresses influence the fatigue behaviour of the core very negatively, so that the crack initiation phase gets much shorter (Figure 8). In most cases however, these local cracks barely influence the strength of the structure.

Some simulations showed however, that it would be too time-consuming to simulate the growth of the cracks (which is very sensitive to imperfections) within this project, in order to see which cracks lead to failure and which cracks not. Therefore, it was assumed that a cyclic buckling of the honeycomb cells is not tolerable if a part is dimensioned against fatigue. In this case, the stresses are distributed more uniformly and the crack growing process is not so important. This assumption does not lead to a big oversizing of the part, because the fatigue curve of the core indentation in Figure 8 is very flat. Therefore, it does not make a big difference if the part is dimensioned for 100,000 cycles or one million cycles (it is assumed, that for

1M million cycles, no buckling is occurring). In the field, core indentation is usually avoided by reinforcing the panel at the position of the load application.

For this reason, honeycomb sandwich structures should be dimensioned so that no buckling occurs, because only in this case can good results be achieved. The buckling load can be calculated by a Finite Element Method in two different ways. First, by a buckling analysis, that calculates the theoretical buckling load for a perfect elastic system (Euler analysis). Alternatively, if nonlinearities have to be considered, the buckling load can be evaluated out of a nonlinear simulation. The contact of the hard load application (Figure 5a) is not very load dependant, so that the linear buckling analysis is possible. However, the soft load application (Figure 5b) causes a nonlinear contact condition, so that in this case a nonlinear simulation is necessary.

Shear failure

After proving that no buckling is occurring, a normal static analysis can be accomplished. In this case, the stress state in the core is quite homogeneous and it will be

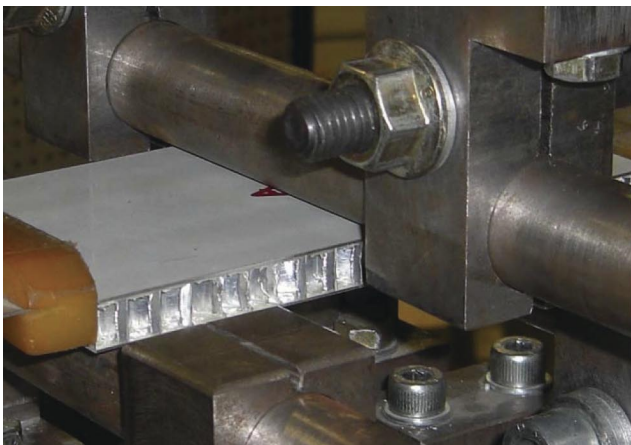


Figure 5a: Hard load application made of steel

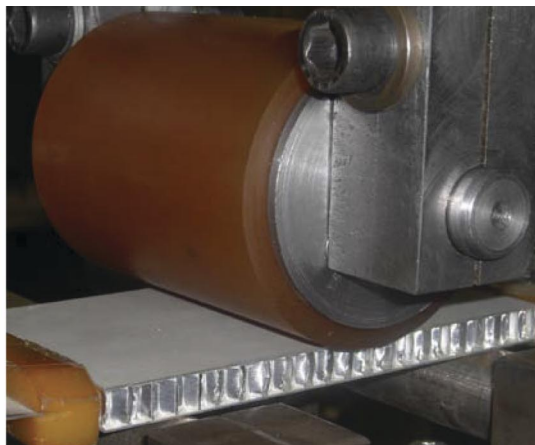


Figure 5b: Soft load application made of Vulkollan

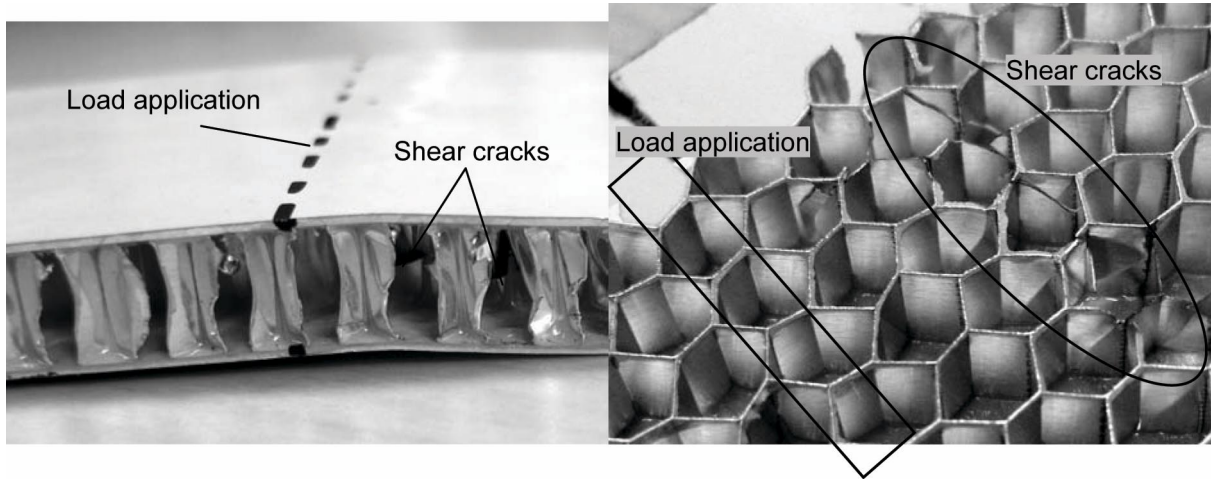


Figure 6: Fatigue Shear failure

possible to do a fatigue prediction with this analysis. Just under the load application, the compression stress dominates, and next to the load application, the shear stress dominates like shown in Figure 3. When no buckling of the core is occurring, the most damaging stress component in the core is the shear stress. Therefore, the critical location can be determined from a shear stress contour plot. At this location, a fatigue prediction can be accomplished using the FKM-guideline [4].

In a 3-point bending test, away from

$$\tau = \frac{Q/n}{t \cdot h}$$

in element coordinates

- τ: shear stress
- Q: shear force
- h: height of specimen
- t: foil thickness of the core
- n: number of cell walls over width

the load application, the shear stress can be checked analytically:

In this formula, it is assumed that the shear stress is distributed uniformly over the honeycomb cells. In the element coordinate system, the angle of the cell walls does not appear in the formula of the shear stress. However, the number of cell walls across the width is important, which implies that the L-samples are much more stable against shear than W-samples (n much bigger for L-samples than for W-samples).

These approximate formulas are just used to understand the influence of the parameters and to check the simulations. In order to have the exact stresses with all local effects, the Finite Element simulations are still needed.

Fatigue analysis of examined specimens

The procedure of the fatigue analysis for the core structure of an

aluminium honeycomb sandwich should be as follows:

- Determine the buckling load of the core. Applied load must not exceed this value
- Determine the stresses in a static Finite Element Analysis
- Locate the critical points (e.g. in a contour plot of shear stresses because these stresses are predominating)
- Calculate the lifetime of the honeycomb core, using the FKM-guideline [4]
- Confirm the results when possible by tests

Buckling loads

The buckling loads of different specimens and different load applications are shown in Table 3.

The buckling loads of the soft load application cannot be compared with the test results, because in these cases, the failure mode is not core indentation, and therefore no

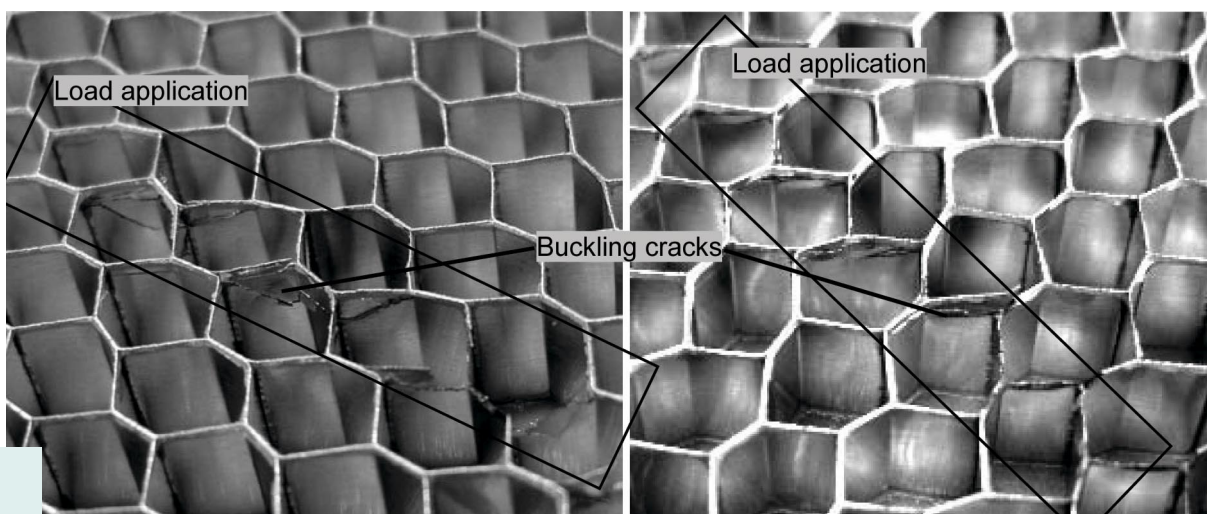


Figure 7: Fatigue buckling failure for W and L specimens

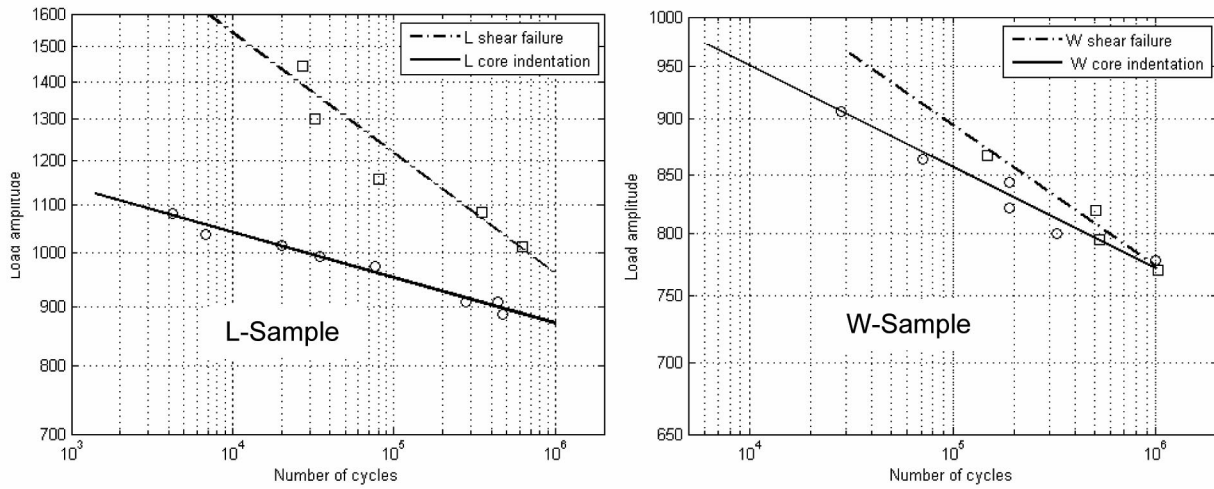


Figure 8: Fatigue strength diagrams for L and W samples

buckling is occurring. These buckling loads are higher than the failure loads in Figure 8, so the failure is not due to buckling effects, as it is also shown in the experiments.

The buckling load of the hard load application is exactly in the area of the fatigue limit found in the experiments. It was assumed that at the fatigue limit no more buckling is occurring, and so in the experiments the load at the fatigue limit is exactly the buckling load. In these cases, the endurance limit can be predicted with an accuracy of approximately 10%.

In Table 3, nonlinear analysis means, that the contact surface is changing with load and that the deflections can grow at the buckling load nonlinearly.

Shear failure

When no buckling is occurring, a fatigue analysis is performed using the FKM-guideline [4]. The hard load application leads to core indentation: here, only the soft load application is examined. In Table 4, the results of an L and a W-specimen are compared with the test results.

The lifetime predictions for the two cases examined in Table 4 are conservative. The durability found in the tests was higher than the prediction by a factor of two. This can be considered to be a good prediction [5].

Conclusions

Two different failure modes of the honeycomb core structure were examined: core indentation and

shear failure. Core indentation induces buckling of several honeycomb cells. This results in high tensile forces, which will quickly initiate cracks. In practice, components should be designed so that no buckling occurs. The buckling load can be calculated easily with a Finite Element simulation.

The shear failure mode can be analysed by doing a static Finite Element Analysis. Afterwards a lifetime analysis can be done using the FKM-guideline. There were only small differences between the fatigue predictions and the experiments.

The differences between the predicted and the tested lifetimes are only 10% based on stress and only a factor of two in real-life.

Load application	Specimen direction	Simulation method	Buckling load	Test results (fatigue limit)
Hard	L	Nonlinear or buckling analysis	2050N	1933N (equals an ampl. of 870N in Fig. 8)
	W	Nonlinear or buckling analysis	1650N	1711N (equals an ampl. of 770 in Fig. 8)
Soft	L	Nonlinear analysis	2250N	
	W	Nonlinear analysis	1850N	

Table 3: Comparison: buckling load / fatigue limit

Load application	Specimen direction	Load Amplitude (R=0.1)	Simulation method	Predicted life-time	Test results
Soft	L	945N	Nonlinear analysis & FKM	500'000cycles	1'000'000cycles
	W	810N	Nonlinear analysis & FKM	240'000cycles	500'000cycles

Table 4: Life comparison: FKM / experiment

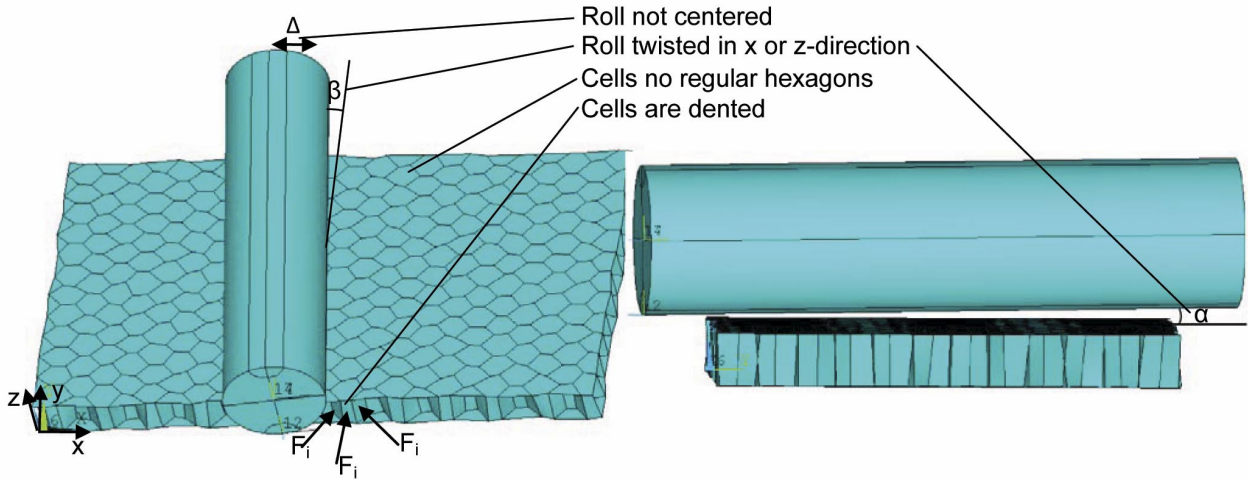


Figure 9: Imperfections included in the simulations (illustrated exaggeratedly)

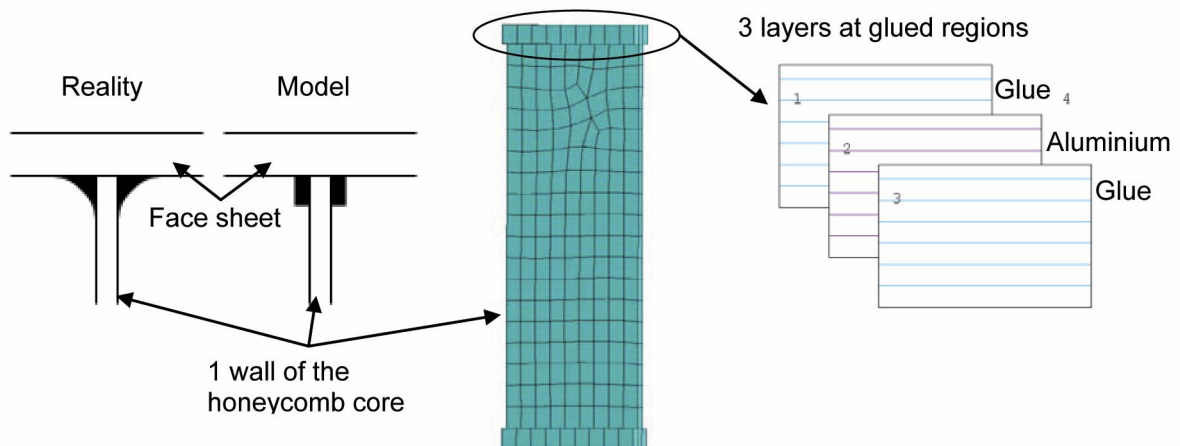


Figure 10: Glue on Honeycomb cells modelled by different layers

References

- [1] Sharma, N.; Gibson, R.F.; Ayorinde, E.O.: "Fatigue of Foam and Honeycomb Core Composite Sandwich Structures: A Tutorial", Journal of Sandwich Structures and Materials 2006 8: pp 263-319
- [2] Blitzer, T.: "Honeycomb Technology, Materials, design, manufacturing, applications and testing", first edition, Chapman & Hall, 1997
- [3] Bauer, J.: "Ermittlung von Schwingfestigkeitseigenschaften für Leichtbaupaneele mit Wabenstruktur", University of Luxembourg, Faculty of Science, Technology and Communication, PhD-FSTC-5-2008, 2008
- [4] Hänel, B.; Haibach, E.; Seeger, T.: "Rechnerischer Festigkeitsnachweis für Maschinenbauteile aus Stahl, Eisenguss- und Aluminiumwerkstoffen – FKM-Richtlinie", 5th edition, VDMA Verlag GmbH, 2003
- [5] Schijve, J.: "Fatigue of Structures and Materials", first edition, Kluwer Academic Publishers, 2001

Acknowledgement

The materials were sponsored by Eurocomposites, Echternach, Luxembourg. Many thanks to them.

Absorbing Rail Impact Assessing the Defect Tolerance of Rail Vehicle Impact Energy Absorbers

A. De Iorio, M. Grasso, F. Penta, G. P. Pucillo;
Università degli Studi di Napoli Federico II – DiME
G. Kotsikos; Newcastle University



This article, based on the winner of the best paper award for most innovative use of simulation technology at the NAFEMS World Congress 2011, investigates the dynamic response of the joints of energy absorbers used in rail vehicles. These energy absorbers are designed to deform in a controlled manner in the event of a collision thereby absorbing some of the impact energy that would otherwise be transferred to the main structure and passengers. The functional requirements of these devices are particularly stringent in terms of their reliability and functionality throughout the life of the vehicle.

The crashworthiness of rail vehicles has improved enormously over the past 30 years. The passive safety requirements for safety of rail passengers are described in the European Standards EN 15227:2008, whose objective is to reduce the consequences of collision accidents. The Standard describes the design requirements that railway vehicle bodies should fulfil in order to withstand certain crash conditions, based on the most common accidents and associated risks. One of these design features is the incorporation of energy absorbing devices at either end of the train. There are several different designs of energy absorbers adopted by rail vehicle manufacturers and their main function is to provide a controlled rate of deceleration of the vehicle in the event of a collision, thereby reducing the impact energy transferred to the vehicle occupants. The legislative European crash scenarios considered in EN 15227:2008 are shown in Figure 1.

The crash process model adopted by rail manufacturers is divided into provisions for both active safety before the collision and passive safety during and post collision. This is shown schematically in the diagram of Figure 2.

The selection of an appropriate energy absorber design relies primarily on the behaviour of the device during the impact (millisecond reaction time) and also the requirements for repair of the vehicle after the impact event. This translates to the rail operator's requirements to be certain that the energy absorber will always perform as designed in the event of a collision (i.e. ease of inspection and maintenance) and how quickly repairs can be made to allow the vehicle to be entered back into service.

This work analyses the collision performance of a common design of energy absorber, assesses the damage tolerance of the design, and investigates through Finite Element Analysis (FEA) a proposed alternative installation method for ease of assembly and repair as well as to aid inspection and maintenance throughout the vehicle service life. The analysis is based on the most common collision scenario described in EN 15227:2008, namely a 36 km/h like for like impact. EN 15227:2008 also includes a like for like impact with 40 mm offset. The 40 mm vertical offset impact represents the difference between a new train and one with worn wheel profiles plus the differential in heights due to maximum and minimum loading conditions. This case could also have been considered but most trains include an anti-rotation device ahead of the energy absorbers to minimise the effects of the misalignment so that the absorbers will behave as a simple like for like impact. An overall deceleration rate of 5 g as a maximum has to be maintained.

Background

The most common design of energy absorber is a circular or square cross-section hollow tube which undergoes collapse under axial loading. This is a relatively simple and inexpensive approach and is used widely in many transport applications ranging from rail, to aerospace. Modelling of the axial collapse of square and circular cylinders has been carried out by many researchers and analytical solutions for dynamic collapse can be found in the literature [1, 2, 3]. The most notable work is that of Abramovicz & Wierzbicki [3] who developed an expression for the dynamic axial crushing force of a square cross-section tube as:

$$P_m = 9.56 \cdot t^{5/3} \cdot C^{1/3} \left[1 + \left(\frac{\dot{\epsilon}}{D} \right)^{1/q} \right] \sigma_0 \quad [1]$$

where C is the tube width, t is the tube thickness, σ_0 is the static yield stress, $\dot{\epsilon}$ is the strain rate, D and q are constants (usual values are: $D = 300 \text{ s}^{-1}$, $q = 5$ for mild steel and $D = 6500 \text{ s}^{-1}$, $q = 4$ for aluminium).

There are also several pieces of work where FEA has been used to predict the collapse of axially loaded tubes of circular and square shape made of both steel and aluminium alloys as well as tubes with geometric features introduced to improve their energy absorption performance [4, 5, 6].

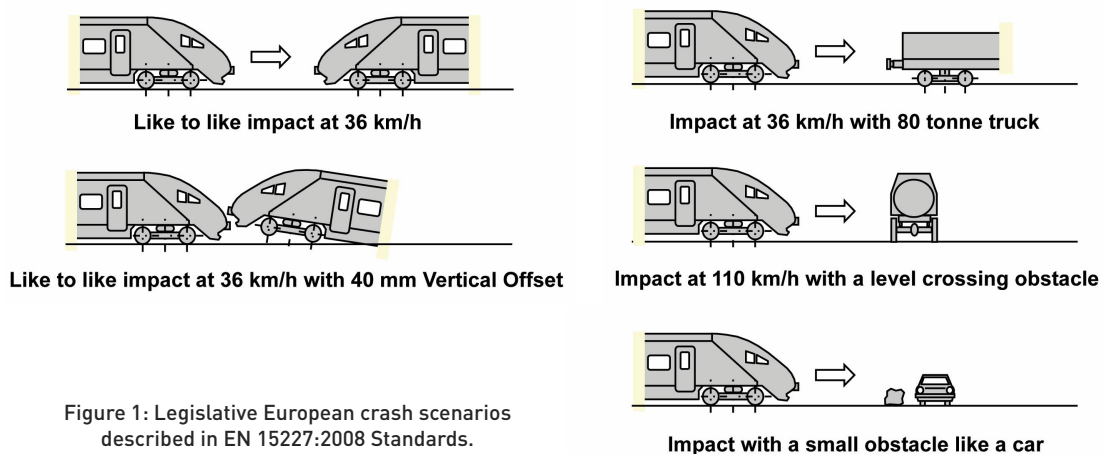


Figure 1: Legislative European crash scenarios described in EN 15227:2008 Standards.

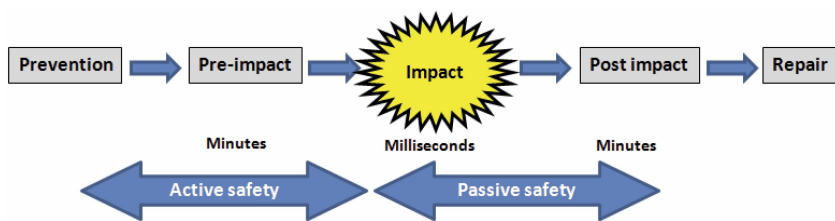


Figure 2: Crash process model (CPM).

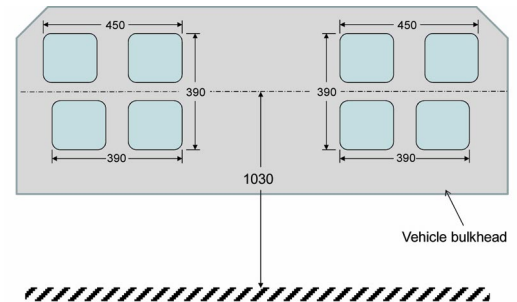


Figure 3: Schematic design of a rail vehicle's energy absorber assembly.

Most studies concentrate in predicting the absorbed energy, the impact force and effects such as the impact velocity and impactor mass on the deformation pattern. What has not been investigated in detail is the behaviour of the joints between the energy absorber and the reaction plate onto which they are attached. An early failure of the joints may compromise the energy dissipation characteristics of the absorber.

In many structures featuring tubular energy absorbers, the tubes are welded onto a reaction plate. But weld defects have been found in some welded joints, arising either from fabrication quality problems or have developed in service. Fabrication problems may arise either from incorrect welding procedures, or difficulties encountered by the welder to correctly position the welding gun due to limited amount of space round a tube (most common when multiple sets of tubes are used in close proximity). Service defects may arise from metal thinning due to general corrosion or crack development as a result of stress corrosion or corrosion fatigue at the weld region. It is therefore important to know how the energy absorbers would behave when the integrity of the welded joints is compromised.

Furthermore, once the tubes are welded to their reaction plates, through life inspection of their condition is difficult because access to the inner surface is difficult. In addition, inspection techniques such as ultrasonics have limitations in identifying any weld defects due to limited space available for the correct insertion of inspection probes.

Modelling

The design considered here is a set of four hollow rectangular tubes placed at either side of a rail vehicle as shown in Figure 3, welded onto the bulkhead. At the front end, a flat plate is welded which incorporates the anti-rotation and anti-climb devices (not shown in the sketch).

Quasi-static and dynamic tests performed on round and square tubes have shown that there is an initial high load until the creation of the first fold due to buckling dropping to a more or less constant load until the tube has fully collapsed. A typical load time plot is given in Figure 5. This initial "spike" in the impact load is not desirable during a collision as its effect would be

transferred to the occupants of the vehicle. For this reason energy absorbers incorporate a "starter" fold to minimise the effects of the initial load spike. Figure 6 shows an example of such a starter fold in an energy absorber.

The modelling investigates the performance of energy absorbers with weld defects, represented by un-joined sides on the tubes (weld integrity completely lost), as indicated by the red lines in Figure 7, and modelled in the FE analysis as untied regions. The analysis examines two cases, the first case showing non welded sections on two tubes and the second case non welded sections on three out of the four tubes, the latter being an extreme case scenario.

The model considers a steel energy absorbing tube system and a lightweight aluminium alloy energy absorbing system. The latter has been included in the investigation because aluminium is gaining ground for lightweight rail vehicle construction.

The problem with aluminium alloys is that unlike steels where "matched" welds can be obtained (weld strength equal to parent metal strength), in aluminium alloys the weld region can exhibit strength almost half that of the parent plate due to the microstructural changes taking place by the heat input to the material as a result of the fusion welding process.

Mechanical tests were performed to obtain the mechanical properties of the parent metal and the welds of both the steel and aluminium alloy used for energy absorption tubes. The properties of the materials considered are given in Tab's 1 & 2. The mechanical tests included the acquisition of material parameters required for the FEA modelling.

After assessing the defect tolerance of the welded design of energy absorber as a method of attachment to the rail vehicle, the modelling is extended to consider a bolted on energy absorbing system, as shown in Figure 8.

All simulations have been carried out using a cluster with 40 CPUs and LS-DYNA version mpp971 R4.2.1. The implemented model for the welded solution is composed of 166310 Belytschko-Tsay shell elements (7) with 5

integration points through the thickness and an average dimension of 4 mm. Also, differed mechanical properties for the weld, the HAZ and the base material has been used. Automatic single surface contact without friction and soft constraint formulation has been used to model the contact between all the parts and accommodate the interactions between the folds within a given tube during collapse. The MPP algorithms have been activated as well.

The nodes of the back plate in correspondence to the surface attached to the train have been completely constrained. The simulations were performed using a 25 tonnes impact mass, modelled with a flat plate with a fictitious density and an impact velocity of 10,000 mm/s (i.e. 36 km/h).

The bolted model is composed of 114470 Belytschko-Tsay shell elements with 5 integration points through the thickness and an average dimension of 4 mm and 80204 solid elements for the back and front plates and the fixing systems. Even if there are different way to model the bolts [8] in the present work the bolts have been modelled using one *CONSTRAINT NODAL RIGID BODY for each bolt as the purpose of the present work is to compare the welded and the bolted solution assuming that the shear failure and the bearing effect can be prevented using a suitable dimension of the bolt and a thicker plate for the fixing system. However, using the Gurson model, if the stress attained around the holes is too high failure occurs causing the tubes to fail without absorbing the impact energy. In this case, the impact mass has been modelled using a *RIGIDWALL PLANAR MOVING with a mass of 25 tonnes and impact velocity of 10,000 mm/s (i.e. 36 km/h).

The constitutive model used for all the simulations is the Gurson model with the Wilkins Rc-Dc fracture model added and is already implemented in LS-DYNA as MAT 120. The Gurson failure model is a sophisticated approach which uses a state variable plasticity law, in which the void volume fraction is an explicit state variable and the yield stress is taken to be a function of the volume fraction of voids in the material. The Gurson flow function is defined as:

$$\Phi = \left(\frac{\sigma_e}{\sigma_y} \right)^2 + 2f^* q_1 \cosh\left(\frac{3q_2 \sigma_H}{2\sigma_e} \right) - 1 - (q_1 f^*)^2 = 0$$

where σ_e is the von Mises equivalent stress, σ_y is the yield stress, σ_H is the hydrostatic stress component, f^* the effective void volume fraction, defined as:

$$f^* = \begin{cases} f & \text{if } f \leq f_c \\ f_c + (1/q_1 - f_c)(f - f_c)/(f_E - f_c) & \text{if } f > f_c \end{cases}$$

where q_1 and q_2 are material parameters, f_c the critical void volume fraction, f_E the damage parameter corresponding to the void volume fraction at failure.

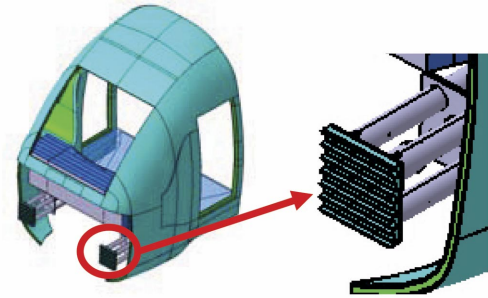


Figure 4: Typical positioning of energy absorbers in a rail vehicle.

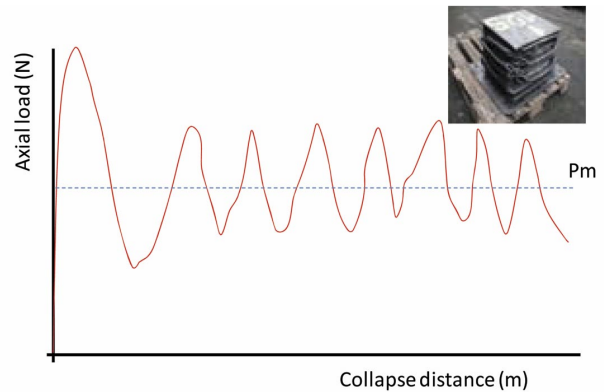


Figure 5: Load vs. time curve during dynamic testing of energy absorbing tube.



Figure 6: Energy absorbing tubes shown in situ in a rail vehicle, starter fold is clearly

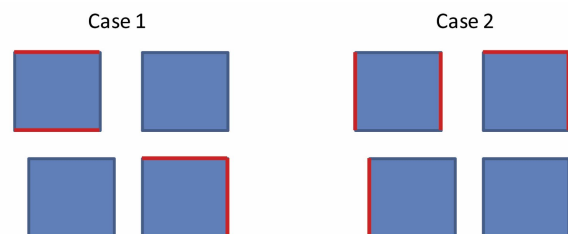


Figure 7: Two cases of weld defects where red lines represent complete loss of weld integrity (non welded regions).

To achieve a good accuracy the parameters defined above have to be obtained from materials tests. For the steel absorbers the following material properties were used determined by experiment.

Parameter	Base material	HAZ	WM
Density	7850 kg/m ³	7850 kg/m ³	7850 kg/m ³
E	206 (GPa)	206 (GPa)	206 (GPa)
Poisson's ratio	0.29	0.29	0.29
σ_y	349 (MPa)	317.6 (MPa)	286 (MPa)
q_1	1.5	1.5	1.5
q_2	1.0	1.0	1.0
f_c	0.027	0.027	0.02
f_0	6e-4	6e-4	5e-4
e_n	0.2	0.2	0.2
s_n	0.1	0.1	0.12
f_n	0.04	0.04	0.03
f_E	0.25	0.25	0.2

Table 1. Steel base material and weld properties.

Parameter	Base material	HAZ	WM
Density	2700 kg/m ³	2700 kg/m ³	2700 kg/m ³
E	70 (GPa)	76 (GPa)	76 (GPa)
Poisson's ratio	0.33	0.33	0.33
σ_y	262 (MPa)	120 (MPa)	165 (MPa)
q_1	1.5	1.5	1.5
q_2	1.0	1.0	1.0
f_c	0.008	0.1	0.015
f_0	0.012	0.01	0.025
e_n	0.1	0.05	0.25
s_n	0.01	0.1	0.1
f_n	0.005	0.01	0.01
f_E	0.25	0.15	0.15

Table 2. Aluminium alloy 6xxx series base material and weld properties.

Analysis of Welded Absorbers

In the following the results of the dynamic analysis related to the weld defects are presented. In the model the defects have been simulated by means of both Gurson model and untying the nodes on the edge between the elements of the weld and the HAZ in order to simulate the lack of fusion [see Fig. 9].

The results show that both the steel and aluminium absorber welded joint integrity is maintained when two tubes have weld defects and the energy absorbers perform as designed. However when the untied sides are significant, the folding starts in a regular manner but, due to the number of unsupported tube sides, the absorber fails in an uncontrolled manner. As example in the following the worst case has been shown.

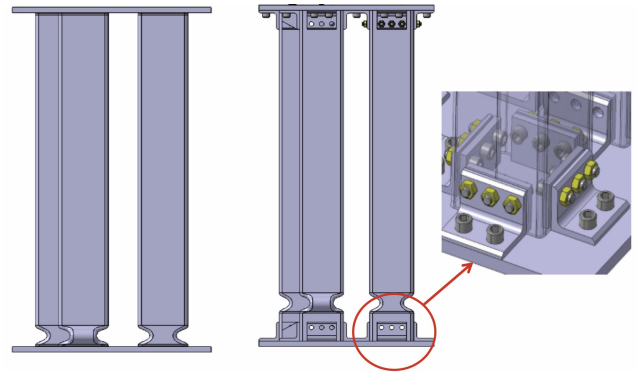


Figure 8: Welded and bolted on tubular energy absorbing system.

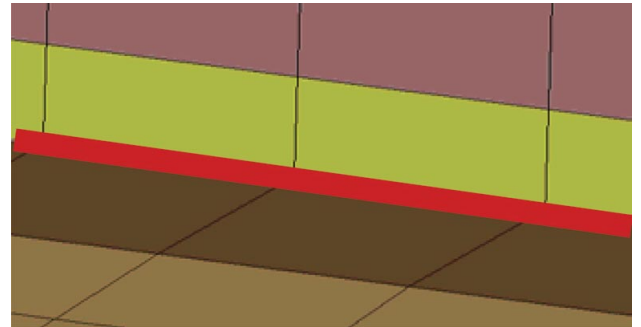


Figure 9: The red line shows the untied side.

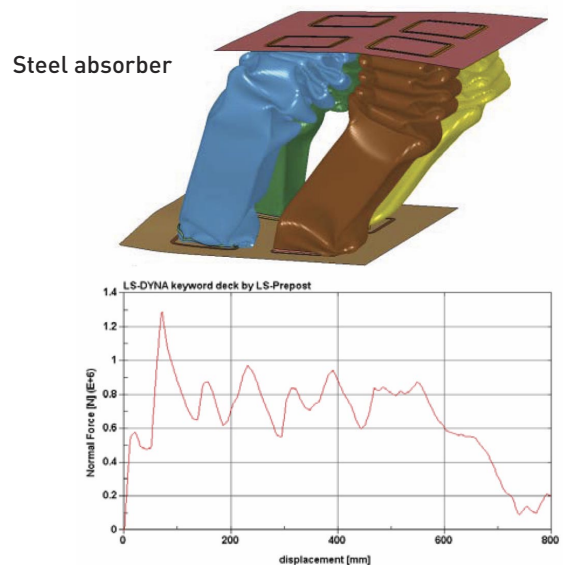


Figure 10: Axial load diagram and deformed configuration of steel welded energy absorber under in line impact at 36km/h with weld defects as for CASE 2.



Figure 11: Axial load diagram and deformed configuration of aluminium welded energy absorber under in line impact at 36km/h with weld defects as for CASE 2.

The simulation of the aluminium absorber with weld defects of case 2 shows that the welds would completely fail on impact. This is the worst case scenario where three out of the four tubes have welded sides with defects (total loss of joint strength). The axial load curve shows that the tubes would not function as intended.

The fact though that the steel absorbers performed better for CASE 2 suggests that both aluminium and steel could be used for a bolted solution and that this approach would be more advantageous for the case of aluminium absorbers because of the fact that the aluminium welds are "undermatched" (strength of weld lower than strength of parent material).

Bolted Energy Absorbers

In order to prevent propagation of cracks around the welds that affect the behaviour of the whole absorber and to improve the maintenance and the inspection aspect, a bolted solution has been proposed. Two solutions have been analysed made of aluminium and steel.

Aluminium bolted absorber

A comparison of the axial load curves of bolted and welded absorbers (steel and aluminium) shows that the bolted solution does not affect the performance of the tubes. It is therefore a feasible solution especially if aluminium absorbers are used which are more prone to failure due to weld defects.

The solution for the mean axial load provided by Wierzbicki and Abramowicz (Eq. 1) was also compared with the FEA results. Equation 1 includes the Cowper-Symonds (9) expression for the dynamic flow stress. What is also required for the solution is the strain rate, $\dot{\epsilon}$, but it is difficult to make an estimate of the strain rate in a square tube because of the complex deformation patterns that develop during axial deformation. However, an estimate was provided in (10) as:

$$\dot{\epsilon} = 0.33 \frac{V_0}{C},$$

where V_0 is the impact velocity, and C the tube width.

The Wierzbicki and Abramowicz equation provides the solution for a single deforming tube. When more than one tubes are simultaneously undergoing dynamic axial compression, mean load for axial progressive buckling is not additive (5). To make the comparison an impact model of a single steel tube was run and the mean axial load obtained.

Pm (FEA): 250 kN;

Pm (Eq.1): 283 kN (using $D = 300 \text{ s}^{-1}$, $q = 5$).

This is a reasonably good agreement, and gives confidence to the results obtained for a set of 4 tubes.

Conclusions

The results show that for multiple welded energy absorbing tubes, partial loss of weld integrity does not affect greatly their performance. The design is therefore damage tolerant.

A bolted on absorber design is a viable alternative to a welded absorber for rail vehicle applications offering advantages of ease of maintenance and quick replacement following a collision with significant economic benefits both in terms of repair procedures and time to return to service.

References

- [1] Hayduk, R. J. and Wierzbicki, T., "Extensional collapse modes of structural members", Computers and Structures, 18(3), 447-58 (1984).
- [2] Wierzbicki, T. and Abramowicz, W., "On the crushing mechanics of thin-walled structures", Journal of Applied Mechanics, 50, 727-34 (1983).
- [3] Abramowicz, W. and Wierzbicki, T., "Axial Crushing of Multicorner Sheet Metal Columns," J Appl Mech, 56(1), 113-20 (1989).
- [4] Jiayao Ma, Yuan Le and Zhong You, 51st AIAA/ASME/ASCE/AHS/ASC Structures, Structural Dynamics, and Materials Conference, April 12 - 15 2010, Orlando, Florida.
- [5] Aljawi A.A.N., "Axial Crushing of Square Steel Tubes", The 6 st Saudi Engineering Conference, KFUPM, Dhahran, December 2002.
- [6] Jones N. and Birch R.S., "Dynamic and static axial crushing of axially stiffened square tubes", Proc Instn Mech Engrs Vol 204, 293-310 (1990).
- [7] Shailesh Narkhede, Nitin Lokhande, Bhavesh Gangani, Ganesh Gadekar, "Bolted joint representation in LS-DYNA to model bolt pre-stress and bolt failure characteristic in crash simulations" Proc. of the 11th International LS-DYNA3D Conference, June 6-8 2010, Dearborn, MI, USA.
- [8] LSTC - LS-DYNA Keyword User's Manual Version 971, Livermore Software Technology Corporation, 2007.
- [9] Symonds, P. S., "Viscoplastic Behavior in Response of Structures to Dynamic Loading", Behavior of Materials Under Dynamic Loading (Huffington, N. J. Editor), pp 106-124, SME, New York (1965).
- [10] Jones N., "Dynamic progressive buckling", Structural Impact, Cambridge University Press, 1989, ISBN 0521301807.

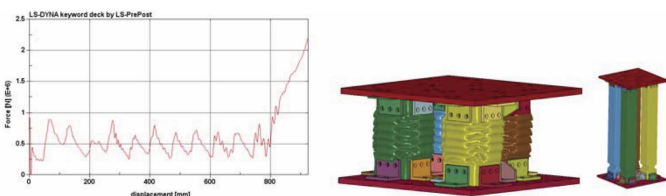


Figure 12: Axial load diagram and deformed configuration of bolted on aluminium welded energy absorber under in line impact at 36km/h. Steel bolted absorber

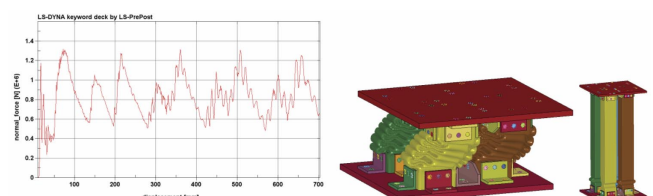


Figure 13: Axial load diagram and deformed configuration of bolted on steel welded energy absorber under in line impact at 36km/h.

Ford Motor Company Accelerates Design for Manufacturability of Conical Joints

Developing high-quality bolted joints is an integral part of vehicle chassis design. Robust joints are critical to improving handling and longevity of vehicle performance. Joints that are loose tend to exacerbate quality issues such as alignment, and ultimately the durability of the joined components. A properly designed joint is more efficient and can support larger loads with smaller size fasteners without loosening.

Engineers at Ford Motor Company were tasked to deliver a robust cantilevered conical joint design for the rear suspension system of a midsize passenger car [Figure 1]. To minimize time and cost while meeting functional targets, the team developed an automated Design of Experiments (DOE) process using Abaqus for CATIA (AFC) for structural analysis and Isight for process automation and optimization, both from the SIMULIA brand of Dassault Systemes.

“Our team chose to deploy standard stress modeling and simulation practices in the form of templates to a broader group of engineers within the design organization,” says Satyendra Savanur, chassis CAE engineer at Ford Motor Company. “We used response surface model, one of the approximation models, for finding optimal parameters to size the joint.”



Analyzing Conical Joint Performance

A bolted joint is the most common type of attachment method used in the suspension of a car. In this application, a conical joint is used for connecting the toe-link to the rear knuckle with a cantilevered type connection. The two mating parts of the conical joint—the bushing inner sleeve and the knuckle—each have unique manufacturing tolerances of the cone angle.

To develop a robust conical joint between a steel inner sleeve and an aluminum knuckle the following aspects were considered:

- manufacturing tolerances of each component
- contact area between the cone and seat
- angle of the cone
- torque loss after the service load is removed.

To perform virtual tests of their design, the Ford engineers created the finite element model of the knuckle and the bushing inner sleeve with the geometry input and material properties from their model created in CATIA. Associativity was maintained to ensure that the model updates were robust when the CAD model is changed within the usable range of design variables.

During the physical assembly process, a forged steel inner cone is forced against an aluminum knuckle seat [Figure 2]. Due to the different manufacturing processes used to make each part, the angular tolerances of the conical design features are different on the inner sleeve and the knuckle mating surface.

“Because of the potential angular mismatch, there are variations in contact area when the two surfaces mate together and the joint is fully torqued,” says Savanur.

Local yielding can occur in the mating materials, leading to changes in contact area and pressure distribution during assembly of the joint. When the service load is applied, further changes to contact area and contact pressure can occur.

“It is therefore important to simulate both the joint assembly, and the loading and unloading, of service loads on the joint during the analysis,” he says. **“Our objective was to deliver a robust conical joint design for the entire range of conical mismatch between the cone and the knuckle.”**

For a robust contact analysis and even contact pressure distribution, the mesh of the inner sleeve was constructed to align with the mesh of the knuckle seat. To facilitate mesh alignment in the contact area, a separate “domain” of the knuckle seat, shown in light blue in Figure 4, was created to simplify meshing. This part was connected to the rest of the knuckle body with a tied contact.

To simulate the bolt assembly process, a virtual bolt between the inner sleeve and the knuckle joint seat was created. External service loads were applied on the sleeve center. Non-linear stress-strain curves for aluminum and steel were imported to facilitate the nonlinear analysis. Contact pairs and bolt tension were then created. Output of contact area and contact force magnitude were used during post-processing. Finally, the analysis file was output and submitted to the High Performance Computing (HPC) cluster for running the analyses.

Managing the DOE Process

Ford’s need to evaluate a large number of designs with different combinations of parameters prompted the engineers to create an automated DOE process. In this process, CAD geometry updates and FEA model updates are completed in the same loop thus allowing a completely automated DOE approach.

At Ford, CAD startup is customized with an external product management system. Scripting is used to strip away the linkages to the product management system before initializing the interface.

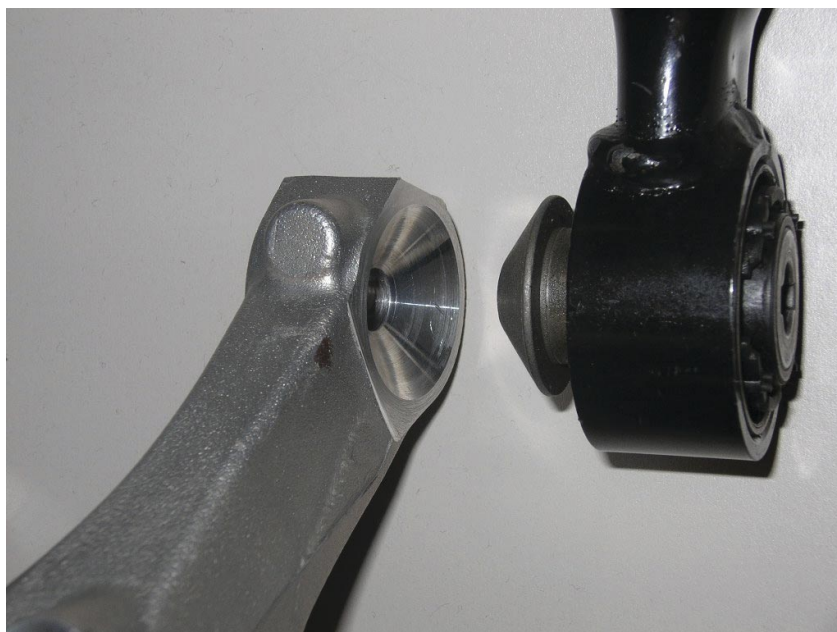


Figure 1: Close-up view of Knuckle Cone Seat and Inner-Sleeve

Design parameters are then fed in with an external Excel file. The input parameters from the Excel file are mapped to the DOE task of the Isight manager. This enabled automatic updates of the excel sheet for each loop. Since Excel is synchronized with the design table, this results in automatic updates of the CAD geometry and FE.

“By developing a single integrated process, we were able to drive automatic updates of the geometry and mesh at the same time,” says Savanur. The process automation manager was used to manage and control the DOE process. The resulting automation loop is completely integrated to run CAD updates, creating the FE models, and job submission for analysis and post-process results.

The FE component inside the process management loop was used to extract outputs, including contact area and contact force magnitude for each run of the DOE. The input parameters from the Excel file are then mapped to these output parameters to create Isight approximation model.

“In our case, we used the response surface model method of approximation,” says Savanur, as seen in figure 6. This approximate model of conical joint behavior can then be used to show how-input affects output and quickly optimize the conical joint.

“This is the first application of an integrated DOE automation loop to morph geometry using CATIA with Abaqus at Ford,” says Savanur.

Isight Enables More Efficient Processes

The set-up and validation of the scripts, HPC job submission batch file, and the windows batch command file took time and resources to develop, but were well worth it as they are re-usable for subsequent projects with minor changes.

“Developing a comparable CAD model with an associated Excel design table, and linked to an associated FE model would take approximately three days to construct,” says Savanur. **“Modifying and debugging the previously developed scripts to run with these new models would take another day.**

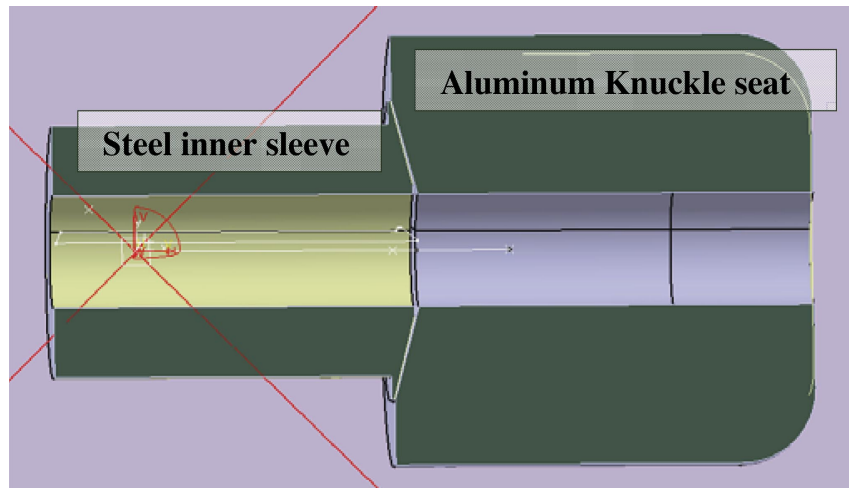


Figure 2: Section of the Conical Joint

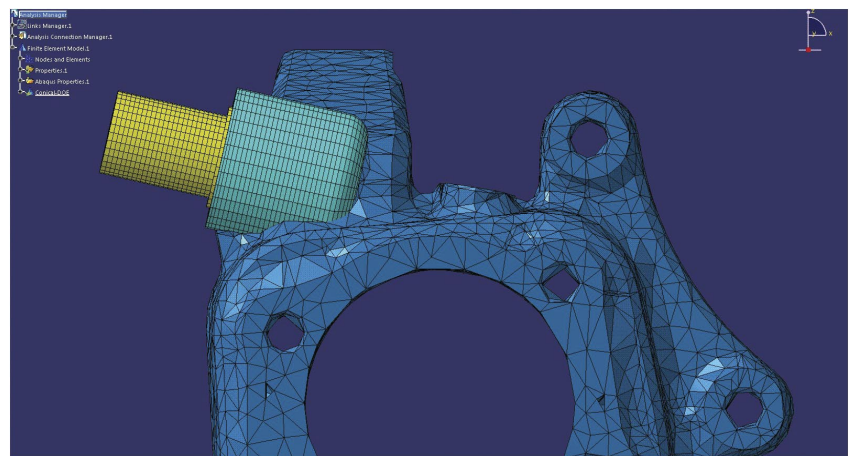


Figure 3: Detailed CAE model

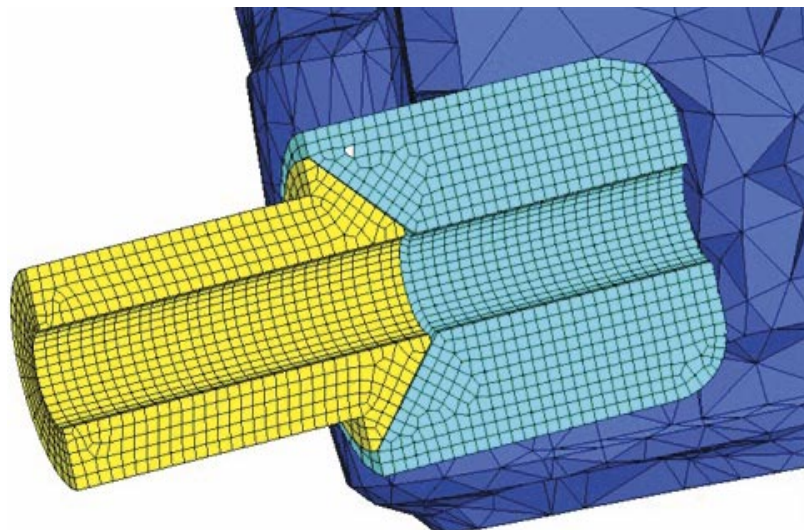


Figure 4: CAE Mesh details of the conical joint

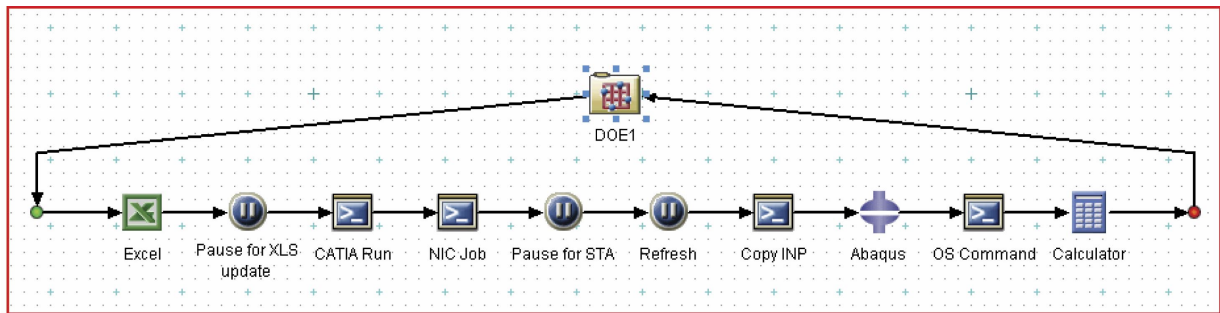


Figure 5: Integrated DOE Automation Loop Using Isight

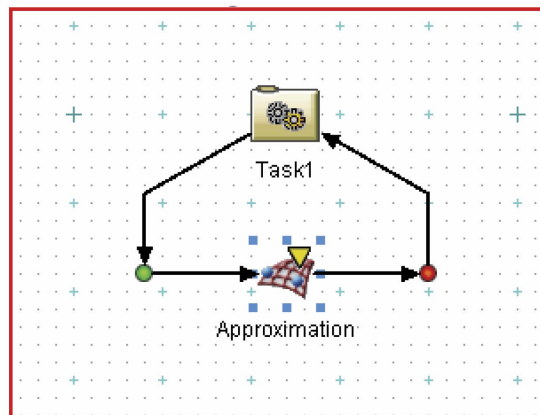


Figure 6: Response Surface Model Method

Using this method, it took about 3.5 hours for the process to complete 35 analysis runs.”

“Typically, the manual CAE process consumes two days just to complete one run. Of course, this timing can be reduced if the project is critical, but this is the typical day-to-day turn-around time balancing several projects per engineer,” says Joe Peters, chassis CAE supervisor at Ford Motor Company.

Time inefficiencies typically occur in the transfer of data back and forth between CAE and CAD organizations, as people have multiple assignments and do not immediately stop their current work when new design iterations are requested; this is analogous to CPU time verses wall clock time.

“It is estimated it would have taken approximately 70 days to complete all 35 runs, while maintaining other day-to-day work; whereas, our new process eliminates the inefficiencies that were part of the manual CAD/CAE procedures,” says Savanur. “By setting up the integrated closed-loop automated DOE loop using Isight, we achieved this task in about four days. This was the only way to help achieve the program objectives of cost and timing with a lean CAE organization”.

“Using the automated DOE process, we were able to drastically cut down the time required to develop a robust conical joint with minimal resources,” says Peters.

By creating an integrated closed-loop DOE process, Ford Motor Company was able to deliver a robust conical joint design. This joint exhibits good contact area and retains clamp load after load removal, within the specified manufacturing tolerances.

Conical Joint Description

Figure 1 shows a close-up view, before assembly, of the toe-link (black) and the rear knuckle (silver) using a conical joint.

CAE Model Details

The CAE model, shown in Figure 3, has three distinct parts:

- bushing inner sleeve (yellow) made of steel,
- knuckle seat (light blue) made of aluminum
- And third is the knuckle body (dark blue) made of aluminum.

RSM approximation based on a polynomial fit via the least squares regression of the output parameters to the input parameters. The R^2 analysis is a measure of how well the model polynomial approximates the actual function. When $R^2=1.0$, the polynomial values and response function values are identical (at all design points).

This case study was developed with the assistance of the following engineering team at Ford Motor Company: Satyendra Savanur, Elaine Hoffman, Rajesh Rajput, Xiaoming Liu, Joe Peters & Kyu Sohn.

Joint Durability on the Rails

Dipl.-Ing. Thorsten Weyh, Dr. Michael Speckert
Fraunhofer Institut für Techno- und Wirtschaftsmathematik (ITWM),
Kaiserslautern, Germany.



This article, taken from the newly released NAFEMS publication “FEM Idealisation of Joints”, takes a look at a project led by the department of “Mathematical Methods for Dynamics and Durability” (MDF) at Fraunhofer ITWM in collaboration with a leading railway company, to analyse multi-bolted joints and their durability behaviour under service loads.

The finite element model that was used includes nonlinear contact formulations and friction between the specific parts of the railway ball joint connection. The service loads were represented by long 3-dimensional time signals, characterising a typical operating day of the railway vehicle.

Due to the length of the time signals a fully transient FE calculation was not an option. In addition, the commonly used linear quasi-static superposition approach could not be used due to the nonlinear contacts.

Within the project, ITWM developed a highly efficient method to compute the stress time signals of multi-bolted joints. The approach enhances the established method of the linear quasi-static superposition such that nonlinear contact formulations can be covered. It is based on the interpolation of suitably chosen static contact problems.

The new approach enables a profound comparison and improvement - in the early stages of the development process - of different design variants undergoing complex varying service loads even in case of nonlinear phenomena such as contact.

Bolted joints are one of the most common detachable connections in mechanical engineering. For the design of a single- or multi-bolted joint, the VDI guideline “Systematic calculation of high duty bolted joints / Joints with one cylindrical bolt, VDI 2230, Feb. 2003 [1]” has been used for many years. The guideline provides all the necessary calculation steps for a standard stress analysis of a bolted joint based on reduced and simplified model assumptions.

Nevertheless, not all possible connection designs are included in the guideline. In particular, the calculation of multi-bolted joints is not fully described. FEA is increasingly being used to assess these multi-bolted joints. On the other hand, there is no common guideline for the usage of FEA regarding modelling, calculation, and durability behaviour of single or multi-bolted joints. Thus, FEA does not replace the VDI guideline, but offers reasonable extensions to those joints, which can't be calculated with the reduced or simplified models of the guideline. Further details for single- and multi-bolted joints see [4].

In the case described here, nonlinear FE analysis is needed due to contact between different parts of the structure. Thus, the well known quasi-static superposition approach does not apply. A separate FE analysis for each time sample would be required. However, this is not possible due to the length of the load signal. Instead, only a few suitably defined combinations were calculated,

building the basis for a new approach to obtain the stress results of the multi-bolted joint for the whole measured time series.

Furthermore, a fatigue life analysis of the multi-bolted joint under the service loads was performed.

Model Details

In order to obtain reasonable fatigue life estimations, the requirements on the accuracy of the stresses calculated by FE models are high. Therefore the FE model has to be detailed enough. On the other hand it is hardly possible to include all the details of the bolted joint model (e.g. single thread turns) due to the increasing size of the FE model and the corresponding calculation time and hardware requirements. In the case described here, a compromise has been implemented to get reasonable stress results within the multi-bolted joints which are accurate enough for a subsequent durability analysis.

In Figure 1, the FE model of the joint investigated in this paper is shown.

The service load was given by measured time series (three forces F_x , F_y , F_z at 200 Hz sampling rate) representing the load of a typical day for this kind of railway vehicle. The time series were measured at the ball joint connecting two railway wagons.

Details of the bolt joint:

- Type: M16 10.9, rolled before heat treatment, tapped thread joint, thread insert
- Tensile strength: 1000 MPa
- Yield strength: 900 MPa

Overview of the FE model:

- Elements: approx. 104.000 (predominantly Hexahedron-Elements)
- Material: Steel and Aluminium parts
- Friction coefficient between the parts: = 0.3
- Assembly preload at the bolts: FM = 41kN
- Solver: ANSYS 10.0 (see [5] for further details)

Analysing the Nonlinear Behaviour of the Structure

For a first overview regarding the model behaviour under service loads, the measured time series were analysed to identify the load range. The time series contains three forces F_x , F_y , F_z within the following range:

F_x [-45kN ... +45kN]; F_y [-60kN ... +60kN]; F_z [-5kN ... -40kN]

F_x acts along the longitudinal axis of the bolt. It mainly represents the load acting on the bolt when the train accelerates (tensile stress) or due to braking events (compression stress).

F_y represents the load when the train is cornering. Depending on the curvature of the track, F_y creates tensile stresses at the bolts located in the direction of the outer curve radius and compression stresses at the bolts located in direction of the inner curve radius. It acts along the lateral axis of the bolt.

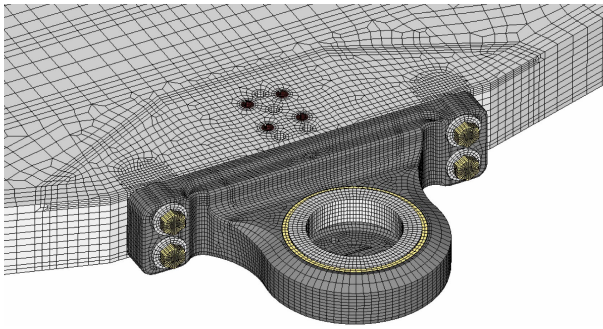


Figure 1: Finite element model of the railway ball joint connected by a multi-bolted joint.

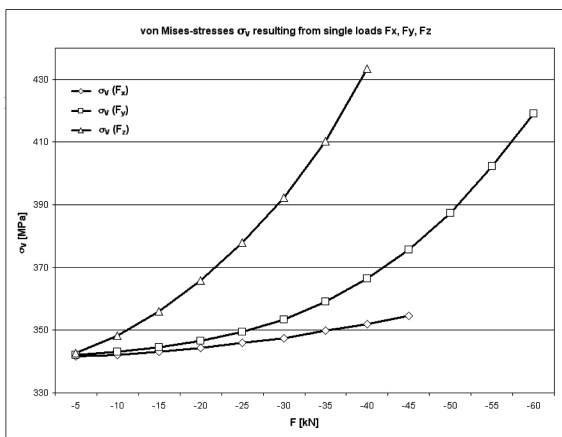


Figure 2: von Mises equivalent stress σ_v under single loads F_x , F_y and F_z .

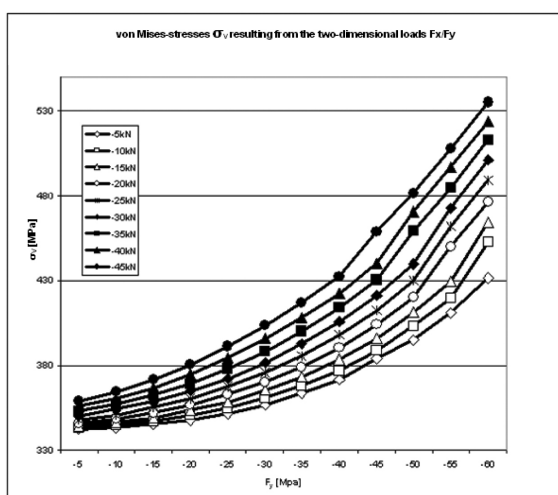


Figure 3: von Mises equivalent stress σ_v under two-dimensional loads F_x and F_y for one selected FE node. The legend refers to the value of F_y .

Finally, F_z represents the part of the applied loads based on outer loads (tare mass and payload). F_z also acts on the lateral axis of the bolt. Depending on the driving condition of the railway vehicle, F_z and F_y may have negative and positive signs while F_x only acts in the negative direction.

To obtain an adequate resolution for the analysis, the load range was divided into 5kN steps and FE computations were performed on that grid. F_x was assumed to act within -5kN to -45kN, F_y within -5kN to -60kN and F_z within -5kN to -40kN. Therefore the total numbers of calculations was $9 (F_x) + 12 (F_y) + 8 (F_z) = 29$. For one single load step including the preceding load step 'pretension', the calculation time is up to two hours. So the overall used calculation time was 58 hours (nearly 2 1/2 days).

The equivalent stress results (von Mises) are plotted in figure 2. In each load direction the FEA model obviously shows nonlinear stress behaviour which is due to the nonlinear contact formulations.

Since linear superposition of these load cases is not allowed here, combinations of several loads had to be calculated in addition. For the combinations F_x/F_y , F_y/F_z and F_x/F_z the same load step size of 5kN was used. Thus, we get $108 + 72 + 96 = 276$ FE calculations, resulting in 552 hours computation time (23 days).

As can be seen easily, the stress depends on the forces again in a nonlinear fashion.

Transferring this fine resolution of 5kN steps to the three-dimensional load combinations, the overall calculation time would add up to slightly more than 144 days which of course was not executed. Nevertheless, the calculations performed so far clearly show the nonlinear behaviour of the stress as a function of the loads. Thus, linear quasi-static superposition is not applicable and a new approach had to be found.

Basic Idea of the Interpolation Approach

As already mentioned, the current state of the art process for calculating the stress time histories due to long load time series in combination with FEA models is the so called "linear quasi-static superposition" approach. For this approach, static unit load cases $\sigma_i(x)$ calculated by an FEA solver are superimposed with measured time series $L_i(t)$ in the form

$$\sigma(x, t) = \sum_{i=1}^L \sigma_i(x) \cdot L_i(t).$$

This linear quasi-static approach requires linear model behaviour. For calculating the i -th unit load case $\sigma_i(x)$ the corresponding i -th load is set to 1 while all other loads are zero and the resulting static problem is solved. In case of nonlinear model behaviour, the quasistatic approach will not deliver correct results. To take the nonlinear effects of the present FEA model into account, the new "interpolation" approach extends the basic idea of the quasi-static approach to nonlinear models. Instead of the

three unit load cases, a set of FE computations have to be performed on a suitably defined grid of loads.

As mentioned before, the main goal is to decrease the overall calculation time whilst keeping the error small. A first attempt to fulfil this requirement is to reduce the fine grid of 5kN steps to a coarser range of load steps. As shown in Figure 2, the nonlinear system response of stresses due to increasing F_x load starts at approximately -20kN. So the first load step is fixed at -5kN, the second one at -20kN where the beginning of a stronger nonlinear behaviour of the stress curves can be observed. The end point of the load range is given by the highest measured load at approximately -40kN. An additional point at -30kN in between -20kN and -40kN completes the F_x -grid. With these four values the nonlinear characteristic of the stress curves can be reproduced with sufficient accuracy as will be shown below. The same procedure was used for the lateral and vertical forces.

Another step to reduce calculation time is to use the symmetry of the FE model. The load range in F_x direction cannot be reduced because of a lack of symmetry (differences in roll off and brake events). Also for F_z (tare mass of the vehicle and payload) which acts only in one direction, no symmetry can be exploited. However, for F_y it is sufficient to calculate only one load direction and reduce the overall effort to one half.

In the current example, the following load steps have been chosen:

- F_x [kN]: -45, -35, -20, -5, 5, 20, 35, 45
- F_y [kN]: -60, -45, -30, -5
- F_z [kN]: -40, -30, -20, -5

For each combination of F_x , F_y , and F_z (grid point in 3D load space) there will be a stress result, calculated by an FEA solver resulting in $8*4*4 = 128$ FE calculations.

At a fixed load in one direction, for instance F_z , the stress results can be plotted as a surface in the remaining load space as shown in Figure 4 for the stress in longitudinal direction of a bolt.

For fatigue analysis, the von Mises stress is not appropriate. Therefore, the tensor component σ_x in longitudinal direction of the bolt is used in the following.

The basic idea of the interpolation approach is to substitute the results of the FE calculation for an arbitrary load combination with an approximation which is found by interpolating the stresses calculated on the

128 grid points in the load space. The system response σ_x depends on

- the given three-dimensional service load F_x , F_y , and F_z ,
- the suspension load FM of the bolted joint, and
- the friction values between the head of the bolt joint and other parts

In the following calculation steps, the pretension force FM and the friction coefficient μ were set to a certain constant value. Thus, from a mathematical point of view the system response σ_x in the bolt joint can be described by a function $\sigma_x = \sigma_x(F_x, F_y, F_z)$. For further investigations it would also be possible to construct an interpolation base with variable values for the pretension and friction coefficient.

The approximation function is required to deliver values which are close to the real system response. The way to find those approximation functions is sometimes called "response surface" method.

The grid decomposes the load range into $7*3*3=63$ cells. Within each cell, the approximate interpolation function can be represented by a spline function $\tilde{\sigma}_{x,local}$ which can be described in the form

$$\tilde{\sigma}_{x,local}(F_x, F_y, F_z) = \sum_{i=0}^3 \sum_{j=0}^3 \sum_{k=0}^3 c_{ijk} \cdot F_x^i F_y^j F_z^k .$$

To evaluate the unknown coefficients c_{ijk} for each cell, several properties are required, namely

- continuity and interpolation: the values at the grid points have to be equal to the values calculated by the FE analysis,
- smoothness: the first and second derivatives at the grid points of two connected cells have to be equal,
- the second derivatives at the boundary have to be zero.

The combination of all local splines for the whole load range is denoted by $\tilde{\sigma}_x$.

Besides this spline interpolation approach there are a lot more ways to find a response surface for instance by "least squares methods" or other interpolation approaches. Some of them have been implemented and compared to the spline $\tilde{\sigma}_x$. Since similar results have been found, these methods are not described in this paper.

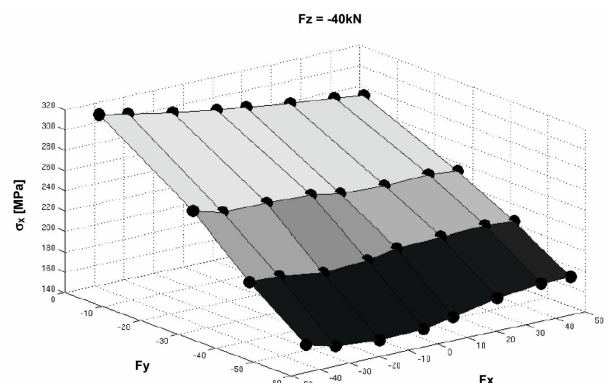


Figure 4: Stress σ_x in direction of the bolt under a three-dimensional load combination of F_x , F_y and F_z .

Error Discussion and Application

To evaluate the difference between the approximation function $\tilde{\sigma}_x$ and the FE system response $\hat{\sigma}_x$ one has to find suitable deviation measures either based on the absolute error $r_{\text{absolute}} = \sigma_x - \tilde{\sigma}_x$ or the relative error $r_{\text{relative}} = \frac{\sigma_x - \tilde{\sigma}_x}{\sigma_x}$.

Here, the maximum error, the mean absolute error, or the mean relative squared error at a certain set of test points $(F_{x,i}, F_{y,i}, F_{z,i}), i=1, \dots, L$ can be used. As mentioned by Schumacher [2] another quality measure is the so called regression parameter R^2 which is defined by

$$R^2 = 1 - \frac{\sum_{i=1}^L (\sigma_{x,i} - \tilde{\sigma}_{x,i})^2}{\sum_{i=1}^L (\sigma_{x,i} - \hat{\sigma}_x)^2},$$

where L is the number of test points, $\tilde{\sigma}_{x,i}$ the value calculated by FE analysis, $\sigma_{x,i}$ the response surface value and

$$\hat{\sigma}_x = \frac{\min(\sigma_{x,i}, i=1, \dots, L) + \max(\sigma_{x,i}, i=1, \dots, L)}{2}$$

the mean value of the highest and lowest stress. This measure is quite similar to the variance reduction mentioned in [3] for which $\hat{\sigma}_x$ is the mean value of all inspected stress values.

To evaluate the error of the approximation function, the grid points can only be used in the case of the least squares approach. For the interpolation approach the error on the grid points is zero by definition.

Therefore, new combinations besides the grid points have to be calculated by FE analysis. The following table gives an overview of the error between interpolated and FE results for 8 chosen test points.

Table 1: Error between interpolated results and FEA results.

Load combination F_x, F_y, F_z [kN]	Error	
	Absolute [MPa]	Relative [%]
-27.5, -50, -30	-1.3	-0.6
-27.5, -50, -15	0.9	0.3
-27.5, -15, -30	-2.7	-0.9
-27.5, -15, -15	2.8	0.8
12.5, -50, -30	0.9	0.4
12.5, -50, -15	-3.1	-1.1
12.5, -15, -30	1.5	0.5
12.5, -15, -15	2.7	0.8

In all of these 8 test points, the relative error is at most 1%, the absolute error at most 3 MPa. Thus, the interpolation approach was judged to be accurate enough to calculate the stress results for the multi-bolted joint.

By evaluation of $\tilde{\sigma}_x(t) = \tilde{\sigma}_x(F_x(t), F_y(t), F_z(t))$ for all time samples t of the measured loads $F_x(t), F_y(t), F_z(t)$ the interpolation approach delivers time series of interpolated stress results for all interesting positions of each bolted joint.

For each bolt 48 spots have been selected which gives in total 192 time series. Once the interpolation function has been obtained, the effort to calculate these stress time series is only several minutes, even for the long measured time series with over 3 mill. sampling points. Based on these results, it is a straightforward task to perform fatigue life estimations for the bolts of the structure under investigation. This step is not described here.

Conclusion

In this paper, an extension of the well established linear quasi-static approach was introduced. It could be shown that the interpolation approach can take nonlinear effects into account, in contrast to the linear quasi-static approach.

It was also shown that the error of the interpolation approach was small enough for the bolted joint structure described here.

The overall time spent to obtain fatigue life estimations of the multi-bolted joint could be limited to a couple of days for the structure under investigation.

The time spent for the FE calculations to build up the interpolation basis took nearly 10 days on a single CPU machine. The calculation of the interpolation function took only several minutes. Also the calculation of the interpolated stress time signals at the spots of interest and the subsequent fatigue life estimation can be done very quickly.

Compared to the standard way of performing an FE analysis for each sample point of the measured load time signals, the interpolation approach decreases the calculation time in a tremendous way.

However, the approach described in this article applies only to loads and structures where a quasi-static behaviour can be assumed. Thus, the loads have to be slowly varying compared to the eigen-frequencies of the structure.

References

- [1] Verein Deutscher Ingenieure e.V.: „Systematic calculation of high duty bolted joints / Joints with one cylindrical bolt“, VDI 2230 Part 1, Feb. 2003, 171 Pages
- [2] Schumacher, A.: „Optimierung mechanischer Strukturen: Grundlagen und industrielle Anwendungen“, Springer, 2005, 308 Pages
- [3] Wolberg, J.: „Data analysis using the method of least squares“, Springer, 2006, 250 Pages
- [4] Wiegand, H., Kloos, K.-H., Thomala, W.: „Schraubenverbindungen“, Springer, 2007, 428 Pages
- [5] ANSYS 10.0 Online help

Engineering Design Optimisation

Peter Bartholomew, of the NAFEMS Computational Structural Mechanics Working Group, discusses the history and future of design optimisation.



Historical context

The concept of structural optimisation, in particular, is not new. Galileo [1] attempted to determine optimal shape of a variable depth beam, despite the fact that it was only during the following century that Parent [2] and Lagrange independently identified the significance of the neutral axis in bending theory of beams and so were able to analyse the loaded beam correctly. Other eminent scientists that worked in the area include Maxwell [3] who in 1869 published a theorem on fully-stressed layouts of pin-jointed frames but it was Michell [4] who in 1904 developed generated families of solutions featuring orthogonal arrays of pin-jointed bars such as the rather elegant arch shown in Figure 1 below. These structures still provides useful benchmark problems for modern-day topology optimisers.

By the time of the Second World War, the design of light alloy compression structures was of interest and Cox et al developed solutions to various aeronautics problems [5], later published within a volume of the ESDU data sheets. At this time optimisation was still applied at component level and only for mass-critical situations such as aerospace. Studies at that time could be characterised as addressing structures of generic interest which may be described by sets of closed-form equations, so allowing the optimum to be determined by assuming the simultaneous solution of constraint equations as equalities.

The state of the art was to change totally during the 1960s with the advent and increasingly widespread availability of the digital computer. Numerical optimisation methods were also developed, under the name of Mathematical Programming [6], to support the Operations Research community. At the same time, the finite element method was being developed, not least by Zienkiewicz and his team at Swansea [7]. By the time of the 1972 conference on the Optimisation of Structural Design [8] held in Swansea, a surprisingly large range of issues of current interest were under consideration, including the treatment of discrete variables and design for reliability. In 1980, however, Petiau was able to report a decade of optimisation applications at Dassault built round the use of Elfini. An increasingly multidisciplinary content was becoming evident with both 2D aerodynamic shape optimisation and aeroelastic considerations appearing.

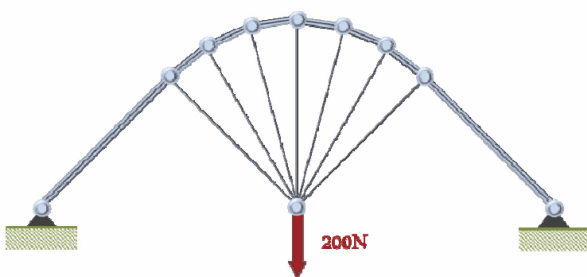


Figure 1: Example of Michell Structure



Figure 2: Ares V Heavy Lift Launch Vehicle

FENet

In August 2001 NAFEMS was funded by the European Commission to lead the FENet Thematic Network, that sought to co-ordinate activities within Europe aimed at improving both the quality of industrial applications of finite element (F.E.) technology and the level of confidence that can be placed in the computed results. In excess of 110 organisations were members of FENet, representing eight separate industry sectors:

The activities of the network were focussed on three technology areas: Durability and Life Extension, Multi-Physics & New Technology and Product and System Optimisation. A principal objective of FENet was to collate and structure existing information and to facilitate the efficient exchange of experience and knowledge within, and between, different industrial sectors within the European Community. A State of the Art report on Product and System Optimisation summarising material gathered during the four years of the FENet Thematic Network formed part of the final deliverables to the Commission.

Applications

That report has now been updated to reflect the expansion in the usage of optimisation that has occurred since that time and is about to be issued in the form of a NAFEMS book. The initial sections covering historical aspects of the subject, basic optimisation theory and the forms of design optimisation are little altered. The major departures come later with the introduction of fluid dynamic optimisation alongside structural design optimisation and the inclusion of an applications section.

A number of vendors were approached to provide user applications which would capture the current state of practice in applying the various categories of optimisation to industrial design problems. Inevitably the number of

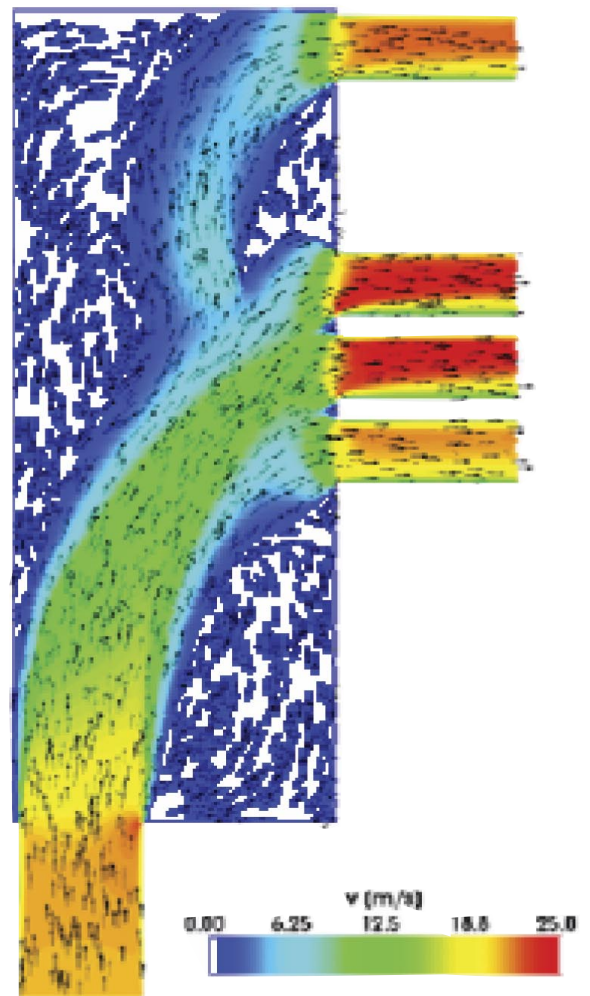


Figure 3: Optimal Flow through a Ventilation Duct

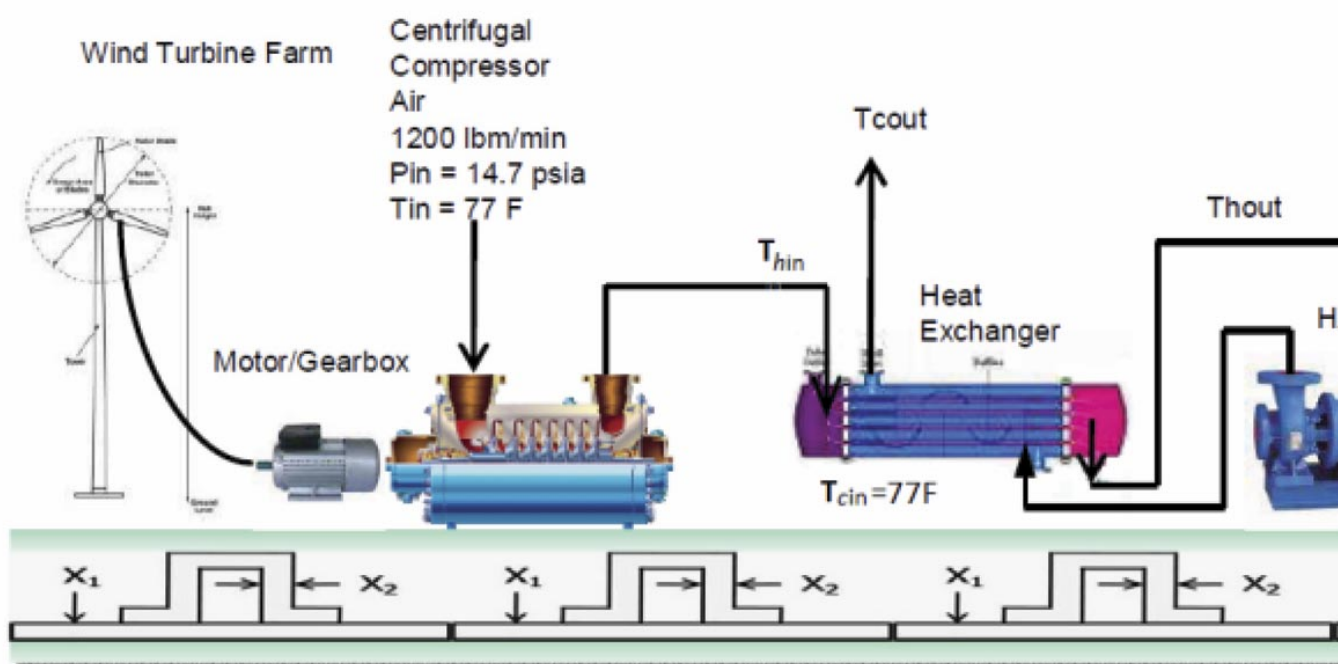


Figure 5: Schematic dra

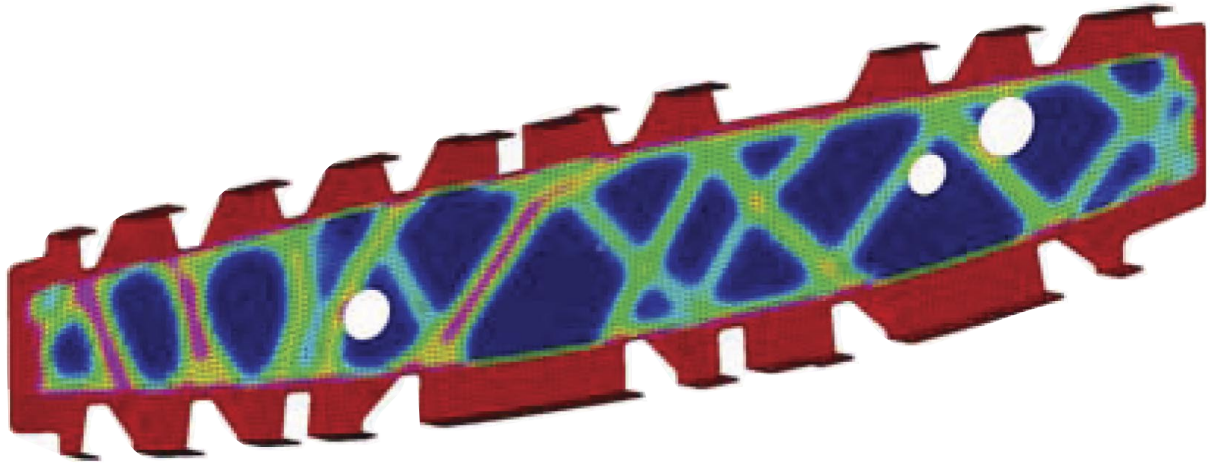


Figure 4: Design Space and Optimised Topology for Wing Rib 11

vendors that eventually contributed was only a proportion of those that expressed a willingness to participate but nevertheless a reasonable coverage of the technology was achieved.

A traditional approach to structural strength design is to optimise the product component by component on the assumption that changes in the load path and other interactions have small effect. Such approaches have evolved to incorporate a sophisticated range of detail-stressing tools that allow the resulting design to be accepted with confidence. The example given in the booklet is provided by Collier Research [9] and describes

the evaluation of composite design concepts for application to a space launch vehicle (NASA's Ares V Heavy Lift Composite Technology Vehicle shown in Figure 2).

For the sake of historical record an example of structural size optimisation that epitomised airframe structural design programs during the 1990 is also provided. This includes strength and stiffness design against multiple criteria including exploitation of the strength of composite materials, the avoidance of flutter and the aeroelastic tailoring of high aspect ratio wings to avoid undesirable aeroelastic effects such as aileron reversal.

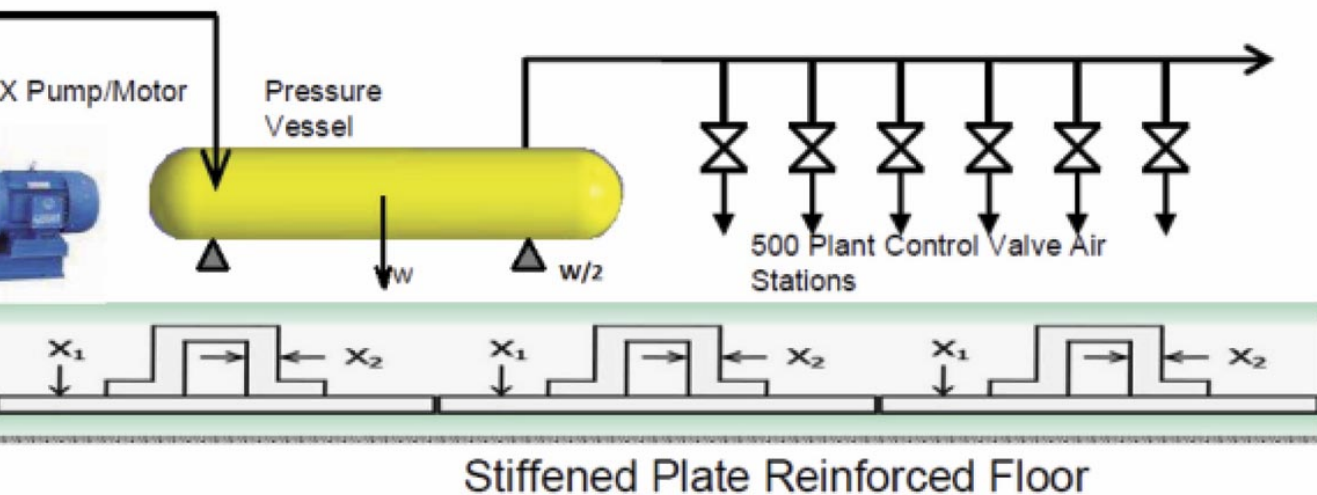


Diagram of air supply system

Shape optimisation is illustrated in an automotive context using an aerodynamic application provided by ICON Ltd [10]. The study has as its objective drag reduction applied to the Audi A6 Avant. The development of adjoint sensitivities showed that the greatest changes could be achieved by modifying the shape of the rear of the vehicle. The gradient-based optimisation procedure converged in 14 iterations, giving a 2.5% reduction in the drag coefficient. The drag reduction is significant and compares well with that achievable by traditional experiment-based optimisation methods.

Topology optimisation is illustrated using both aerospace and automotive applications. The aerospace application [11] was provided by Altair and addresses the design of a wing rib. Through the initial use of topology optimisation a radical rib design was achieved, involving a novel mix of stiffened panel and truss concepts, which satisfied buckling and stressing. After refining the design using shape and size optimisation, the final CAD model showed a mass saving of about 10% over that achieved through the use of traditional design approaches.

The automotive application [12] was an internal ducted flow problem in which the objective was to minimise the power dissipation as the flow is split across ventilation ducts. In the structural topology optimisation it is the material density that drops to zero for ineffective structural paths; in the case of fluid optimisation it is an artificial porosity term that is increased to block the flow.

The optimised flow (Figure 3) corresponded to more compact ducting than in the base-line case, with negligible amounts of flow in recirculation regions. In addition, the approaches to the outlet sections have been tapered, which has the effect of removing the previously observed small recirculation regions downstream of the outlet duct throats. A power dissipation of 60.8 W was calculated for the baseline case, while the optimised duct displays a dissipation of 34.8 W, an improvement of 43%.

The final application shows a system optimisation problem which is modelled using a Process integration tool developed by Phoenix Integration [13]. This application addresses the selection of pre-built engineering components which are combined to provide an integrated system for supplying shop air to a chemical plant.

The system comprises a centrifugal compressor, an associated electric motor and gearbox, a heat exchanger, and a pressure vessel. The equipment is located in the upper floor of a plant building and is supported by a stiffener-reinforced floor. The motor is partially fed from the mains grid and, to reduce energy costs for the plant, supplemented by electricity from a wind turbine.

Thus the problem is one of sizing each piece of equipment, including the wind turbine, to meet shop air requirements and minimise cost, all subject to safety constraints. In this case the traditionally designed system was found to be close to the optimum and cost reduction achieved by optimisation was a relatively modest 3%; the total cost being reduced from \$13.34M to \$12.92M.

Conclusions

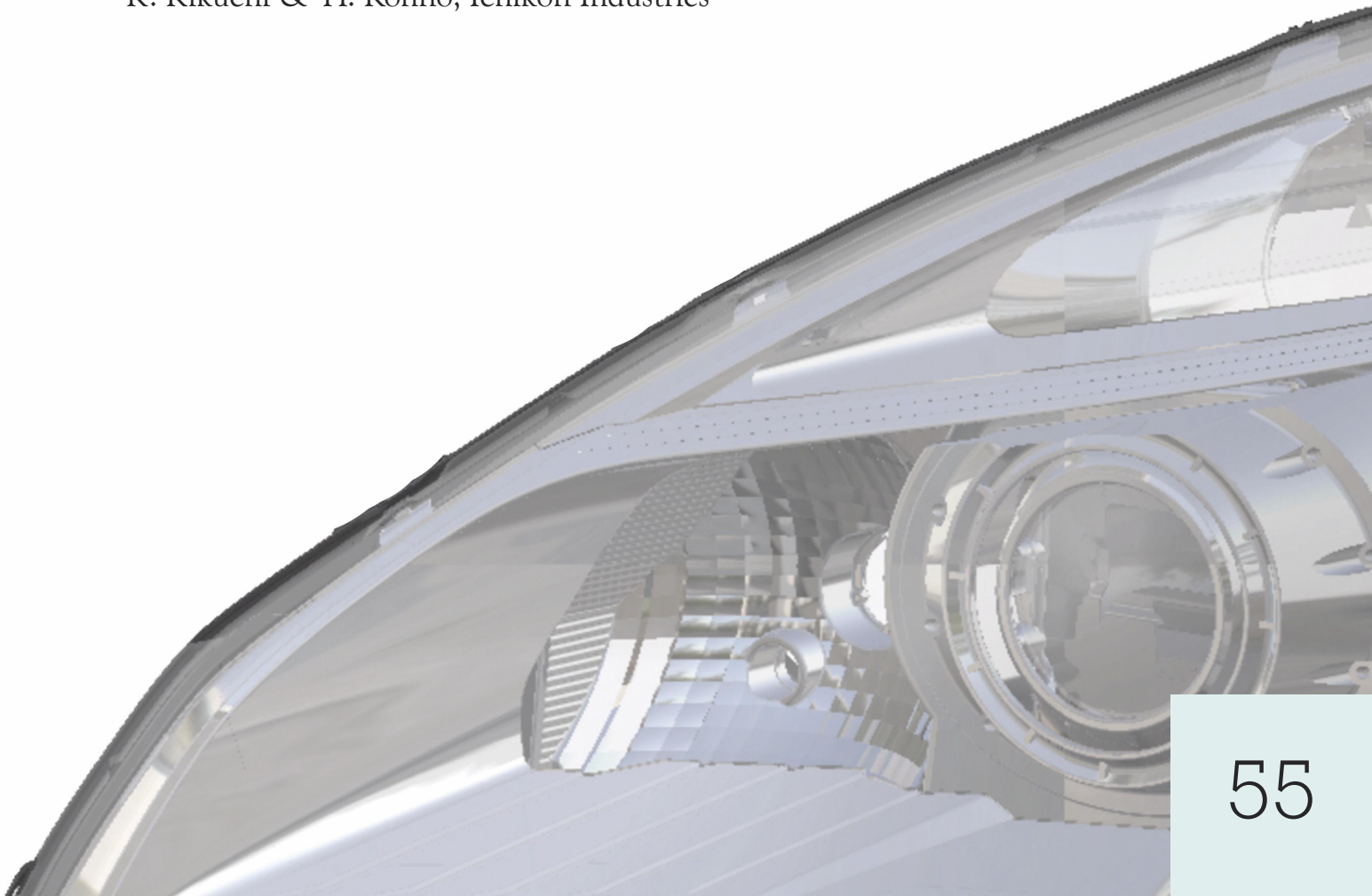
A judgement drawn from the FENet project is that Product and System Optimisation does not represent a single technology, so there are no simple measures of technological maturity and industrial uptake. Rather the subject may be characterised by a range of techniques, beginning with highly restrictive but computationally efficient techniques for size optimisation, through to somewhat heuristic approaches to topological design and, finally, reaching the new generation of process integration tools capable of supporting design at a systems engineering level. The 'best' design optimisation approach is highly specific to the intended application.

References

- [1] GALILEO G L, 'Discorsi e dimostrazioni matematiche intorno a due nuove scienze attenenti alla meccanica et i movimenti locali', Leida, 1687.
- [2] PARENT A, 'Des points de la rupture des figures. D'en deduire celles qui sont partout d'une resistance egale', Mem Acad Roy Sci Paris, 1710.
- [3] MAXWELL C, Scientific Papers 11, p175, Cambridge University Press, 1890
- [4] MICHELL A G M, 'The limit of economy of material in frame structures', Phil Mag 8, 589-597, 1904.
- [5] COX H L and SMITH H E, 'Structures of Minimum Weight', Aeronautical Research Council Reports & Memoranda, No 1923, Nov 1945.
- [6] BEALE E M I, 'Mathematical Programming in Practice', Pitmans London, 1968.
- [7] ZIENKIEWICZ O C, 'The finite element method (Third edition)', McGraw-Hill, 1977
- [8] 'Proceedings of the International Symposium on Computers in Optimisation of Structural Design', University of Swansea 1972.
- [9] COLLIER C., AINSWORTH J, YARRINGTON P, JOHNSON D, and LUCKING R, "Ares V Interstage Composite Panel Concept and Ringframe Spacing Trade Studies", AIAA-2010-2782, 51st AIAA/ASME/ASCE/AHS/ASC Structures, Structural Dynamics, and Materials Conference, Orlando 2010.
- [10] de VILLIERS E and PETROPOULOU S, "An Efficient Adjoint-Based Method Applied on Vehicle Aerodynamic Optimisation", ICON London, 2009.
- [11] BUCHANAN S, "Development of a Wingbox Rib for a Passenger Jet Aircraft using Design Optimization and Constrained to Traditional Design and Manufacture Requirements", Altair Engineering, 2007.
- [12] OTHMER C., A continuous Adjoint Formulation for the Computation of Topological and Surface Sensitivities of Ducted Flows, Int. J. Num. Meth. Fluids, submitted, 2007.
- [13] MENEGAY P, MOSQUERA A, 'Multi-disciplinary Design Optimisation of an Energy Efficient Compressed Air System', NAFEMS UK Conference, Oxford, 2010.

Prediction of Headlamps' Light Beam Deviation Angle by Thermomechanical Simulation

N. Pluy, Valeo Lighting Systems,
K. Kikuchi & H. Konno, Ichikoh Industries



The principal function of a headlamp is to provide light on the road for the driver especially at night while driving. Although the main function of the headlamp is for the driver to see safely at night, the light from the headlamp should not dazzle the oncoming drivers. The standard regulations specify that under driving conditions, its low beam deviation is restricted to a limited angle, above which the visibility and security of other car drivers is compromised. The beam angle deviation is due to the temperature gradient and the materials used in the headlamp. Indeed, a headlamp is an assembly of parts made from different polymers, each of them deforms with temperature increase due to internal heat when the source of light is on. As a consequence, the light beam is deviated from its original direction. One approach to check the regulation is to do tests once the headlamp parts are available. However, when a headlamp is not meeting the regulation requirement, design modifications must be done: they are costly due to mold modifications and cause delays in the planning of the project. The other approach is to use simulation during the design phase. Simulation methods are currently used to predict thermal or mechanical behavior during the design phase. The advantage is then to identify the components or materials which need to be modified to meet the product specification and regulation requirement.

This article explains a method to predict the low beam deviation by simulation. As beam deviation angle is the result of a multi-physic phenomenon that mixes thermal and mechanical effect, the aim is to develop a simulation process involving the coupling of thermal and mechanical simulation. The other requirement is to assess the accuracy of the simulation prediction in order to use this simulation method in the design phase of new headlamp project. First a description of the product is given followed by the regulation test and its requirement. Then the simulation process and results is presented. Test results are then described as well as the limitation of those results. Finally, the comparison of the test and simulation results is done.

An automobile's headlamp can be simplified in four main sub-assemblies: the housing which supports the internal components and which is also the interface with the vehicle; the lens which closes the volume of the headlamp as it is fixed on the housing; the optical module called the projector which is the source of light and heat; and the masks which have an esthetic function. The headlamps technology has impressively evolved in the past 20 years, from simple design in 1980's to more complex products nowadays.

The headlamp studied (Figure 1) has a Xenon projector module that produces a light beam. The projection of the light on a wall creates a specific shape composed by a horizontal and an inclined line. This "V" shape is called the "cutoff" line (Figure 2).

As previously mentioned, the aim of the test is to look at the beam deviation angle due to the temperature created by the bulb. The regulation requires that after one hour,

with the low beam turned on, its beam vertical deviation is restricted to 1mrad (0.057°, Figure 3).

The materials used are thermoplastics (housing in PP, lens in PC...) and their properties are different according to the molecular structure (amorphous or semi-crystalline) [1,2]. These properties are shown in Figure 4. The three main properties to consider for a thermo-mechanical simulation are: Young's modulus (rigidity of the part), thermal expansion (deformation with temperature), and thermal conductivity (heat transfer through the material). Most of the headlamp's materials can be considered as isotropic, except polymers reinforced with glass fibers which have anisotropic behavior. Some components participating in the fixation of the optical module in the headlamp, called screws, are made of PA66 GF30. Indeed, the mechanical and thermal properties are different whether their impact is considered along or in the transverse direction of the fibers.

To summarize, the problem is to solve a thermo-mechanic analysis using materials that have a high dependency on the temperature variation, and which are not necessarily isotropic.

Model Description

As the aim is to predict the beam deviation after one hour, it is assumed that the thermal state of the headlamp can be calculated from a stationary thermal simulation. As a matter of fact, after one hour of headlamp low beam switched on, measured temperature of components are stabilized. The method consists in calculating the temperatures of the full headlamp with a CFD code, FLUENT, in stationary. The stabilized temperature components are then imported in a mechanical software, ANSYS Workbench, in order to get the deformations of the assembly due to the temperature.

CFD Calculation

The thermal simulation takes into account the three classic heat transfer modes: radiation, convection and conduction [3,4]. The xenon projector module is the heat source emitting light from visible to long infrared by radiation. The optical module is composed of specular surface (high reflective surface) and optical lens made of transparent material, which transmits light. To simulate those conditions, the radiation is modeled by a discrete ordinate model. The radiation and thermal properties of each component are defined by their emissivity and diffuse fraction. Conduction is calculated in the component. Most of the parts are meshed in 2D (inner surface of the housing, bezels), the

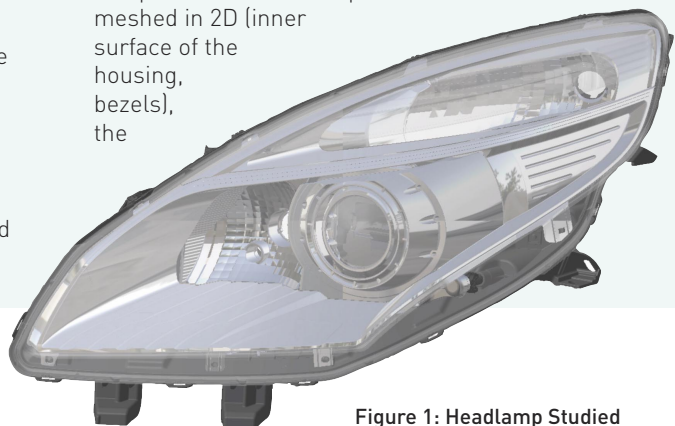


Figure 1: Headlamp Studied

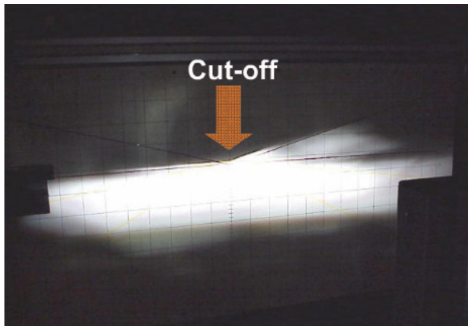


Figure 2: Cutoff Line

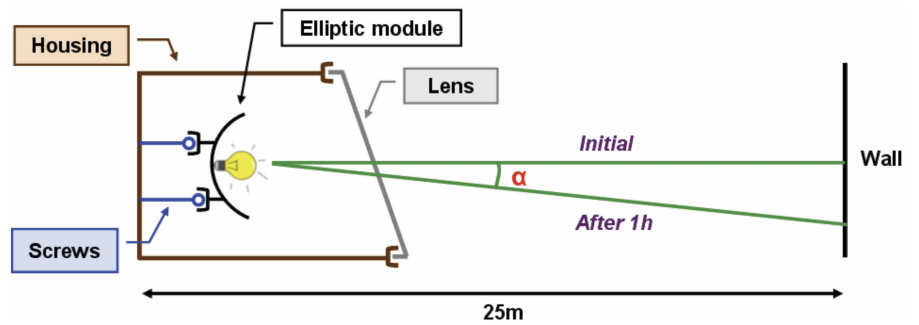


Figure 3: Cutoff Stability Test

projector module and lens are in 3D (Figure 6). The air is modeled with 3D tetrahedral elements so that both the radiation and the convection are calculated. This model is composed of 1 500 000 3D elements. The thermal state of the components is calculated in stationary and requires 11h of calculation using a cluster due to the resolution of the radiation. The maximum temperature respectively on the housing and on the reflector of the elliptic module is 62° and 130° (Figure 7).

Physical Explanations

This results shows that heat is emitted by the xenon source. This energy is transferred to the other components through radiation, convection with the air and conduction (Figure 8). As the bulb is on, a gradient of temperature is established between the source and the housing. These temperatures are exported as surfaces' temperatures later in the mechanical simulation.

Mechanical Calculation

The headlamp assembly is imported from CATIA to workbench. All the parts are meshed using 3D quadratic tetrahedral elements (700 000 elements) small enough to assure good temperature propagation through the parts. The main difference between the thermal simulation and mechanical simulation is that the fluid is not modeled. Then, contacts are created to define the assembly definition between the components. It contributes to transmit the movements and the thermal energy from part to part.

The material's properties definition is a crucial step of the preprocessing. The properties must be known for a wide range of temperatures (up to 200° average).

- The Young modulus is deduced from tensile tests made at various temperatures. Considering that the displacements are small (less than 1mm), the tensile curves can be simplified as linear.
- The thermal expansion is the most important parameter and must be carefully set. For a 1D case, it can be expressed as follows: $DL = a.L0.DT$ [5,6]. a is the coefficient of thermal expansion, $L0$ is the initial length and DT is the temperature variation.

For isotropic materials, the thermal expansion has only one value, but for anisotropic materials (screws and bracket with glass fibers reinforcements), two coefficients have to be distinguished: in the direction of the fibers, the expansion is smaller than in the transverse direction. Since the material law used is linear, a choice must be made on either using the longitudinal or transversal thermal expansion, based on a rheological analysis [7,8].

- Finally, the conductivity of the materials is important. As the imported temperature from the CFD software is the surface temperature, conductivity is necessary to calculate the temperature distribution in on

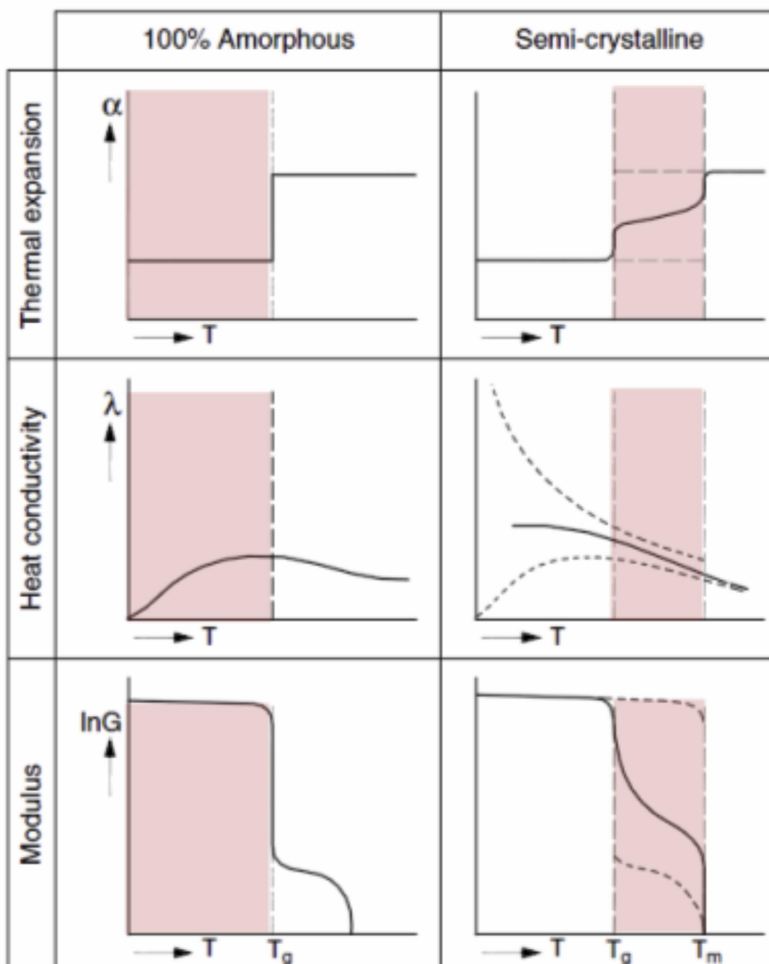


Figure 4: material properties dependence to the temperature [1]

all components. Only the conductivity needs to be set because the surface temperatures imported are the result of radiation and convection with the air.

When the model is finished, temperatures can be imported. This is the "mapping" process whose aim is to interpolate the temperatures from the CFD mesh (2D) to the mechanical mesh (3D). After the mapping is completed, the mechanical calculation will be launched with only the gravity as external force.

Experimental Study

The headlamp is fixed on a test bench and turned on, facing a wall 25m away, and the vertical displacement of the cutoff line is monitored after 3min and 60min. For precision reasons, the displacement cannot be measured visually: indeed, 1mrad angle represents a vertical displacement on the wall of 2.5cm only. Therefore, displacement measurement is made by optical sensors which are going to measure the light intensity and deduce the angle by using a contrast criterion. The angle variation is given when the contrast is maximum (difference between dark and bright colors). The small displacement of the light makes this kind of test sensitive and variable. The angle is impacted by two main factors:

The first one is measurement error which is characteristic of the test bench: it is characterized by measuring the reproducibility of the measurement process. For that purpose, only one headlamp is used and measured five times by the same operator under the same conditions. After applying the statistic "Student distribution" [9] on the results, with a confidence level of 95%, the average error found is $\pm 0.2\text{mrad}$ (20% of the 1mrad regulation limit).

The second one is the error coming from the dispersion in dimension and assembly, specific to production process of headlamps. This error is more difficult to measure because the test sample needs to be representative of the population, here, the entire production parts.

The result of the angle variation is given in Figure 10. After 60min, the cutoff moved down by 2.09mrad ($\approx 0,12^\circ$).

Results

The angle variation simulated is deduced from the displacement of the reflector: 2.14mrad ($\approx 0,122^\circ$). In this example, the correlation between the simulation and the laboratory test is within 2% difference, which is acceptable regarding the measurement error.

The simulation method has been applied on 5 different products and the results are presented in the table above.

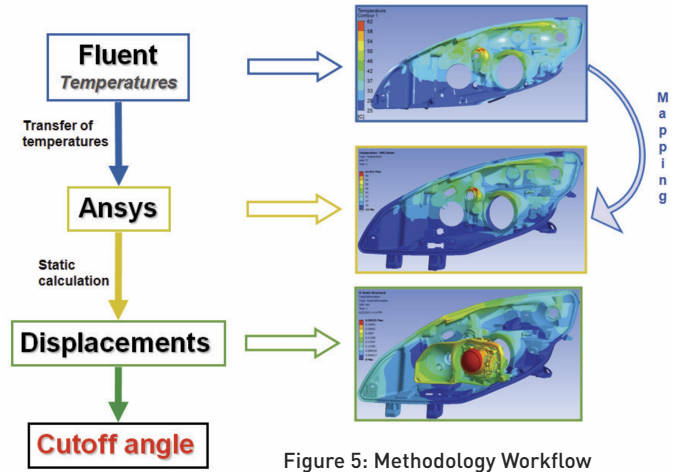


Figure 5: Methodology Workflow

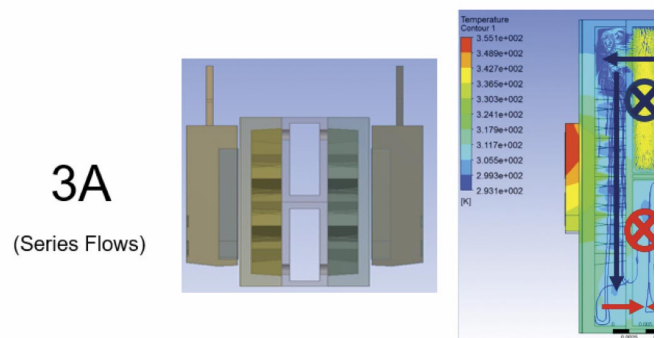


Figure 6: CFD Mesh

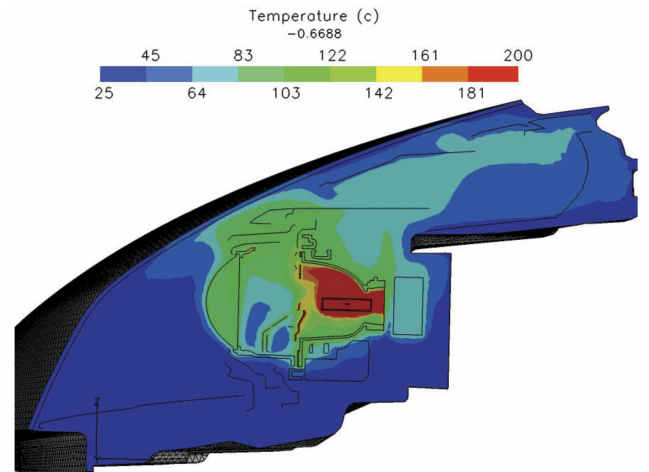


Figure 7: temperature inside the headlamp

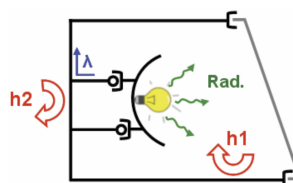


Figure 8: Heat Transfers in a Headlamp

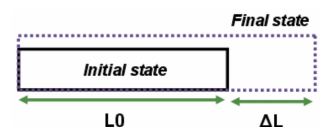


Figure 9: Thermal Expansion

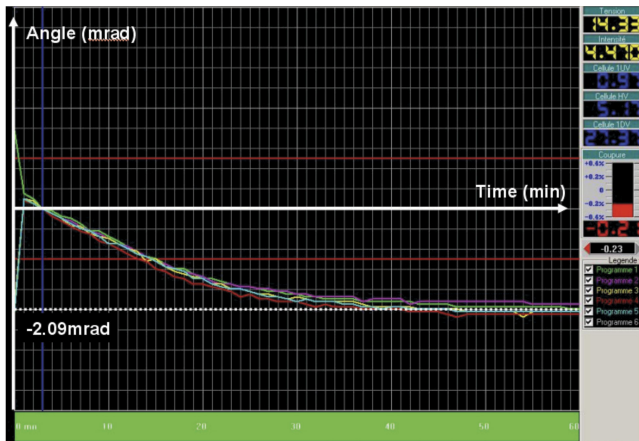


Figure 10: Test Result

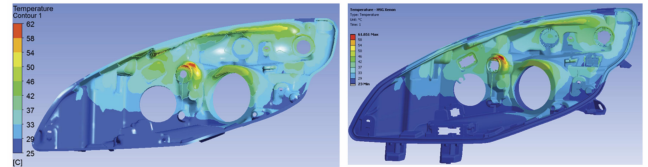


Figure 11: Mapping of the Housing (Fluent on the Left, Ansys on the Right)

Projects	Test (mrad)	Simulation (mrad)	Difference (%)
Project 1	2.09	2.14	+2%
Project 2	1.79	1.25	-32%
Project 3	0.89	1	+12%
Project 4	1.13	1.01	-11%
Project 5	1.5	1.42	-5%

The simulation results predicts within 12% the beam deviation measured in tests using linear materials and contacts.

Discussion

The temperature mapping is verified by comparing the temperature results from CFD results and mapping results in Ansys on every part. The difference in temperature distribution is less than 0.2% on each part (Figure 11).

Concerning the materials, the thermal expansion is the parameter which has the biggest effect on the result. For instance, if the housing's thermal expansion is divided by two, the angle drops by almost 30%. If the housing's conductivity is divided by 2, the result is only reduced by 1%. If the young's modulus of the housing is considered constant (no temperature dependency), a variation of 5% is observed. The boundary conditions also affect a lot the result. The housing has three fixations and one support that block the vertical displacements. After suppressing this support, a variation of +58% of the angle was observed.

Conclusion

Coupled thermal with mechanical simulation was set up in Ansys to simulate the beam deviation of a headlamp. The important parameters to take into account in the simulation are the boundary conditions, mapping and material definition. Thermal expansion is the parameter which contributes the most to the accuracy of the simulation results.

Five projects were correlated in order to estimate the accuracy of this tool and the average difference between test and simulation found is 12%. The difference between simulation and experimental results is smaller than the

measurement error except for one product. This indicates that this simulation process can be used in project development to anticipate potential beam variation issues.

Acknowledgment

The laboratory measurements were conducted in partnership with Ichikoh (Isehara office, JAPAN) and Angers office (FRANCE).

I would like to thank Kazushige Kikuchi, Hiroshi Konno and Takao Dodo for providing me with detailed information about cutoff stability tests.

Thank Xie Guoliang (Wuhan office, CHINA) for running the Fluent simulations.

I would also like to express my gratitude to Christine Roucoules, Malik Bakacha and Cédric Mayer for their support during this project.

References

- [1] Tim A. Osswald, Juan P. Hernández-Ortiz, Polymer Processing Modeling and simulation, Hanser, 2006.
- [2] Patrick Heuillet, Polymères, cours de l'Ecole Supérieure des Techniques Aéronautiques et de Construction Automobile.
- [3] C Chenevier, Thermal simulation in lighting systems -5 days/5degrees, PAL Symposium Darmstadt, 2001.
- [4] Natti S. Rao, Günter Schumacher, Design Formulas for Plastics Engineers, Hanser, 2004.
- [5] Article 067026 Chapter 2: Thermal expansion, ASM International.
- [6] Tim A. Osswald, Georg Menges, Material science of Polymers, Hanser, 2003.
- [7] Hychem Boukehili, Design, Cours MEC6306 : Production et Application des Composites, cours de l'Ecole Polytechnique de Montréal, 2005.
- [8] A. Guidoum, Matériaux composites, cours de l'Ecole Polytechnique Fédérale de Lausanne.
- [9] Jacques Baillargeon, Application et interprétation des techniques statistiques avancées, cours de l'Université du Québec à Trois-Rivières.

Understanding the Effects of Nonlinear Preloads on Engine System Dynamic Response

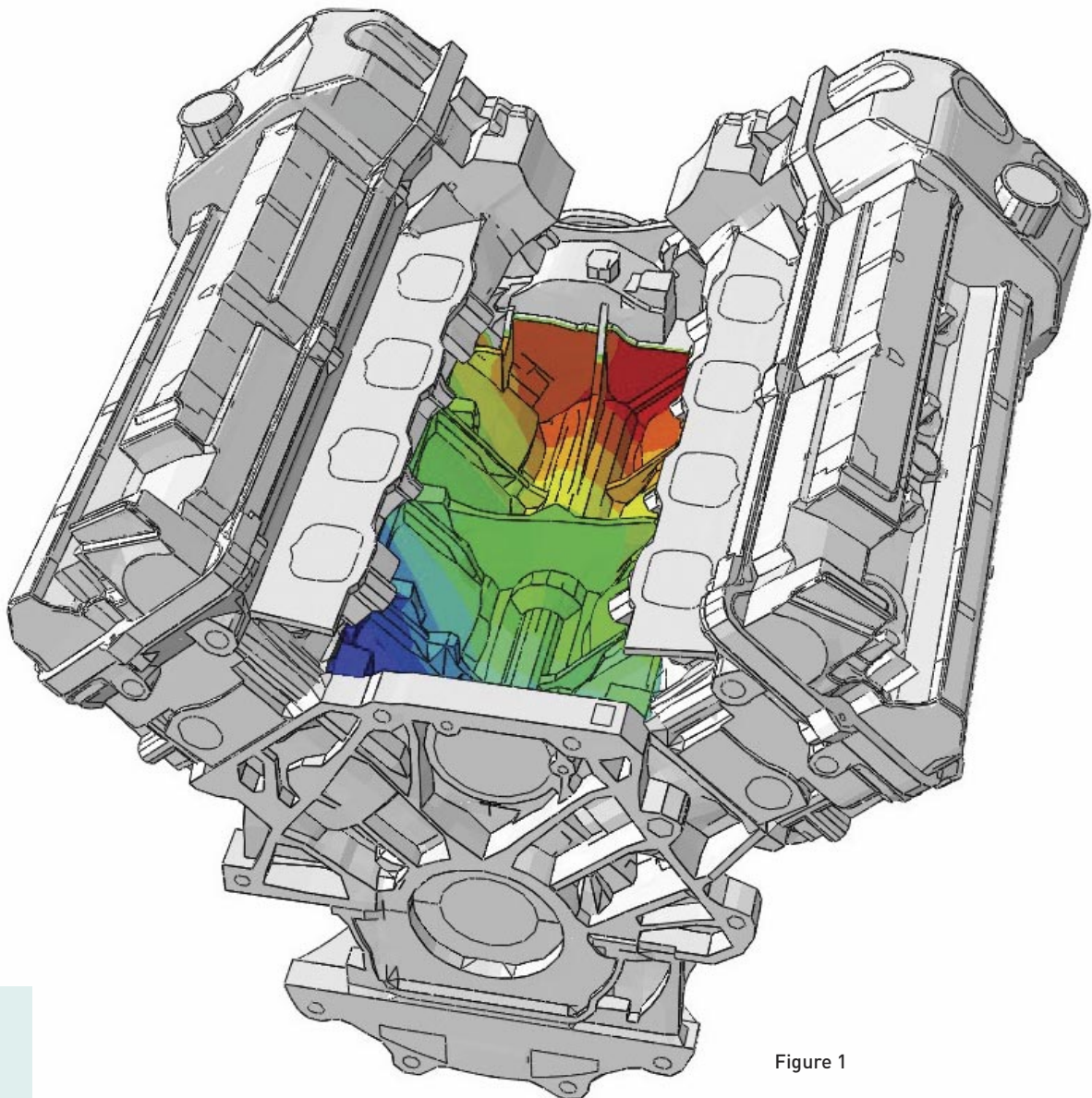


Figure 1

It is well understood that stress stiffening affects the dynamic response of a structure. Just as tightening a string changes the tones produced by a violin, tightening head bolts changes the dynamic response of an engine block assembly. While fundamental to nonlinear static stress analysis, stress stiffening effects are most often ignored when evaluating the steady-state dynamic response of engine assemblies.

This article highlights the impact of various bolt loading assumptions on the flexibility and steady-state dynamic response of an engine head and block assembly. Including assembly load effects in the simulation workflow allows for more accurate prediction of system-level performance, such as engine radiated noise.

FEM is broadly used in the automotive industry for structural assessments across the entire design life of a vehicle. Prior to 1990, the bulk of powertrain FE analyses utilized linear assumptions, which limited the ability to capture key physical features such as contact, gasket nonlinearity, advanced material laws, and nonlinear geometric effects.

Since the mid-1990s, there has been a progressive adoption of nonlinear analysis techniques within the engine and powertrain sealing & durability community. Today, the vast majority of major automotive manufacturers and engine suppliers utilize, to varying degrees, nonlinear assumptions within their structural FEM workflows. The importance of including the effects of nonlinearity in modal response has been acknowledged and reported [1], but for complex geometric structures it is difficult to account for such effects within the confines of a “traditional” linear code.

The simulation presented in this article demonstrates the effect of bolt pre-tension on the forced frequency response of an engine assembly. The Abaqus/Standard automatic multi-level substructuring (AMS) eigensolver is used to extract the eigensolution of the engine assembly, which is then subsequently used in the steady-state dynamic analyses.

Analysis Approach

We will consider a V8 engine model representative of a typical sealing & durability analysis — with 3 million elements and 12 million structural degrees of freedom

(Figure 1). The head and block are modeled as individual components, and are assembled with bolts. A representation of a gasket, consistent with simplified properties of a multi-layer steel (MLS) construction, lies between the head and block. Contact conditions are enforced between the individual components.

Sources of Nonlinearity

There are several potential sources of nonlinearity in the model, any of which could lead to stiffness changes and subsequent changes in the eigenmodes of the structure. For the purposes of this study, aluminum was treated as purely elastic, thus eliminating material plasticity as a source of nonlinearity. The remaining key features that could give rise to stiffness changes are contact and geometric nonlinearity (also commonly referred to as “stress stiffening” or “differential stiffening”).

MLS gaskets used for head and block applications tend to have an initially low stiffness, followed by a “bottom out” stiffness which is often an order of magnitude higher. These gaskets can be modeled with varying degrees of complexity within the FE model. In this study, the gasket is simplified with a linear (constant) stiffness to allow for the isolation and investigation of other forms of nonlinearity. Given this assumption, it is expected that after initial assembly loading, the gasket allows the head and block to behave as a singular unit. This source of nonlinearity is thus dominated by contact stiffness — the two entities (head and block) transition from being individual entities to being a single unit (in terms of stiffness). Beyond the initial loading and contact resolution, there should be no progressive stiffening of the gasket (nor significant changes to contact), but there is the possibility of geometric nonlinearity (“stress stiffening”) and progressive loading across the gasket interface.

Loading

The bolt assembly loads are defined through pre-tension sections. For all bolts, a series of tension loads is applied in four separate analyses: (i) 0.1% of nominal load (“0.1%”), (ii) 50%, (iii) 100%, and (iv) two times the nominal load (“200%”). These four loading conditions will provide a reasonable indicator of the degree of nonlinearity to which a “normal” engine may be subjected. The 0.1% case is artificially low, but allows one to confirm the assumptions of contact and gasket behavior under marginal loads. The other loads

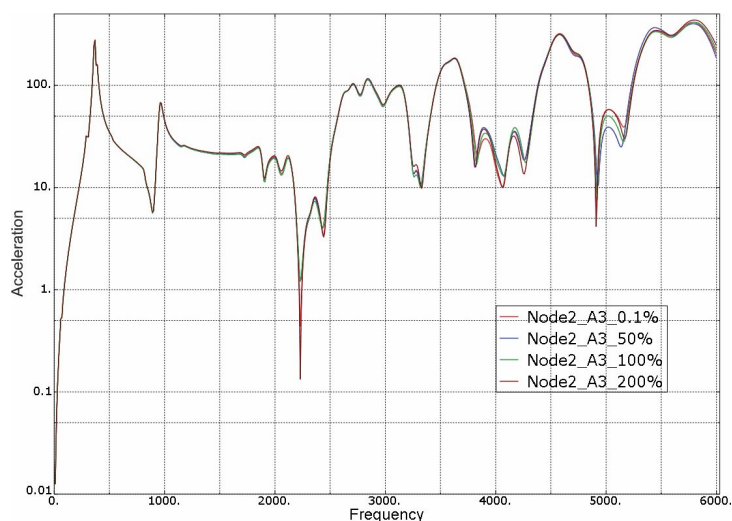


Figure 2

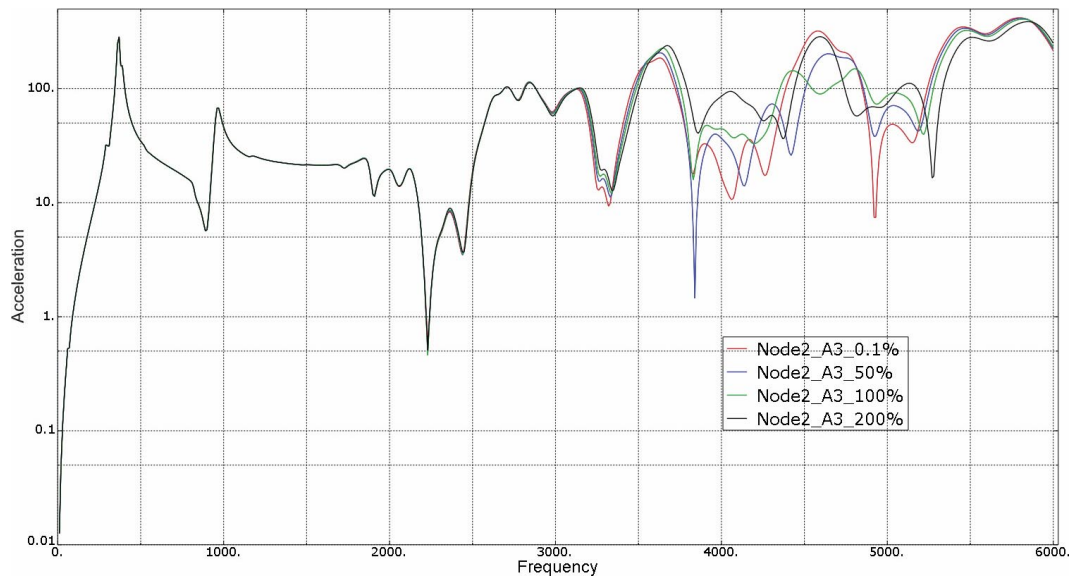


Figure 3

more accurately capture realistic behavior and loading profiles. Scatter in pre-load has been demonstrated in tests and has been noted to vary by a factor of two or three, depending on conditions and the bolt tightening processes employed [2,3]. While the 50% and 200% cases represent extreme values, such scatter is reasonable across real-world scenarios and allows one to understand the impact of this range on system response. To understand the effect of geometric nonlinearity, the model was analyzed with and without this capability enabled.

The bolt loads are applied in an initial non-linear static step. For each bolt loading scenario, an eigenvalue extraction was performed to compute all modes up to 9,000 Hz. A frequency response analysis was then performed out to 6,000 Hz. A vertical unit load was defined near the main journal bearing and responses were measured at various points. For the frequency response analysis, modal damping of 2% was used (which is within the range of commonly utilized assumptions for such a system).

Results and Discussion

For all loading conditions and assumptions, two sets of data were evaluated. The first set was associated with the engine cylinders. For each of the eight cylinders, a set of nodes associated with an upper, lower, and middle ring were used for output. The three rings of each cylinder allow us to evaluate “ovalization” and other mode shapes. These modes are of significant interest in assessing dynamic performance, and are also indicators of local stiffening changes. The second set of variables was the acceleration of various nodes on the outside of the cylinder bank. Not only are these accelerations indicators of system stiffness changes, they are also directly associated with radiated noise from the engine.

A set of trends was observed for all bolt loading scenarios: for frequencies below 3,000 Hz, there were negligible results differences, independent of the inclusion geo-metric nonlinearity. This would suggest that, for this model with simplified linear gasket stiffness, the dominant lower frequency effects are sufficiently captured once contact is established and the gasket transfers load. Above 3,000 Hz, there are noticeable but modest differences between the four loading scenarios when geometric nonlinearity is neglected (Figure 2). However, when geometric nonlinearity is included, there are substantial differences in the various responses. Calculated accelerations are dramatically different above 3,500 Hz (Figure 3). Focusing on the frequency range of 3,000 – 6,000 Hz, it can be further seen that the four bolt loading conditions tend to form “bands” of increasing and decreasing responses—the 0.1% and 200% loads tend to form minima and/or maxima, while the 50% and 100% loads fall between them respectively. To further evaluate and understand these effects, we focus on the specific relationships between the 100% and 200% loading scenarios.

For both the 100% and 200% load scenarios, there were exactly 200 modes below 6,000 Hz. The previously mentioned engine cylinder node set was used to evaluate specific mode shapes and compare them by means of the Modal Assurance Criteria (MAC) [4]. The function of the MAC is to provide a measure of consistency, or similarity, between estimates of a modal vector. The MAC varies between 1 and 0, with 1 representing perfect consistency and 0 representing no consistency. The MAC in Abaqus can be calculated using an Abaqus/CAE plug-in [5]. Given two output database (.odb) files that contain displaced shape field output from frequency extractions (mode shapes), the Abaqus/CAE plug-in computes the MAC and displays the results in bar graph or contour plot form.

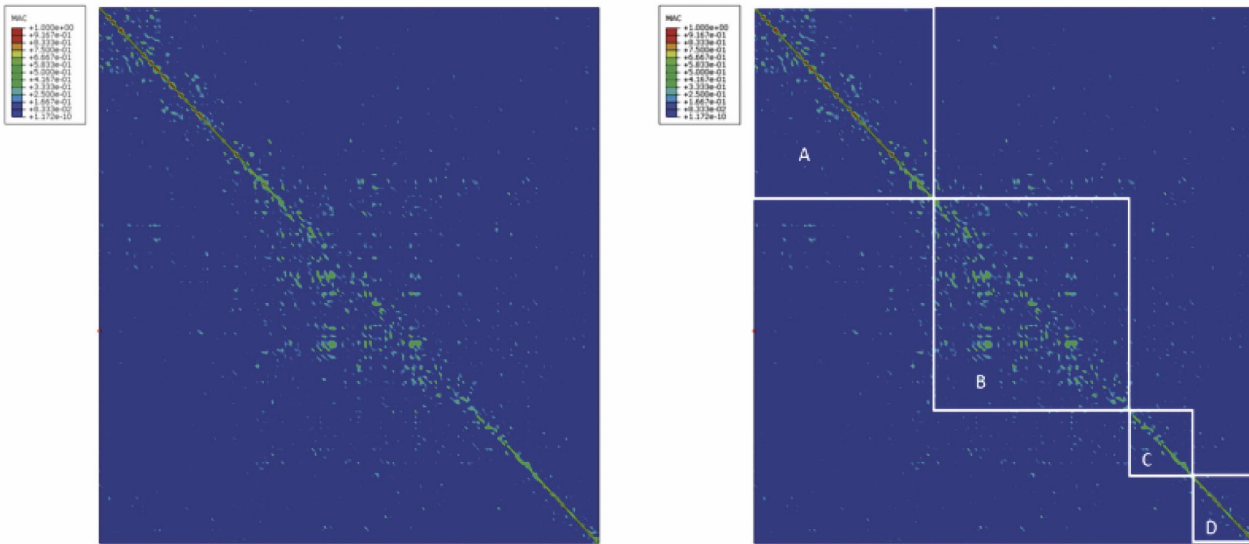


Figure 4

Evaluating the MAC of the 100% vs. 200% cases (Figure 4), it is clear that there is a region in the middle of the mode range for which the mode shapes are substantially different. Not only is there a lack of diagonal terms, but there are no sets of modes that show significant correlation with any other modes. To further understand the degree of disconnect in the two mode sets, the MAC data can be broken into four regions (Figure 5):


- A: 0 – 3,800 Hz: This region shows very high correlation, with the MAC generally \rightarrow 0.95 and frequencies from the two models consistently within 0.25% of each other. Nearly all of the modes have a MAC of 0.99-1.00 until 3,600 Hz, at which point the MAC values still remain above 0.90 (indicating high correlation).
- B: 3,800 – 5,000 Hz: After a quick degradation between 3,600 – 3,900 Hz, the two models show virtually no correlation. The MAC for all modes in this range is generally below 0.6, with only four pairs of modes (out of 82) showing correlation above 0.7. Many respective modes in this range have near-zero correlation.
- C: 5,000 – 5,500 Hz: This frequency range transitions from no correlation to an area of relatively good correlation, with most modes exhibiting MAC values above 0.75. While this represents a modest MAC value, it suggests enough correlation to infer modal similarity. For these similar eigenvectors, the associated frequencies are generally within 0.5% of each other.
- D: 5,500 – 6,000 Hz: After the transition of C, the modes return to quite high MAC values, with most mode pairs in this region exhibiting a MAC above 0.90. For these modes, the respective frequencies are generally within 0.2%.

Individual modes of the various models were evaluated, with special attention paid to the cylinder liners. As would be implied by the MAC values, there was clear discrepancy in mode shapes for different loading scenarios when geometric nonlinearity was considered. However, when geometric nonlinearity was omitted, the models behaved quite consistently, with only modest differences in response and with consistently high MAC values.

For the area of high deviation between the different models (3,800-5,500 Hz), the cylinders tend to be undergoing some combination of 2nd order cylindrical modes ("ovalization") and 3rd order cylindrical modes ("triangular modes"). Upon visual inspection, it is clear that the 100% and 200% load scenarios result in quite distinct oval and triangular modes within the cylinder liners. It appears that stress stiffening in the region of the cylinders is quite significant in accounting for higher-frequency structural vibration, both of the cylinders themselves and of the system as a whole.

Conclusions

These results suggest that including geometric nonlinearity in engine assembly models is particularly important if one wishes to more accurately capture higher-frequency linear dynamic responses. This observation is noteworthy because in general practice, engine durability workflows tend to neglect this aspect. For stresses, strains, and static stiffnesses (of primary interest to durability groups), it has been generally found that geometric nonlinearity only modestly impacts the results for most passenger vehicle engines. However, based on the results presented here, its impact for higher-frequency calculations is considerable.

A photograph of the open trunk of a silver car, showing the interior of the trunk and the rear hatch. The trunk is empty, and the car is parked in front of a modern building with many windows. The text is overlaid on the right side of the image.

Reverse Engineering Made Simple

Dipl.-Ing.(FH) Alexander Krauß
Prof. Dr.-Ing. Uwe Fischer
West Saxon University of Applied Sciences of Zwickau

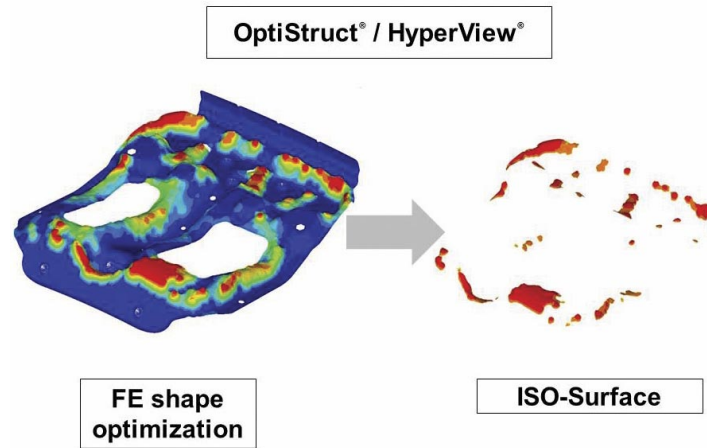


Figure 1: Results of FE shape optimization and created ISO-Surface

The dimensioning of thin walled parts within automotive construction is highly influenced by Finite Element Analysis and Optimization. The common targets are to improve stiffness or eigenfrequencies. The FE Model which is based on the concept CAD geometry of the designer is mostly created by a specialized computational engineer. The data exchange is done with universal non-parametric CAD data formats, like IGES. At this stage a direct update of the FE geometry, by changing the CAD geometry and vice versa, is impossible, so the necessary variation of the shape is achieved by deforming the FE mesh. These deformations are called beads in technical language, and they must be rebuilt in CAD geometry by hand. This so called "reverse engineering" is very time consuming for the designer. Within the research project "Automation of optimization tasks inside the construction process of thin walled parts", at the University of Applied Sciences Zwickau (Germany), in association with FES Zwickau and Volkswagen Kassel, we created a new workflow which allows for more simple reverse engineering. The process will be demonstrated in this article by using an automotive body part, namely a car tailgate.

Initial Situation

To increase the fourth eigenfrequency of the tailgate, a FE shape optimization was performed using the commercial software OptiStruct® (Altair®). The result is a distorted finite element mesh, where necessary changes are shown by the red areas (figure 1). They have to be transferred from the computational engineer to the designer.

Process Overview

Our aim is to support the designer in his daily workflow and to reduce time consuming steps, but not to create a one-click solution. Therefore a step by step process is used to create parametric CAD geometry out of distorted finite element shapes. The method is focused thereby on producibility. The process can be divided into the following steps, as shown in Figure 2. The individual actions will be discussed later in further detail.

Step 1: Data Transfer

Within this first step only the necessary red areas will be transferred to CAD. With HyperView®, the postprocessor for OptiStruct® results, a so-called "ISO-Surface" can be generated (Figure 1). Using the "export as STL-File" function, a triangulated mesh will be created, which is then imported into CATIA V5® R19 (Dassault Systems®). Dealing with such data in CATIA® is not easy, since extra licensed workbenches are normally necessary. To give the designer the ability to use this STL-file within the Generative-Shape-Design workbench, we programmed an STL-To-IGES-Converter. The converter is accessed by a VBA Macro and allows a direct import into CAD, while using the data format IGES. The designer only chooses the given STL-File and a geometrical set, where the optimization surface will be inserted. But the converter also runs as standalone software with GUI. Therefore it can be used with other CAD or FE optimization software. The result is a single, non-parametric surface which can be seen in the structure tree (Figure 3).

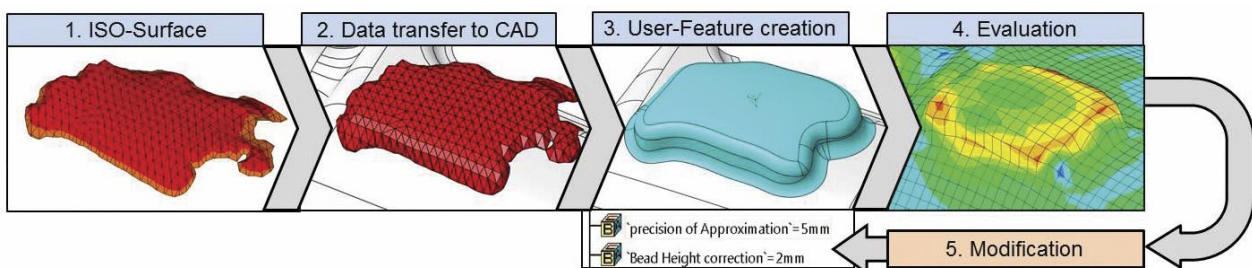


Figure 2: Process overview

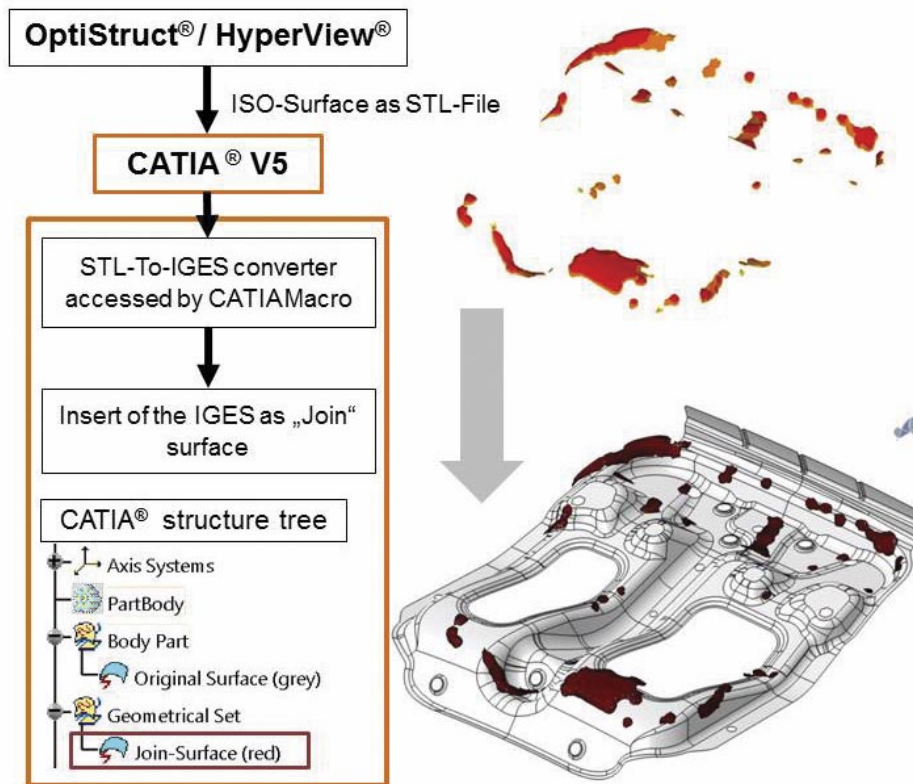


Figure 3: Data transfer OptiStruct® – CATIA® V5

Step 2: Data Filtering and Surface Disassembly

For further editing the “join” surface has to be “disassembled” into its domains. Small pieces which remain after the transfer process also have to be filtered out. Therefore we developed another VBA Macro which combines disassembling and filtering. With an interactive preview the user can define the size of the filter. Each single domain is now able to be selected. The process is shown in Figure 4.

Step 3: Parametric Feature Creation

The construction of a bead is mostly a compromise between producibility and approximation of the optimization results. The bead geometry is mainly characterized by its top surface and contour. These are represented by the transferred optimization surfaces. We created CATIA® User-Features for some standard cases in bead constructions. The so-called Bead Construction Toolkit is an easy to use feature catalogue. It allows the designer to pick the right feature for his case.

User-Feature 1: Line Bead

In some special cases the optimization surface shows a distinct direction and a nearly constant profile (Figure 5). The designer creates a guideline which approximates the middle curve of the optimization surface. He can then choose a feature from the catalogue which fits best into the profile, e.g. a semi-circle or trapeze bead. After selecting the guideline and the base surface, the feature will be created. With just a few parameters, like the height and width of the bead, the geometry can be easily controlled and optimized, but normally a distinct direction is not provided. Therefore the next two features have been created to suite a wider range of cases.

User-Feature 2: Custom Bead Contour, Based on Original Surface

This feature uses a custom contour which is drafted by the designer. The easiest way to do this is to place a sketch on the plane of the local inertia axis system of the optimization surface (Figure 6). In this case a feature is also provided. The sketch is then transferred to the original surface by the feature and cuts out the

Our aim is to support the designer in his daily workflow and to reduce time consuming steps, but not to create a one-click solution. Therefore a step by step process is used to create parametric CAD geometry out of distorted finite element shapes.

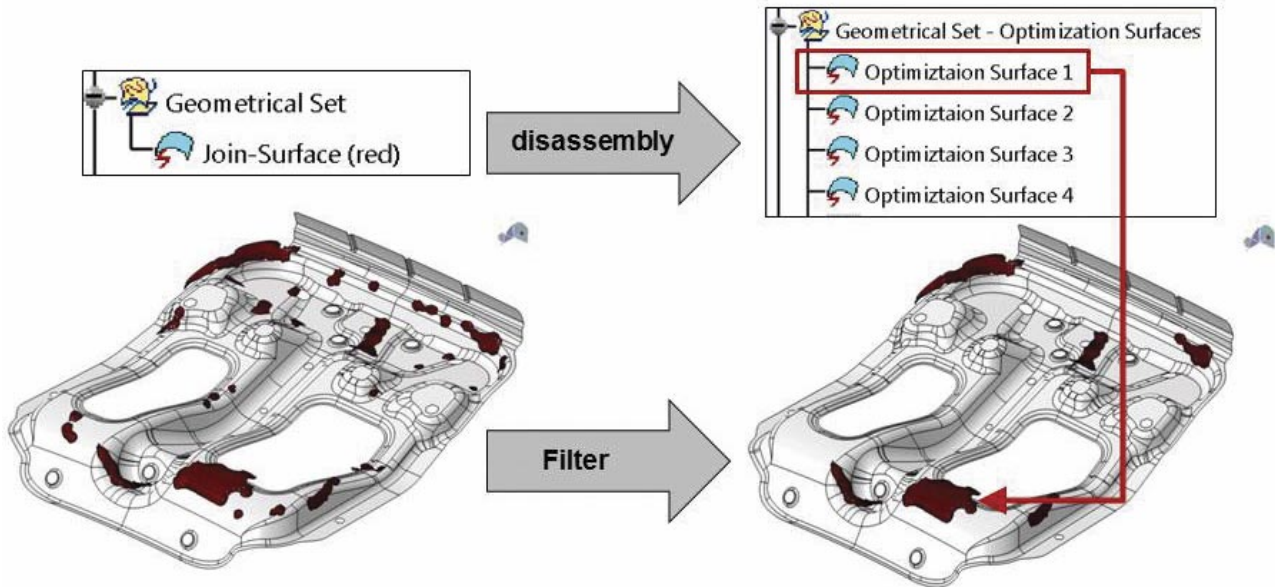


Figure 4: Disassembly and filtering of the join surface with a CATIA® Macro

top surface of the bead. This piece is then translated along the draw direction and so the bead is created. If the original surface changes, the bead will follow. But this assumes a high quality original surface, which applies to the most parametric shapes created using CATIA®.

User-Feature 3: Bead contour and Surface, Based on Optimization Surface

To approximate the optimization results in a more accurate way, the last feature is based directly on the triangulated surface. The designer is now independent from the quality of the original shape. With a feature integrated surface recognition, the top surface of the bead is created, with reference to the optimization surface. Using the parameter "precision of approximation", the shape can be controlled as shown in Figure 7. Besides this, the height of the surface and thus the height of the bead can be changed. Furthermore, the discontinuous border is adapted with control points for a continuous spline. If the automatic approximation is not suitable for production, the contour can be easily modified. The designer can do this by removing or adding control points to the spline. In connection with other construction elements, the bead is created with a Power Copy.

Evaluating the Results

The most interesting question is: how close can we come to the optimization results? CATIA® V5 has the ability to calculate and import results from multipurpose FE-Solvers like MSC.Nastran® and ABAQUS® with special workbenches. An import of the FE mesh created by the computational engineer is also

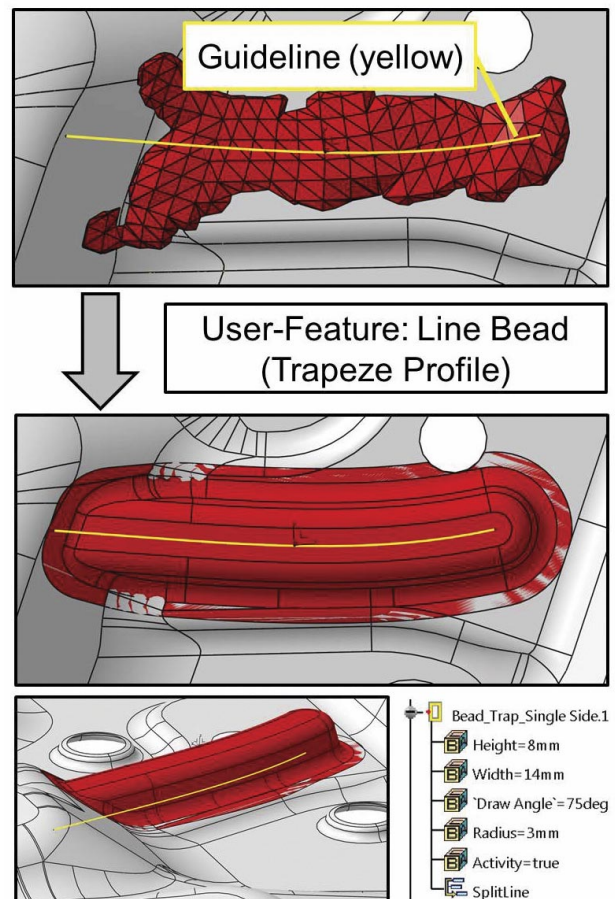


Figure 5: Creation of Line Beads
 Figure 6: Bead with sketched top surface contour
 Figure 7: Bead with surface approximation

possible in some cases. To get a quick evaluation of the results, a Hybrid FE model can be used. This consists of an imported FE-mesh and remeshed areas which are based on the CAD geometry which has been changed by the designer. After building up a finite element model and FE analysis, the designer can evaluate the effectiveness of his beads and correct them if necessary, e.g. modify the height to improve stiffness. If there are small changes in CAD geometry, the designer can try to restore the original results with a parameter optimization of the beads. So there is no need for FE shape optimization in every case, which is a big advantage. If a new FE shape optimization was performed, the new ISO Surface can be easily used to update the bead feature.

The remeshed part can also be used to evaluate producibility. Therefore, we created a CAD integrated template for deep drawing simulation which gives a surface impression of critical areas on the part.

Summary and Discussion

The process shown gives an overview of how to create parametric CAD geometry out of non-parametric FE shape optimization results by using a CATIA® User-Feature. The method focus on producibility, where the designer themselves can define what the bead looked with respect to optimization results. The biggest advantage of this method is a much more efficient design cycle in product development. With result evaluation using CAD integrated FEA systems, the designer can calculate the effectiveness of the created beads. The computational engineer is then able to concentrate on more specific tasks. But our research is not finished at this point. There are some problems like multi-domain beads, surface borders and holes that have to be solved. Besides this, the whole process is only really efficient when the computational engineer and designer work together as closely as possible.

Acknowledgements

The editors take this opportunity to gratefully acknowledge the German Federal Ministry of Education and Research (BMBF) for sponsoring this project (Number: 17N2011). Our very special thanks go to Christoph Schleicher and Ronny Kubik for the support by programming the converter. For careful reading and correction of the text a special thanks go to Tina Singer and Tristan Lodge.

The biggest advantage of this method is a much more efficient design cycle in product development. With result evaluation using CAD integrated FEA systems, the designer can calculate the effectiveness of the created beads.

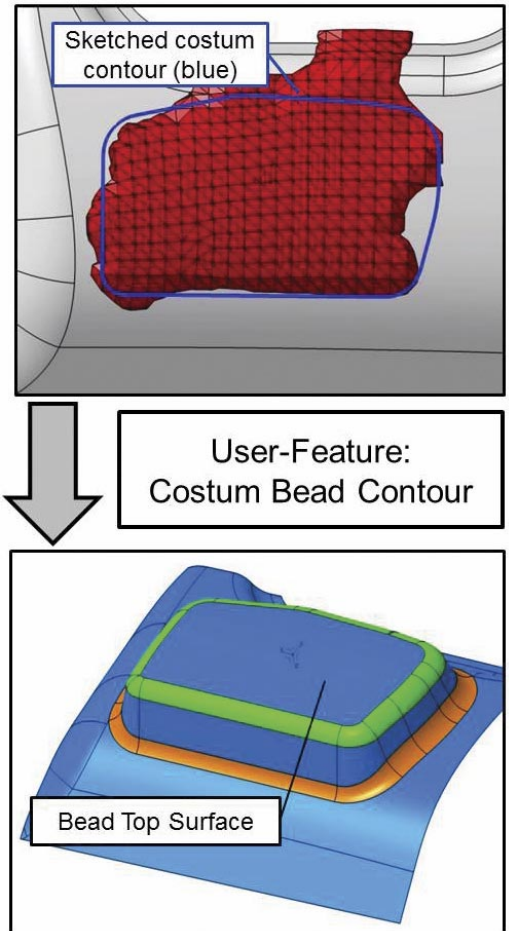


Figure 6: Bead with sketched top surface contour

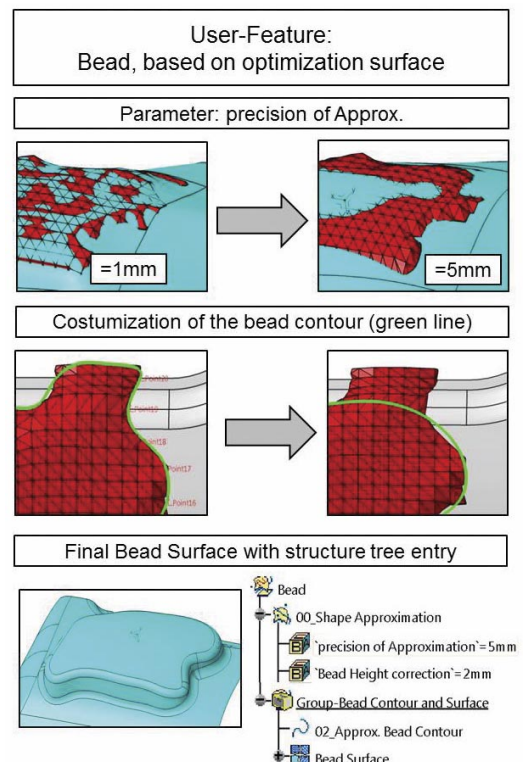


Figure 7: Bead with surface approximation

Composite Process Simulation – Digitally Reinforcing High-Rate Composite Manufacture

Dr. Peter Giddings CEng MIMechE

Research Engineer, Manufacturing Process Simulation, National Composites Centre UK

Miroslav Stojkovic MSc CEng MRaes

Engineering Capability Manager, Design Stress and Simulation, National Composites Centre UK

Fibre reinforced polymer composites have been a mainstay of research and development in aerospace and motorsport industries for decades. With mass reduction and increased structural efficiency becoming a key priority in the transport, renewable energy, marine and construction sectors, the composites industry faces new challenges to meet the growing demand and cut component costs.

Developing highly repeatable automated production lines is critical for composite manufacturing industries to make the transition from low volume business models to the high volume cost-efficient manufacturing these new markets demands.

The National Composites Centre UK (www.nccuk.com) is the UK hub for composites manufacturing industry and provides a focal point for research and development into automated composite processing. The Bristol-based centre houses a multidisciplinary team of over 140 staff who are successfully supporting industrial partners in understanding and solving a range of issues facing composite manufacturers.

As part of the NCC technology development, manufacturing process simulation plays a key role in developing insight and guiding the development of composites manufacturing processes to accelerate innovation and reduce the cost and risk associated with process development. Among the wide ranging research into automated manufacturing, automated fibre placement, resin infusion and induction welding of thermoplastics stand out as examples where challenging simulations have provided real benefit to NCC members.

Automated fibre placement (AFP)

Automated fibre placement (AFP) is used in the manufacture of high-value composite components, where precision and repeatability of fibre placement are key to the performance of safety-critical components.

Tapes of composite material, between 6.35mm and 25.4mm wide, are compacted onto a tool using a compliant polymer roller mounted to a robotic positioner. Most AFP systems also heat the incoming material via laser, infra-red light or Xenon Flash-lamp (a system manufactured by Heraeus NobleLight and developed in collaboration with the NCC) to achieve the ideal processing conditions.

AFP is a key technology at the NCC, with live development programs for thermoset composites (such as carbon/epoxy), dry fibre materials as well as thermoplastic matrix composites already yielding industrial benefits.

Simulating the AFP process presents many challenges, with large gradients in both pressure and thermal fields around the rapidly moving roller. However, by addressing specific manufacturing issues, the NCC simulation engineers are providing real benefits on the shop floor.

Recently, the NCC has developed efficient methods for predicting the maximum achievable course width (the number of tapes deposited in a single pass) and also how changes in applied heating power influence the as-deposited material state.



Figure 1: The NCC has two Coriolis Composites AFP machines (pictured with GKN composite winglet) and an additional Accudyne machine with choice of laser, infrared and patented Xenon FlashLamp heat sources.

The method developed to predict maximum course width provides clear programming rules for manufacturing engineers that ensure material will receive sufficient compaction pressure. This critical information is extracted from local quasi-static finite element simulation describing the compaction of a roller onto a tool surface at critical locations (simulated boundary of positive contact pressure shown as green ellipse in Fig. 2. Built-in modelling options describing materials behaviour, geometric non-linearity and sliding contact within Abaqus Standard (provided by NCC member Dassault Systèmes) efficiently capture the complex physical behaviour. By taking component geometry, fibre orientation and experimentally measured load-deflection response of the roller [1] as inputs, these models return maximum course width within around 90 minutes for each desired fibre orientation and feature on the tool. For a complex component, just 2.5 days of simulation effort is required to generate design rules to guide process specification and ensure good manufacturability. These rules reduce operator uncertainty and variability in programming while saving days or weeks of costly on-machine trials.

The prediction of as-deposited material state has begun by tackling AFP manufacturing using thermoplastic composites as part of the Core

Research Program.

Dr. Peter Giddings, simulation engineer responsible for that effort explains "Our objective was to quantify how we could manipulate heater power to maximise quality of the deposited material by predicting material state parameters like degree of bonding between layers or percentage of voids".

The underpinning simulation method is an in-house finite difference code, written in MatLab, that predicts heat diffusion within the deposited material as the thermal and pressure boundary conditions imposed by the roller move across a component. To enhance predictions for temperature and material state distributions, the code updates key material properties that influence thermal diffusion [2,3], for example density, during each solution increment.

Today these coupled thermo-chemical simulations are helping to define process windows for high quality carbon fibre/PEEK composites for aerospace structures. As the capability is extended to cover the full range of materials and heat sources used in AFP it will help more customers, " these simulations can offer guidance on effective machine settings and usable design rules for AFP manufacturing to help broaden the viability of

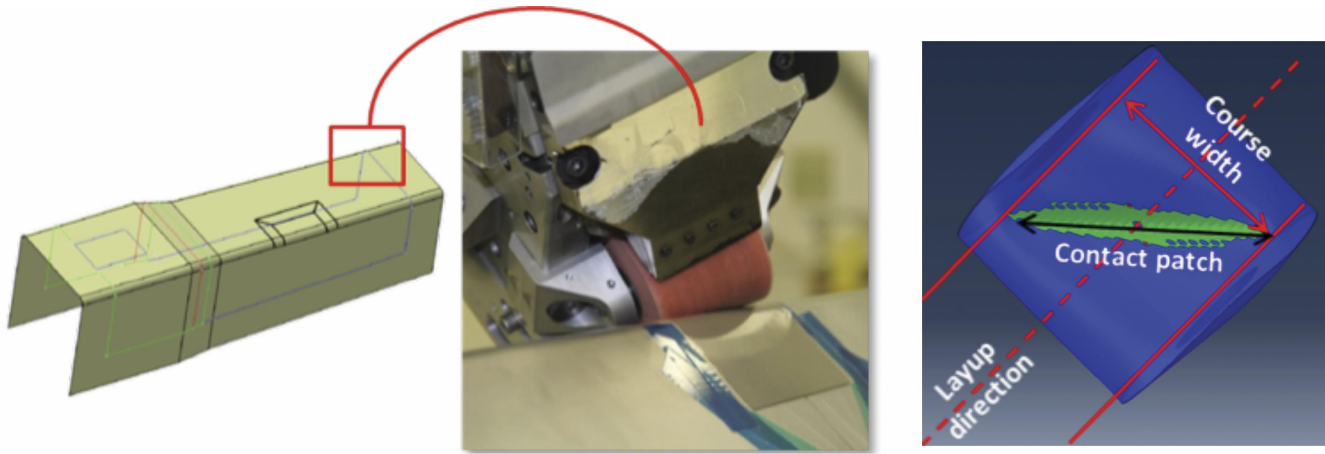


Figure 2: Simulation of critical features in AFP layup to determine maximum course width showing manufacturing challenge and an example FE contact patch output with extraction of maximum course width

Resin flow

Many composite components begin as preforms of dry reinforcing fibres before being impregnated with an uncured liquid resin and heated to cure the resin. For components requiring excellent surface finish and increased mechanical performance, that impregnation occurs in a closed metallic tool in a process called resin transfer moulding (RTM). Prediction of how the resin flows through the preform to fill the mould, whether any areas will fail to be completely impregnated and the optimisation of injection location and pressure are all challenges that the NCC is working toward resolving. Over the past two years NCC core research has developed effective RTM simulation approaches as Dr. Christian Lira explains: “today, if a customer comes to us with a problem in their infusion, even if it is thick or highly curved, we can help. Tooling design, where you inject the resin and how you adjust the pressure can all be included to guide them to a solution”.

These successes have been achieved using ESI’s software PAM-RTM which Dr. Lira says “provides a finite element solution to Darcy’s flow equation (flow through porous media) and allows us to make useful simulations within industrial timescales. With infusion, the process has inherent variability, small but unavoidable changes in material permeability cause big changes in flow rate so any simulation is indicative, not perfectly predictive”[4]. However, the simulations are still extremely valuable for comparing the effects of various parameter changes on process outcomes.

The understanding of material and process variation built up at the NCC has made it clear that flow simulations cannot predict the exact dimensions of a defect but do indicate whether defects may occur and their likely locations. Within these limits, Dr. Lira’s infusion simulations are already guiding engineers through more efficient test plans and have made simulation-led process design for traditional RTM a reality at the NCC.

To meet the tight timescales demanded by high volume automotive customers and produce cured composite parts in less than 5 minutes, resin infusion technology is moving to higher injection pressures and faster curing resins. High pressure RTM (HP-RTM) injects resin into a preform at pressures of up to 140 bar to fill moulds in seconds before the fast curing resin systems begin to harden. The speed and violence of the HP-RTM process means that the understanding of infusion simulation, built up in traditional RTM development, is no longer enough to effectively guide manufacture.

The challenges posed require new approaches as Dr. Lira describes “we have to update material permeability and fluid viscosity during the simulations as resin pressure deforms the fibres and fast reacting resins begin to cure during injection. We’re working with software providers to help extend RTM simulation techniques to deal with these effects, but the effects of small quantities of polymeric compounds applied to the dry fibres to hold performs together, known as binders, is not so simple”. The methods for capturing the influence of binders within HP-RTM are not well understood even within the scientific community and so arriving at a predictive

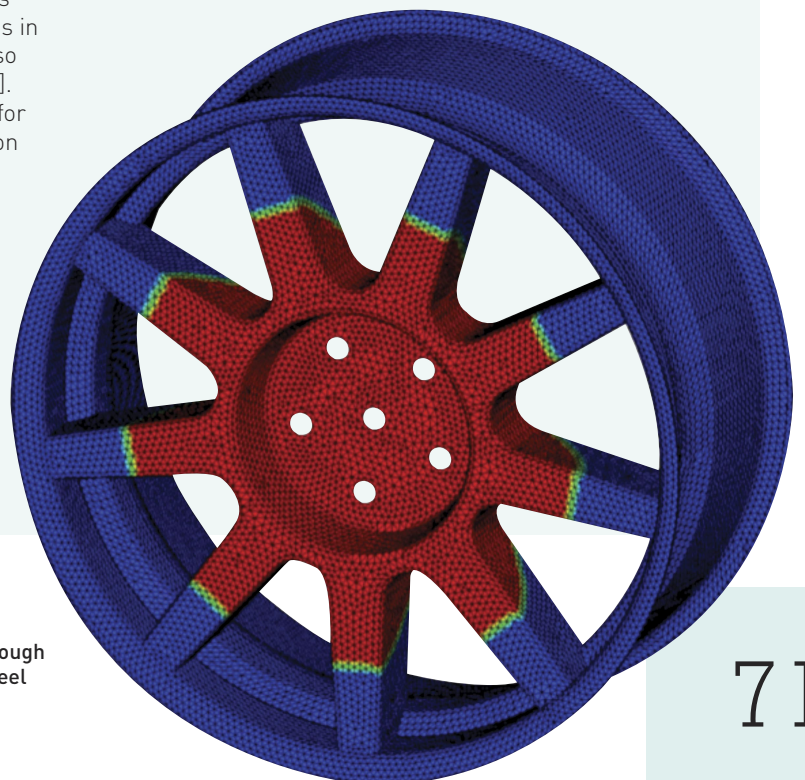


Figure 3: Prediction of resin infusion through a carbon fibre preform of a vehicle wheel using ESI’s PAM-RTM software



Figure 4: Europe's only open-access 3.4m x2.6m press installed and making parts at the NCC

simulation of HP-RTM requires a longer-term commitment to develop and refine the simulation capability. That commitment has already begun as the NCC works with academics, software vendors and manufacturers around the world to bring insightful simulation of HP-RTM towards industrial implementation.

These efforts are made possible by the installation of a Schuler 36-Kilotonne press in December 2014 at the Bristol site to explore the infusion of large composite components via HP-RTM. The unique combination of open-access industrial scale equipment together with on-site laboratory mean that the novel simulations necessary to support rapid development of HP-RTM processes can be grounded in high quality experimentation. That industrial scale validation is critical to understand how machinery and processes will respond under the extreme conditions that HP-RTM imposes.

Multiphysics simulation of induction welding Together with enhanced environmental resistance, recyclability and novel processing routes, one of the benefits for thermoplastic composites is that components may be joined structurally by welding two components together. The resulting joints can replace mechanical fasteners to help components retain more of the strength of the pristine laminate by eliminating drilled holes as well as reducing part count in large composite assemblies.

A particular interest at the NCC is induction welding of carbon fibre composites. In this emerging composites process, a magnetic field is used to heat the carbon fibres within composite materials through electrical eddy currents generated by electromagnetic induction within the conductive fibres. Through controlled application of an oscillating magnetic field the heating effect can be managed so that the polymer matrix melts in the desired locations to permit welding to take place.

For simulation engineers at the NCC, capturing the induction heating effect in layered anisotropic materials has proven to be a hugely satisfying project. The process simulation team chose MSC MARC Nonlinear FEA software (supported by MSC Software Ltd, Frimley) to build simulations for induction heating of thermoplastic composite joints.

The task of improving simulation results to be of use in process specification for composite welding required coupling of thermal and electromagnetic models, and careful specification of material parameters. The research posed challenges to the materials test and tooling manufacture supply chains as well. Materials tests were identified or developed to provide unusual but necessary simulation input data over describing properties such as dielectric permeability, among others, for anisotropic composite materials. Once preliminary models were validated against literature data, more detailed analyses were developed with MARC to design test fixtures and induction coils suitable to experimentally characterize the induction heating process [5,6].

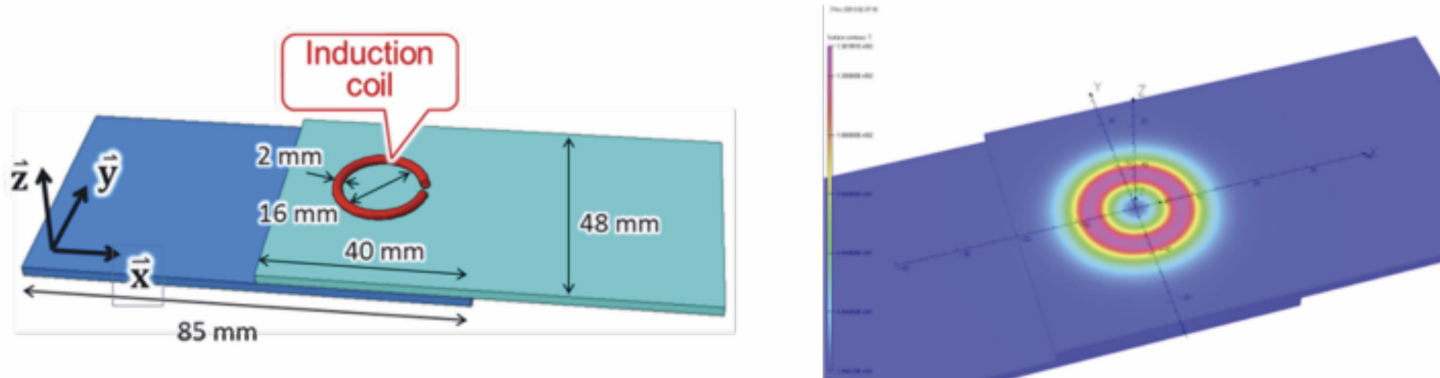


Figure 5: Induction welding simulation of lap shear test specimen conducted at the NCC showing specimen dimensions and resulting heated area

The simulation of induction heating is a strong first step towards developing the predictive tools for induction welding of composites, and is already helping tooling suppliers to refine fixture designs that retain components without impacting the delivered magnetic field. The effort expended in building these capabilities has allowed the NCC to validate methods for predicting heat input within induction heating of composite plates as the centre moves towards simulation of real industrial welding processes.

Conclusion

The outlook for process simulation in composite manufacture is incredibly bright. There is vibrant academic research activity extending our fundamental understanding and coupled with strong growth in industrial demand for composites. Automation technology is becoming established in a broader range of industrial applications and simulation tools from ESI, Dassault Systèmes, MSC Software and others offer suitable platforms in which to build useable and powerful process simulations.

The simulation successes at the NCC are just the tip of the iceberg for composite process simulation; there are some fascinating challenges and tangible commercial opportunities for simulation engineers within composites. However, real progress is needed in bringing these complex simulations into the supply chain to aid in industrialisation of automated composite manufacture.

The NCC aims to pave the way for the simulation supply chain to effectively support the composites sector and help demonstrate that the fascinating multiphysics problems bring real returns on the shop floor and also in the finished product.

References

- [1] Helenon, F. D. H.-J. A. Lukaszewicz, Ivanov, D and Potter, K. "Modelling slit tape deposition during automated fibre placement". 19th International Conference on Composite Materials (ICCM19), Montreal, Canada, 2013
- [2] Cogswell, F. N. "Thermoplastic aromatic polymer composites". 1st Edition, Elsevier Science and Technology, 1992
- [3] Stokes-Griffin, C.M. Compston, P. "A combined optical-thermal model for near-infrared laser heating of thermoplastic composites in an automated fibre placement process". Composites Part A (In Press) .
- [4] Arbter, R. "Experimental determination of the permeability of textiles: A benchmark exercise." Composites: Part A 42: 1157-68, [2011]
- [5] Moser, L. "Experimental Analysis and Modelling of Susceptorless Induction Welding of High Performance Thermoplastic Polymer Composites", PhD Thesis, Institut für Verbundwerkstoffe (2012)
- [6] Rudolf, R. Mitschang, P. & Neitzel, M. "Induction heating of continuous carbon-fibre-reinforced thermoplastics". Composites: Part A 31: 1191-1202 (2000)

About the NCC: www.nccuk.com

The NCC is a £25m investment supported by: the Department for Business, Innovation and Skills (£12m); the South West RDA (Regional Development Agency) (£4m); and £9m from the European Regional Development Fund (ERDF). It is owned and hosted by the University of Bristol. The Government announced a further £28m in the 2012 Autumn Statement for the expansion of the NCC. The NCC is a partner of the High Value Manufacturing Catapult.

Addressing Automotive Engineering Challenges in Composite Development by Simulation

Michael Hack, Laszlo Farkas, Christophe Liefoghe, Michaël Bruyneel & Alexander Szatecsny Siemens PLM Software

During the past decades, the ecological footprint caused by various human activities has largely increased with a clear tendency to further grow. This global socio-economic problem triggers environmental action plans in order to attenuate the ecological impact of the human activities. As a result, manufacturers in the transportation sector are under increasingly large pressure to reduce the ecological footprint of their products and to comply with the ever more stringent emission requirements of the European Union. The deployment of advanced lightweight materials (especially in the aerospace and automotive sector) is a response of the transportation industry to deal with this challenge. It is widely acknowledged that there is large weight-saving potential in the new composite materials that lead to increased energy efficiency and less emissions. Further strong socio-economic relevancies (next to cleaner vehicles) can be linked to the application of new composite materials such as improved products in terms of safety and reliability.

► Lightweight potential of metals and CFRP

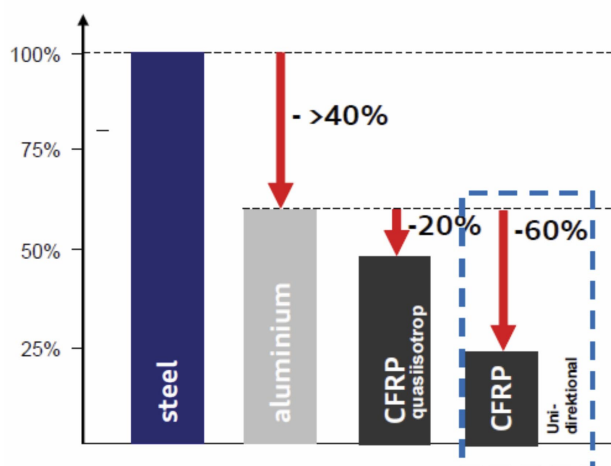


Figure 1: ©Audi, IQPC Conference Automotive Composites, Munich, Germany, 7-8 December, 2011

Motivation

According to the automotive sector, a weight saving of approximately 60% can be achieved on the body-in-white with the application of composite materials (see Figure 1). This important advantage w.r.t. metal car bodies is attributed to the higher specific stiffness and specific strength (or specific energy absorption capacity) of composites (see Figure 2).

At present, the massive deployment of lightweight composite materials is limited by three major bottlenecks in the automotive sector:

1. In the industrial manufacturing process such materials cannot be produced with the production rates common for the metal-based structures and furthermore the industrial manufacturing processes are very expensive as compared to the metal-dominated manufacturing technologies; this means that manufacturing processes for composite materials, and joining techniques for composite materials (with composite and other components) still have to be fine-tuned and matured to the level of industrial applicability.
2. The industrial engineering design and development process is limited by the lack of predictive modelling tools that are able to accurately mimic the real-life behaviour of lightweight material structures. This aspect is more apparent for design attributes such as crashworthiness and fatigue, which require the material predictions beyond the elastic limits (strength and damage under dynamic loading conditions); this means that the industry has to largely rely on expensive tests for which the results become available only very late in the product development process. Furthermore the full lightweight potential cannot be exploited as the uncertainties in the performance predictions are typically compensated by safety factors, leading to oversized components.
3. The integration of predictive tools with manufacturing simulation and the manufacturing process that allows an efficient implantation of new materials in the production process.

In order to address the CAE challenge, experience from other industries is being leveraged in the traditional automotive domains like NVH (Noise, Vibration & Harshness) & Durability to develop advanced solutions in damage, fatigue, NVH & Crash. At the same time full computer aided integration of the manufacturing process from definition of the laminate through like in Figure 3 is being implemented.

State of the art

For simulation of the various automotive performance attributes, the basic physical phenomena driving the composite material's behaviour need to be understood. Accurate predictions of stiffness and also failure and damage are necessary to be able to achieve a virtual CAE-based development process of composite-intensive vehicles. While stiffness prediction models are well developed, reliable and available in commercial FEM packages, the strength and damage predictions are still rather inaccurate nowadays, based on approximate descriptions of the relevant phenomena.

Currently large research efforts are dedicated to the study and analysis of composites mechanical behaviour at different scales:

- the micro-scale is focusing on the physical phenomena at the fibre level and fibre-matrix interface level,
- the meso-scale is concerned with the details at the level of a representative volume element (RVE) or unit cell, while
- macro-scale is focusing on the homogenized continuum.

In the typical mechanical product manufacturing industries, state of the art is the macro-scale modelling approach as it is today the only feasible way to model the behaviour of complex structures such as a car body that is discretized in multi-million finite elements. As homogenized finite element modelling (FEM) has its limitations in terms of the detailed representation of the mechanical behaviour, the authors believe that a breakthrough in predictive CAE of composite structures can be achieved by multi-scale modelling.

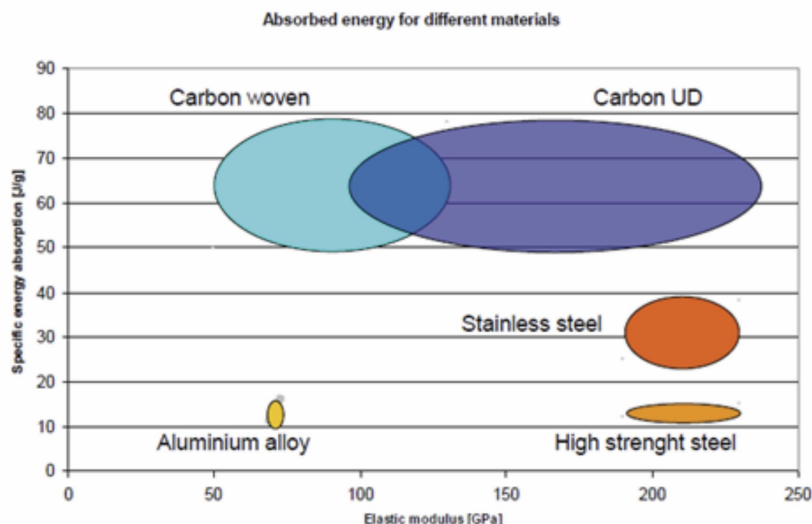


Figure 2: ©Dallara, Altair Americas HTC – Detroit, USA, May 16th 2012

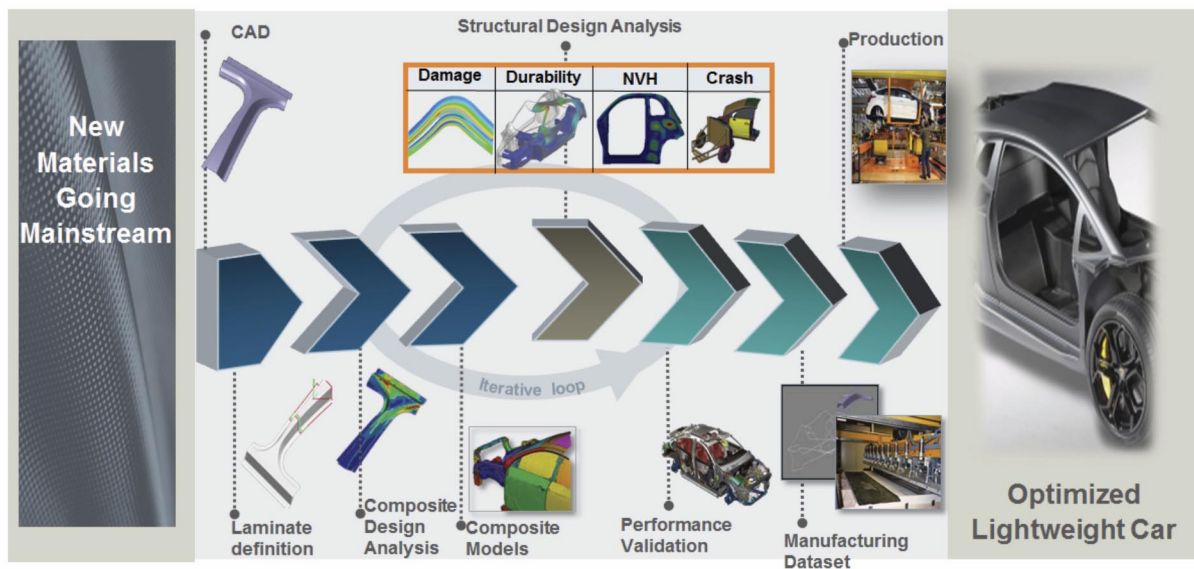


Figure 3: Integrated design process for laminated carbon fibre reinforced composites

Damage modelling

Continuum damage modelling (CDM) is the current state of the art for the progressive failure predictions of composite materials (See e.g. [2]-[5]). Based on CDM theories, the complex phenomena of damage initiation and propagation under static or dynamic loads can be efficiently modelled at the level of a homogenized composite cell. This macro-level modelling approach for composite laminates captures both the intra-ply and inter-ply damage evolutions by stiffness degradation laws. Figure 4 shows the typical damage modes accounted in CDM models for ply damage (intra-ply). Inter-ply (delamination) damage captures the stiffness degradation at the interface between plies (see Figure 5).

Damage models capability are implemented in finite element solver technology and need to include intra- and inter-laminar damage progression in complex composite lay-up [1]. Latest developments in advanced FE codes include the ability to study the progressive damage inside the ply [2]-[3], accounting for fibres breaking, matrix cracking and fibre-matrix de-cohesion. On the other hand, delamination can also be studied with the cohesive elements approach [4]. Cohesive elements models are based on continuum damage mechanics. A new non-local model has been developed recently, coupling the two kinds of damages, meaning that the transverse micro-cracking appearing inside the plies will influence the initiation of delamination at the interface of the plies [5]. With this new model, delamination occurs earlier in terms of load level, which is closer to what is observed in physical tests. The available solution for the non-linear damage modelling of composites has been validated on different industrial structures [6]-[8].

An important point to mention is that all CDM need material parameters that today need to be estimated from experiments. The correct setup and conduction of the experiments are key for successful parameter identification and therefore also highly important for good simulation results. (The NAFEMS Composite Group sees this as a point of high importance [9]) Only the combination of well defined experiments, material parameter identification, and finite element modelling allows predictive simulation [10]-[12].

The material behaviour and therefore the material parameters are highly influenced by the manufacturing process. For the future a virtual testing procedures should replace a large part of the physical tests.

Fatigue modelling

Following the state-of-the-art analysis presented in references[13] - [16] one can state that fatigue models for composites are still in their "infancy". The main approaches are based on SN-curves, a methodology adopted from the fatigue of metals. They are typically based on fatigue experiments in the main load direction. Modelling of fatigue in cross-ply laminates and especially for textile composites is difficult, as all models are based on experimental data for the full laminate, which requires that each change in the laminate structure leads to expensive experimental programs.

Damage modelling for fatigue of composites is an emerging research field. Relevant publications refer to damage models that are based on CDM approach [17]-[19]. Damage state variables are evolving in function of the fatigue stresses and are typically linked to the degradation of the elastic orthotropic properties on ply level. This approach has a number of advantages as compared to the classical SN approaches:

- Representation of the correct global behaviour by stiffness degradation
- The simulation can follow the full life of the components, so profiting from the typically good fatigue behaviour of composite structures
- Cross influences between damages can be considered (multi-axiality)
- Stress redistribution can be accounted for during the cycling
- No re-testing is needed for a change in layup (while keeping the same ply properties)

The main challenge today in this approach is to make it feasible for industrial applications in terms of computational efficiency. All state of the art implementations (like so called N-Jump based methods, that extrapolate (jump) the damage accumulation and stiffness reduction of a given load cycle for N cycles) are

limited to simplified block loads. E.g. Siemens has implemented methodologies for composite-specific fatigue and stiffness degradation, both for short fibre as well as for long fibre applications based on combining progressive damage models with hysteresis operators allowing accurate and efficient fatigue life predictions of composites structures with complex, multi-axial, long-duration loading cycles as typically encountered in automotive full vehicle and body applications [20].

The damage models for fatigue rely basically on the same CDM mechanisms as the static damage. Hence a similar process for material testing and parameter identification is used. Elastic properties on ply level can be re-used when identified for static damage behaviour.

NVH modelling

In the NVH (Noise, Vibration and Harshness) domain, the main research focus currently is on assessing the effect of the complex material geometry (e.g. fibre orientations in short fibre composite structures, micro-level material topology in poroelastic materials) on the stiffness properties and vibro-acoustic performances of lightweight material systems, on dynamic correlation and updating of lightweight numerical models using experimental data and on simulating the vibro-acoustic properties of complex lightweight material systems, including noise and vibration control treatments. [See [21]- 24]] Through manufacturing simulations, highly accurate models for the stiffness properties of composite components can be incorporated to augment the vibro-acoustic prediction accuracy of numerical models. In order to further increase the fidelity of dynamic model of often complex assemblies of composite components, numerical-experimental correlation and model updating techniques can be applied. In this way the impact of hard

to model features such as complex joints and manufacturing defects can be introduced in the numerical models. In a next step, these models can be incorporated in e.g. system-level vibro-acoustic models.

The lightweight nature of composite structures presents additional challenges for the design of effective noise control treatments. Due to their decreased weight, the acoustic transmission properties of such structures are significantly degraded. Moreover, due to the lower weight of the structural components, adding one kilogram of sound package has a much higher impact on their dynamic behaviour than in metal constructions. In a recent paper [25] the applicability of these formulations is experimentally validated based on two test rigs dedicated to NVH analysis of automotive trim components.

In the past decades modal representation techniques have been applied extensively to reduce model sizes in computational dynamic analysis at component and system level. This has become the default approach for dynamic analysis of industrial sized models. Nevertheless, many advanced materials (like some epoxy based composites for instance) exhibit a highly frequency dependent behaviour which prohibits the use of such approaches. Additionally, the modal superposition technique also fails to provide an accurate dynamic representation of structural components when noise or vibration control treatments such as visco-elastic patches are locally applied. It also cannot work if many composite components are assembled through bonding techniques whose properties are both frequency and position dependent. To address these limitations, efficient direct solution strategies are developed and significant research effort is invested in the development of advanced non-modal model reduction strategies [24].

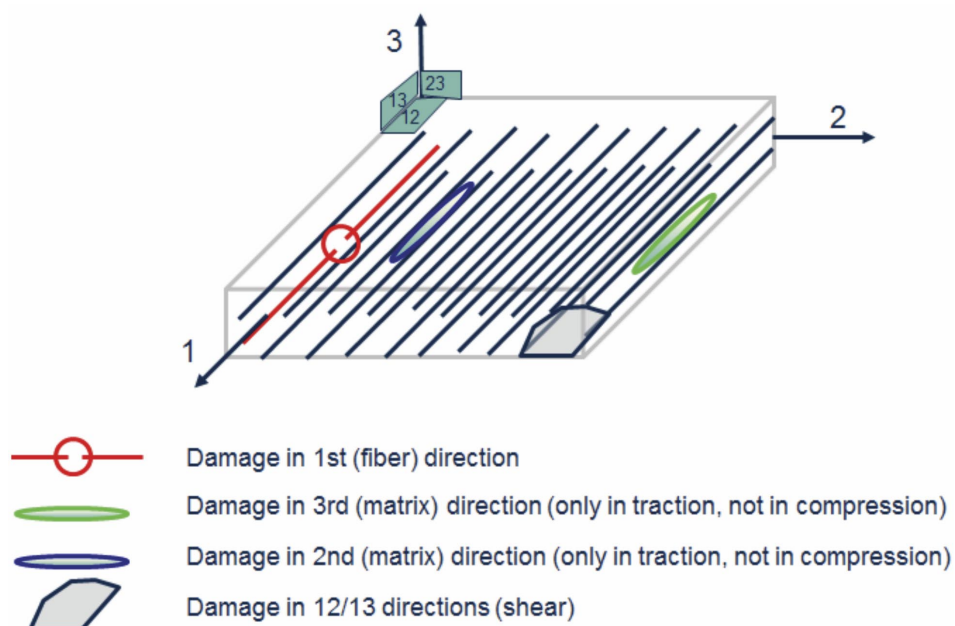
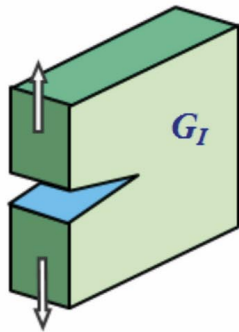
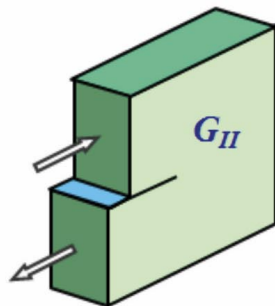


Figure 4: Damage inside the ply

MODE I
Interlaminar tension

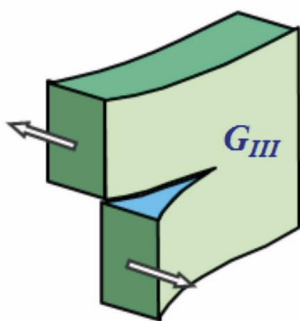


Interlaminar fracture toughness G_{IC}



Interlaminar fracture toughness G_{IIC}

MODE III
Interlaminar scissoring shear



Interlaminar fracture toughness G_{IIIC}

Figure 5: Damage between the plies

Crash modelling

In the automotive industry, the crashworthiness is one of the major driving attributes for vehicle development programs in general and for lightweight vehicle development in particular. Optimal balancing between conflicting design objectives such as weight, impact resistance and energy absorption capability is necessary. For transport applications, crashworthiness involves basically two different ways of expected component behaviour, namely components designed for optimal crash behaviour and components designed for optimal crush behaviour. The passenger compartment should provide passenger protection and should therefore resist to the high impact loads involved, meaning that the structural integrity is (approximately) conserved during a crash; it should hence show optimal crash behaviour. On the other hand, the large amounts of kinetic energy involved in such an accident should adequately be absorbed; this is most often achieved through adequate crush behaviour of front and back elements such as crush cones.

Predictive CAE of composites in automotive crashworthiness scenarios is not yet possible in an industrial context, which means that industry has to rely on expensive experimental tests for which the results become available only very late in the product development process. Internationally, much research effort has been devoted and currently still being dedicated to understand and simulate the behaviour of composite materials and composite structures under impact loading. Various aspects increase the simulation complexity of composites under dynamic loading conditions that make the necessary predictive property highly challenging. Also the behaviour of composite materials and composite structures under impact loading is being studied intensively [26]-[29].

However, it is a strong belief of many companies that currently, industrially relevant tools for adequately and accurately simulating the outcome of an impact are still in their "infancy". In the automotive sector, manufacturers like Mercedes-Benz for example state "that the state-of-the-art in the accuracy of prediction capabilities of current CAE tools for composites is the lowest, when durability and crashworthiness are concerned" [30]. Similarly Volvo "demands for better CAE for carbon composites, as crash simulation packages were originally designed with metallic structures in mind". "Regarding aluminium and safety, we have all of the tools we need and we can predict crash performance, but when it comes to CFRP the situation is quite different: CAE capabilities are much poorer; we don't have the tools yet – they are not mature enough" [31]. Depending on the exact nature of the involved types of impacts, the situation may be slightly different in other sectors, like aerospace or ballistic, but the general statements are also valid there [32].

The highly dynamic simulation of composite structures is challenged due to the high complexity of the damage mechanisms, geometrical non-linearities with contacts, multiple material combinations, stacking sequences. Furthermore the large number of impact scenarios (e.g lateral impact, axial impact or crushing) that manifest in numerous possible failure mechanisms (e.g. fibre/matrix debonding, fibre tensile failure and buckling, inter-ply delaminations) are characterized by a large number of associated model-specific physical or non-physical variables (e.g. fibre/matrix tensile strength, strain-rate coefficients, delamination mode coupling coefficient).

Manufacturing simulations

In order to fully cover the CAE-based virtual design engineering process for advanced lightweight materials such as composites, the process of manufacturing needs to be considered in the simulation chain. Various fabrication methods target different materials dedicated to applications that require specific properties, cost and cycle time. The large varieties of manufacturing processes have important influences on the mechanical properties of the composite components. The designed composite (micro)structure is often altered by manufacturing influences that result in scatter such as variations in local material properties, fibre misalignment or imperfections such as inclusions and voids. These factors have

significant impact on the mechanical performances. Therefore, a crucial point for accurately incorporating the often complex micro-structure of composite components on their structural stiffness and strength related performance is the link between the manufacturing process used to construct such structures and their predicted mechanical properties.

While simulation tools (see Figure 6) can enable high fidelity prediction of the (local) stiffness and inertia properties of composite structures, the incorporation of the complex inherent damping properties is far less understood and remains a field of active research.

Conclusions & Outlook

Conclusions

The pursuit for lightweight in the automotive sector implies a much more complex transition than just a simple material replacement (this simple metal replacement process is often called “black metal” approach). The massive deployment is currently hindered by two large technological bottlenecks: lack of efficient and cheap manufacturing processes on the one hand and efficient and lack of predictive CAE methodologies and tools on the other hand. When these key challenges are solved, large-scale deployment of composite structures will be possible. In addition, the full lightweight potential can be also exploited due to the more accurate performance predictions.

Addressing the challenges associated to the efficient and accurate multi-attribute CAE of composite-intensive vehicles requires advances on the scientific, on the upscaling and on the application level which can only be achieved by leveraging multi-decade experience in the aerospace sector related to the advanced simulation of composites and by teaming up between key academic and industrial R&D partners. Addressing this way the key challenges in the CAE of composite products will result in a major reduction of risks related to the insertion of such lightweight materials in the transportation sector.

Outlook

A breakthrough in the predictive simulation of complex composite materials is expected with advances in multi-scale modelling. The physical phenomena can be correctly captured by thoroughly understanding the mechanisms driving the material behaviour at different scales. The homogenized macro models applied in the context of FE modelling are based on empirical and phenomenological postulates. Instead, the application of the multi-scale concept in the modelling asks for a highly detailed physical representation of the material for fibres, matrix and fibre-matrix interface.

Well-developed geometrical models of textile reinforcements form a basis for meso-level finite element models of textile composites [33]-[35]. The existing meso- and micro-level methods and tools efficiently and accurately aid the stiffness predictions, while this multi-scale approach for strength and damage predictions is currently being developed. Further advances in multi-scale modelling will augment the existing benefits in different ways. On the one hand the further reduction of the complex and expensive physical tests needed for the identification of the macro-model

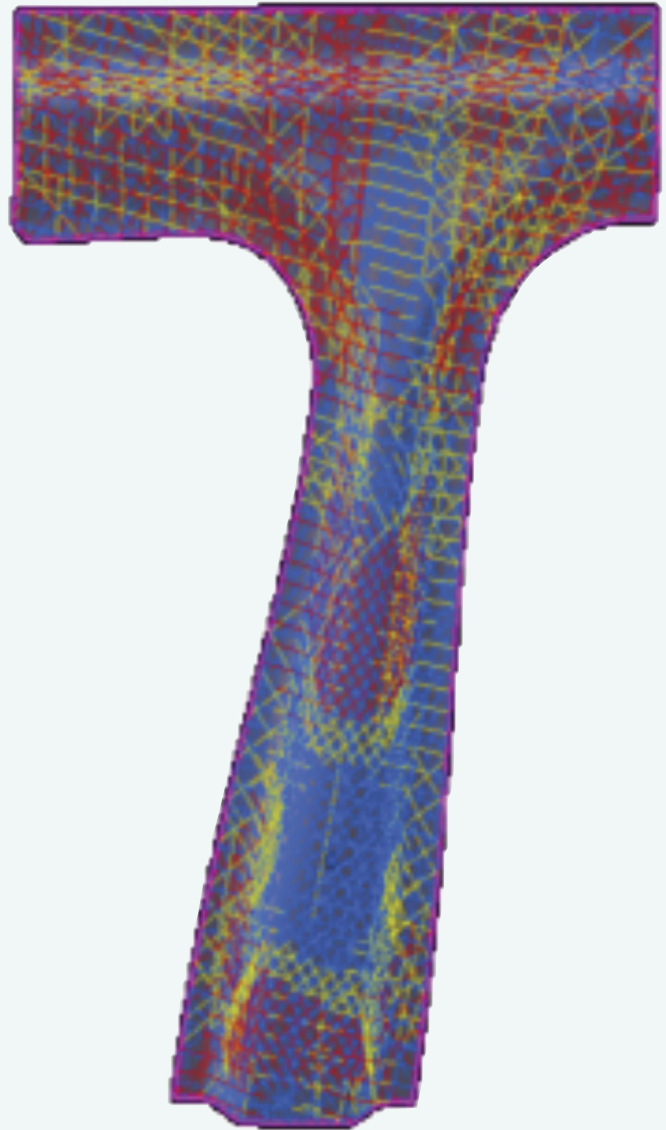


Figure 6: Draping simulation in FiberSim

parameters is expected. On the other hand, the simulations at a lower scale with a high physical resolution will further increase the fidelity and trustworthiness of predictions.

Acknowledgments

The authors gratefully acknowledge the support of IWT Vlaanderen (Agency for Innovation by Science and Technology) and of the Strategic Initiative Materials (SIM, see www.sim-flanders.be). Furthermore, the academic partners KULeuven (Be), UGent (Be), LMT-Cachan (Fr) and Faserinstitut Bremen (De) are gratefully acknowledged for their collaboration. Finally, the European Commission is gratefully acknowledged for their support of the EC FP7 Marie Curie projects ITN 290050 “GRESIMO” (“Best Training for Green and Silent Mobility”, see www.gresimo.at) and IAPP 285808 “INTERACTIVE”, see www.fp7interactive.eu).

References

- [1] Bruyneel, M., Delsemme, J.P., Jetteur, Ph. and Remouchamps A., "SAMCEF for composites: innovative numerical methods for analysis and optimisation", Proc. NAFEMS NORDIC Seminar: "Simulating Composite Materials and Structures", Esbjerg, Denmark, February 2-3, 2010.
- [2] Ladevèze P. and Le Dantec E. (1992). "Damage modelling of the elementary ply for laminated composites", *Composite Science and Technology*, 43, pp. 252-267.
- [3] Hochard et al. (2007). "A ply scale non-local fibre rupture criterion for CFRP woven ply laminated structures", *Composite Structures*, 80, pp. 321-326.
- [4] Lévêque D. (1998). "Analyse de la tenue au délaminage des composites stratifiés", PhD Thesis, LMT-Cachan, France.
- [5] Lubineau G. and Ladevèze P. (2008). "Construction of a micromechanics-based intralaminar mesomodel, and illustrations in Abaqus/Standard", *Computational Materials Science*, 43, pp. 137-145.
- [6] Bruyneel M., Delsemme J.P., Degenhaerd R.: An industrial solution to simulate postbuckling and damage. *JEC Compos. Mag.*, 48, 38-39 (2009).
- [7] Bruyneel M., Delsemme J.P., Jetteur P., Germain F.: "Modelling inter-laminar failure in composite structures: illustration on an industrial case study". *Appl. Compos. Mater.* 16(3), 149-162 (2009).
- [8] Bruyneel M., Delsemme J.P., Jetteur Ph. and Mertens T. (2011). "Recent results in damage modelling of composites", NAFEMS World Congress, May 23-26, 2011, Boston, USA.
- [9] NAFEMS Composite Group:
http://www.nafems.org/publications/tender/material_properties_for_structural_analysis_of_composites
- [10] Bruyneel M., Delsemme J.P., Goupil A.C., Jetteur P., Lequesne C., Naito T., Urushiyama Y. (2014). "Damage modeling of laminated composites : validation of the intra-laminar damage law of SAMCEF at the coupon level for UD plies", *European Conference on Composite Material, ECCM16*, Sevilla, Spain, 22-26 June, 2014.
- [11] Bruyneel M., Delsemme J.P., Goupil A.C., Jetteur P., Lequesne C., Naito T., Urushiyama Y. (2014). "Damage modeling of laminated composites : validation of the inter-laminar damage law of SAMCEF at the coupon level for UD plies", *World Congress of Computational Mechanics, WCCM11*, Barcelona, Spain, 20-25 July, 2014.
- [12] Urushiyama, Y; Naito, T. : Strength Calculation of Composite Material Considering Multiple Progress of Failure by Ladevèze Model, JSAE, paper JSAE_397-20145205, 2014
- [13] Talreja, R. and C. V. Singh (2012). "Damage and Failure of Composite Materials". Cambridge, Cambridge University Press.
- [14] Jain , A.; Verpoest, I; Hack, M. Lomov, S. Adam, L.; van Paepegem, W.: "Fatigue Life Simulation on Fibre Reinforced Composites - Overview and Methods of Analysis for the Automotive Industry", SAE 2012 - World Congress, Detroit, USA, April 24-26, 2012
- [15] Rohwer, K.: "Predicting fiber composite damage and failure", *Journal of Composite Materials* published online 26 September 2014, DOI: 10.1177/0021998314553885
- [16] Jain, A., Hack, M., Lomov, S., Abdul, Y., Van Paepegem, W., & Verpoest, I. (2013). Micromechanics and fatigue life simulation of random fiber reinforced composites.. NAFEMS World Congress, Salzburg, 2013.
- [17] Degrieck, J. and Van Paepegem, W. (2001), "Fatigue Damage Modelling of Fibre-Reinforced Composite Materials: Review", *Applied Mechanics Reviews*, 54(4): 279-300.
- [18] Van Paepegem, W. (2010). "Fatigue damage modeling with the phenomenological residual stiffness approach". In: Vassilopoulos, A.P. (ed.). *Fatigue life prediction of composites and composite structures*. Woodhead Publishing, United Kingdom, July 2010 (ISBN 978-1-84569-525-5), p. 102-138.
- [19] Nouri, H., Meraghni, F. and Lory, P. (2009). "Fatigue damage model for injection-molded short glass fibre reinforced thermoplastics". *International Journal of Fatigue*, 31(5), 934-942.
- [20] Hack, M.; Nuhn, P.; Liefoghe, C.; Sträßer, S.; Bruyneel, M.; Donders, S.: A Process for calculating fatigue and fatigue failure of structures, patent pending.
- [21] M. Tournour, F. Kosaka, H. Shiozaki: "Fast Acoustic Trim Modeling using Transfer Admittance and Finite Element Method" SAE 2007 Noise and Vibration Conference and Exhibition, St. Charles (IL), USA, 2007
- [22] J.F. Allard, N. Atalla: "Propagation of sound in porous media", Wiley, 2009
- [23] M.A. Hamdi, N. Atalla, R. Panneton: "Enhanced weak integral formulation for the mixed (u,p) poroelastic equations", *J. Acoust. Soc. Am.* 109 (6), 3065-3068, 2001
- [24] Lenzi, M., Lefteriu, S., Beriot, H., Desmet, W. (2013). A fast frequency sweep approach using Padé approximations for solving Helmholtz finite element. *Journal of Sound and Vibration*, 332 (8), 1897-1917
- [25] Van Genechten, B., Geslain, A., Tournour, M., Bruyneel, M., Hack, M.: "Finite Element-based simulation approaches for NVH assessment of lightweight system", SIA conference on Light-weighting and acoustical materials in vehicles, October 22, 2013, Compiègne, France
- [26] Karim, M.R. (2005). "Constitutive Modeling and Failure Criteria of Carbon-fiber Reinforced Polymers Under High Strain Rates". PhD thesis. University of Akron, Department of Mechanical Engineering.
- [27] Palanivelu, S., Van Paepegem, W., Degrieck, J., Kakogiannis, D., Van Ackeren, J., Van Hemelrijck, D., Wastiels, J., et al. (2010). Parametric study of crushing parameters and failure patterns of pultruded composite tubes using cohesive elements and seam, Part I: Central delamination and triggering modelling. *Polymer Testing*, 29(6), 729-741.
- [28] Palanivelu, S., Van Paepegem, W., Degrieck, J., Van Ackeren, J., Kakogiannis, D., Wastiels, J., Van Hemelrijck, D., et al. (2010). Parametric study of crushing parameters and failure patterns of pultruded composite tubes using cohesive elements and seam: Part II - Multiple delaminations and initial geometric imperfections. *Polymer Testing*, 29(7), 803-814.
- [29] Batra, R.C., Gopinath, G., Zheng, J.Q. (2012). "Damage and failure in low energy impact of fiber-reinforced polymeric composite laminates", *Composite Structures*, Volume 94, Issue 2, January 2012, Pages 540-547.
- [30] Kögl, M. "Influence of fibre waviness on the stiffness and strength of CFRPs", *Automotive Composites* 2011.
- [31] Fermer, M., "Volvo demands better CAE tools for carbon composites", *AE*, July 2012.
- [32] Qiao P., Mijia Y., Bobaru F., 2008, "Impact Mechanics and High-Energy Absorbing Materials: Review", *JOURNAL OF AEROSPACE ENGINEERING*, 235-248.
- [33] Lomov, S. and et al, "Meso-FE modelling of textile composites: Road map, data flow and algorithms", *Composite Science and Technology*, vol. 67, no. 9, pp. 1870-1891, 2007.
- [34] Verpoest, I. and Lomov, S.: "Virtual textile composites software WiseTex: integration with micro-mechanical, permeability and structural analysis.", *Composite Science and Technology*, vol. 65, no. 15-16, pp. 2563-74, 2005.
- [35] Jacques, S. and Van Paepegem, W.: "New approach for the construction of meso-scale finite element models of textile composites with periodic boundary conditions", *TexComp-11*, 19-20 September, 2013, Leuven, Belgium.

A Practical and Reliable Solution for the Damage Analysis of Composite Structures, with Applications to Automotive

Michaël Bruyneel, Cédric Lequesne, Benoit Magneville & Michael Hack
Siemens PLM Software

Yuta Urushiyama & Tadashi Naito
Honda R&D

Laminated composite materials have been successfully used in the aerospace industry for years. Today, the automotive sector must produce vehicles that satisfy strong regulations on gas emission. Carbon fiber-reinforced plastics, because of their high stiffness and strength to density ratio, represent a serious alternative to classical metallic approaches but generate the need to revisit the design, structural sizing and manufacturing methodologies of the parts. Concerning structural sizing, composites exhibit complex material behaviours, especially for heavily loaded structures when the assumption of linearity cannot be done anymore. Moreover, composite materials and structures show specific failure modes, which must be well controlled in the structural sizing process to exploit the full capacity of the material. In this context, and in order to reduce the development time and cost, simulation can become an interesting companion to the physical tests in the building block approach (pyramid of tests, Figure 1). There is a need to develop predictive material models able to represent the different modes of degradation of the plies forming the laminate. Delamination, that is the ply separation, must also be taken into account in the problem. The solution available in LMS Samtech Samcef is described in this paper, and demonstrated in the automotive context. Only static computations are carried out in this paper. Fatigue is also briefly discussed.

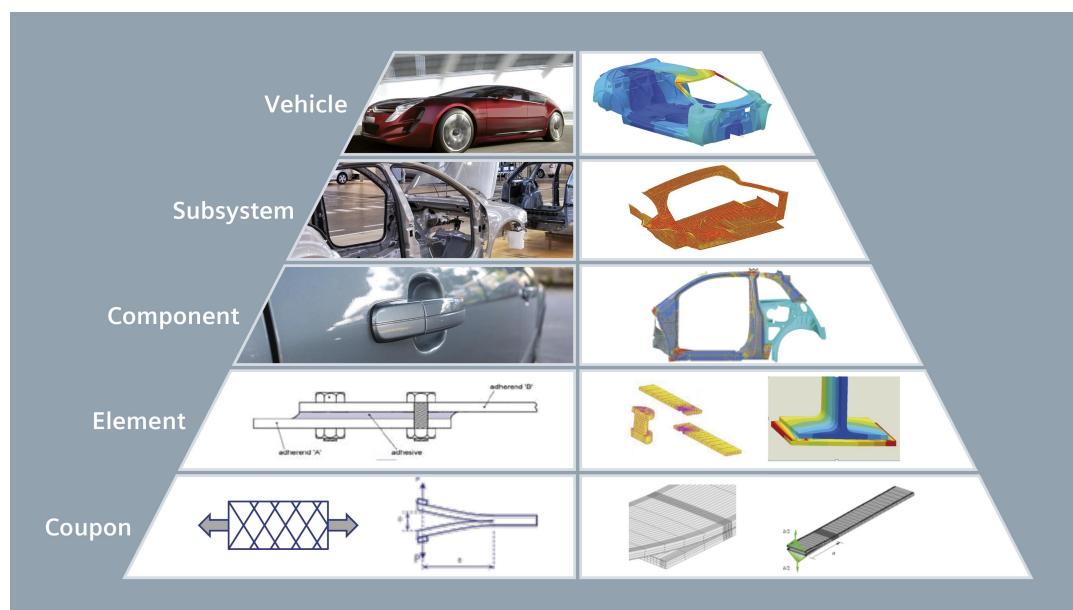


Figure 1. The pyramid of tests: physical and predictive virtual prototypes

Material Models for Inter and Intra-Laminar Damage

The intra-laminar damage model for the unidirectional ply is described in detail in references [1,2]. It is based on the continuum damage mechanics. In this approach, damage variables taking their values between 0 and 1 are introduced in the formulation to penalize the material stiffness.

The model includes 23 parameters (to be identified): the 9 elastic orthotropic properties in 3D ($E^0_1, E^0_2, E^0_3, \nu_{12}, \nu_{23}, \nu_{13}, G^0_{12}, G^0_{13}, G^0_{23}$) and specific parameters associated to damage and plasticity (like $Y_{II}, Y_{012}, Y_{s12}, R_0, \beta$ and n in Figures 2 and 3).

The potential e_d in (1), written here in plane stress for the homogeneous ply, includes the damage variables d_{II}, d_{22} and d_{12} related to the fibres, the transverse and the shear directions, respectively. The damage in the transverse direction only appears in tension, not in compression, as cracks get closed in the matrix under a compressive loading.

$$e_d = \frac{\sigma_{11}^2}{2(1-d_{11})E_1^0} - \frac{\nu_{12}^0}{E_1^0} \sigma_{11}\sigma_{22} - \frac{\langle \sigma_{22} \rangle_+^2}{2(1-d_{22})E_2^0} + \frac{\langle \sigma_{22} \rangle_-^2}{2E_2^0} + \frac{\sigma_{12}^2}{2(1-d_{12})G_{12}^0} \quad (1)$$

The so-called thermodynamic forces Y_I (see reference [1]) are the derivatives of the potential e_d with respect to the damage variables d_i . They can be seen as the loading in the different directions. They manage the evolution of the damages via relations $d_{II}(Y_{II}), d_{22}(Y_{12}, Y_{22})$ and $d_{12}(Y_{12}, Y_{22})$, see Figure 2a and 2c. In the fibre direction (Figure 2a), the behaviour is brittle, and the damage increases suddenly from 0 to 1 when the material strength (expressed in terms of Y_{II}) is reached. In the matrix, the damage produces a decrease of the material stiffness (Figure 2b), and its evolution with respect to the loading (here $\sqrt{Y_{12}}$) is more complex (Figure 2c). The two damages in the matrix, d_{12} and d_{22} , are coupled.

Besides damage, non-linearity is also taken into account in the fibre direction (Figure 3a). For the matrix, inelastic effects are considered in the form of a plastic law, which captures the permanent deformations (Figures 2 and 3). These material behaviours come from the tests interpretation.

The inter-laminar damage model for delamination is based on cohesive elements [3,4]. A potential is assigned to the interface elements, and three damage variables d_i are related to modes **I**, **II** and **III** (opening, sliding and tearing modes, respectively).

$$e_d = \frac{1}{2} \left[k_I^0 \langle \varepsilon_{33} \rangle_-^2 + k_I^0 (1-d_I) \langle \varepsilon_{33} \rangle_+^2 + k_{II}^0 (1-d_{II}) \gamma_{31}^2 + k_{III}^0 (1-d_{III}) \gamma_{32}^2 \right] \quad (2)$$

k_i^0 in (2) is the undamaged stiffness. Thermodynamic forces Y_i are obtained by deriving (2) with respect to d_i . For mixed mode loading, the damage evolution is related to the inter-laminar fracture toughness (G_{IC}, G_{IIC} and G_{IIIc}) in an equivalent thermodynamic force Y taking the following form:

$$Y = \sup_{\tau \leq t} G_{IC} \left\{ \left(\frac{Y_I}{G_{IC}} \right)^\alpha + \left(\frac{Y_{II}}{G_{IIC}} \right)^\alpha + \left(\frac{Y_{III}}{G_{IIIc}} \right)^\alpha \right\}^{1/\alpha} \quad (3)$$

In (3), α is a coupling coefficient, and t represents the time (pseudo-time when static analysis is addressed). The *sup* symbol in (3) means that the thermodynamic force can't decrease over time, so reflecting that damage is irreversible. In the model, the three damage variables have the same evolution over the loading and a unique damage d is therefore defined. The damage is related to Y via a function $g(Y)$. Three different functions $g(Y)$ are available leading to exponential, bi-triangular and polynomial cohesive laws.

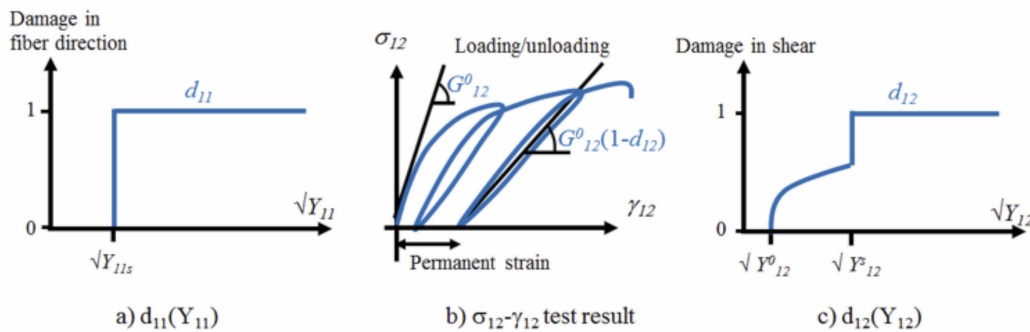


Figure 2. Damages in the fiber direction (left) and in the matrix

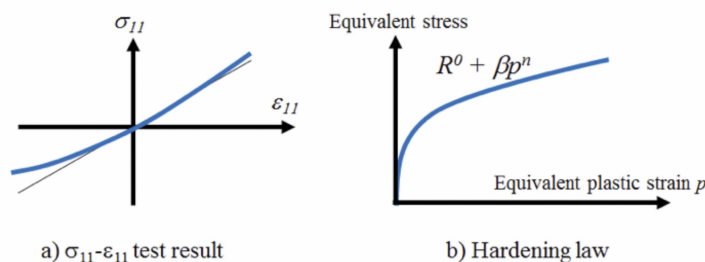


Figure 3. Non linearities in the model

Parameter Identification Procedure

From the coupon testing performed on classical machines according to some standards (e.g. ASTM D3039, www.astm.org), the longitudinal stress σ_L and the axial and transversal strains ϵ_L and ϵ_T are obtained. Based on this information at the coupon level, the 23 parameters of the ply model are determined. In practice, four series of tests are conducted, each series on a specific (well-defined) stacking sequence and/or loading scenario. As 5 successful tests are usually required, it results that 20 (= 4 x 5) successful tests must be conducted to cover the 4 series, that is a total of 20 tested coupons only. This is enough to identify the 23 parameters of the progressive damage ply model, i.e. the damage, plastic and initial elastic properties. The identification procedure is done without extensive use of simulation. It is a simple procedure based on EXCEL sheets, which can be sped up by some very simple programming. A comparison between an ASTM D3039 test and simulation is used to validate the identified values on a stacking sequence not used for the identification (Figure 4).

For the cohesive laws, specific DCB, ENF and MMB tests (www.astm.org) are performed. Finite element models are developed and a fitting between experiments and numerical results is conducted (Figure 5) to get the value of the parameters. Analytical solutions based on the beam theory are also used to fine tune these values.

Validation at the Upper Stage of the Pyramid

The previously identified parameters of the inter- and intra-laminar damage models are now used in simulations at the upper stage of the pyramid of Figure 1. Solid shell finite elements with EAS and ANS formulations are used. The element height is equal to the ply thickness. Interface elements are defined between each ply.

In a first application, a $[45/0/-45/90]_s$ plate is submitted to an impact. Test results are obtained with a C-scan. The simulation determines the amount of damage in each interface; red meaning completely broken while blue corresponds to no local damage. The damaged interfaces

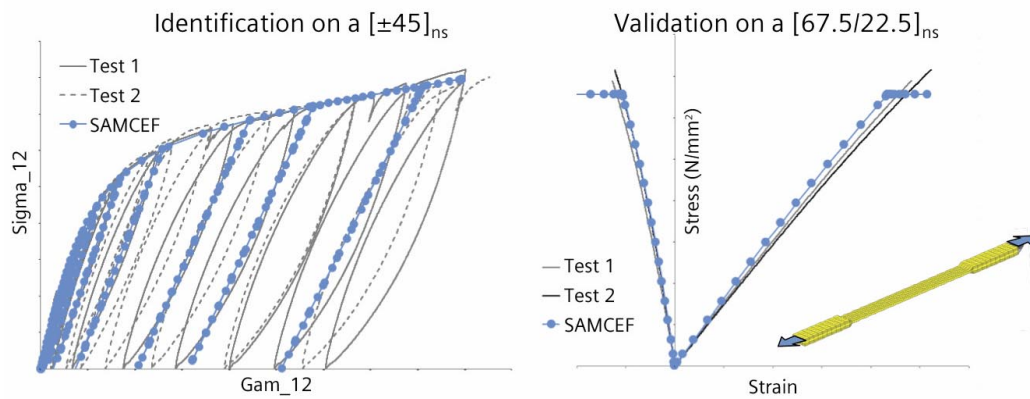


Figure 4. Comparison between test and simulation for the identification and validation at the coupon level (intra-laminar damage model)

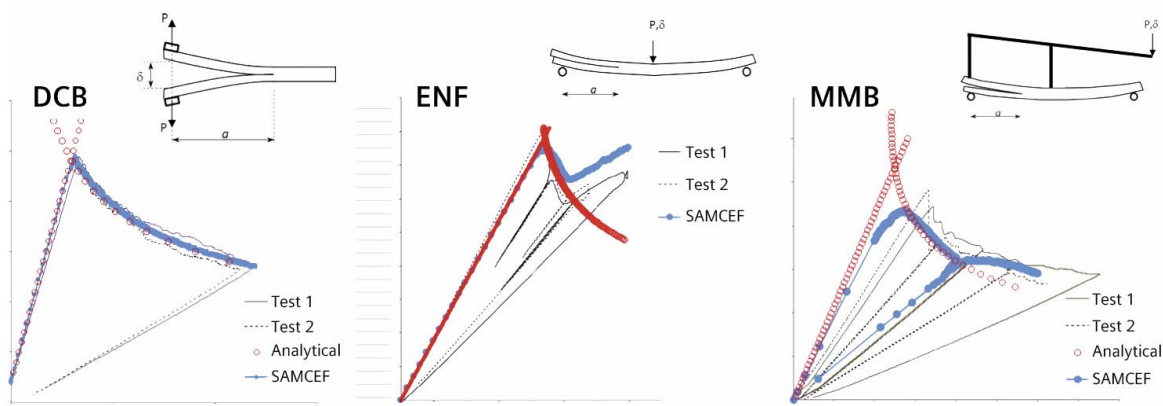


Figure 5. Comparison between test and simulation for the identification of the inter-laminar damage model parameters at the coupon level (delamination)

are illustrated in Figure 6. The agreement between test and simulation is very good.

In the second application, an L-shaped beam submitted to two different load cases and boundary conditions is considered (Figure 7). The laminates are made up of 12 plies with the following stacking sequence [60/-60/0/0/-60/60]s. Even if ply damage is present, the failure is mainly driven by delamination leading to large sliding of the plies. In Figure 8, a comparison between tests and simulations is done. The global behaviors are very similar. In Figure 9, the load-displacement curves show that a very good agreement is obtained between test and simulation.

Fatigue Analysis of Laminated Composites

Besides the static case described in the previous sections, fatigue is another attribute to consider in the structural sizing of composites. Even if laminated composites are known to have a good behaviour in fatigue, it is anyway interesting to study for instance the degradation occurring during the first cycles as tests reveal a (possibly large) stiffness decrease during that period.

The fatigue framework available in the LMS Samtech Samcef finite element code was adapted here in order to study laminates made up of unidirectional plies submitted to intra-laminar damage. It is based on the cycle jump approach proposed in [5], and relies on the

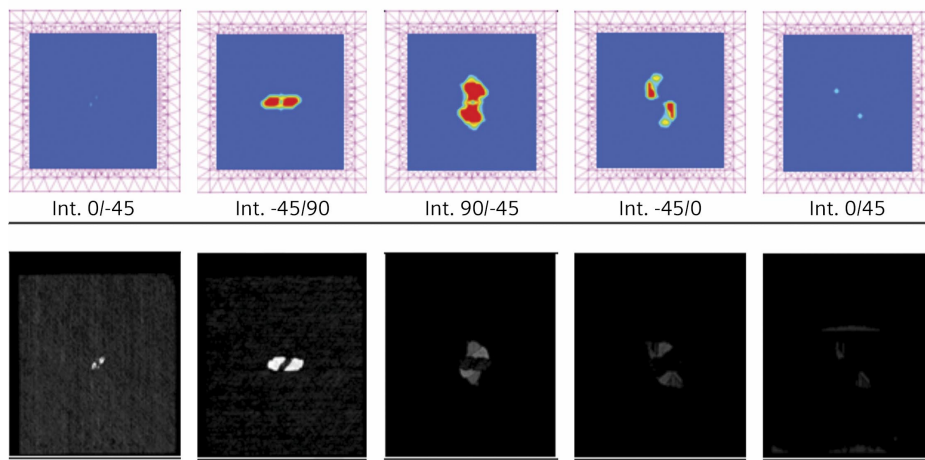


Figure 6. Results of the impact on the laminated plate

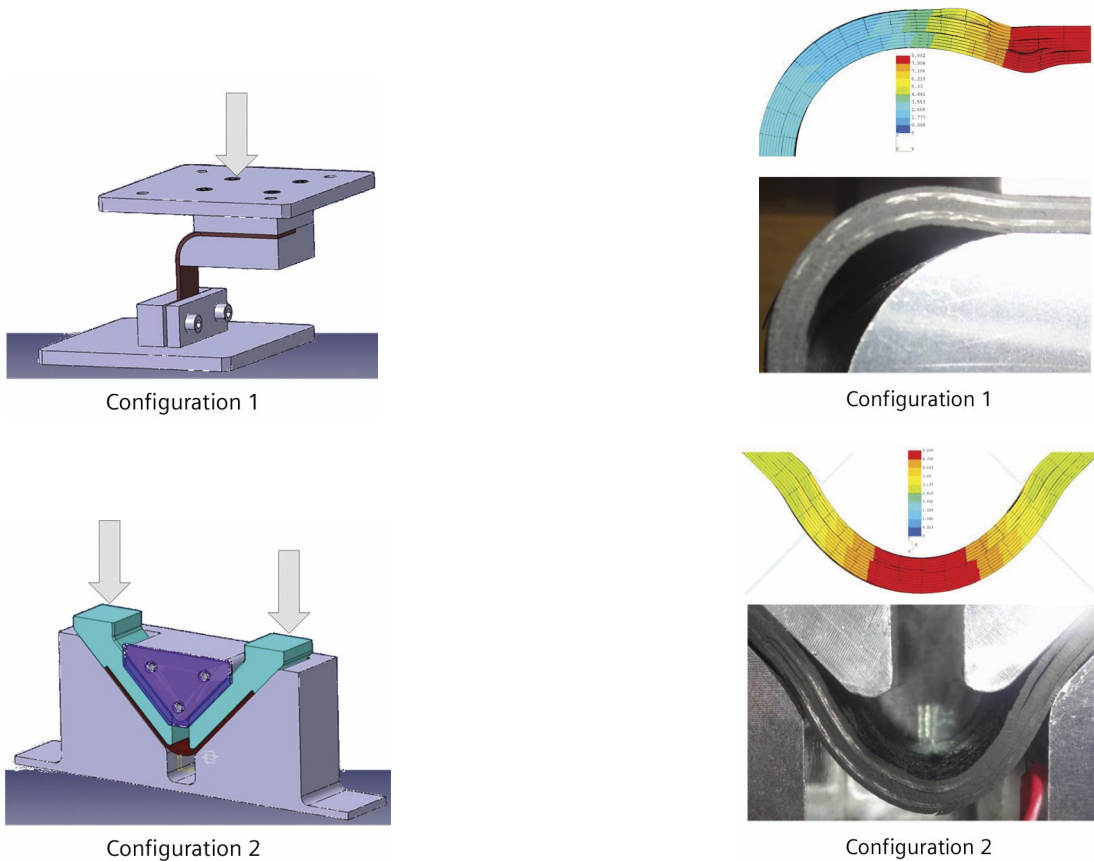


Figure 7. Two configurations for the L-shaped beam

Figure 8. Delamination resulting from the loading

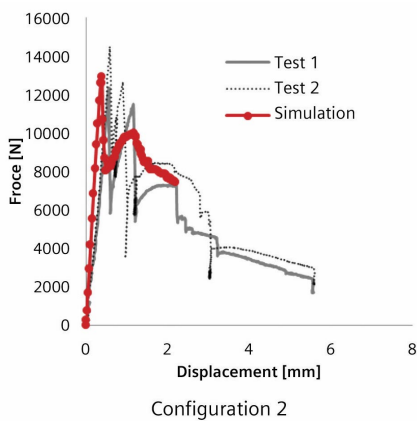
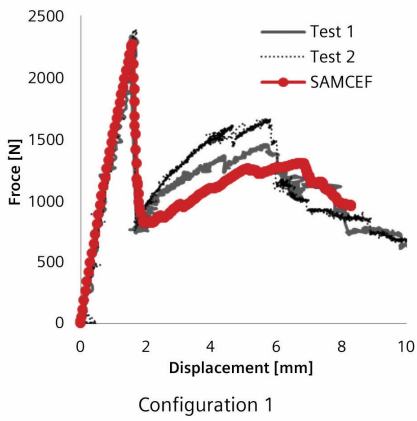


Figure 9. Load-displacement curves

continuum damage mechanics described in the previous sections, as stiffness decrease is also observed in fatigue. In the developed formulation, the cyclic loading is limited to constant amplitude. An extension to variable amplitudes is developed in LMS Virtual Lab Durability. With the specific fatigue law $\partial d/\partial N$ (where N stands for the number of cycles) and the cycle jump strategy, the computation of each cycle is avoided, saving large computational times. In Figure 10, the resultant reaction force of the coupon submitted to a fatigue membrane loading is recorded: it decreases over time, demonstrating that damage appears in the plies. First comparisons between physical tests and simulations for intra-laminar fatigue damage appearing after few cycles in coupons made up of plies oriented at either 0° or $\pm 45^\circ$, and submitted to membrane loading, are reported in Figure 10.

Summary and Concluding Remarks

In this paper, we have described the damage models for laminates made up of UD plies available in the LMS Samtech Samcef finite element software. Both inter and intra-laminar damages are addressed. The formulations and the methodology were presented and the parameter identification procedure at the coupon level was explained. Very good agreements were found between tests and predictive simulations at the coupon level and at the upper stages of the pyramid.

The methodology described for laminates made up of unidirectional plies and the static case was also demonstrated for woven fabrics and NCF materials [6,7]. Solutions of aerospace applications are available in [8-10].

References

- [1] Ladeveze P., Le Dantec S. (1992). Damage modeling of the elementary ply for laminated composites, *Composites Science & Technology*, 43, pp. 123-134.
- [2] Bruyneel M., Delsemme J.P., Goupil A.C., Jetteur P., Lequesne C., Naito T., Urushiyama Y. (2014). Damage modeling of laminated composites: validation of the intra-laminar damage law of SAMCEF at the coupon level for UD plies, *European Conference on Composite Material, ECCM16, Sevilla, Spain, 22-26 June 2014*.
- [3] Allix O., Ladevèze P. (1992). Interlaminar interface modelling for the prediction of laminate delamination, *Composite Structures*, 22, pp. 235-242
- [4] Bruyneel M., Delsemme J.P., Goupil A.C., Jetteur P., Lequesne C., Naito T., Urushiyama Y. (2014). Damage modeling of laminated composites: validation of the inter-laminar damage law of SAMCEF at the coupon level for UD plies, *World Congress of Computational Mechanics, WCCM11, Barcelona, Spain, 20-25 July, 2014*.
- [5] Van Paepeghe W. (2002). Development and finite element implementation of a damage model for fatigue of fibre-reinforced polymers. PhD Thesis, University of Ghent, Belgium.
- [6] Bruyneel M., Delsemme J.P., Goupil A.C., Jetteur P., Lequesne C., Naito T., Urushiyama Y. (2014). Damage modeling of woven-fabric laminates with SAMCEF: validation at the coupon level, *International Conference on Advanced Computational Methods in Engineering – ACOMEN 2014, Ghent, Belgium, 23-28 June, 2014*.
- [7] Bruyneel M., Delsemme J.P., Jetteur P., Lequesne C., Sopelsa L., Naito T., Urushiyama Y. (2015). Validation of the LMS Samtech Samcef material models for inter- and intra-laminar damages in laminated composites made of NCF plies, *ICCS18 International Conference on Composite Structures, June 15-18 2015, Lisbona, Portugal*.
- [8] Bruyneel M., Delsemme J.P., Jetteur P., Germain F. and Boudjema N. (2014). Damage modeling of composites: validation of inter-laminar damage model at the element level, *JEC Composites Magazine*, 90, June 2014.
- [9] Bruyneel M., Degenhardt R. and Delsemme J.P. An industrial solution to simulate post-buckling and damage of composite panels, *JEC Composites Magazine*, 48, May 2009.
- [10] Galucio A.C., Jetteur P., Trallero D., Charles J.P. Toward numerical fatigue prediction of composite structures: application to helicopter rotor blades, *3rd ECCOMAS Conference on the Mechanical Response of Composites*, 21-23, Hannover, Germany, 2011.

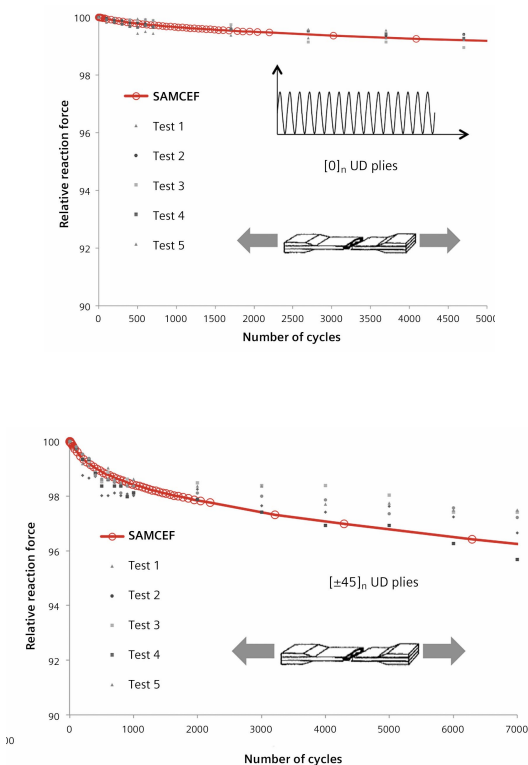


Figure 10. Fatigue in a $[0]_n$ and in a $[\pm 45]_n$



An Investigation of London Skyscraper's Unexpected Scorching Effect

By Dr. Svetlana Shtilkind, Dr. Andrey Ivanov and Maxim Popov,
Mentor Graphics, Mechanical Analysis Division

Sometimes even the most deeply considered engineering creations such as architectural structures can exhibit unpredictable behaviors. One such example, is the commercial skyscraper in the center of London, 20 Fenchurch Street. Nicknamed The Walkie-Talkie Building or The Pint because of its distinctive top-heavy shape, this impressive building provides 680,000ft² of exclusive office space that offers unrivalled panoramic views of London. The only problem is that the £200million skyscraper has a dazzling effect on passers-by. As a result of its unusual shape, the architectural structure reflects blinding rays of sun onto the street below, damaging the vehicles parked beneath it.

In the summer of 2013, the United Kingdom experienced unusually hot and sunny weather. On the 29th of August, Martin Lindsay, director of a tiling company, parked his Jaguar XJ for one hour opposite The Walkie-Talkie Building only to return to find a rancid smell of burning plastic and that parts of the car, including the wing mirror and side panels had melted and warped. We later calculated that Mr Lindsay had, by coincidence, parked in the 30m area with the most intensive sunlight exposure from Walkie-Talkie. This article investigates this phenomenon with the aid of Mentor Graphics' FloEFD analysis software.

To begin a full-scale CAD-model of building and the surrounding landscape was reconstructed with the maximum correspondence to its parabolic surface (Figure 1). The area topology data is taken from Google maps. All the top views are oriented with north upwards. The solar radiation parameters (location and actual time) were defined in FloEFD automatically.

FloEFD is equipped with three models of radiation: Discrete Ordinates, Monte-Carlo and Discrete Transfer. Taking into account the importance of the optical effects in concentrating the solar radiation as well as high-temperature conditions the Discrete Transfer model of radiation was chosen. This model solves the radiative transfer equation for a finite number of discrete solid angles, each associated with a vector direction. This method also allows the solution of radiation in case of refractive media. Three types of the incident flux reflection can be taken into account: diffusive reflection on the basis of Lambert's law, Fresnel law reflection on a refractive media interface and 100% specular (mirror) reflection.

The heat radiation leaving a radiative surface or radiation source is defined as:

$$Q^{out} = \varepsilon \cdot \sigma \cdot T^4 \cdot A + (1 - \varepsilon) \cdot (Q^{in} + Q^{source})$$

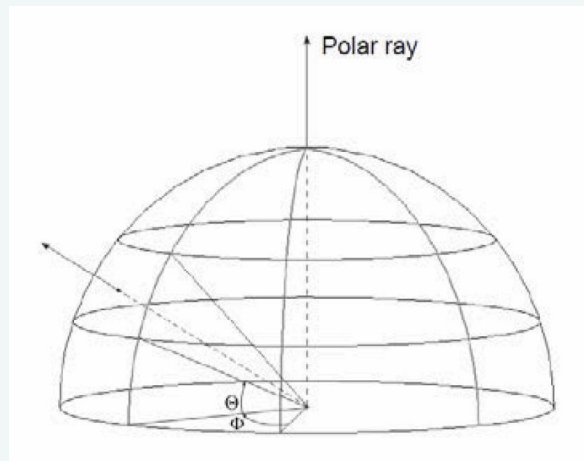
where: ε is the surface emissivity; σ is the Stefan-Boltzmann constant, T is the temperature of the surface; A is the radiative surface area; Q^{in} is the incident solar radiation arriving at this surface; Q^{source} is the radiation arriving at this surface from solar sources. The net radiation Q_{net} being the difference between the heat radiation Q_{out} leaving this surface and the incident heat radiation Q_{in} arriving at it:

$$Q_{net} = Q_{out} - Q_{in}$$

are calculated for each of the surfaces participating in the radiation heat transfer.

In order to reduce memory requirements, the problem of determining the net heat radiation fluxes is solved

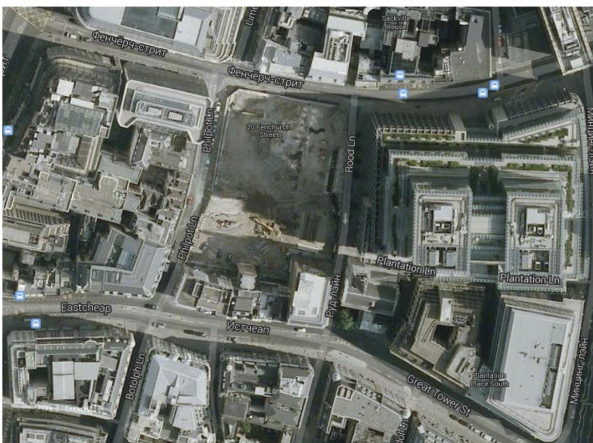
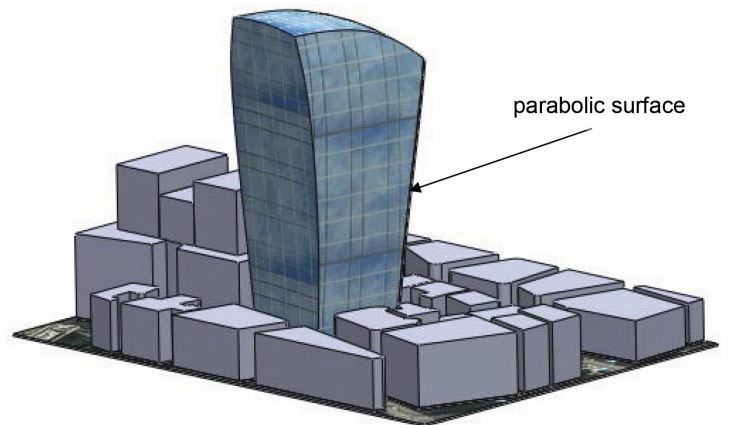
using a discrete ray Monte-Carlo approach. The computational mesh cells containing faces approximating the radiative surfaces are divided into clusters by a special procedure that takes into account the face area and angle between normal and face in each partial cell. For each of the clusters, the hemisphere governed by the ray's origin and the normal to the face at this origin is evenly divided into several nearly equal solid angles generated by several zenith (latitudinal) angles Θ (at least 3 within the 0...90° range, including the zero zenith angle of the normal to the face) and several azimuth (longitudinal) angles Φ (at least 12 within the 0...360° range).



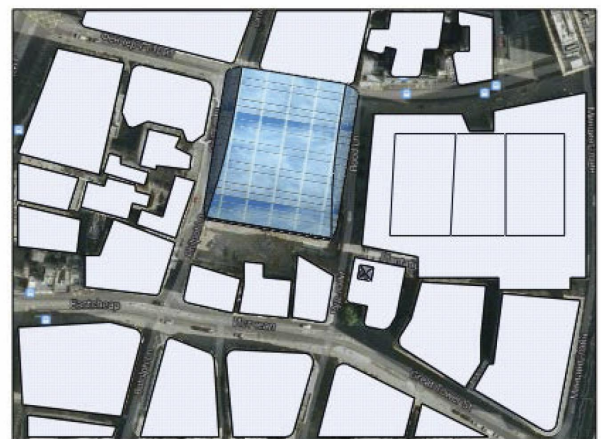
A radiation ray is emitted in each of the solid angles in a direction that is defined randomly within this solid angle. Each ray is traced through the fluid and transparent solid bodies until it intercepts the computational domain's boundary or a cluster belonging to another radiative surface defined as a 'target' cluster. When a radiation ray intercepts another cluster of radiative surfaces, the radiation heat carried by this ray is evenly distributed over the area of this cluster. The same procedure is performed if several radiation rays hit the same cluster. The two clusters interact according to their exchange factor. The total radiation energy emitted from one of the clusters is intercepted partially according to the visibility of clusters surfaces to each other.

As a first step in the investigation we estimated the ray exposed area dynamics as a result of the sun's position in 29th of August. Distribution of the calculated solar net radiation flux, W/m² (indicated here as Insolation), for the expanded time interval from 10:10 to 15:10 is shown in Figure 2. We can see the complicated shadow distribution changing its configuration as the rays shift. The sunlight focus spot illustrating via insolation maximum moves from west to east heating the pavement and any objects on it.

As a result of its unusual shape, the architectural structure reflects blinding rays of sun onto the street below, damaging the vehicles parked beneath it.



actual view (the photo is taken in June, 2012)



CAD-model

Figure 1. 20 Fenchurch Street Skyscraper and its CAD-model.

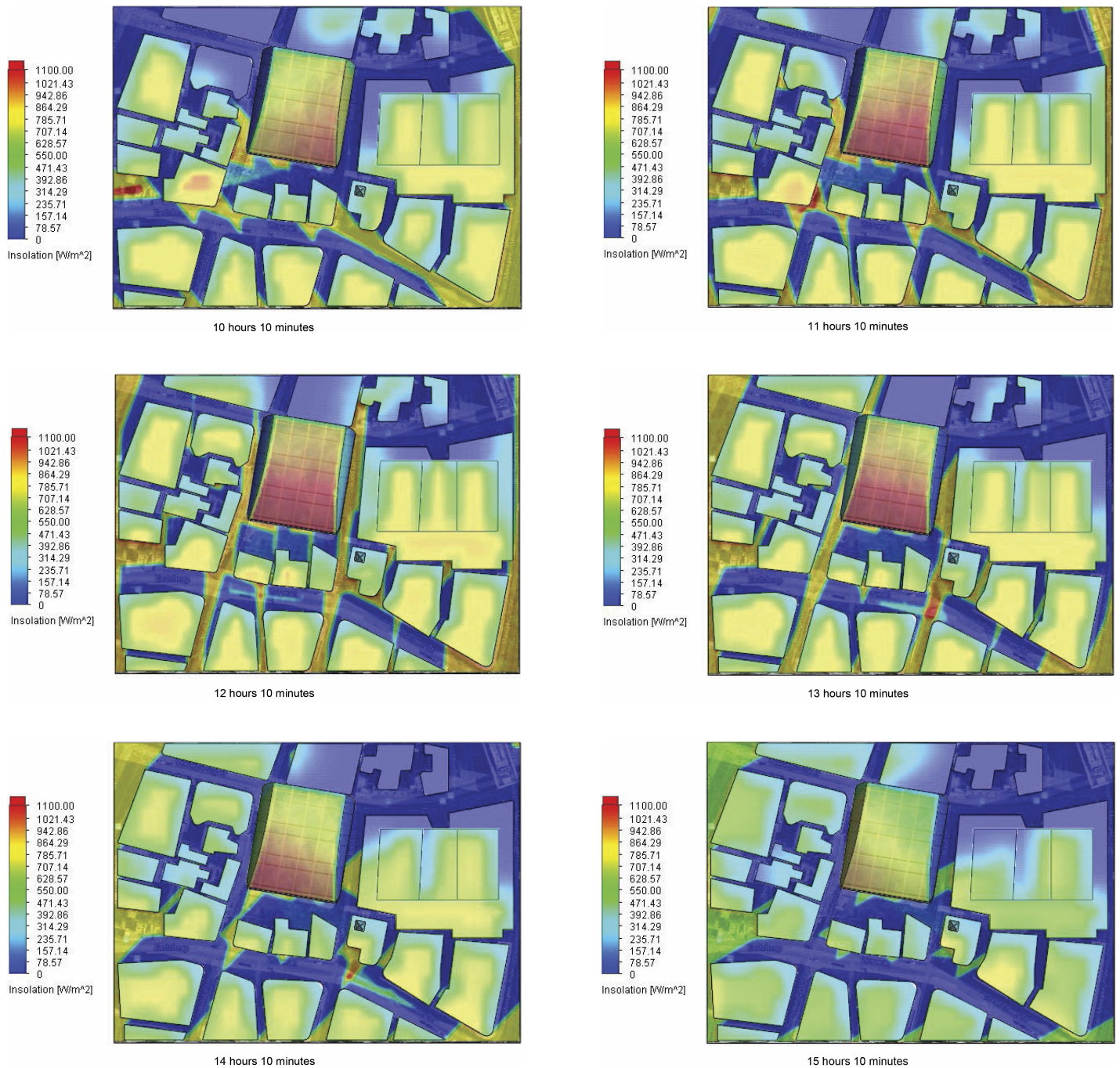


Figure 2. Solar net radiation flux (insolation) as a function of time.

By analyzing the results obtained, one can see that the most heated area at the time of incident (between 12:00 and 14:00) is the section of Eastcheap Street between St. Mary in Hill street and Botoph-lane (Figure 3).

The next step in the calculation, was to place the sunlight focus area in the CAD model. (Figure 4)

A more exact car position was defined by the focus trajectory analysis. For a deeper understanding of the optics specific to this case, we compared the results of the solar radiation flux calculation both with and without

reflection. In the first case, the parabolic surface of the skyscraper was defined as reflecting glass and at the second case as absorbent concrete. Figure 5 illustrates the focusing effect of parabolic glass surface. Glass is treated like semitransparent medium with refractive index of 1.45. Its reflecting properties are defined on the basis of Fresnel formula. As a result the incident sunlight is reflected and focused onto a small area. Concrete is simulated as diffusely reflecting surface so it has no focusing abilities. As we can see parabolic glass surface is a necessary condition to focus the sunlight.

When a radiation ray intercepts another cluster of radiative surfaces, the radiation heat carried by this ray is evenly distributed over the area of this cluster.

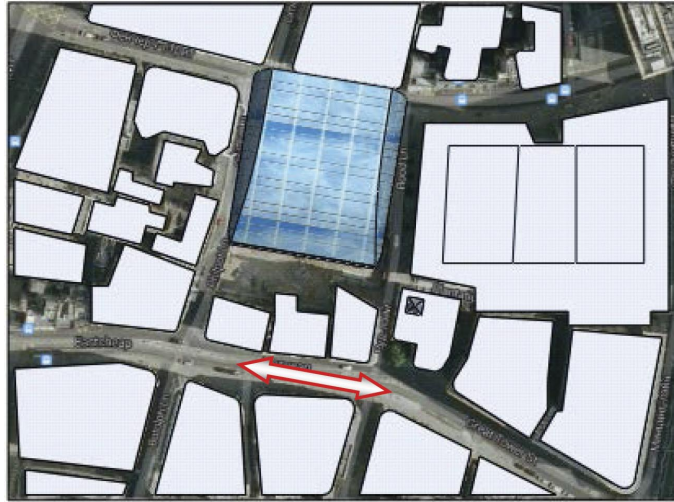


Figure 3. Spread of probable Jaguar positions between of 12.00 and 14.00.

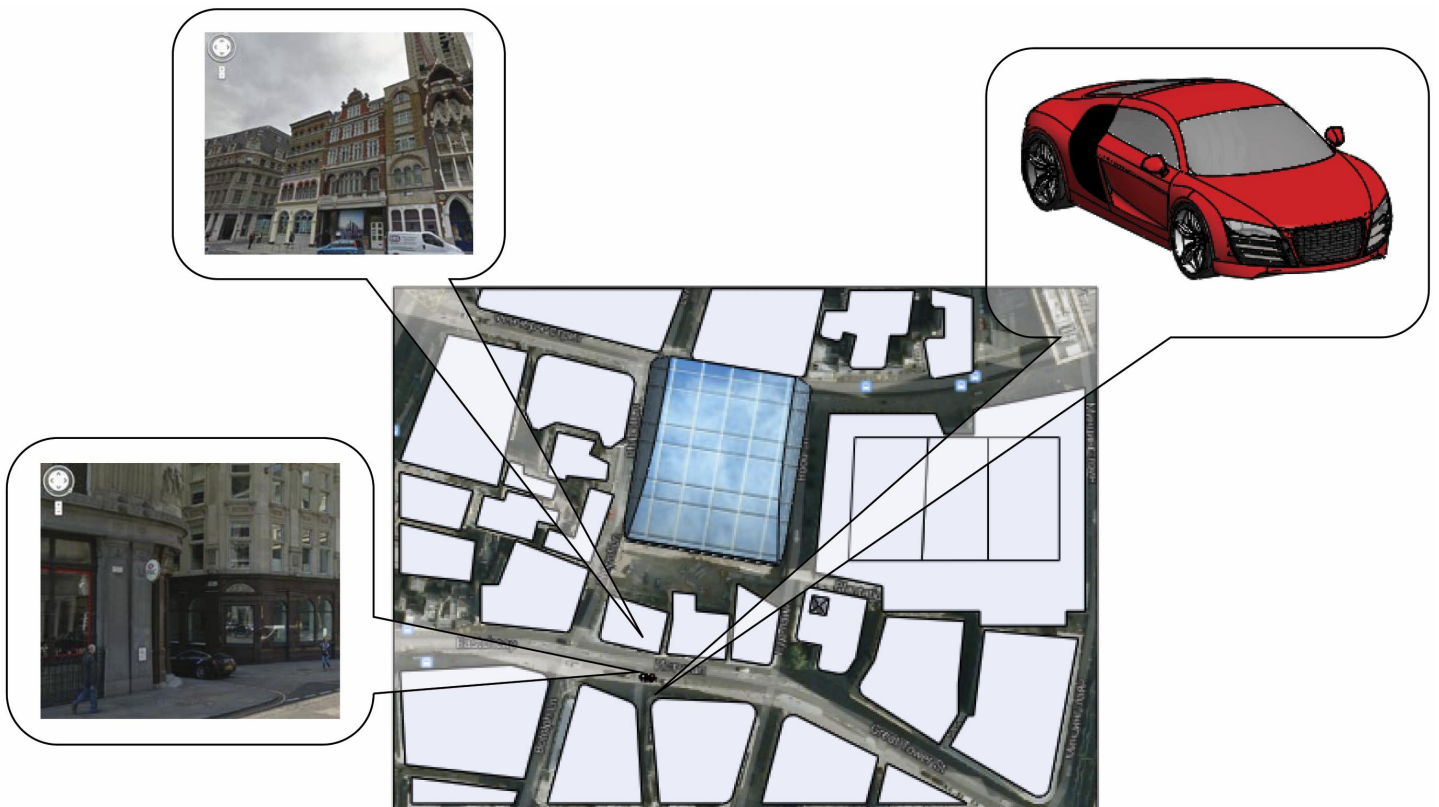
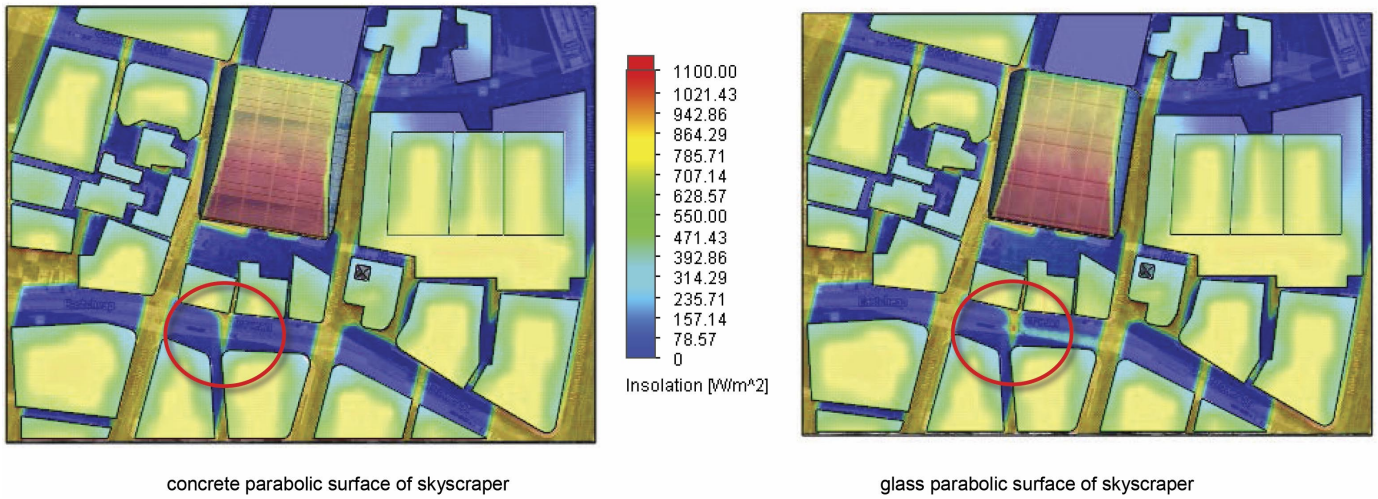


Figure 4. The CAD-model of the car parked on the Eastcheap Street on 29th of August.



concrete parabolic surface of skyscraper

glass parabolic surface of skyscraper

Figure 5. Comparison of solar radiation influence with or without focusing effect. The time is 12.40.

In order to simulate the melting effect of the wing mirrors, their materials were defined as plastic. For the car's shell material, steel was used. Figure 6 illustrates the solar radiation influence on the car parked on the southern side of Eastcheap Street near the crossing with Botolph-lane at 12:40. The focused insolation maximum reaches the car's bonnet (hood) and left wing mirror shell at this point. Its value is around 1300 W/m² which is about 1.5 times higher than the average solar radiation flux value (about 850 W/m²) relative to current location, day and time. According to the calculations, the focused insolation maximum is reached within the morning hours of the time period of 10:00 and 15:10. It is an incredible feat of luck for pedestrians that the focused area (about 2600 W/m²!) is occupied by buildings which is preventing more dramatic damage.

The temperature distribution shows the hottest area on the left wing mirror shell. The solar influence on the wing mirror surface lasted just ten minutes. This short time is enough to cause a considerable heating effect. Typically, a wing mirror has a hollow construction with thin plastic outer shell. Given these variables it is rather difficult to remove the heat inside the construction and therefore the plastic shell is forcibly heated. The softening temperature of the typical plastic materials used for wing mirror shells is around 100 °C, with the melting temperature at around 220 °C. The result in the simulation model exactly mimics the effect on Mr Lindsay's Jaguar: the most heated parts of wing mirror are hot enough to change shape or even melt (Figure 6).

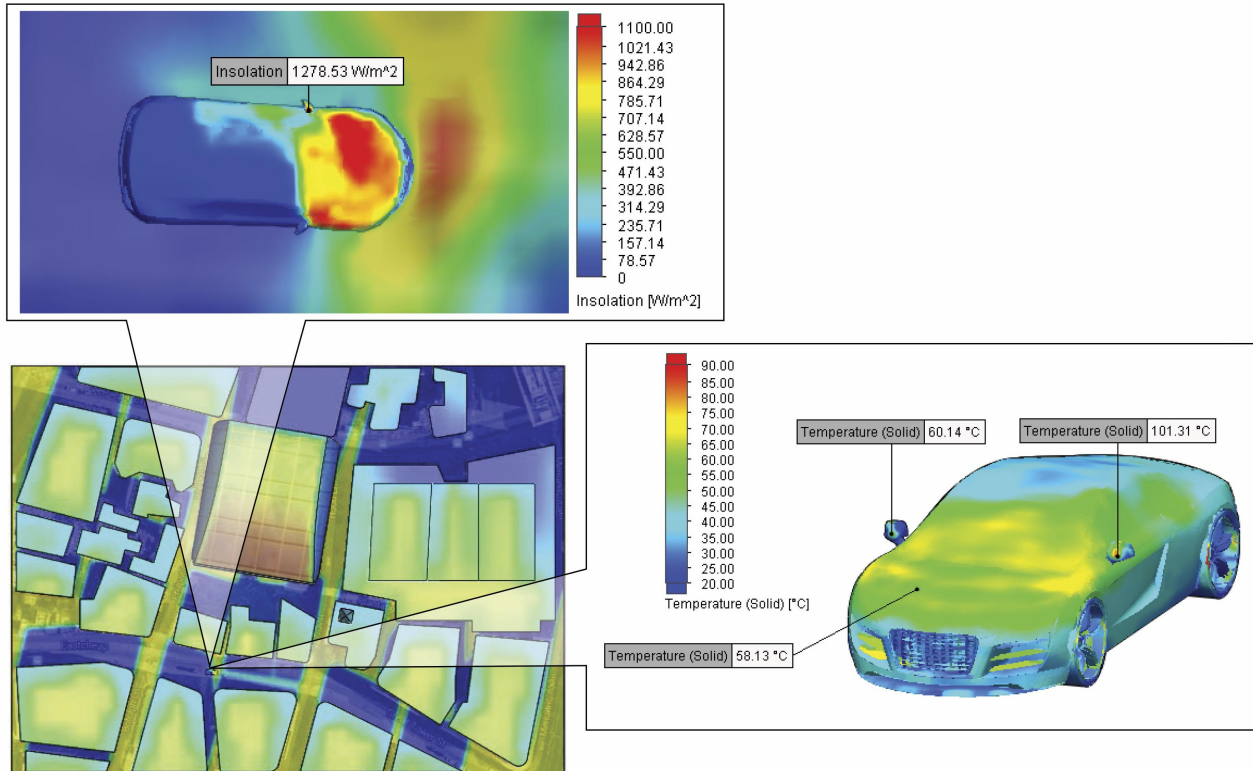
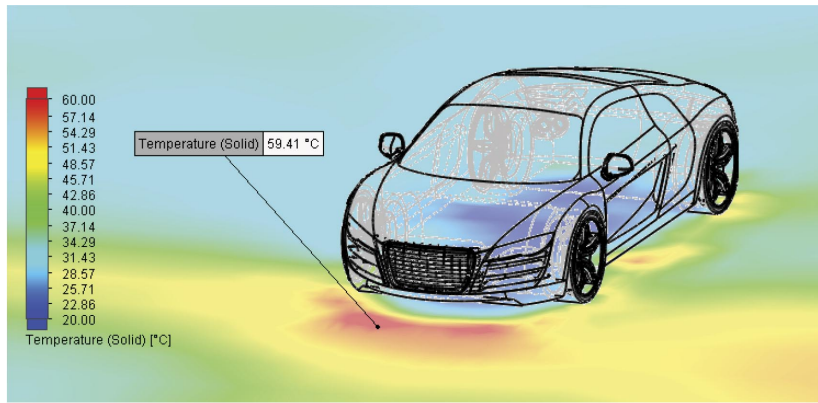


Figure 6. Insolation of all model surfaces and the temperature distribution on the car.



calculated temperature distribution

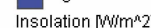
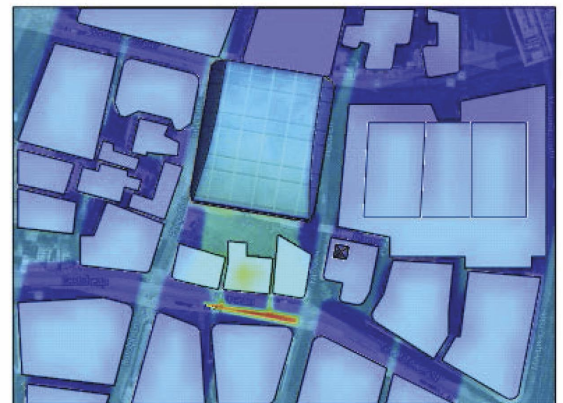
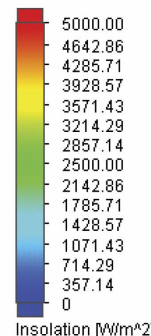
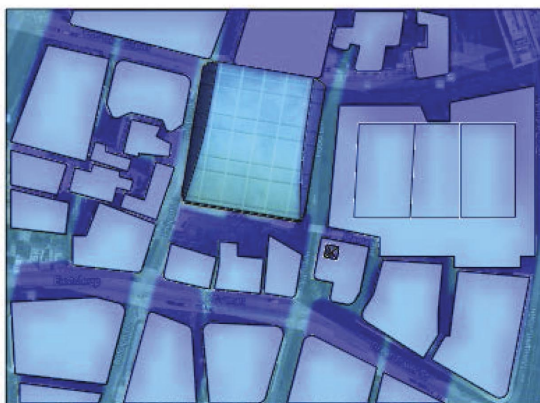
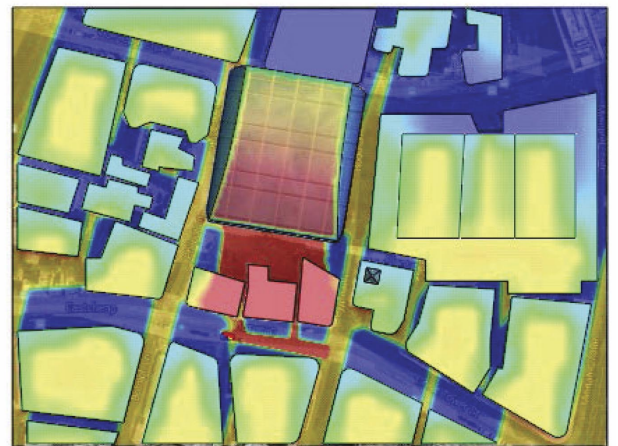
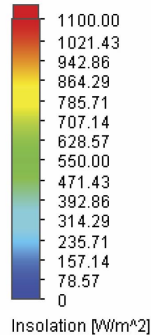
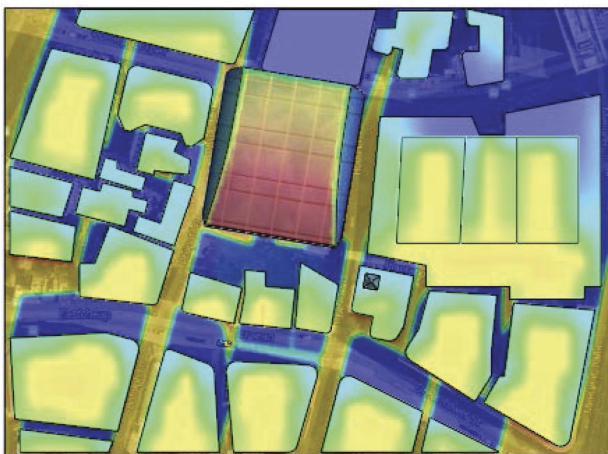
Figure 7. The pavement temperature distribution.

The measurement of the pavement temperature at the focused rays area was reported by local press as being around 59.5 °C. This fact was obtained in FloEFD calculations (see Figure 7):

The retrospective of the focus position and intensity was obtained under the assumption that the skyscraper front surface is made of ordinary glass. Its reflective properties are dependent on the incidence angle and other factors. Glass reflection forms a complex interaction pattern which is defined by ray optics principles. Perhaps this consideration was not completely taken into account in the design of the skyscraper. If even the ordinary parabolic glass surface

working as a giant mirror can scorch plastics, then how dangerous could it be with more reflecting materials?

Let us consider the extreme situation where the solar radiation flux value in focus reaches its physically feasible maximum. Obviously this is a case of total or mirror reflection when energy of incident solar flux is returned completely without absorption, and the angles of incidence and reflection for each surface are equal. The FloEFD simulation of total reflection shows that maximum of insolation at 12:40 is about 6000 W/m² (Figure 8). No doubt the consequences of such exposure would be more dramatic.



reflection of glass surface

mirror reflection

Figure 8. The pavement temperature distribution.

It is an incredible feat of luck for pedestrians that the focused area (about 2600 W/m²!) is occupied by buildings which is preventing more dramatic damage.

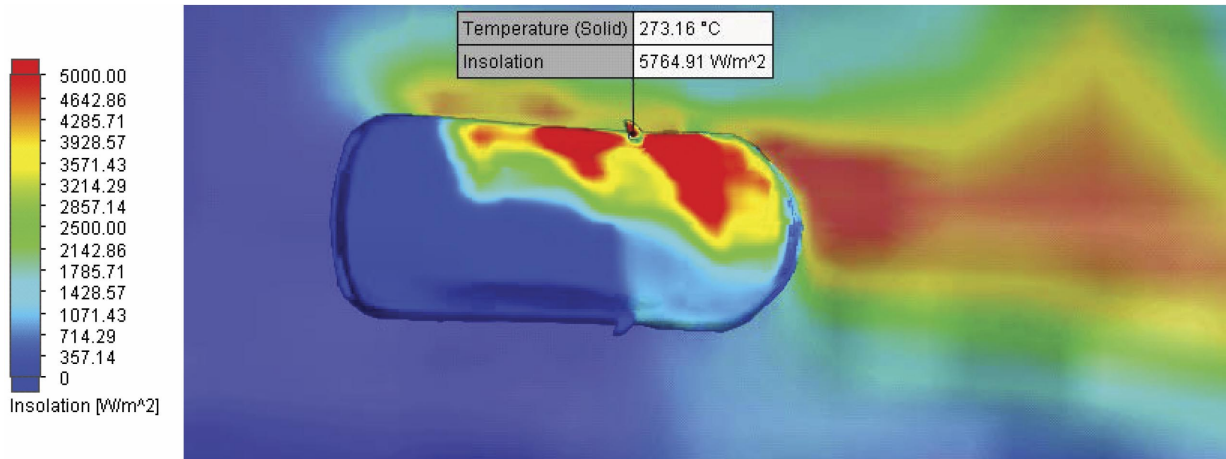


Figure 9. Insolation in the vicinity of the Mr Lindsay's Jaguar at 12 hours 40 min in the case of mirror reflection.

Conclusions

This example effectively illustrates designers and architects should not neglect the engineering analysis when designing complex structures. While designing an embedded item the interference of all components becomes a very important factor that can have an influence in all assembly operations. Using FloEFD, it is quite simple to explore various constructions under different conditions in detail. The reliable results of calculations are based on a consideration of geometrical optics as well as heat transfer specific data. The amount of engineering reference data that is available in FloEFD makes the designer's task easier.

For example in this task the parameters of solar radiation as well as the material's physical properties were defined by means of FloEFD's database. The use of FloEFD in the design of new structures is an effective way to prevent costly failures in the future.

References

1. <https://maps.google.com/>
2. <http://www.bbc.co.uk/news/uk-england-london-23930675>
3. <http://www.dailymail.co.uk/news/article-2410972/Walkie-Talkie-building-Walkie-Scorchie-skyscraper-firm-scaffolding-protect-nearby-shops.html>
4. FloEFD Technical Reference (2013)



/nafems



@nafems



/nafems

nafems.org

Characterization and Model Validation of Laminate Failure and Partial Damage in Industrial Applications

F. Köster and D. Moncayo
Daimler AG, Sindelfingen, Germany

Prof. Dr. F. Henning
Karlsruher Institut für Technologie (KIT), Germany

For an efficient analysis of the post-critical material behavior of fiber composites an appropriate balance between accuracy and abstraction is required to model the complex failure of composite structural parts under crash loads. The goal is not only a lightweight design of automotive components, but the best possible prediction of material damage and the correspondent failure modes. Based on current research studies, the presented validation strategy involves a standard material model and a recent constitutive model for laminated composites based on fracture mechanics and a set of physical based model parameters. An appropriate parameter identification and a necessary adjustment by using coupon tests and principle components is demonstrated for various laminate types and laminate thicknesses. These represent a contribution for a robust model validation in an early status of the model design.

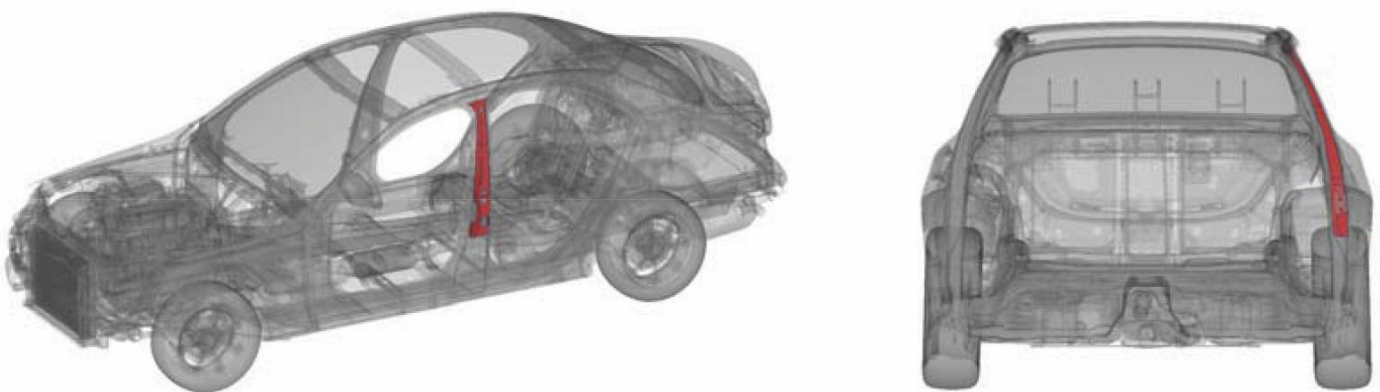


Fig. 1: Limousine with a glass fiber reinforced B-pillar

Introduction

After the successful application of fiber-reinforced components as structural components in the aerospace and aviation industry, the attention of automobile industry was drawn to the same light and stiff materials. The increased interest is driven by the potential to achieve a reduction of CO₂ emissions and an optimal consumption, while using the extreme lightweight potential of hybrid material configurations in structural parts. While for both industries the strength and stiffness values are considered for the design of parts, it is the automotive industry that orients its structural development towards achieving a damage tolerant solution through a very dynamic development process sui generis for the automotive sector. Hence, an understanding of the post-critical behavior of the laminate, as well as macroscopic deformations that lead to a partial degradation of the material properties have a crucial influence in a composite design. In order to achieve a high prediction quality in the crash simulation of fiber composite materials, the simulation methods require a high degree of effort. The use of valid material models, physically well-documented material parameters and an adequate discretization, especially for moderately thick laminates, is crucial for the development of computational methods. The representation of the morphological fracture in inhomogeneous materials is influenced by a variety of factors. In this study, the presented strategy requires a physical understanding of the correspondent parameter identification and model validation of each of the used material models, the specification of the used materials as well as the relevant details from the manufacturing process. In order to derive an appropriate interpretation from the simulation results using physical based material models leads, an extensive scope of experiments is required. Therefore, dealing with a new fiber-matrix configuration, a fast and efficient validation process is necessary, in a first phase of the material characterization process, as well as to develop a reasonable strategy for cumulative model validation.

The transferability of a defined set of material parameters depends on numerical robustness through the model validation process. In order to be accurate

enough for a certain material configuration and to be representative enough for similar fiber-matrix architectures, it has to be noted that the experimental characterization as a basis for the material properties, remains within certain limits, always an approximation of the physical reference.

Fig. 1 depicts a concept study for a limousine based on a glass fiber prepreg reinforcement laminated to the steel structural part.

This study presents an exemplary application of the material characterization process for this kind of glass fiber reinforcements. After a correspondent model validation, a step-by-step strategy (Fig. 2), through the different levels of part complexity, is followed until the final correlation in a full crash vehicle level is attained. An adequate method development for hybrid crash structures at the DAIMLER AG is not only focused on a mere part design but also on attaining an increased understanding in the development of damage tolerant structural parts. Achieving a better compromise between functional efficiency and manufacturing costs, will enable the analyst to develop a better and broader understanding of the utilization of composite materials.

Predictability of FRP components under crash loads

While metallic components depict a more distinctive plastic flow behavior before fracture occurs within the vehicle body, the laminate behavior of fiber-reinforced structures is characterized by a rather brittle heterogeneous and anisotropic behavior. A load path optimized laminate design is gained by multilayer composite parts. These utilize several unidirectional single layers with different angular orientations in order to allow a multi-axial load capacity. Under crash loads the structural response shows its highest stiffness at small deformations as the elastic regime in Fig.3 illustrates. In the subsequent phase the stiffness of the part reduces due to the initiation of damage. Partial damage defines the progressive concatenated failure of the laminate layers (see Fig. 3). The failure and fracture of further layers leads to a total laminate failure which results in a brittle chaotic fracture evolution.

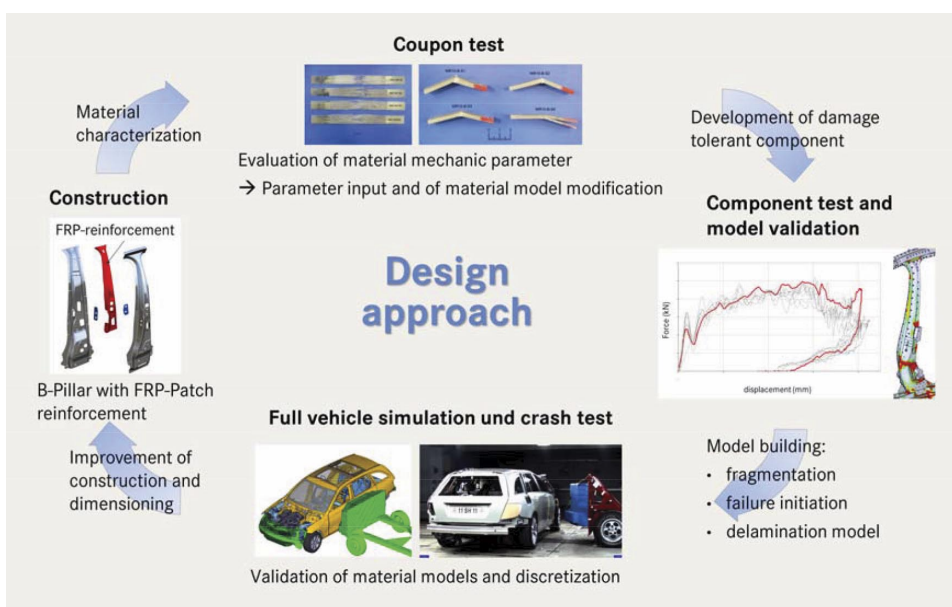


Fig. 2: Component development process with new materials

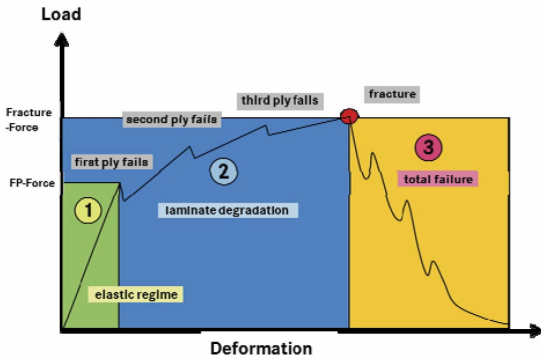


Fig. 3: Structural behavior of a multidirectional laminate under bending

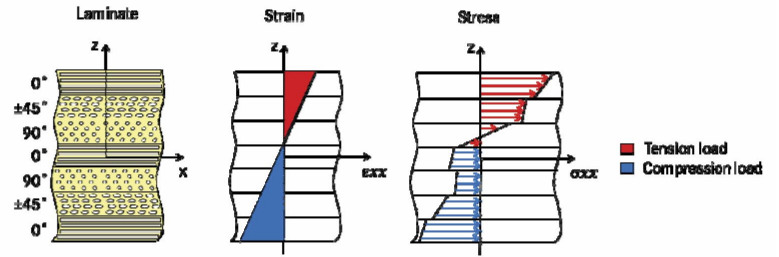


Fig. 4: Stress and strain distribution of a multidirectional laminate under bending [2]

A component design that is developed in order to prevent a "first ply failure" as maximum allowable laminate load, leads in consequence to an unnecessary over-dimensioning of the laminate. Therefore, the following criteria have to be considered (been introduced) for a weight-optimized design:

1. The material can be sufficiently exploited, then and only then, when all deformation states in areas of critical loads are taken into account.
2. All occurring possible loads of the component must lead to a homogeneously distributed laminate effort in order to prevent the oversizing of individual areas. This design usually leads to a more complex laminate layout with local reinforcements in critical areas. However, such a complex fiber layup-design complicates a cost-reduced industrialized manufacturing process due its increasing complexity. On the contrary, the analyst needs to reach a good compromise between both approaches for an adequate optimized layout design.
3. A load-path oriented design takes into account the highest amount of tolerable damage in the laminate and ensures a robust residual load capacity. The latter is decisive for the technical integrity of a structural supporting function for body-in-white components.

The above mentioned criteria present also a goal conflict between the geometrical component design and its functional response that has to be solved through an engineering process. For realistic evaluation of digital prototypes under crash loads, a correct prediction of the laminate behavior and the expected failure modes is crucial when choosing an adequate FEM tool. The quality of the structural analysis by simulation of different load cases has nowadays a direct impact on a fair use of composite materials within a conceptual design.

Limits of the classical laminate theory for Crash: Differences between thin laminates and moderately thick laminates

Due to the high complexity of current vehicle models and their digital representation, the calculation of crash load cases in the automotive industry is based on a single shell model structural representation. In the commonly used under integrated shell elements (ETYP 2), the through-the-thickness stress components are neglected [1]. The same plane stress state builds the basis for the "classical laminate theory" (CLT) to calculate the stresses and strains of the individual layers within large shell like composite structures (see Fig. 4). This simplification reduces the discretization effort, while increasing the expected numerical efficiency.

$$\begin{pmatrix} \sigma_1 \\ \sigma_2 \\ \sigma_6 \end{pmatrix} = \begin{bmatrix} Q_{11} & Q_{12} & 0 \\ Q_{12} & Q_{22} & 0 \\ 0 & 0 & Q_{66} \end{bmatrix} = \begin{pmatrix} \varepsilon_1 \\ \varepsilon_2 \\ \varepsilon_3 \end{pmatrix}$$

mit: $Q_{11} = \frac{E_1}{1 - \nu_{12}\nu_{21}}$, $Q_{12} = \frac{\nu_{12}E_2}{1 - \nu_{12}\nu_{21}} = \frac{\nu_{21}E_1}{1 - \nu_{12}\nu_{21}}$

$$Q_{22} = \frac{E_2}{1 - \nu_{12}\nu_{21}}$$
, $Q_{66} = G_{12}$

Fig. 5: Stress-strain relationship in laminate [2]

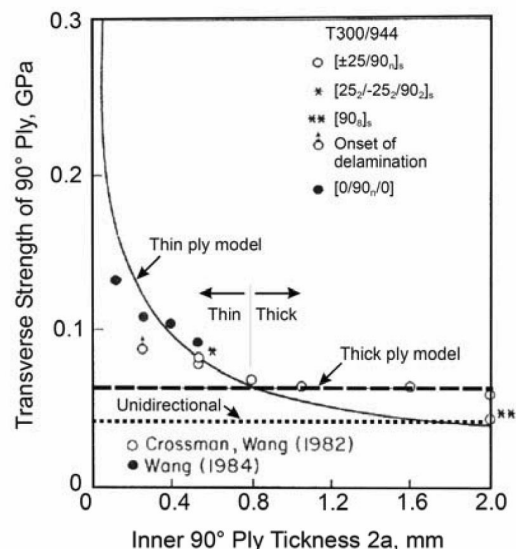


Fig. 6: Transverse tensile strength as a function of number of plies clustered together [4]

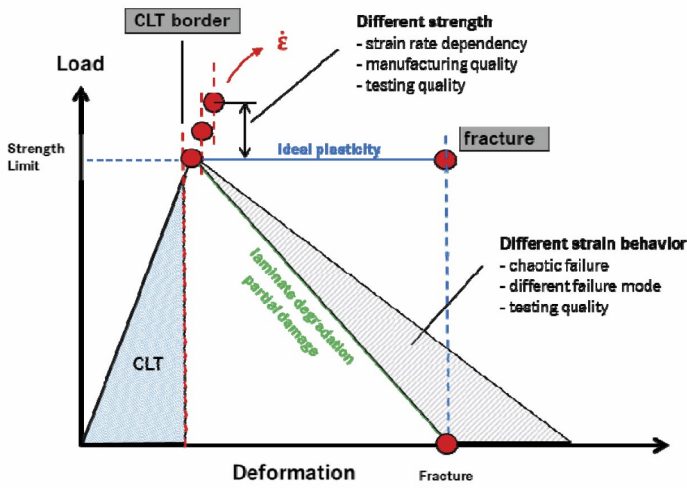


Fig. 7: Boundary of CLT and insecurities of material behavior

As direct consequence, all transverse strains ($\epsilon_{zz}, \epsilon_{xz}, \epsilon_{yz}$) and stresses ($\sigma_{xz}, \sigma_{yz}, \sigma_{zz}$) are neglected in moderate thick plates, as required are required for structural parts. [2]

Based on the homogenized young's modules E_1, E_2 and the correspondent poisson ratio ν_{12} for the orthotropic lamina, a set of macroscopic material relations for the elastic regime can be formulated.

For the stress-strain relationship in dependence of the elastic moduli and transverse contractions, the following relationship can be formulated (see Fig.5):

Applying the Kirchhoff plate theory, the following criteria prevent an erroneous calculation, and have to be considered:

1. The consideration is limited to an infinitesimally small element with single plies oriented parallel to the plane mid-surface.
2. Macroscopically homogeneous single layers with orthotropic elastic behavior and constant thickness are assumed.
3. The surrounding layers in the laminate have no effect on the elastic constants of the single layers. All plies are perfectly bonded to each other [3].
4. All forces and stresses cause only in-plane distortions ($\epsilon_{xx}, \epsilon_{yy}, \gamma_{xy}$). This means that a straight line to the mid-surface of the plate remains straight and normal to the deformed mid-surface.
5. These theoretical relationships are only valid for small deformations.
6. In-situ effects acting over the physical properties of the laminate correspondent to a particular manufacturing process are not considered.

Obviously, for crash analysis, there are several limitations through the above postulates that influence the further strategy for an appropriate model validation. Historically the CLT postulates applied for thin plates under in-plane loads and under

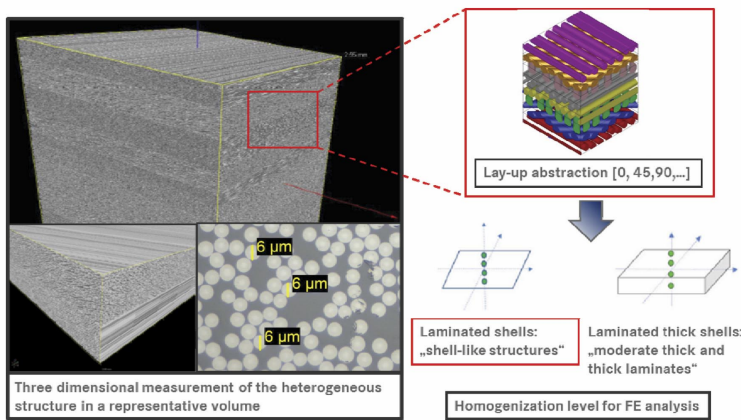


Fig 8: Microscopic analysis [6]

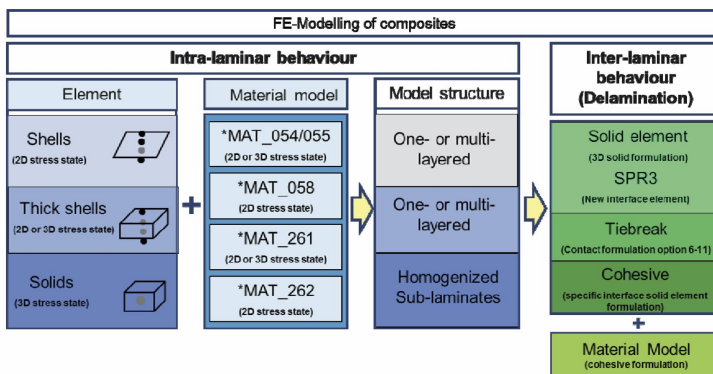


Figure 9: FE-Modelling of Composites [5]

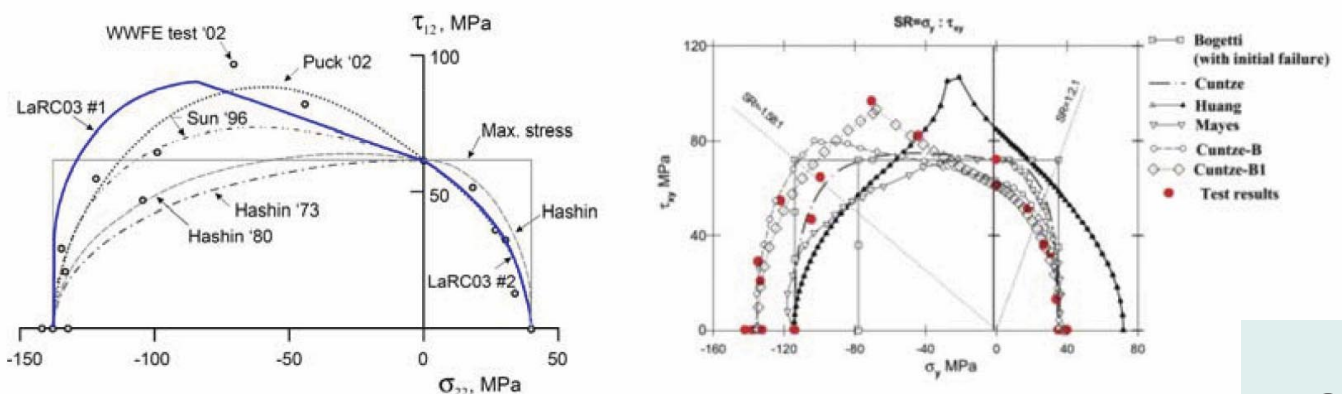


Fig. 10: Failure criteria [7]

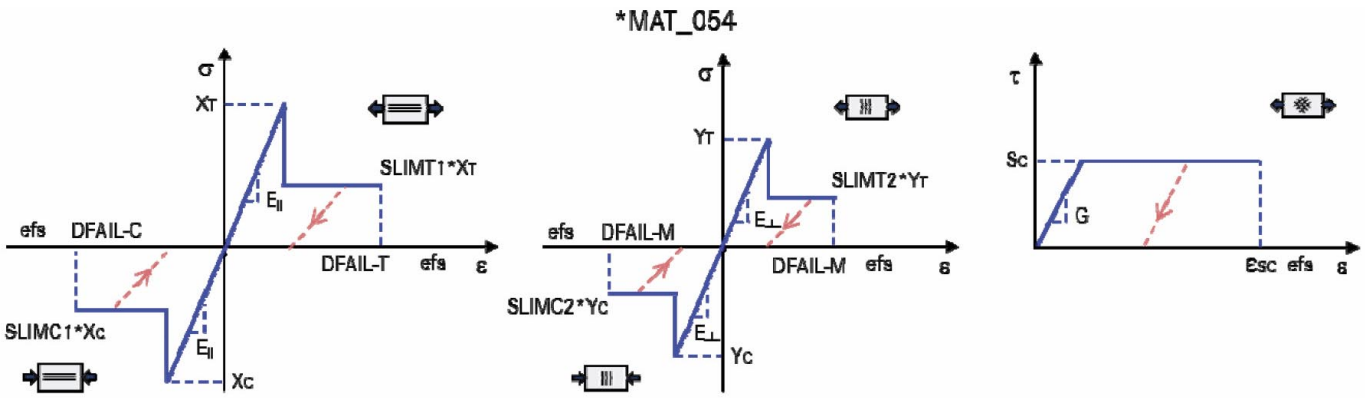


Fig. 11: *MAT_054 [8]

bending loads. Since this approach represents only a first evaluation of the laminate behavior, the crash analysis needs to be carefully reviewed. The validity through the evaluation of simulation results, at this stage, significantly depends on the interpretation quality of the analyst.

Considering the current structural composite parts for the automotive industry, the range of application represent the one correspondent to moderate thick shell like structures. The current computational efficiency considers characteristic element sizes in a range between 2 and 8 mm. If the characteristic element size is smaller than the overall laminate thickness, care has to be taken, since these approximation error would lead to a clearly loss of the prognosis capability of the numerical results. Structural components in automotive applications undergo bending and in-plane loads as well as a partial degradation of the material properties. This clearly defines the limitation of the CLT for the purpose of the crash analysis. The ply thickness within the laminate lay-up should also maintain a certain suitable range. Otherwise, the evolution of the through-the-thickness stresses in structural parts induces a partial degradation far lower than the correspondent strength limits for the ply. This, in consequence leads again to a non-linear material behavior which is out of scope of the CLT [5].

Materialmodels in LS-DYNA

Usually constitutive material models represent the laminate lay up in simple manner Fig. 8. Therefore the quality of abstraction while depicting a partial degradation of the laminate under crash loads depends on the quality of the homogenization process.

Prior to the characterization process for parameter identification, several factors have to be considered during the homogenization process:

- Fabric quality, (fiber topology, material, waviness, tow size)
- Manufacturing process (matrix infiltration, resin volume)
- Geometrical influence (draping, tailoring, adequate CAD)

While abstracting the physical unidirectional layer in an ideal configuration (Fig.8), the analyst has to evaluate and prioritize a set of parameters for a robust representation of the material properties. Not only in the elastic regime, but also in the post critical material behavior, where the conventional theories i.e. CLT do not apply anymore.

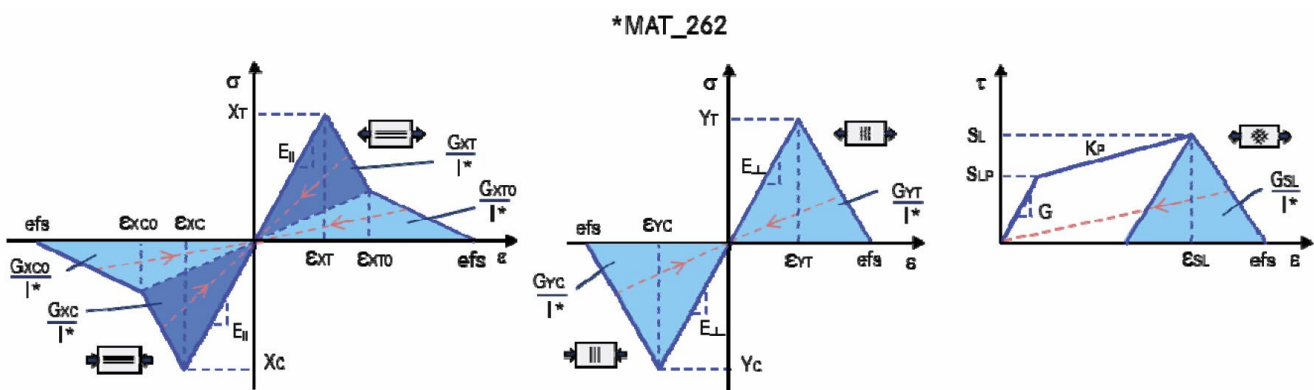


Fig. 12: *MAT_262 [8]

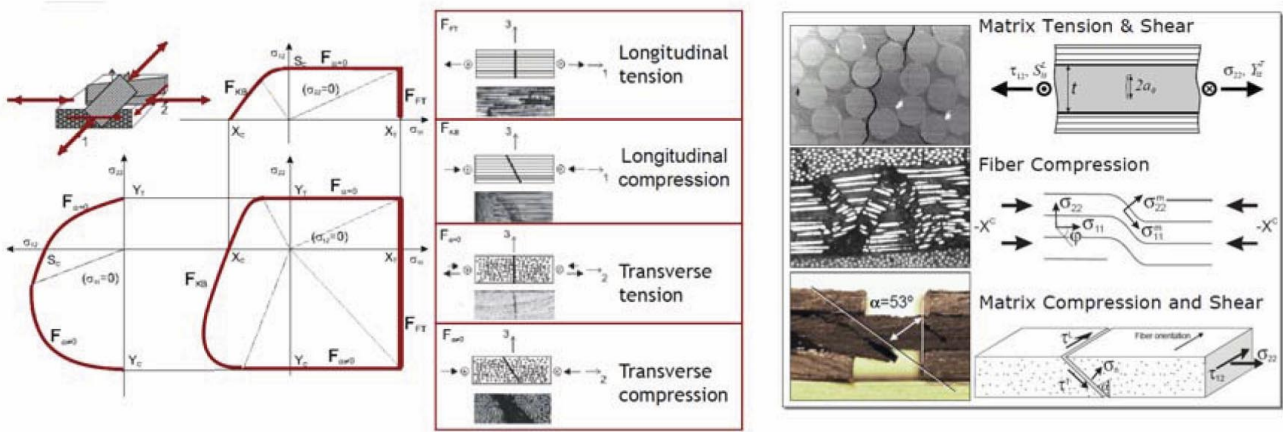


Fig. 13: LaRC Failure Criteria [11]

Further, the material properties should apply for a single ply, in order to reach an adequate prognosis of the laminate behavior independently of a lay-up configuration, material definition or a particular load case. Nevertheless an appropriate approach with sublaminates definitions can lead to a considerable increase of computational efficiency, while taking into account some loss of accuracy in the local material behavior unless an additional complexity for including interlaminar failure is introduced (Fig. 9)

An appropriate failure criterion for the crash analysis of composite materials has been discussed by several research studies over the past decades as depicted in Fig. 10. Although there are many publications that deal with important progresses [6], there is still a lack of consensus for an adequate multiscale approach in the analysis of composite structures for the automotive industry. The mere overview and diversity of theories available today does not create sufficient transparency to address the requirements of this continuously growing industry.

In this study two material models in LS-DYNA have been discussed. An adequate parameter identification, experiments on different structural levels and a comparison in their prognosis capability, lead to an improved step-by-step pragmatic understanding and handling of composite material parts in digital prototypes for automotive applications.

***MAT_ENHANCEDCOMPOSITE_DAMAGE**

This material model is an enhancement of the definition *MAT_022 which depicts a more sudden failure after exceeding the strength limits of the ply. This model is common used to represent unidirectional plies of a composite laminate. *MAT_054 [8] uses a Chang Chang criterion as the *MAT_022 definition.

The *MAT_054 definition has also other parameters to control the element erosion in a more numerical manner.

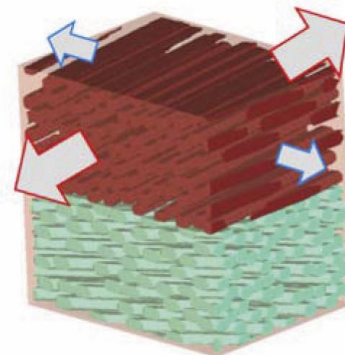
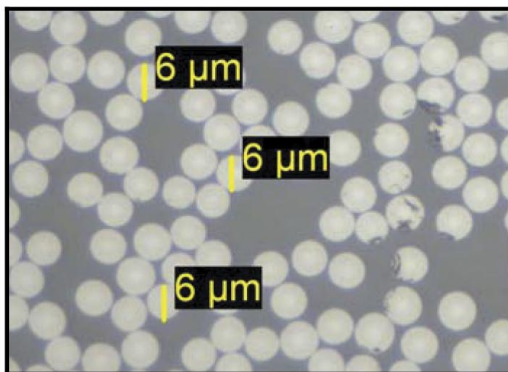


Fig. 14: real and statistical distribution of the fibers in the laminate [5].

Tensile fiber mode:

$$e_f^2 = \left(\frac{\sigma_{11}}{X_t}\right)^2 + \beta \left(\frac{\sigma_{12}}{S_c}\right) - 1$$

where $E_{11} = E_{22} = G_{12} = \nu_{21} = \nu_{12} = 0$

Compressive fiber mode:

$$e_c^2 = \left(\frac{\sigma_{11}}{X_c}\right)^2 - 1$$

where $E_a = E_b = \nu_{ba} = \nu_{ab} = 0$

Tensile matrix mode:

$$e_f^2 = \left(\frac{\sigma_{22}}{Y_t}\right)^2 + \beta \left(\frac{\sigma_{12}}{S_c}\right) - 1$$

where $E_b = \nu_{ba} = G_{ab} = 0$

Compressive matrix mode:

$$e_d^2 = \left(\frac{\sigma_{22}}{2S_c}\right)^2 + \left[\left(\frac{Y_c}{2S_c}\right)^2 - 1\right] \frac{\sigma_{22}}{Y_c} + \left(\frac{\sigma_{12}}{S_c}\right)$$

where $E_b = \nu_{ba} = \nu_{ab} = G_{ab} = 0$ and $X_c = 2Y_c$ for 50% fiber volum

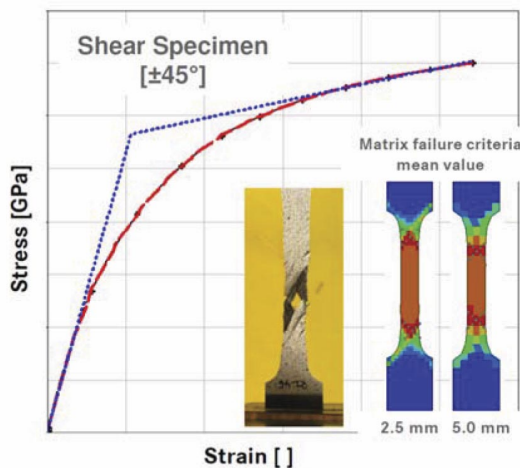


Fig. 15: Tensile test [+/- 45°] for model validation of the shear plasticity [6].

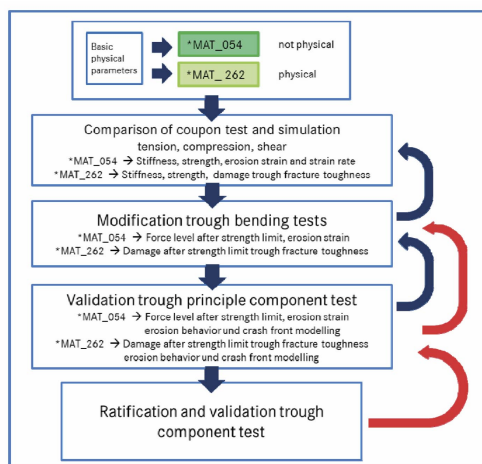


Fig. 16: Model validation strategy for industrial applications (robust conservative approach)

The *MAT_054 definition has also other parameters to control the element erosion in a more numerical manner.

Model parameters:

- DFAILM for limiting the strain of matrix in tension and compression
- DFAILS for limiting the strain in shear
- DFAILT for limiting the strain in fiber tension
- DFAILC for limiting the strain of fiber compression
- SLIMxx for reducing the stress level beyond the strength limit
- EFS defines an effective strain to control element erosion

Damage in the laminate can be represented through an ideal plasticity beyond the limits for strength. This can be explained by the fact, that local regions of a laminate undergo a common loss of strength in the fiber-matrix compound during a process of partial degradation of the laminate properties before a catastrophic fragmentation occurs. The strain values, for the failure of each ply, can be defined by a more ad-hoc manner. After the failure of all plies in the element has occurred, the numerical fade out of the element (element erosion) is triggered. A robust calibration of these values for the post-critical behavior (DFAILxx, EFS) leads to a tedious effort. Nevertheless this implementation represents a very pragmatic abstraction for layered materials and has been improved in the last years for its use in shell elements as well as for thick shell elements.

***MAT_LAMINATED_FRACTURE_DAIMLER_CAMANHO**

This is the *MAT_262 Definition in LS-DYNA based on the material model developed by Camanho [9], [10]. Here a constitutive model for the prediction of the onset and growth of intralaminar failure mechanisms in composite laminates under plane stress has been enhanced for industrial applications at a coarse mesh level. This definition applies for non-crimp fabrics as depicted in Fig. 12. Under tension, in fiber and matrix direction, the stress-strain relationship depicts a linear behavior until the strength of the ply. Under shear loads, this implementation depicts shear plasticity as it can be observed through experiments and presented in [6] before (Fig 12). This model can be used for shell element as well as for thick shell elements.

This Material considers four different failure mechanisms [8] that form the failure surface. Under longitudinal compression and transverse loads, a fracture plane is assumed and the loading functions are evaluated using a set of stress transformations. A 1-D elasto-plastic shear behavior is also considered to capture a pseudo-plasticity of partial damaged layered laminates under shear loads.

After reaching the limits of failure, a set of scalar damage evolution laws rule the degradation of the

physical properties. This material model assumes a plane stress state, a suitable assumption for shell like structures made of laminated fabrics.

The constitutive law of the material is expressed by:

$\boldsymbol{\varepsilon} = \boldsymbol{\sigma}$

H is the compliance tensor of the lamina, it is expressed by:

$$H = \begin{pmatrix} \frac{1}{(1-d_1)E_{11}} & -\frac{\mu_{21}}{E_{22}} & 0 \\ -\frac{\mu_{12}}{E_{11}} & \frac{1}{(1-d_2)E_{22}} & 0 \\ 0 & 0 & \frac{1}{(1-d_6)G_{12}} \end{pmatrix}$$

In this tensor, d_i represents the damage parameter. The different failure criteria are described as follow [8]:

Longitudinal fiber tension, (LaRC04)

$$\phi_{1+} = \frac{\sigma_{11} - \nu_{12}\sigma_{22}}{X_T} = 1$$

Longitudinal fiber compression, (transformation to fracture plane)

$$\phi_{1-} = \frac{\langle |\sigma_{12}^m| + \mu_L \sigma_{22}^m \rangle}{S_L} = 1$$

with:

$$\mu_L = -\frac{S_L \cos(2\phi_0)}{Y_C \cos^2(\phi_0)}$$

$$\sigma_{22}^m = \sigma_{11} \sin^2(\varphi^c) + \sigma_{22} \cos^2(\varphi^c) - 2|\sigma_{12}| \sin(\varphi^c) \cos(\varphi^c)$$

$$\sigma_{12}^m = (\sigma_{22} - \sigma_{11}) \sin(\varphi^c) \cos(\varphi^c) + |\sigma_{12}| (\cos^2(\varphi^c) - \sin^2(\varphi^c))$$

and

$$\varphi^c = \arctan \left(\frac{1 - \sqrt{1 - 4 \left(\frac{S_L}{X_C} + \mu_L \right) \frac{S_L}{X_C}}}{2 \left(\frac{S_L}{X_C} + \mu_L \right)} \right)$$

Traverse matrix failure, traverse compression / shear

$$\phi_{2-} = \sqrt{\left(\frac{\tau_T}{S_T} \right)^2 + \left(\frac{\tau_L}{S_L} \right)^2} = 1 \quad \text{if} \quad \sigma_{22} < 0$$

with:

$$\mu_T = -\frac{1}{\tan(2\phi_0)}$$

$$S_T = Y_C \cos(\phi_0) \left[\sin(\phi_0) + \frac{\cos(\phi_0)}{\tan(2\phi_0)} \right]$$

$$\theta = \arctan \left(\frac{-|\sigma_{12}|}{\sigma_{22} \sin(\phi_0)} \right)$$

$$\tau_T = \langle -\sigma_{22} \cos(\phi_0) [\sin(\phi_0) - \mu_T \cos(\phi_0) \cos(\theta)] \rangle$$

$$\tau_L = \langle \cos(\phi_0) [|\sigma_{12}| + \mu_L \sigma_{22} \cos(\phi_0) \sin(\theta)] \rangle$$

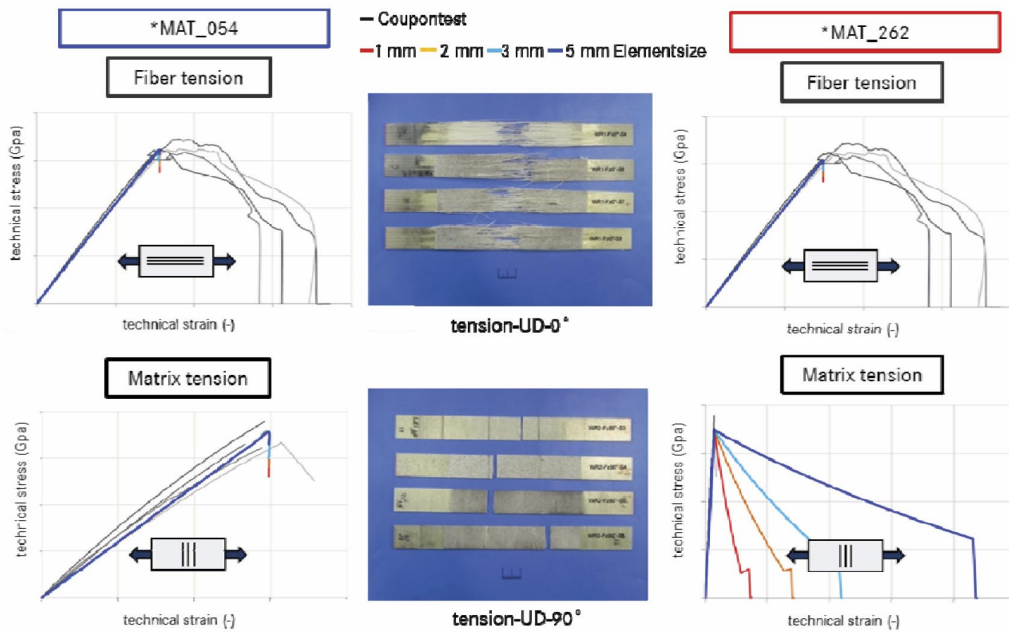


Fig. 17: Correlation of tension test and simulation

Appropriate material characterization for CAE Crash

The presented CLT applies to a macro-mechanical approach for modeling the material behavior and takes into account the different angular orientations of a laminate with single layers of anisotropic fiber-matrix material. In recent publications several approaches present a more detailed micromechanical model of the fiber matrix architecture. This kind of discretization can be used for a better physical homogenization of the material properties. Within this study, a pragmatic strategy has been chosen with focus on a user friendly representation of composite parts in large scale models to meet the needs of the automotive industry. From today's perspective, however, a micromechanical approach will lead to a very effective instrument in the homogenization procedure considering the current progress of the computational efficiency. This study

considers uni-directional prepregs with a high stiffness and strength in fiber direction and matrix-dominated properties with relatively low values in perpendicular to the fiber direction (Fig. 14)

Within this study the homogenization of the micromechanical components, represents a set of "smeared" orthotropic material properties for the ply. In micromechanics, the strength and stiffness are usually calculated by using the rule of mixtures and the resulting fiber volume contents. The basis for this homogenization relies on several simplifications such as the assumption of an ideal fiber-matrix adhesion and an ideal, homogeneous distribution of the fibers in the laminate which depict the reality only within certain limits. According to Schürmann [3], it is more productive to perform an adequate parameter identification of the material-mechanical properties by using coupon tests or so-called elementary test samples as shown in Fig 15.

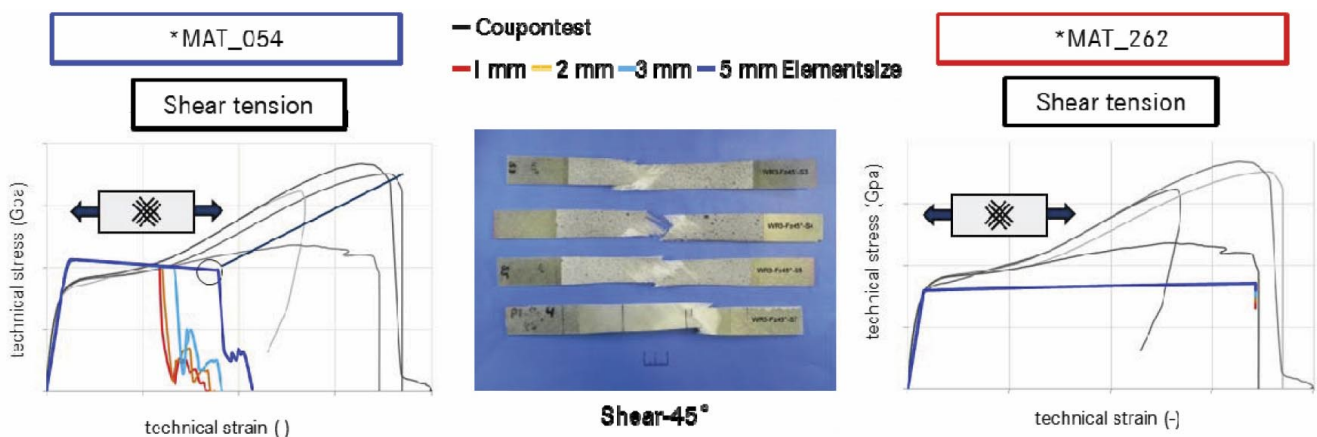


Fig. 18: Correlation of shear tension test and simulation

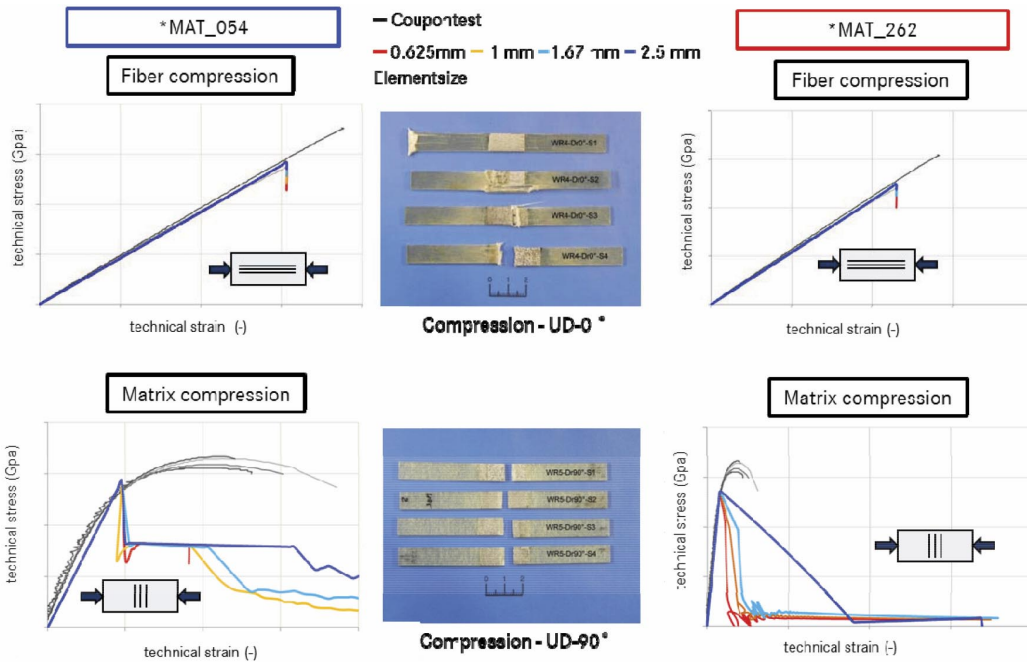


Fig. 19: Correlation of compression test and simulation

Material Characterization

As part of the development of methods for the simulation of crash structures, different fiber composites were tested for the reinforcement of metallic structures. In addition to the required mechanical properties of the laminate, the adequate selection of materials for a use in automotive structures plays a crucial role in terms of manufacturing, efficient draping, tailoring and costs. Within this study, a specific E-glass fiber prepreg containing boron is discussed, which is embedded in an epoxy matrix and processed into unidirectional prepregs. A pressing process at 160°C is used to drape the preform into a curing tool. The result is a final shape of a layered laminated structure with a fiber volume fraction of about 60%.

Material	Fibertype	Matrixtype	Fiber volume fraction	Single layer thickness
GRP-Prepreg	E-glass fiber	Epoxy-resin	60%	0.2 mm

Test program for material characterization

The initial test program of the material characterization for determining the physical material properties is based on a sample of coupon tests. Since both material models discussed here apply mainly for calculation of unidirectional non-crimp fabrics, the related parameter identification is conducted by unidirectional planar coupon tests. Five well known standard coupon tests for fiber tension, fiber compression, matrix tension, matrix compression and for shear tensile stress are performed.

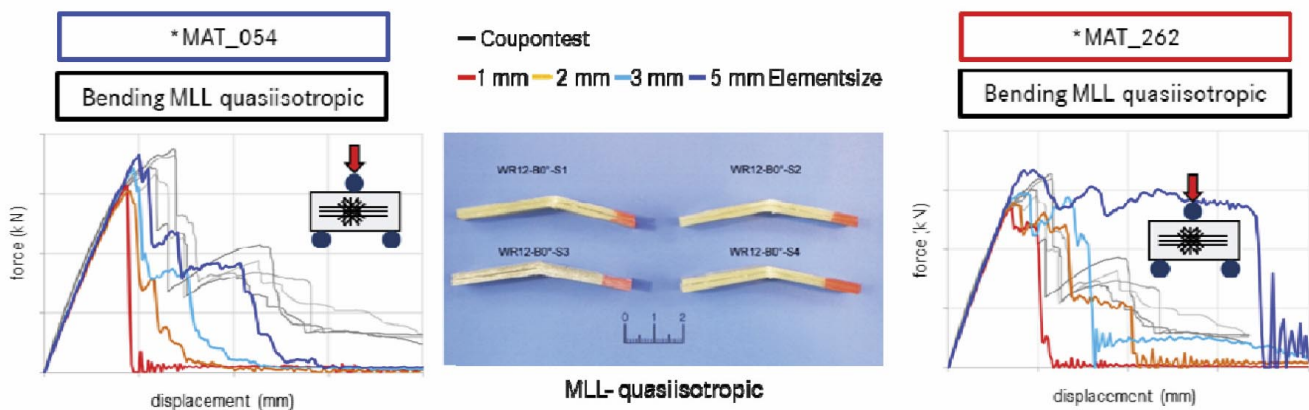


Fig. 20: Correlation of bending test and simulation

Tension longitudinal	Tension transvers	Compression longitudinal	Compression longitudinal	Shear tension
UD 0° 10 layers	UD 90° 10 layers	UD 0° 10 layers	UD 0° 10 layers	UD ± 45° 10 layers(sym.)

Tab. 2: Standard test for determining characteristic values

For the purpose of an adequate parameter characterization for the crash analysis, the strain measurements are taken out from a digital visual correlation using ARAMIS. The mere use of strain gauges for the strain measurement is rather counterproductive for crash analysis.

The related material parameters represent the effective macroscopically values in the specimen. This cannot be achieved by limiting the strain measurement to the simple local strain-gauge measurement and its failure. This again, especially for moderate thick laminates, is of high interest in industrial applications and crash analysis.

The experiments presented above are used for the measurement of the strength limits, the measurement of the in-plane young moduli (E_{II} , E_{\perp}) the poisson ratios (ν_{ab} , ν_{bc}), and for the measurement of the respective elongations (ϵ_{II} , ϵ_{\perp}) and the shear moduli (G_{II} , G_{\perp}) as well. The conducted tension and compression tests are carried out according to the standards DIN EN ISO 527-5 and DIN EN ISO 14126 as usual for the testing of fiber reinforced plastics. While for the simple parameter identification of the material *MAT_054 five of the conducted test are enough for gaining first approximation, physical based models like the development in *MAT_262 require an adequate identification of the fracture energies [12], as described before.

Therefore additional material tests as described in the literature by Pinho [4] are performed as well and considered for a first approximation. The following coupon tests for material fragmentation are conducted for the characterization of the material characteristics and for the measurement of the correspondent fracture toughness:

- Compact Tension
- Compact Compression
- DCB [ASTM D5528.01]
- ENF [DIN EN ISO 14180]

With the above mentioned experiments, a first approach for the mode I, mode II and mixed mode fragmentation and delamination is achieved. The values in the material card represent therefore a smeared homogenization of the intralaminar and interlaminar failure and fracture of the ply. These tests are discussed in [12], [13].

The theory shows that, the physical values of the fracture energy apply to a specific element size. Here the use of these homogenized values would limit the crash simulation of larger models with coarse mesh sizes. Therefore a calibration of these values with respect to the desired level of abstraction and mesh sizes is required. Fig. 16 shows the validation procedure for the input

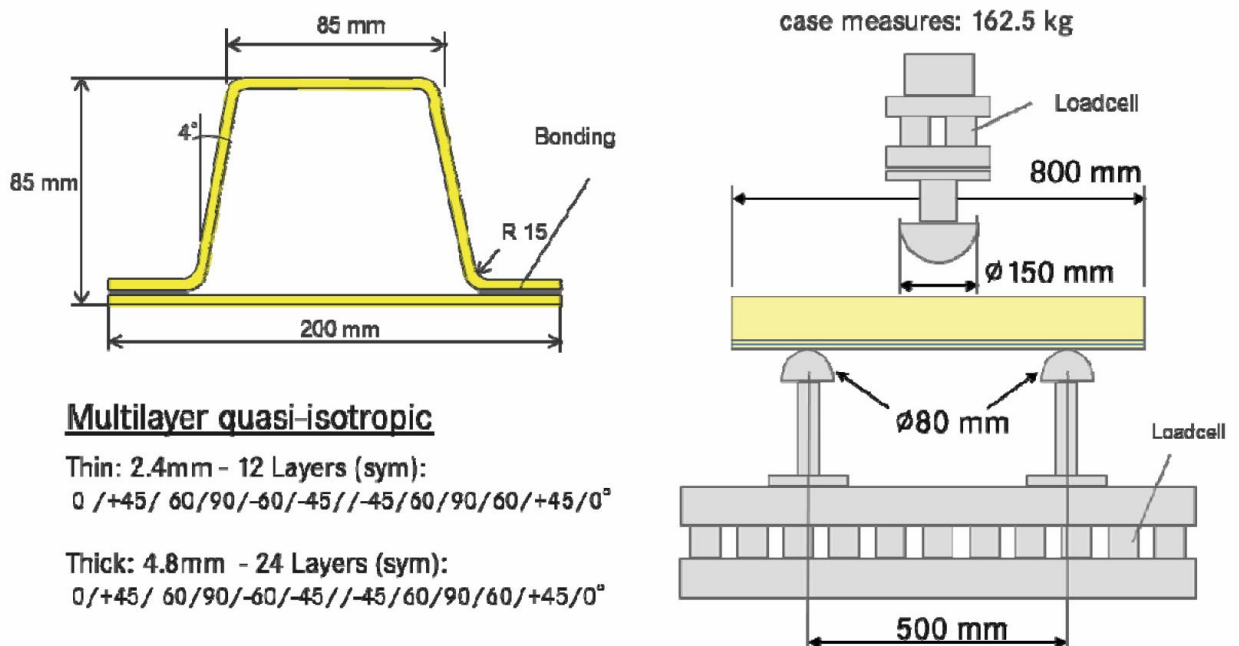


Fig. 21: Experimental set up, hat profile dynamic - principle component test

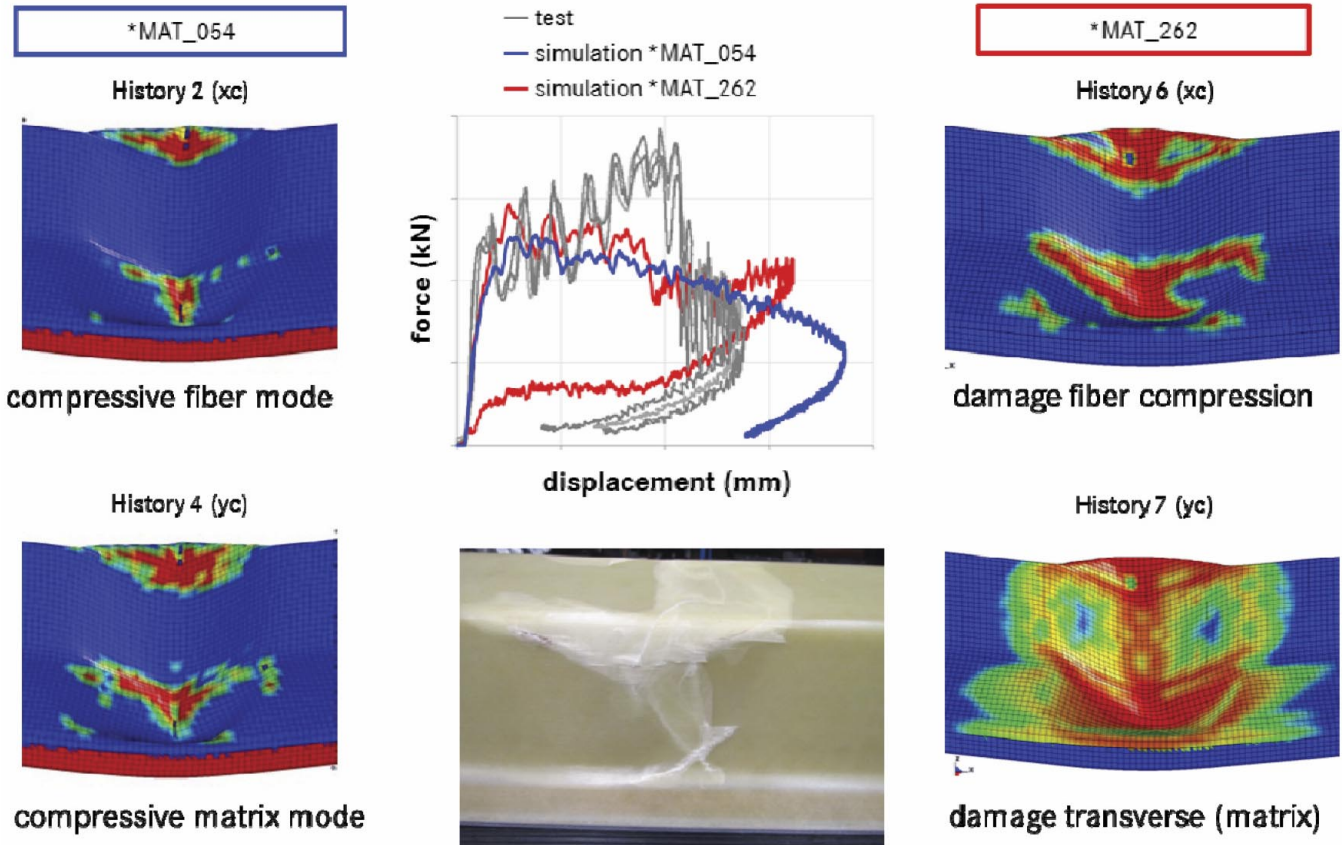


Fig. 22: Correlation component test and simulation of 2.4 mm hat profiles

parameters in the material card as proposed in this study, in order to guarantee a robust, cost efficient and conservative prognosis of the material parameters for industrial applications. The adjustment and calibration of the pseudo-plastic elongation in *MAT_054 and the correspondent fracture toughness in *MAT_262 are validated using bending coupon tests and hat profile tests under dynamic three point bending. The fracture toughness and the morphology of the fragmentation behavior need to be adapted to the real occurring post-failure behavior of the whole laminate. In a further phase of the presented model validation loop, component tests that show a higher geometrical complexity are used for a final model validation and correlation of the smeared mechanical properties of the laminate.

This captures, in very pragmatic way, certain inhomogeneities related to the manufacturing process into a robust prediction of the structural behavior of automotive parts in a digital prototype at larger scales.

Modeling of FRP parts for the crash simulation

The use of an appropriate modelling technique in automotive applications depends on the geometrical complexity of the parts. Reaching an adequate compromise between geometrical representations

(holes, flanges ...) and their structural answer under crash loads for depicting a robust prediction in CAE models represents the main challenge when dealing with different mesh sizes. To analyze a mesh size dependency of the material models all tensile coupons and 3-point-bending test coupons are simulated using element sizes of 1, 2, 3 and 5 mm. Compression test coupons are, modeled using element-sizes between 0.625 mm and 2.5 mm, due to a small width of 10 mm. Triggering a representative failure in the middle region of the homogenous mesh can be achieved with inducing a slight localization by a reduction between 0.01 and 0.1 mm of the coupon width. The strain analysis is geometrically similar to the test coupon by measuring the nodal displacements within the measured length of the coupon specimens.

Simulation results of model validation

Coupon tests in the simulation

The simulation of the tensile coupon tests shows for both material models, a correct reproduction of the used stiffness values. The main target of the presented modeling method is to keep the material parameters as far as possible unchanged within a physical based range. It can be observed, that the simple coupon tests from

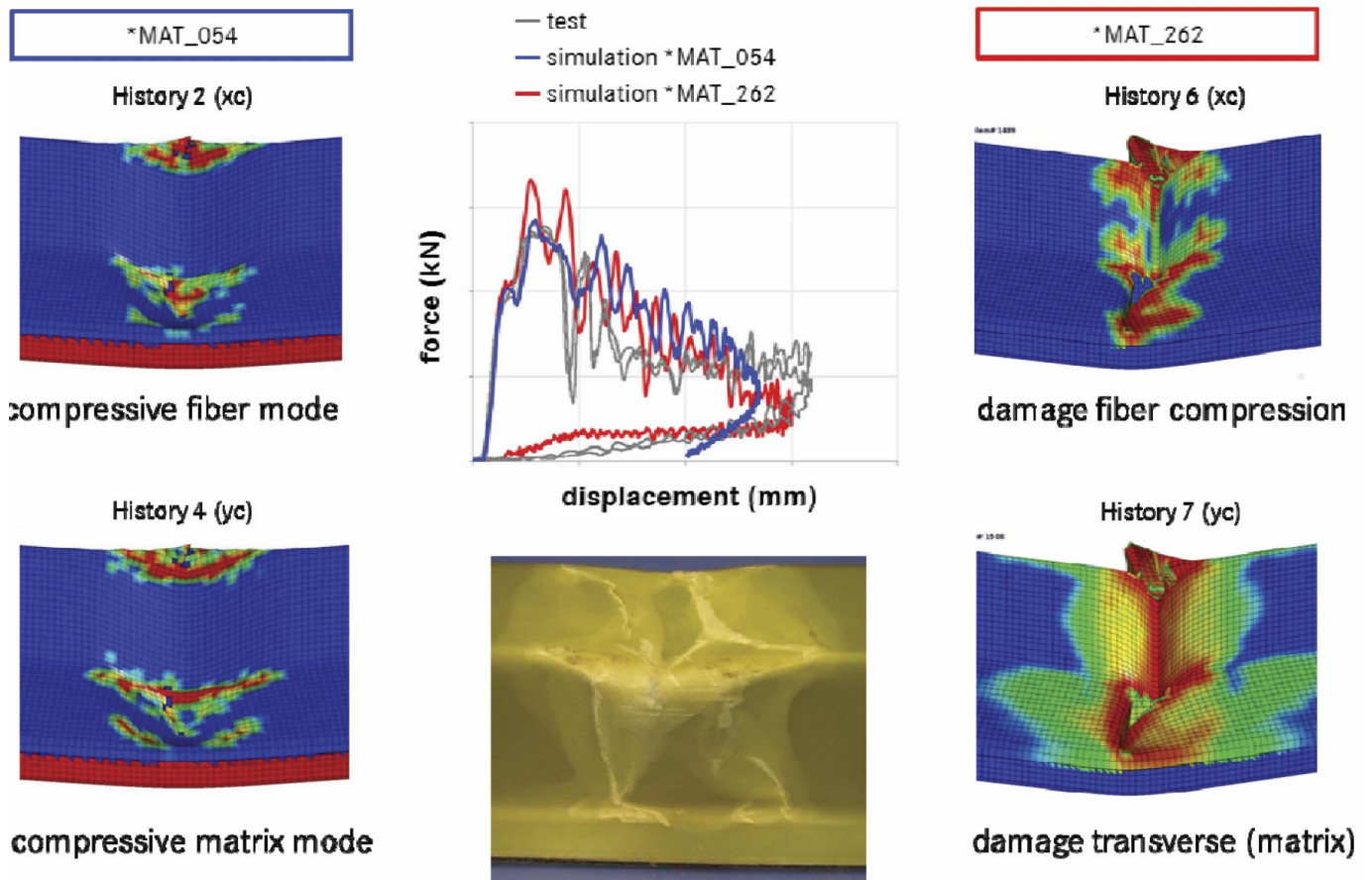


Fig. 23: Correlation component test and simulation of 4.8 mm hat profiles

simple unidirectional laminates are, in terms of stiffness, strength as well as the for the related failure strains are well represented in the analysis. Based on one-element tests and the results of [14], [15], [16], these results were expected. The depicted curves show the results for the simulation of the coupon tests after an extensive validation that is based on the correlation with principle component tests, such as the mentioned hat profiles. Therefore, a better representation of the real damage tolerance in multi-layer composites leads to an increase of the correspondent failure strains and fracture toughness for larger models and coarse meshes. This will be discussed later in this article. While the strength-strain relationship is correctly represented by the implemented criteria's in the unidirectional tensile coupons, an increase of the post-critical values in matrix direction is necessary within *MAT_262. The modified values related to the degradation of the material properties enable a high level of laminate abstraction using single shell layered models. This leads to a representative physical partial damage for coarse meshes that can be achieved considering the influence of the effective elongation of the elements at their mid-surface

The effect described as a "localization effect" is mentioned in the related Literature for the explicit solver LS-DYNA [17]. This kind of effect leads to an equal, percental elongation of all element sizes. In the simulation, a homogeneous damage development induces a properly functioning regularization of fracture energies. In the simulation of the shear tensile coupon tests, a good correlation for the first phase of the shear strength- strain relationship can be observed for *MAT_054 as well as for *MAT_262. Therefore, a certain amount of the physical strength values are increased, as considered through the material model definition in *MAT_054 for the shear. Until 8% strain within the strength -strain relationship for the shear is captured in an acceptable way. The main reason for this modification is to avoid a far too pessimistic pseudo-plastic behavior of the laminate at high strain values that would occur by the post failure characteristic beyond the shear strength limit.

For the component simulation of multi-layer composites with *MAT_054 the values for the shear stresses are considered to be small, for a pure shear plasticity and its

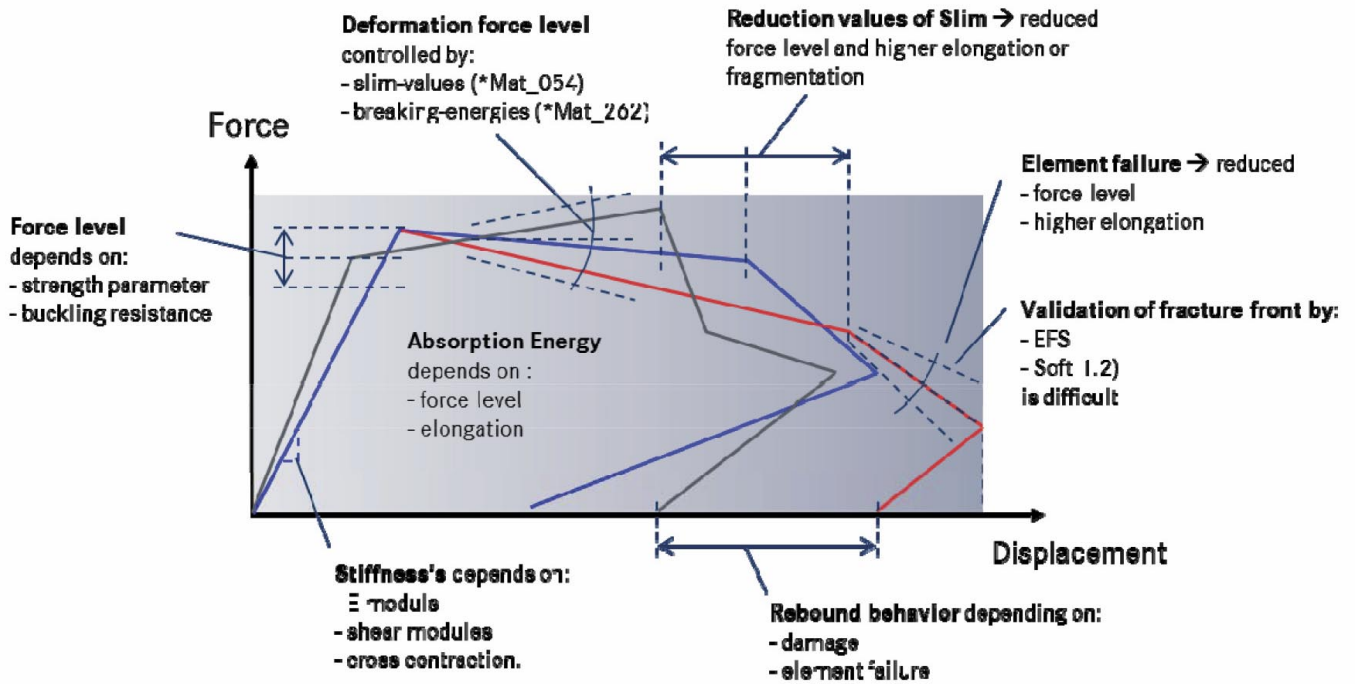


Fig. 24: Influence factors of the model validation in the force displacement diagram

incomplete correlation as depicted in Fig. 18 is considered less critical because elongations of more than 5% are usually not practically achieved. The rise of the non-linear force levels for the shear caused by the change in fiber orientation at high strain values can be adjusted by a pragmatic implementation of the bilinearity due to a shear plasticity implementation, as captured only by *MAT_262. The simulation of the compression coupon tests in fiber direction shows that both material models can fulfill the strength criterion in an ideal manner. In the experiment, a sudden buckling failure of the 10mm wide coupons occurs, and due to the high fiber stiffness a clean experimental capture of the compressive properties is difficult to attain. A further discussion on the proper geometry and physical test procedure for the compression coupon tests goes, at this stage, beyond the scope of this study. The force curves for the compression coupon tests evaluation also show a perfectly planar behavior and the correspondent linear result is captured in the simulation including, obviously, the correspondent in-plane element failure. In the compression coupon tests in matrix direction, the experimental procedure induces a slight buckling of the laminate, which is, in a strict manner, not intended within this test procedure. This leads to a diffuse strength limit and a non-linear force-displacement characteristic in the experiment. Both material models show the conducted validation through the presented hat profiles, a strong plastic, element size-dependent strain curve. Numerically, both models maintain within this study physical values and model parameters based on the experimental measured strength and strain limits. This strictly conservative pragmatic way is a requirement for a physical correct abstraction. It is well known that matrix failure caused by

delamination or intralaminar matrix cracking does not lead automatically to the catastrophic failure of the laminate, but it induces a partial degradation of the laminate which requires a higher abstraction level, when dealing with the compressive behavior of single layered shell models. A damage tolerant adaptation of the material card with a larger plastic matrix strain and increased fracture energy is attained by the validation process and shows some discrepancies for the correlation with the experimental behavior of pure unidirectional coupon tests under sole unidirectional loads.

For this validation procedure with *MAT_054, the failure parameters DFAIL_M and DFAIL_C are increased by a factor of three. In consequence, an early matrix failure of the elements for the simulation of three-point bending test of a quasi-isotropic lay-up is avoided on the compression side of the coupon. However, a compromise must be found. Under this circumstances, an increase of these parameter values lead to a pessimistic localized failure at smaller element sizes. When using fully integrated elements (Element-type 16), a significant improvement of the above mentioned effects can be achieved. Caused by cracking effects occurring in the matrix and delamination of the layers, the coupon specimen loses its bending stiffness. By reducing the correspondent slim-factor (SLIM2_C) for matrix compression the pseudo-plastic strain considering a reduced force level represents a more realistic material behavior. In *MAT_262 this effect is accomplished by increasing the fracture energy for the matrix fraction, in a more pragmatic way.

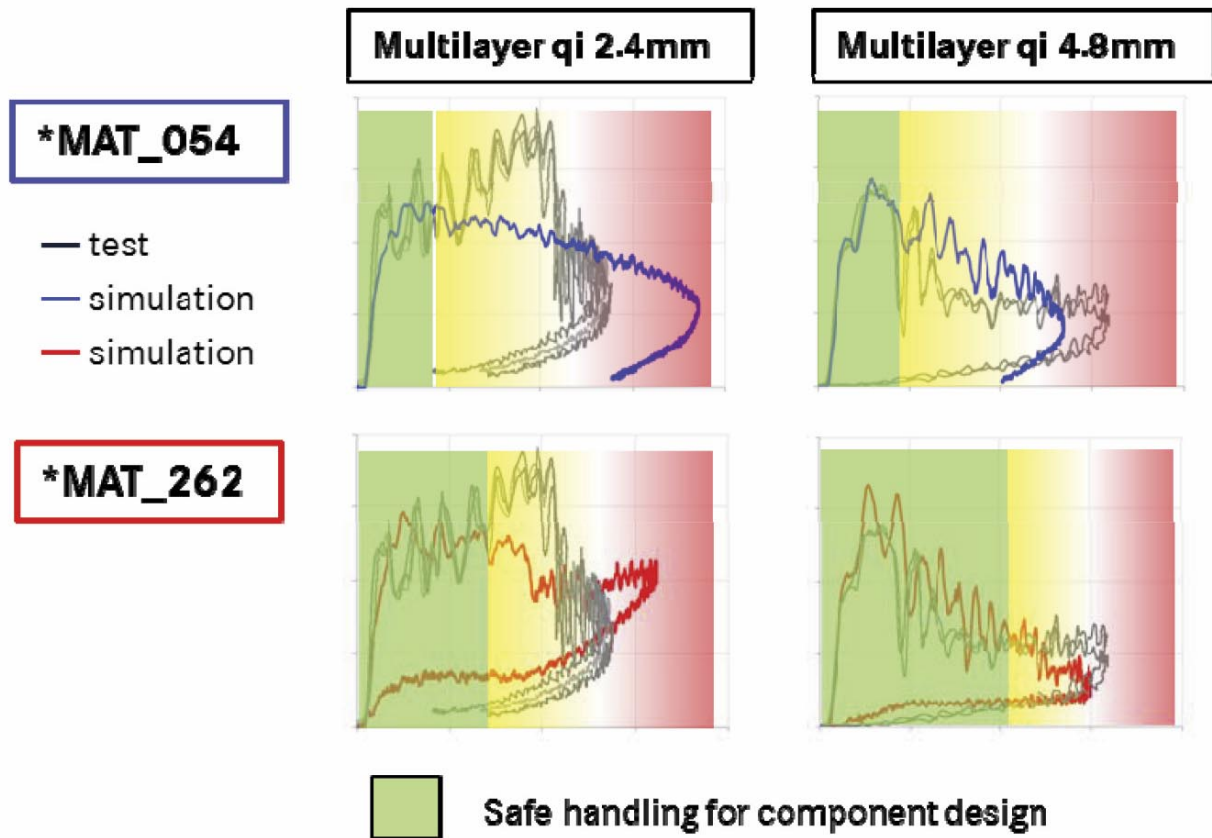


Fig. 25: Areas of prediction quality in the force displacement diagram

Considering element sizes through the correspondent parameter identification between 3 to 5 mm is part of the presented procedure for an effective model validation that meets the requirements of an industrial application. Therefore, as mentioned before, it must be noted, that small element mesh sizes (1-2 mm) are not suitable for an effective analysis of moderate thick composites, such as 3.2 mm thick laminates, due to the lack of improper accuracy (limits of the CLT) by the use of these mesh sizes for predicting the laminate behavior.

Hat profiles in the simulation

At a higher level of geometrical complexity, dynamical three-point-bending tests were conducted using hat profiles as depicted in Fig. 21. For the model validation capturing the effects through the laminate thickness in the macroscopic laminate behavior, two kinds of laminates, a 2.4 mm and a 4.8 mm thick, quasi-isotropic layered structures are tested. To avoid the pull-through of the different hat profiles, all the thin profiles were tested with 450 J, the thick profiles were tested with 1800 J.

The goal is to reach a similar deformation behavior of all different profiles. Maintaining a constant mass for the impactor leads, due to different energies, to a different correspondent impact velocity and therefore to a bandwidth of strain rates considered in the proposed procedure for model validation. In the experiment, some areas undergo clearly a tension load; also a compressive

failure is clearly visible with the induced areas of delamination failure. The most important point in the validation of the material card, at this phase, is to reach a good agreement among the force level F and the correspondent deformation S . For the final prognosis and the achieved accuracy are crucial, limiting and representing the application range of the material cards, this considers:

- a high predictive quality of the force displacement curve for different laminate thicknesses
- a layup independent prediction quality
- a good evaluation of the failure modes by history-variables (structural integrity)
- a correct prediction through the loading and the unloading performance of the laminate, the rebound of the impactor and after impact.

The hat profile simulations and the three-point bend coupons have shown a good agreement of the initial stiffness and the initial force levels with the experiments. Both models can represent the increasing level of force, which is based on the delayed buckling failure of the profile edges. The necessary higher SLIM values and correspondent increased fracture toughness lead, for thick laminates, to a predicted raised force levels in post strength area. In the scope of this paper, influences through the manufacturing process are neglected. In a

first step, the goal is to achieve a set of parameters that are representative enough for thin laminates and moderate thick laminates as well. This is necessary in order to avoid a not over-optimistic structural behavior at different laminate thicknesses.

By using the history variables of the correspondent material routine, the individual laminate loading and the correspondent damage states can be verified. The damage, mainly induced by compression loads and superimposed with bending stresses of the hat profile, can be well evaluated for *MAT_054 by the damage variables "compressive fiber mode" and „compressive matrix mode ". For *MAT_262 the damage variable "damage fiber compression and" damage transverse direction" depict well the damaged areas. The damage variable "damage in transverse direction" shows for *MAT_262 a better resolution of the laminate effort and can be used as an indicator for delamination prediction and tendency. The significantly stiffer profiles show in experimental and simulation almost the same buckling behavior of the side flanks. But the developing kink failure and deformation mode shows one buckle instead of two.

The 4.8 mm thick laminate specimen shows zones of a massive laminate degradation without exhibiting a macroscopic cracking. In the simulation the significant crack development, which is triggered by the parameters of the "effective failure strain" (EFS) and by the concerted crash-front parameters (soft 1 u. 2) achieve a rather conservative element erosion as depicted in Fig. 23. While both models represent the intralaminar matrix failure adequately, a realistic prediction of interlaminar delamination behavior is still conservative with *MAT_262 but not adequate for *MAT_054. The force level after the laminate strength limit controls the adjustment of the correspondent slim factors and fracture toughness, and lead to a reduced displacement correlation compared to the thinner hat profiles. An increase of the mentioned values, in order to achieve a good correlation for thin and moderate thick laminates, shows the need of a compromise, as result of the chosen discretization bandwidth to be covered, and the used material modeling. Again, important differences between the different model approaches depict obviously the need of a closer look into the discretization method. Fig. 24 describes the factors that influence the model correlation between experiment and simulation for a typical application in the automotive industry, considering here, a shell like structure under bending loads.

Fig. 25 shows the areas of good correlation between simulation and test results. For the analyst it is finally important to know the limits and quality of the calculated simulation. According to current state *Mat_262 shows a better forecasting accuracy with regard to force-displacement correlation and the laminate evaluation by using the history variables.

Conclusion:

The material modeling of continuous-fiber reinforced composites requires usually a material characterization

and a tedious simulation validation process due to a very complex failure and an heterogeneous material degradation. In addition to a comprehensive understanding of the micro-mechanical structure and the correspondent fracture modes, the use of valid numerical models gain a crucial importance for the automotive industry. Because of the diversity of the possible fiber textures - matrix material configurations, a fast prediction capability through valid digital prototypes at larger scales increase the efficiency through the technical development process. This is, for the component development of damage tolerant automotive structures, of special interest, since crash load cases are part of the structural requirements to be fulfilled and are not just a misuse scenario. To exploit the weight-reducing potential of introducing fiber-reinforced, shell-like structures in the dimensioning process induces also the need to allow and represent an adequately tolerable partial fragmentation of highly loaded areas of structural components. This study has the goal of developing a robust pragmatic procedure in order to achieve an acceptable representation of the structural behavior of composite parts beyond the elastic regime. It demonstrates that, for certain applications, the prognosis capability achieves an acceptable quality for the use of digital prototypes in an early stage of the dimensioning process. A defined method for the abstraction of composite structural parts can be applied to new material configurations, within a range of diversity, and thus reducing as far as possible the complexity through the presented validation process. Again, this leads to the need for a robust prediction capability. The presented method introduces a pragmatic parameter identification for two common material models in LS-DYNA. Comparisons between the implemented failure criteria have been shown as well. *MAT_054 depicts a "pseudo-plasticity" after the failure criteria in the element is reached. The further failure of the element is strain-controlled on a reduced pre-defined constant strength level. *MAT_262 considers an effective damage model implementation with a bilinear softening of the stress values and a progressive crash destruction after the strength limits.

As conclusion, it can be remarked that the physical based implementation of the postulates from [9], [10] achieve a good description of the material behavior as observed in the conducted experiments. In addition, the implemented damage variables show a more accurate representation of integrity of the laminate and its damage development. Taking advantage of the introduced history variables for evaluation purposes in the *MAT_262 definition, the analyst can take now conclusions about the interlaminar, intra-laminar and trans-laminar failure propagation. These prediction capability leads to an efficient abstraction for shell like structures using single layer shell models. Finally, the presented procedure has been ratified successfully through an extensive model validation in larger applications, dimensioning structural components. Nevertheless, further investigations at the DAIMLER AG will be used for a continuously increase of the predictive power in crash simulations.

References

- [1] Livermore Software Technology Corporation (LSTC), LS-DYNA theory manual, 2006
- [2] Reddy, J.N.: Mechanics of Laminated Composite Plates and Shells, 1997
- [3] Schürmann, H.: Konstruieren mit Faser-Kunststoffverbunden, Springer Verlag, 2007, S.220
- [4] Pinho, S.: Modelling failure of laminated composites using physically-based failure models, 2005
- [5] Moncayo, D.: A semi-analytical approach for the homogenization of the physical properties in unidirectional laminates, based on the classical laminate theory, DAIMLER AG, to be published
- [6] Moncayo, D.; Kögl, M.: Challenges for the Structural Analysis of Composite Structures in Automotive Applications, (Daimler AG), Moncayo, Dyna-Forum, 2012
- [7] Hinton, M.; Soden, P. D.; Kaddour, A.: „Failure Criteria in Fiber-Reinforced-Polymer Composites: The World Wide Failure Exercise“, Elsevier Science, Auflage 1, 2004
- [8] Livermore Software Technology Corporation (LSTC), LS-DYNA keyword user's manual Volume II - Material Models, 2014
- [9] Maimi, P.; Camanho P.P.; Mayugo, J.A.; Davila, C.G.: A continuum damage model for composite laminates: Part I – Constitutive model. Mechanics of Materials 2007, 39:897-908
- [10] Maimi, P.; Camanho, P.P.; Mayugo, J.A.; Davila, C.G.: A continuum damage model for composite laminates: Part II – Computational implementation and validation. Mechanics of Materials 2007, 39:909-919
- [11] Camanho, P.P.: Analysis models for advanced composites, Workshop on Composite Laminates, University of Porto and DAIMLER AG, 18.09.2009
- [12] Catalanotti, G.; Camanho, P.P.; Xavier, J.; Davila, C.G.; Marques, A. T.: Measurement of resistance curves in the longitudinal failure of composites using digital image correlation, Composites Science and Technology 70 (2010), 1986-1993
- [13] Gomes, J.: Crashsimulation / Modelling and Simulation of Compact Compression (CC) and Compact Tension (CT) Tests for CFRP and GFRP Materials, FEUP / DAIMLER AG
- [14] Mildner, C.: Numerische und Experimentelle Untersuchungen des Crashverhaltens von FVK-verstärkten Metallstrukturbauteilen, 2013
- [15] Schweizerhof, K.; Weimar, K.; Münz, Th.; Rottner, Th.: Crashworthiness Analysis with Enhanced Composite Material Models in LS-Dyna – Merits and Limits, 2001
- [16] Maimi, P.: User material damage model for laminated composites, User Guide, Daimler AG
- [17] LS-DYNA Composite Notes, DAIMLER AG, 2014

HPC - The Genesis of SDM

Mark Norris, the SDM Consultancy

The first commercial SDM platform was deployed into production on BMW's HPC on 19 December 2000 (ref 1). Virtual Insight, the platform for BMW's CAE Bench solution, had been developed by a visionary team at Silicon Graphics, the HPC provider. The Munich-based SGI Professional Services team had decided to develop a technology framework to enable the development of domain solutions for HPC users. Virtual Insight was designed to enable the automation of data-set management; to assemble sets of data, transfer the data to the HPC and then collect and collate the results. The idea was to reduce the data management overhead on simulation experts whilst providing traceability of results, thus enabling analysts to submit more jobs on HPCs.

BMW and SGI pioneer SDM

At BMW, Dr Michael Holzner and his team had refined vehicle crash simulation to the point that it was sufficiently accurate to replace physical testing for business decisions. This meant that multi-hundred-million-dollar decisions were to be taken based on numerical simulation alone. Only later would these be validated by crash testing of pre-production vehicles. Simulation was now business critical and Dr Holzner successfully argued that a "Simulation Data Management" solution was required to ensure the quality and traceability of business-critical simulations. It was unthinkable that a data or process error could be allowed to adversely impact business decisions of this magnitude. Michael Schlenkrich, then of SGI, managed the project to develop the CAE Bench SDM solution on the Virtual Insight platform to deliver the quality assurance and traceability that Dr Holzner sought. CAE Bench reduced the data management overhead on expert users as predicted by Dr Schlenkrich, who, with Dr Holzner, maintained a focus on helping engineers to do their work throughout the project. The many automation scripts developed by individual analysts were validated and deployed in the SDM solution so that all analysts could benefit.

Audi take SDM to the next level

Dr Holzner left BMW to join Audi and further develop their vehicle simulation capability. He repeated the success of CAE Bench by commissioning a Virtual Insight-based SDM solution for Audi. This time the emphasis was on growing engineering throughput, initially by automating process documentation by automatic meta-data capture. Dr Holzner acknowledged a 35% gain in engineering throughput with the same staff(ref 2). Audi took SDM for automotive vehicle simulation to the next level by co-developing with MSC Software the Simulation Generator which automates the assembly of the FE model. This enables part changes to be incorporated with minimal effort. This approach was then modularised at Audi with the use of LoCo for assembly(ref 3&4) The Audi SDM solution automatically assembles the FE model and collects an average 200 meta-data objects to define the audit trail(ref 5). The

implementation of model assembly, results extraction and the creation of lightweight viewables next to the HPC minimises the data traffic between the analyst's workstation and the HPC. This is an important enabler for HPC or cloud computing. It also enables global working, as analysts can be located anywhere.

SDM helping the Analyst

Analysts are not only freed from the laborious task of recording ~200 items of information per simulation manually, but a capable SDM system can also manage the Information Lifecycle (ILM). Whilst the metadata, key results and viewables are retained, large files of raw data are automatically deleted after a set period, unless the analyst sets a flag to retain them. Some output files are compressed using lossy compression tools such as FEMzip. Reichender reported that BMW currently persists 700 terabytes of mainly compressed simulation data which equates to automatically deleting more than a petabyte per year(ref 1). BMW migrated from its custom CAE Bench solution to the standard, configurable SIMmanager SDM2.0 solution in 2013. Using extended data management automation, BMW recently passed the milestone of 2,000,000 vehicle simulation data sets created and under management. This equates to an 800 gigabyte database holding close to 200 million objects.

Airbus brings SDM to CFD

In the European aerospace domain, the Airbus teams had improved their CFD algorithms to the point that they were "able to deliver quantitative results such as flight drag/lift values with quite a high precision in large parts of the flight domain" in an overnight run, replacing wind tunnel testing. As numerical simulation became the basis for engineering and business decisions, Thierry Chevalier echoed the same thought process as Michael Holzner: once simulation replaces physical testing for important engineering and business decisions "strong data management, with trace-ability and to enable repeatability of numerical simulation" is a high priority. Airbus elected to develop a specific SDM, AeroCity, for their distributed European CFD teams.

Top Down or Bottom Up?

While Audi chose to adopt the first commercial SDM platform and build functionality on top of it, Airbus chose to use a commercial workbench, ModelCentre, and underpin it with a solution built from standard, industrial strength data management building blocks from Oracle(ref 6). Most importantly they built the capability which is at the core of SDM: to create the simulation process history in the database, independent of the individual files. CFD engineers on any site can trace processes and data and then re-run processes when inputs change. They have the freedom to re-run automatically if the change is minor, or repeat the analysis adapting their assumptions and methods to the

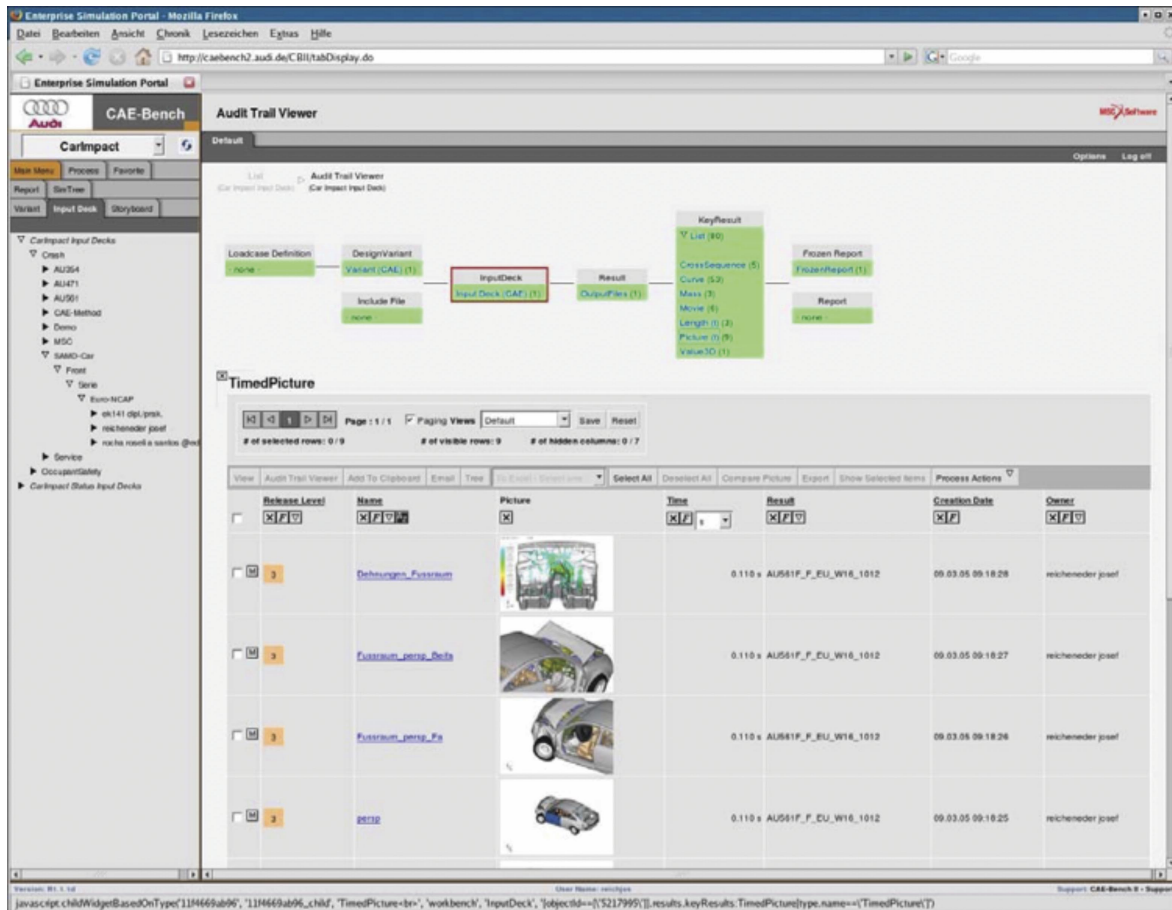


Figure 1: Access to Intellectual Property through search or audit trail at Audi (ref 3)

modified physical situation.

At the recent SimBest conference in Manchester, England, Nadir Ince of GE Power asked the audience "How long it would take them to find the data to re-run that analysis?" without an SDM solution. At BMW, Audi and Airbus a decade or more of simulation data and millions of results are available instantly through a browser see figure 1. The Intellectual Property of the engineering organisation is searchable, accessible, traceable, verified and secured. Beyond appropriate governance, increased productivity and the elimination of laborious non-value added tasks, it's access to the IP from the HPC that is the true added value of SDM.

References:

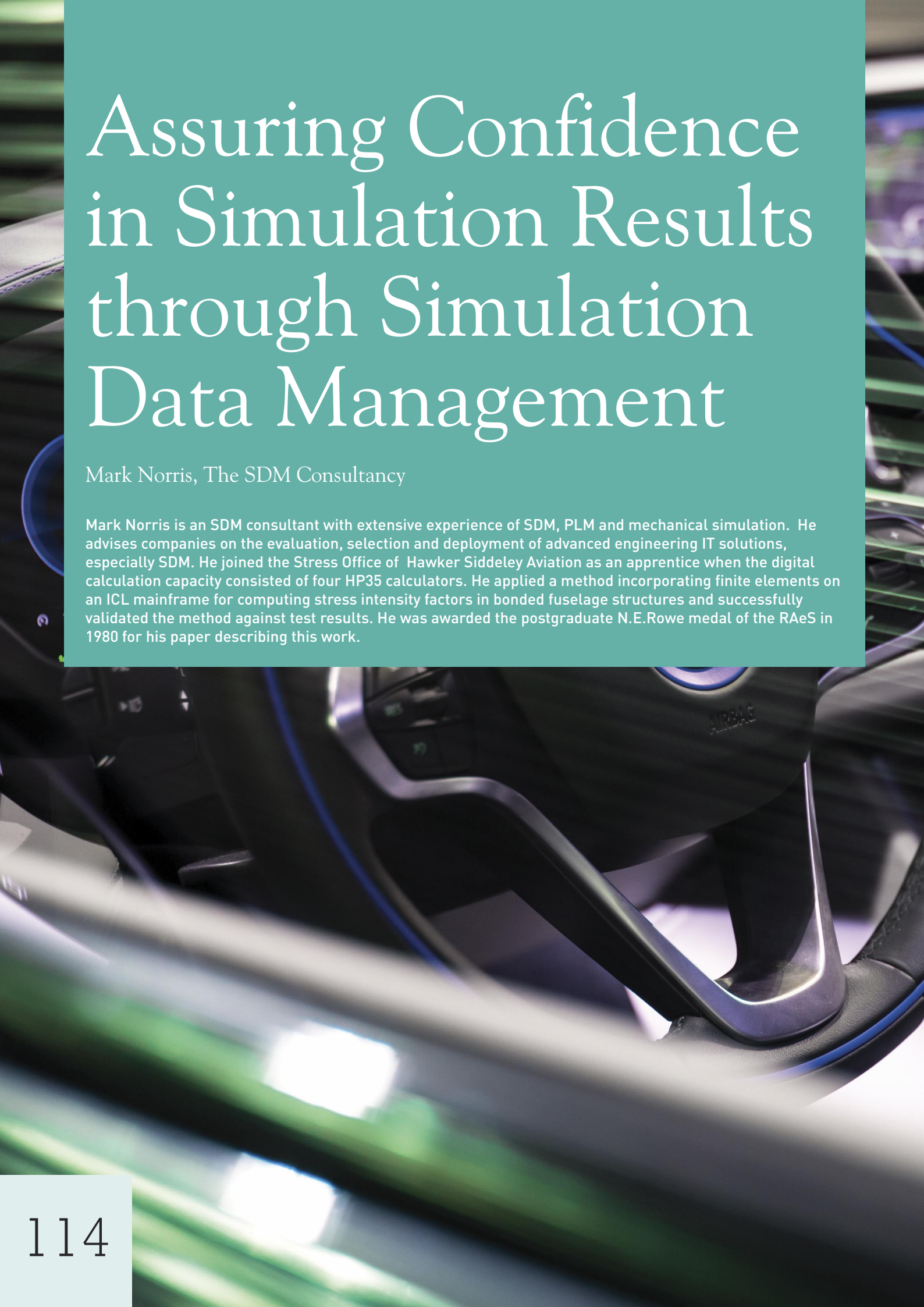
- [1] REICHENEDER, Josef 15 Years SPDM@BMW, NAFEMS European SPDM conference, December 2015
- [2] NORRIS, Mark Business Value from SDM, A Decade of Production Experience NAFEMS White Paper 2012
- [3] GRUBER, Karl REICHENEDER, Josef BAUER, Stefan KEUL, Manfred. CAE Process and Data Management at Audi. NAFEMS Weisbaden 2009.
- [4] BECK, A J GRUBER, K Simulation Data Management and Process Chain at Audi NAFEMS European SPDM conference 2015

- [5] LAYFIELD, Dale MCINTOSH, Larry MAYER, Stefan, NORRIS, Mark ROSINA, Milan. Oracle Database Optimisation for MSC SimManager using Oracle's Sun Flashfire Technology. www.oracle.com 2010
- [6] CHEVALIER, Thierry Airbus Aerodynamic Framework: AeroCity International Conference on Trends in Product Life Cycle Modelling, Simulation and Synthesis, PLMSS Bangalore 2006

NAFEMS SDM Bibliography

These presentations are now accessible to NAFEMS members through the NAFEMS SDM bibliography on the SDM WG web-page nafems.org/SDMWG which contains some 200 papers. I would like to thank the staff members at BMW, Audi, Airbus and MSCSoftware as well as all those from other organisations who took the time to present their SDM projects and lessons learnt.

Mark Norris is an SPDM consultant and member of the NAFEMS SDM Working Group. He can be reached at mark.norris@theSDMconsultancy.com



Assuring Confidence in Simulation Results through Simulation Data Management

Mark Norris, The SDM Consultancy

Mark Norris is an SDM consultant with extensive experience of SDM, PLM and mechanical simulation. He advises companies on the evaluation, selection and deployment of advanced engineering IT solutions, especially SDM. He joined the Stress Office of Hawker Siddeley Aviation as an apprentice when the digital calculation capacity consisted of four HP35 calculators. He applied a method incorporating finite elements on an ICL mainframe for computing stress intensity factors in bonded fuselage structures and successfully validated the method against test results. He was awarded the postgraduate N.E.Rowe medal of the RAeS in 1980 for his paper describing this work.

The first Simulation Data Management solution built on a commercial SDM platform was implemented to assure the quality of simulation results for multi-million \$ business decisions. Back in the year 2000, BMW had taken a lead in developing crash simulation methods that were sufficiently accurate to replace physical testing. Dr Holzner asserted that an information system was needed to assure the quality of results and provide appropriate governance for a product development process that used simulation-based experimentation. The two key SDM capabilities deployed were the automated recording of the Audit Trail and the management of digital complexity, providing confidence that the simulation was run on the correct data files.

This SDM solution was implemented to support a simulation process that was already defined and validated to assure the quality of results. However, the last fifteen years has seen dramatic advances in product technology, for example the usage of new materials especially Carbon Fibre Reinforced Plastic (CFRP), see Figure 1, in passenger cars and commercial aircraft, as well as in simulation technology. Simulation Data Management platforms have not just kept up, but have been used as the platforms for process and technique development, verification and validation.



Figure 1: BMW's revolutionary i8 Hybrid CFRP sports car, 6000 simulations on the SDM platform

Assuring Simulation Quality in the Face of Extreme Digital Complexity

Clearly an SDM solution can't make value judgments about the quality of work, it's just a sophisticated database. What SDM can do is to assure that the right data is used. This is no trivial task when 400 engineers are performing experiments on 50 virtual vehicle prototypes [1]. There is wide recognition that manual management of files in folder structures and shared drives is no longer up to the task of tracking data-sets of many hundreds of mesh files through simulations for a hundred design iterations.

Digital complexity has expanded beyond geometry data to materials definitions, fastening methods as well as thickness and residual stress distributions from the sheet metal stamping process. The proliferation of material types in use in a passenger car; pressed, cast

and extruded aluminium, hot and cold formed steel and now glass- and carbon-fiber reinforced composites, requires each meshed component to be associated with the correct material model file. These new structural materials have led to an ever widening range of fastening methods, 64 at the last count [2], to add these further layers of complexity to the file management problem. This scale of the problem is not limited to Automotive and Aerospace OEMs. Christophe LeMaitre cited the 2000 analyses necessary to assure the quality and fitness for purpose of a set of car seats in his presentation of Faurecia's Simulation and Test Data Management systems [3]. Steve Howell of Abercus, in an article in the April edition of this magazine, described how an SPDM solution for CFD assured quality and saved the engineers time by setting up individual simulations, launching runs and then collating the CFD predictions in the SDM database. He explained that SDM enhanced the success of applying CFD on an HPC because of the large numbers of simulations needed, hundreds to thousands, for probabilistic explosion assessments for the oil and gas industry [4]. It's interesting that both Faurecia and Abercus developed their own SDM solutions in-house to save engineers time managing a large number of similar simulations.

File system privileges are simply inadequate to assure confidence in today's simulation environments, especially where method development is proceeding in parallel with product development. A cautionary tale concerns a simulation run to refine a material model for vehicle engineering. This promising novel approach proved not to be representative of the material behaviour. Unfortunately the material file, which had the same name as the standard material model, was left on a shared drive and used for every subsequent product simulation. The company then complained to their FEA supplier that their code was giving erroneous results. It took a week for an expert engineer to find the cause of the problem and identify that it was a rogue file. During which time all the HPC runs on products incorporating this material were compromised. Fit-for-purpose version and configuration control has long been a necessity for the simulation domain and it's not deliverable without an appropriate information system.

Beyond Version Control

File version control incorporating an approval workflow and the replication of files are basic capabilities of any fit-for-purpose SDM solution. But the challenges of Simulation Governance extend way beyond file management which, though a serious and visible issue, is actually the simplest to solve. Simulation is a multi-stage engineering process. It needs to be planned methodically [5]. Consistent modelling and discretisation decisions need to be made. All this meta-data, together with the relevant data sets for each iteration, need to be recorded with the minimum overhead on the analyst. Sylvain Castellani of Peugeot-Citroen commented that an SDM solution was being implemented to replace their

SDM solution was being implemented to replace their existing content manager to address the number one question that engineering managers ask simulation engineers: “How did you validate this simulation result for that vehicle program”[6].

The capability of an SDM solution to capture meta-data and then to provide interactive, web browser access to the audit trail of any set of results is invaluable for generating confidence in simulation results. This is especially valuable when the work is being done remotely, which otherwise can require as much as one supervisor for three remote engineers. SDM can provide a project supervisor with a dashboard showing how simulations are progressing. He can directly access information on Work In Progress (WIP), reassuring him on project progress or flagging up areas of concern.

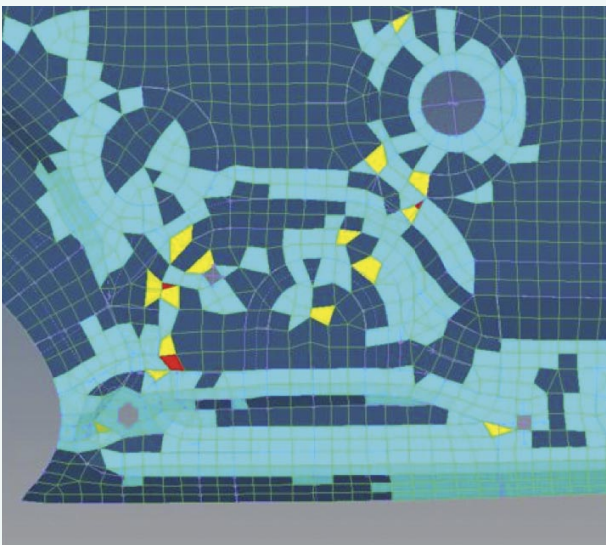


Figure 2: Plot showing element distortions to characterise mesh quality

As well as capturing metadata, SDM can be used to launch programmatic quality checks, display quality plots for review and then store them with approved mesh files. Thorsten Pohl of GM Europe described how the mesh management functions of TeamCenter had been extended to provide interactive access to quantitative and visual Quality Criteria of Finite Element meshes of automotive CAD models, see Figure 2, [7]. The aim of this project was to save time and money by eliminating re-meshing of already meshed parts when a further analysis was to be performed on a different site. Analysts were reticent to use meshes created elsewhere until they could readily see quantitative quality indicators and be assured of the quality of the mesh.

Verification, Validation, Industrialisation

For simulation to come of age as an industrial process in a particular domain, processes need to be captured, documented, refined, verified and validated. This is particularly important when testing is impractical, such

as in nuclear industries or for large scale CFD, or where new product architectures, such as the CFRP i8, are being developed. Dr Dirschmidt described BMW’s stepwise validation strategy in his keynote to the NAFEMS 2015 World Congress [8], see Figure 3.

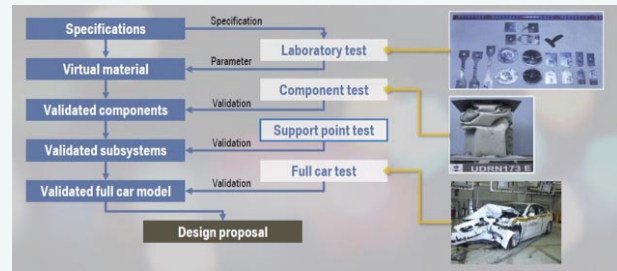


Figure 3: Interaction of testing and simulation for method validation at BMW

Other technical domains have already encountered the need to move from heroic individual efforts by a few specialists to repeatable, defined and managed processes to assure the quality of results. In particular, process improvement in Software Engineering, Systems Engineering and Integrated Product Development have been addressed by an approach called the Capability Maturity Model (CMM), originally developed at Carnegie-Mellon University’s Software Engineering Institute. CMM was sponsored by the US Department of Defense, which wished to achieve more reliable and fit-for-purpose weapons system, but has found widespread civilian use. This has been refined over two decades into CMMI, see Figure 4, and a wealth of know-how, guides, case studies and checklists are available [9]. Dr Joe Luxmore of Siemens PLM proposed an SPDM-specific 5 stage maturity model for SPDM in his paper to the NAFEMS UK conference [10].

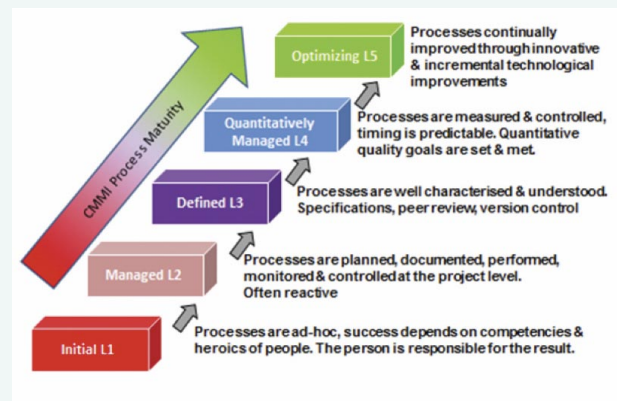


Figure 4: The Capability Maturity Model (CMMI) approach to delivering assured results

Being at level 1 as a Simulation group is not in itself “bad”, the majority of clinical consultants are there also and we rely on them for our health. It’s a function of the difficulty of the tasks performed and the duration of the learning process to become a competent practitioner. Here, programs like NAFEMS Professional Simulation Engineer (PSE) accreditation are valuable since the

practitioner is relied upon for the validity of the result. The implementation of Best Practice processes such as "How to plan a CFD analysis"[5], and the NAFEMS Quality Systems Supplement (QSS 2008) [11] combined with appropriate SDM technology provide a route for simulation groups to move to Level 2 and beyond. Level 3 requires formal version control which can't realistically be achieved using file system permissions but in the 21st century it would be aberrant to embark on such a global process improvement initiative without an information system to underpin it.

A recent SDM project in the nuclear industry addresses the issues of Verification and Validation. Chetwynd & Nurbhai of the UK AWE described a custom implementation of NAFEMS QSS001 process implemented as a workflow in their PLM system [12]. The workflow they had developed enables engineers to record assumptions, approximations and decisions, provides version and configuration control of documents and a link to the archived results. It replaces a paper document which required 17 ink signatures. Best Practice processes and xLM technology have been combined to build a system to record the process steps, approvals and information gathered to verify the codes and validate the results. AWE typically deals with unique problems which can't be tested, such as risks in transporting nuclear weapons, so a rigorous digital verification and validation process and formal version control of key data-files are essential components of their Governance approach. .

Verification is a subject where SDM is ideally placed to help. The test data-sets, test conditions and expected results can all be stored in the SDM together with documents describing the mathematical basis for the methods. This information can then be accessed by anyone concerned about the verification of the code. Subsequently, verification tests of new software versions or models can be run with just a few mouse clicks and compared with previous results. And without the risk of leaving in-development methods on a production server! SDM is therefore a good platform for methods development. The progress of the validity of the method under development can be tracked and displayed in a dashboard.

Supporting Method Development

Dr Ferdinand Dirschmid presented the advanced simulation methods developed on the BMW SDM platform for the functional development of the BMW i8 hybrid sports car. The i8 is the first example of a new product architecture with a Carbon Fibre Reinforced Plastic Body In White (BIW) [8], which is produced in a new, entirely automated, CFRP body shop, with front and rear aluminium structures for energy absorption. He commented that SDM has been essential to enable the timely development and validation of new simulation

techniques, a new product architecture and a first new product. He described a systematic process of progressive validation of material models, components and sub-systems. This rigorous methodological approach culminated in the successful validation of the crash simulations of the i8 see Figure 5.

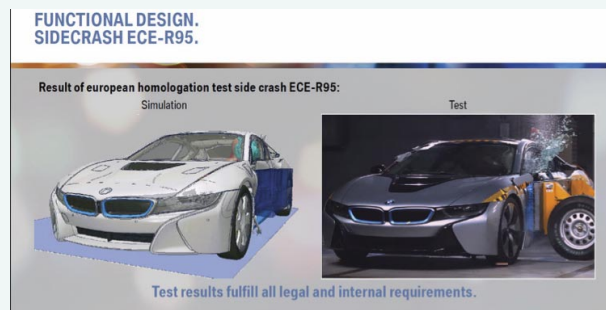


Figure 5: Validation of simulation models of side test crash simulation of the i8

BMW's achieved and planned simulation engineering throughput gains were presented at NWC13 after their move to an SDM2.0 configurable SDM solution set [1]. BMW's measurement of simulation program data and prediction of future process performance for the 50 or so virtual vehicles under development is indicative of Level 5 Capability Maturity. It's perhaps un-surprising that process rigor and early adoption of information systems go together.

McCoy described Ford's use of an integrated SDM environment, VDSS, to develop and deploy a suite of simulations for Roll-Over testing of safety systems [13]. Once these simulation processes had been verified and validated in the USA, they were rolled out globally within the SDM solution. McCoy reported that the global rollout had been accelerated by the SDM environment because the training times for analysts to become proficient were reduced by 50% since they could easily browse all aspects of the process approach as well as previous data- and result-sets.

Conclusion

In conclusion, SDM solutions are not just systems of record to support regulatory compliance. They are structured information and process management environments which enable organisations to gain better control of their simulation processes and data thus providing greater assurance in results delivered. SDM can also support process and method development and provide the necessary infrastructure for attaining the higher levels of Capability Maturity.

Forming Complex Shaped Components Using High Strength Aluminium Alloys

Mohamed Mohamed, Strathclyde University, Glasgow & Helwan University, Egypt
Damian Szegda, Impression Technologies Ltd.
Rajab Said, ESI Group
Jianguo Lin, Imperial College London

In this article the challenges of an innovative forming process are discussed and a simulation strategy that has been implemented in a commercial software code that captures the thermo-viscoplastic material response and formability of the component is described.

In 2009, a new EU regulation on emissions targets was passed which committed European vehicle manufacturers to cut average CO₂ emissions in new cars to 95 g/km by 2020. Average CO₂ emissions from new cars sold in the EU in 2015 were 119.6 g/km, 8% below the 2015 target and 3% lower than in 2014 [1]. Vehicle weight-reduction has been identified as one of the most effective ways of addressing the reduction of energy consumption and CO₂ emissions in the transportation industry. A 10% reduction in vehicle weight can result in a 6% to 8% fuel economy improvement.

Replacing cast iron and traditional steel components with aluminium alloys can reduce the weight of a vehicle's body and chassis by 40% to 50%. Use of high and ultra-high strength aluminium alloys in particular, such as 6XXX and 7XXX series alloys, can reach the upper bound here, or even higher. On the other hand, forming of aluminium alloys is known to be more challenging than steel, and it is significantly more challenging for these high and ultra-high strength alloys. The 6XXX and 7XXX series alloys exhibit low ductility at room temperature - making the forming of complex structures using Deep Drawing techniques virtually impossible. In addition, due to lower than steel elastic modulus and high residual stresses, springback after forming becomes a very difficult issue to manage.

The HFQ® process in a nutshell

A process which combines high formability with virtually no springback for (ultra-) high strength aluminium alloys was developed and patented by a team of researchers based at Imperial College London [2] and commercialised by a spin-out company - Impression Technologies Ltd (ITL) [3]. The process is called Solution Heat Treatment, Forming and in-Die Quenching, or HFQ® for short. It consists of heating an Al-alloy blank sheet to its Solution Heat Treatment (SHT) temperature to produce a homogeneous solid solution with high ductility and hence good formability. The blank is then transferred to the press where the tool speed is set to a value that enhances the work hardening and strain rate hardening of the material. The formed part is held in the tool for a few seconds to quench it in order to avoid the formation of precipitates in the microstructure (see Figure 1).

This is a hot forming technology that combines mechanical deformation with alloy tempering where die forming and quenching are done in one step. This doesn't only reduce production steps but also facilitates the production of high strength, high precision, and complex-shaped lightweight Al-alloy panels in an efficient and cost-effective way.

Simulation of HFQ: Associated Challenges and Continuum Damage Mechanics Model

There are a few more challenges in simulating and modelling hot-stamping/forming processes than conventional cold-processes in general, which is mainly due to the complexity in physics that high temperature and heat flow bring into the task. The material response is thermo-viscoplastic: heat transfer from the blank to the tools and cooling needs to be accounted for, and temperature effects on friction also require additional consideration. Investigating all these aspects in association with the HFQ® process in particular has been subject to extensive R&D activities for more than a decade by researchers at Imperial College London.

The formability of sheet metal is a critical measure of its ability to form complex-shaped components, and is influenced by the stress state of the material during deformation. The traditional set of uniaxial constitutive equations can't predict the forming features in real hot stamping processes with varied stress states of the formed component during the process. Due to this, a multi-axial viscoplastic constitutive model based on continuum damage mechanics (CDM) has been developed to describe the deformation behaviour of aluminium alloys and address the complex response of precipitation hardening aluminium alloys under hot/warm stamping conditions [4, 5].

The CMD model in a nutshell

Over the last couple of years, the CDM model has been extended to account for the effect of stress state on damage accumulation and failure. Different shapes of forming limit diagrams (FLCs)

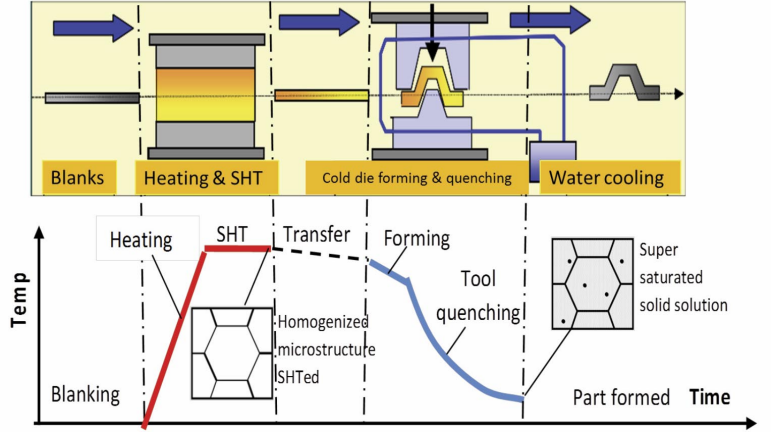


Figure 1: The HFQ process in a nutshell

under hot stamping conditions could be predicted with different temperatures and strain rates. Implementing this CDM-based constitutive equation into the FE code (PAM-STAMP) with a user-defined subroutine, allows the formability for any process conditions, cold or hot and low or high forming speeds, to be predicted by the FE simulations.

A viscoplastic-damage constitutive model has been developed that takes the mechanisms of dislocation-driven evolution processes such as hardening, dynamic and static recovery and damage into account is presented below [4, 6]

$$\dot{\epsilon}_p = \left(\frac{\sigma / (1 - \omega) - R - k}{K} \right)^n \quad \text{Equivalent plastic strain rate} \quad (1)$$

$$\dot{\epsilon}_{ij}^p = \frac{3}{2} \frac{S_{ij}}{\sigma_e} \dot{\epsilon}_e^p \quad \text{Plastic strain rate} \quad (2)$$

$$\dot{R} = 0.5 B \bar{\rho}^{-0.5} \dot{\bar{\rho}} \quad \text{Strain hardening} \quad (3)$$

$$\dot{\bar{\rho}} = A(1 - \bar{\rho}) \left| \dot{\epsilon}_p \right| - C \bar{\rho}^{n_2} \quad \text{Normalised dislocation density} \quad (4)$$

$$\sigma_{ij} = (1 - \omega) D_{ijkl} (\epsilon_{ij} - \epsilon_{ij}^p) \quad \text{Stress matrix} \quad (5)$$

$$\dot{\omega} = \frac{\Delta}{(\alpha_1 + \alpha_2 + \alpha_3)^{\phi}} \left\langle \frac{\alpha_1 \sigma_1 + 3\alpha_2 \sigma_{II} + \alpha_3 \sigma_e}{\sigma_e} \right\rangle^{\phi} \cdot \frac{\eta_1 \sigma_e}{(1 - \omega)^{n_3}} (\dot{\epsilon}_p)^{n_2} \quad \text{Damage} \quad (6)$$

Integration of the CDM Model into a Comprehensive Hotforming Solution

ESI Group has developed a comprehensive solution for hotforming of steel based on its flagship software PAM-STAMP for Sheet Metal Forming [7]. The global strategy adopted for addressing all physics involved in the forming process itself, as well as the incorporation of traditional CFD tools to address design and optimisation of cooling channels to control thermal profile throughout quenching and cyclic loadings is presented in Figure 2. Integration of the CDM model into this global framework, in order to deliver a complete industrial solution for simulating the HFQ® Process, has been an essential part of an EU collaborative R&D project during the last three years [LoCoLite: Low Cost forming of Lightweight structures for transportation industries] [8].

The CDM model was initially coupled as an external subroutine following a standard process for defining User Defined Material (UDM), i.e. USERMAT-184 in this particular case, as illustrated in

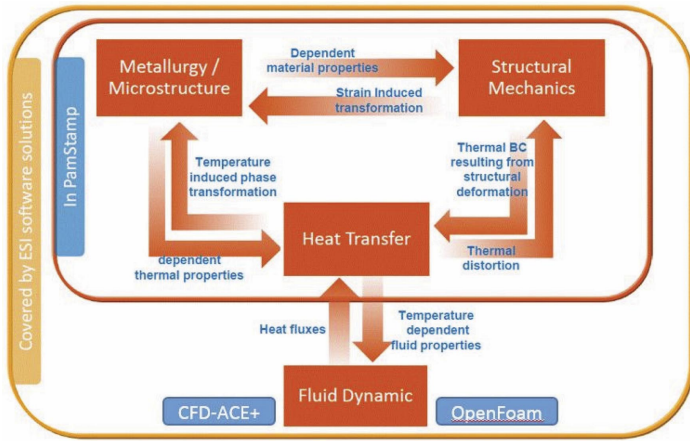


Figure 2: Sketch of the global strategy adopted by ESI to simulation the HFQ Process

USRMAT184_INI

(Initialisation)

This routine function receives parameter from IUSER/RUSER array and stores them in internal arrays CM
The user can print his variables in this function

USRMAT184_SLV

(Solving – Explicit Integration)

Core function to compute stresses, damage, from an incremental strain value.
This function is dedicated to the Explicit Solver

IMP_USRMAT184_SLV

(Solving – Implicit Integration.)

Not used in the current project.
It's equivalent of function USRMAT184_SLV for the Implicit Solver

USRMAT184_OUT

(UDM results output)

The aim of this function is to let the user the possibility to write some element values (plastic strain, equivalent stress, damage...) which will be displayed in post-processing in PAM-STAMP

Figure 3: The template of UDM (USERMAT-184) as followed to introduce the CDM model



Figure 4: Industrial case, Door Inner panel provided by Lotus Cars, as successfully HFQed using Al-6082 alloy.

Figure 3 below. Further refinements of the CDM model parameters and extensive verification studies have been carried out before the model was eventually fully integrated inside the main solver of PAM-STAMP [7].

Industrial Applications and Validation

Several studies were performed during LoCoLite, and through other projects at ITL, to validate the simulation of the HFQ® process. Studied cases were mainly for Automotive body-panels but also included a couple of small-scale cases from Aerospace. A real-life industrial case based on a complex deep-drawn door inner provided by Lotus Cars was selected for this article, shown in Figure 4, and simulations were performed using PAM-STAMP 2015.1 with the CDM model being coupled as an external UDM.

Starting with an initial design of the blank outline, the simulations have predicted failure with a clear split as well as wrinkling in two separate zones, which was then proved to be correct by experimental trials. A thorough investigation based on various cross sections with thickness measurements using Vernier callipers was carried out. An example of correlation between the simulation results and the actual measurements from these initial trials is shown in Figure 5, where good agreement in predicting the split (top) and wrinkling (bottom) is pretty clear.

Learning from experience gained through the trials based on the initial design of the blank, and increasing confidence in the simulation results, a new optimised shape of the blank was achieved after two iterations only, and several panels were successfully formed by AP&T who is also a partner in LoCoLite. Similar comparison of thickness based on the simulation results of the optimised blank is shown in Figure 6; and the photos shown in Figure 4 are for two, out of many, successfully formed panels at the end.

Current Status and Future Work

The boxes marked with a red outline in both figures 5 and 6 highlight areas where the deviation between the simulation prediction of thickness and the actual measurement is greater than the acceptance target of 5% that was set at the time of these initial trials. Two more industrial demonstrators in LoCoLite (B-Pillar case and armrest of aeroplane seat) have been produced since then, and ITL has also been successful in delivering several parts to small volume production OEMs in the automotive sector. Unfortunately, due to confidentiality agreements, none of these cases can be shared at the time of writing this article. It can be reported, however, that the target of 5% above has already been reduced to 2%, and parties involved in this article with another 15 partners from academia and industry across Europe are already involved in a follow up R&D Project (LoCaMaTech under Horizon 2020) where both simulation and manufacturing processes will be developed further. Simulation developments in particular will look into further improvements of the representation of contact and friction under various thermal and lubricant/coating conditions, and it will also expand the material model to cover all major aluminium alloys used across transportation industries.

Acknowledgement

The work described in this article is supported by the European Commission (Grant no: 604240 under FP7) for the LoCoLite project (Low Cost forming of Lightweight structures for transportation industries). <http://www.localite.net/>.

The Authors would like to thank all LoCoLite Partners for their support during the project, and in particular the team of researchers and engineers at ESI (Jean-Luc Babeau, Daniel Vieilledent, Patrick Saillard and Vladimir Cerny), ICL (Liliang Wang and Nan Li), and ITL (Alistair Foster) for their contribution to this article.

References

1. International Council on Clean Transportation, <http://www.theicct.org/spotlight/eu-2020-vehicle-targets>.
2. Jianguo Lin, and et al; A method of forming a component of complex shape from aluminium alloy sheet, UK Patent (GB2473298), European (09785115.8) and International (WO2010/032002)
3. <http://www.impression-technologies.com/>
4. Mohamed Mohamed, Alistair Foster, Jianguo Lin, Daniel Balint and Trevor Dean, Investigation of deformation and failure features in hot stamping of AA6082: Experimentation and modelling, Int. J. of Machine Tools and Manuf. Vol. 53 pp27-38, 2012.
5. Alistair Foster, Mohamed Mohamed, Jianguo Lin and Trevor Dean. An investigation of lubrication and heat transfer for a sheet aluminium heat, form-quench (HFQ) process, Steel Res. Int. 79-11-VII, 133-140, 2008.
6. Jianguo Lin, Mohamed Mohamed, Daniel Balint and Trevor Dean, The Development of CDM-based theories for predicting FLD for hot stamping applications, Int. J. of Damage Mechanics. Vol. 23 [5], pp. 707 – 724, 2014.
7. PAM-STAMP-2G; User Guide and Technical Reports, ESI Group: <http://www.esi-group.com/software-services/virtual-manufacturing/sheet-metal-forming>
8. Jean-Luc Babeau, Daniel Vieilledent, Patrick Saillard, Vladimir Cerny and Rajab Said. Technical Reports D4.2 and D4.4 Deliverables by ESI Group under LoCoLite, FP07-NMP-2013-SME-7 [604240-2], 2013. ■

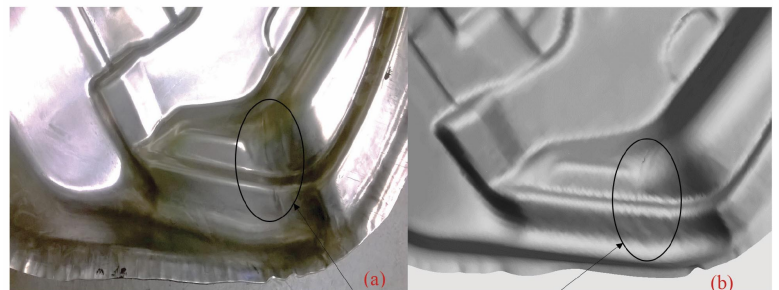
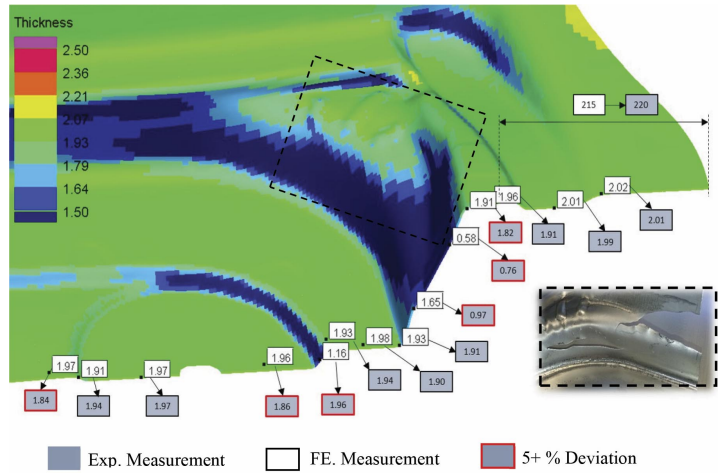


Figure 5: Comparison between PAM-STAMP and the experimental results based on the initial design of the blank: (top) zoom-in of the split zone and (bottom) one of the wrinkling areas; (a) HFQed panel and (b) simulation prediction.

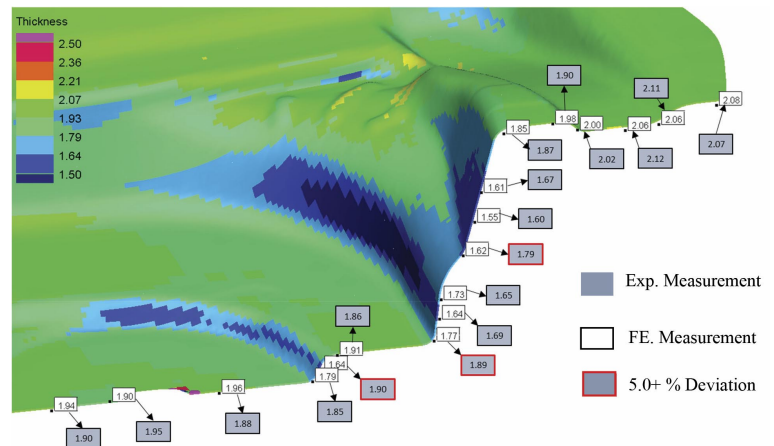


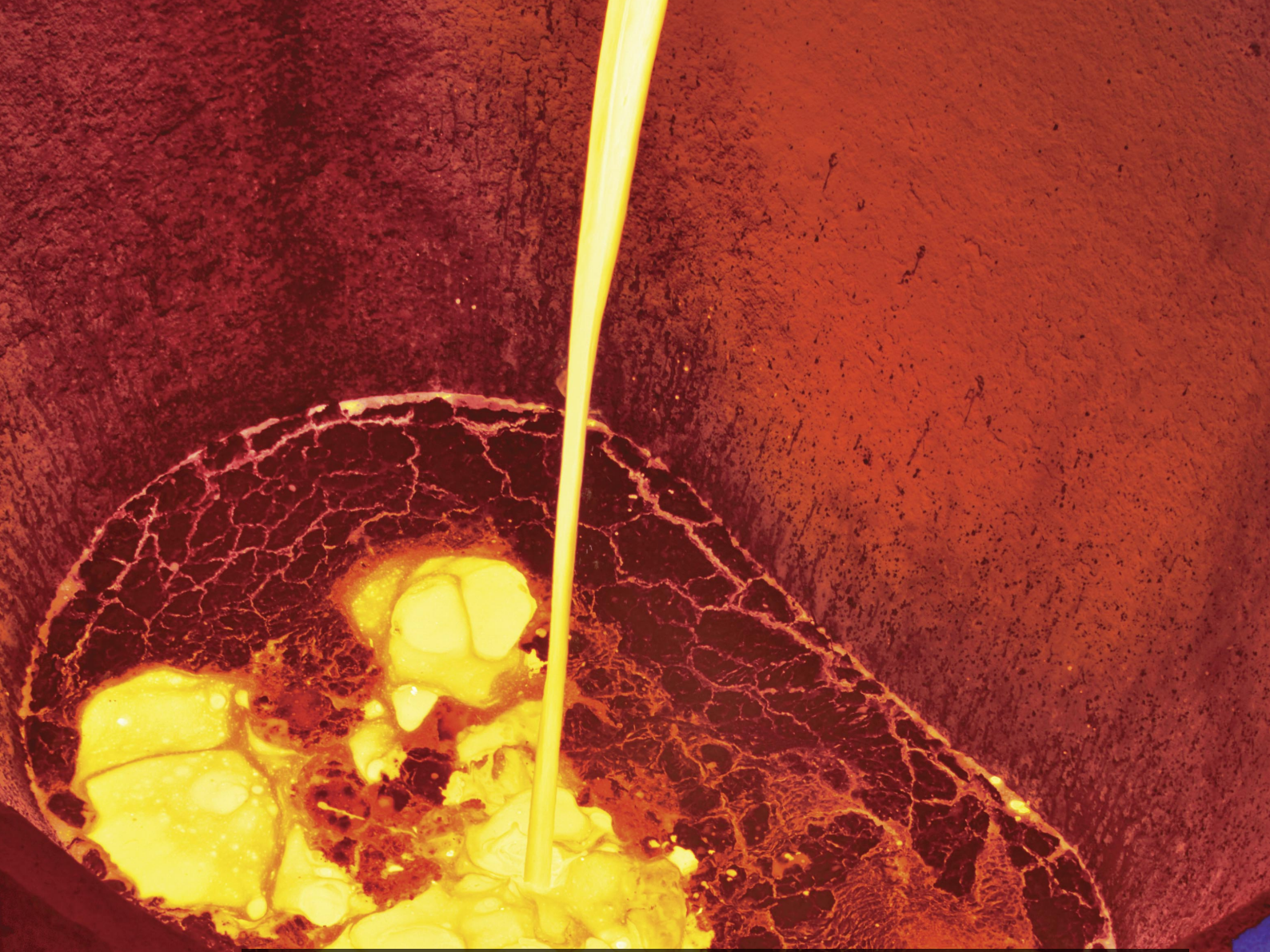
Figure 6: Comparison between simulation and experimental results of the optimised blank. Photos of the successfully HFQed panels can be seen in Figure 4 above.

Dr. M. Mohamed is a Research Fellow, and leader of the Modelling Team at Advanced Forming Research Centre (AFRC), University of Strathclyde. He received his PhD from Imperial College London in 2010".

Dr D. Szegda is responsible for tool design and virtual manufacturing at Impression Technologies Ltd. His background is in product design by FE analysis for defence, aerospace and automotive industry. Damian received his PhD from Brunel University in constitutive and mathematical modelling of thermoforming process"

Dr R. Said has an MSc and a PhD from Swansea University, and more than 20 years' experience across the Computational Simulation & Modelling field. He now works as the Academic and R&D Collaboration Manager for ESI Group.

Prof J. Lin, is a Fellow of Royal Academy of Engineering (FREng), TATA Steel and Royal Academy of Engineering Research Chair, and he is the Head of Mechanics of Materials Division, Department of Mechanical Engineering, at Imperial College London (ICL). He joined ICL from the University of Birmingham in 2008 and established the Metal-forming and Materials Modelling Group.



Simulation in the Die Casting Manufacturing Process

Changhua (Joshua) Huang, Exco Engineering

Die casting manufacturing is a low cost high efficiency manufacturing technology for mass-production of light metal components, such as those widely used in automotive, aerospace and white goods industrial sectors. It uses high pressure to inject molten metal such as aluminium and magnesium into a steel mould cavity under high velocity. The process contains many complicated physical phenomena under high pressure, high temperature and high speed, which cause difficulties for manufacturing engineers to control the quality of die casting parts. So, it is also a “defect-prone” manufacturing process. Due to its mass production feature, any defect can result in a large financial loss. In order to master this efficient but “defect-prone” manufacturing process engineers use simulation tools to design the die casting part and its manufacturing process.

Industrial practices have proved that simulation can significantly improve the success rate of the die casting manufacturing process, which can yield a very high return on investment (ROI). For example, in the automotive industry, a one million transmission case program costs about \$100,000,000. The simulation of this type of die casting program costs about \$50,000 (about 400 engineering hours). If simulation saves 10% of the manufacturing cost that is \$10,000,000, the simulation yields a stunning 20,000% ROI. Actually the average potential improvement percentage is much higher than 10% normally. This does not even include the financial benefits of preventing a potentially catastrophic program failure or major delay.

Simulations are used at three levels of die casting manufacturing process engineering. Top level is up-front engineering for die casting part design. Middle level is die engineering. Foundry level is "Fine-tuned" die casting process engineering.

Top Level: Up-front Engineering

Up-front engineering plays the most critical role in defining the success rate of the whole die casting project and determining the overall manufacturing cost of a die casting product. There are two major tasks at the top level: die casting part castability engineering and requirement engineering.

At this level, the die casting part designer, die caster and die casting tooling engineer should carefully examine the castability of the part geometry for the following, wall thickness, draft angle, split lines, die casting machine capability, etc.. For these purposes certain conceptual simulation models can be employed such as solidification analysis and conceptual flow analysis. These simulation analyses can be performed as long as the die casting part geometry is ready. Based on the results of simulations, the opportunities for improvement can be found. As a result, a manufacturing process-friendly die casting part can be designed in the context of die casting part functionality design. Subsequently, engineers

involved in requirement engineering can develop a reasonable and cost-effective requirement package for the die casting manufacturing process, including the casting quality specification document, design criteria and constraints for the die design if the condition applies.

Middle Level: Die Engineering

Die engineering has three major functionality designs: die casting flow design, die structural design and die casting thermal process design. These designs require intensive simulations. All of these simulations should be carried out concurrently as the die casting die system design progresses.

Die casting flow design is to first determine the best casting orientation in the die casting machine in order to achieve the best die casting quality, considering the ease of the overall die structural building and the stability of die casting manufacturing process. This could be an iterative design process between die casting flow design and die structural design in order to satisfy both functionality design targets. However, die casting flow design has higher priority than die structural design. Die casting flow design includes finding the best in-gate locations and sizes, metal entrance angles, runner shape and overflow locations and sizes using Computational Fluid Dynamics (CFD) simulation to minimize the air entrapment porosity risk to achieve the best casting quality at the lowest cost.

Die structural design is normally decomposed into global assembly design and subassembly design to make it feasible for concurrent CAE. FEA simulations are used to ensure the die structure integrity and die casting manufacturing process stability at the maximum material efficiency. Global assembly design is carried out at a very early stage after the die casting orientation in the die casting machine is initially selected. A global assembly FEA model that includes all major components, from stationary machine platen to movable machine platen, is employed to optimize the overall structural configuration design (subject to the initial die casting process proposed

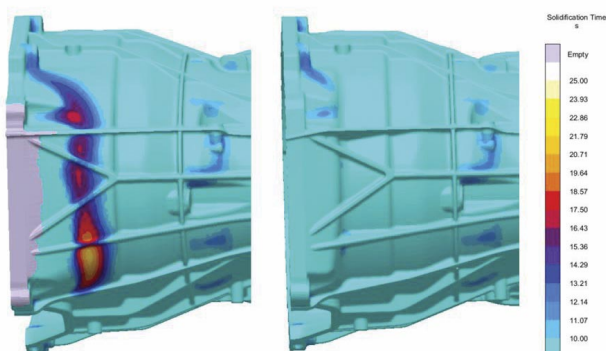


Figure 1: Results of die casting solidification simulation.
Left - Superhot spot in the solidification process is detected.
Right - Superhot spot is removed via casting geometry modification.

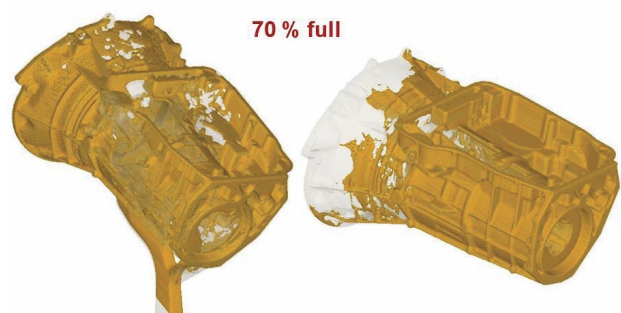


Figure 2: Die casting flow simulation showing the flow pattern results of two die casting cavity filling strategies for a transmission case. Different cavity filling strategies serve different die casting manufacturing process styles and die casting quality requirements.

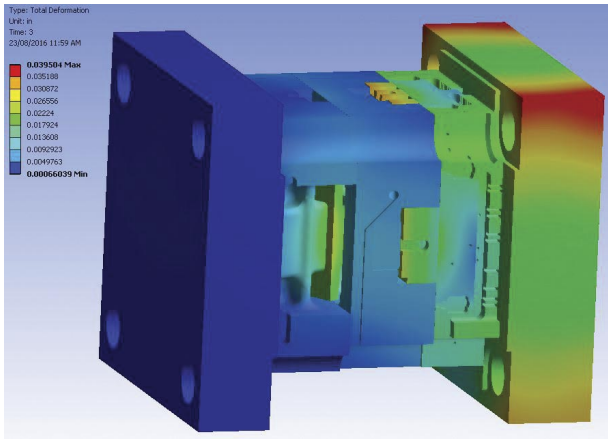


Figure 3: A global FEA model of a V6 die casting die plus die casting machine platens showing the total displacement result; used to evaluate the stiffness and integrity of the die casting die system.

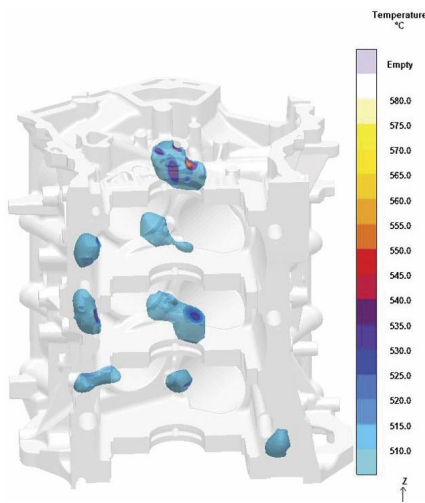


Figure 4: Last solidified zones of a V6 engine block die casting. This result is used to evaluate the risk of shrinkage porosities of the die casting product and to search for ways to minimize these defects.

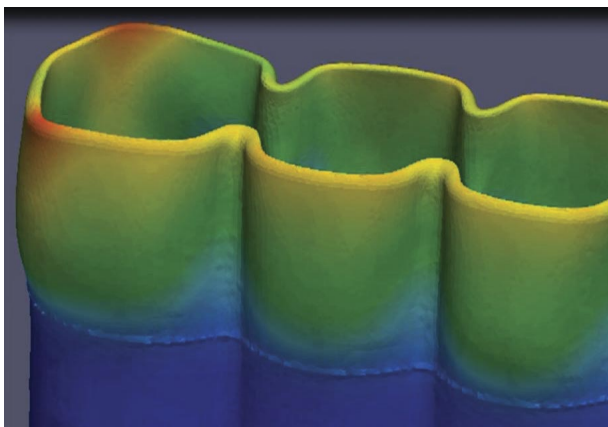


Figure 5: The deformation pattern of a water-jacket insert for an engine block die casting die as the result of the thermal CFD and mechanical FEA coupled simulations of the solidification process. The simulated deformation pattern matches the failure pattern observed in the foundry.

at the top-level), and to determine the material sizes for long lead items required for purchasing at the early stage of project. Sub-assembly design is carried out at a later detailed design stage. The sub-assembly simulation model can be big or small and depends on the purpose of analysis and locations of interest.

Die casting thermal process design is the core of die engineering. All other actions serve the solidification process of molten metal to achieve best part quality at the lowest cost. All key die casting process parameters such as cycle time definition, thermal control parameters and shot profiles have to be taken into consideration in the simulation model for thermal process design. The simulation model can be conceptual or virtually realistic and has to be compatible with the die casting die engineering progress. Die casting thermal process simulation can reveal many possible defects including shrinkage porosity, soldering, heat sink and cold flow line.

Proper thermal process design using simulation can eliminate or minimize these defects and maximize manufacturing productivity at the same time. The simulations of the three key functionality designs can be performed in parallel such as conceptual flow simulation and thermal process simulation, structural FEA simulation and thermal process simulation. They can be coupled, for example flow simulation and thermal process simulation or die structural FEA simulation and thermal process simulation. They can be overlapped, for example die casting flow simulation and die structural FEA simulation. The concurrent CAE can be performed flexibly according to the interests, questions and concerns at the time of die engineering. More advanced simulation tools have been developed or are under development for these co-simulations and/or coupled multi-physics simulations.

Foundry Level: “Fine-tuned” Die Casting Process Engineering

Simulations via concurrent CAE at the top and middle levels will have designed the die casting process with a big stable operational window and will have significantly increased the success rate of “Right the First Time”. However, during the die development phase, die casting part engineering changes might happen or die caster foundry conditions might change, plus other unpredictable changing conditions not taken into design consideration. These factors acting together might make the designed die casting process no longer optimal for the new operational conditions. So, a “Fine-tuned” die casting process for mass production with updated foundry conditions is recommended and sometimes mandatory. In addition, during die casting process development in the foundry real production data feedback can be obtained, which can be used to fine-tune the simulation models. For example, the die cavity surface thermal images taken during thermography inspection can be used to verify the simulation model of

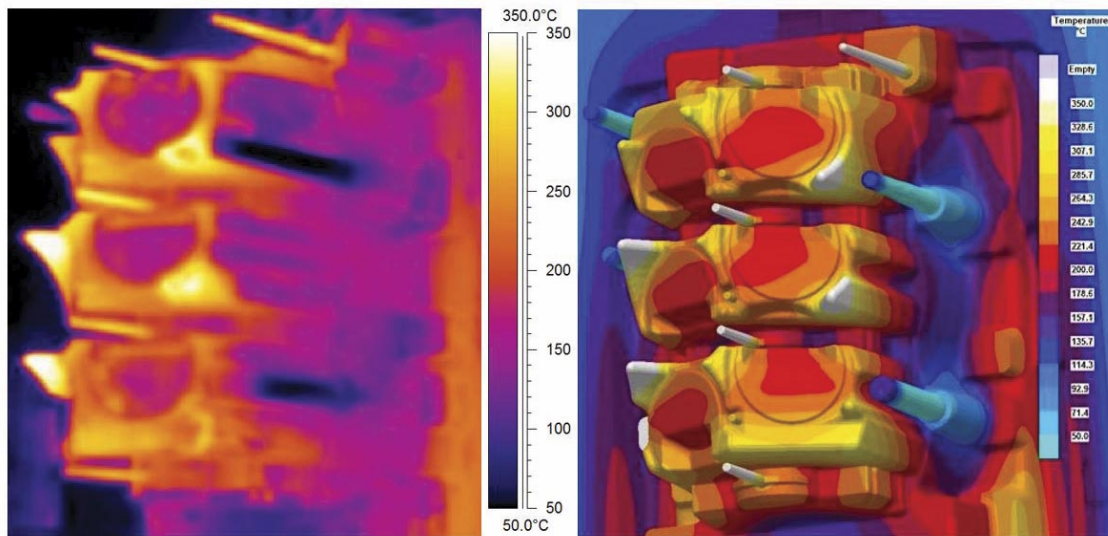


Figure 6: Die cavity surface temperatures of a V6 engine block die. Left - thermal image of thermography inspection, right – result of thermal process simulation.

die casting thermal process design. Some optimization or design of experiment (DOE) tools associated with die casting process CFD simulation software can be used to fine-tune die casting process parameters. From there, an optimal die casting manufacturing process can be designed to achieve the best die casting quality with the lowest cost in the foundry.

Summary

This article briefly discusses the role of simulation at different levels of die casting manufacturing process engineering. It starts from the top level - the up-front engineering of die casting part design, at which the die casting solidification simulation is used to optimize the die casting geometry design for manufacturing (DFM) in the context of casting functionality design. The middle level is for die engineering, which includes three major functionality designs: die casting flow design, die structural design and die casting thermal process

design. At this level three types of simulation (flow simulation, thermal simulation and structural FEA simulation) and/or their combinations are employed to concurrently address design concerns and/or optimize design parameters as the die engineering progresses. At the foundry level simulations are used to “fine-tune” the die casting process based on the actual operational conditions at the die casting foundry. At each level there are different combinations of CAE programs harmoniously employed to simultaneously address the design concerns and/or to search for the optimal solutions in the context of the whole die casting manufacturing process.

Simulation plays a key role at all levels of modern die casting manufacturing process engineering. In order to gain competitive advantages more and more foundries and tooling companies have been acquiring the simulation capability for die casting manufacturing process engineering. ■

Since 2000 Dr. Changhua (Joshua) Huang has been working for Exco Engineering as a senior research & development engineer and head of CAE and simulations. His work includes the conceptual design of die casting die systems, process development and new technology exploration, which includes flow analysis, thermal analysis/thermal inspection, structural stress analysis and beyond. In 2014 he received the NADCA Best Paper Award. He is currently a member of the NADCA Computer Modelling Committee and a member of NAFEMS Manufacturing Process Simulation Working Group.
joshuah@excoeng.com

Exco Engineering is a world leader in the design, build and development of large high pressure die cast tooling, serving our powertrain, body and structural component customers globally in the automotive industry.

Virtual Engineering to Ensure Excellent Customer Experiences for Life

Dr.-Ing. Prashant Khapane, Jaguar Land Rover

One of the biggest challenges for automotive manufacturers is to achieve higher levels of reliability and durability for what is accepted as being the life of the vehicle (10 years or minimum of 150,000 miles with 4-7 years warranty), under a greater variation of use due to a widening consumer base. New vehicle lines addressing new segments of the market, with different characteristics in terms of vehicle use and expansion are the key factors. The purpose of design verification is to ensure that a product has met its design requirements, which are set to ensure that a product will satisfy the customer not only in terms of performance, but also in terms of the time period over which it gives this performance, i.e. product reliability.

The traditional approach to testing automotive components and systems was very much based on subjective criteria; using established "custom and practice", intelligent guesswork, worst casing, basic road load data / customer usage information, and legal requirements. In particular, understanding customer usage is a critical issue, as experience has shown that there is a net difference between what engineers think the customer does and what the customer actually does.

With shorter product development cycles and late physical prototype availability it is absolutely necessary to have virtual methods to predict design loads for automotive OEMs. At Jaguar Land Rover (JLR) a new department was conceived to manage vehicle durability, robustness, and capability requirements using a virtual and systems engineering based approach. Various mega-projects were initiated to develop Virtual Road Load Data (VRLD) capability for design loads prediction. We have used such commercial CAE tools as Multi-body dynamics (SIMPACK), Structural Dynamics (LS-Dyna and Abaqus) and Computational Fluid Dynamics (STAR-CCM+). It was necessary to use a multi-physics approach for many of the problems we were solving.

Jaguar Land Rover's business purpose is to give every customer an experience they love for life. Our customers have high expectations from our products; be it wading through deep water or driving through desert. Although the two low speed impact requirements, deep water wading and robustness to impact with sand dune, are as different as chalk and cheese the challenges we faced were similar. Let's start with defining the problem.

Historically off road vehicles were built on a ladder sub frame; and the steel cross beam at the front provided robust protection for the cooling pack. With the move to monocoque construction, the cooling pack became vulnerable to low speed grounding damage. This led to the development of what became known as the 'Bunny Bar', validated at Cranfield University with the newly-created dune impact test.

Unfortunately this vulnerability can't be confirmed until later in the programme when fully representative vehicles are available. This results in late engineering change that is expensive, time consuming and stressful. And, like all late change, it is rarely optimised for cost and weight.

The recent very heavy rain in the North of England has provided a timely reminder of just how damaging flooding can be. Thankfully for the west this tends to be a rare occurrence, but for many markets monsoon flooding happens every year and having to drive through deep water simply cannot be avoided. Also for some Land Rover customers the spirit of adventure encourages them to seek out opportunities to go wading.

One area that has proved difficult to optimise for wading requirement is trim, especially under-trays, these are now essential in reducing aero drag and hence lowering CO2 emissions, but they are vulnerable to scooping large volumes of water when driving through deep floods. What material, what gauge, how many fixings and where to put them has always been difficult to optimize as we had no method to predict the water dynamics other than trial and error, which again results in costly redesigns.





With no historic literature or procedure available, the challenge was to model the physics of sand and water media and also solve the complex multi-physics problem of vehicles impacting these media.

Our first challenge to model sand was to get accurate material properties. The tri-axial testing was carried out to determine the relationship between hydrostatic pressure and volumetric strain. A friction angle test was carried out using a motorised soil shear rig. Static and dynamic drop rigs were used to determine impact force against displacement.

We also benchmarked various methods in structural dynamics CAE tool LS-Dyna including Arbitrary Lagrangian Eulerian (ALE), Discrete Element Solid (DES), Solid Finite Element Method (Solid FEM) and Smoothed Particle Hydro dynamics (SPH). SPH is an N-body integration scheme developed by Lucy, Gingold and Monaghan (1977). The method was developed to avoid the limitations of mesh tangling encountered in extreme deformation problems with the FEM. The difference between the classical approach and SPH is the absence of grid. In SPH, the location of neighbouring particles is important. Also the particles are uniformly distributed in space. The results of which were clearly in favour of SPH for simple plate tests done at Cranfield University.

However computational effort at vehicle level modelling using SPH was unrealistic so we came up with a unique approach; a hybrid modelling of SPH and Finite Elements. The clever optimisation of using SPH elements in the region of impact and solid/FE elements outside the impact zone enabled us to reduce the computational effort by more than 83% and also correlate design loads.

Computational Fluid Dynamics (CFD) is used for wind tunnel based aerodynamic analysis; the vehicle is stationary and the fluid is moving. However in order to capture the pressure flow field accurately and replicate the vehicle motion effects we decided to use a non-traditional CFD approach.

We developed a unique method to model vehicle motion using an overset mesh technique. The concept is simple. There are two grids, a background grid for the fluid and a field grid for the vehicle. Fringe cells exchange the data as the vehicle moves through the water. For sophisticated usage of the method and some internal programming done by JLR engineers to replicate physics we have filed two patents protecting components of this method (PAT14019GB0 / GB1-1505504.9).

This innovative virtual tool set replicates complex physics phenomena at vehicle level. It has played an instrumental role in risk assessment due to design changes and optimisation of key components enabling weight reduction. This in turn enabled us to deliver a key goal as a responsible business - reducing tailpipe emissions and carbon footprint.

Besides reducing reliance on physical prototypes and whole vehicle verification tests it also enables us to deliver the brand promise and robust products so our customers can have experiences they love for life.

This innovation has been applauded at prestigious conferences and publications. It has won three Innovation awards at various levels within the TATA group. It has also been chosen as Business Innovation of the Year 2016 by the Institute of Physics. ■

Dr.-Ing. Prashant Khapane received his PhD in multi-body simulation from Technical University of Braunschweig and his masters degree in computational fluid dynamics / Aeroacoustics from RWTH Aachen and IIT Kanpur. In his current role as a virtual engineering manager of vehicle attributes at Jaguar Land Rover he has developed a concept of digital proving ground and virtual road-load data generation reducing reliance on physical prototype testing for failure mode detection and avoidance. He has built a team of passionate CAE analysts and together managed virtualisation of attribute requirements including extreme strength and durability events, discrete off-road events such as wading and under-body robustness and development of new requirements for electric and special vehicle operations.

Multi-Objective Design Optimization of an Inverter for Electric Vehicles

Alberto Bassanese, Barnaby Lewis and David Moseley, Lucid Motors Inc.



Electric Vehicle drivetrains offer numerous advantages in respect to conventional internal combustion engines including higher energy efficiency, lower emissions and decreased dependency upon oil. At the heart of the development of a new Electric Vehicle is the necessity of converting electricity from Direct Current (DC) source to Alternating Current (AC) for use in electric motors. An inverter carries out this task. The ideal EV powertrain is small in size, has high efficiency, high output, and is reliable. In this article, we present the methodology that we have successfully applied at Lucid Motors for the design optimization of the Lucid Air's inverter.



Figure 1: Lucid Air.

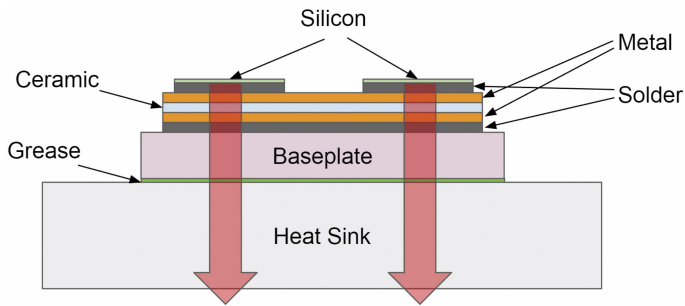


Figure 2: IGBT cooling.

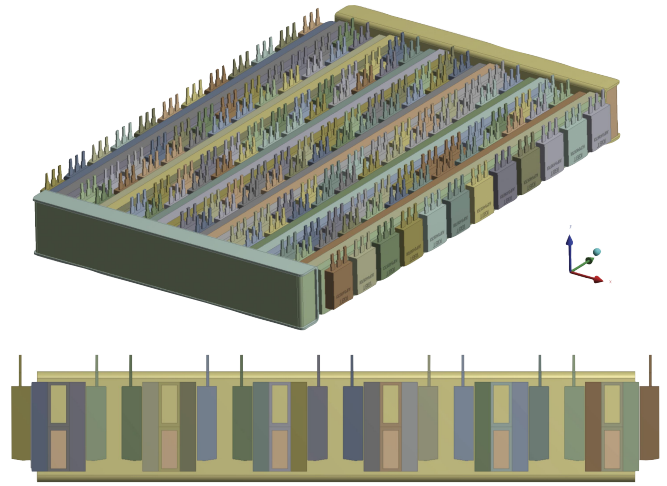


Figure 3: Initial inverter design concept.

IGBTs (Insulated Gate Bipolar Transistors) are commonly used as power devices in medium to high current rating power converters. An inverter consists of an array of IGBTs, each of which is paired with an anti-parallel diode. A single IGBT and diode pair form one bi-directional switch and, in combination with the other switches in the inverter, generate the AC waveforms necessary to control the motor. IGBTs dissipate electrical energy as heat and the total loss is the sum of conductive and switching losses. In this regard, a key parameter that has to be kept under control is the maximum junction temperature.

From a simulation point of view, thermal modeling of electronic systems can be a challenging task since it involves a hierarchy of length scales ranging from 1m down to 10⁻⁴ m and results in a wide range of time scales in the simulation. Heat is generated at the junction regions of the IGBTs, which have a characteristic dimension of the order of micro-meters. From there, the heat will go through a multilayer structure in the device (see Figure 2) and eventually will dissipate into a heat sink, whose size is of the order of centimeters. Heat is then transferred to coolant via forced convection. Most of the heat is therefore dissipated by conduction and convection, whereas heat radiation can be considered as negligible [1-3]. The electrical phenomenon (switching) occurs in several nanoseconds while the heat transfer process occurs over minutes if not hours. The simulation time step should therefore be small enough to catch the transient

detail while the total simulation time should be long enough to obtain the long-term temperature profile. This requirement makes the electro-thermal simulation very time consuming thus a compromise between speed and accuracy has to be made: the fast switch events and the long-term simulation have to be balanced in building the power loss model.

From an optimization standpoint, the objective is to determine the most thermally efficient design configuration. Given that many hundreds of designs will have to be evaluated, a steady state model is used. Instantaneous power losses will be replaced by average values, calculated from the Root Mean Square (RMS) values of the electric currents. For the optimization study the coupled electro-thermal problem is simplified into a conjugate heat transfer one.

All the Computational Fluid Dynamic (CFD) models employed throughout the present study are 3-dimensional and have been simulated using ANSYS Fluent. The original multi-objective optimization problem had four objectives: minimize peak junction temperatures, minimize junction temperature variance, minimize volume of the overall package, and minimize the coolant pressure drop across the whole inverter. Constant coolant flow rate and IGBT heat generation were assumed. As a starting design concept for the device, six cooling channels are used as heat sinks, see Fig 3. IGBTs were attached to each of the two vertical faces of those channels.

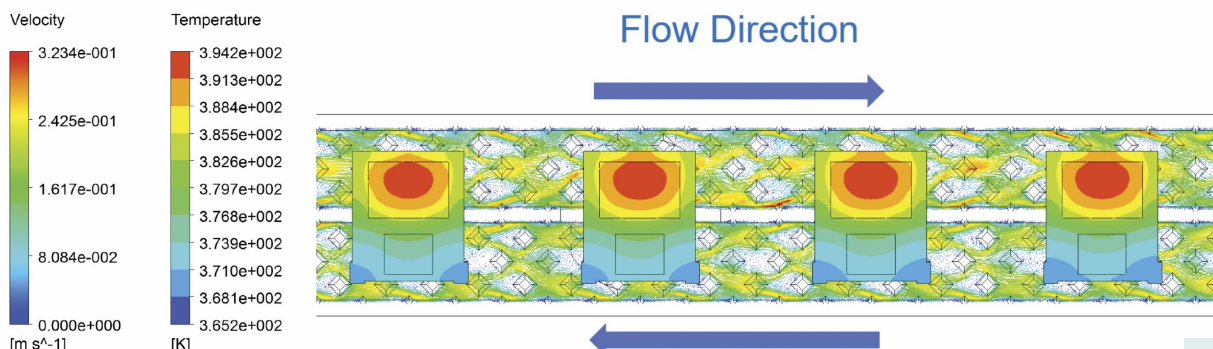


Figure 4: IGBT counter-flow cooling (temperatures and velocity vectors).

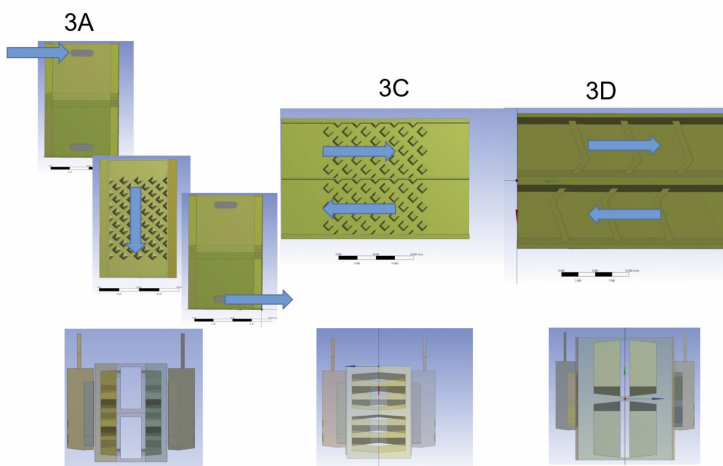


Figure 5: Different Concepts of Cooling Channel.

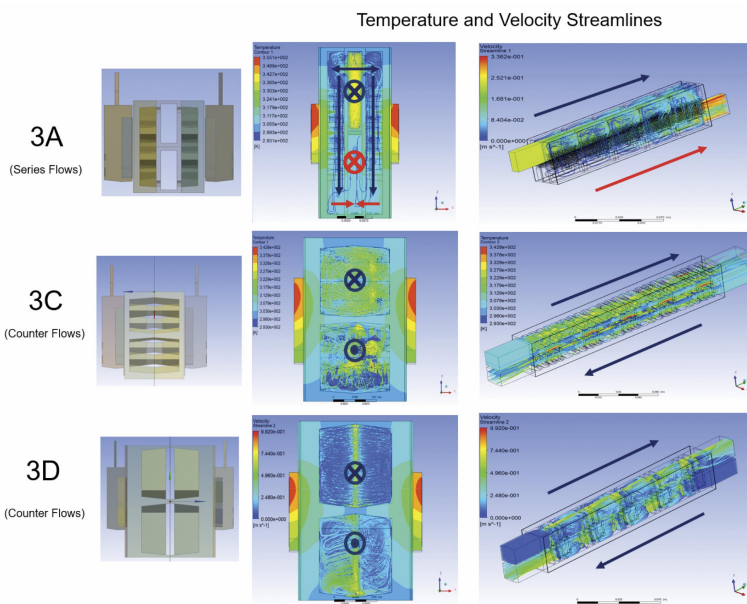


Figure 6: Different Concepts of Cooling Channel.

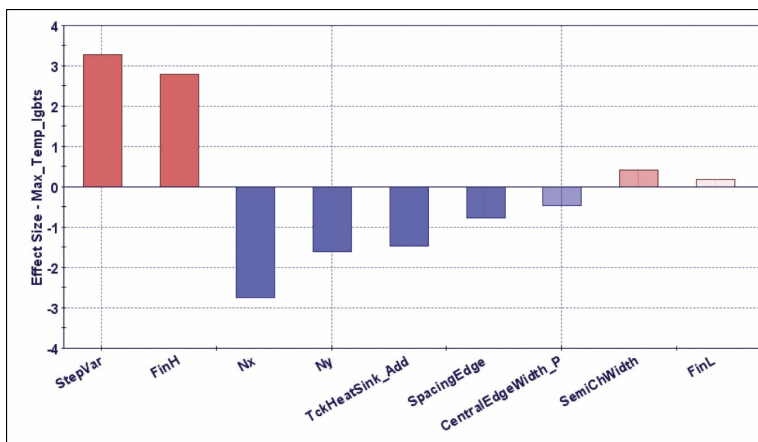


Figure 7: Junction Temperature Main Effect for Channel Configuration 3D.

Within each cooling channel (or stick), two inner sub-channels are conceived. The topology of these sub-channels is allowed to vary freely, but only two main concepts have been considered: series flow and counter flows. In the counter flow configuration, we have two independent sub-channels (top and bottom) and the coolant flows independently in opposite directions to minimize thermal gradients (see Figure 4). In the series flow configuration, upper and lower sub-channels are connected so that the coolant can flow only in one direction from one side of the main channel to the other one (see Figure 5). Fins (turbulators) of different shapes are placed on the inner side of the channel to increase surface area and induce turbulence improving fluid mixing which results in better thermal performance. The different concepts, labeled as 3A, 3C and 3D are reported in Figures 5-6. The precise details of the designs are not crucial, but in broad terms design 3A has central distribution channels to feed finned heat exchanger regions on the outer walls of each stick. 3C simply has upper and lower finned channels and 3D has flow tripping features on the walls of the upper and lower channels rather than fins.

We chose to implement a two-stage optimization strategy:

- 1) Optimize the topology for each channel configuration;
- 2) Optimize the shape of the manifold, which connects the upstream and downstream coolant piping.

The main advantage of this approach relies on the modularity of the whole inverter design. Indeed, once an optimal design of the channels has been identified, one could readily reduce the number of the IGBTs and therefore the length of each cooling channel so as to obtain inverters that are suitable for lower power levels. When the power level (or number of IGBTs) is changed, only the second optimization study, of the final manifold shape, needs to be performed, as the main channel optimal design can be re-utilized. One additional advantage is that during the first channel optimization phase, only a limited number of IGBTs needed to be modeled in order to assess the performance of the cooling topology and this reduced the computational time to evaluate each configuration. Parameterization of the CAD for the three different channel topologies was carried out in ANSYS Design Modeler, see Figure 6. A total of 20 geometrical input variables for each configuration have been considered. Ad-hoc coded Python and Scheme scripts managed the model generation, analysis submission, and post-processing.

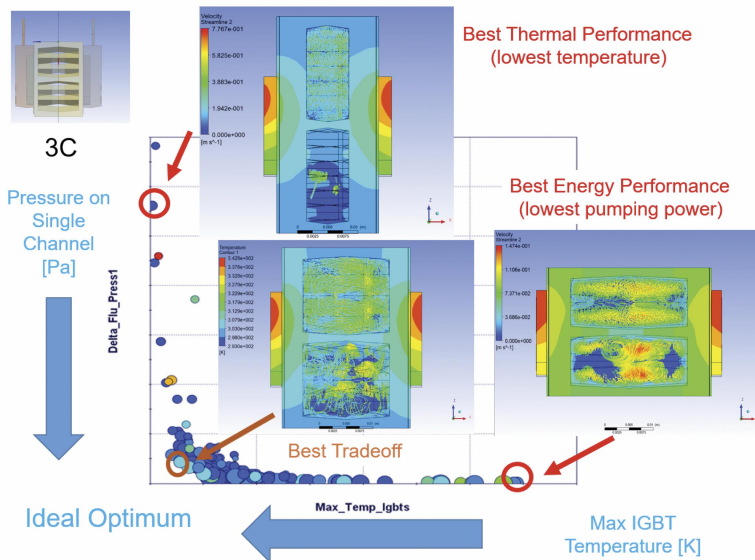


Figure 8: Pareto Front for Channel Configuration 3C.

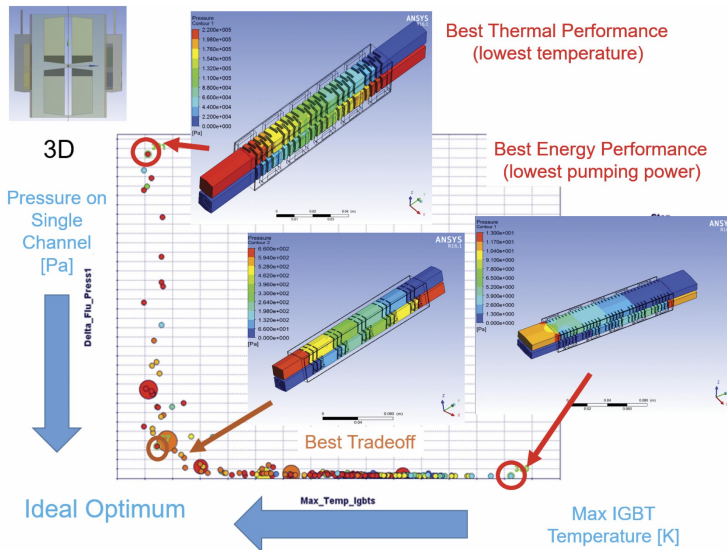


Figure 9: Pareto Front for Channel Configuration 3D.

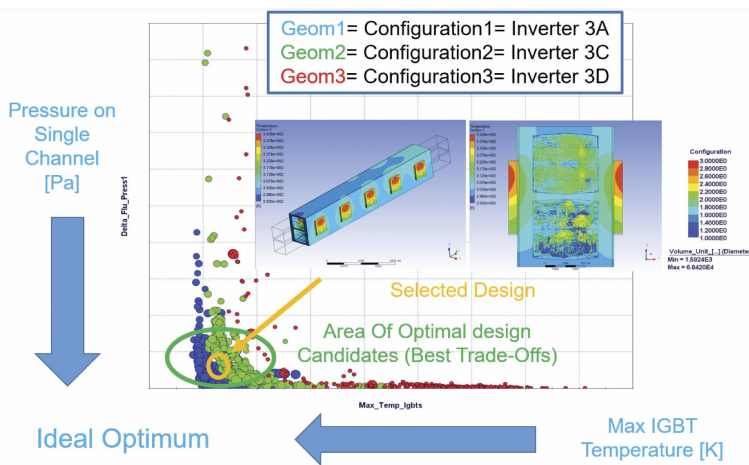


Figure 10: Comparing the Pareto Fronts for all the Channel Configurations.

The channel optimization study has been carried out using Esteco’s modeFRONTIER. For each of the three topologies, an initial set of 100 Uniform Latin Hypercube designs Design Of Experiments (DOEs) were evaluated to perform a sensitivity analysis: the main effect of each input variable with respect to each of the output variables was determined. In Figure 7 we report the main effect chart for the most important input variables with respect to the maximum IGBT junction temperature. The length of the bars indicates the significance of each of the input variables in reducing the IGBT junction temperature. Red bars indicate a variable whose increase will increase junction temperature and blue bars indicate variables whose increase will decrease junction temperature. This helps quickly identify which variables are the most important for the optimal solution. Similar charts were obtained for all the other optimization objective functions.

After this initial design space exploration, the MOGA-II algorithm (multi-objective genetic algorithm [4]) was used for the optimization. A total of 1200 channel designs were evaluated. A set of optimal (non-dominated) design solutions (Pareto Front) was therefore determined for each one of the three channel topologies. In Figure 8-9 we report the Pareto fronts for the channel configurations 3D and 3C respectively.

The underlying chart shows many individual bubbles. Each bubble represents a different design. Just three of the bubbles, or designs, have been circled. The top left red circle is a design which minimizes the peak temperature – but it requires a lot of pumping pressure. The bottom right red circle is a design which requires little pumping pressure, but at the expense of higher peak temperature. A preferred tradeoff design is shown by the brown circle in the bottom left, which gives a combination of low temperature and low pumping pressure.

The radius of each circle is proportional to the size of the channel. Optimal designs are therefore those characterized by a small circle and located near the origin of the axes. There is no single optimal solution, but rather a set of optimal solutions along a multi-dimensional trade-off curve, which represents the mentioned Pareto front. Along those fronts, thermal

improvements (lower junction temperature) can only be achieved at the expense of other objectives (for example higher required pumping power). In Figure 10 we overlay all the three Pareto fronts in the same chart: blue circles refer to configuration 3A, green circles refer to configuration 3C and lastly red circles refer to configuration 3D.

In performance terms configuration 3A offer the best set of solutions. The pareto front offers options with lower pumping pressure / lower temperature combinations. However, subsequent exploration of manufacturing options ruled out this design on grounds of cost. The family of solutions based on configuration 3C provides the second-best family, and significantly better manufacturability. For this reason, a design was chosen from the family 3C.

Now that a channel design has been selected, we need to proceed with the second stage of the optimization, shaping of the manifold. Keeping a single inlet and single outlet solution, we came up with an initial double Y-shaped manifold solution as depicted in Figure 11.

The final manifold optimal shape configuration was determined by employing a hybrid approach: starting from the initial design of topology of Figure 11, we used ANSYS Fluent's Adjoint solver to identify regions that would improve the design with respect to the already defined optimization objectives. We then used modeFRONTIER to perform a multi-objective optimization study on the manifold. Fluent's Adjoint Solver [5] is a specialized tool that extends the scope of the analysis provided by a conventional flow solver by providing detailed sensitivity data for the performance of a fluid system.

Two "observables" (quantities of interest, in this case to be minimized) were defined for the adjoint calculation: the variance of the velocity within the control box domain defined in Figure 12 (as a measure how the cooling channels are working altogether), and the pressure variation between inlet and outlet. As seen in Figure 12, improving those two objective functions has a physical meaning: reduce/eliminate fluid regions where recirculation occurs. The results of the adjoint calculation are shown in Figure 13 as (logarithmic) shape sensitivity magnitude indices. As one

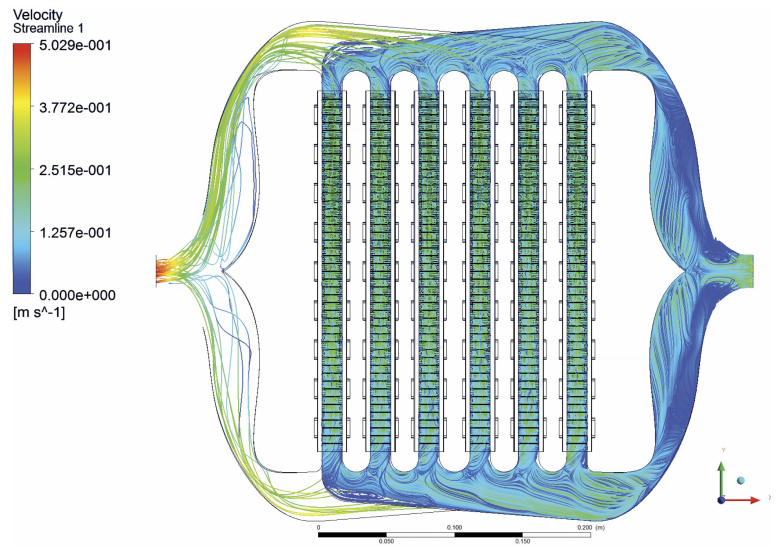


Figure 11: Y-Shaped initial manifold design.

Optimize the shape of the manifolds connecting with up-/down-stream piping

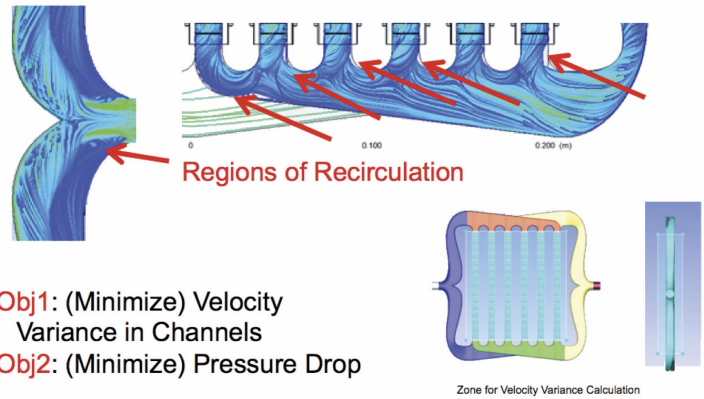


Figure 12: Adjoint Observables definition.

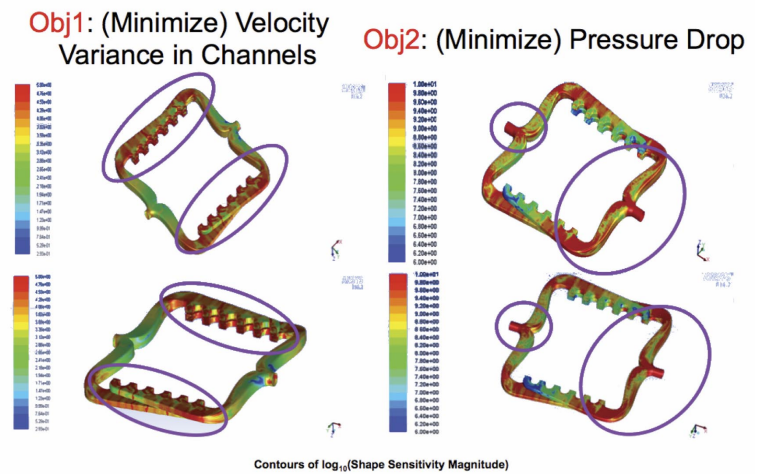


Figure 13: Adjoint Shape Sensitivities.

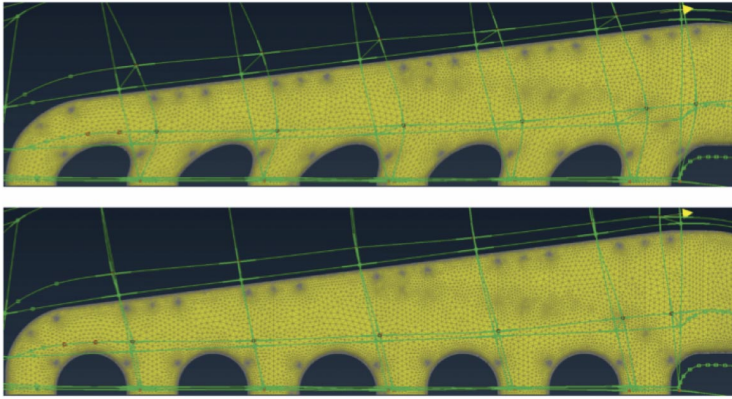


Figure 14: Manifold mesh morphing.

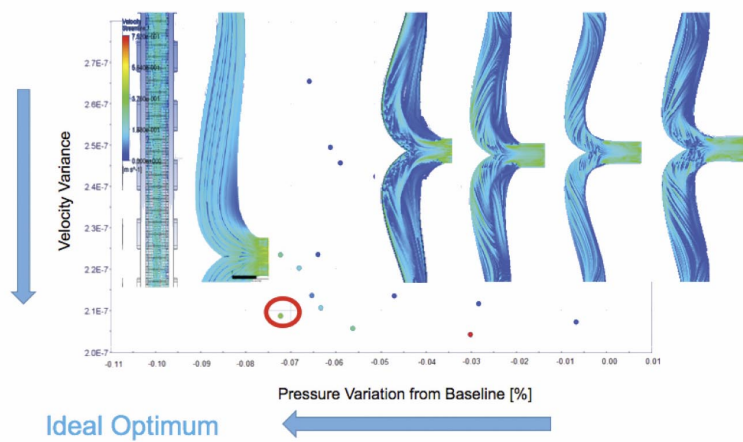


Figure 15: Final Manifold Pareto Front.

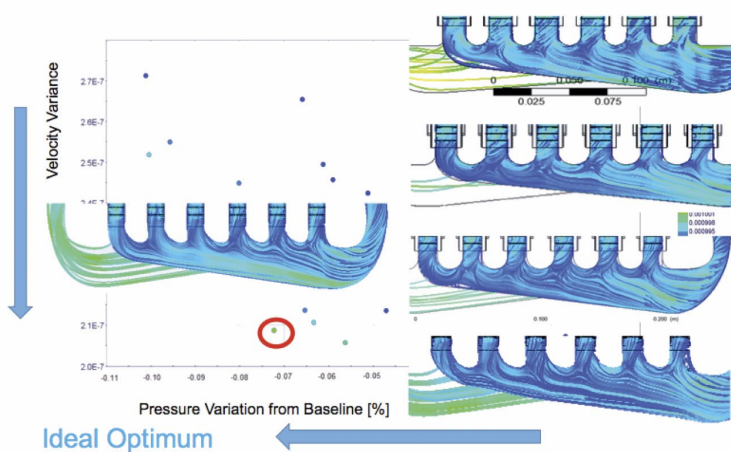


Figure 16: Final Manifold Pareto Front.

would expect, the flow variance across the different channels is strongly dependent upon the local shape of the manifold; the pressure drop is instead strongly dependent upon the inverter's y-shapes boundaries near the inlet and the outlet.

Using software tools Sculptor [6] and Ansa [7], we were able to parametrize the inverter's manifold model directly at the mesh level with 16 morphing variables. Different manifold (meshed) geometries were obtained without the need of generating/updating any additional CAD model. This resulted in a tremendous saving in terms of computational time. Part of the mesh morphing process is represented in Figure 14.

The final optimization was conducted once again via modeFRONTIER. In Figure 15-16 the Pareto front is reported as a function of the fluid velocity variance across the different channels (y-axis) and the percentage of pressure variation from baseline/initial configuration (x-axis). Velocity streamlines are shown for the optimal solution along with other configurations.

The chosen optimal solution is also reported in Figure 17 as temperature contour plot and velocity streamlines. The optimal solution turned out to give almost uniform (within 3.5°C) junction temperatures across the different IGBTs. This new optimized inverter proved to outperform our older inverter design in every metric: peak junction temperatures are now 18°C lower and required pumping power has been reduced by 1/3. In fig 18 we depict the final inverter-motor package assembly; from here we can clearly appreciate the compactness of the optimized solution.

Conclusions

A novel inverter cooling system was developed with the use of several advanced simulation optimization techniques. Pressure drop, maximum temperature, and temperature range across IGBTs were all reduced. The simulation was validated through physical testing, demonstrating the impact a simulation-driven design optimization can have. ■

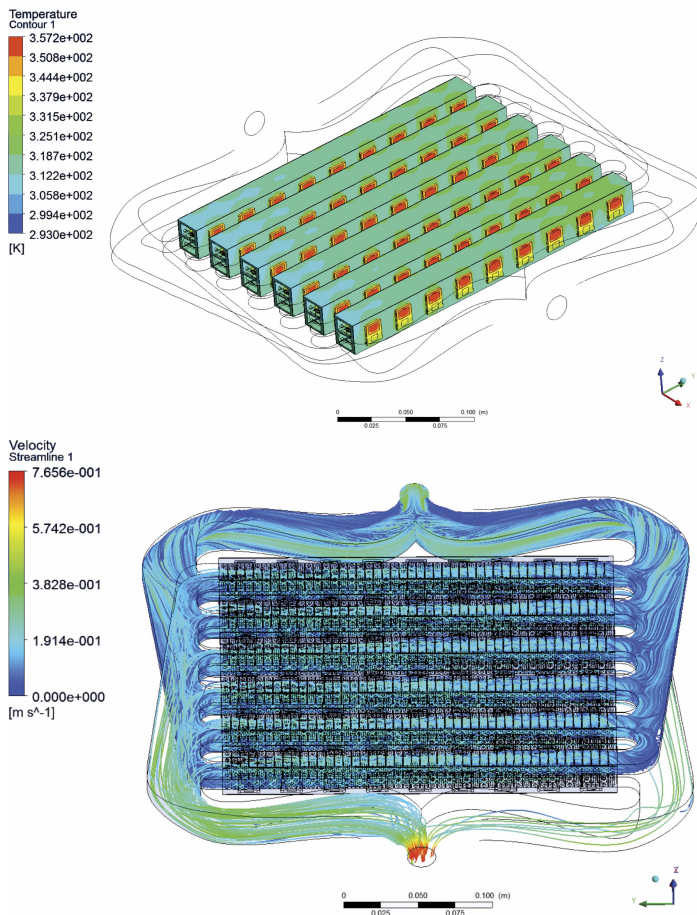


Figure 17: Chosen Optimal Solution.

References

- [1] "A Simple Approach for Dynamic Junction Temperature Estimation of IGBTs on PWM Operating Conditions", Masayasu Ishiko and Tsuguo Kondo 1-4244-0655-2/07 IEEE;
- [2] "Thermal management of electronics: A review of literature," Shanmuga and Velraj, Thermal Science, 12, -2, 5-26, Feb. 2008;
- [3] "Thermal modeling of diamond-based power electronics packaging," Fabis and Shum, In Proc. 15th IEEE Semiconductor Thermal Measurement and Management Symposium, San Diego, CA, Mar. 1999, pp. 98-104;
- [4] "MOGA-II Performance on Noisy Optimization Problems" Silvia Poles, Enrico Rigoni, <https://dis.ijs.si/tea/Publications/Poles04MOGA.pdf> ;
- [5] ANSYS Fluent 18.1 Manual Chapter 35.1 The Adjoint solver;
- [6] Sculptor <http://gosculptor.com/Products.html>;
- [7] Ansa <https://www.beta-cae.com/ansa.htm>

David Moseley is the Director of Powertrain for Lucid Motors Inc..

davidmoseley@lucidmotors.com

Alberto Bassanese is the Manager of the Multi-Physics and Optimization Team at Lucid Motors Inc.

albertobassanese@lucidmotors.com

Barnaby Lewis is a Project Engineer in the Multi-Physics Team at Lucid Motors Inc.

barnabylewis@lucidmotors.com

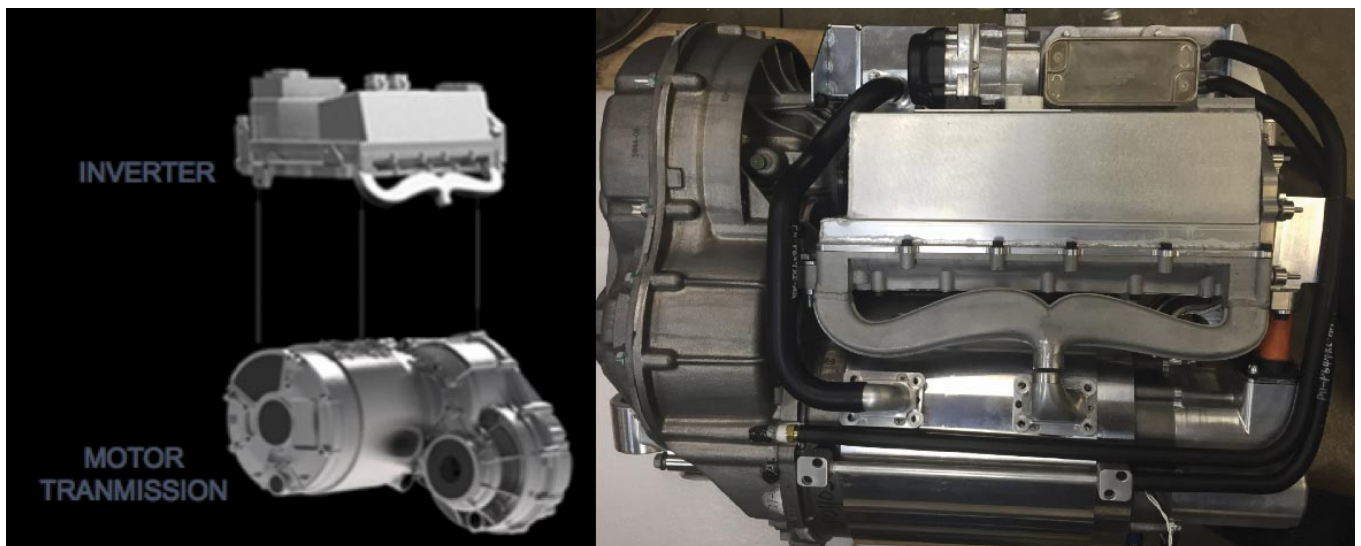


Figure 18: Final Optimal Inverter Design.

A detailed close-up photograph of an engine's intake manifold, showing several polished metal intake ports and valves. The lighting highlights the metallic textures and the complex geometry of the components.

Multi-objective Adjoint Optimization of Intake Port Designs

Gregor Kotnik & Matthias Rainer, AVL

Performance, fuel consumption, raw emissions and thermal load of modern internal combustion engines with Gasoline Direct Injection (GDI) strongly depend on the engine's intake ports. Their design affects the amount of charge delivered to the engine's cylinder and it defines the tumble motion of the charge in the combustion chamber. Respectively, key parameters characterizing intake ports are the *Discharge Coefficient* and the *Tumble Ratio*.

This article describes the optimization of an intake port of a 4-valve, 4-stroke GDI Engine with a bore of 83 mm by means of adjoint solver technology. Contrary to the already widely used 'conventional' technique of coupling *CAE Simulation software* with a *CAD Software* and an *Optimization tool*, shape optimization by means of adjoint solver technology is performed as an integral part of the CAE Simulation itself. If objective functions are available, the adjoint solver approach simplifies and accelerates the task of finding the optimum solution for a given problem as no coupling (data exchange) between different tools is required and design sensitivities are directly derived from a concurrently running CAE Simulation.

The base design used to accomplish the work described in this article is the result of a previously performed conventional optimization task, that was carried out using an automated optimization loop with a parametrized CAD model coupled with FIRE CFD tools and a genetic algorithm. This required over 300 designs to get some improvement. Each of the 300 designs / simulations required around 3000 solver iterations. However this approach did not succeed in increasing the tumble to the desired level while maintaining the achieved discharge coefficient. This occurred, because the parameterization of the CAD Model limited the geometrical changes possible. Thus continuation of the optimization work by deploying adjoint solver technology appears to be the right way to proceed.

Theory

The optimization problem uses the incompressible, stationary Navier-Stokes equations as *Constraints*. The *Boundary* of the problem is partitioned in the **Wall**, which can be moved during optimization, see Figure 2, the **Inlet** and the **Outlet**.

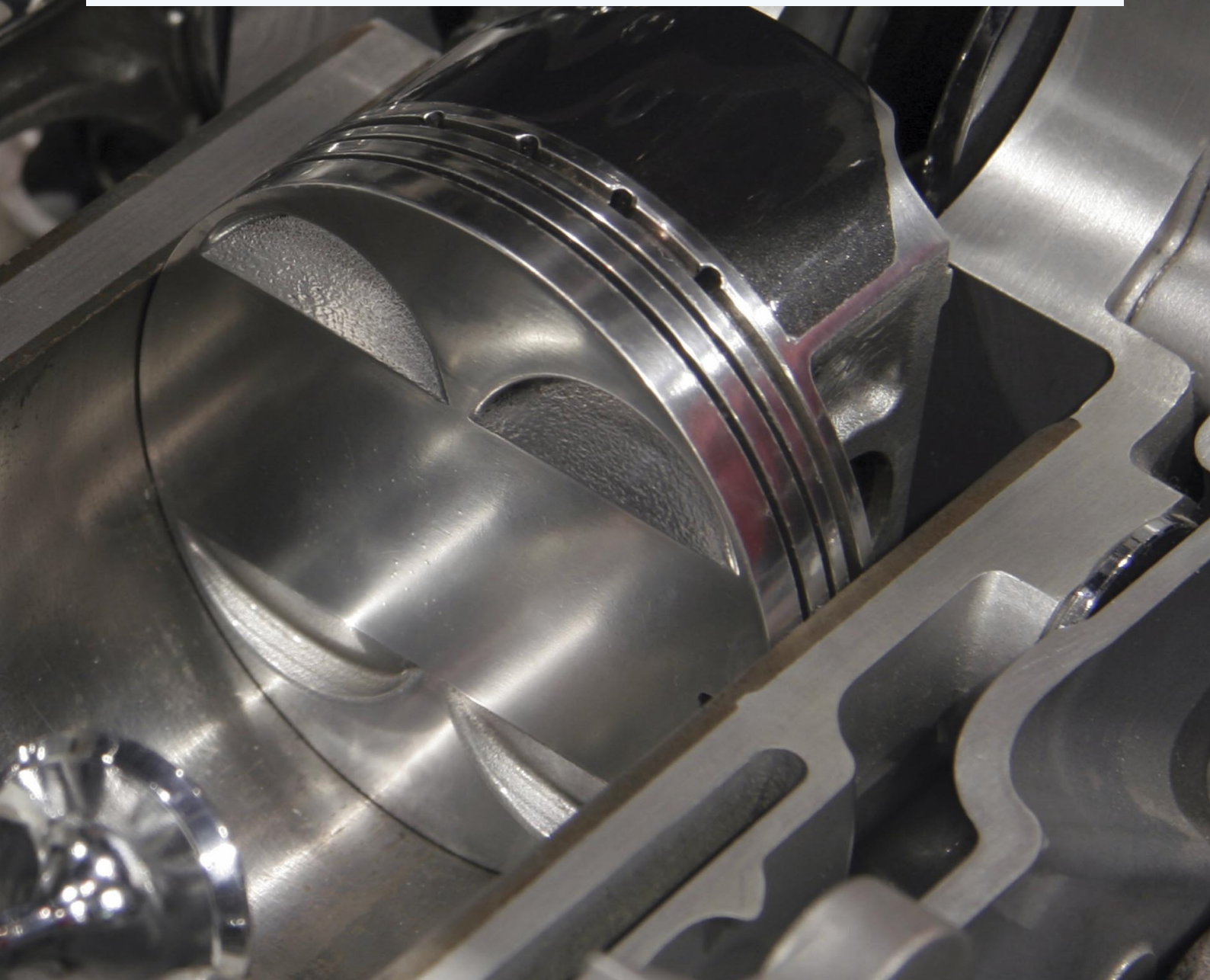
To execute the optimization task, two objective functions, namely **Energy Dissipation** and **Angular Momentum**, are introduced and inserted in the constraints and boundary conditions, while

- ▶ minimizing the Energy Dissipation (ED) leads to an increase of the Discharge Coefficient
- ▶ maximizing the Angular Momentum (AM) leads to an increase of the Tumble ratio

During the multi-objective optimization the two objective functions are combined by using weights ω_i with the sum of the weights being equal to unity.

Simulation Model

The CAD Model and the corresponding computational mesh (generated as 'half model' due to given symmetry) is presented in Figure 1.



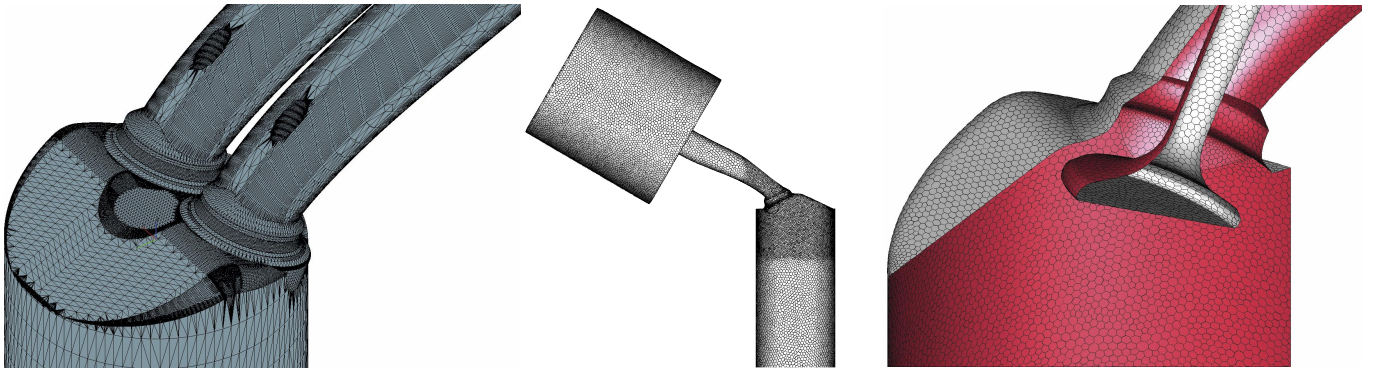


Figure 1: CAD Model (left) and computational grid (centre and right)

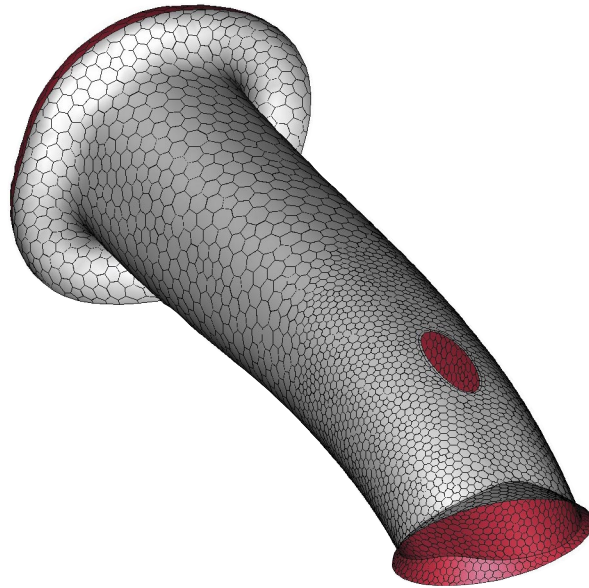


Figure 2: Area of the Wall boundary permitted to be changed during the optimization (the inside surface is coloured red)

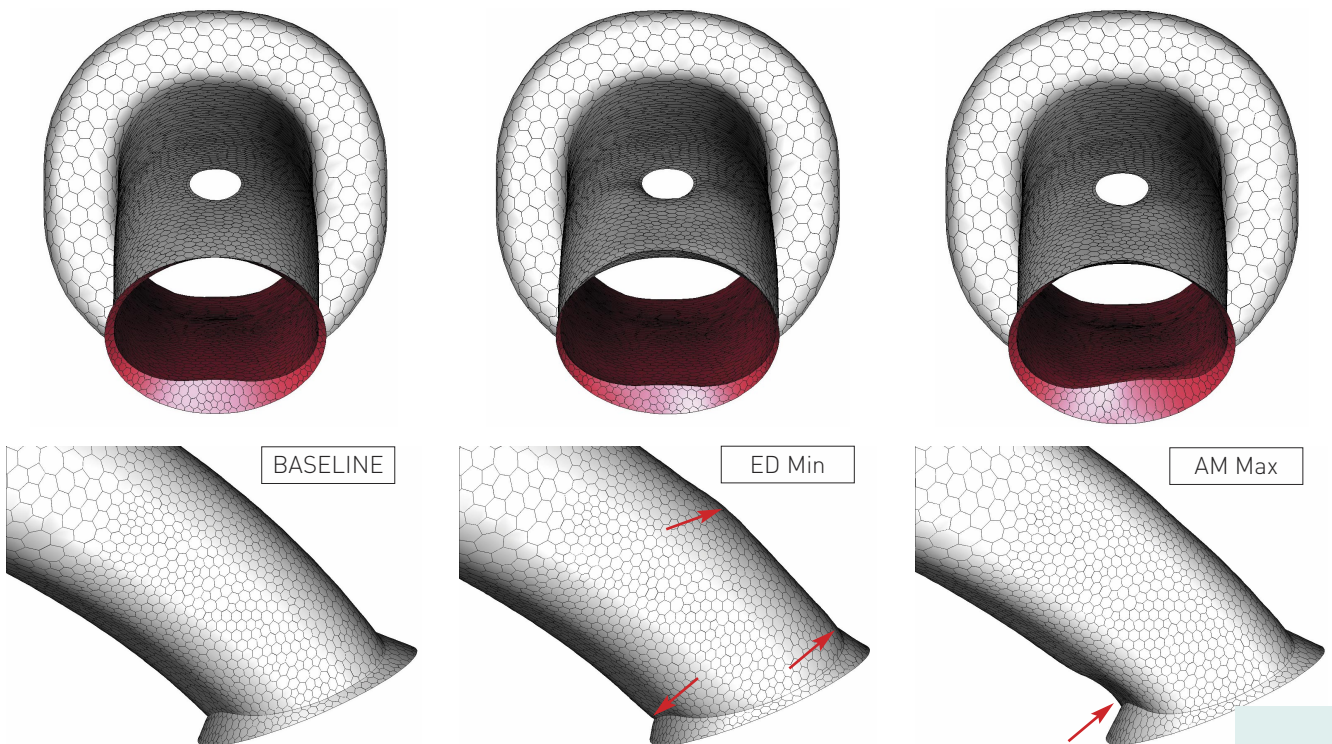


Figure 3: Baseline shape compared to the results of the individual adjoint optimizations

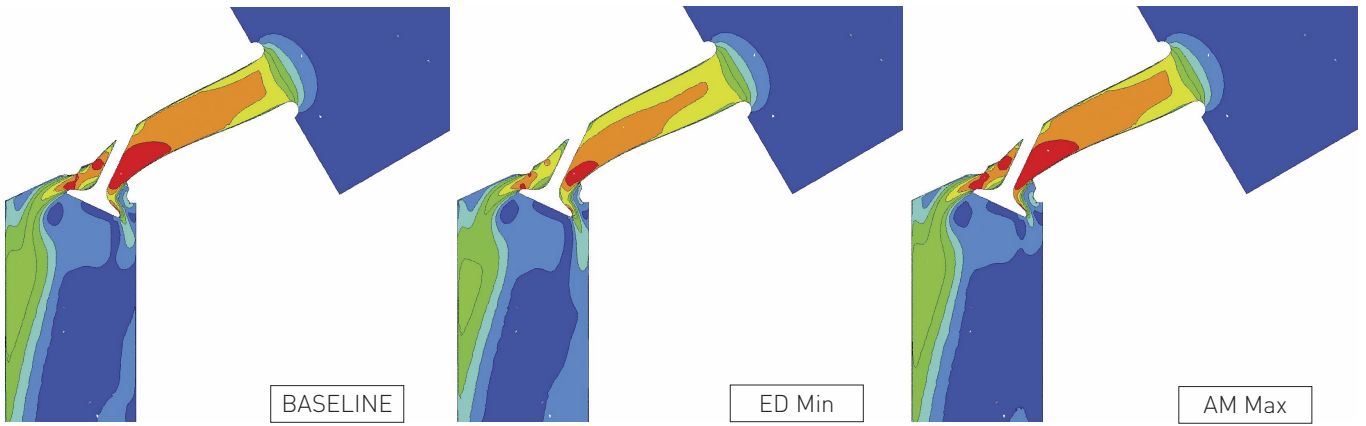


Figure 4: Velocity field in the mid-intake valve-section

The simulation setup is outlined in Table 1. A mass flow of 0.04791kg/s was applied as Inlet boundary condition. Simulations have been executed using AVL FIRETM [6].

Stationary, compressible, iso-thermal flow	
Inlet boundary	0.04791kg/s, 293K
Turbulence model	k- ζ -f
Linear solver	AMG
Differencing scheme	MINMOD
Wall treatment	HYBRID

Table 1: Numerical setup

Single Objective Optimization

Sensitivity analysis was done first for both objectives, Discharge Coefficient and Tumble Ratio, individually. Results are shown in Figures 3, 4 and 5.

Minimizing the Energy Dissipation required less than 30 adjoint steps to achieve convergence. The observed parameters, Discharge Coefficient and Tumble Ratio, show an almost linear response to the changes in the port shape. The finally obtained Discharge Coefficient is increased by ~10%, while the Tumble Ratio has dropped by ~20%.

Maximizing the Angular Momentum required almost 100 adjoint steps to complete the simulation. Considering the primary goal of the task, the outcome seems to be more

favourable. The Tumble Ratio is ~17% higher compared to the Baseline, while the Discharge Coefficient dropped by ~3%. These numbers are reflected in the flow fields shown in Figures 4 and 5.

In Figure 4, a reduced maximum flow speed can be seen when minimizing Energy Dissipation only (ED Min). Additionally the outflow on the rear side of the valve appears stronger compared to the Baseline. This leads to a lower pressure drop and a higher Discharge Coefficient, but a reduced Tumble Ratio.

Maximizing the Angular Momentum (AM Max), a reduced flow over the rear side of the valve, resulting in a clearly higher Tumble Ratio than in the other two simulations, can be observed.

Figure 5 shows the velocity field in the tumble evaluation plane, which is located 1x cylinder diameter below the fire deck. The velocity normal to the plane, the z-velocity, is recognized through the colour scheme with blue representing upwards and red representing downwards flow. The x- and y- velocities in this plane are represented through black vectors with larger vectors corresponding to larger velocities.

A diminishing normal velocity on the exhaust side is observed for the ED Min-case. For the AM Max-case, the area with high absolute normal velocities occupies a larger portion of the cross-section as for the Baseline and the ED Min-case. This corresponds to the higher Tumble Ratio delivered with this configuration.

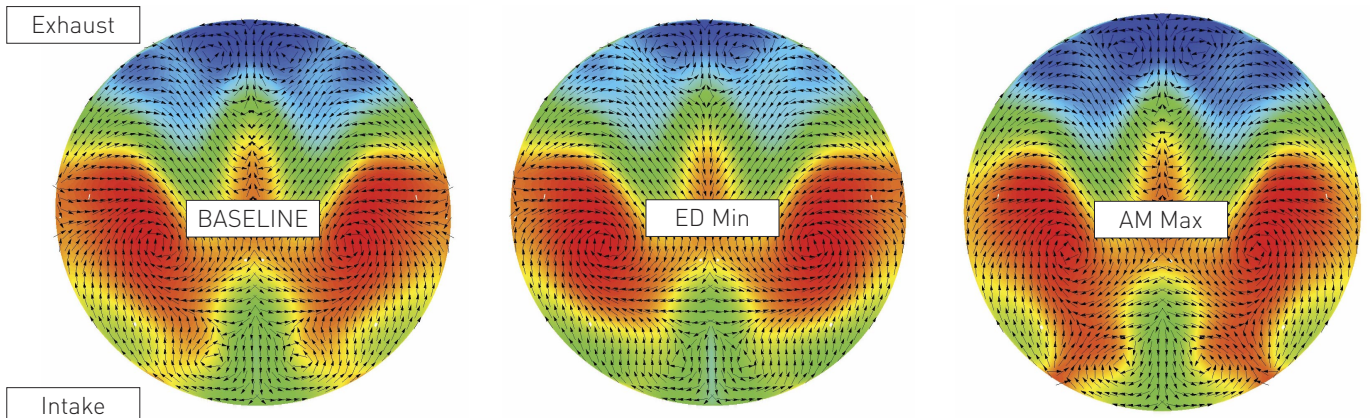


Figure 5: Velocities in the tumble evaluation plane

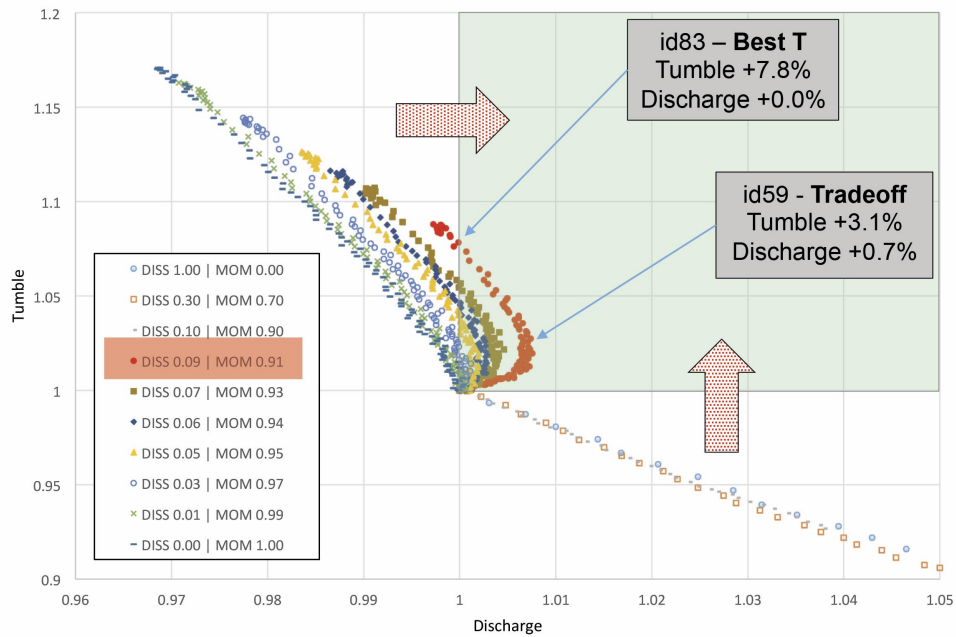


Figure 6: Trade-off between Tumble Ratio and Discharge Coefficient obtained from multi-objective optimization for different weighting factors

Multi-Objective Optimization

From the adjoint optimization of each objective separately one could recognize wall areas sensitive to each specific objective. Additionally it became clear that the pursued objectives are in a trade-off relationship, which requires a weighted objective function.

The shaded area in Figure 6 represents the design space that meets the goal of this optimization task: increased Tumble Ratio while maintaining Discharge Coefficient.

The best results are obtained with a weighting factor of 91% on Angular Momentum and 9% on Energy Dissipation [DISS 0.09 | MOM 0.91]. The design id59 from that run shows ~1% increase of the Discharge Coefficient and an increase of the Tumble ratio for ~3%, which appears to be a good compromise. The design id83 although, allows to increase the Tumble Ratio for ~8%, while maintaining the Discharge Coefficient of the Baseline. The maximum deformation for id83 is a shift of 1.4 mm inwards and 0.7 mm outwards.

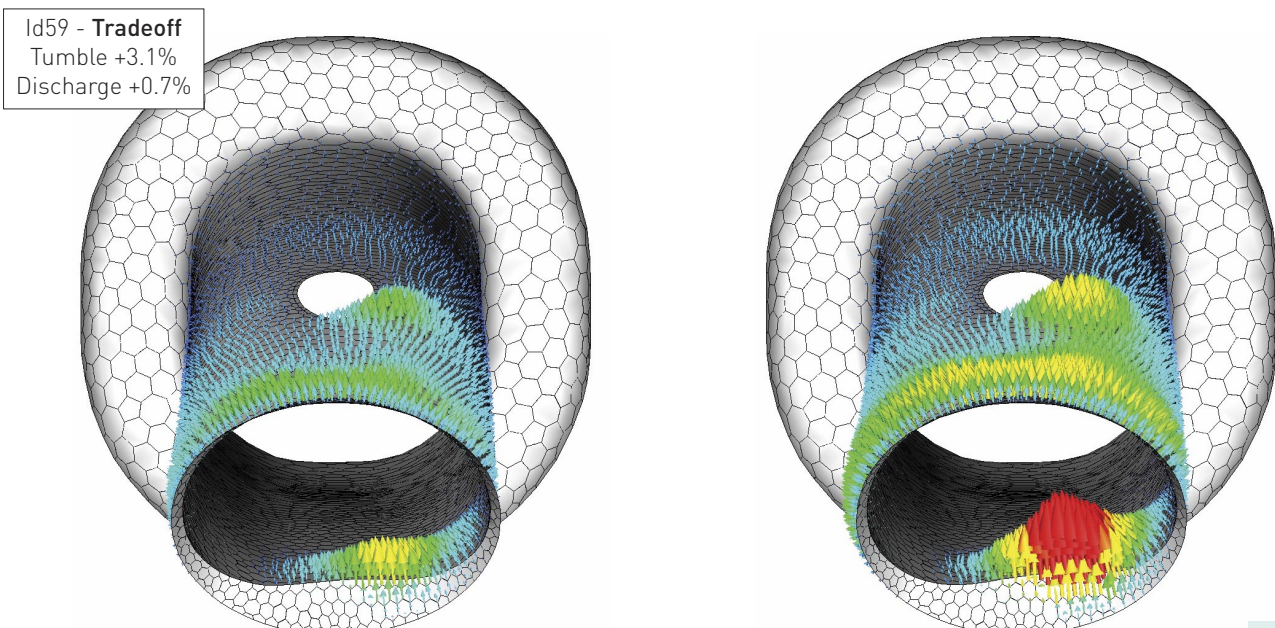


Figure 7: Comparison of 'Best Designs'

Conclusions

The main motivation for this study was the inability to satisfy given targets by deploying a conventional optimization workflow. Consequently, adjoint solver technology was applied to enhance the Tumble Ratio of the Baseline design while maintaining the Discharge Coefficient.

In a first step, single objective adjoint optimization was carried out individually for each objective, Energy Dissipation and Angular Momentum, with the following results:

Minimizing Energy Dissipation:	Discharge Coefficient +10%,	Tumble Ratio -20%
Maximizing Angular Momentum:	Discharge Coefficient -3%,	Tumble Ratio +17%

In a second step multi-objective adjoint optimizations with varying weighting factors for the cost function were performed. Applying a weighting factor of 91% on Angular Momentum and 9% on Energy Dissipation fulfilled the optimisation goal. The Tumble Ratio increased by ~8% while the Discharge Coefficient was kept unchanged. The maximum deformation hereby resulted in a move of 1.4 mm inwards and 0.7 mm outwards.

The adjoint optimization approach was carried out with a single simulation, compared to the 3000 used for the previous conventional approach. Although more iterations were required for the adjoint simulation (3000+2000) it required significantly less overall computational effort. Those two approaches should be considered as complimentary though – the adjoint technique allows unrestricted optimization, which is useful for “local” improvements, while the conventional method allows investigation of a large design space.

The low computational effort and the successful outcome are proof that shape optimization with an adjoint solver is an effective method for searching local extremes. With an increasing choice of built-in objectives the method is expected to be applied in future for a wide range of applications. ■

References

- [1] Rainer, M., Haase, G., Basara, B., and Offner, G., "Shape Optimization by an Adjoint Solver based on a near-wall Turbulence Model," SAE Technical Paper 2015-01-1358, 2015
- [2] Schmidt, S., Schulz, V., "Shape derivatives for general objective functions and the incompressible Navier-Stokes equations," Control and Cybernetics 39, 2010, p. 677-713
- [3] Heywood, J.G., Rannacher, R., and Turek, S., "Artificial Boundaries and Flux and Pressure Conditions for the Incompressible Navier-Stokes Equations," International Journal for Numerical Methods in Fluids 22, 1996, p. 325-352
- [4] Leifert, T., Moreno-Nevaldo, F., Fairbrother, R., Prevedel, K., "Optimizing the dynamic operation of a gasoline engine with high flexibility by means of AVL-GCA", Engine Process Simulation and Turbocharging, Berlin, 2011
- [5] Kotnik, G., Priesching, P., Suffa, M., Hatayama, K., "Diesel Engine Emissions Prediction and Gasoline Engine Knocking Estimation by CFD Methods", JSAE, Yokohama, 2016
- [6] FIRE™ User's Manual v2014, AVL List GmbH, 2016
- [7] Kotnik, G., Rainer, M., "Multi-objective Adjoint Optimization of Intake Port Designs", NAFEMS, Germany 2016

Gregor Kotnik is a Senior Analysis Engineer at AVL. For the last twenty years, he has been active in computational fluid dynamics applying advanced simulation methods especially in the automotive field. He specialises in combustion and emission modelling in internal combustion engines (both, diesel and gasoline). Additionally, in the last decade he is focusing in optimization related to CFD - either conventional (parametrized geometrical design optimizations) or non-restricted (adjoint methods). He is currently leading methods development projects for 3D CFD code FIRE®.

For further information, please contact Gregor Kotnik at gregor.kotnik@avl.com.



SIMCenter - *Advancing the State of CAE in the Transportation Industry*

Amber Pasternak, Ohio State University SIMCenter

As undergraduate engineering education strongly emphasizes fundamentals, students are going into the workforce where they'll be using simulation software often without the required skills to work independently. The Simulation Innovation and Modeling Center (SIMCenter) at The Ohio State University has developed a multi-tiered approach to this challenge in major part through a close partnership with Honda R&D Americas. An undergraduate internship program provides students an opportunity to learn hands-on with faculty members who are working with companies like Honda on immediate research needs while mentoring the next generation of engineers.



Launched in 2013 with a \$5 million gift from Honda, SIMCenter's objective is to train students through applied simulation. Not housed in a specific department or discipline, SIMCenter pulls expertise from several departments within the College of Engineering and works in concert with other University entities. This interdisciplinary approach benefits students, staff, affiliated faculty members and labs, and research sponsors.

Honda didn't just cut a check and sit back. Allen Sheldon, Principal Engineer at Honda and a SIMCenter Honda Official, maintains an office at SIMCenter where he spends part of his workweek and thus is available to interface with students, staff, and faculty. To facilitate work on Honda projects SIMCenter's main office features secure connections to the Honda network that can be used by Honda employees on campus, as well as students and research staff working on Honda projects. Similarly, the SIMCenter conference room also has a direct connection to Honda, so researchers on campus—including students—can participate in meetings about their projects without having to travel off campus.

To address the immediate need for Computer Aided Engineering (CAE) experts, SIMCenter started with a core staff of researchers with expertise in acoustics, aerodynamics, CFD, controls, engines and combustion, finite element simulation, friction, heat transfer, materials joining, and optimization. These staff members are available as researchers on projects, software training, proposal writing, and consultation. Research staff members often oversee undergraduate and graduate students both formally and informally. Spend any amount of time in the SIMCenter office and you'll

hear researchers guiding students on ways to approach problems, what to do when results aren't what's expected or wanted, and communicating with project sponsors.

Emerging Researcher Initiatives

Working to meet immediate industry needs are researchers like Senior Research Associate Sheng Dong and Research Specialist Emily Nutwell who are respectively leading the center's engineering services and professional development initiatives. Sheng and Emily both started at the center in 2015 and through their work have found ways to pursue their specific interests in line with the center's growth. Sheng earned his B.S. in Civil Engineering and M.S. in Bridge Engineering. During his master's program he was first introduced to ANSYS. Sheng then came to Ohio State for his PhD. He gained exposure to additional CAE software and began a project with Honda involving friction characterization and modeling which has become his focus. Traditionally, friction is treated as more of an afterthought. Textbook values are often employed in modeling, but Sheng's work has revealed discrepancies with these coefficients. Now a researcher with SIMCenter, he continues to work with friction research on Honda and Chrysler sponsored projects using his in-house pin-on-disc tribometer.

Taking a different path to SIMCenter, Emily went right to work at Honda R&D Americas as a Vehicle Test Engineer after earning her undergraduate degree. At the end of 1999 she was able to move into a CAE Engineer position. In 2015 Emily joined SIMCenter which allowed her to have significant flexibility and an opportunity to pursue a graduate degree. She began working toward her master's in mechanical engineering and soon discovered the newly



formed Department of Engineering Education at OSU whose course offerings have helped define the next branch of her career.

Before coming to Ohio State, Emily had already started teaching LS-DYNA training classes for other engineers at Honda. She continued to be the lead person for training after joining SIMCenter and was the obvious choice for leading the design of a professional development program. The initial phase of the program, a fully online non-credit certificate with tracks to meet multiple needs, is on set for a January 2018 start. When asked who she sees as the intended audience for the program, Emily answered, "I see me - someone who is in one job, but needs additional skills to move within their company." Engineers not looking to change roles could also benefit. As Allen Sheldon explains, companies like Honda are also putting more of an emphasis on virtual testing before moving on to the physical stages, so there's a need for more test engineers with a fluency in CAE modeling and simulation. Emily emphasizes this is a level beyond software training. Enrollees will already need to know how to use the software they'll be using on the job. What they'll be learning is how to apply techniques and analyze results.

Building the Future

Many early SIMCenter initiatives focused on meeting immediate needs for companies and their engineers, but the center also serves the needs of student engineers. Through the undergraduate internship program SIMCenter helps develop skills and exposure to CAE software. Professors who have hosted interns have said they feel the program works to move students beyond the fundamentals and "raise up undergrads and prepare them

to be grad students." The center recruits students academically on track to get into graduate school. Students selected either work in a lab of an affiliated faculty member or work on a project within the center itself.

Reflecting on his first year as an intern Mark Varner shared, "I learned a lot from the year and it influenced my decision to apply to graduate school." While not every student decides to go on to graduate school, the reality is even the students graduating and going on to industry have gained skills they wouldn't have had otherwise. With any exposure to CAE software, they're more aware of the capabilities and less likely to feel intimidated when they encounter the software on the job. Even if they're not working directly with simulations and modeling, the familiarity they've gained provides a literacy so they're better able to communicate with those who do. Students report that working closely with grad students and faculty in the labs provides skills and comprehension they can apply directly to their classes. Holly Rhodes, a second-year intern, shared, "I think the work I have done, and the things my professor and graduate student have taught me, have increased my engineering thought process and technical skills."

Clayton Thomas, a current master's student, responded to the first call for undergraduate internship applicants. Although concerned about the time commitment, he didn't want to miss out on an opportunity. An argument often made to undergraduates who are on the fence about graduate school involves earning potential with a master's degree versus a bachelor's and the ability to start their career on a higher rung. Clayton had already decided he would get his master's degree right away to avoid

disrupting his career later. However, his experiences as a SIMCenter intern and direct relationship with Honda R&D helped Clayton form a more concrete reason for graduate school. "After diving into the work through SIMCenter, I realized how much more there was to learn that I would have never been able to get to without furthering my education."

While the breadth of subjects covered in the undergraduate curriculum is helpful from a modeling perspective, Clayton's field of automotive powertrain modeling, simulation, and control doesn't allow much of an opportunity for depth at the undergraduate level at Ohio State. To really get into powertrain dynamics and control, graduate school was a necessity. Clayton's research focuses on powertrain control verification and validation through hardware-in-the-loop testing (HIL), which allows for testing control strategies on a virtual vehicle in a controlled environment before the real vehicle is built. In addition to the change in development cycles (earlier, quicker, and less expensive), there is an added safety benefit since the simulations allow for near or over limit testing without the usual dangers of driving at high speeds or in hazardous conditions. His positive experiences working with Honda R&D as an undergraduate and graduate student keep the company at the top of his short list for post graduate plans.

New this academic year is a partnership with Caterpillar. For the first time outside of Illinois, Caterpillar summer interns from Ohio State will have the opportunity to continue their relationship with the company into the academic year. SIMCenter provides dedicated work stations to selected Ohio State students, who will continue their Caterpillar work through a network connection similar to Honda's. Two students started at the beginning of the academic year in August, and another two will join them in January.

Thinking back to when he first heard about Ohio State and Honda partnering to create SIMCenter, faculty member Dr. Scott Noll shares, "I recognized the value such a concentrated center would have on student education and professional development as well as industry research at an academic institution and wanted to be involved." His first introduction to simulation occurred while he was working for a tire manufacturer. The code was written in-house, the interface was clunky and buggy, and it ran on a terminal with the VAX

operating system, but he was hooked. "At my fingertips was all of the company's simulation knowledge in a single place. I could virtually test all types of scenarios for design changes, material properties, etc., and have relatively immediate results." His curiosity led him to graduate school and the memory of those early experiences is what inspires him as he works with students. Scott's research areas include nonlinear structural mechanics, vibrations, inverse identification, experimental modal analysis and dynamic substructuring, applied finite element modeling, and design. He regularly works with students at the undergraduate and graduate levels and believes one of the biggest benefits for students is the opportunity for multiple mentors. In the SIMCenter environment "a graduate student is mentored by a world class academic researcher, industry user experts that have the breadth of simulation experience, and full-time PhD research staff with tremendous depth of knowledge in simulation technology." Students also work on challenging industry problems and network with industry experts.

Director Shawn Midlam-Mohler has been a part of the center since its beginning, first serving as associate director until his promotion in June 2017. Also an associate professor, Midlam-Mohler says, "being involved in the leadership of SIMCenter has been a great addition to my more traditional teaching and research duties. It has the same feel as launching a new business and I am excited to have the opportunity to continue moving SIMCenter forward over the next several years." Midlam-Mohler takes as much a personal interest in guiding permanent research staff through career decisions as he does advising students on classes, long term academic plans, and networking academic and industry connections. His overarching vision that includes strengthening research relationships and moving forward with new initiatives is consistently communicated to all involved.

SIMCenter was started to address an immediate area of concern identified by Honda R&D - a gap in knowledge concerning CAE. Through the growth of research services and professional development initiatives, as well as continuing to improve the internship program and partnerships with faculty labs, SIMCenter's collaborations help place students, faculty, and our industry partners on the best course for innovation. ■

Amber Pasternak started with Ohio State's SIMCenter in January 2017. With the University since 2007, she previously worked in the Academic Programs office of the College of Food, Agricultural, and Environmental Sciences. Amber earned her B.A. in English with a minor in biology from Hiram College in Hiram, Ohio. She lives in Columbus, Ohio with her husband, twin sons, and 2 cats. pasternak.6@osu.edu

Multiphysics Analysis of Lithium Ion Battery

Xinran Xiao & Miao Wang,
Michigan State University

Light-weight, long lasting rechargeable batteries are desired in many applications and lithium ion batteries (LIBs) dominate the market today. Nevertheless, the current LIB technology is still far from satisfactory in meeting the power demands and safety requirement. As in the cases of other products, numerical simulations can help to improve the design of LIBs.

Multiphysics in LIBs

Figure 1 presents a schematic showing the operation of LIBs. It uses two Lithium (Li) storage materials of different thermodynamic potential as a positive and negative electrode. A membrane separator prevents physical contact between the electrodes while enabling ionic transportation. The movement of the ions is driven by the thermodynamic force. When an external electrical potential is imposed, a Li ion is forced to move from the positive electrode to the negative electrode and the battery is charging. Remove the external power source, a Li ion moves back to the positive electrode and the battery is discharging.

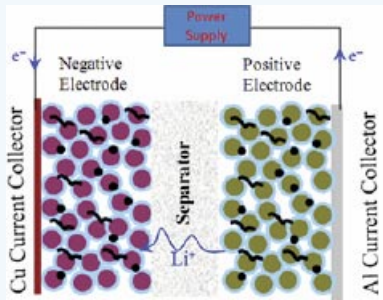


Figure 1: Schematic of a lithium-ion battery being charged.

For a LIB cell during normal operation, the main events are the species/charge transport and electrochemical reaction [1-3]. In the electrolyte, a Li ion is transported through diffusion and migration, governed by the Nernst-Planck equation. In the electrode, the movement of Li ion is described by the diffusion equation. The electrochemical reaction occurs at the electrolyte / electrode interface following the Butler-Volmer equation. These processes generate heat and the process parameters are temperature dependent [4]. Inside solid electrodes, the Li concentration gradient will induce stresses in the material. The stress, in turn, can affect Li diffusion in the host material [5]. Figure 2 depicts these physical phenomena and their coupling relationships in a LIB during normal operation [6].

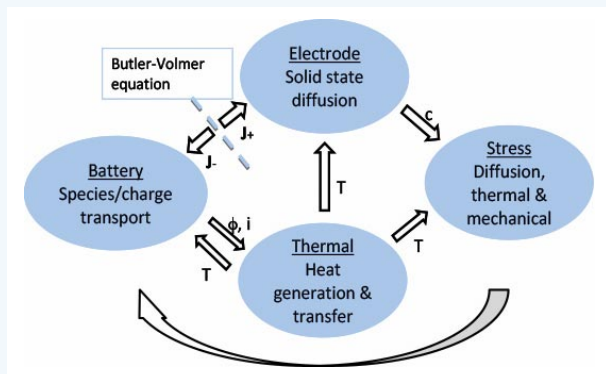


Figure 2: Multiphysics in a LIB cell under normal operation [6].

Stress and Deformation

A unique problems of LIBs is its volume variation. Most materials will experience volume variations during Li insertion and deinsertion. The higher the Li storage capacity of the material, the greater the volume variation. For example, Si offers the highest Li storage capacity besides pure Li itself [7]. Each Si atom can accommodate up to 4.4 Li atoms. Nevertheless, this is accompanied by over 300% volume variation. Figure 3 shows the dramatic volume change of an amorphous Si (a-Si) disk after Li insertion captured by Transmission Electron Microscopy (TEM) [8] and reproduced below by simulation. The Li concentration gradient induced stresses in Si are very high which can pulverize the material [9]. This problem can be solved by making an electrode with nano-sized Si powder and a binder. However, the large volume fluctuation will induce high stresses in other components such as the binder and the interfaces between binder/active material and active material/current collector. Failure at these locations leads to loss of electrical contacts in local areas and rapid capacity fading of the battery. The large volume change of the electrode also poses problems for battery packaging.

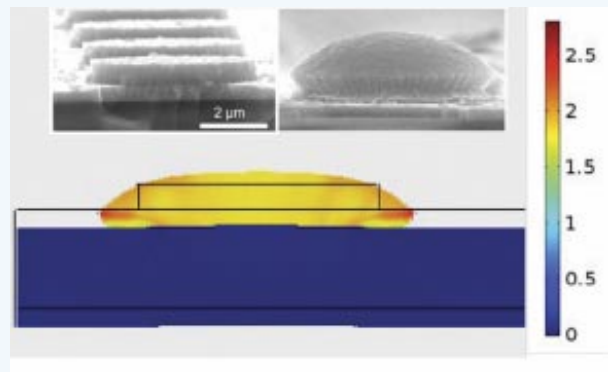


Figure 3: Upper image, before and after images captured by in-situ experiment in TEM [8]. Lower image, simulation results with the black outline showing the original position and shape of the Si disk/current collector. Contours indicating volumetric strain.

To reveal the stress in the electrode, a microstructure resolved Multiphysics (MRM) battery model has been developed in COMSOL, a Multiphysics finite element (FE) solver. The model is composed of two sub-models: "battery" and "stress", as shown in Figure 4. The "Battery" sub-model computes electrochemical kinetics, mass transport, and charge balance. The "Stress" sub-model computes the Li intercalation induced strain, the mechanical strain, and the stresses in the active particles and other battery components. The two sub-models share the same FE mesh and are coupled through Li concentration field and deformation field. This model is capable of revealing the stress and deformation in each battery component throughout operational cycles, as shown in Figures 5 and 6 for a $\text{Li}_x\text{C}_6\text{Li}_y|\text{LiPF}_6(\text{EC}/\text{DMC})|\text{Mn}_2\text{O}_4$ cell [3].

Figure 5a shows a galvanostatic cycle consisting of a discharge (0-1000s), Open Circuit Period (OCP) (1000-1500s), charge (1500-2500s), and OCP (2500-3000s). Figures 5b and 5c present the stress history at the current collector/negative electrode interface for two binders with elastic modulus of $E=184$ MPa and $E=1.1$ MPa, respectively. As seen, the stress is cyclic. The maximum stress occurs at the end of discharging. The magnitude of the maximum stress is about two orders higher in the higher modulus binder.

Figure 6 presents the Li concentration distribution in the electrodes and the 1st principal stress in the negative electrode at different time intervals. It is interesting to note that during OCP, the Li concentration continues to evolve and the stress in the electrode particles and in the binder relaxes.

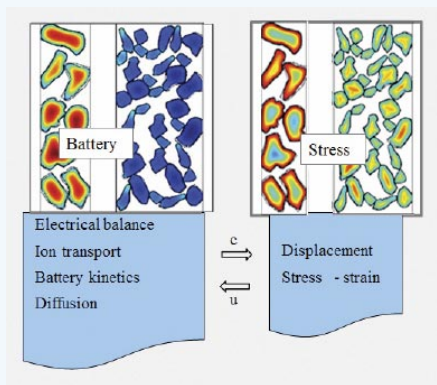


Figure 4: Microstructure resolved Multiphysics battery model

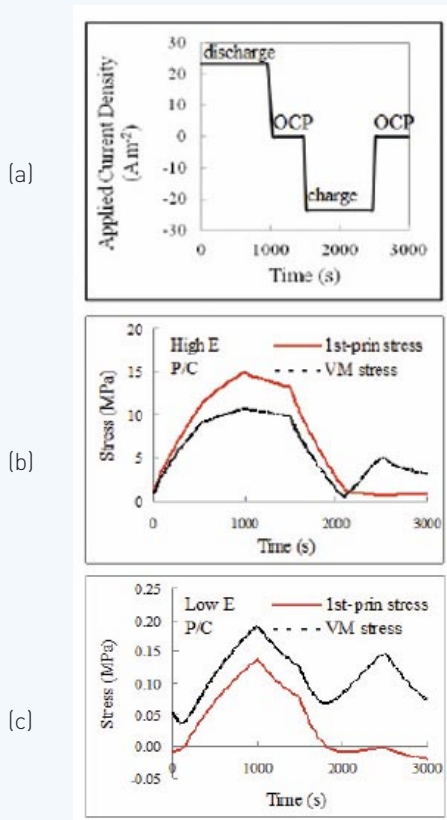


Figure 5: a) A galvanostatic discharge-charge cycle
 b) Stress history for binder with $E=184$ MPa
 c) Stress history for binder with $E=1.1$ MPa

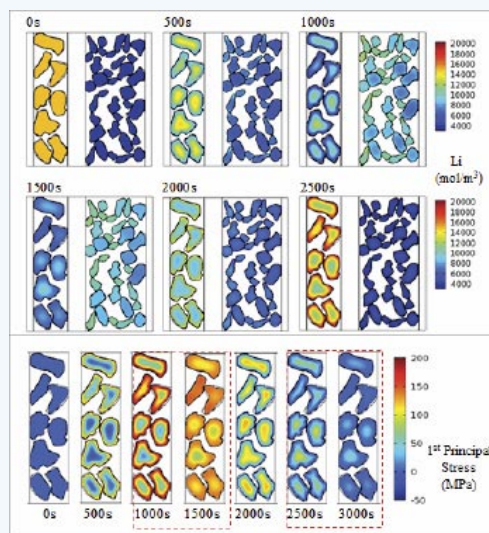


Figure 6: The evolution of Li concentration evolution in the two electrodes and the evolution of 1st principal stress in negative electrode particles during the galvanostatic cycle in Figure 5a.

In LIBs with Si electrode, the stress-diffusion coupling can be significant. It was observed that amorphous Si (a-Si) in the form of thin films exhibit a strong asymmetric rate behavior between lithiation and delithiation [10]. However, this phenomenon was not reported for other geometries, such as Si nanospheres [11]. The MRM model with stress-diffusion coupling was able to reproduce the different rate behaviour of Si electrode in different shapes [5]. The result revealed that the asymmetric rate behaviour is the consequence of the unique stress state in the thin film on a rigid substrate and the stress-diffusion coupling.

Design Optimization

Multiphysics battery models have great potentials for design optimization. Figure 7 shows a parameter study on electrode design for a $\text{Li}_x\text{C}_6\text{Li}_y|\text{LiPF}_6|\text{Mn}_2\text{O}_4$ cell [4]. The parameters investigated are for the negative electrode ($\text{Li}_x\text{C}_6\text{Li}_y$) with a thickness of 0.5L and 1L and a particle size of 0.1R and 1R. Discharge at 1C (complete discharge in 1 hour), the effect is relatively small. At 4C (complete discharge in ¼ hour), the capacity of the LIBs with thick electrode (1R/1L) and (0.1R/1L) has reduced by about 60%.

Another example is a study on the electrode design with Si nanowalls [12]. The results show that the maximum achievable capacity of a cell under a given charging rate depends on the electrolyte potential and overpotential. These two potentials are affected by the concentration polarization. The factors reducing the concentration polarization can enhance the achievable capacity of the cell. Such factors include increasing the space ratio and Li^+ concentration in the electrolyte, and reducing the aspect ratio and the nanowall thickness. Furthermore, the optimal values of design parameters depend on the specific target. Figure 8 compares the effect of aspect ratio and spacing ratio on the achievable specific capacity and volumetric capacity at 1C and 4C. Computer simulations provide a clear picture on how different parameters affecting these capacities at different rates.

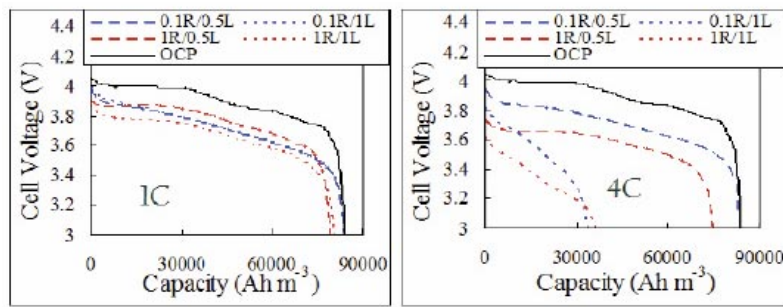


Figure 7: Parameter study investigating the design of the negative electrode at 1C (left image) and 4C (right image)

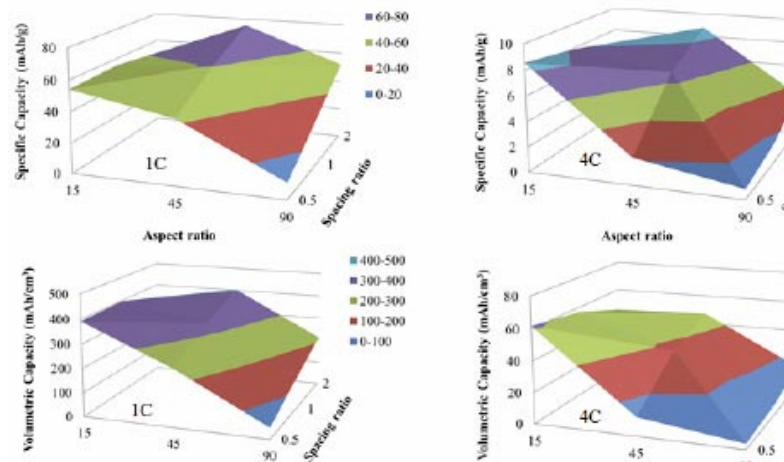


Figure 8: Study comparing the effect of aspect ratio and spacing ratio on the achievable specific capacity.

Summary

In summary, the finite element based Multiphysics simulation has the potential to be used in a wide range of applications beyond the traditional civil and mechanical structures. The application in the analysis LIB is one of them. Even for this particular device, the current work only touches its surface. For example, the models presented here can be extended for design analysis concerning the potential occurrence of short circuit, which is a rather serious concern for LIBs. ■

References

1. Newman, J., *Electrochemical Systems*. 1991, Prentice-Hall.
2. Doyle, M., T.F. Fuller, and J. Newman, Modeling Of Galvanostatic Charge And Discharge Of The Lithium Polymer Insertion Cell. *J. Electrochem. Soc.*, 1993. 140(6), p. 1526-1533.
3. Wu, W., Xiao, X., Wang, M., Huang, X., A Microstructural Resolved Model for the Stress Analysis of Lithium-Ion Batteries, *J. Electrochem. Soc.*, 161 (5), [2014], A803-A813.
4. Wu, W., Xiao, X., and Huang, X. The Effect of Battery Design Parameters on Heat Generation and Utilization in a Li-Ion Cell. *Electrochimica Acta* 83, 227-240 [2012].
5. Wang, M., Xiao, X., Investigation of the chemo-mechanical coupling in lithiation/delithiation of amorphous Si through simulations of Si thin films and Si nanospheres, *J. Power Sources*. 326 [2016] 365-376.
6. Wu, W., Xiao, X., Huang, X., Yan, S. A Multiphysics Model for the In-Situ Stress Analysis of the Separator in a Lithium-Ion Battery Cell, *Computational Materials Science*, 83 [2014] 127-136.
7. Larcher D, Beattie S, Morcrette M, Edström K, Jumas J, Tarascon J, Recent Findings and Prospects In The Field Of Pure Metals As Negative Electrodes For Li-Ion Batteries, *J. Mater. Chem.*, 2007, 17, 3759.
8. Wang, J.W., Y. He, F. Fan, X.H. Liu, S. Xia, Y. Liu, C.T. Harris, H. Li, J.Y. Huang, S.X. Mao, T. Zhu, Two-Phase Electrochemical Lithiation in Amorphous Silicon, *Nano Lett.* 13 [2013] 709-715.
9. Tirado JL, Inorganic Materials for the Negative Electrode of Lithium-ion Batteries: State-of-the-art and Future Prospects, *Materials Science and Engineering R* 40 [2003] 103.
10. Li, J., N.J. Dudney, X. Xiao, Y.-T. Cheng, C. Liang, M.W. Verbrugge, Asymmetric Rate Behavior of Si Anodes for Lithium-Ion Batteries: Ultrafast De-Lithiation versus Sluggish Lithiation at High Current Densities, *Adv. Energy Mater.* 5 [2015] 1401627.
11. Liu, N., H. Wu, M.T. McDowell, Y. Yao, C. Wang, Y. Cui, A Yolk-Shell Design for Stabilized and Scalable Li-Ion Battery Alloy Anodes, *Nano Lett.* 12 [2012] 3315-3321.
12. Wang, M., Xiao, X., and Huang, X., A Multiphysics Microstructure-Resolved Model for Silicon Anode Lithium-Ion Batteries, *J Power Sources*, 348 [2017] 66-79.

Xinran (Sharon) Xiao is a Professor of Mechanical Engineering at Michigan State University (MSU), a member of the MSU Composite Vehicle Research Center, and a Fellow of the American Society for Mechanical Engineers (ASME). She worked at General Motors (1999-2008) and supported crashworthiness predictions of composites, plastics and adhesive bonded vehicle structures. Xiao's research is focused on modeling of mechanical behaviors of materials and structural responses under different loading conditions using finite element (FE) simulations, including impact, crash, fatigue, creep, thermal, diffusion and during manufacturing.

Aero-Vibro-Acoustics for Wind Noise Applications

Marco Oswald, ANSYS Germany GmbH
Sandeep Sovani, ANSYS Inc., USA

Wind noise is high on automotive customers' minds when they judge the quality of a vehicle. In the J.D. Power 2014 U.S. Vehicle Dependability Study [1], excessive wind noise is listed as no. 1 amongst the top 10 problems most commonly experienced by vehicle owners. Whereas automobile manufacturers have a good handle on optimizing aerodynamics for minimizing drag force, reducing wind noise has remained a stiff challenge. Wind noise comprises three advanced physical problems, making it more complicated to simulate and predict. As a result, until now automakers have had to rely heavily on costly and time-consuming wind tunnel testing for wind noise reduction. A new simulation method - Deterministic Aero-Vibro-Acoustics - has now been developed to solve all three physical problems involved in wind noise as a single set. This method is based on first principles not requiring statistical or empirical techniques such as transfer functions, and can be used by engineers to predict wind noise with accuracy and confidence.

Challenges

Wind noise is a physical problem that involves the three complicated aspects each governed by a different physics:

- Sound generation: governed by fluid dynamics
- Sound transmission: determined by structural mechanics
- Sound propagation: governed by acoustics

Sound Generation: Wind noise is generated on the vehicle's outer surface due to turbulence in the surrounding air flow. Obstructions such as the A-pillar, side view mirror, and wipers disrupt the air flowing past the car and produce intense turbulence. As turbulent eddies move past or impinge on flat surfaces, they create pressure fluctuations on the side window, windshield and other body panels. These pressure fluctuations are the source of wind noise and are governed by the fluid dynamics of the air flow.

Sound Transmission: The pressure fluctuations acting on the vehicle body's outer surface create minute vibrations transmitted through the thickness of the body panels, glass and trim and reach inside the cabin. These vibrations and their transmission are determined by structural mechanics of the body structure.

Sound Propagation: The vibrations that reach the vehicle body's inner surface excite the air in the passenger cabin and propagate as sound waves from the inner body structure to the driver's ears. This propagation is governed by the acoustics of the cabin air cavity.

The main challenge in wind noise simulation for passenger cars and commercial vehicles lies in computing the sound transmission through the vehicle body structure. Whereas tools for simulating the unsteady external airflow have reached a high level of maturity and are able to reliably predict external turbulent pressure fluctuations that serve as the source

of wind noise, previous methods for computing sound transmission have proven unreliable. Popular methods that have attempted to calculate sound transmission to-date are transfer functions and Statistical Energy Analysis (SEA).

The major drawback of these techniques is that they employ assumptions, empirical correlations and model constants that rely heavily on specific test data. As a result their applicability is quite narrow. They can make reasonable predictions only when used in cases closely similar to the case where the test data was measured. For instance, if empirical correlations in these methods are formulated using wind tunnel test data for one vehicle program, then their accuracy is likely to be unreliable for another vehicle program, or even for major design changes within the same vehicle program. Typically, some amount of testing is essential to give confidence in the model parameters and predictions of SEA methods [2]. Particularly, SEA methods requires testing for confirming acoustic-acoustic and structural-acoustic transfer functions, which can vary significantly with design changes in body shape and design. Since the predictive range of these methods is narrow and centered around test measurements, car makers have to incur the time and expense of performing extensive testing during wind noise related vehicle development.

New Deterministic Method

In contrast to SEA, a deterministic method is based on first-principles and does not require empirical correlations such as transfer functions. A classic example of a deterministic method is Computational Fluid Dynamics (CFD) used for simulating air flow around the vehicle. The method is based on rigorous solution of fundamental physical equations and the only required inputs are simple case specific parameters such as vehicle speed, ambient temperature, and material properties of air.

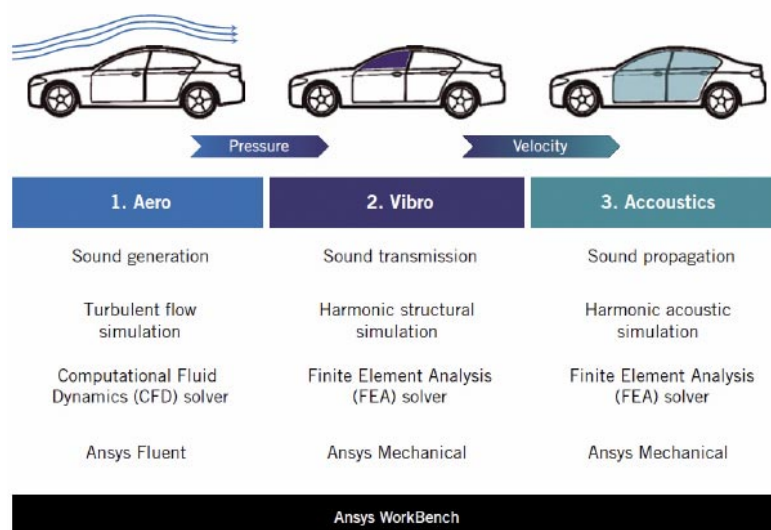


Figure 1: Deterministic Aero-Vibro Acoustics (DAVA) – implementation of DAVA simulation in three steps

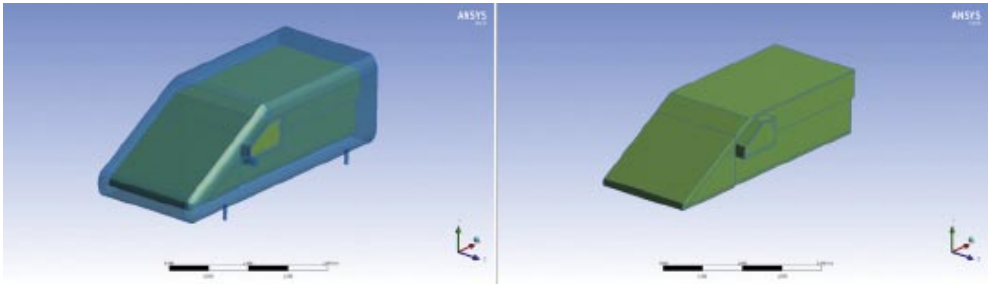


Figure 2: Left: SAE-Body with generic side-view mirror. Right: Vehicle cabin volume

Such a deterministic method has now been developed by ANSYS for predicting automotive wind noise. It solves fundamental physical equations of fluid dynamics, structural mechanics and acoustics, to compute all aspects of wind noise in unison: generation, transmission, propagation. It is referred to as Deterministic Aero-Vibro Acoustics (DAVA), where "Aero" represents aerodynamics of the external air flow which generates sound, "Vibro" stands for vibrations of the vehicle body structure which transmit outside sound to the interior of the vehicle, and "Acoustics" represents acoustic wave propagation inside the vehicle cabin that takes sound from the vehicle body to the driver's ears.

A DAVA simulation is implemented in three steps as visualized in Figure. 1. First a transient CFD simulation of the external airflow is conducted with scale-resolved turbulence models such as Large Eddy Simulation (LES). Time-varying pressure which acts as the source of sound is recorded at every grid point on major sound transmitting surfaces such as the side window and windshield. The pressure signals at each grid point are transformed with Fast Fourier Transformation (FFT) and applied as excitations to a structural model of the vehicle body in a structural solver. A harmonic analysis of the vehicle body structure is conducted with Finite Element Analysis (FEA) in the structural solver to compute sound transmission through the body structure. Vibration velocities at all grid points on the inside surface of the vehicle body obtained from the structural acoustic analysis are applied as excitations to a model of the cabin air cavity. A harmonic acoustic analysis of the cabin air is conducted in a FEA solver to compute propagation of sound through the cabin to the driver's ear. Optionally, the body structural vibration and the cabin acoustic simulations can be conducted simultaneously in the FEA solver with a single combined model of the body and cabin air. This approach is referred to as strong vibro-acoustic coupling, in contrast to the weak vibro-acoustic coupling described earlier.

The key requirements for DAVA are

- (a) comprehensive robust physics solvers for each of the three underlying physics and
- (b) seamless interconnection between the solvers so that the geometry models, boundary conditions and results from one physics solver can be easily and robustly applied to another solver.

ANSYS Fluent (CFD solver) is used for the Aero solution and ANSYS Mechanical (FEA solver) is used for the Vibro and Acoustic simulations, see Figure 2. These solvers are hosted inside the ANSYS Workbench platform that manages the interconnections between solvers. The interface between the Aero and the Vibro solutions automatically records pressure in time domain at all grid points of relevant vehicle body surfaces in the CFD solver, transforms them into the frequency domain, interpolates them to the grid point locations of the structural model and applies them to the relevant surfaces of the FEA solver. Likewise, the interface between the Vibro and Acoustic solvers seamlessly interpolates and transfers vibration velocity data.

The DAVA method is only practical for low-frequency acoustics. The higher the frequency, the more expensive the CFD-part is. Especially higher frequencies are exciting certain Eigenmodes of the side window (depending on the glass material and the mounting of the glass panel). In contrast, Statistical Energy Analysis (SEA) has best insight at higher frequencies. Furthermore, the DAVA method is time-consuming compared to SEA because DAVA is based on accurate solution of fundamental physical equations of fluid dynamics, structural mechanics and acoustics solved in unison and does not rely on assumptions, empirical correlations and model constants that depend heavily on specific test data as for SEA.

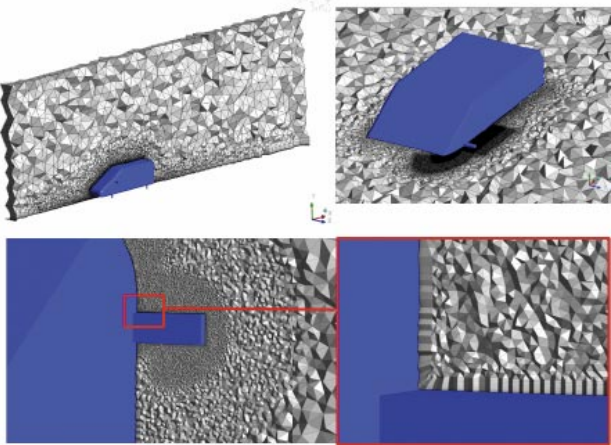


Figure 3: CFD- mesh including tetrahedral cells, 30 prism-layers near the wall and refined region of interest

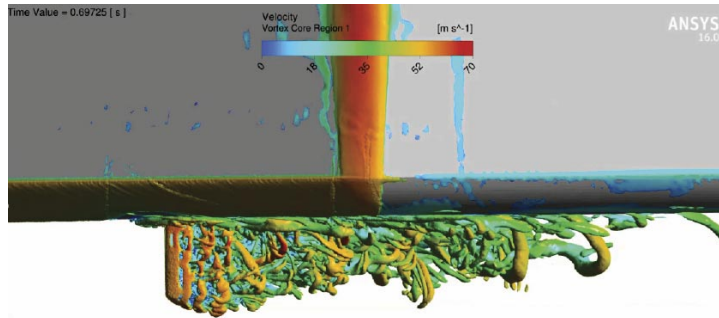


Figure 4: Instantaneous flow-field - iso-surfaces of the Q-criterion (colored by velocity magnitude; view from top)

Validation Example

The Friedrich-Alexander University Erlangen-Nuremberg recently conducted detailed experimental measurements with the SAE body [3]. The extensive data set could be used for validating generation, transmission and propagation of wind noise, see Figure 2.

The SAE body generates wind noise generating fluid structures similar to a commercial vehicle shape, including an A-pillar vortex, a generic side-view mirror and separation and reattachment regions on the roof. The model has a float-glass sheet on driver's side as well as an inner hollow space lined by sound absorption materials that acts as the cabin. Key material properties such as a density, Young's modulus, Poisson's ratio and frequency-dependent absorption coefficients are reported for all materials involved.

Wind tunnel tests were conducted at 150 km/h. Time varying static pressure was reported on 39 probe positions on the outer surface of the model. Likewise, sound pressure was reported at a microphone placed in the cabin at a point representing the driver's ear. An 87 million cells CFD model with first cell height of 0.05 mm was used for the Aero (CFD) portion of the DAVA simulation. Figure 3 shows several cuts through the hybrid computational mesh.

Transient flow simulation was conducted with the Delayed-Detached-Eddy-Simulation (DDES)-SST k-omega model at a 30 μ s time step with the ANSYS Fluent CFD solver. Unsteady RANS-models often fall short of capturing coherent structures that are responsible for significant tonal and broadband noise. Evidently, LES and RANS/LES-hybrid approaches are better suited for that task [4]. Figure 4 shows the instantaneous turbulent flow-field. Near the wall, turbulence is modelled, away from the wall, it is resolved.

Surface dB maps from the CFD simulation, Figure 5 (left), show the location of prominent sound sources in two different frequency bands (100 and 1000 Hz). After transforming the time-signals of the pressure into the frequency domain by means of FFT, this complex pressure will be mapped as loads onto the structure-side of the interfaces. The real part represents the resistance and the imaginary part represents the reactance. Figure 5 (right) shows the resistance for same two frequency bands. Structural harmonic simulations were conducted with the ANSYS Mechanical solver at 333 frequencies from 0 to 1000 Hz.

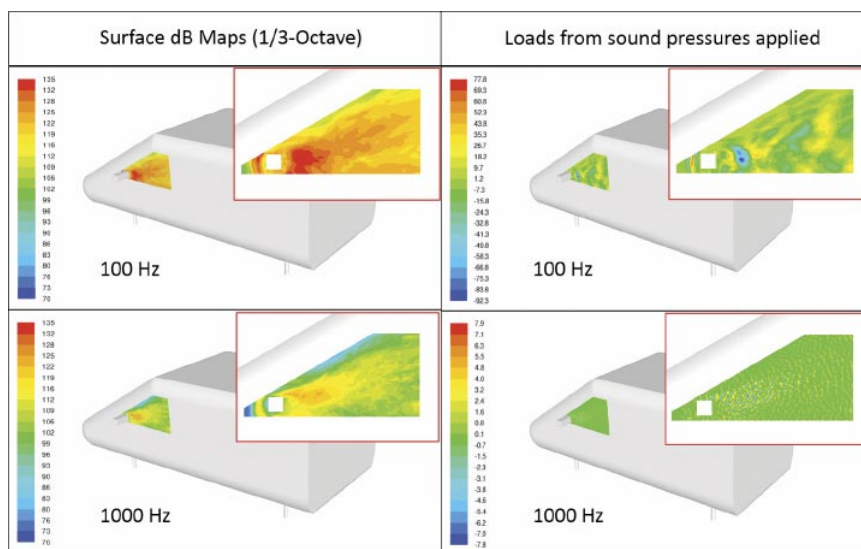


Figure 5: Surface dB maps on side window (left); real part (resistance) of the mapping quantity (right)

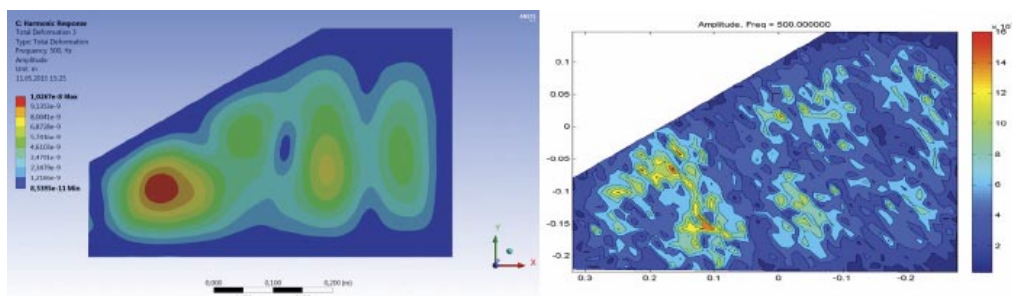


Figure 6: Simulated displacements (left) of side window at 500 Hz; comparison with experimental data (right).

Displacements of the float-glass sheet, Figure 6, computed from these simulations were applied as loads to a model of the cabin air cavity with 660,000 elements. The absolute difference between simulation and experimental data is only about 1.5e-07m. The right plot in Figure 6 is spotted because there were only 1426 measuring points for the laser-scanning vibrometer setup. In FEA we have about 22,000 elements for the side window, hence the plot is much smoother.

A harmonic acoustic analysis of the cabin air, which represents the final acoustics simulation, was conducted with the ANSYS Mechanical solver. This yielded sound pressure levels at the microphone location in the cabin, Figure 7. DAVA simulation predictions are seen to predict same trends vs. frequency as experimental data.



Figure 7: Sound pressure level at driver's ear compared with measured data

Conclusions

Though wind noise is the top quality concern of automotive customers, it has been challenging to simulate accurately since rigorous wind noise computation methods were not available, until recently. For a first-principles computation of wind noise without use of empirical correlations, transfer functions and experimental calibration, three physical problems need to be solved in unison – aerodynamics for sound generation, vibration for sound transmission through the vehicle body, and acoustics for propagation of sound in the vehicle cabin.

A new Deterministic Aero-Vibro-Acoustics (DAVA) method has been developed by ANSYS that performs simulations of each of these three aspects with rigorous CFD and FEA methods. This DAVA method runs in the ANSYS Workbench platform that hosts the CFD and FEA solvers and seamlessly interconnects them for ensuring efficiency and robustness of the solution process. Test cases confirm that computed sound spectra inside a vehicle cabin shows good trends as compared with test data up to 1000 Hz. ■

References

- [1] J. D. Power and Associates (Ed.): J.D. Power 2014 U.S. Vehicle Dependability Study, 2014
- [2] Musser C. T., Manning J. E., Peng G. C.: Predicting Vehicle Interior Sound with Statistical Energy Analysis. In: Sound and Vibration, December 2012, <http://www.sandv.com/downloads/1212muss.pdf>
- [3] Müller, S., Gabriel, C., Ullrich, F., Lerch, R., Becker, S.: Analysis of Flow-Induced Noise at a Simplified Car Model Depending on Various Setup Parameters. In: Proceedings of the International Conference on Acoustics AIA-DAGA 2013, Deutsche Gesellschaft für Akustik e.V., 2013. – ISBN 978-3-939296-05-8, S. 1884–1887. – Merano(Italy), March 2013
- [4] Menter F. R.: Best Practice: Scale-Resolving Simulations in ANSYS CFD, December 2012



Marco Oswald studied of Mechanical Engineering at Technical University of Darmstadt/Germany with focus on Aerodynamics and Numerical Methods in Mechanical Engineering, graduating in 2002, when he joined Fluent Germany, now Ansys Germany. In the early years, he acted as support and consulting engineer for aerospace and automotive accounts with a focus on Aerodynamics and Aero-Acoustics.

From 2011 until 2015 he has been teamleader in the Ansys Customer Excellence Team. Responsible for training and support of CFD-related workflows in aerospace and automotive industries.

Since December 2015, he has worked as the Technical Account Manager for the Volkswagen Group, responsible for coordination of technical activities related to Ansys simulation in all 12 group brands (flow-, structural, electromagnetics and system-simulation).

Using Artificial Intelligence to Analyze Crash Simulations

Constantin Diez, Lasso GmbH

In recent years, Artificial Intelligence (AI) has disrupted almost every industrial branch, be it Robotics, Medicine, Marketing, Geology, Astronomy and many more but Computer Aided Engineering (CAE) is still only beginning to incorporate AI technology. This article demonstrates how AI-technology is already being used at Lasso GmbH to analyze crash simulations. The results shown in this article originate from a doctoral thesis done at Opel Automobile GmbH, which emphasizes the industrial relevance of the topic

Why use Artificial Intelligence for Postprocessing?

In general, there are two core questions when postprocessing simulations:

1. What notable effects are occurring?
2. How to avoid or trigger specific effects?

Humans can answer these questions for one or two big models, but if confronted with five or six models at once, this usually exceeds our capabilities. Unfortunately, as a general trend of digitalization, the amount of simulations being performed is steadily increasing. For many companies, it is already impossible to analyze every simulation result thoroughly and in consequence, important issues get overlooked every day.

AI has the capabilities to alleviate the burden of postprocessing by enabling algorithms to compare results without human input. The need to deal with the increasing amount of data is not the only benefit, but also attaining deeper insights into our existing data. Therefore, future postprocessing will inevitably incorporate AI technology in order to not lose sight of what's important in our simulation data and keep analysis costs low.

Case Study of a Full-Frontal Crash

As an example, the simulation model of a 2007 Chevrolet Silverado will be used. The simulation model is freely available on the website of the National Highway and Traffic Safety Administration (NHTSA) [1].

In order to investigate the behavior of the car under uncertainty, 24 sheet thicknesses, the impact velocity and the impact angle were varied heavily in a Design of Experiments (DOE) study. The sheet thicknesses are

taken from the crash absorbing structure shown in Figure 1, which ought to have a high influence on the deformation behavior. 1000 simulation runs were performed. The similarity cloud shown in Figure 2 can be created from far fewer samples without any problem or quality issues. The rule mining also works well on low sample counts (it was especially designed for this) but the effectiveness is strongly dependent on the data. Obvious trends can be found at low sample counts (e.g. 50-80), whereas rare effects require many more. Note that we do not necessarily need a lot of samples of one cluster to derive recommendations. In this case 11 out of 1000 samples showing a particular undesirable trait was sufficient to develop a design recommendation. For explanatory purposes we will focus in the rest of the article only on the left rail (red) from Figure 1.

What Notable effects are Occurring?

Manually analyzing and categorizing 1000 simulation results is not feasible and thus requires automation. Using simple scripting to extract some system responses would be an incomplete approach, since important effects at locations where measurements are not being taken might be neglected.

Another approach is to use an AI algorithm [2] to automatically cross-compare every simulation result. In order to visualize its findings, the algorithm returns a similarity cloud (Figure 2), where every marker represents a simulation result. The exact coordinates of a simulation result in this cloud does not matter, what matters is the relative positions of the simulation results. The shape of the cloud inherently describes how the entirety of runs behaves. For example, continuous regions will reveal continuous behavior transitions as will be shown later on.

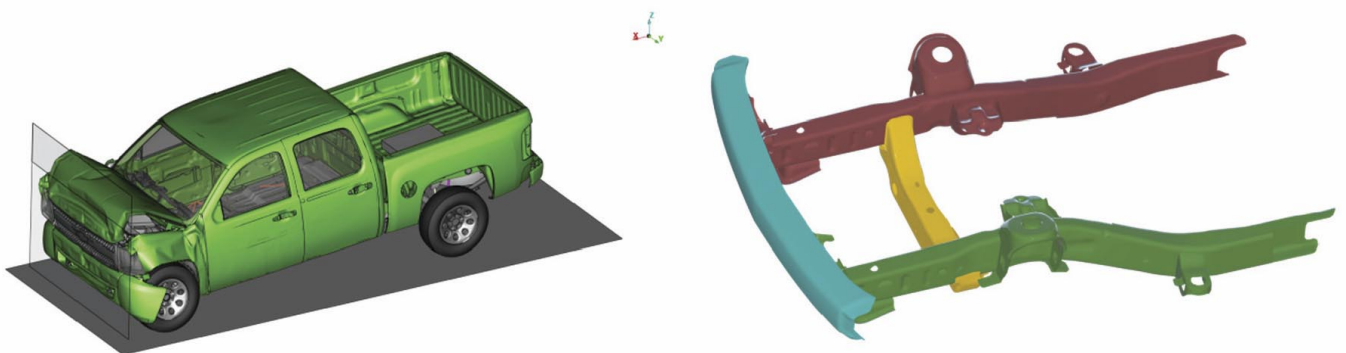


Figure 1: Full frontal crash of a 2007 Chevrolet Silverado (left). For data analysis, the crash absorbing structure (right) was divided into four sub-components: the bumper (cyan), the crossbeam (yellow), the left rail (red) and the right rail (green).

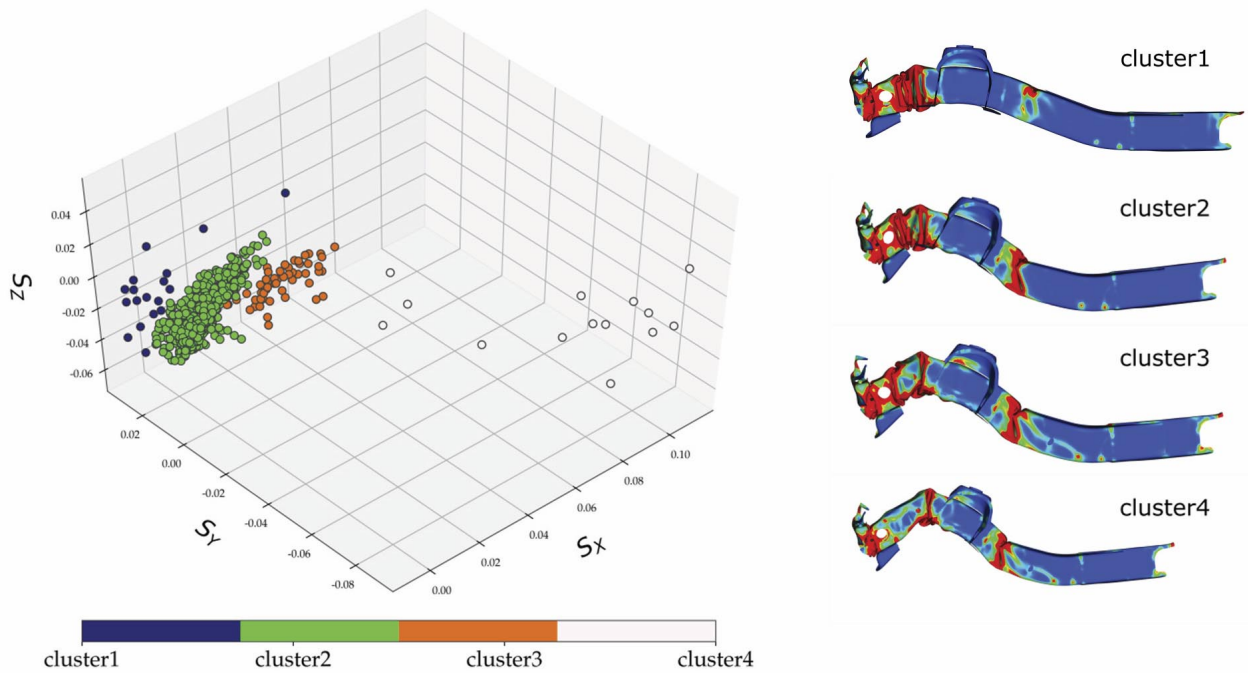


Figure 2: Similarity cloud of 1000 left rail simulations (left). In order to understand the overall behavior, one can cluster the data and view the most centric samples of the clusters (right). The samples are colored according to effective plastic strain.

The similarity cloud of the left rail (Figure 2, left) has four obvious clusters, which are the major deformation modes. In order to understand the cluster differences, it is helpful to view the effective plastic strain for one representative sample for each cluster (Figure 2, right). Cluster 1 reveals good behavior for keeping the rail relatively straight during impact, whereas the samples of cluster 2 and 3 bend upwards more, which is not perfect but still acceptable. Cluster 4 contains ~1% of the samples and deforms very inefficiently in terms of energy absorption, since the rail is bending upwards rather than being crushed. Later on, we will investigate how to avoid this rare but still very dangerous type of deformation. At this point it's obvious how fast this method actually is to analyze such a vast number of simulation runs.

The similarity cloud of Figure 2 can also be analyzed on a much finer scale. For example, if samples are chosen along a path in cluster 2, one can view the transitional behavior inside the cluster (Figure 3).

How to Avoid or Trigger Specific Effects?

From the previous analysis, one is able to determine not only the overall deformation behavior of the structure, but also detect undesirable types of deformation. We found the behavior of cluster 4 to be especially undesirable, since the rail is bending upwards (Figure 2, right), thus does not absorb the kinetic energy sufficiently well.

To investigate the issue, we will use Rule Mining. Rule Mining is a technique from the field of Knowledge Discovery in Databases (KDD) and has the goal to identify a Boolean rule "if D then T " where a design D is results in the target T . An example rule is

$$\text{if } X_7 < 4 \text{ then intrusion} < 100$$

which simply states, that if we would keep the design variable X_7 smaller than four, that we would always

achieve an intrusion smaller 100. Before performing Rule Mining, the target condition T is specified by the user and the algorithm will search for multiple corresponding designs D_i .

What are the Advantages and Disadvantages?

An interesting property is that the algorithm doesn't necessarily return one specific design, but in contrast to optimization, may return multiple design spaces. The user can select a specific design from these design spaces, which allows them to incorporate additional information. Our algorithm [3] is designed in such a way, that it returns only the most important rules and may also return none if the data is not obvious enough. Additionally, as few variables as possible are used to explain the data and the design rules are also simplified in such a way, that an engineer can understand them. By using Decision Tree Learning as background technology, Rule Mining is applicable on low sample counts, which is very common in the field of CAE.

How to Avoid the Bending Behavior of the Left Rail?

In order to avoid the bending of the left rail (Figure 2, cluster 4), we define the target as:

$$T := \text{not cluster 4}$$

For this target the Rule Mining algorithm returns two design recommendations:

$$D_1 = t_{\text{rail}} < 2.65$$

$$D_2 = t_{\text{rail}} > 2.65 \wedge t_{\text{crossbeam}} > 2.3$$

The first recommendation is to reduce the thickness of the rail itself, which lowers the stiffness. This makes sense from a mechanical point of view, since lowering the stiffness makes the rail soft enough to be crushed instead of bending upwards.

The second recommendation simply states, that if the

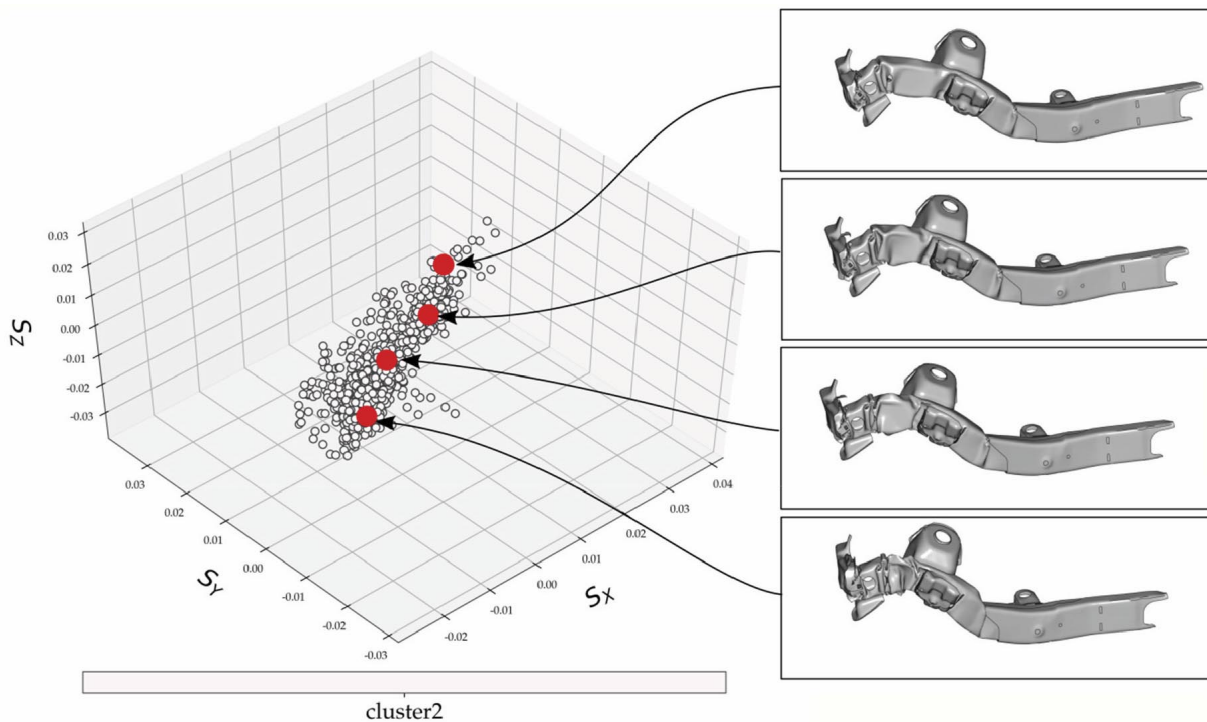


Figure 3: Choosing samples along a cluster in the similarity cloud reveals the transitional behavior of the simulation results.

left rail needs to have a high stiffness, then one could also reinforce the crossbeam by increasing the thickness to keep the rail in place.

These design recommendations can also be visualized as zones in the design space (Figure 4).

Summary

Keeping track of the steadily increasing amount of simulation data is a difficult task. In this article we were able to not only understand the overall behavior of 1000 simulations but could also detect a rare but dangerous deformation mode. Even though only 11 simulations showed the specified behavior, Rule Mining was able to give reasonable design recommendations in order to avoid the undesired behavior.

As a conclusion, by using Artificial Intelligence it is possible to gain insights faster, and in more detail, than ever before. AI will not only help to keep simulation costs low but will also help engineering departments deliver higher quality solutions. ■

References

- [1] United States Department of Transportation. Crash Simulation Vehicle Models. Available at: <https://www.nhtsa.gov/crash-simulation-vehicle-models>.
- [2] C. Diez, L. Harzheim, A. Schumacher, "Effiziente Wissensgenerierung zur Robustheitsuntersuchung von Fahrzeugstrukturen mittels Modellreduktion und Ähnlichkeitsanalyse", VDI-Reports Vol. 2279, SIMVEC 18, November 2016, Baden-Baden, Germany
- [2] C. Diez, L. Harzheim, A. Schumacher, "Efficient and automated comparison of crash simulations with geometry based dimensionality reduction", Technical Report, November 2016, Ruesselsheim, Germany, DOI: 10.13140/RG.2.2.29234.91844 available on Research Gate.
- [3] C. Diez, et al., "Big-Data Based Rule-Finding for Analysis of Crash Simulations", 12th World Congress of Structural and Multidisciplinary Optimization, June 2017, Braunschweig, Germany

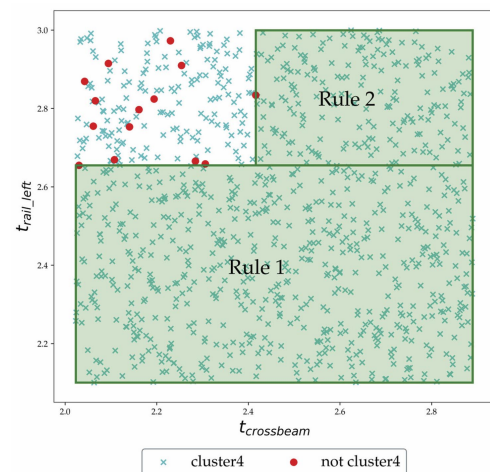


Figure 4: Visualization of all samples in the design space. The red samples belong to cluster4 as shown in Figure 2, which shall be avoided. The two rules can be visualized as two design-subspaces in which no rail yields bending behavior. When choosing a specific design, a safety distance to the rule bounds should be incorporated.

Constantin Diez is a passionate CAE engineer who is responsible for CAE Machine Learning Software and Services at Lasso GmbH Germany (www.lasso.de). Recently the company has also started offering CAE services utilizing Artificial Intelligence. Constantins dedication to CAE extends beyond his job, as he is part of the qd engineering team, which builds new and advanced CAE Tech for fun. qd also maintains a News Website (www.qd-eng.de), a Youtube Channel, and a Github Repository. constantin.diez@lasso.de

Virtual and Augmented Reality

The Future of how we Interact with Computers?

Richard Schweet, Kinetic Vision

With the notable exception of mobile computing, not much has changed in how we interface with computers since the development of the mouse and graphical user interface (GUI) over forty years ago. In fact, nearly two generations of users have no idea that at one time the only way to access the power of a room-sized computer was to feed a stack of punched cards into a reader and examine pages of printed output. Nor do they know that next came monochrome terminals and command line input, which somehow has continued to live on for system administrators, Linux users and others today.

Of course, the big breakthrough that brought the power of desktop computing to the masses was the invention of the mouse and GUI by Douglas Engelbart in the 1960s, while he was working at the Stanford Research Institute on a U.S. Department of Defense grant. Engelbart's work directly led to advances at Xerox PARC, who in 1973 developed the Alto computer, shown in Figure 1. During that time the first GUI was developed by Alan Kay, Larry Tesler, Dan Ingalls, David Smith, Clarence Ellis and several other researchers. A sample screenshot from a UI version known as SmallTalk-76 is shown in Figure 2.

Some may remember the transition from the command line interface, but few remember that the mouse and GUI languished in obscurity for over twenty years prior to the mainstream interest that came with the 1984 introduction of the Apple Macintosh desktop computer. Public acceptance and demand finally occurred because of the rise of a "killer" application (desktop publishing), effective marketing by Apple, and porting of successful programs to GUI interfaces.

Are we at another inflection point today? Many claim that Virtual and Augmented reality are the "future" of how humans will interact with computers, but even though "modern" VR/AR technology has been available for over a decade, that revolution hasn't yet occurred. Are we waiting for the killer application or do we need a hardware breakthrough like the iPhone? The author examines those questions and presents evidence that, yes, this is the beginning of the end for our rodent friend.



Figure 1: Xerox PARC Alto computer, circa 1973
By Joho345 - Own work, Public Domain

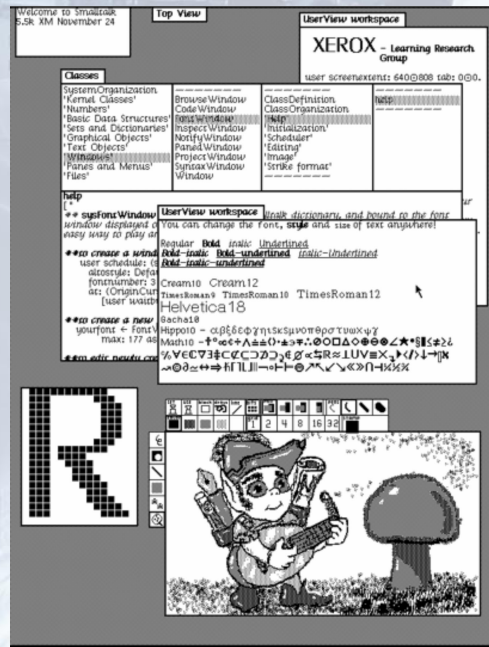


Figure 2: The interim Dynabook environment desktop (1976; aka Smalltalk-76 running on Alto).
By SUMIM.ST [CC BY-SA 4.0 from Wikimedia Commons]

The concept of a “virtual reality” is considered to have begun in the 1950’s but actually can be traced back to 360-degree murals in the 1860’s. During the 60’s the head-mounted display (HMD) was developed by Philco Corporation as a means for helicopter pilots to see at night, and in 1968 Ivan Sutherland created the first HMD connected to a computer. Although it allowed users to experience a virtual world, the headset was so heavy it had to be supported with a suspension system.

Today popular VR headsets are made by Facebook-owned Oculus, HTC, Sony, Samsung, Google and others. These systems are completely immersive, leaving users with no visual connection to their physical environment. Augmented and mixed reality (MR) systems include those made by Google, Microsoft, Meta, Magic Leap and others. AR overlays digital content, which may appear as either two or three dimensional, over the user’s actual physical environment, whereas MR enhances this experience by allowing this content to appear behind objects within the environment.

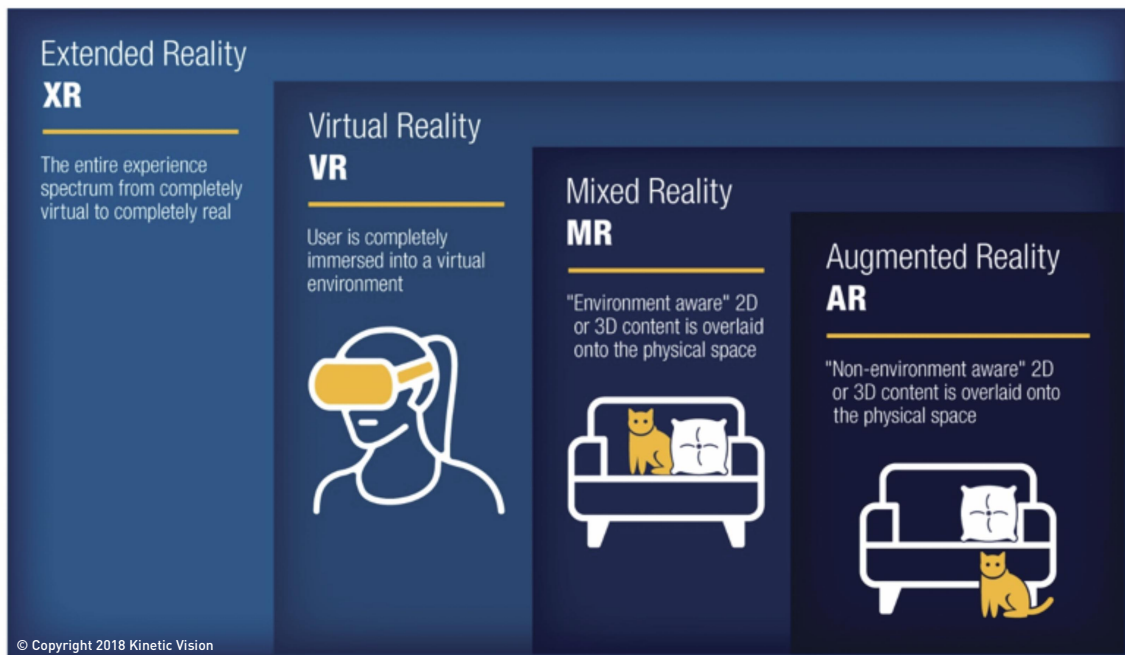


Figure 3: The intersections between XR, VR, MR and AR.

Video Games Lead the Way

Just a decade ago realistic real-time 3D computer graphics existed only in military and aerospace simulators that might have cost millions of dollars. Video game consoles rapidly became more powerful and paved the way for widespread adoption of realistic real-time 3D content, and it may be video games that finally pulls us into the VR world. Sony's PSVR headset for the Playstation 4 leads the way, with sales of over two million units in the last year. Impressive as that might be, it's miniscule to the over 70 million PS4 consoles in use today. The list of VR titles grows every day, but there's been nothing even close to megahits like Epic Games' Fortnite, Rockstar Games' Grand Theft Auto or the EA Sports' Madden NFL football series. By far the most successful AR game to date is Pokémon GO, which uses a mobile device's GPS to locate, capture, battle, and train virtual creatures, which appear as if they are in the player's real-world location. While a huge success to the creator, Pokémon GO influences the lives of just a small fraction of the population and has not created a paradigm shift in how people live their daily lives by any measure.

What are XR, VR, MR and AR?

The terminology for virtual and enhanced environments is evolving, but currently the most widely accepted terms are Extended Reality (XR), Virtual Reality (VR), Mixed Reality (MR) and Augmented Reality (AR). Each is a subset of the other, with XR covering the entire spectrum from completely virtual to completely real. VR completely immerses the user into a virtual environment, but the virtual experience might also include feedback mechanisms other than just purely visual, e.g. the user might interact with physical objects that are depicted virtually, or wear gloves or suits that provide haptic feedback to actions. As with all virtual environment systems, the user's head motion must be accurately tracked, and the imagery rendered at a sufficient rate for the effect to seem real and not cause motion sickness. In spite of these efforts, "VR sickness" remains a problem for some users.

MR and AR differentiate themselves from VR in that the user is able to experience both the virtual and physical simultaneously. Usually the physical space represents the majority of the user's visual experience and 2D and/or 3D graphics are overlaid onto their visual view. Both MR and AR require some sort of headset or "glasses", or a handheld mobile device. Mixed Reality, sometimes called hybrid reality, differs from Augmented Reality in that the the display device is "environment aware". This allows virtual objects to be aware of and interact with the physical space. A simple example is object awareness: overlaid imagery is occluded to make it look like virtual objects are "behind" physical objects. AR systems in general do not have this capability. An infographic that defines the intersections of XR, VR, MR, and AR is shown in Figure 3.

Corporations are Slow to Adapt but are Moving Now

Like all new technologies, growth in the business world is guided by "What's my ROI?". Without a return on investment that can be quantified, road-mapped and budgeted, corporations tend to adopt new technologies cautiously. Recently, General Electric was dropped from the Dow Jones Industrial Average, leaving none of the original 30 companies on the list. Once dominant companies like Eastman Kodak, Blockbuster and most print media businesses hang by a thread. Balancing "Where's my ROI?" with "Innovate or Die" is the key, but finding the fulcrum of that teeter-totter is often difficult.

More success stories appear every day. Ford uses VR to design new vehicles [1]. AR has helped Boeing to speed airframe wiring harness assembly by 25% [2] and GE wind turbine technicians by 34% [3]. Museums [4] are using AR to engage a younger demographic. You can even immerse yourself with the characters of Star Wars [5] or Lego [6].

VR/AR Case Studies

Augmented Reality Business Card

Even a smartphone can create a very realistic AR experience. Here the concept of an "AR Business Card" [7] is presented. While running a free app, the device camera recognizes a target printed on the card to start the experience, shown in Figure 4.

Robot Training Using Real-Time Simulation and Machine Learning

VR provides the means to create immersive simulations that extend beyond spatial environments. Modern game development platforms such as Unity and Epic Games' Unreal Engine provide "real-time" (unnoticeable to the user) rendering of complex environments, but also basic physical behavior, such as collision detection, gravity and friction.

Plugins from NVIDIA and others can add behavior of particles, fluids, cloth, mechanisms, elastic bodies and much more, enabling developers to create virtual worlds that closely replicate the physical space they are designed to represent. In addition, the behavior of machinery, sensors and other devices can be represented via custom software or by utilizing the same software that drives and monitors the devices in the physical environment.

That allows robotic systems, manufacturing operations, drones and other advanced systems, *and the software to drive the components*, to be virtually designed, tested and debugged within the digital twin. This greatly speeds up the development process of complex systems as all of the design configurations, performance optimization and control software are directly transferred to the physical space.

In this simplified example, shown in Figure 5, a pick-and-place robot is simulated in Unity and driven under user control. Unity's Machine Learning Agents are utilized to train the robot to locate, pick, move and place the bottles sequentially on the moving conveyor, first using imitation learning and then reinforcement learning [8]. During the training process, shown in Figure 6, multiple instances of the system are utilized to speed the process; after each cycle the best performing robot's behavior is used in each instance for the subsequent cycle.

Although machine learning isn't required to train simple pick-and-place robots (or equivalent dedicated systems), more complex situations can benefit greatly from the beyond-human intelligence created by this revolutionary technology.



Figure 4: Augmented Reality business card [7].



Figure 5: Still-frame from pick-and-place robot interactive VR simulation.

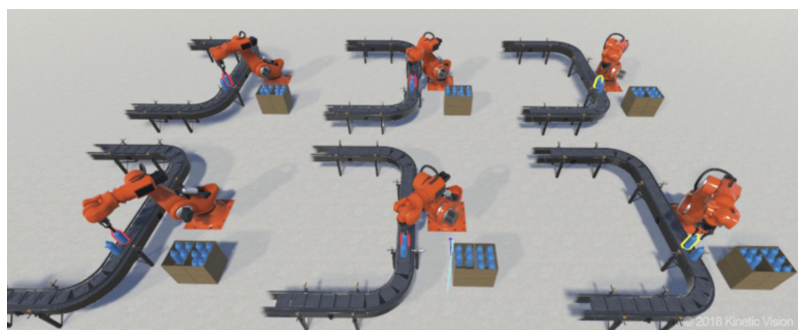


Figure 6: Robots being trained using machine learning algorithms.

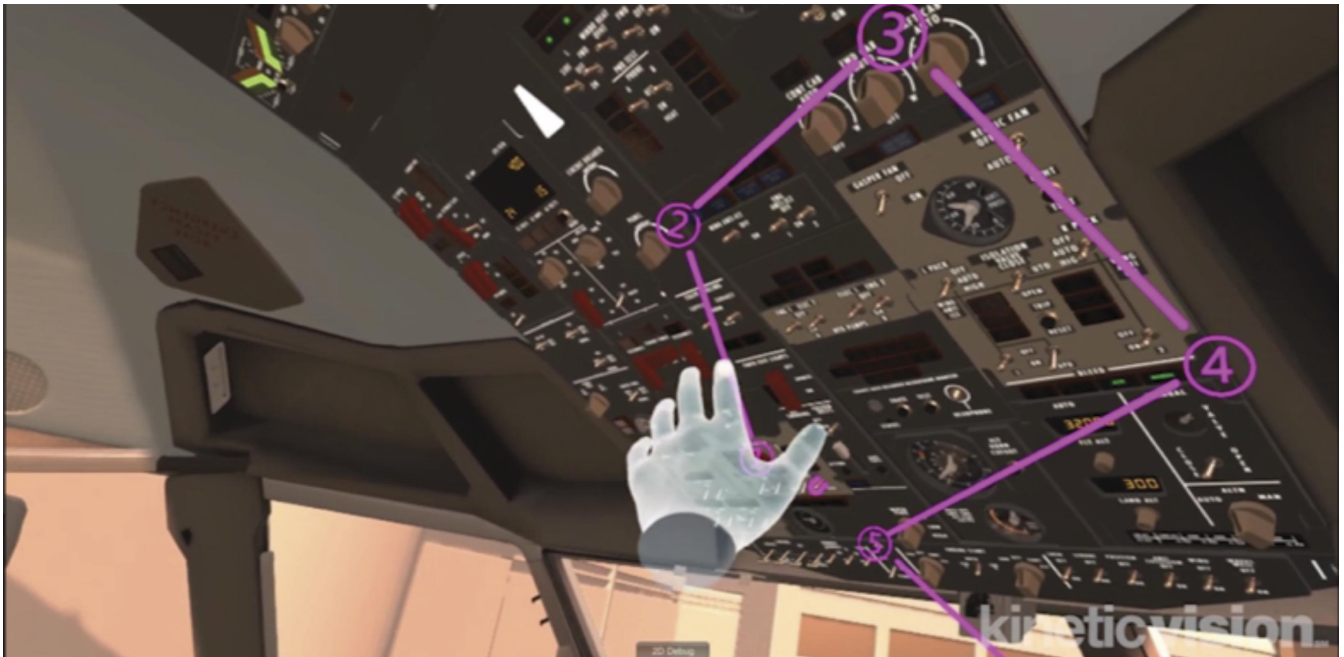


Figure 7: Pilot cockpit procedure VR training system screenshot [9].

Pilot Cockpit Procedure VR Training

A fully-immersive 737 cockpit environment enables pilot VR training of ground tasks by utilizing both declarative and procedural memory learning. Muscle memory, a form of procedural learning, is created by repetitively performing an assigned sequence of events while a virtual guide cues the user in Practice Mode. In Training Mode, the same tasks are requested with no cues until the task sequence is memorized.

This VR training example demonstrates how low-cost systems can be used to augment more expensive traditional simulators and training platforms. Although a pilot on-ground workflow example is shown here, this technology translates well to medical, industrial, automotive, manufacturing and other training requirements - any situation where the use of physical labs, training facilities and systems is inflexible, costly, time-consuming or involves personnel travel. A screenshot of the Pilot Cockpit Procedure VR Training system is shown in Figure 7.



Figure 8: Screen capture from Andretti Autosport AR Experience app from pit row in Indianapolis [10].



Figure 9: Screen capture from Andretti Autosport AR Experience app showing car scaling capability.

Andretti Autosport AR Experience Engages New Fans

Andretti Autosport® the namesake company of one of the most famous families in racing, was looking for a way to place photorealistic scale or full-size cars from each race series into any environment, enabling them to provide additional value to existing sponsors, find new partners, and increase fan engagement. The resulting app, titled Andretti Autosport AR Experience, enables racing fans or anyone interested in motorsports to virtually experience the cars from four different race series: IndyCar, Indy Lights, Global Rallycross and Formula E. The app allows the user to place each car into any environment and walk completely around it, or even go “sit” in the cockpit. A screen capture from the app is shown in Figure 8. Using the app’s scaling feature, users are able to place virtual race cars literally anywhere, as shown in Figure 9.

Communicating with Computers: from Points to Lines to Pages to Environments

Augmented, Virtual and Mixed Reality provide us the means to communicate with and extract information from the computers of the future. History shows that this process has followed an almost geometric progression: punch cards (points) to command line (lines) to mouse and gui (planes). What’s left are three dimensional experiences where the environment is the interface. The dumb rodent that only does what we tell it to will soon be replaced by real-time simulations that are intelligent and

able to learn by our actions. Whether the breakthrough comes as an “iPhone moment” or some killer app, this progression is inevitable. It took over two decades for the mouse/GUI combination to gain acceptance. Is the adoption of virtual environments as the computer interface of the future around the corner or still years away? Only time will tell. ■

References

- [1] Democratic design day 2018 Lugano: Tim Spears. Designboom, January 2017 nafe.ms/2xt9MRy
- [2] Boeing is using Google Glass to build airplanes, Nick Slatt, The Verge, July 2016 nafe.ms/2xvzbz99
- [3] Looking smart: Augmented reality is seeing real results in industry: Kristin Kloberdanz, GE Reports, May 2017 nafe.ms/2xvHJkL
- [4] Augmented reality in museums: 6 success stories: Camila Kohles, Wikitude, October 2017 <https://nafe.ms/2xuQkV6>
- [5] Star Wars app augmented reality instructions: StarWars.com nafe.ms/2xto9pA
- [6] New app brings Lego® bricks to life: December 2017 nafe.ms/2xqL0C4
- [7] Augmented Reality Business Cards nafe.ms/2xsiYpW
- [8] User driven robotics simulation: July 2018 nafe.ms/2xpyB0K
- [9] Virtual Reality 737 Cockpit Pilot Trainer: October 2017 nafe.ms/2xqLQ1G
- [10] Andretti Autosport AR Experience: October 2017 nafe.ms/2xwPwPg

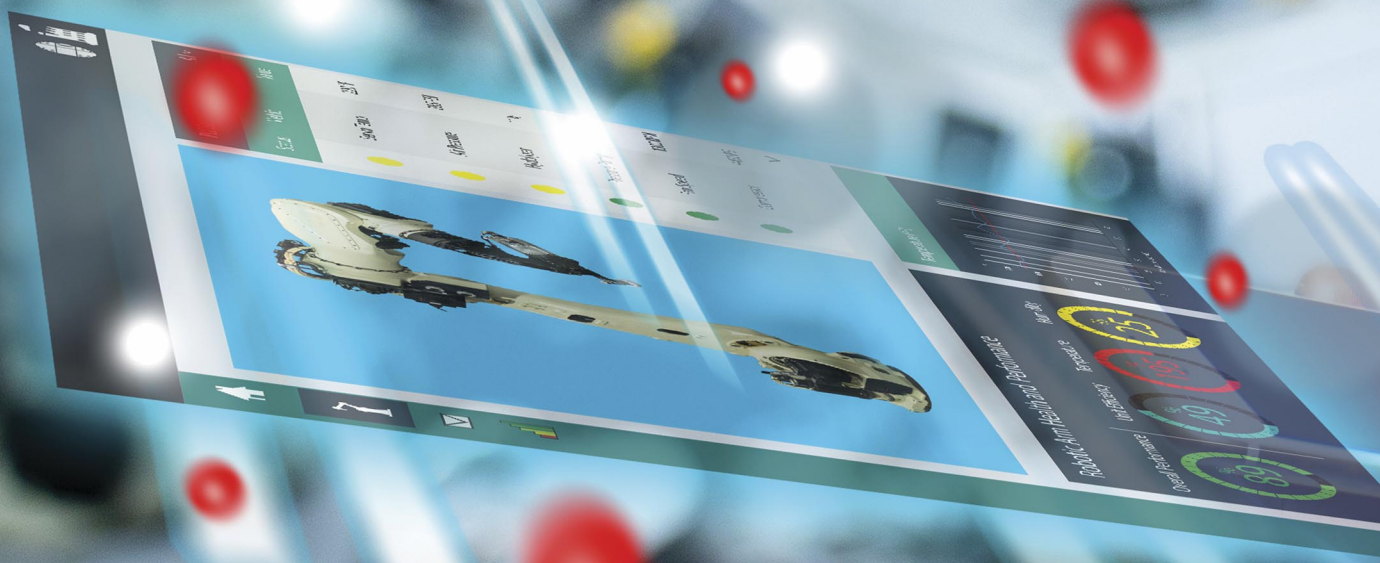
Richard Schweet is President and founder of Kinetic Vision, an industry leader in innovative product development, modeling and simulation, visual communication, software and app development, augmented and virtual reality, game engine-driven simulators, IoT innovation and industrial scanning. Kinetic Vision provides services to an international customer base and currently has 140 employees. In 2018 Deep Vision Data was formed as a division of Kinetic Vision to focus on the development of synthetic training data for machine learning systems.

He received a Bachelor of Science in Mechanical Engineering from the University of Kentucky and a Master of Science in Engineering from Florida Atlantic University while working for Motorola Communications in Plantation, Florida. He subsequently worked for Structural Dynamics Research Corporation (SDRC) in Milford, Ohio prior to starting Kinetic Vision in 1985.

Interactive Modelling and Simulation for Virtual Engineering Design and Analysis

Dr Adrian R. G. Harwood, The University of Manchester, UK

Engineering simulation is an essential tool for design and analysis. Typically, its emphasis is on achieving a high-fidelity representation of reality and hence, the resources required in terms of time, money, skill, training and power consumption, are not insignificant. However, over recent years, we have seen huge advances in low-power computing hardware and intuitive user-interfaces (UIs) with technology such as smartphones, tablets and virtual reality both available and affordable to the everyday consumer. It has made me question whether there is a place in engineering simulation for this technology and, if so, whether it can offer some form of transformative power to allow simulation to be used in new and exciting ways.



A Power Struggle

As exciting as smartphones and tablets are, with their combination of touchscreens, cameras, connectivity and innovative applications, their hardware is understandably geared towards a delicate balance between performance and power consumption. They simply don't have the compute capacity that desktops or workstations have, on which we would normally run simulations. However, the computational cost of simulation usually scales with accuracy and so reduced-accuracy modelling, used in the right way, may be a solution. Alternatively, we can "divide and conquer" – why not give a small bit of the problem to one device and then have a whole bunch of them compute the solution. After all, why buy a new workstation when we could have every smartphone and tablet in the office share the calculation instead? Engineers are potentially carrying around part of a 'smartphone computer' in their pocket, with the collective power to easily rival a serious workstation [2].

Real-time, Interactive Simulation

My research examines the potential of low-power devices for providing a new range of simulation tools for engineering. In this article, we consider real-time, interactive CFD using Graphics Processing Units (GPUs) with in-situ visualisation and user-interaction via virtual reality (VR). Time stepping is performed instantly and run-time touch and mouse input allows manipulation of the simulation configuration without the need to re-initialise. With real-time, interactive simulation, a parameter space can be explored quickly, results analysed and communicated efficiently. Using simulation in this way is an entirely different use-mode to what we usually see. However, increasing the speed always comes at a cost. In most cases, this price is paid in terms of a reduction in accuracy. But lower accuracy doesn't have to mean it is any less useful.

Before proceeding, it is beneficial to give the term "real-time" a strict definition in this context. Strictly speaking, a real-time simulation ought to be one where the time we are simulating takes the same amount of real-world time to simulate. In other words, if we wish our simulation to simulate 1s of physical behaviour, it should take 1s. Clearly the ability to achieve this is going to depend on the numerical method, the time step chosen for each iteration (how much physical behaviour each time step simulates), the implementation of the method, and the computing hardware on which it is run.

However, not every application will require a simulation that adheres to this strict definition. It may be beneficial to have a simulation that steps through time at a rate suitable for visualisation at 24 frames per second regardless of how much physical behaviour is being simulated at that rate. Given this, as a minimum we just

need a simulation where iterations (time steps) take at most $1/24$ th of a second = 42ms. We term this the "threshold of interactivity". In other words, our simulation is advancing such that an observer can see a smooth "video-like" evolution of behaviour. Our target, therefore, becomes "interactive" simulation.

Where Could we Use it?

Anyone who has played a video game will know that very fast simulation, capable of representing a plausible reality is essential for providing the gamer with a sense of immersion in a virtual world. But outside the field of entertainment, there are some more serious applications where instantaneous simulation of a physical problem might be beneficial. At the University of Manchester, we use GPU-powered, real-time, interactive flow simulation tools on desktops, tablets, projectors and in VR as teaching, communication and analysis tools. They provide an intuitive means of simply communicating the invisible to students and allows them the freedom to explore flow around different shapes through touch input. Depth-sensing cameras can be coupled to the applications to acquire new geometry to put in the flow. This way, objects can be refined both physically and digitally to design a solution. However, there are many other conceivable applications. What if the user were a machine? Accurate modelling of air flow within hospital wards, operating theatres, data centres could be used to inform real-time, adaptive control, with simulation "filling in the blanks" where sensors cannot detect physical information. If simulation is run faster than real-time, we can perform forecasting, with simulation results used to inform artificially intelligent systems.

Realising an Interactive Simulation Infrastructure

Of course, all these applications depend on a developed infrastructure which offers all the capabilities they require. At its heart, fast simulation can be provided by a real-time compute engine which can process input and provide output instantaneously. The hardware required would not need to be fixed but could adapt depending on the end-user requirements and simulation demands. However, it is expected that parallel computing of some form will be necessary to achieve the computational performance required for interactive simulation. The compute engine may be local, running on one or more energy-efficient mobile devices, or may be built around a traditional high-performance computing (HPC) system. It must also be able to respond to steering activity, such as a user adjusting the geometry or physical parameters such as flow speed or structural stiffness at runtime, and present data for real-time rendering. A possible system is shown in Figure 1.

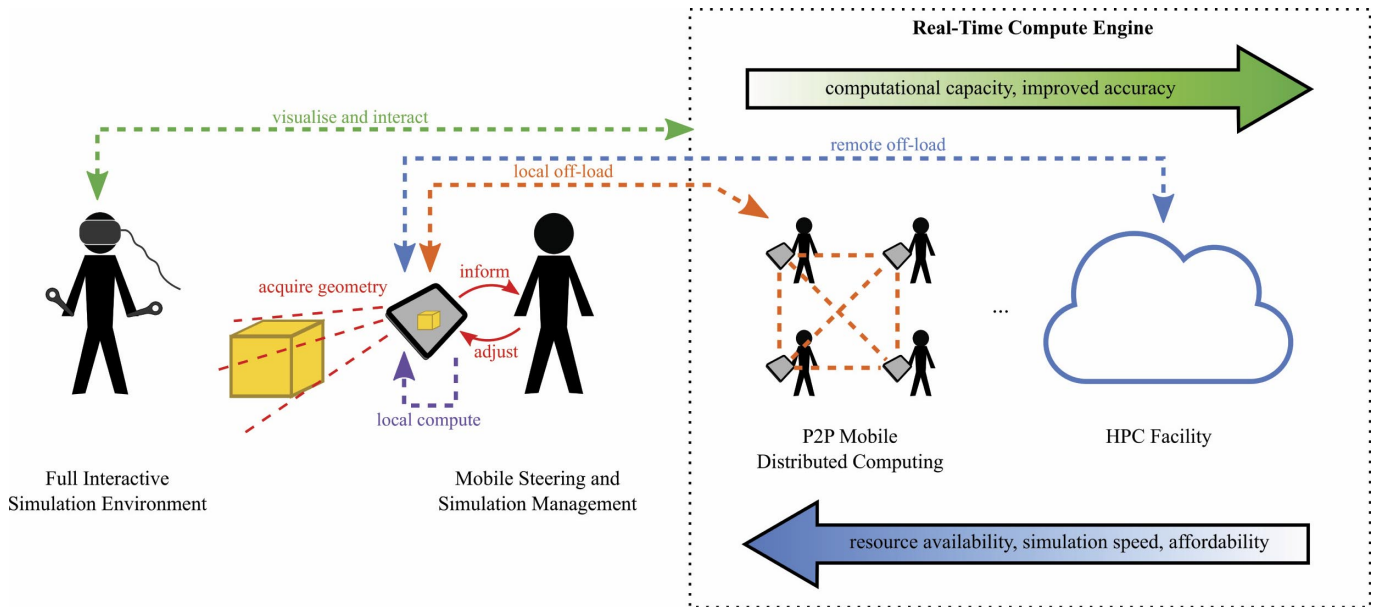


Figure 1: Interactive simulation infrastructure offering geometry acquisition, VR visualisation and a range of computational resources including mobile devices adapted from [3].

Realising Real-Time CFD: LBM & GPU

In addition to hardware, simulation software is a critical part of realising an interactive simulation infrastructure. Some methods are more amenable for implementation on parallel computing architectures than others. Key characteristics include data locality, access patterns and computational intensity. In our work to date, we have used the combination of GPUs and a numerical method well-suited to parallel execution – the Lattice-Boltzmann Method (LBM) [1] – to simulate fluid flow in 3D.

The LBM is remarkably simple in its formulation even though it is capable of simulating even complex turbulent flow given enough resolution, as can be seen from the validation study results for a 3D channel flow at $Re_c=180$ (equivalent to $Re_c=3300$) in Figure 2. GPUs are very efficient at conducting arithmetically-simple, parallel computations on highly-local data. They are less efficient if data associated with a given thread is to be accessed by other threads. In addition, global memory access on GPUs is a relatively expensive operation and memory bandwidth per thread is much more limited than on a

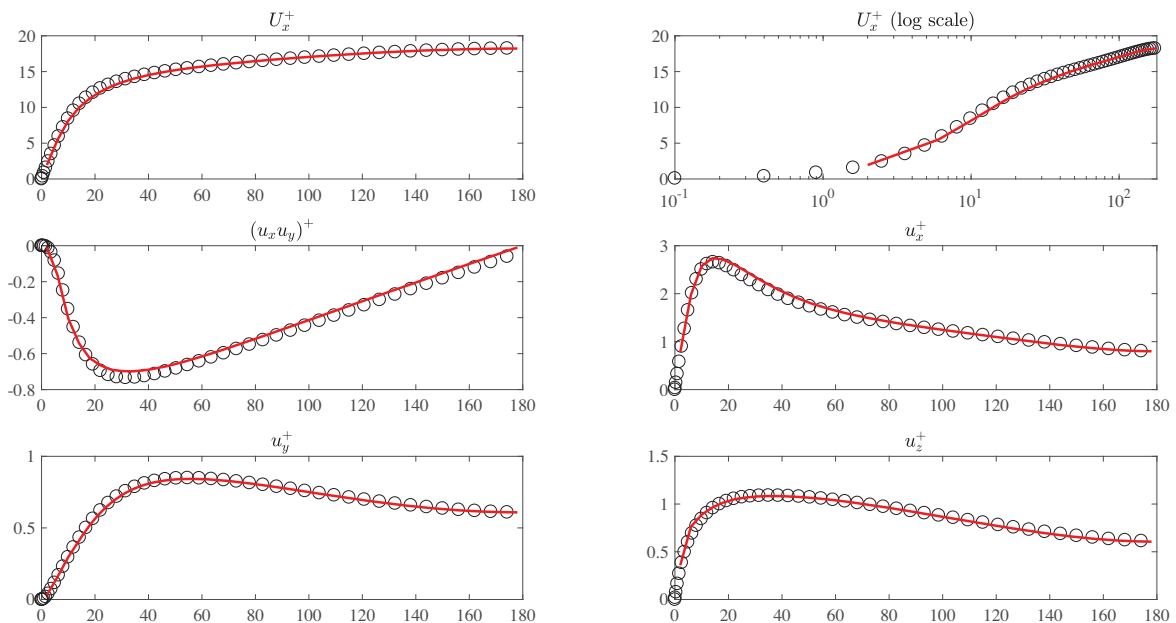


Figure 2: Comparison between 3D turbulent channel flow Reynolds stress and stream-wise velocity results from LBM (red line) and DNS results of Kim, Moin and Moser [4].

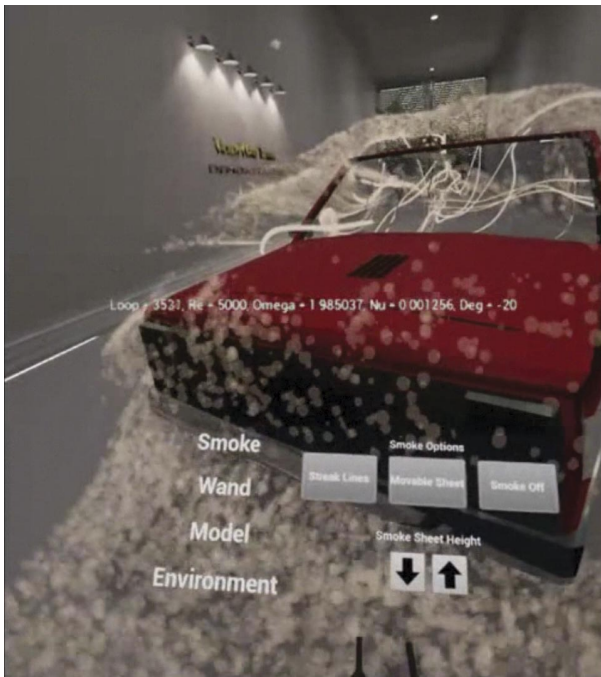


Figure 3: Floating UI for user interaction.

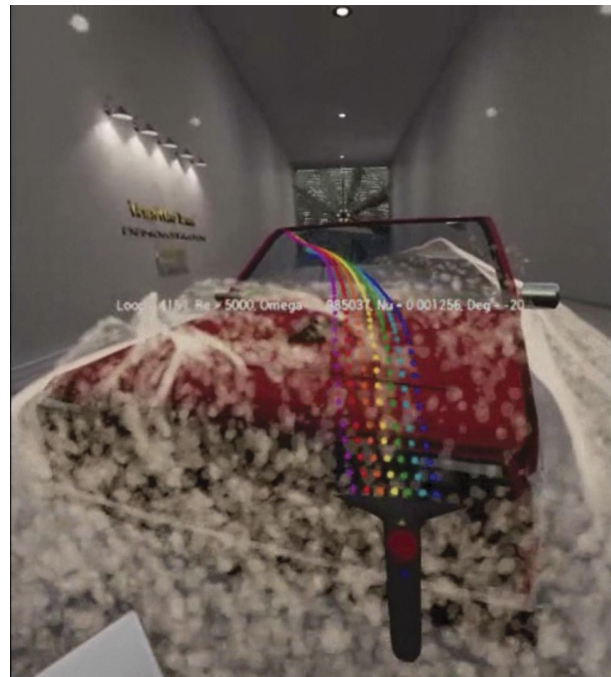


Figure 4: Coloured streak-lines injected into the flow by the user through the VR motion controllers.

CPU. Fortunately, the LBM can be performed using highly local operations, using small amounts of data in a given cell and its immediate neighbours only. To maximise GPU performance, our implementation follows established best practice. First, GPU threads in each workgroup access GPU memory infrequently and efficiently. This is achieved by:

- 1 Restricting read/write operations to only those which are essential for functionality;
- 2 Taking care to structure data in GPU memory such that arrays fit neatly into cache lines to minimise the lines read per memory transaction;
- 3 Refactoring code to ensure GPU threads in a workgroup access the same cache line at the same time if possible.

Furthermore, we minimise branch divergence by ensuring threads in a workgroup are not working off separate instructions due to diverse “if...elseif...else” constructs with large bodies. This would slow down execution due to serialisation of instructions in a workgroup. Finally, as it takes a finite number of clock cycles for values read from GPU memory to become available, we hide this memory latency by performing additional compute on cached data while data is being fetched.

A Virtual Wind Tunnel in VR

The virtual wind tunnel is a 3D video game, built using the Unreal Engine 4 game engine. Game engines offer a wide range of capabilities for developing and executing 3D games, with real-time graphics and built-in support

for human-interface devices such as controllers and VR headsets. In our application, we use point cloud data of real objects to produce a static mesh visualised in the game world. Games are built in game engine editors using a collection of software objects known as actors which interact with each other when the game runs. We use a custom actor implemented using the Unreal’s domain-specific C++ to link our own GPU-LBM library to the game, with simulation data passed from the library to actor each frame. The game engine then uses its own particle systems to visualise the physics data given to it from our library. Other elements of the game engine are used to provide an interactive user-interface with the actor and our physics library, handling interactive inputs in real time. Figures 3 and 4 show the view of a user using the virtual wind tunnel game to investigate the flow around a car at an angle to the oncoming flow.

Although only a prototype, the tool allows us to demonstrate how interactive simulation might be used in the not too distant future. Our research has proposed solutions to many of the problems associated with integrating all the hardware and software components necessary for an interactive simulation tool. However, managing the scalability of these solutions across the infrastructure discussed earlier remains a key challenge. In particular, the data transfer bottleneck between solver and visualiser limits the throughput of the simulation. This problem is only exacerbated as the resolution increases due to the need to decrease the simulation time step accordingly. Spreading the calculation across multiple GPUs will increase throughput, and offset the demand for more timesteps but at the expense of making the data transfer bottleneck worse and there is plenty of scope for alternative solutions.

So, is there a Place for Interactive Simulation?

Well I certainly think so. There are many applications, some of which we haven't even thought of, which can benefit from fast simulation even if it involves sacrificing some accuracy in order to achieve it. The key to using interactive simulation for engineering, is to know how much accuracy is "enough" rather than doggedly pursuing the best we can get.

However, one thing this tool does teach us, is that sometimes, real-time simulation is not really what you want. Consider simulating a turbulent flow in real-time where an observer wishes to monitor the size and development of large coherent structures. The structures of interest will have convected from view long before an observer can interpret them in a real-time simulation. In this scenario, only interactive speeds are necessary, and accuracy needs to be sufficient to capture the structures of interest.

But there is also a lower limit as to how slow evolution can be before simply waiting for these structures to convect exceeds the patience of a user. We therefore close by refining our initial interactive target with a minimum rate at which flow need to be displayed to the user in order to satisfy their application requirements.

In conclusion, the realisation of real-time simulation is

coming. For some applications it is already here. As engineers we need to keep our minds open to the possibilities offered by emerging hardware and new numerical methods. The proliferation of real-time simulation is going to be an interdisciplinary pursuit between computer scientists, engineers and others, and I look forward to exciting times ahead. ■

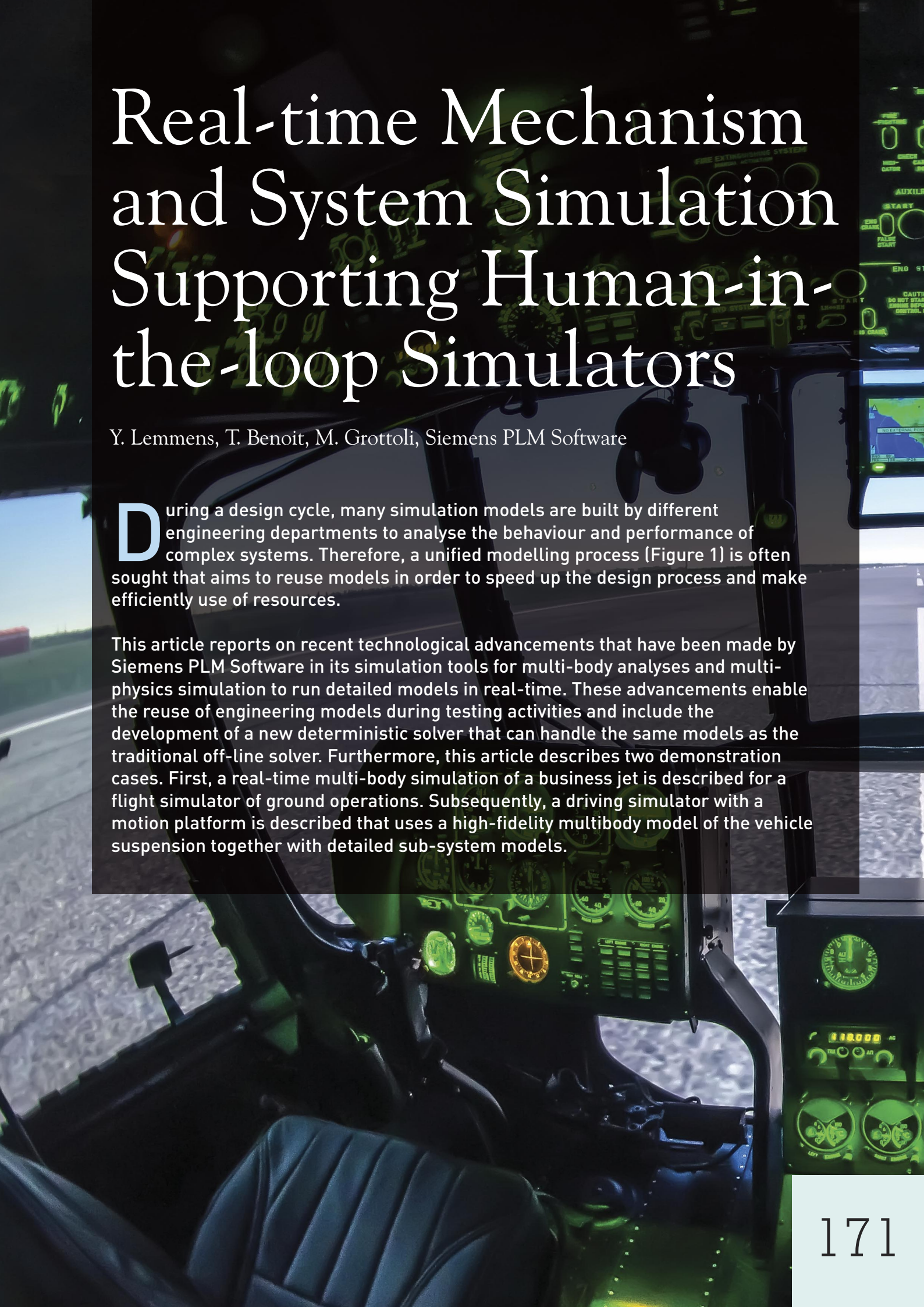
Bibliography

- [1] Chen, S. & Doolen, G. D., 1998. Lattice Boltzmann Method for Fluid Flows. Annual Review of Fluid Mechanics, Volume 30, pp. 329-364.
- [2] Harwood, A. R. G. & Revell, A. J., 2017. Parallelisation of an interactive lattice-Boltzmann method on an Android-powered mobile device. Advances in Engineering Software, Volume 104, pp. 38-50.
- [3] Harwood, A. R. G. & Revell, A. J., 2018. Interactive flow simulation using Tegra-powered mobile devices. Advances in Engineering Software, Volume 115, pp. 363-373.
- [4] Kim, J., Moin, P. & Moser, R., 1987. Turbulence statistics in fully developed channel flow at low Reynolds number. Journal of Fluid Mechanics, Volume 177, pp. 133-166.

Adrian has been part of the School of Mechanical, Aerospace & Civil Engineering (MACE) at The University of Manchester since starting as a student in 2006. Since joining he has completed his MEng in Aerospace Engineering, PhD in acoustic wave propagation and held research associate and fellow positions. During his undergraduate degree he worked for Rolls-Royce (and later Aero Engine Controls) throughout the UK on the design of safety-critical systems including thrust reverser control systems for corporate aviation gas turbine engines. He is currently a Lecturer in MACE and a Fellow of the Higher Education Academy teaching numerical and computational methods as well as programming to students at all levels.

Adrian's interest in real-time computing developed while he was lead research software engineer (RSE) of the open-source LUMA (Lattice-Boltzmann @ the University of Manchester) project, a multi-grid, many-core FSI solver in C++ based on the Lattice-Boltzmann Method nafe.ms/20mNgBy. Adrian led the LUMA-inspired Virtual Wind Tunnel project, backed by Jaguar Land Rover, where he uncovered and tackled head-on the challenges associated with integrating fast simulation with interactive hardware through 3D virtual environments. Through this work, he applied knowledge of GPGPU programming in CUDA, OpenGL and GLSL, as well as mobile application development in Android (Java/JNI) to deliver tractable solutions. He also has several publications in the development of real-time simulation on Android devices and organises an international symposium for other researchers interested in the broader field of virtual engineering every two years.

Away from academia, Adrian enjoys playing the clarinet in two local orchestras, creating the "Eddie Engineer" LEGO animation series nafe.ms/20gHJw9 and spending time caravanning throughout the UK.



Real-time Mechanism and System Simulation Supporting Human-in-the-loop Simulators

Y. Lemmens, T. Benoit, M. Grotoli, Siemens PLM Software

During a design cycle, many simulation models are built by different engineering departments to analyse the behaviour and performance of complex systems. Therefore, a unified modelling process (Figure 1) is often sought that aims to reuse models in order to speed up the design process and make efficient use of resources.

This article reports on recent technological advancements that have been made by Siemens PLM Software in its simulation tools for multi-body analyses and multi-physics simulation to run detailed models in real-time. These advancements enable the reuse of engineering models during testing activities and include the development of a new deterministic solver that can handle the same models as the traditional off-line solver. Furthermore, this article describes two demonstration cases. First, a real-time multi-body simulation of a business jet is described for a flight simulator of ground operations. Subsequently, a driving simulator with a motion platform is described that uses a high-fidelity multibody model of the vehicle suspension together with detailed sub-system models.

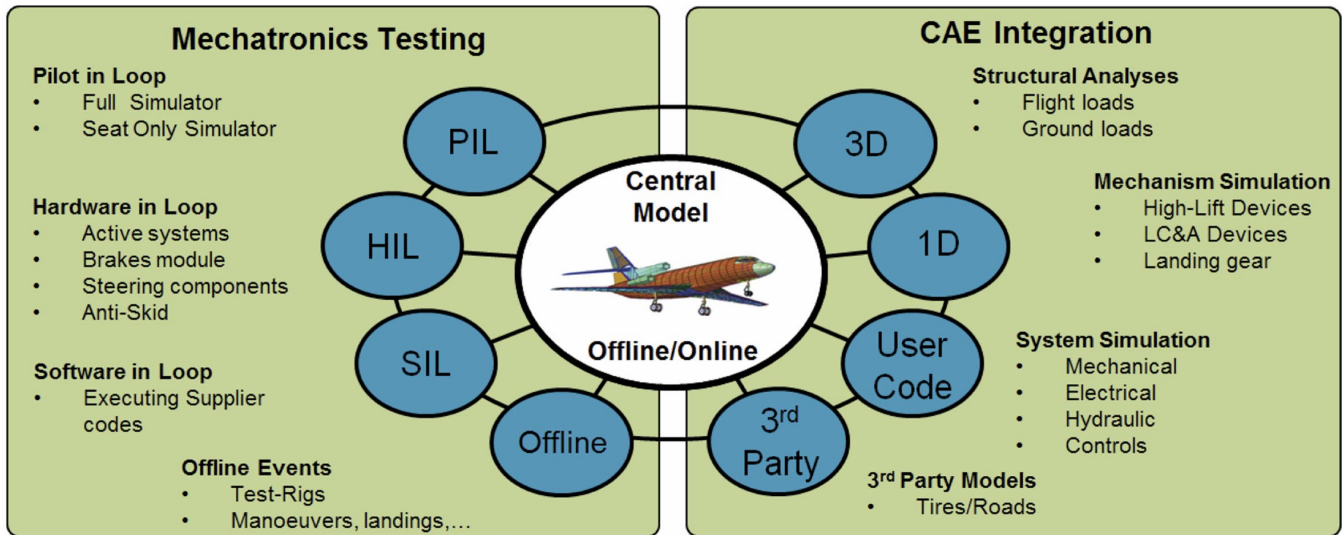


Figure 1: Unified modelling approach.

Solver advancements

First of all, the time integration scheme was modified. In real-time simulation, the time it takes to compute the system state at the next time step has to be less than the simulated time step. In implicit time integration schemes, the formulation is composed of Differential-Algebraic Equations (DAE). Although explicit schemes guarantee a known computational load, implicit schemes are preferred for their superior numerical stability and accuracy in stiff systems. To make the integration schemes deterministic, the number of iterations is limited and the order of the time integration scheme is fixed [1]. This can lead to less accurate results and to instability of the computation process. Hence not every model can be computed in real-time.

Furthermore, every iteration step in every time step of an implicit time integration scheme involves the evaluation of the system Jacobian, and the factorization of this matrix. Classically, the Jacobian is obtained by finite differencing, but this is only feasible for low-fidelity models in real-time simulation. To overcome the cost of the Jacobian evaluation, analytical expressions for the Jacobian have been implemented in the multi-body simulation software, reducing the cost of Jacobian evaluation dramatically and enabling real-time simulation of significantly more complex models.

Moreover, drift or violation of the constraint equations might occur during the solution process. Therefore, Baumgarte's stabilization, which uses a proportional-derivative controller to correct the constraint violations

[2], is included. Since the sparsity pattern of the Jacobian does not change, it does not add significantly to the computational load.

Finally, the duration of simulations can be reduced through parallelization of parts of the simulation. The model is subdivided in pieces such that co-simulation on separate cores is used. To ensure the same response as the original single model, parameter states are exchanged at the interface between the two mechanisms.

For multi-body simulations, a dedicated element has been developed based on a stiff bushing element to connect sub-models [3]. Because an implicit time integration scheme handles the resulting higher numerical stiffness, using a bushing element does not adversely affect the timestep.

Flight Simulator

The real-time capabilities are demonstrated in a Pilot-In-the-Loop (PIL) simulator using a digital twin of a business jet. Figure 2 shows an overview of the total system and the physical setup. The user provides joystick, pedal and throttle movements, which are sent as input signals to the models coupled through co-simulation. Finally, the outputs are visualized for feedback. The models each run on a separate core for parallel computation. Data is exchanged between the models by using standard UDP network protocol in each time step.

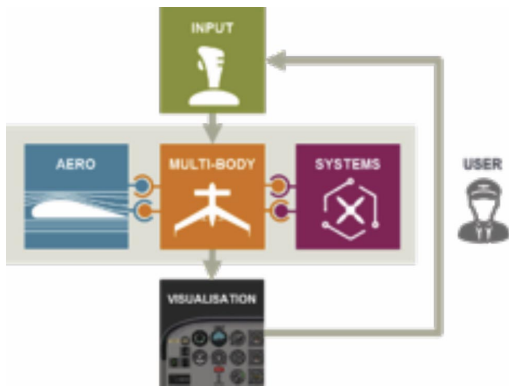


Figure 2: Overview of business jet co-simulation models (Left) - Demonstrator setup (right)

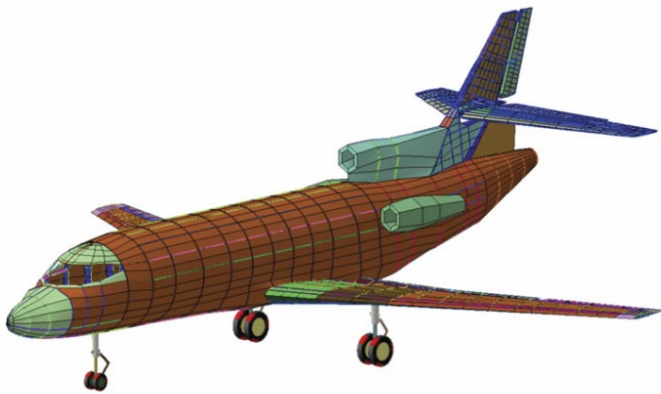


Figure 3: Multi-body model of a business jet type aircraft

The aircraft multi-body model (Figure 3) contains an airframe represented by a rigid body. The landing gear is a tricycle undercarriage that is composed of tire models, vertical struts with non-linear stiffness and damping and steerable nose landing gear. The engines are modelled with force elements that can be reversed for thrust reversal. The aerodynamic forces are applied at the centre of gravity and obtained from a different model. This resulted in a model with 29 rigid bodies, 204 generalized coordinates and 16 Degrees of Freedom (DoFs).

The aerodynamic forces are computed in a system simulation model (Figure 4) and are based on the traditional coefficient look-up.

There are two modes of visualization. Firstly, there is the open-source flight simulator game FlightGear showing a 3D scene with a cockpit

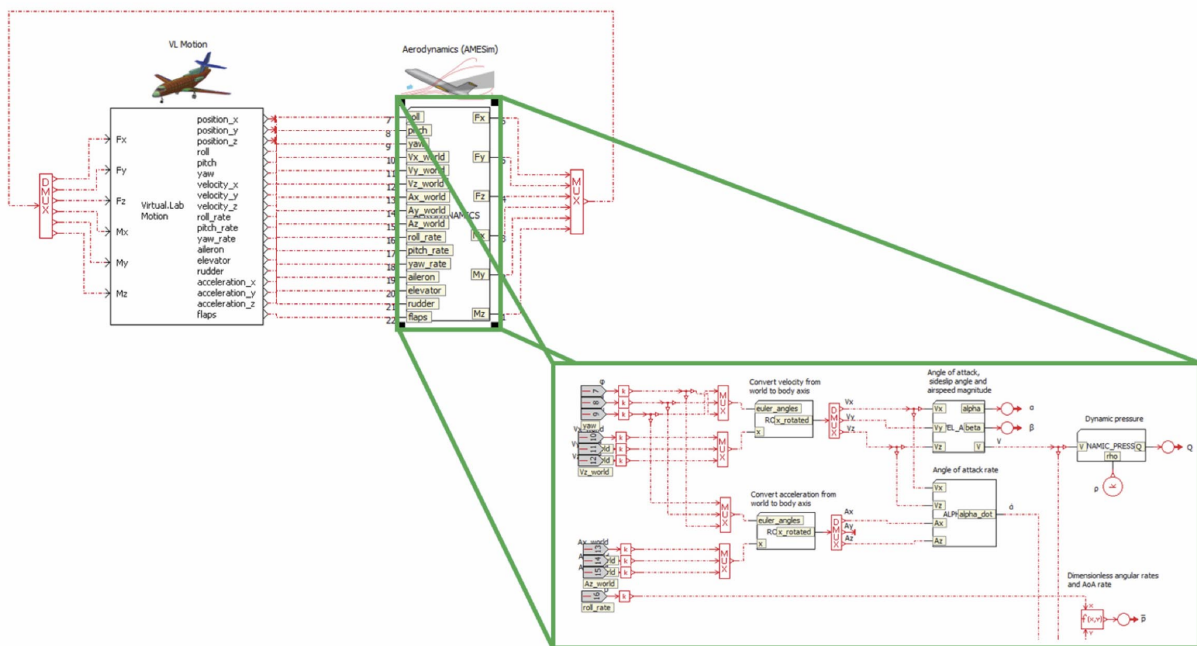


Figure 4: Aerodynamics model in Simcenter Amesim

The model is controlled directly by the driver with steering wheel and pedals. The signals are acquired and sent to the simulation models. From the integration of the complete model relevant data (like vehicle position and orientation) is used for visualization of the environment and other traffic.

All the models are combined in a co-simulation environment and the code is automatically exported to solve the complete model on a real-time machine. The input/output communication between different machines uses UDP for input acquisition and visualization, and to the real-time controller for the motion system (Figure 8).

Conclusions and outlook

This article reported on recent advances in multi-body and multi-physics simulation software that enables real-time simulation of complex systems. The motivation is to support a more unified modelling approach during the design of complex systems.

Two demonstration cases for human-in-the-loop simulations were presented. A flight simulator was presented to demonstrate the use of an aircraft model with the non-linear behaviour of the landing gear for flight and ground manoeuvres. Secondly, a driving simulator with a motion platform, that uses a high-fidelity multi-body model of the vehicle suspension together with detailed sub-system models, was discussed.

Currently, the driving simulator setup is used to investigate human perception of advanced driving assistance systems. In the future, the setups will be extended for hardware-in-the-loop and hybrid

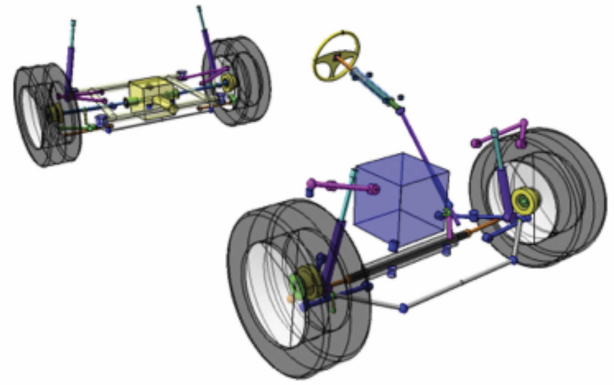


Figure 7: Real-time Multi-body Model of the Vehicle

applications. In these applications, physical hardware controllers or mechanism parts are combined with virtual models. ■

References

1. Garcia de Jalon, J. and Bayo, E., "Kinematic and Dynamic Simulation of Multibody Systems: The Real-Time Challenge", Springer-Verlag, New York, NY, 1994.
2. Arnold, M., Burgermeister, B., Eichberger, A., "Linearly implicit time integration methods in real-time applications: DAEs and stiff ODEs. Multibody System Dynamics", Vol. 17, No. 2-3, pp. 99-117, 2007.
3. Prescott, W., "Parallel processing of multibody systems for real-time analysis", Proceedings of the ECCOMAS Thematic Conference on Multibody Dynamics 2011, Brussels, Belgium, 4-7 July 2011.

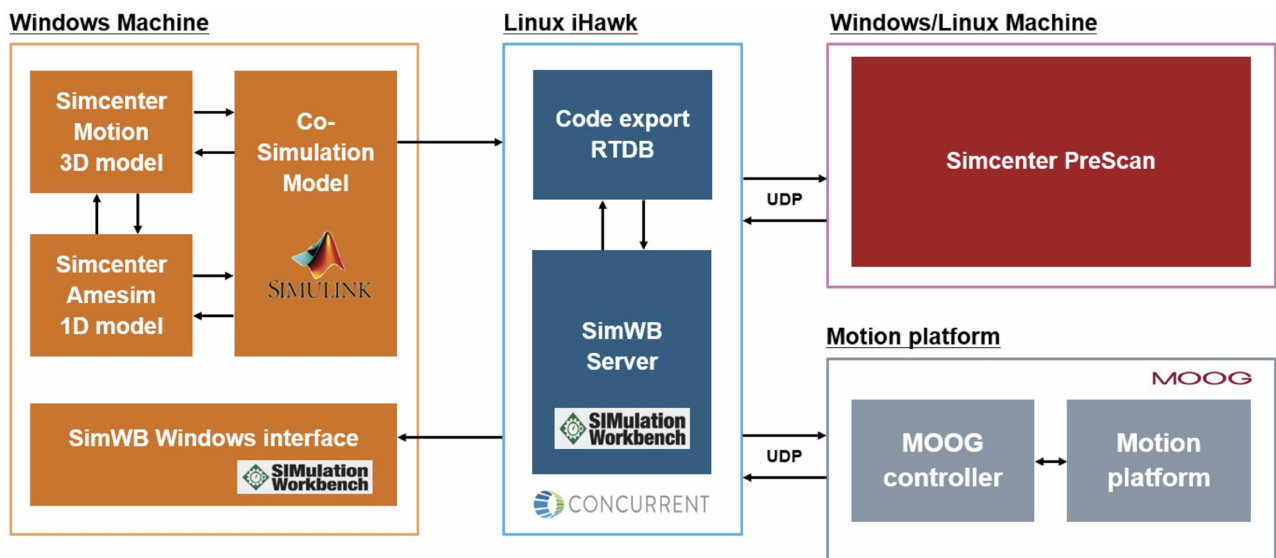


Figure 8: Driving simulator software architecture

Dr. Yves Lemmens has a degree in Aviation and Space Technologies from the University of Brussels and a PhD from the Department of Aerospace Engineering of Cranfield University (UK). He is currently a senior research manager at the Industry Solutions team of Siemens PLM Software in Belgium. His research activities are focussed on simulation methods of structures, mechanisms and systems for aerospace and automotive applications in support of the development of the Simcenter simulation software.

More info at nafe.ms/2QFGmc7

Simulation Data Management - The Next Challenges

A Summary of the 3rd International SPDM Conference

Mark Norris, NAFEMS SDM Working Group

The 3rd International NAFEMS SPDM Conference was held in June 2017 in Stockholm, Sweden alongside the NAFEMS World Congress 2017 (NWC17). With a packed programme of presentations, training courses and workshops, NWC17 was the largest NAFEMS event to date, and the SPDM Conference gave all attendees an excellent opportunity to learn more about SDM, how the industry is moving forward, and what the next steps may be.

The conference was kicked off by Dirk Ruschmeier of Porsche whose keynote title, "Simulation Data Management – The Next Challenges" [1], summarises the theme of the conference. He described the classical challenges of user acceptance and integration into the IT landscape based on a decade of SDM experience at Porsche. He then described the evolving challenges of integration into a Systems Engineering landscape with increasingly complex simulations with new model types, new domains and new simulation scenarios. The increase in the number and complexity of simulations and simulation types carried out each week by analysts at automotive companies is a recurring theme of NAFEMS SPDM conferences.

Dr Ruschmeier described how the increasing use of simulation upstream of a vehicle program is driving the need for collaboration between OEM and their tier 1 suppliers. Three papers were presented on the management of simulation collaboration of which more later. Likewise simulation is increasingly used downstream for Virtual Testing, the simulation of the physical test process, as described in the keynote on Smarter Testing by Steven Chisholm of Boeing [2] and by Tobias Ulmer of Airbus [3] in his paper on Virtual Testing of High lift Systems.

SDM for CoreProduct Development

For traditional simulation in the core of the product development process we saw more papers that ever before describing substantive SDM deployments. This is clear evidence of increasing adoption of SDM as more organisations recognise the need to evolve from a paper trail to a Digital Thread. We also saw more solution vendors represented in the SDM deployments as well as a diversity of solution approaches.

The best paper award was won by Carsten Eller of Eberspracher Exhaust Technology [4] who described their successful deployment of SPDM on the 3D EXPERIENCE PLM platform as well as the effort required and the challenges encountered. This paper is well worth reading for those considering such a deployment. Eberspracher built an internal team to deploy and support SDM as did SAFRAN Landing Systems with the benefits of deep understanding of the organisation's simulation Processes and Data to be managed as well as strong alignment with the needs of the Analysts and the Enterprise. The SAFRAN deployment described by Vincent Raimbault [5] was perhaps the most impressive SDM project of the conference.

Vincent and his team successfully deployed Ansys EKM to support the certification of the A350 Landing Gear system, building a database of more than 1 million objects. Not only did the SPDM system meet its objectives for the certification of the system, it's proving invaluable to support manufacturing and repair concessions. For this program, it's now possible to rapidly simulate the Digital Twin of a particular landing gear since the entire calculation set can be re-run as necessary in the managed environment so crucial in regulated industries. This is a great story of unintended positive consequences of SPDM deployment. A further example of the expansion of SDM in tier-1 suppliers is ZF. Martin Pährisch of ZF, the automotive powertrain supplier, co-authored a paper with Stefan Mayer, MSC's Munich-based SDM Services Director on the integration of SDM into a PLM and SAP environment [6]. They describe both the IT integration aspects as well as the replacement of paper-based reporting with audit trails in the SDM database, see Figure 1. It's noteworthy that the Proof of Concept was designed to address the key concern of ZF for their SDM selection, namely that an SDM system could be successfully integrated into their IT landscape.

Since the conference was in Sweden, it was good to hear of China Euro Vehicle Technology's deployment of SPDRM, Simulation Process Data and Resource Management [7]. CEVT is better known by its consumer brands such as Volvo. SPDRM is the brainchild of BetaCAE and it's an integrated SDM solution from this well-known CAE vendor. CEVT described their use of the integrated Load Case Configurator to select CAE sub-assemblies and Load Cases for a particular run. SPDRM, like SimManager from MSCsoftware, includes an optional Load Case Configurator module in an integrated SDM solution. In contrast, Dr Müllerschön of SCALE described their Load Case Configuration module LoCo [8] which is interfaced to the PD Tec Pre-Processing SDM platform at Audi and has been used to generate 800,000 simulation runs. He also

addressed the important topic of eliminating duplicate and redundant data in the face of the exponential rise of simulation data in highly productive SDM-powered environments.

Desktop or Cloud?

Audi have adopted a building block approach to SDM incorporating best in class modules such as the LoCo desktop application. A key feature of this approach is that the analyst can keep working if disconnected from the network and the SDM backbone; the analyst can cache the data locally and save back to the SDM when the connection is restored. Analogous workbench approaches were presented by JJ Billings of Oak Ridge National Laboratory and Robert Clay of Sandia Labs (Figure 2).

Since it's neither desirable, remember Chernobyl, nor possible to test these engineering systems, Analysts at Sandia perform exhaustive multi-domain simulations with upstream Design Space Exploration using their Dakota plug-in and then Design Optimisation and Robust Design to validate solutions. Once again the analyst can continue work on the workbench and connect to the Sandia SDM solution which underpins SAW as needed. This intensive use of simulation is indicative of where the simulation world is headed so the data management approaches that Sandia have adopted may be the shape of things to come for the rest of us. It's noteworthy that the Airbus flight Physics SDM is also a workbench underpinned by a repository.

In complete contrast, Michael Schlenkrich of MSCsoftware and Mr Lieb of BMW presented a sophisticated SDM solution for managing Multi-Body Simulations (MBS) vehicle suspensions. SimManager already has very large SDM implementations such as BMW with 2,000,000 vehicle simulation datasets, where model assembly, job submission and automated post-processing are all managed on the server-side. The MBS SDM solution takes the move to locating processes in the Cloud one step further. Whereas MBS has typically been a desktop application, solving has been moved to the "Cloud" so critical Intellectual Property such as control algorithms and suspension performance characteristics never leave the Cloud. This ensures that Intellectual Property of "the Ultimate Driving Machine" is not shared on every suspension engineers desktop but is completely secure as a "black box" model on the server.

Secure Collaboration

The approach of consolidating processes and data on a Private cloud begs the question; "how do I integrate my suppliers?" At present large automotive SDM deployments at Audi and BMW use the security of the SDM system to permit controlled supplier logons. This was effective when SDM was a new technology and many tier 1 suppliers did not have an SDM solution. In the evolving SDM world, where companies are equipped with their own different SDMs, different collaborative solutions are required. Three different approaches for simulation collaboration were presented at the conference. Dirk Ruschmeier presented FDX a file-based format for Functional Data eXchange that will become the VDA5550 standard [9]. This is analogous to the **xMCF** Master Connection File approach pioneered by

Ford and standardised by VDA for weld, rivet, bolt definition exchange which was presented by Carsten Franke of ProStep at the 2015 eSPDM conference.

Adrian Murton of Airbus presented the progress of MoSSEC web-services-based collaboration standard that has been elaborated between Aerospace OEMs and suppliers [10]. MoSSEC is on track to become a STEP standard and the results of the TOICA project to further refine the data model are now available. The third solution to be presented was KARREN from DPS in collaboration with Valeo [11], the automotive equipment supplier. KARREN is a revolutionary and pragmatic approach which enables a CAD designer at an OEM and an Analyst in a supplier to collaborate based on a parameterised definition of a functional component. The designer can request a performance evaluation of a set of CAD design and duty-cycle parameters and the analyst can respond with his simulation of performance. The volume of data that is exchanged is extremely small and the users interfaces are within the engineers CAD and CAE tools. Additionally, either person can interrogate the KARREN database to see if this parameter combination has already been simulated.

Conclusion

It was encouraging to see a growing number of SDM implementations presented using SDM software from a wider range of vendors. It's clear that SDM has joined the mainstream as organisations replace their paper trails with a Digital Thread. This not only provides traceability for regulatory compliance but also provides a sound foundation for Digital Twins of specific real world systems to be rapidly assembled to respond to manufacturing or operational requests. As always, NAFEMS is a public forum which enabled a robust exchange of views on the real challenges of SDM deployment. We look forward with interest to the European SPDM conference in 2018 nafe.ms/SPDM18. ■

References

- [1] Ruschmeier, D. "Simulation Data Management – The Next Challenges", NAFEMS World Congress 2017 nafe.ms/2N5zcuS
- [2] Chisholm, S. "Smarter Testing Through Simulation for Efficient Design and Attainment of Regulatory Compliance", NAFEMS World Congress 2017 nafe.ms/2lotbZs
- [3] Ulmer, T. "Virtual Testing for High Lift Systems – Efficient and Traceable Parameter Variations", NAFEMS World Congress 2017 nafe.ms/2Dz7sJj
- [4] Eller, C. "Introduction of SDM at Eberspächer Exhaust Technology", NAFEMS World Congress 2017 nafe.ms/2DDrxVb
- [5] Raimbault, V. "StressApps - A SPDM System for Aircraft Landing Gears Classical Analyses", NAFEMS World Congress 2017 nafe.ms/2Dyuhmy
- [6] Pährisch, M. "Integration of Manual and Automated Activities into a Commercial SPDM System – A User's Experience", NAFEMS World Congress 2017 nafe.ms/2DD1BJe
- [7] Makropoulou, I. "SDM System Implementation at China Euro Vehicle Technology", NAFEMS World Congress 2017 nafe.ms/2DEi7sn
- [8] Müllerschön, H. "New Developments on Compression and Transfer of Simulation Data within an SDM System", NAFEMS World Congress 2017 nafe.ms/2DDv0Db
- [9] Ruschmeier, D. "FDX – A Data Format for Functional Data Exchange and Process Chain", NAFEMS World Congress 2017 nafe.ms/2DBBtH5r
- [10] Murton, A. "MoSSEC: a Standard for Sharing Modelling and Simulation Information in a Collaborative Systems Engineering Context", NAFEMS World Congress 2017 nafe.ms/2DDwCNf
- [11] Grimberg, P. "Simulation Driven Design: How to Improve Collaboration?", NAFEMS World Congress 2017 nafe.ms/2Dzg5tD

Mark Norris is a PLM and SDM consultant, he is a long-standing member of the NAFEMS SDM Working Group and author of the NAFEMS SDM Business Value White Paper. He can be reached at e.mark.norris@gmail.com



Figure 1: The Graph browser which answers the question: "How and from what data did you get this result?"

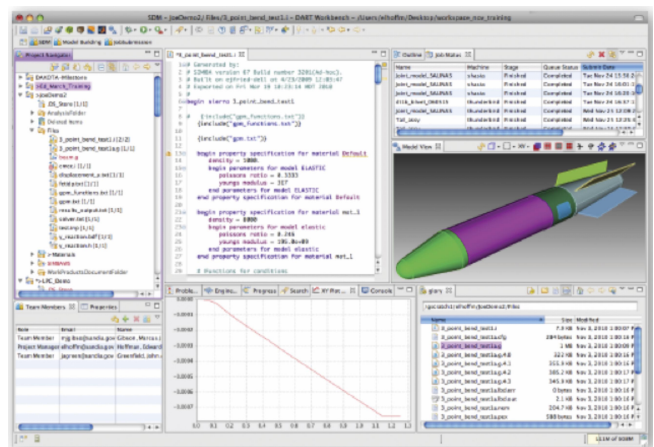


Figure 2: Sandia Analysis Workbench (SAW) for high consequence engineering systems.

The Future of Working in F1

Marco Einöder & Leire Apraiz, Totbox

Imagine an automotive company with more than 5,000 employees where around 15-20% of the workforce resides almost every fortnight in a different country, moving through the year from Australia to Canada or from Japan to Brazil.

Suppose now that the 500 people working in each project team include 14 different managing and functional profiles and that each project, itself, covers more than 10 different engineering branches, from chemical, mechanical, materials or telecommunications, to aerodynamics, ergonomics, electronics, structural engineering or data science and computing.

Think now that every 15 days (often including back-to-back weekends), this organisation must produce and launch 20 cars to the race track and that at any time hundreds of gigabytes of information have to be scanned in fractions of a second to take strategic decisions and to avoid accidents and injuries.

Complete the picture with a noisy working environment, with maximum stress situations and varying atmospheric conditions depending on the season and country. That's Formula 1, the most challenging working place in the world (Figure 1).

The yearly new regulations force teams to develop innovative solutions for the car design every year. Every thousandth of a second is potentially the difference between winners and losers, so teams invest a lot of time and money to deploy and apply the latest technologies not only to the development of the monocoques, but also to ease the management of such a large and geographically dispersed team and information set.

Real-time streaming of VR-360° images is something that has ceased to be science fiction and has become a reality. Formula One Management (FOM) begun this year

to use this technology in its sports broadcasts, allowing fans to live the races in a completely new and customizable way, enjoying the race from perspectives never before dreamed off. For the fans, names like Oculus, Vibe or Magic Leap or Play Station VR are now well known and it is likely that we will soon move from the World Wide Web (WWW) we know to a new World Virtual Web (WVW) where FOM and teams will create and share more and more VR content, maybe including VR-orientated websites.

On the other hand, some F1 teams will soon be using VR streaming technology for their team meetings, enabling them to gather in the same virtual space the team at the track and the engineers working simultaneously in their UK headquarters.

This VR environment where meetings take place, not only gathers people geographically distanced, but also all the team's relevant information and documentation: telemetry, photos, videos, CAD parts and models. During sessions, engineers working in such Assisted Virtual Reality Environments can abstract themselves from the distracting physical working conditions (small 2D laptop screens, noisy environment...) to work in a virtual world, with numerous aids and where everything can be easily found and shared.

One of the greatest challenges is that there is now so much data continuously received from the cars and the track that it is impossible for anyone to search through it to find the information needed sufficiently quickly. The information is there but if it can't be found, it is no better than not having it at all. So beneath the VR interface, an artificial intelligence core system, analysing track and car conditions and based on the team strategies, would automatically display to the engineers the pertinent information needed at every stage of the race, Figure 2.



Figure 1: Formula 1 racing

pxhere.com image under Creative Commons License



Figure 2: Images from the F1 Connectivity Innovation Prize Web, [1]

VR is becoming the new interface for other systems too, such as training. Mechanics and engineers learn and practice protocols and procedures to be used to repair the car without needing to damage it first and drivers test the ergonomics of the steering wheel controls even before it has left the drawing board. VR can be used everywhere to test in less time and at a lower cost.

But we must not forget that Formula 1 is a championship, and teams must not lose sight of their opponents' improvements. VR is also perfect for reverse engineering. Taking pictures of other cars, processing them using computer vision and photogrammetry to obtain a complete CAD model and evaluating it with CFD/FEA simulation software gives a team valuable information about the behaviour of their competitor's aerodynamics.

Testing the CAD model inside a VR wind tunnel where engineers are side-by-side with the parts during tests, manipulating 3D geometries with their own hands and seeing in real time and from any angle the behaviour of materials and fluids, is the next step.

To end, we can't forget the VR driving simulators that every F1 driver uses to explore the limits of a track before each race. Where to brake, how to take each turn, compound strategies; everything is tested a thousand times to find the right place to shed that thousandth of a second and reach the podium.

VR is here to stay in Formula 1, but what about in your company?

This article is written by the authors, based on their winning proposal for the "2016 Mercedes-AMG Petronas Challenge of the F1 Innovation Prize" set by Tata Communications, the Mercedes-AMG Petronas Formula One Team and Formula One Management (Figure 3). ■

F1, Formula One, Formula One Management and Mercedes-AMG Petronas Formula One Team are trademarks of their owners.

References

- [1] "F1 Innovation Prize," 2016. nafe.ms/2xqA2fS



Figure 3: Challenge 2 winners of the F1 Connectivity Innovation Prize Web

Marco Einöder, is a Computer Engineer with an MBA and has more than 25 years' experience working in Germany and Spain. He currently works as Senior Innovation Engineer designing artificial intelligence, computer vision and virtual reality systems.

Leire Apraiz, is a Computer Engineer with more than 25 years' experience working in consultancy and digital marketing.

Their interest in innovation and Formula 1 has made them participate in the following contests:

- 2018 - F1 Connectivity Innovation Prize - "My F1 Experience" Challenge. **Finalist**
- 2016 - F1 Conectivity Innovation Prize - Mercedes AMG Petronas Formula One™ Team Challenge. Virtual Reality Challenge. **Winner**
- 2015 - F1 Conectivity Innovation Prize - Mercedes AMG Petronas Formula One™ Team Challenge. Real Time Display Challenge. **Winner**
- 2013 - Scuderia Ferrari - Bco Santander Forza Ferrari marketing-video contest. **Winner**

Other awards and innovation prizes won are:

- 2017 - Aixé Getxo Award in the "Innovative Culture" and "Science Culture" categories
- 2014 - Innocentive Marketing Challenge: Maximizing Retail Merchandising Space
- 2010 - "Euskaltel Challenge" at the Baske Innovation Community

www.totbox.es
totbox4u@gmail.com

Simulation Limited:

How Sensor Simulation for Self-driving Vehicles is Limited by Game Engine Based Simulators

Zoltán Hortsin, Almotive

Simulating the images of unique cameras used for self-driving was a driving force behind the development of a new engine for a simulator designed for autonomous vehicle development.

Over the last 18 months, the importance of simulation in the development of autonomous vehicle technologies has become widely accepted. Industry experts and analysts alike are claiming that enormous distances must be covered by self-driving systems to achieve safe operation in varied road conditions and environments. Meanwhile, certain weather conditions and traffic scenarios are extremely rare, resulting in limited test opportunities. The only way to cover the distances and reach the diversity required for the safe operation of highly automated vehicles is through testing these systems and their modules in virtual environments. The demands of simulation for self-driving cars are extremely high and not all simulators are created equal.

Simulation for Self-driving

Simulators for autonomous technologies must be comprehensive and robust tools, offering at the least:

1. A diversity of maps, environments, conditions and driving cultures.
2. Repeatability of tests and scenarios for the continuous development of safety-critical systems.
3. Ready access for self-driving developers and engineers to accelerate iteration times and development loops.

However, these requirements only scratch the surface. The demands of self-driving are unique, as a result, only a purpose-built virtualization environment can become a full solution. Several industry stakeholders have built proprietary solutions based on game engines. While game engine rendered simulators can provide the above-listed characteristics, they do not solve all the challenges of self-driving simulation. Beyond the basic demands listed above a true self-driving simulator has to offer more:

1. The utmost level of physical realism in vehicle and road models, weather conditions, and sensor simulation.
2. Pixel-precise deterministic rendering to ensure that minor differences in simulated environments do not affect the results of repeated tests.
3. The efficient use of hardware resources including the ability to run on any system from laptops to servers or utilizing the performance of multiple CPUs and GPUs.

The Limitations of Game Engines

These more specific demands cannot be answered efficiently by game engine based simulators. Their focus is inherently different. A game engine is designed with a commercial end-user in mind and is built to utilize average hardware setups while being optimized to offer the best game performance. Furthermore, it is often 3D and graphic artists that create the final visual effect to ensure a spectacular world for the consumer, rather than a physically correct environment.

Almotive encountered several problems while using a game engine-based simulator. One of the most notable was how game engines are not prepared to simulate the images of unique sensors such as ultra-wide field of view fisheye lenses or narrow view long-range cameras. This is fundamentally because such views are almost never used in games. As a result, the previous iteration of our simulator contained custom modifications to the engine. However, as these were not organic elements of the code they were also a bottleneck. On the one hand, they affected the performance of the simulator. On the other hand, certain effects built into the game engine could not be used on intermediary images, only on the final render, which resulted in less realism. Of these more unique sensors, ultra-wide field of view fisheye cameras were the most exciting challenge. The following sections will outline the approach we took to overcome these difficulties.

Synthesizing Camera Images

A camera's operation can be divided into two parts: the optics and the sensor. Rays of light move through the lens and arrive in a given pixel of the sensor. When simulating camera images, it is this process that has to be recreated. There are several mathematical models for this projection, the commonality between them being that they all result in a 2D pixel position from 3D data.

However, when discussing images taken with ultra-wide-angle lenses, further difficulties arise. We use fisheye lenses to cover ultra-wide field of views which do not create rectilinear images, but exhibit barrel distortion. As a result, projecting them onto a two-dimensional plane is a slightly more complex process as the distortion must be accounted for. Figure 1 illustrates how this distortion is mapped to a 2D plane.

Simulating a Fisheye Image

The most obvious solution to simulate such an image would be to simulate the exact paths of the rays of light as they move through a simulated lens and onto the

sensor. However, this approach relies on ray tracing, a technology currently only available in a few select GPUs. Most GPUs employ rasterization for image synthesizing (Figure 2), a solution that does not allow for a robust fisheye projection. While there are certain workarounds that make the projection possible, the nature of these solutions mean that the projection will not be robust, thus, rendering may be incorrect, or the performance of the engine may be affected. To find a solution the problem has to be reexamined.

Reexamining the Problem

To achieve a robust projection the task at hand has to be divided into two parts. In the first step, data for rays of light reaching the lens is generated. In the second step the corresponding data for the rays that reach the sensor must be found. Naturally, the high distortion of fisheye lenses causes difficulty in the projection.

Step one – This is the most demanding part of the process, which relies most heavily on the rasterization performance of the GPU. Based on the calculated location of the sensor, images must be generated that cover the area of space from which light can enter the lens. This can be a single image or a total of six, depending on the characteristics of the simulated camera, as shown in Figure 3. The hardware demands of the process are heavily dependent on the quality of these images, and to achieve the highest degree of reality high-quality images and physically based High Dynamic Range (HDR) rendering must be employed. As several cameras and other sensors are being simulated concurrently by the simulator, this can lead to huge demands on memory and compute capacity. Hence the ability to efficiently utilize multiple CPUs and GPUs if needed is vital. However, to ensure flexibility, the system should also be able to run on more everyday systems such as desktop PCs. This is to allow developers and self-driving testers to have proper access to the simulator and use it as a development tool. Naturally, high-quality tests have to be run on heavy performance setups, but not all tests require such resolutions.

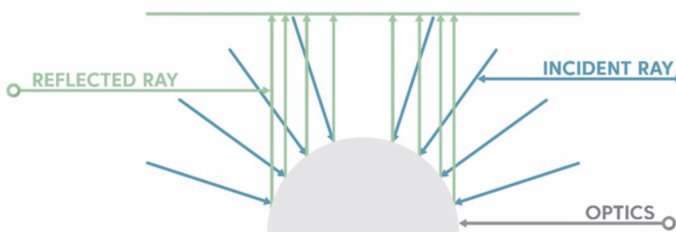


Figure 1: Fisheye projection illustrating rays and final pixels

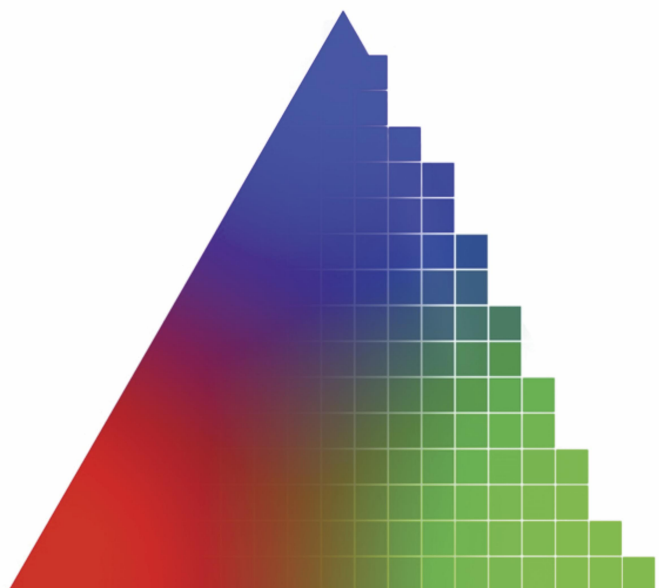


Figure 2 : GPU rasterizing



Figure 3: Six images forming a cube with a camera placed in the center

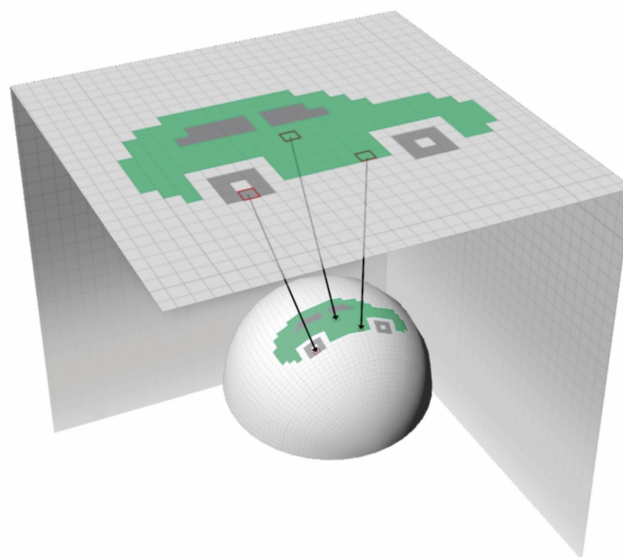


Figure 4: Pixels from images are projected onto a sphere

Step two – In essence, the task at hand is to simulate the lens distortion of the camera and create the image that appears on the sensor itself. The resolution of this image matches the resolution of the sensor. The data used to create the image is obtained from the 1-6 images generated in step one. The GPU is used to calculate the characteristics of the 3D rays that correspond to the 2D pixels on these images (Figure 4). Further characteristics of the simulated camera (exposure time, tonemapping etc.) are also added in this step. These are needed to create a simulated sensor image that is the closest it can be to the image the real sensor would provide to the self-driving system in the real world. Only through a high correlation can simulation truly be a viable tool for the development and validation of self-driving systems.

The Simulated Image

Following these steps, we can create a virtual representation of an image that a fisheye camera would provide to the self-driving system. The robustness of this solution is based on recreating the problem in a way that allows GPUs to compute the simulation effectively without relying on niche technologies. The method is also extremely precise, allowing for pixel-perfect

deterministic rendering: each scene will be calculated and rendered in entirely the same way, every time it is loaded.

If simulators are to be used as a platform for not only testing but also validation, they must be the closest possible representation of the real world in every regard. The example given above clearly presents how the inherent limitations of game engines cannot serve as a reliable platform for this. Fisheye cameras are an important element of a vision-first self-driving setup as they can be used to create a wide (or ultra-wide) field of view around the vehicle easily. Without the ability to properly simulate these there will be limits to the correlation between the real world and the simulated test environment. Beyond this highly technical difficulty and the required level of physical fidelity, the limitations discussed above regarding the flexibility and scalability of the simulator, the efficient use of hardware are also important factors. Building on our experience with self-driving technology and working with a game-engine-based simulator in the past we strongly believe that in the future simulators for autonomous technology testing and verification must be purpose built. ■



Zoltán Hortsin is a self-trained game engine development and OpenGL ES 2, 3 and Vulkan 3D API specialist who originally studied Dentistry at Semmelweis University, Budapest. After discontinuing his university studies during his final semester, he joined Almotive's predecessor, Kishonti Informatics Ltd, where he served as a team leader to work on the company's mobile GPU benchmarks. Zoltan is the technological mentor of Almotive's internal simulation engine development team. His favorite area of research is real-time global illumination. Zoltán is a chocolate connoisseur, and spends his free time reading up on paleontology and collecting fossils.

To read more about Almotive visit aimotive.com

Event Review

“New Methods in CFD – Alternatives to Finite Volumes”

Arzu Avci, Festo

Jens Iseler, ABB

Arthur Stück, German Aerospace Center (DLR)

Uwe Janoske, University of Wuppertal

On November 12th and 13th 2018 the NAFEMS seminar “New methods in Computational Fluid Dynamics (CFD)” took place in Wiesbaden, Germany. The seminar was organized by the NAFEMS CFD Advisory Board for Germany, Austria and Switzerland [1] with the goal of presenting a brief overview of alternative methods in CFD besides the well-known Finite-Volume based method. Nearly 60 attendees had the chance to benefit from four keynote and twelve presentations. The presentations covered Lattice-Boltzmann Methods (LBM) and mesh-free methods such as Smooth Particle Hydrodynamics (SPH) and Finite Point Methods (FPM). The seminar was rounded off with presentations on unconventional Finite-Element/Volume techniques and applications differing from main-stream CFD approaches.

Finite Point Methods

The first block of lectures regarding Finite Points Methods was opened by Dr. Jörg Kuhnert from the Fraunhofer Institute ITWM in Kaiserslautern [2] who gave a keynote presentation on a “Meshfree-Generalized simulation tool in CFD”. The approach of a generalized mesh-free finite-difference method was demonstrated for various applications ranging from filling simulations up to detailed simulations of cars on wet roads (Figure 1). Fabian Nick and his co-authors from the Fraunhofer Institutes SCAI and ITWM presented a number of parallel performance test simulations made in conjunction with the in-house finite pointset method (FPM), MESHFREE [3].

The developments and improvements were aimed at scaling parallel solution methods for mid-sized compute clusters with some hundreds of cores, which are used in many industry applications. In the subsequent talk by Dr. Matthias Schäfer and co-authors from ESI Software Germany GmbH [4], a meshless FPM-based simulation method was presented that was used to predict the interaction of water with car structures in the context of complex water crossing scenarios (Figure 2). As a summary, finite point methods showed interesting options especially for the simulation of free-surface flows where only a small part of the domain is covered by the second phase.

Presentations from this event are available for NAFEMS members to download at nafe.ms/CFD18DACH





Figure 1: Comparison of FPM simulation and experimental results

Smooth Particle Hydrodynamics

Several applications of SPH were shown in three different talks. Gernot Maier and his colleagues from AVL List GmbH/Italia S.r.l. [5] evaluated and compared classic finite-volume methods against SPH for flow simulations in automotive transmissions (Figure 3). Oil splashing in basic single-gear setups and complex transmission configurations were considered. In these studies, the SPH method allowed for huge time savings due to the omission of the mesh generation phase. The studies were able to plausibly predict the resulting oil distributions, although torque loss predictions obtained from standard finite-volume calculations were considered superior to the SPH counterparts. Michael Ehlen from AVL qpunkt [6] presented the application of SPH to simulate the air intake of the air-conditioning unit of a vehicle in heavy rain. Different models including the movement of wipers, gave an insight in the behaviour of water in the air intake system. Simon Härdi (University of

Wuppertal) [7] presented the simulation of thin water films using a combination of SPH and the FPM. The motivation of the study was to provide a precise and fast method to predict wall films (Figure 4). Mr. Härdi explained during his talk, that a pure SPH approach is not sufficiently accurate for the prediction of thin films due to non-negligible surface tension effects, which depend on the third order derivative. However, by combining SPH with a FPM, those limitations can be overcome. The proposed procedure solves the field variables via SPH whilst the derivatives are computed via FPM. A validation of this approach was conducted by predicting the behaviour of a drop resting on a flat surface. The results obtained showed a good match with the analytical solution. A good comparison with experiment was also achieved with the other two application cases – namely free surface wetting flow on a cylinder between two walls and on a sphere.



Figure 2: Virtual car prototyping in a realistic driving environment

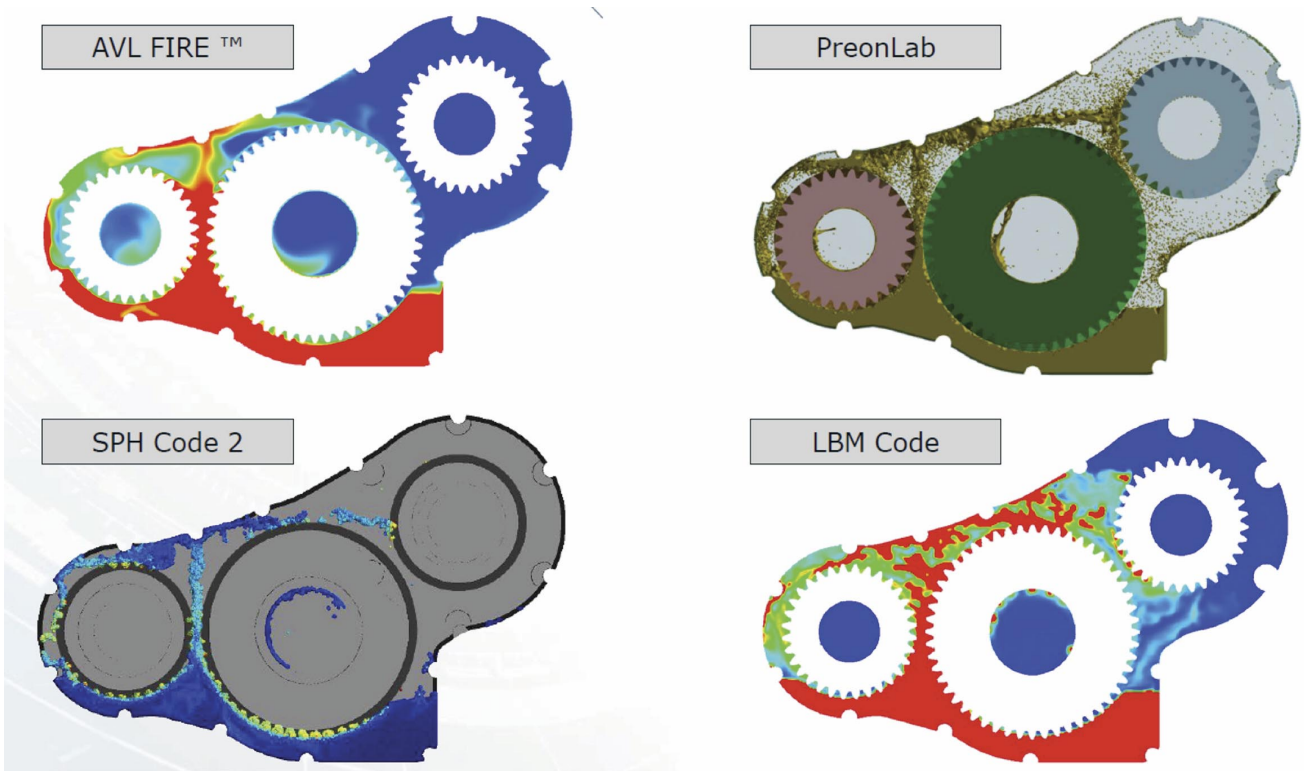


Figure 3: Comparing different methods for oil distribution simulation

SPH methods are deemed to have a good potential, similar to FPMs, for many scenarios of free-surface flows. In particular, if a visualization of transient and often violent free-surface flow patterns are the main interest of the simulation, these methods can be very efficient compared to finite volume methods.

Lattice Boltzmann Methods

LBM have been used for several years in industrial applications and the interest is growing in different fields. Professor Martin Böhle from the Institute of Fluid Mechanics and Fluid Machinery (University of

Kaiserslautern) [8] presented the application of an in-house LBM code in turbomachinery applications. In particular, the combination of flow and acoustics gives interesting opportunities for the development of rotating machinery. Manfred Krafczyk, Professor at TU Braunschweig, focused on a newly developed 4th-order accurate LBM for the simulation of scale-resolving turbulent flows [9]. Among the examples shown were GPU-enabled simulations of turbulent flow around spheres, automotive aerodynamics and urban wind engineering problems as well as massively parallel CPU computations with a 7×10^{10} DOF LES for the analysis of noise damping for airfoils (Figure 5).

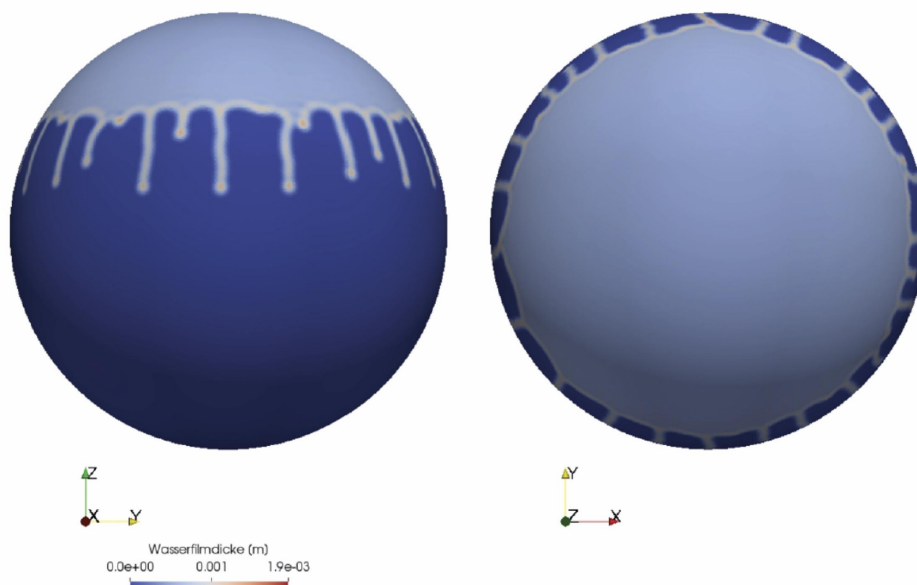


Figure 4: Simulating thin water films

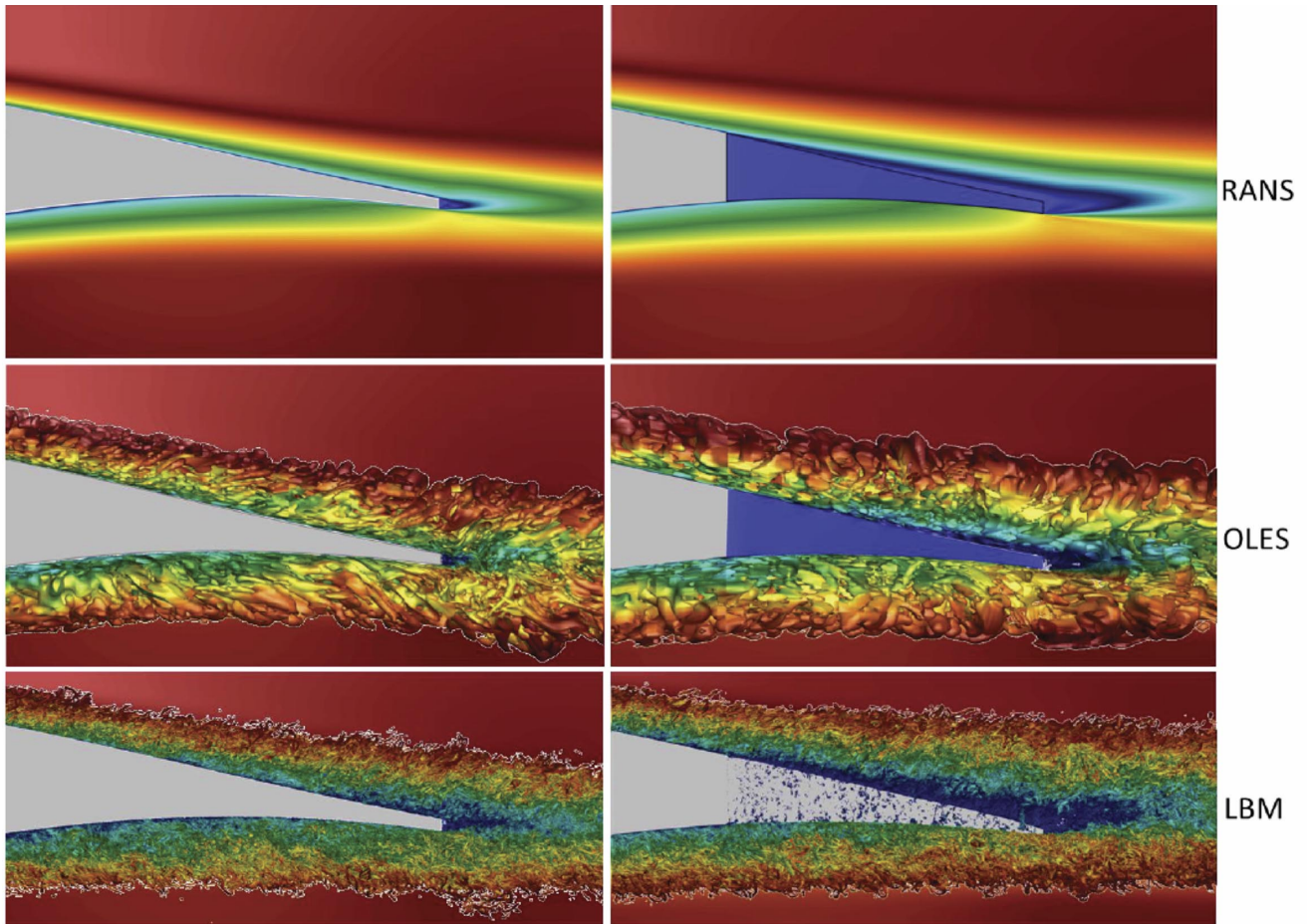


Figure 5: Different CFD models addressing the same problem [13].

Moreover, Professor Krafczyk used the opportunity to make some comments on “so-called” mesh-free methods and requirements for the consistent comparison and assessment of established and alternative CFD methods from a numerical perspective. Dr. Christian F. Janßen, Altair and Hamburg University of Technology [10], presented LBM high-performance computing simulations in different fields of automotive and marine applications. They used a free-surface software extension, implemented in the in-house LBM code “ELBE” that allowed for predictions of violent sloshing in a deck-mounted pool of a cruise ship or for the simulation of a ship passing through ice. Prof. Feuchter presented the LBM applied at the University of Aalen, Germany [11]. Results were shown for an engine air intake system and compared to physical measurements of mass flow rate.

The goal of the study was to reproduce measured deviation of the mass flow rate in the intake system. The intake system included an inflow area, a filter, a section with ribs followed by a section with the sensor. A high lattice-resolution allowed the capturing of vortex structures developed at the ribs near the sensor (Figure 6). The isosurface of the Q-criterion showed that those

structures are still present at the sensor and therefore affect the measurement. Similarly to the experiment, two different rib configurations with different thicknesses were considered. Both the experiment and LBM simulation showed a very similar increase in mass flow rate when the thicker rib was used. Gerhard Öttl (Dassault Systemés) [12] presented results of a flow analysis for an unmanned aerial vehicle (UAV) using a LBM.

The presentation was split into two parts. Within the first part, the flow behaviour of the drone was investigated for different angles of attack. The aerodynamic parameters deduced from the simulation results showed good agreement with the ones obtained from wind tunnel testing.

The second part of the presentation dealt with a dynamic analysis. Here, a pitch oscillation of the UAV was initialized by applying a sudden displacement to the elevons at the beginning of the analysis. The prediction of the oscillation was conducted by coupling the LBM method with an internal 6-DOF motion solver. The results revealed – as expected – a stable oscillation with a decreasing pitching moment in time.

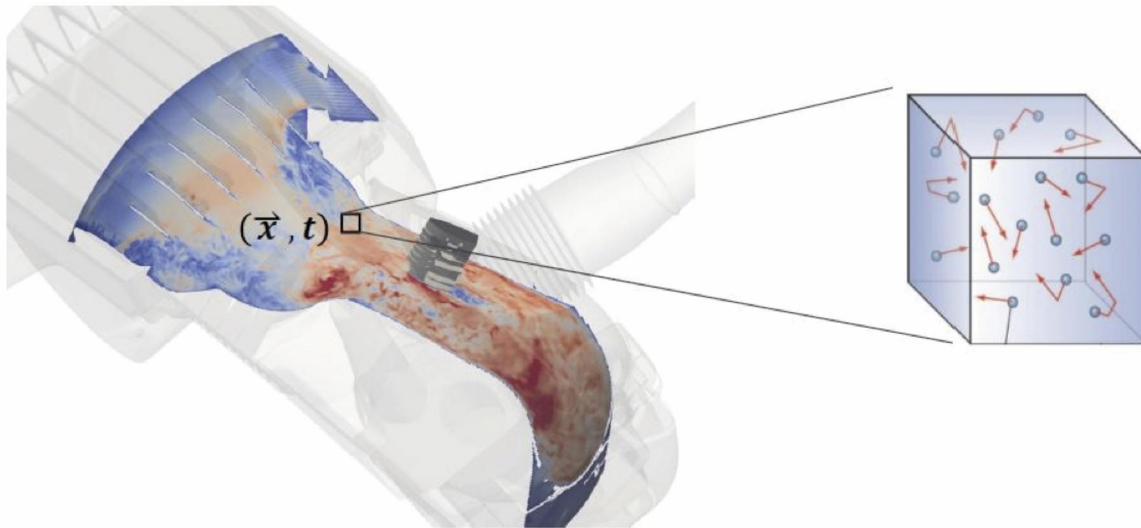


Figure 6: Using LBM for Large-Eddy Simulations

The presentations showed the possibilities and capabilities of LBM predominantly in unsteady simulation scenarios and their potential regarding the simulation times if GPUs are used.

New Methods

In the final part of the seminar, new simulation approaches were presented. Dr. Sabine Baumbach from the Volkswagen company [14] presented an incompressible time-spectral CFD method for the simulation of viscous time-periodic flows. Industrial applications with time-periodic flow regimes like the flow around a ship propeller and an oscillating airfoil were investigated comparing the time-spectral method against conventional time-stepping methods. Dr. Sven Linden from Math2Market GmbH [15] demonstrated specialized

methods for direct numerical simulations of porous media (Figure 7). The shown method is designed to compute the properties directly on very large 3D images of porous materials. Kamil Braschke, Chair of Fluid Mechanics from the University of Wuppertal in Germany [16], presented an in-house developed library ABSFoam (Arbitrary Body Simulation), which enables implementation of the immersed boundary method into OpenFOAM. Complex interactions of volumetrically resolved particles, such as in the process of filtration were shown.

As a summary, the seminar gave delegates the chance to learn about advantages and disadvantages of new and unconventional CFD methods with a focus on industrial applications. The feedback from the audience was positive. ■

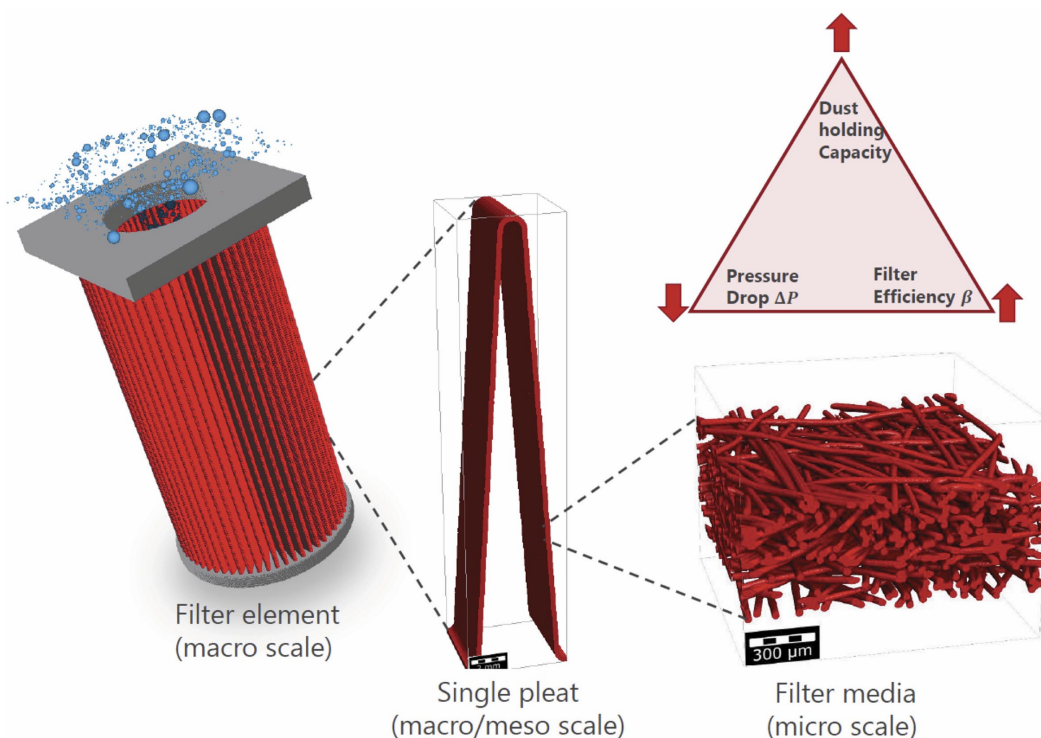


Figure 7: Filtration simulation at different scales

References

- [1] NAFEMS, "NAFEMS DACH CFD Advisory Board (CAB)," [Online]. Available: nafe.ms/cab [Accessed 2019].
- [2] J. Kuhnert, MESHFREE-echt gitterfreie Strömungssimulation, Wiesbaden: NAFEMS, 2018. nafe.ms/2W0JFwF
- [3] B. Metsch, F. Nick and H. Plum, Performanceaspekte in gitterfreien CFD-Methoden, Wiesbaden: NAFEMS, 2018. nafe.ms/2W77EdO
- [4] M. Schäfer, Virtuelle Fahrzeugentwicklung unter realistischen Fahrbedingungen am Beispiel von Wasserdurchfahrt, Wiesbaden: NAFEMS, 2018. nafe.ms/2W4baWa
- [5] G. Maier, F. Testa, A. Diemath and W. Baier, Anforderungen und Grenzen traditioneller FV- und neuer SPH-Methoden für Strömungsuntersuchungen in Fahrzeug-getrieben, Wiesbaden: NAFEMS, 2018. nafe.ms/2W8ha0s
- [6] D. Bäder and M. Ehlen, Simulation der Luftansaugung des Klimageräts eines in Starkregen stehenden Fahrzeugs, NAFEMS, 2018. nafe.ms/2W1NS3i
- [7] S. Härdi, M. Schreiner and U. Janoske, Simulation von dünnen Wasserschichten auf beliebigen, Wiesbaden: NAFEMS, 2018. nafe.ms/2W5cdVR
- [8] M. Böhle, Die Lattice-Boltzmann Methode zur Simulation von Strömungen in Turbomaschinen-Anwendungen, Wiesbaden: NAFEMS, 2018. nafe.ms/2W5co3t
- [9] M. Geier, K. Kutscher, M. Schönherr, H. Safari and M. Krafczyk, GPU-basierte Lattice-Boltzmann-Methoden höherer Ordnung für DNS/LES Simulation, Wiesbaden: NAFEMS, 2018. nafe.ms/2W27CUA
- [10] C. F. Janßen, D. Mierke and M. Gehrke, Anwendung innovativer LB-Verfahren für simulationsbasiertes Design im Schiff- und Automobilbau, Wiesbaden: NAFEMS, 2018. nafe.ms/2W2t8bD
- [11] C. Feuchter, A. Stief and O. Wagner, Anwendungen von Lattice-Boltzmann Methoden für Large-Eddy Simulationen, Wiesbaden: NAFEMS, 2018. nafe.ms/2W2GfJV
- [12] G. Öttl, CFD Analyse zum Flugverhalten einer Drohnenkonfiguration mittels Lattice-Boltzmann Methode, Wiesbaden: NAFEMS, 2018. nafe.ms/2W3dT2l
- [13] TU-Braunschweig, "SFB 880 at TU-Braunschweig," [Online]. Available: nafe.ms/2VwtqqZ [Accessed 2018].
- [14] S. Baumbach and A. Stück, Zeitspektrales Verfahren zur Berechnung viskoser, inkompressibler Strömungen in der industriellen Anwendung, Wiesbaden: NAFEMS, 2018. nafe.ms/2W2MjIH
- [15] S. Linden, C. Cheng and A. Wiegmann, Spezialisierte Methoden zur direkten numerischen Simulation in porösen Medien, Wiesbaden: NAFEMS, 2018. nafe.ms/2W1Nxx2
- [16] K. Braschke and U. Janoske, Eine Immersed Boundary Methode zur Berechnung komplexer Partikelinteraktionen für volumetrisch aufgelöste Partikel, Wiesbaden: NAFEMS, 2018. nafe.ms/2W2Gp3Z

The article was written by four members of the Germany Advisory Board in CFD (CAB) for Germany, Austria, and Switzerland (DACH) - Arzu Avci, Jens Iseler, Arthur Stück and Uwe Janoske.

Arzu Avci is a simulation engineer at Festo working in the field of fluid dynamics. She is particularly interested in deeper insight into and achievable simulation of coupled fluid and structural phenomena. She is a member of the NAFEMS Multiphysics Working Group and CFD DACH Advisory Board (CAB). The family-owned automation company Festo offers a wide range of pneumatic and electric components and system solutions.

Jens Iseler was a project engineer at ABB in the field of power generation and is now a Senior Solution Consultant at DS/FE-DESIGN. His fields of activities are non-parametric optimization, RANS- and LBM based flow simulations on different industries as well as Fluid-Structure Interaction (FSI). He is a member of the NAFEMS Multiphysics Working Group and CFD DACH Advisory Board (CAB). He has a PhD in Aerospace Engineering (Simulation of turbomachinery flows for axial compressor and turbine blades with turbulent or transitional BL).

Arthur Stück developed high-performance CFD methods and algorithms for aerodynamic flow simulation and CFD-based optimization at the German Aerospace Center (DLR), Institute of Aerodynamics and Flow Technology in Braunschweig. Currently he is head of the Department Simulation Frameworks, DLR Institute of Software Methods for Product Virtualization in Dresden. He has a Dipl.-Ing. in Ship Studies from Hamburg University of Technology (TUHH) and a PhD from TUHH (development of adjoint CFD methods for hydrodynamic shape optimization). He is a member of NAFEMS Computational Fluid Dynamics Advisory Board (CAB).

Uwe Janoske is professor for Fluid Mechanics at the University of Wuppertal. His research interests are multiphase and coupled multiphysics flow problems. He is also head of the Steinbeis Research Centre Virtual Testing (www.virtualtesting.de) which offers consultancy and services in the field of modelling and simulation. He chairs the NAFEMS CFD Advisory Board for Germany, Austria and Switzerland [1] and offers two courses in CFD for NAFEMS in Germany and the UK. He has a Dipl.-Ing. in mechanical and process engineering from the University of Mosbach and Stuttgart (1993, 1995), a PhD in process engineering (Univ. Stuttgart, 1999) and a post-doctoral lecturer qualification (Habilitation, Univ. Wuppertal, 2006).

Validation of Electromagnetics Simulations for Vehicle-to-Everything Applications using Measured Results

Ushe Chipengo, ANSYS

The automotive industry has seen a recent surge in the development and deployment of Advanced Driver Assistance Systems (ADAS). This trend has seen ADAS become one of the fastest growing markets in the technology sector. The automotive industry is seeing a shift in ADAS implementation and adoption from low volume, high end vehicles to high volume, low end vehicles. Projections are that by 2021, Original Equipment Manufacturers (OEMs) will be spending over \$37 billion on ADAS and safety related electronics [1]. With fully autonomous vehicles being the ultimate manifestation of ADAS, much of the growth in the ADAS market has been attributed to OEMs racing to deploy the first, commercially available, fully autonomous vehicle. According to Allied Market Research, the global autonomous vehicle market is projected to be valued at \$54.23 billion in 2019. This number is expected to rise to \$556.67 billion by 2026 [2]. Therefore, there is an enormous financial incentive to develop advanced driver assistance systems that will serve as the backbone of fully autonomous vehicles.

Another driving factor in ADAS development has been the need to make roads safer. According to the National Highway Traffic Safety Administration (NHTSA), 37,133 people lost their lives in traffic accidents in the US in 2017 [3]. Furthermore, over 90% of traffic accidents are caused by human error [4]. There is clearly a case for equipping vehicles with safety related ADAS.

Vehicle to Everything (V2X) is an ADAS enabled, wireless technology that allows vehicles to communicate with other vehicles and road infrastructure. Vehicles and road infrastructure equipped with V2X capabilities will enable low latency transfer of safety-critical and commercial information. For example, V2X can be used to deliver 'do not pass', 'blind curve ahead' and 'road works ahead' warnings, among others. The NHTSA has estimated that safety applications enabled by V2X will eliminate or reduce the severity of up to 80% of non-impaired traffic accidents [5]. In 1999, the U.S. government allocated 75 MHz of spectrum for Dedicated Short-Range Communication (DSRC) technology centered at 5.9 GHz to support V2X applications [6], [7].

Experimental works have been conducted to investigate various aspects of establishing reliable communication between vehicles and road infrastructure at 5.9 GHz [8]–[13]. Test and measurement is very valuable, however, it is expensive, time consuming and difficult to use to measure all the possible corner case scenarios. Furthermore, test and measurement usually lack insight into the physics involved. On the other hand, simulation is relatively low cost by comparison. Using simulation, it is possible to rapidly simulate multiple corner cases and, more importantly, gain physical insight into the root cause of engineering problems.

Past works have used simulation to evaluate the impact of antenna placement and time varying propagation channels on the received signal strength in V2X scenarios [14], [15]. However, the simulation solvers used lacked a comprehensive, full physics approach. Specifically, the work in [14] only accounted for first and second order reflections using a 3D ray tracing model to save time. Furthermore, the simulation model in [15] neglected to include the effects of the vehicle bodies on the radiation patterns of the antennas themselves. By acting as secondary ground planes, vehicle bodies can significantly modify the far field radiation patterns of antennas and their effects need to be accounted for. Finally, the simulation solvers used in [14], [15] failed to account for advanced physics principles such as creeping waves, Physical Theory of Diffraction (PTD) and Uniform Theory of Diffraction (UTD) which can significantly affect simulation results.

This article looks at one particular work where three independently published field tests [8], [11], [12] were virtually recreated and simulated using ANSYS HFSS SBR+, an asymptotic, full physics electromagnetic solver that can efficiently simulate electrically large electromagnetics problems. For each of the cases, the simulated results were compared with the independently

obtained measured results. In the first case [8], the impact of vehicular obstructions on the received signal strength in V2X applications was investigated. Here, both measurements and simulations demonstrate how vehicular obstructions can lead to over 20 dB loss in signal reception. In the second case [11], the impact of ground induced multipath is investigated and shown to cause signal drops of almost 10 dB when compared to free space propagation. Finally, vehicle to vehicle communication in urban Non-Line-Of-Sight (NLOS) conditions is investigated [12] and shown to heavily depend on the physical widths of the streets making up the NLOS intersections. The good correlation between measured and simulated results in this study demonstrates how simulation can be used to rapidly model various V2X scenarios with great accuracy.

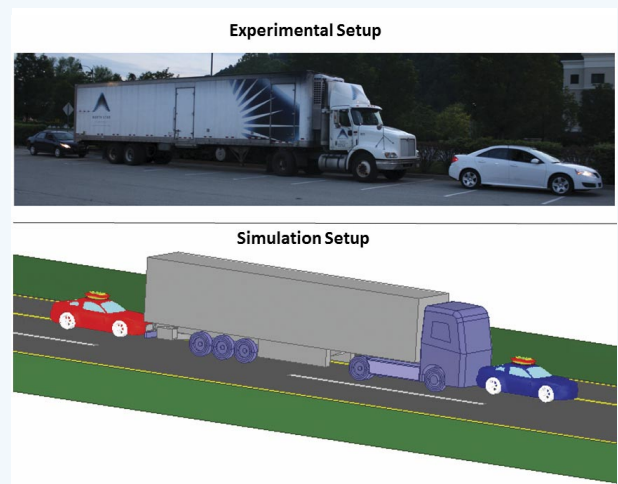


Figure 1: Experimental setup for physical testing done in [8] and a simulation setup of the same scene.

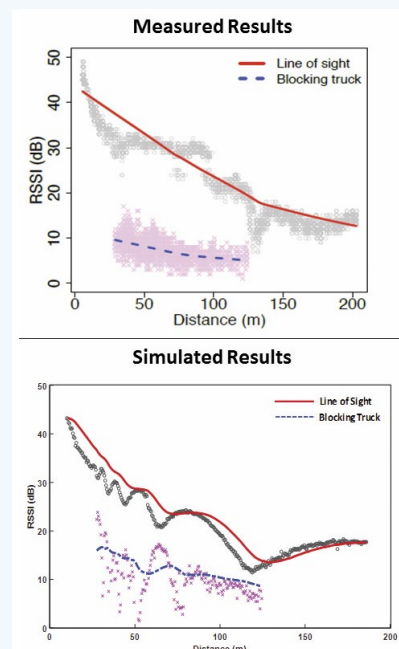


Figure 2: Measured results of the Received Signal Strength Indicator (RSSI) from [8] and simulated results obtained by recreating the experiment as shown in Figure 1

Shooting and Bouncing Rays (SBR+)

Solver: Concept & Simulation Setup

High Frequency Structure Simulator, Shooting and Bouncing Rays (HFSS SBR+) is a high frequency, asymptotic electro-magnetics solver that uses Geometric Optics (GO) ray tracing in conjunction with Physical Optics (PO) to solve electrically large problems [16]. In addition to GO and PO, SBR+ takes into account physics such as Physical Theory of Diffraction (PTD), Uniform Theory of Diffraction (UTD) and creeping waves. It is used to model antenna to antenna coupling problems in electrically large environments. It is also used to model the effects of electrically large platforms on the radiation characteristics of antennas. In this work, HFSS SBR+ was used to evaluate the impact of a full vehicle body on the radiation characteristics of a monopole antenna mounted on top of sedan type vehicles. This modified far field radiation pattern was then mounted on the vehicles and placed in the virtually recreated scenes as shown in Figure 1. From here, simulations were run to obtain the received signal strength between transmitting and receiving antennas.

Virtually Recreating Measurement Test Setups

Evaluating Impact of Vehicular Obstructions on Vehicle to Vehicle (V2V) Communications

Vehicular obstructions between two communicating vehicles can eliminate a direct line of sight link between them. According to experiments conducted in [8] a single vehicular obstacle can reduce the received signal between two communicating by 20 dB when they are 10m apart. It has also been shown that at longer distances, vehicular obstacles can effectively halve the distance at which packets are transmitted with 90% chance of reception. The experiment in [8] was reproduced as shown in Figure 1. Figure 2 shows the received signal strength between two vehicles when they have no obstacle between them (line-of-sight) and when there is a truck between them (non-line-of-sight). As shown in Figure 2, the simulation results also validate the 20 dB drop in signal strength observed in previous experiments. Over all, there is a good level of agreement between measured and simulated results.

Evaluating Impact of Ground Induced Multipath on Received Signal Strength for V2V Links

A typical vehicle to vehicle communication link is characterized by multiple dynamic and static obstructions that serve as secondary reflection surfaces. Such unintended reflections of the direct signal can lead to constructive and destructive interference at the receiver. The ground is an ever-existing obstruction that serves as a source of multipath signals. Unexpected nulls in received signal strength profiles of V2V links have been observed and attributed to ground induced multipath. To investigate this, the experiments in [11] were virtually recreated. Two vehicles with antennas

mounted on them were driven towards and away from each other at 55mph and the received signal strength was recorded. Figure 3 shows the experimental and simulation setups. Figure 4 shows a comparison between the simulated and measured results from [11]. The simulation results accurately show the received signal strength and the distances where the nulls occur.

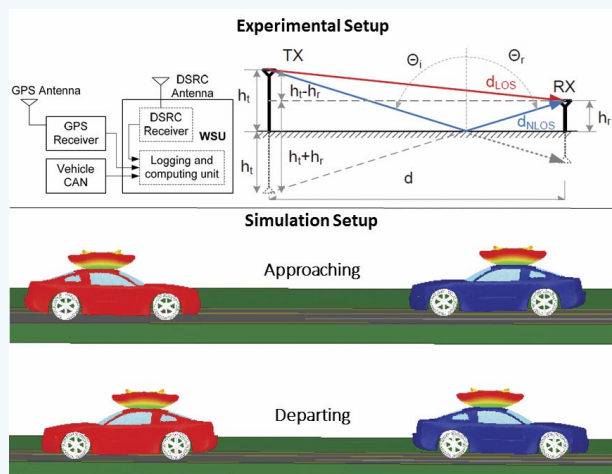


Figure 3: Experimental setup for physical testing done in [11] and a simulation setup of the same scene using HFSS SBR+.

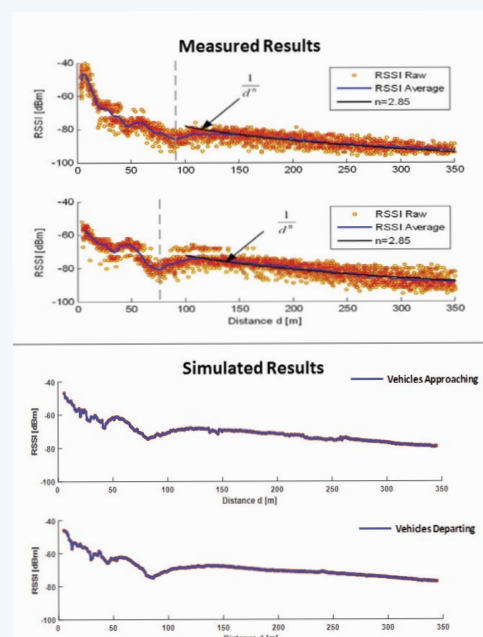


Figure 4: Received Signal Strength Indicator (RSSI) vs. range for approaching and departing vehicles. Measured results were obtained from [11].

Investigating Non-Line-of-Sight (NLOS) V2V Communication Links on City Intersections

City intersections create complex propagation channels for V2V communication links due to the non-line-of-sight conditions that can be created by buildings at intersections. This loss in received signal strength between two vehicles approaching an intersection as

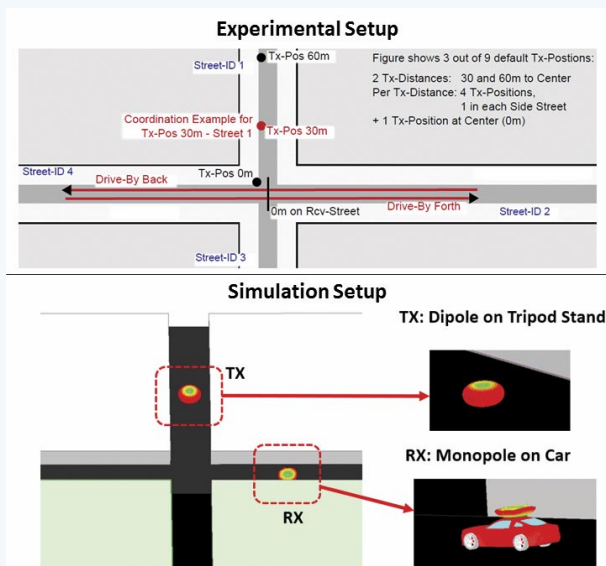


Figure 5: Experimental setup for physical testing done in [12] and a simulation setup of the same scene.

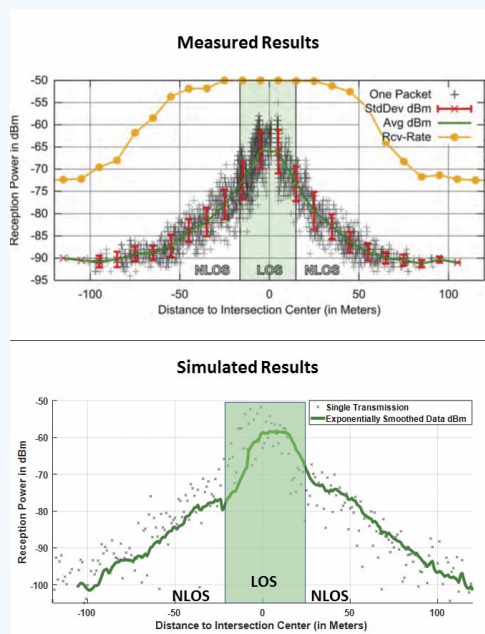


Figure 6: Received signal power in dBm for vehicle approaching and departing an intersection. Measured results were obtained from [12].

shown in Figure 5 can lead to an unreliable communication channel. Unreliable communication links at blind intersections can prevent vehicles from sharing crucial safety information. An example of such safety information can be an impending red-light violation by a vehicle in one of the intersecting streets. Communication in NLOS conditions was investigated in [12] by placing a transmitter and vehicle-mounted receiver on two roads that intersect. The receiving vehicle [RX] was then driven from one end of the street to another while the received signal strength and the packet reception rate were

measured. Figure 5 shows the experimental setup and the simulation setup. The results from simulation and measurements are shown in Figure 6. Results from this setup demonstrate that the received signal strength drops sharply once the receiving vehicle falls into the NLOS distance regions. This leads to a corresponding drop in the packet reception rate. It is important to note the good level of agreement between the measured and simulated results. Using such results, it can be evaluated if two vehicles travelling towards an intersection would be able to get safety information related to the state of the intersection when they are sufficiently far enough to avoid a collision.

Conclusion

Vehicle to Everything is one of the leading technologies that have been enabled by advanced driver assistance systems. Various works have sought to measure the received signal strength for various vehicle-to-vehicle communication links. Such measurements, though reliable, are expensive, time consuming and impractical for evaluating all the possible corner case scenarios that could arise. Simulation of vehicle-to-vehicle communication links is a viable alternative.

In all three of the setups discussed in this article, both measurements and simulations demonstrated the 20dB loss in signal strength that can arise from vehicular obstructions in vehicle-to-vehicle communication links. In addition, nulls in received signal strength were observed and attributed to ground-induced multipath fading. Finally, the impact of non-line-of-sight communication links in urban canyons on the received signal strength was investigated. Results from this study demonstrated the sharp drop in received signal strength that is experienced by two vehicles that do not have line-of-sight communication at urban intersections. For all three cases, a good level of agreement between measured and simulated results was observed. Such good agreement demonstrates how simulation can be an accurate, cost effective and practical alternative for modelling V2X test scenarios.

References

- [1] Miller, L., Connected Car for Dummies, New Jersey, John Wiley & Sons, 2018.
- [2] "Autonomous Vehicle Market Outlook-2026," Allied Market Research. Available Online: <https://www.alliedmarketresearch.com/autonomous-vehicle-market>
- [3] "U.S. DOT Announces 2017 Roadway Fatalities Down," NHTSA. Available Online: <https://www.nhtsa.gov/press-releases/us-dot-announces-2017-roadway-fatalities-down>
- [4] Yadav, A. K. and Szpytko, J., "Safety problems in vehicles with adaptive cruise control systems," Journal of KONBIN, Vol. 0035, pp.389-398, 2017.

- [5] "Proposed rule would mandate vehicle-to-vehicle (V2V) communication on light vehicles, allowing cars to 'talk' to each other to avoid crashes," NHTSA. Available Online: <https://one.nhtsa.gov/About-NHTSA/Press-Releases/ci.nhtsa.v2v.proposed.rule.12132016.print>
- [6] Kenney, J. B., "Dedicated Short Range Communications (DSRC) Standards in the United States," Proceedings of the IEEE, Vol. 99, No. 7, pp.1162–1182, July 2011.
- [7] Jiang, D., Taliwal, V., Meier, A. and Holfelder, W. "Design of 5.9ghz dsrc-based vehicular safety communication," IEEE Wireless Communications, Vol. 13, No. 5, pp.36–43, October 2006.
- [8] Meireles, R., Boban, M., Steekinste, P., Tonguz, O. and Barros, J. "Experimental study on the impact of vehicular obstructions in VANETs," 2010 IEEE Vehicular Networking Conference, Jersey City, NJ,2010, pp.338– 345.
- [9] Otto, J. S., Bustamante, F. E. and Berry, R. A. "Down the Block and Around the Corner the Impact of Radio Propagation on Inter-vehicle Wireless Communication," 2009 29th IEEE International Conference on Distributed Computing Systems, Montreal, QC,2009, pp.605–614.
- [10] Kaul, S. et al "Effect of Antenna Placement and Diversity on Vehicular Network Communications," 2007 4th Annual IEEE Communications Society Conference on Sensor, Mesh and Ad Hoc Communications and Networks, San Diego, CA,2007, pp.112–121.
- [11] Miucic, R., Popovic, Z.and Mahmud, S. M., "Experimental characterization of DSRC signal strength drops," 2009 12th International IEEE Conference on Intelligent Transportation Systems, St. Louis, MO,2009, pp.1–5.
- [12] Mangel, T., Klemp, O.and Hartenstein, H., "A validated 5.9 GHz Non-Line-of-Sight path-loss and fading model for inter-vehicle communication," 2011 11th International Conference on ITS Telecommunications, St. Petersburg,2011, pp.75–80.
- [13] Cheng, L., Henty, B. E., Stancil, D. D., Bai, F.and Mudalige, P., "Mobile Vehicle-to-Vehicle Narrow-Band Channel Measurement and Characterization of the 5.9 GHz Dedicated Short Range Communication (DSRC) Frequency Band," IEEE Journal on Selected Areas in Communications, Vol. 25, No. 8, pp.1501–1516, October 2007.
- [14] Kornek, D., Schack, M., Slottke, E., Klemp, O., Rolfes, I. and Kurner, T., "Effects of Antenna Characteristics and Placements on a Vehicle-to-Vehicle Channel Scenario," 2010 IEEE International Conference on Communications Workshops, Capetown,2010, pp.1–5.
- [15] Adhikari, N., and Noghianian, S., "Multiple antenna systems for vehicle to vehicle communications," IEEE International Conference on Electro-Information Technology, EIT 2013, Rapid City, SD, 2013, pp.1–6.
- [16] "ANSYS HFSS SBR+," ANSYS. Available Online: <https://www.ansys.com/-/media/ansys/corporate/resourcelibrary/brochure/ansys-sbr-plus.pdf>

Ushe Chipengo received his B.S. degree in electrical engineering (summa cum laude) from the University of Nicosia, Cyprus in 2013. He received his MSc. and Ph.D. in electrical engineering from The Ohio State University in 2017. With a focus on electromagnetics, he has conducted research on slow wave structures for high power microwave sources, antennas, microwave circuits and computational electromagnetics. Since 2017, he has been with ANSYS as an Application Engineer II. His current research interests include antenna design for automotive applications and automotive radar for advanced driver assistance systems (ADAS).

From Simulation to Reality

The Bloodhound Land Speed Record Car

Dr Ben Evans, Associate Professor in Aerospace Engineering & CFD
Engineer for Bloodhound LSR, Swansea University



Over a decade ago I stood on a stage in the Science Museum in London along with Andy Green and Richard Noble to announce that a new British Land Speed Record attempt was on the horizon. We promised that we would be raising the Land Speed Record to 1,000 mph by 2011 – how naïve we were!

In reality, the technical (and financial!) challenges involved in developing a project that would deliver a vehicle as complex as a fighter jet and capable of travelling across the surface of the Earth at Mach 1.3 turned out to be greater than any of us could have imagined. The journey that we've been on over the last 10 years has been well documented. My role in it all, as the CFD engineer and part of the aerodynamic design team, has been to ensure that the design evolution of the car was always leading us to a minimum drag and, more importantly, zero/minimum lift solution. The aerodynamic design has been carried out entirely using the Swansea University FLITE3D Computational Fluid Dynamics software suite [1].



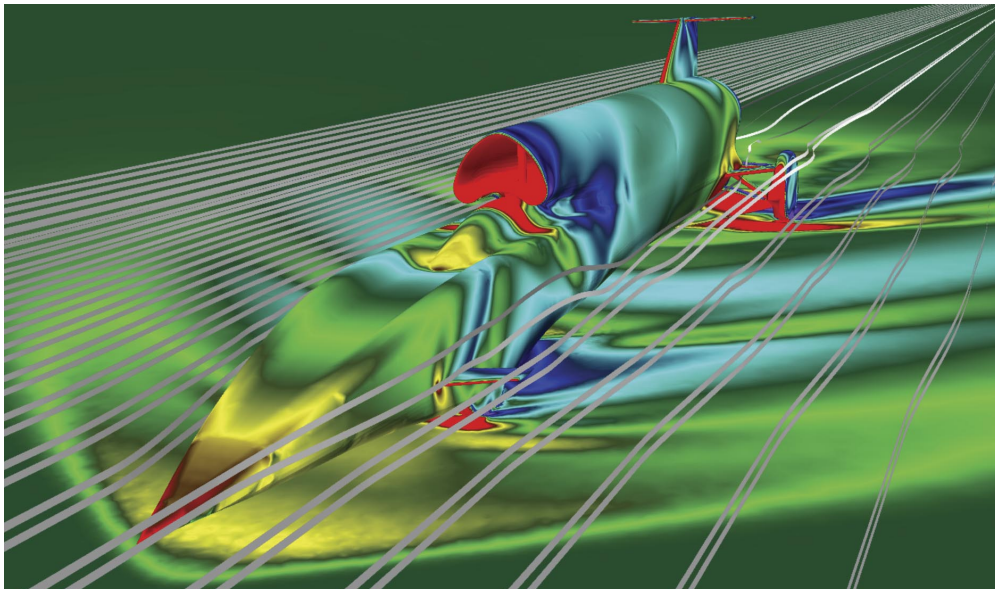


Figure 1: An early CFD render of Bloodhound showing simulated pressure distribution at Mach 1.3

One of the questions always in a modeller's mind, especially when applying techniques to a completely novel and unique application, is 'can we trust these computational predictions'? When simulation becomes reality, how good will our computational predictions turn out to be? So, over the decade of design development from 2007 – 2016, whilst Bloodhound lived in the virtual world, mainly in the form of CAD models and CFD post-processing renders on my computer screen, I was dreaming of the day when Bloodhound would come alive in the real world and we could start answering these questions.

Bloodhound Low Speed Testing – Newquay 2017

Bloodhound finally became a physical reality in 2017. After a year of 'car build' we took the car to Newquay Airport in Cornwall to commence the test programme.

The objectives of the low speed UK runway tests in 2017 were quite simple. We wanted answers to three questions:

- 1) Could we achieve maximum (reheat/afterburner) thrust from the EJ200 jet engine from a standing start?
- 2) Would the wheel brakes survive when applied at 200mph?
- 3) Could we persuade some new sponsors to join the adventure?

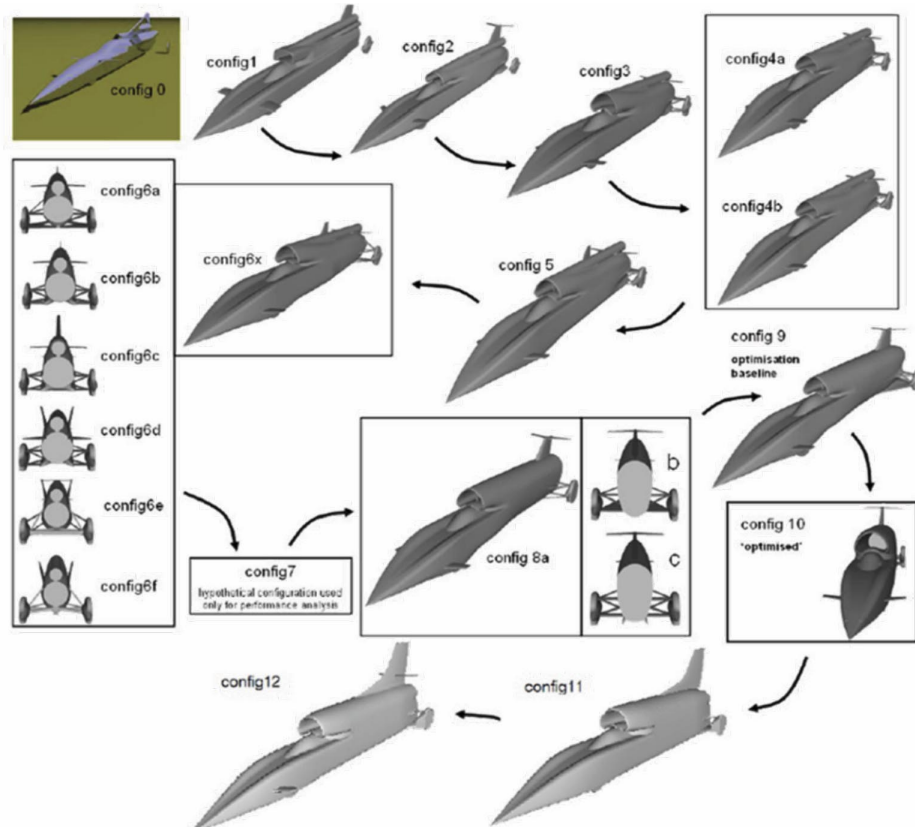


Figure 2: Evolution of the Bloodhound design from config 0 (2007) to config 12 (2016)



Figure: 3 Bloodhound during the UK runway testing at Newquay Cornwall Airport 2017

The answers to the first two questions were exactly what we wanted to hear. Bloodhound delivered, and exceeded, our expectations. However, the project was, yet again, in a precarious financial situation (that's putting it politely) and ended up coming very close to being scrapped – very frustrating for the engineering team as, technically, the car had demonstrated its ability to do everything we were asking of it. At the 11th hour, a new investor and now owner of the Bloodhound LSR project, Ian Warhurst, stepped in to provide the cash injection needed to rescue Bloodhound from its looming date with the scrapyard. In late 2018, planning for the high speed test programme went into top gear or, more appropriately in the context of Bloodhound, into afterburner mode.

High Speed Testing (HST) – Hakskeen Pan, South Africa 2019

The HST campaign in October/November 2019 was treated primarily as a data gathering exercise. This, for me, essentially meant the first opportunity to answer some of those nagging questions about how much trust we could place in our RANS (Reynolds-Averaged Navier Stokes) CFD models – we could finally carry out some CFD validation. We fitted out Bloodhound with one of its two propulsion systems, the EJ200 jet engine, with the ambition to explore how it would behave at speeds up to 500 mph. We went with no ambition to set a new record but, rather, to gather enough data and, therefore, evidence to convince ourselves, and the rest of the world (including future potential sponsors) that we were credible and Bloodhound had what was needed for a realistic shot at breaking the current record (763 mph) by a substantial margin.

There were several things we wanted to understand;

- How well the CFD modelling that we had used to design the car in the first place was predicting the aerodynamic loads on the car.
- How the EJ200 jet engine performed at high speeds and inside a completely different environment to its usual home, the Eurofighter Typhoon.
- How effectively and predictably our primary braking systems (airbrakes and parachutes) behaved; getting an LSR vehicle to stop is as big a part of the problem as getting the car to go fast in the first place.
- How, as the ultimate speed of Bloodhound is track-limited, fast can you go whilst having sufficient track length to accelerate and decelerate back to zero.

So, we flew Bloodhound out to the hot and dusty Kalahari Desert in the northwestern-most corner of South Africa, a surreal but beautiful location called The Hakskeen Pan, in September 2019 and commenced 6 weeks of testing. Tests started with static tests of the jet engine, learning procedures for starting the EJ200 at the high altitude (low air density) and high temperatures of the Kalahari desert and then, methodically, we stepped up the speed of the car on successive runs, after each of which, we carried out extensive data analysis. This data was examined by a team of engineers (and Andy, the driver!) to make a decision on whether we were comfortable pushing faster on the next run.

It turned out that in the end, once again, Bloodhound exceeded all of our expectations and easily reached a peak speed of 628 mph (1011 kph) or Mach 0.83 before reaching the track-limited peak speed of the car with only the jet engine propulsion system installed.



Figure 4: High speed testing of Bloodhound at Hakskeen Pan, South Africa (October 2019)

Wheel Load Monitoring

Obviously, one of the key concerns about taking a vehicle to extremely high speed is the question of whether we can keep it on the ground. The CFD predictions were consistently [i.e. independent of choice of turbulence model] indicating that up to approximately Mach 0.7 (~ 550 mph) we should have been steadily increasing the downforce across the vehicle. Not until accelerating through Mach 0.8+ did the CFD predict that the effect of transonic/supersonic shock waves leads to a switch from downforce to some, manageably small, lift on the vehicle.

To test this prediction, and provide reassurance that Bloodhound wasn't getting anywhere close to the vehicle lifting off the desert surface due to aerodynamic lift, wheel load monitors were installed in each of the four wheels. Sensors measured the suspension deflection and then we were able to correlate, via a look-up table, the measured deflections to wheel loadings.

An example of this data output for 'run 33' (peak speed 550 mph/Mach 0.72) is shown in the figure below.

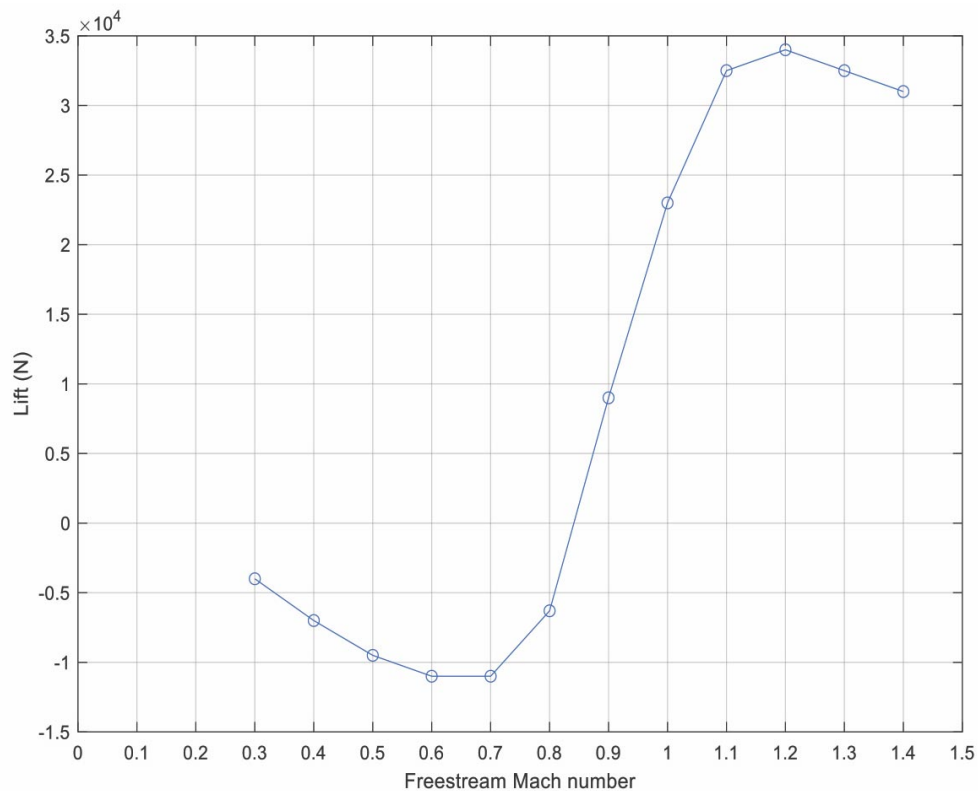


Figure 5: Lift/downforce prediction of Bloodhound as a function of Mach number (assuming $p_{\infty}=921\text{mb}$, $T_{\infty}=25\text{C}$) using HLLC numerical flux [1] and SST turbulence model

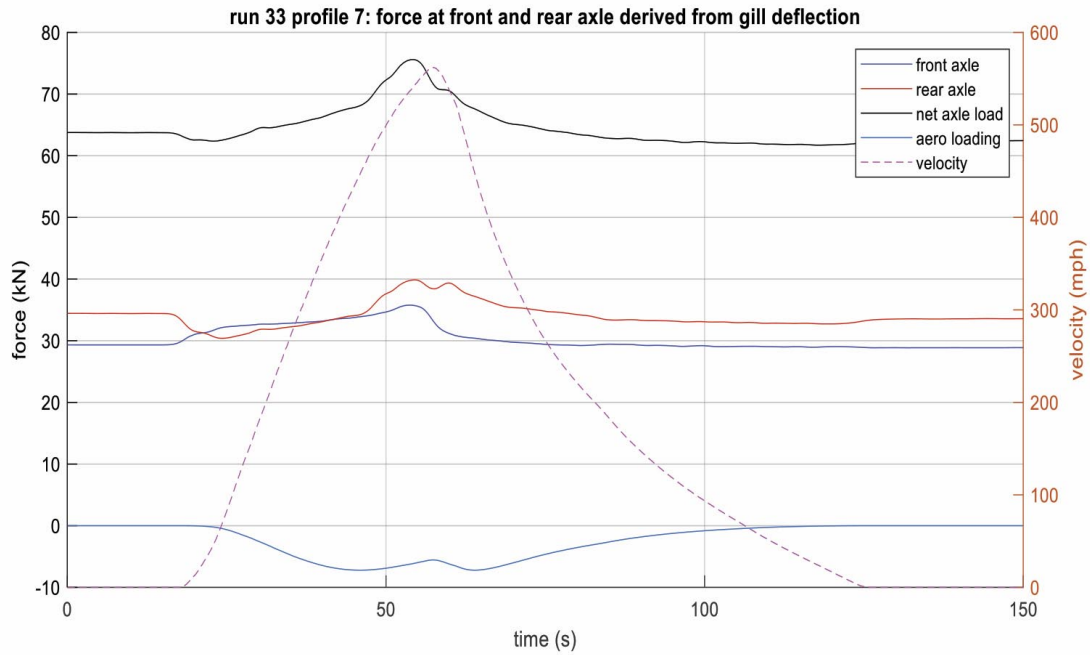


Figure 6: Measured loads on the front and rear axles during 'run 33' of Bloodhound (peak speed 550 mph)

The net axle loading (black) and front (blue)/rear (red) breakdown is shown alongside a plot of the vehicle speed (dashed purple). We started seeing an odd 'camel hump' feature on the rear axle load on runs above 500 mph near peak speed. As soon as we realised that this feature corresponded perfectly to the CFD prediction of passing through the point of maximum downforce (see previous figure), we started getting some real confidence that the CFD model seemed to be working well. (Note that there are a range of factors affecting the wheel loads: vehicle mass loss due to fuel burn, moments generated by engine thrust, aerodynamic loading.)

Pressure Sensor Data

Of course, the net aerodynamic loading on the vehicle is a result of the net/integrated effect of the pressure (and to a lesser extent skin friction) distribution across the vehicle's surface. So, to support the validation of the CFD modelling, Bloodhound is fitted out with over 150 pressure sensors across its surface. Each sensor measures the real-time pressure experienced throughout a run of the car at a frequency of 10Hz.

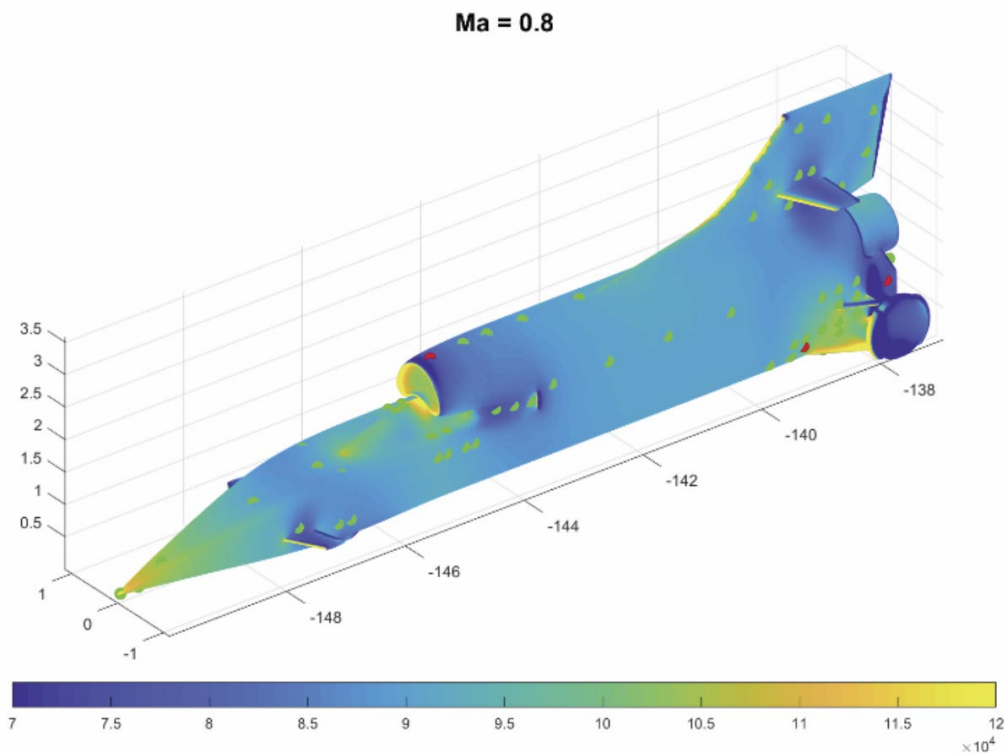


Figure 7: CFD predicted pressure distribution across Bloodhound at Mach 0.8 (HLLC numerical flux, SA turbulence model) showing the position of pressure sensors – green sensors are measuring pressures within 5% of the CFD prediction, red sensors are outside this tolerance

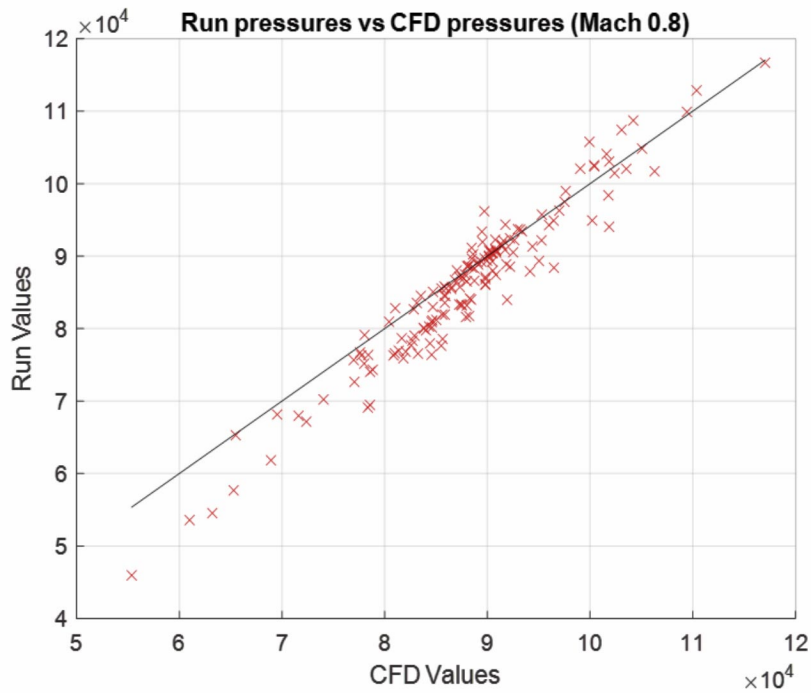


Figure 8: CFD prediction vs measured ('Run Values') pressures (in Pa) for run 34 (peak speed 628 mph) as Bloodhound accelerates through Mach 0.8

On any particular test run we were able to use this data to explore to what extent the CFD-predicted pressure distribution over the surface of the car was matching the HST measurements. Overall, the level of agreement between the CFD predictions and HST measurements was impressive – over 90% of the sensors on the car continuously measured pressures that were within 5% of the CFD predictions. Part of the ongoing research work that is now being undertaken is to identify where on the

car (and why) we observed outliers and if there are particular assumptions in the CFD modelling that generates better fits to the measured data than others. We expect to be publishing the findings from this work later in 2020.

We were also able to identify the point at which Bloodhound exceeded the 'critical Mach number'. This is the speed at which the flow around the vehicle first

M=0.8 CFD – HLLC/SST (accel)

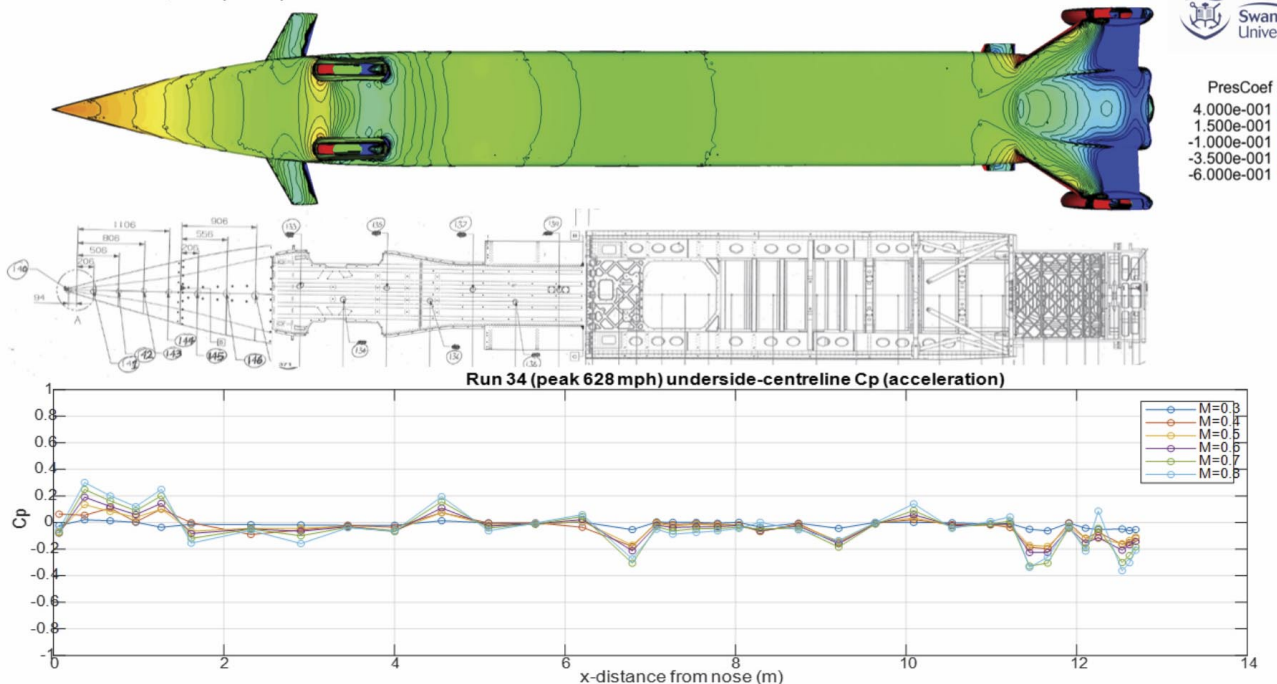


Figure 9: CFD render of the underside predicted pressure distribution (HLLC flux, SST turbulence model) and the measured pressures on sensors on the underside centreline at Mach 0.8 (accelerating)

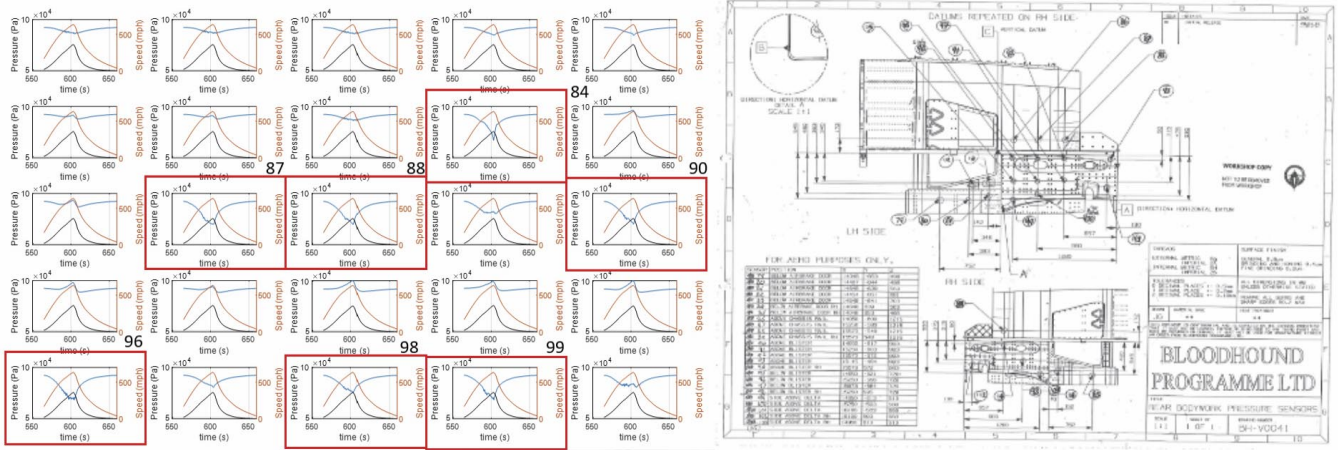


Figure 10: Outputs of measured pressures (blue) on sensors close to the position on the side of the car where the flow first went sonic. Black curves show the theoretical sonic pressure.

exceeds Mach 1.0 even though the vehicle itself is still below Mach 1.0. By looking at the pressure measurements on individual sensors and comparing the measured pressure (blue lines in the plots in the figure below) with the theoretical pressure corresponding to sonic velocity for a given freestream speed (black lines in the plots in Figure 10) we identified that the first point on the car to experience sonic air velocity was on the side at the rear close to the rear wheel suspension system at approximately Mach 0.72. This was followed by sonic flow on the underside of the car just aft of the front wheels.

Airbrake Performance

Time-accurate CFD simulations of Bloodhound's airbrakes had identified that we were likely to experience some extremely turbulent and unsteady downstream flow when the airbrakes are fully deployed. So, we decided that we needed to run Bloodhound at a range of steadily increasing speeds with airbrakes fully deployed (at 60 degrees) to measure the effect on the pressure field downstream and examine any damage to the rear wheel and suspension system.

It turned out that the wake effect from fully deployed airbrakes was not anything nearly as damaging as we had been concerned it would be. We also used these runs to identify the drag increment experienced by the car due to airbrake deployment by comparing acceleration and

deceleration of the car with and without airbrakes. In our overall vehicle performance model (a simple momentum balance model developed in MATLAB Simulink) we compared the predicted (using CFD data) performance of the car with what we observed and, at first, were a little concerned that the airbrakes seemed to be far more effective at generating drag than our CFD model had predicted (leaving me feeling a little concerned about what I was getting wrong!). We slowly cranked up the drag prediction in the performance model until the model performance curves started matching the real car data. Our data analysis engineer came into my office and said, "Ben, it seems that the airbrakes are generating twice as much drag as your CFD model is suggesting". And this was the 'lightbulb moment' when I realised that there were in fact two airbrakes on the car and all the data that I was inputting into our performance model was from a 'reduced' CFD model of a single airbrake!

Particle Entrainment

One of the challenging complications in understanding the fluid dynamic problem of flow around a vehicle like Bloodhound is the reality that the car isn't in fact moving through pure air. Any footage you see of Bloodhound at high speed during HST clearly highlights large quantities of dust entrainment. We were aware that this would be the case early on in the R&D phase of Bloodhound and so we developed a CFD model [2] that attempts to capture

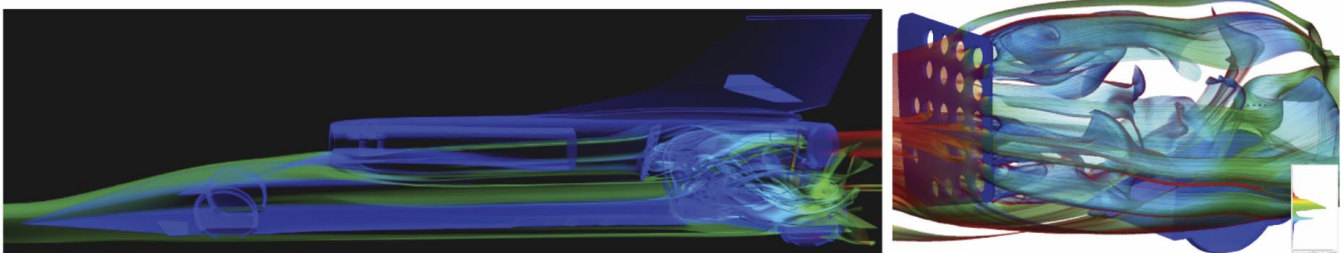


Figure 11: CFD renders of a snapshot from an unsteady flow simulation around a fully deployed airbrake at Mach 0.8

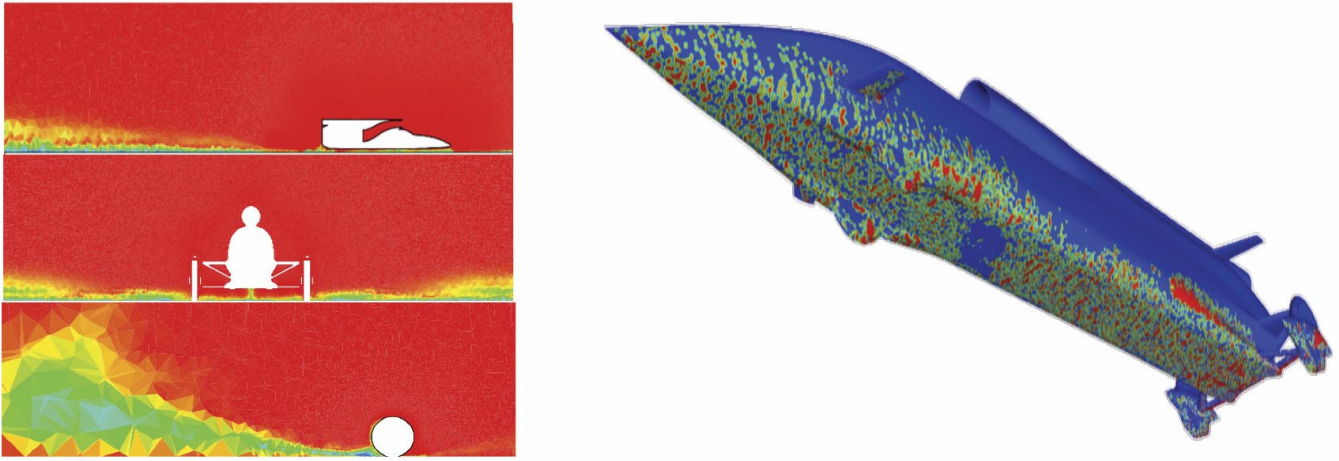


Figure 12: Dust entrainment patterns and dust impact prediction from the Bloodhound particle entrainment 'spray drag' CFD model [2]

the effects of high-speed particle entrainment. Qualitatively, in terms of the dust cloud shape that is predicted by this model, the simulations seemed to match reality fairly well. However, the impact of dust entrainment on overall vehicle drag was found to be highly dependent on the assumption made in the model about the rate of particle entrainment (and location of particle entrainment). Now that we have detailed

performance data for the car, which allows us to break down the various drag components and predict what percentage of the drag is related to the dust/particle entrainment (potentially as much as 30%) some of our ongoing research is to 'tune' our 'spray drag' model and gain improved predictions of the effect of spray drag at higher (supersonic) speeds.

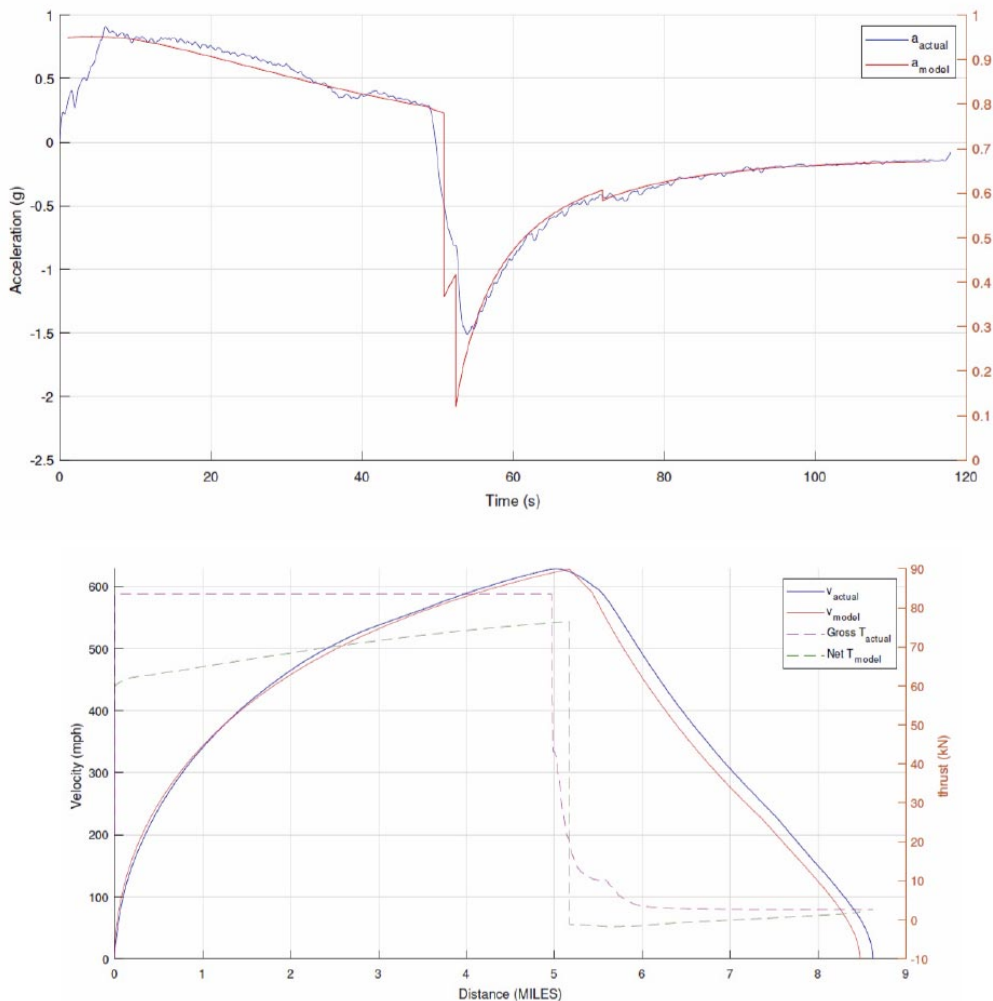


Figure 13: Model (red) and actual performance (blue) curves showing the final (run 34 - peak 628 mph) test of Bloodhound

Overall Vehicle Performance

Ultimately, the critical thing that we can now do with a high level of accuracy is use a simple (momentum balance) performance model for Bloodhound to predict exactly how much thrust (and for how long) and what braking combination will be required to hit a specific target speed and, crucially, how much track will be used up in doing so. This has allowed us to provide a very detailed specification for the rocket system that will be needed to take the car beyond Mach 0.8 and through Mach 1.0 to a new Land Speed Record.

What Happens Next?

And now, following on from the high speed testing of Bloodhound in South Africa in 2019 we are in a position to start providing a detailed answer to the question of how good RANS-based CFD is for extremely complex, aerodynamic / fluid dynamic problems like prediction of the flowfield around a jet / rocket propelled supersonic car.

We are learning about the impact of 'variables' and assumptions within any RANS-based CFD simulation and how this correlates to the real world on a complex geometry application such as this. Early suggestions indicate that moving from the simple, tried and tested turbulence models (such as Spalart-Allmaras) to more complex turbulence models doesn't justify the additional computational expense. Further, more conclusive, analysis on this will be published later in 2020.

And what next for Bloodhound?

We are now looking for corporate backing to take the project into the final stages, which at the next visit to South Africa in 2021 will involve a record attempt targeting a speed over 800 mph. For that we will need to boost thrust with a monopropellant (steam) rocket currently being developed by Nammo in Norway.

We are also committed to making Bloodhound the 'greenest' Land Speed Record car in history. So, along with a zero-carbon output steam rocket (boosting our peak thrust by an additional 60 kN) we are switching from an internal combustion engine to drive the rocket pump to an electric motor. That design work is going on throughout 2020 and we are exploring the option of running the EJ200 jet engine using biofuel.

We also now know that the car will require the addition of small winglets on the tail fin and, potentially, also on the nose to act as vertical force trimmers as we accelerate up through Mach 1. But, essentially, we are ready to go and confident that we have a new Land Speed Record directly in our sights.

Watch this space...

References

- [1] B.J. Evans, O. Hassan, J.W. Jones, K. Morgan, L. Remaki, 'Computational Fluid Dynamics Applied to the Aerodynamic Design of a Land-Based Supersonic Vehicle.' *Numerical Methods for Partial Differential Equations*, Vol 27, pp. 141 – 159, 2011 (MAFELAP 2009 Special Issue)
- [2] L. Remaki, O. Hassan, B.J. Evans, K. Morgan, 'Spray drag effect of fluidized sand for a supersonic vehicle.' *J. Coupl. Sys. and Mult. Dynamics*, Vol 2 (3), pp.169-177, 2014

Dr Ben Evans is an Associate Professor in Aerospace Engineering and sits on the design team for the BLOODHOUND SSC Land Speed Record project. Dr Evans's research interests range from computational shape optimisation and high speed aerodynamic modelling to molecular gas dynamics simulation. He also has interests in engineering public engagement and engineering education.

He is a Director of the Engineering Education Scheme in Wales (EESW), the Director of the Bloodhound Education Programme and a Fellow of the Higher Education Academy.

bloodhoundlsrc.com



Human-Inspired Generative Design

Dr Richard Ahlfeld, CEO and Founder of Monolith AI.

Marc Emmanuelli, Algorithmic Design & Simulation Engineer, Monolith AI.

Engineering is a highly creative discipline. Every iteration of simulations or tests provides engineers with new learning on how to best refine their design, based on complex goals and constraints. Finding an optimum solution means being creative about what designs to evaluate and how to evaluate them.

When trying to build an understanding of how a non-linear and multi-variable physical system works, all engineering efforts (simulations or physical tests) are journeys to learn functional relationships by analysing data. This data is based on ineradicable governing physical laws and relationships. Unlike financial data for example, data generated by engineers reflect an underlying truth - that of physics, as first described by Newton, Bernoulli, Fourier or Laplace.

The fact that this data is abundant (generated from numerous design iterations) and based on fundamental scientific principles means that it can often be an excellent subject for a Machine Learning study: Predicting the behaviour of a new design under new testing conditions, or optimising the design and conditions for a target behaviour.

Researching this possibility has been our focus for the last few years, and we have today built numerous AI tools capable of considerably accelerating engineering design cycles.

In particular, our main focus has been to develop deep learning models to learn from 3D data (CAD designs and simulations). The early adopters of our technology have found it to be a breakthrough. We strongly believe that the methods outlined in this article will revolutionise Engineering in a similar way that AI for facial recognition has revolutionised public security, biometric hardware authentication and synthetic media (*deepfake* technology).

Up until today, engineering companies have traditionally devalued the need to form databases from the results of simulations or physical tests because of the variety of applications and the iterative/creative nature of an engineer's day-to-day work. Engineering information, and most notably 3D designs/simulations, are rarely contained as structured data files. Using traditional data analysis tools, this makes drawing direct quantitative comparisons between data points a major challenge.

Thankfully, the Engineering community is quickly realising the importance of Digitalisation. In recent years, the need to capture, structure, and analyse Engineering data has become more and more apparent. Learning from past achievements and experience to help develop a next-generation product has traditionally been predominantly a qualitative exercise. This is particularly true for 3D data which can contain non-parametric elements of aesthetics/ergonomics and can therefore be difficult to structure for a data analysis exercise.

The aim of our research is to adopt and adapt algorithms from other areas of deep learning such as image processing to create expert AI systems that can learn from 3D Engineering data, for design validation and performance-based optimisation.

For clearer understanding, let's draw a direct comparison with face recognition technology.

Using deep learning algorithms such as Generative Adversarial Networks (GANs), it has become easy for companies such as Facebook or Apple to recognise which of your friends is featured on your latest profile picture, or to unlock your iPhone with your face. These algorithms have gathered learning from millions of images (or point clouds), from which they were able to identify the distinct features which characterise a human face. In a neural network, these 'distinct features' take the form of a structured set of numerical parameters. When presented with a new image, they can synthesise it to identify the face's gender, age, ethnicity, expression, etc.

Beyond simply recognising a human face, these algorithms are also capable of generating new, synthetic images of human faces called deepfakes. With new combinations of the numerical parameters which represent the distinct physical attributes which characterise a human face, highly realistic images can be generated. It is for example possible to generate a 'hybrid' of two faces or change a male face to a female (see Figure 1).

The same concept can be applied to engineering data, with 3D CAD files as the data to synthesise and performance/quality metrics as the attributes to recognise (design validation) or optimise against (generative design).

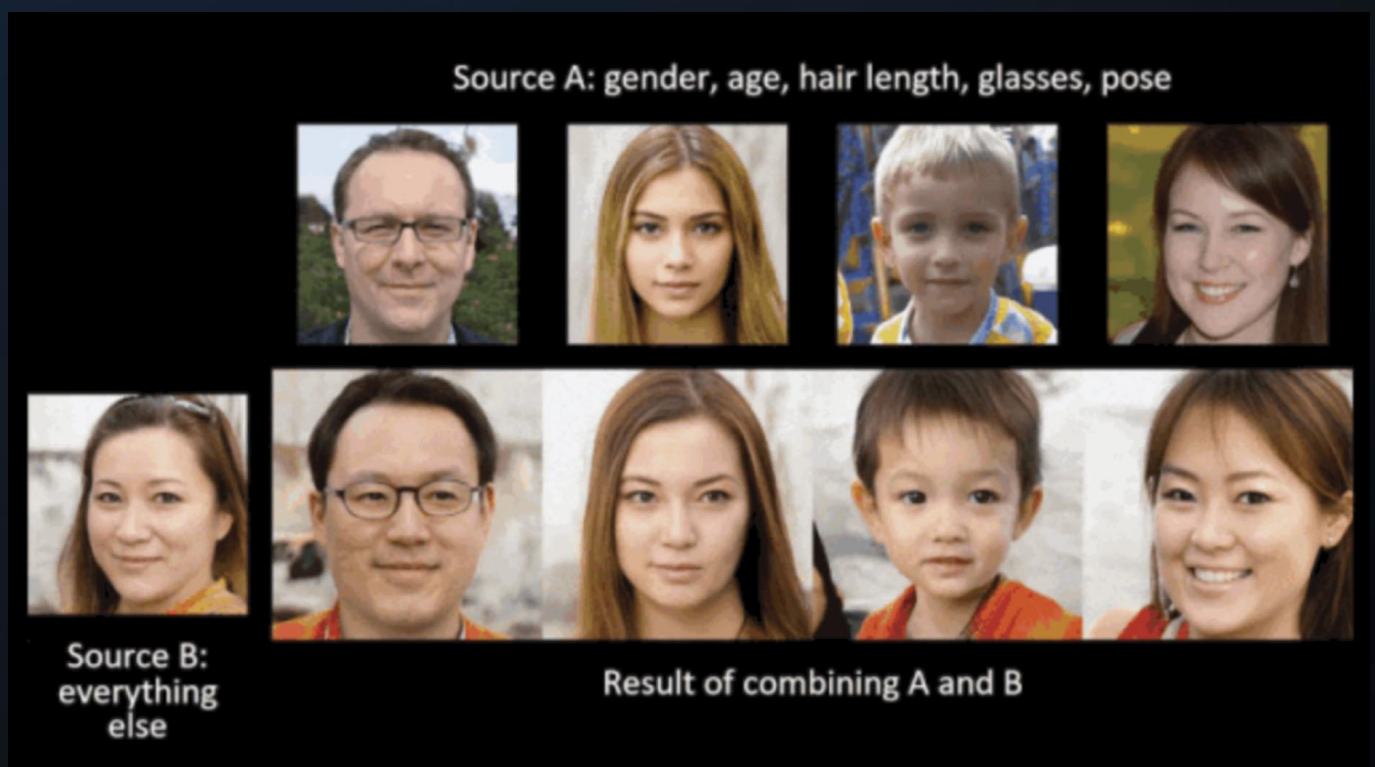


Figure 1: Open-Source Face Generator 'StyleGAN', by NVIDIA

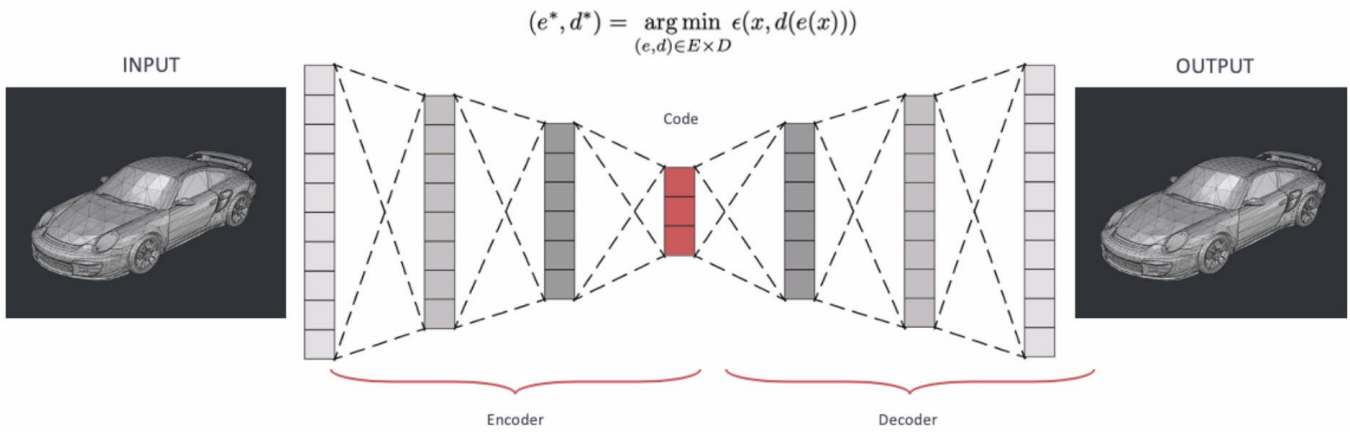


Figure 2: Overview of an Autoencoder's network structure

There are added challenges to developing these methods for 3D Engineering data, among which are the need to structure individual CAD data files and associate to them the boundary conditions in which they were simulated. Compared to image processing, working with CAD data also requires higher computational resource per data point, meaning there needs to be a strong emphasis on computational efficiency when developing these algorithms.

Figure 2 shows an illustration of the algorithmic framework we use to apply this technology for the purpose of Generative Design. First, a neural network is formed on an Encoder model, which 'compresses' the 3D data of the cars into a structured set of numerical latent parameters. We like to call this the '3D DNA' of the geometry. Then, a Decoder model is a second neural

network which can use these parameters to 'regenerate' a 3D car. The fascinating thing is that just like with the human faces above, it can create different combinations of cars it has seen making it seem creative. In the context of Generative Design, the Encoder model can be used for design validation: making a performance prediction for the outcome of a new test or simulation, and the Decoder can be used for design optimisation: generating new 3D geometries which satisfy target performance attributes.

As an example of design validation using this technology, Figure 3 shows a prediction for the contribution to a vehicle's drag coefficient from a wheel design. The Encoder can scan the 3D data, identify its geometric DNA and make an instant prediction based on a dataset of historic wind tunnel tests.

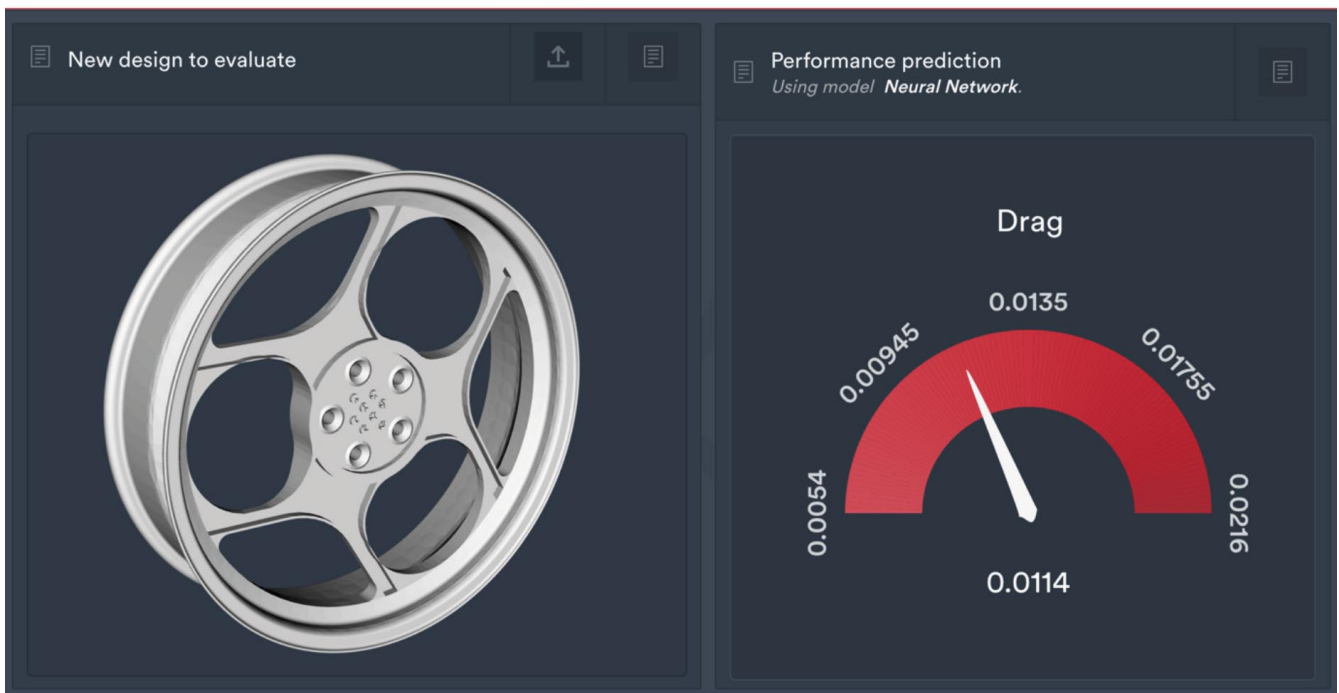


Figure 3: A prediction for Drag is made on an encoded 3D design of a wheel, using a neural network trained on historic wind tunnel data.

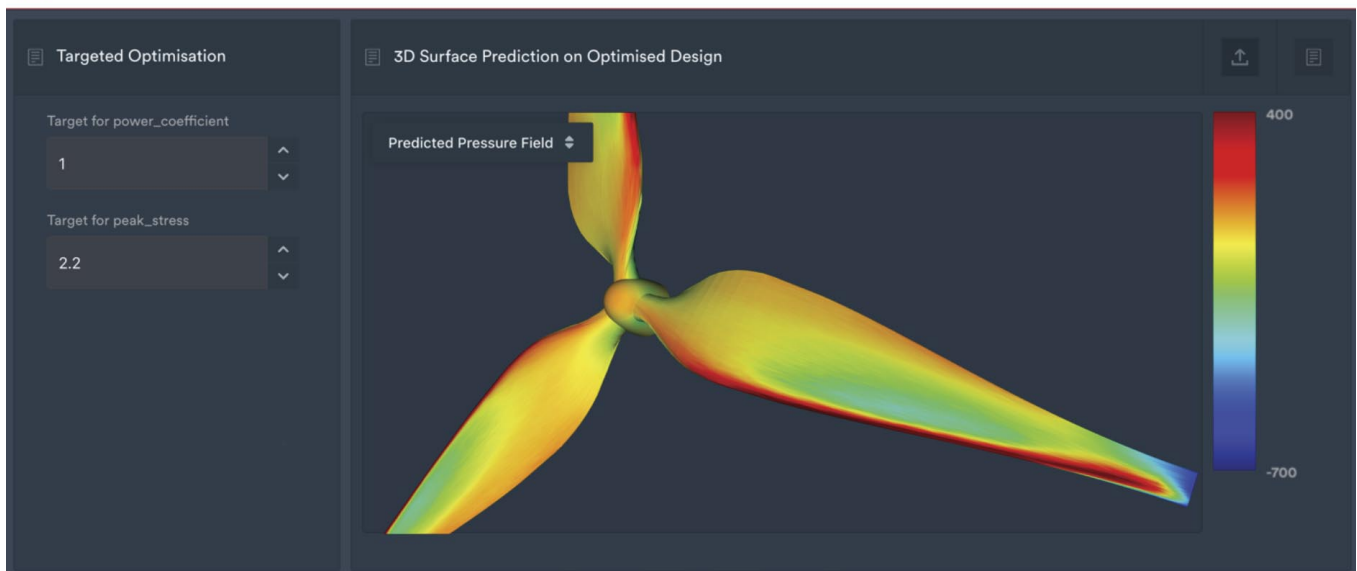


Figure 4: An optimum 3D geometry of a wind turbine is generated according to custom performance attributes. The surface pressure field is also predicted.

As an example of design optimisation, Figure 4 shows a performance-optimised 3D CAD model of a wind turbine which has been fully generated with AI. In this case, the pressure field on the surface on the geometry can also be predicted for this new design, as it was part of the historical dataset of simulations used to form this neural network.

This new method of evaluating and optimising 3D designs has properties that no other generative algorithm has: it is not based on PDE solvers and it has no hard-coded functions. Instead, it purely learns from human inspiration. Engineers have spent decades developing CAE simulation technology which allows them to make highly accurate virtual assessments of the performance and quality of their designs. Our new methods do not replace these tools – on the contrary: the AI algorithms will be as good as the data they learn from. In other words, the engineer's expert intuitions and the quality of simulation tools they use both contribute to enriching the quality of these Generative Design algorithms and the accuracy of their predictions. Therefore, we talk about 'Human-Inspired Generative Design'.

This also means these algorithms are compatible with any simulation software and are applicable to virtually any engineering problem for which there exists a structured dataset of historic tests (or an automated process to generate simulation data in batch), including Computational Fluid Dynamics (CFD) applications. As the algorithms are 'trained' on existing engineering experience, they can learn simulation outcomes (such as aerodynamic forces) but also past judgement calls from engineering experts (such as visual manufacturability assessments).

Perhaps even more impactful is the new avenues which adopting these new methods can open for entire R&D processes. Engineers need fewer testing iterations to converge to an optimum solution, and prototyping can be dramatically reduced.

We strongly believe that in the age of Digitalisation, with ever so accurate virtual prototyping tools, and with ever so complex engineering systems to design, a Siri or Alexa-like artificially intelligent Assistant for Engineers will become increasingly feasible and increasingly necessary.

Dr Richard Ahlfeld graduated summa cum laude with a double degree in Aerospace and Applied Mathematics from Delft University of Technology. He went on to complete a PhD in Machine Learning for Aerospace Engineering at Imperial College London during which he worked at NASA on the Mars rocket. Richard is the CEO and Founder of Monolith AI.

Marc Emmanuelli graduated summa cum laude from Imperial College London, having researched parametric design, simulation and optimisation within the Aerial Robotics Lab. He worked as a Design Studio Engineer at Jaguar Land Rover, before joining Monolith AI in 2018 to help develop 3D functionality.

Monolith AI's software platform is currently being used by engineering companies such as BMW, Honda, L'Oréal and Siemens, for applications ranging from predicting the outcome of wind tunnel or track tests, to generating performance-optimised 3D CAD designs with AI.



Ahead of the Curve

*Classifying Guardrail System Radar
Signatures using High Fidelity Physics
Simulation for 77 GHz Automotive Radar*

Ushemadzoro Chipengo, ANSYS



The recent surge in advanced driver assistance systems (ADAS) in the automotive industry has been mainly motivated by two factors. First is the need to make roads safer by equipping vehicles with technology that relieves drivers of fatigue inducing, repetitive driving actions while providing the vehicle with even more situational awareness. This is crucial since research has shown that approximately 90% of road traffic accidents are due to human error [1]. In the US, the National Highway Traffic Safety Administration (NHTSA) reported that 36,560 people lost their lives to road traffic accidents in 2018 alone [2]. An even more staggering statistic is the 1.25 million fatalities recorded worldwide in 2016 [3]. The second pushing factor in ADAS development has been the race by automotive manufacturers to deploy an autonomous vehicle (level 5) that is capable of fully conducting all driving operations without a driver's intervention. According to Allied Market Research, the global autonomous vehicle industry was valued at \$54.23 billion in 2019 and is projected to be valued at \$556.67 billion by the year 2026 [4]. Beyond the obvious advantages of self-driving cars such as time savings during commutes, autonomous vehicles will provide safe and reliable transportation to the disabled and elderly.

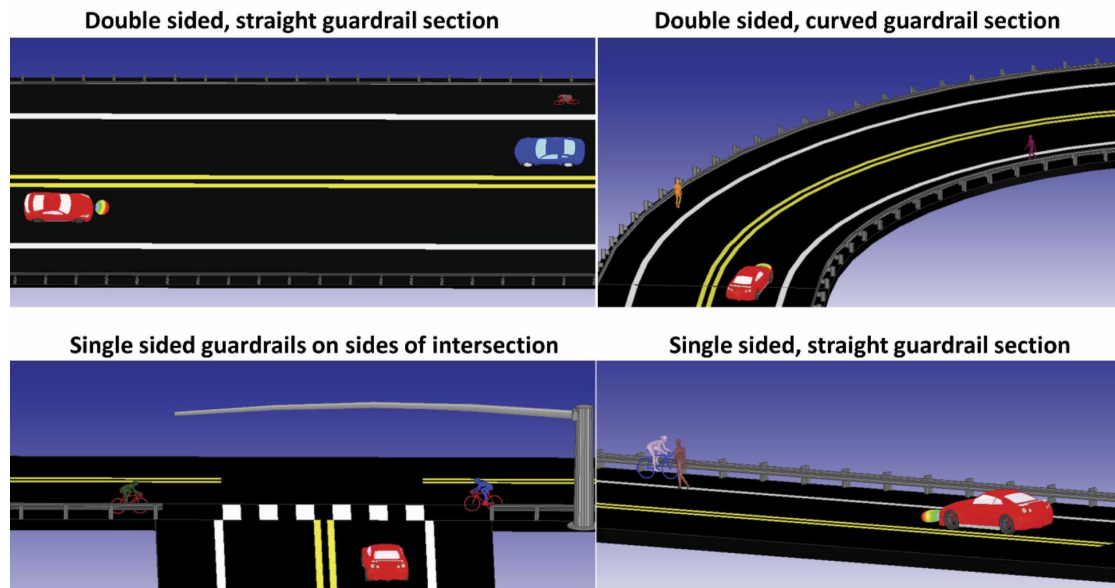


Figure 1: Different road settings where guardrails are employed. The guardrail system geometry and arrangement relative to the road affects its overall radar signature.

For a fully autonomous vehicle to become a reality, the vehicle will need to have a high level of situational awareness. Specifically, in addition to knowing its own position and state, the vehicle will need to map out the range, velocity and angle of arrival of any crucial actors in the surrounding environment while filtering out any clutter. In order to achieve this, autonomous vehicles are equipped with radio detection and ranging (Radar), light detection and ranging (Lidar), optical cameras and ultrasonic sensors [5] [6] [7] [8]. Of these sensor technologies, 77 GHz radar has emerged as the backbone for advanced driver assistance systems that will enable autonomous vehicles. This is because radar is a mature, relatively cheaper (compared to Lidar) and robust sensing technology that can determine the range, velocity and angle of arrival of multiple targets simultaneously even in inclement weather and poor lighting conditions [9]. Radar is employed in automatic emergency braking (AEB), adaptive cruise control (ACC), blind spot monitoring (BSM) and parking assist applications, among others in today's vehicles.

Before any of the mentioned sensor technologies are deployed in vehicles, they need to undergo rigorous testing to determine their reliability and accuracy in mapping out the environment of the vehicle. This burden of reliability will increase since level 5 autonomous vehicles need to make millions of crucial maneuvers based on the data being provided by these sensors. It is estimated that 8.8 billion miles of driving and testing will need to be completed before autonomous vehicles are deemed safe for mainstream consumers and full deployment [10]. Recently, researchers and automotive manufacturers have built and tested radar sensors in live traffic conditions [9] [11] [12] [13] [14] [15]. While building and testing are valuable, they can be expensive, time

consuming, risky and impractical for testing the large number of miles that are necessary. Simulation has emerged as a practical solution as it allows engineers to conduct virtual drives that greatly accelerate testing. A high fidelity, full-scale simulation workflow for 77 GHz automotive radar was presented in 2018 [16].

Another valuable aspect of simulation is that it allows the study of corner cases. Corner cases are scenarios that arise when various environmental and operational factors combine to create a response outside the normal operation of a system. In depth discussions of several automotive radar corner cases are available online [16], [17]. Of these corner cases, guardrails are particularly challenging to deal with. This is because of their high radar cross section and proximity to vehicles. This can cause them to reflect strong signals that mask the presence of pedestrians, cyclists and other vehicles. Furthermore, guardrails can introduce ghost targets in range and velocity that can confuse perception algorithms linked to the radar sensor. A simulation study investigating the impact of guardrails on 77GHz radar was carried out in [18]. Here, it was shown how radar returns from guardrails can mask the presence of vulnerable road users (VRUs) such as pedestrians.

In 2015, Acura recalled 48,000 vehicles equipped with automatic emergency braking due to sudden braking maneuvers by the vehicle without any nearby obstacles. This was observed to occur when the ego vehicle was moving next to guardrails or fences [19]. Therefore, there is a need for the perception algorithms behind the various sensors on board the vehicle to be able to identify guardrails, filter out their ghost target effects and detect real VRUs/traffic in the vicinity of the guardrails.

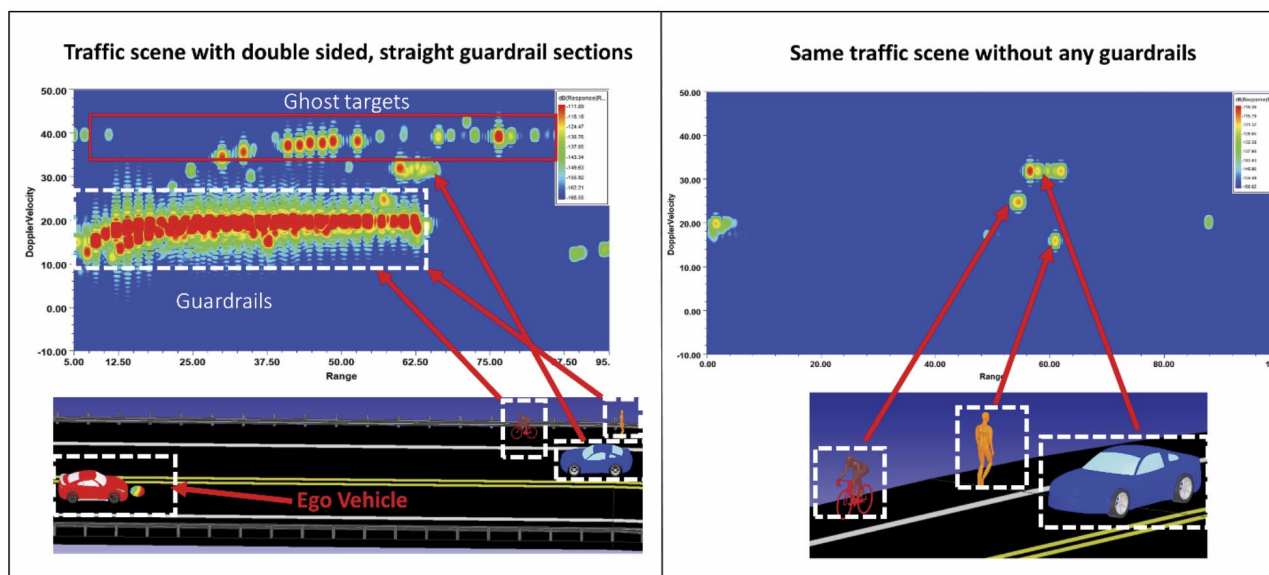


Figure 2: Range-Doppler maps of the same traffic scene with and without guardrails. The guardrails used here are double sided, straight sections.

Probabilistic tracking algorithms and sensor fusion have been used to detect guardrails [20] [21] [22] with varying degrees of accuracy that depended on the traffic scene. Another approach is to use Machine Learning (ML)-based perception algorithms to detect and classify actors in radar scenes [23] [24]. Recently, a perception algorithm based on ML was trained to accurately detect and classify cars and pedestrians using range-Doppler maps from high-fidelity physics simulations [24]. It was observed that the accuracy of the perception algorithm depends on the traffic scene under investigation. This is because each of the actors in the scene and the associated environment have varying radar cross section that depends on their orientation. Such variations can create a complex electromagnetic environment that is difficult for the algorithm to accurately deconstruct. Guardrails have complex radar signatures that are heavily dependent on the physical placement of the guardrail system. This means that a perception algorithm that has been trained to detect guardrails on a straight road may fail to detect the same guardrails if they appear on a curved road due to their drastically different radar signature.

This article presents a comprehensive study of the 77 GHz radar signatures of guardrails in four key configurations. This study was conducted using Ansys' High Frequency Structure Simulator (HFSS), Shooting and Bouncing Ray solver (SBR+), a high-fidelity physics, asymptotic electromagnetic solver. Four full-scale road traffic scenarios were created and interrogated by a 77 GHz radar sensor. Figure 1 shows the four cases that were created and whose range-Doppler maps were obtained via simulation. These four cases were chosen as they represent most of the road traffic scenarios where

guardrails are employed. By comparing the range-Doppler maps of traffic scenes with and without guardrails, ghost targets and the guardrail radar signatures were identified. Furthermore, it was observed that each of these guardrail configurations have distinct range and velocity profiles when shown on a range-Doppler map. It is this distinct behavior that can be exploited by machine learning based perception algorithms to detect and classify targets [24].

This study has two main contributions. First, it presents a comprehensive, high-fidelity physics study of the radar signatures of key guardrail configurations present in today's roads. To the best of the author's knowledge, such a study is the first of its kind. Second, it demonstrates the differences in the range, velocity and ghost target behavior of each of these guardrail systems. The data obtained from this study can be used to better train perception algorithms to not only detect but also classify the type of guardrail system in question. Such capability can prevent accidents and potentially save lives.

Radar Basics and Simulation Setup

The radar cross section (RCS) of a target is a measure of its ability to scatter incident energy in the direction of a radar receiver. It essentially represents a fictitious, equivalent area in space that intercepts and reflects the incident radar signal for a specific target. A guardrail consists of two key parts: a w-beam and the dihedral posts that support it. It has been shown that the high radar cross section of guardrails is attributed to the dihedral posts [17]. This high RCS is fairly constant over a wide range of incidence angles. It has also been shown

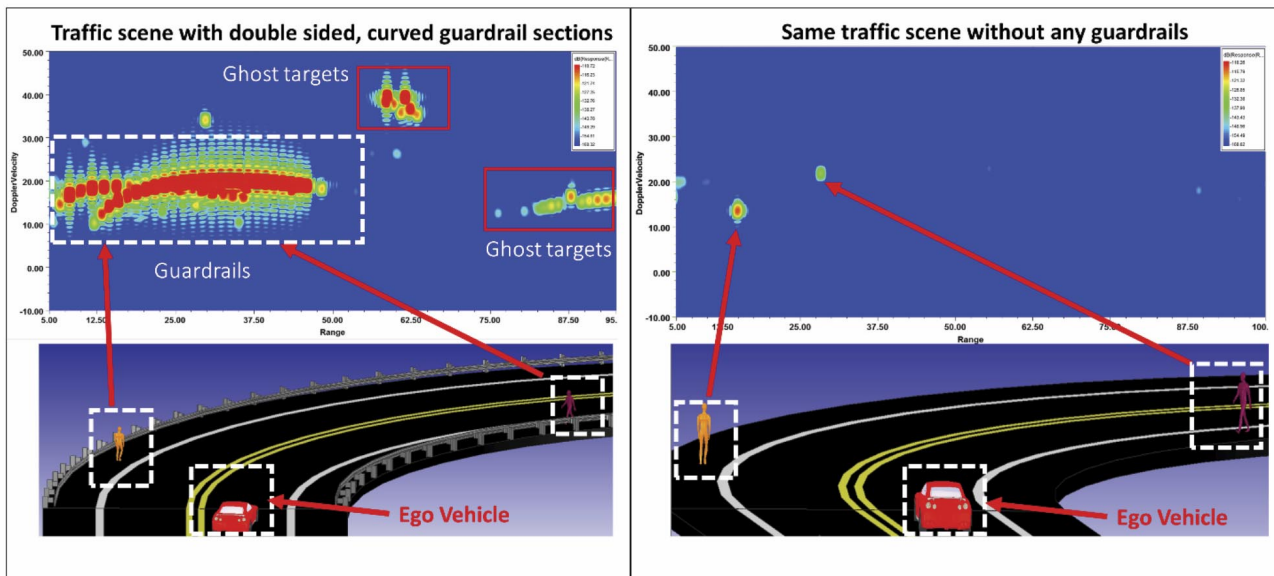


Figure 3: Range-Doppler maps of the same traffic scene with and without guardrails. The guardrails used here are double sided and curved.

that the RCS of guardrail systems can be reduced by covering up these posts with a flat metal sheet [17]. The maximum RCS of a metallic dihedral is given by [25]

$$\sigma_{RCS\ max} = \frac{8\pi w^2 h^2}{\lambda^2}$$

Here w and h represent the width and height of the two orthogonal faces that form the dihedral, respectively. A key point to note is how the RCS of a dihedral is inversely proportional to wavelength, λ . This means that the RCS increases as the interrogation frequency increases. For a monostatic radar sensor with a peak transmitted power of P_t , the received power P_r is given by [26]

$$P_r = \frac{P_t G_t G_r \lambda^2 \sigma_{RCS}}{(4\pi)^3 d^4}$$

Here G_t , G_r , σ_{RCS} and λ represent the transmit antenna gain, receive antenna gain, target radar cross section and free space wavelength of the emitted signal. Guardrails blind radar sensors by reflecting more energy in the direction of the radar sensor than targets with weaker RCS such as pedestrians. Ghost targets emanate from the multipath propagation incurred by some reflected signals as they make their way back to the radar receiver. Such reflections create ambiguities in the phase and time delay of the reflected wave leading to ghost targets in both velocity and range.

The radar scenes shown in Figure 1 were simulated using HFSS SBR+. Depending on the type of problem, HFSS SBR+ can employ Geometric Optics (GO), Physical Optics (PO), Uniform Theory of Diffraction (UTD), Physical Theory of Diffraction (PTD) and Creeping Waves (CW) to accurately solve electromagnetics problems [16] [17] [18] [24]. The vehicle bodies and guardrails were modelled as perfect electrical conductors. The road was modelled as asphalt while the pedestrians used the dry skin model that describes the dielectric constant and conductivity as $\epsilon_r=6.6$ and $\sigma=38.38$ S/m, respectively [27]. The radar sensor used a Frequency-Modulated Continuous Waveform (FMCW). Four traffic scenes were created to describe the typical scenarios where guardrails appear (Figure 1). For each of the scenes, two simulations were run, one with guardrails and one without. The range-Doppler maps of each of these scenes were compared in order to identify guardrails and ghost targets.

Simulation Results & Discussion

A. Double-Sided, Straight Guardrail Section

The first case to be studied was a 60m long, double-sided, straight guardrail section. A cyclist, pedestrian and vehicle were placed in the scene to determine their visibility in the vicinity of the guardrails (Figure 2). The ego vehicle (where the radar sensor was mounted) had a velocity of 20m/s. The range-Doppler (RD) map of the scene with guardrails shows a 60m long train of radar returns at an apparent velocity of 20m/s. The radar

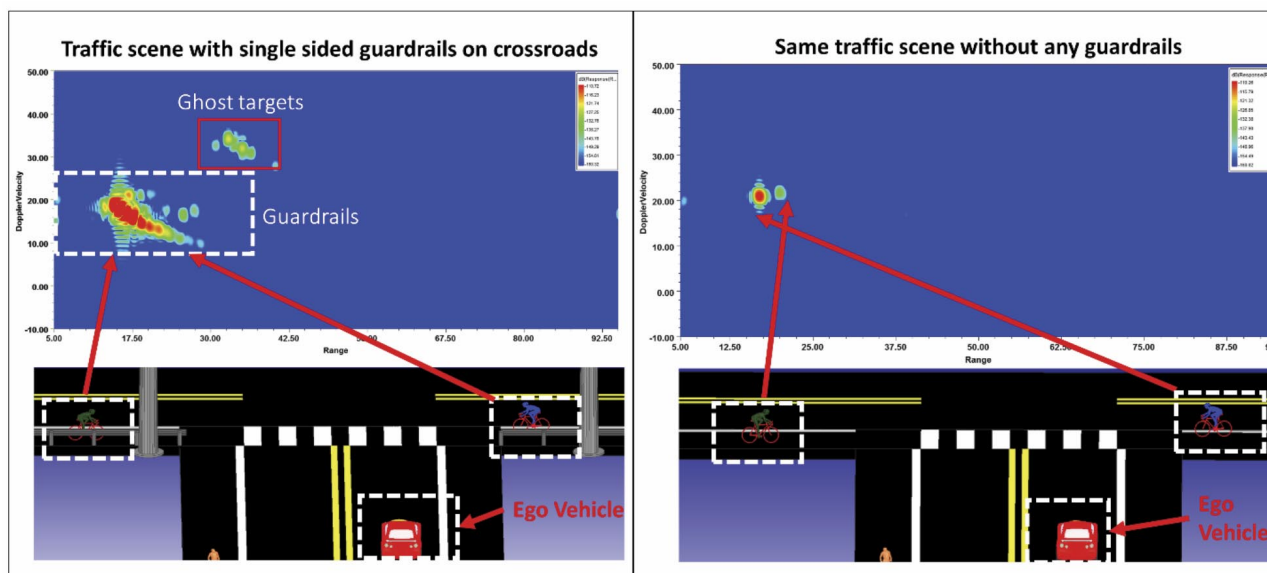


Figure 4: Range-Doppler maps of the same traffic scene with and without guardrails. The guardrails used here are single-sided guardrails on both sides of an intersection.

returns start as two distinct, curved profiles that increase in velocity and eventually merge at around 25m. The profiles merge because the difference in range between two guardrail posts on either side of the road becomes relatively smaller compared to their absolute distance from the radar sensor as one moves away from the ego vehicle. The velocity profile can be explained by observing that the guardrail sections closest to the ego vehicle have a small relative radial velocity since they are almost perpendicular to the vehicle's direction of motion. The range extents of the guardrail section on the RD map correspond to their physical length while their apparent velocity corresponds to that of the ego vehicle. A secondary train of radar returns is observed on top of the guardrail returns in the RD map at a velocity of 40m/s. These are the ghost targets. Of interest is how the ghost targets seem to be at ranges that extend the physical length of the guardrails by over 20m. This is due to the multiple reflections (additional time delay) being encountered by some signals as they return to the radar sensor. As seen in Figure 2, the guardrails completely mask the presence of the cyclist and the pedestrian. On the other hand, the vehicle in Figure 2 can easily be mistaken for a ghost target and be ignored by the perception algorithm. This is an example where sensor fusion would be crucial for target detection since radar might be unreliable at this point.

B. Double-Sided, Curved Guardrail Section

In the second case, double-sided, curved guardrail sections were placed on a road curve (Figure 1). Two pedestrians were also placed to determine their visibility. The inner and outer guardrail sections were 34m and 56m long, respectively. Figure 3 shows the range-Doppler (RD) map of the traffic scene with and without curved guardrails. The RD map shows two curved profiles that do not merge but rather intersect around 25m. Since radar measures the radial distance of a target, the guardrail profile range extents on the RD map are slightly shorter since they have curvature that hides the farthest posts at the end of the section. As in the straight section case, the guardrails mask the presence of the pedestrians while introducing their own ghost targets. The RD profile of curved guardrails differs from that of a straight section in three key ways. First, the RD map profile is curved, compared to the straight profile of a straight guardrail section. Second, while the two profiles in Figure 2 eventually merge to become one, the RD profiles of guardrails at a curve remain as two distinct profiles with one being evidently shorter than the other. Finally, the ghost targets induced by the curved guardrails are tightly localized compared to those of the straight guardrails. This is because signals reflecting on the curved guardrail have limited reflection paths that they can use to return to the radar sensor. This reduces the overall number of ghost targets and their extents.

This was observed using visual ray tracing in HFSS SBR+. Such information can be used to update the perception algorithm so that it accurately identifies the guardrails as the ego vehicle negotiates a curve.

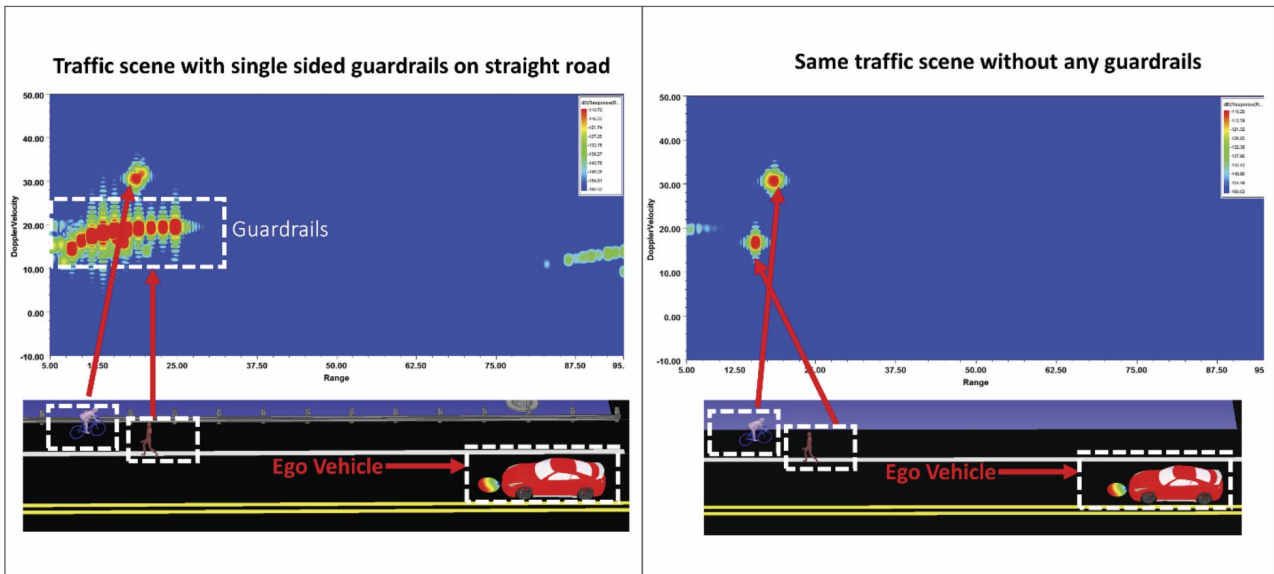


Figure 5: Range-Doppler maps of the same traffic scene with and without guardrails. The guardrails used here are single-sided, straight sections.

C. Single-Sided, Straight Guardrail Sections on Either Side of Intersection

Two 32m long sections of guardrails were placed on a road perpendicular to the ego vehicle (Figure 1). Two cyclists were placed on either side of the intersection to investigate their visibility. This is a very important corner case in which the ego vehicle must accurately detect pedestrians and cyclists who may be trying to cross the road and stop in time. Figure 4 shows the RD maps of the same scene with and without the guardrails. Here, as in the previous cases, the guardrails completely mask the presence of the cyclists on either side of the road. Visual ray tracing studies using HFSS SBR+ reveal that the guardrails at the intersection have very limited multipath propagation paths that can return to the radar receiver.

This leads to even weaker ghost targets. The profile of the guardrails shown in Figure 4 has three distinct properties. First, the profile exists as a single trail even though there are two physical guardrails on either side of the road. This is due to the symmetry of the guardrail placement which superimposes returns from either side at the same range in the RD map. Second, while the RD profiles studied in the past sections have positive velocity slopes, the RD profile shown in Figure 4 has a negative velocity slope. This means that the guardrail posts nearest to the ego vehicle seem to have the highest velocity. Such behavior is expected since the relative (to the ego vehicle) radial velocity of each post decreases as the angle of arrival of that post increases. Specifically, as we move away from the center of the intersection, the angle of arrival of each dihedral post increases and thus decreases its radial velocity (relative to the ego vehicle).

Finally, the guardrails shown in Figure 4 have an RD profile that extends for 15m, less than half of their physical length. This is an artifact introduced by the directivity and limited field of view of the radar sensor antennas. The limited field of view of the sensor antennas means that the guardrails at wider angles of arrival are not heavily illuminated by the sensor.

D. Straight Guardrail Section on One Side of the Road

A single 32m long section was placed on one side of the road a (Figure 1). To account for the length of the vehicle, only 26m of the guardrail section is remaining in front of the vehicle. The RD map of the scene is shown in Figure 5. As shown here, the profile of the single guardrail section is similar to that of the double-sided, straight guardrail section in Figure 2. The range extents of the profile are equal to its physical length and it also has a positive velocity gradient before leveling off at the velocity of the ego vehicle. The RD profile for a single sided section differs from that of the double-sided section (see Figure 2) in two key ways. First, the near-range end of the single-sided guardrail section RD profile has only one tail compared to the two tails of the double-sided section as expected. The second observation is that the single-sided guardrail section has no ghost targets at all. This should be compared to the train of ghost targets that results from double-sided guardrails (Figure 2). In previous sections, ghost targets were attributed to multiple reflections between the guardrail sections on either side of the road that eventually make it back to the radar receiver. Without another guardrail panel on the other side of the road to serve as a reflection surface, multipath propagation of the reflected signals is mitigated and the ghost targets disappear.

E. Discussion

Investigating the range-Doppler (RD) maps of each of the scenes reveals that each of the guardrail systems in the cases shown in Figure 1 can potentially mask the radar returns of pedestrians, cyclists and vehicles in their vicinity. However, the guardrail systems do not have the same ghost-target inducing behavior. Specifically, ghost targets were observed to be most prevalent when the guardrails existed on both sides of the road in the same direction as the ego vehicle (Figure 2 & Figure 3). Having guardrails on both sides of the road created reflection planes that presented more multipath propagation paths for signals to find their way back to the receiver. Multipath propagation was found to be most prevalent in the straight, double-sided guardrail sections (Figure 2). On the other hand, single-sided guardrail sections on one side of the road did not create any appreciable ghost targets (Figure 5) due to their single panel.

Another key observation was that parallel guardrail systems (Figures 2, 3 & 5) have positive velocity gradients that level off at the ego vehicle velocity. On the other hand, perpendicular guardrail sections (Figure 4) have negative gradient velocity profiles. Radar sensors calculate the radial velocity and therefore, the guardrail section next to the ego vehicle would have a very small radial velocity while the ones further away would have higher velocities in (Figures 2, 3 & 5). This situation is reversed when the guardrails are perpendicular to the road where the ego vehicle is travelling on. The highest radial component of the velocity is possessed by the guardrail posts nearest to the intersection since they have the smallest angle of arrival relative to the ego vehicle.

Conclusion

Automotive radar is one of the key sensor technologies for advanced driver assistance systems that will enable the deployment of a fully autonomous vehicle while making roads safer. Testing and validating radar sensors in practical traffic scenes is one of the key challenges in design validation. Simulation has emerged as the most practical, safe and cost-effective way to investigate the performance of radar sensors in traffic scene corner cases.

Guardrails present a unique corner case challenge due to their high radar cross section and physical arrangement which can mask the presence of crucial targets while creating ghost targets. Furthermore, the range-Doppler map profiles of guardrails change drastically depending on their physical placement. In this study, Ansys' HFSS SBR+ was used to create and conduct four, high-fidelity physics electromagnetic simulations of real-world traffic scenes where guardrails normally appear. By inspecting range-Doppler profiles of traffic scenes with and without the guardrails, the crucial target-masking and ghost-target inducing characteristics of the guardrails were demonstrated. Furthermore, the unique range and velocity behavior of the guardrail sections in each of the different scenes were discussed.

Results from this study showed that straight guardrails had different range and velocity behavior compared to curved guardrail sections. Guardrail sections parallel to the ego vehicle's direction of motion also had a significantly different behavior when compared to guardrails running perpendicular to the ego vehicle at an intersection. The conclusions made in this study can be used to train machine-learning based perception algorithms to not only identify guardrail systems but to classify their physical arrangement and predict their range-Doppler behavior. Accurate identification, classification and filtering-out of guardrails can help prevent accidents and save lives.

References

- [1] A. K. Yadav and J. Szpytko, "Safety problems in vehicles with adaptive cruise control system", *Journal of KONBiN*, Vol. 0035, vol. 42, no. 1, pp. 389-98, 2017.
- [2] NHTSA, "U.S. Transportation Secretary Elaine L. Chao Announces Further Decreases in Roadway Fatalities", Available online <https://www.nhtsa.gov/press-releases/roadway-fatalities-2018-fars>, Accessed on: Sep.17,2020, Washington, DC, 22 October, 2019.
- [3] R. Sagar, "Making cars safer through technology innovation", Texas Instruments Inc., 2017. [Online]. Available: <https://www.ti.com/lit/wp/sszy009a/sszy009a.pdf?ts=1600332887748>. [Accessed 17 September 2020].
- [4] A. Jadhav, "Autonomous Vehicle Market Outlook-2026", Allied Market Research, May 2018. [Online]. Available: <https://www.alliedmarketresearch.com/autonomous-vehicle-market>. [Accessed 17 September 2020].
- [5] R. H. Rashoffer and K. Gresser, "Automotive radar and lidar systems for next generation driver assistance functions", *Advances in Radio Science*, vol. 3, p. pp.205-209, 2005.
- [6] D. M. Gavrilu, "The visual analysis of human movement: A survey", *Computer Vision and Image Understanding*, vol. 1, no. 73, pp. 82-89, 1999.
- [7] T. B. Moeslund and E. Granum, "A Survey of advances in vision based human motion capture and analysis", *Computer Visual Image Understanding*, vol. 104, no. 2-3, pp. 90-126, 2006.
- [8] R. Poppe, "Vision based human motion analysis: an overview", *Computer Visual Image Understanding*, vol. 108, pp. 4-18, 2007.
- [9] G. Reina, D. Johnson and J. Underwood, "Radar sensing for intelligent vehicles in urban environments", *Sensors*, vol. 15, pp. 14661-14678, 2015.
- [10] A. Ohnsman, "Toyota's Robot-Car Line In The Sand: 8.8 Billion Test Miles To Ensure Safety", *Forbes*, 3 October 2016. [Online]. Available: <https://www.forbes.com/sites/alanohnsman/2016/10/03/toyotas-robot-car-line-in-the-sand-8-8-billion-test-miles-to-ensure-safety/#4ce2a64116f0>. [Accessed 17 September 2020].

- [11] J. Hasch, R. Topak, T. Schnabel, T. Zwick, R. Weigel and C. Waldschmidt, "Millimeter-wave technology for automotive radar sensors in the 77 GHz frequency band", *IEEE Transactions on Microwave Theory and Techniques*, vol. 60, no. 3, pp. 845-859, 2012.
- [12] K. Ohguchi, M. Shono and M. Kishida, "79 GHz band ultra wideband", *Fujitsu Ten Technical Journal*, vol. 39, no. 2, pp. 9-14, 2013.
- [13] J. Singh, B. Ginsburg, S. Rao and K. Ramasubramanian, "Texas Instruments Inc.", May 2017. [Online]. Available: https://www.ti.com/lit/wp/spyy006/spyy006.pdf?ts=1600343615767&ref_url=https%253A%252F%252Fwww.ti.com%252Fensors%252Fmmwave-radar%252Fautomotive%252Fapplications.html. [Accessed 17 September 2020].
- [14] B.-H. Ku, P. Schmalenberg, O. Inac, O. D. Gurbuz and J. S. Lee, "A 77-81 GHz 16 element phased array receiver with +/-50_ beam scanning for advanced automotive radars", *IEEE Transactions on Microwave Theory and Techniques*, vol. 62, no. 11, pp. 2823 - 2832, 2014.
- [15] Altera Corporation, *Implementing digital processing for automotive radar using SoCs*, San Jose, CA, pp. 1-5., 2013.
- [16] U. Chipengo, P. M. Krenz and S. Carpenter, "From Antenna Design to High Fidelity, Full Physics Automotive Radar Sensor Corner Case Simulation", *Modelling and Simulation in Engineering*, vol. 2018, pp. 1-19, 2018.
- [17] U. Chipengo and M. Commens, "A 77 GHz Simulation Study of Roadway Infrastructure Radar Signatures for Smart Roads", in 16th *European Rada Conference (EuRAD)*, Paris, France, pp.137-140, 2019 .
- [18] U. Chipengo, "Full Physics Simulation Study of Guardrail Radar>Returns for 77 GHz Automotive", *IEEE Access*, vol. 6, pp. 70053-70060, 2018.
- [19] C. Isidore, "CNN Business", 11 June 2015. [Online]. Available: <https://money.cnn.com/2015/06/11/autos/automatic-braking-recall/index.html>. [Accessed 17 September 2020].
- [20] T. Kim and B. Song, "Detection and Tracking of Road Barrier Based on Radar and Vision Sensor Fusion", *Journal of Sensors*, vol. 2016, pp. 1-8, 2016.
- [21] G. Alessandretti, A. Broggi and P. Cerri, "Vehicle and Guard Rail Detection Using Radar and Vision Data Fusion", *IEEE Transactions on Intelligent transportation Systems*, vol. 8, no. 1, 2007.
- [22] C. Adam, R. Schubert, N. Mattern and G. Wanielik, "Probabilistic road estimation and lane association using radar detections", in *14th International Conference on Information Fusion- Chicago*, 2011.
- [23] X. Cai and K. Sarabandi, "A Machine Learning Based 77 GHz Radar Target Classification for Autonomous Vehicles", in *2019 IEEE International Symposium on Antennas and Propagation and USNC-URSI Radio Science Meeting*, Atlanta, Georgia, PP. 371-372.
- [24] A. P. Sligar, "Machine Learning-Based Radar Perception for Autonomous Vehicles Using Full Physics Simulation", *IEEE Access*, vol. 8, pp. 51470-51476, 2020.
- [25] M. A. S. Miacci, E. L. Nohara, G. G. Peixoto, I. M. Martin and M. C. Rezende, "Indoor radar cross section measurements of simple targets", *Journal of Aerospace Technology and Management*, vol. 4, no. 1, pp. 25-32, 2012.
- [26] C. A. Balanis, "Fundamental Parameters of Antennas", in *Antenna Theory: Analysis and Design*, New Jersey, Wiley, p.98,2013.
- [27] T. Wu, T. S. Rappaport and C. M. Collins, "The human body and millimeter-wave wireless communication systems: Interactions and implications", in *2015 IEEE International Conference on Communications (ICC)*, London, 2015.

Ushe Chipengo received his B.S. degree in electrical engineering (summa cum laude) from the University of Nicosia, Cyprus in 2013. He received his MSc. and Ph.D. in electrical engineering from The Ohio State University in 2017. With a focus on electromagnetics, he has conducted research on slow wave structures for high power microwave sources, antennas, microwave circuits and computational electromagnetics. Since 2017, he has been with ANSYS as an Application Engineer II. His current research interests include antenna design for automotive applications and automotive radar for advanced driver assistance systems (ADAS).

Shift Towards Electric Vehicles:

*What does it mean
for Simulation?*

Cecile Pera | OROVEL Ltd

Call it evolution or revolution, the automotive industry is currently facing its biggest transformation from traditional thermal engines (gasoline / diesel) towards electrification (hybrids, fully electric vehicles, batteries, fuel cells, etc.). This sudden and massive change brings a lot of uncertainty and fears to most car manufacturers (OEMs) and related suppliers. Mixed with the COVID-19 pandemic crisis, there is, at the moment, a lot of confusion (and panic) in R&D departments who have very little experience in these new technologies. This radical shift presents a lot of risks but also numerous opportunities for everyone – for investors, for stakeholders and also for engineers in terms of career reorientation.

In this context, simulations could play a significant role at the core of development. But what does this transformation mean for the world of simulation? Here, we briefly present some of the technical changes from classical powertrain to new e-mobility. We will discuss the challenges for modelling, not only for software but also for engineers and companies.



Implications for R&D Departments

There are still some internal combustion engine developments needed for hybridisation and other applications (commercial vehicles, marine, etc.), but this article focuses on the largest segment, i.e. passenger cars, that is currently rushing towards more electric/battery vehicles.

This change from fuel-based powertrains towards battery and electric vehicles requires massive investment. This is not only true for R&D and the manufacturing side of things (new plants with new technologies), but also for marketing, workload, etc. By itself, simulation is not at risk because fundamental understanding and upstream optimisation is still required. Nevertheless, the developed applications and the approaches required in terms of modelling are quite different from traditional engines.

For many years, powertrain development has been the preserve of an elite research group including simulations of complex and intricate phenomena such as turbulence, atomisation, combustion, chemistry of pollutant formation, etc. The introduction of consecutive, increasingly more stringent pollutant emission standards has led to the development of new technologies constantly pushing the need for more advanced simulation: knocking control, higher pressure

of injection, urea injection for after-treatment, etc. Some 15 years ago, R&D departments at OEMs were employing dozens, sometimes hundreds of simulation engineers, busy working at optimising the combustion or at enhancing mechanical properties of conrods, bearing, crankshaft, etc.

But all of a sudden, things have dramatically changed. Everyone is now busy speeding up their electric portfolio. Some OEMs (GM, Ford, Jaguar Land Rover and others) have already announced their ambition to produce only zero-emission vehicles in the near-term future (2030-2035) following multiple declarations by governments (UK, Japan, etc.) to phase-out sales of thermal engines. This has resulted in a lot of confusion – even panic – in some companies.

Implications for the Simulation Community

A major current problem is the imbalance between available and required skills or tools to support electric development. There are plentiful skilled engineers trained in classical powertrains using dedicated tools developed over decades. Conversely, development in new technologies rests upon key knowledge that is completely new and only superficially accounted for in the most well-known software suites (at least those usually used at OEMs).



When dealing with traditional technologies, their ever-increasing complexity imposes the need to hire multitasking project leaders with experience in various domains and/or companies. For new technologies, there is a clear lack of well-trained individuals, almost no one with long experience, and no established path to train existing engineering teams in new concepts.

Aside from historic car makers, several new players coming directly from the electric world are entering the game: names like Lucid, RIVIAN, NIO, Rimac, and of course the most famous, Tesla. They have been developing their own methods and using some secretive software out of reach of the traditional automotive software suppliers.

Implications for Technical Developments

Simulations are as crucial for electric vehicle development as they are for conventional vehicles, but the focus point is different. The first key element is the battery. If battery development mainly deals with new chemistries (cathode with more Nickel, less Cobalt, anode with Silicon additive, etc.), thermal management is definitively at the centre of battery technology and here simulation is very important.

Simulation can help on two levels: at the cell level (locally) and at the pack level (when cells are grouped in modules and then encased together in larger packs). Cell cooling simulation is generally conducted at battery suppliers or research groups. Car manufacturers usually only know the global specification of cells: size, charge, discharge profile, surface temperature, geometrical modification (swelling for example), etc. When designing a battery pack, car engineers are usually interested in keeping the temperature in the optimal range and uniform along the pack. Otherwise, cells would age differently, and hot spots would create higher risk of thermal runaway (inducing battery fire).

Thermal management is not only about heat extraction: batteries do not only need to be cooled down, they also need to be warmed up. The first reason is that the optimal temperature range in which batteries should work is very narrow, ideally between 15°C and 25°C for the best energy storage capacity. Below or above this range, the battery energy storage is less efficient and battery ageing is accelerated, reducing the number of useful lifecycles. Such a narrow range of operation asks for precise heat exchange simulation.

Battery packs can be made from various cell formats (cylindrical, prismatic, pouch cells) presenting different sizes and chemistries. The packs can be organised in very different ways and their cooling can be based on air

or liquid flow either underneath the pack or intricately in between the cells. In order to test and to optimise the battery pack architecture, CFD including flow simulation and conjugated heat transfers is used.

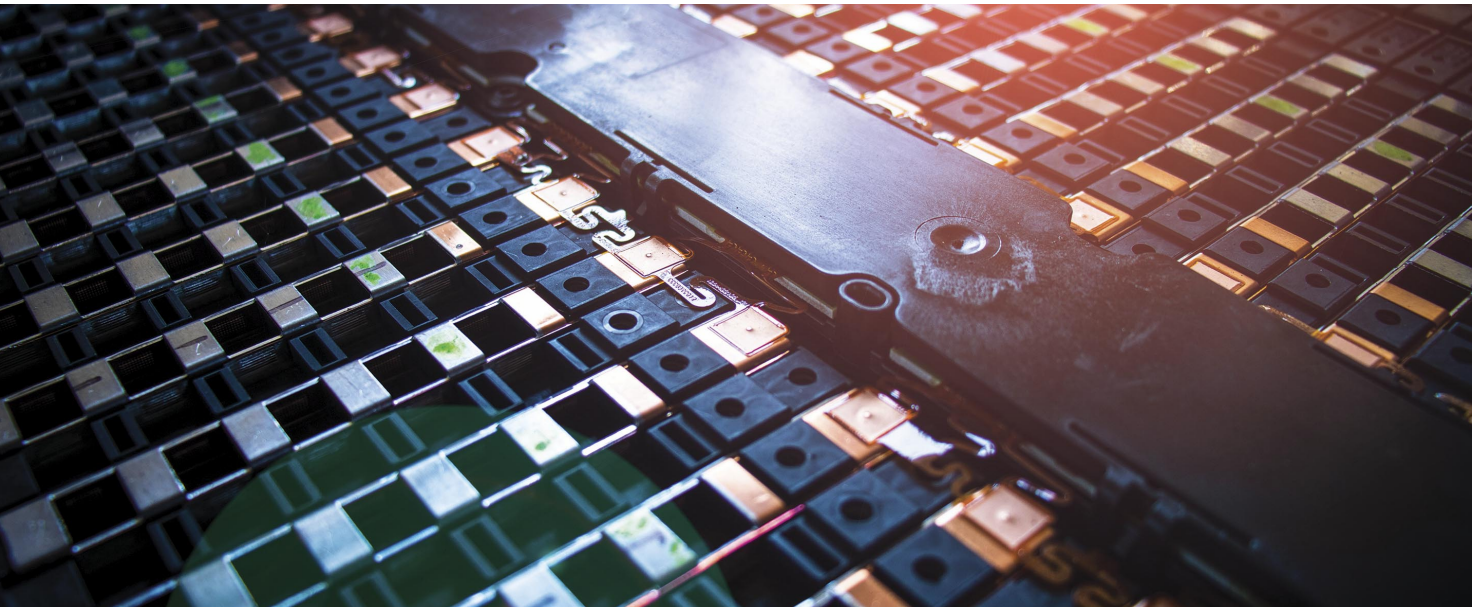
Beyond normal operation, runaway scenarios as well as thermal propagation are very serious concerns for OEMs because they can lead to vehicle fires. Being potentially destructive and dangerous, there is an incentive to better analyse these scenarios with CFD. There are also other concerns, for example, keeping the pressure inside the battery pack safe or limiting the local heat release that could put the battery cell structure at risk.

Fast charging is the second key element of success for electric vehicles. The main challenge is also to keep the temperature under control because left unchecked it can damage the battery and create a fire hazard. Once again, thermal management and optimal cooling strategies are key.

Understanding mechanical properties is also very important for battery safety because of constant vibrations and/or the crashworthiness requirement. It is understood that mechanical deformations can initiate thermal runaway and cause fire or an explosion. FEM can be used to study local deformation at the cell level and to understand how mechanical stresses contribute to induce a short-circuit. Mechanical deformation is also of interest on the full pack and in particular on the battery casing which should be light but still able to protect the battery cells from impacts, for example in case of a side pole impact.

Beyond batteries, a lot of effort, including modelling effort, is focused on the development of the electric motors. While e-motors are nothing new, their optimisation and reliability is becoming more challenging in a context of modularity and scalability to facilitate use in multiple vehicle platforms. In particular, their cooling is once again very strategic because anything electric generates a lot of heat to dissipate. Cooling strategies are multiple with various cooling fluids (glycol-water, refrigerant, dielectric oil).

While, in theory, usual models similar to spray injection or, more generally, two-phase flow could be applied, in practice it is not as straightforward. Among the difficulties, we can cite the use of non-Newtonian fluids, the density of spray dispersion, etc. Yet, the major problems are the lack of data for model validation as well as the coupling with the electro-magnetism properties. Of course, basic approaches imposing heat fluxes as consequences of electrical fields could be considered but this is missing the point of electric motor optimisation.



Implications for Software Suites

This highlights one of the principal issues in simulation for electric vehicles: the lack of availability of models describing electrical components. The development of such models and integration in existing CFD software will take time not only for isolated implementation but also for ensuring compatibility with existing models, notably pre-existing cooling capabilities. Some major companies have anticipated these new needs and have acquired smaller companies to absorb their development within their platform. Some others have been slower to move on and will probably struggle for some time to catch up with the coming trend.

These companies will need to update their decades-long communication strategy as the key messages they have used to build up their success are fast becoming outdated. If in the past complex turbulent models, accurate boundary layers, advanced combustion models and other forms of hydrocarbon detailed chemistry were key in powertrain component development, today there is a shift towards other focus points including electromagnetic fields and battery ageing. Yet, older models are still fundamental to cooling flows, so much so that the ability to couple more and more elements might become a defining factor.

A key aspect of electric vehicle simulation is the absolute necessity to consider the system as a whole. One of the most important aspects of electric vehicles is their global thermal management system which imposes interaction between the various parts on the vehicle making it impossible to separately consider the powertrain as you would in a traditional vehicle. For example, the HVAC circuit (Heating, Ventilation and Air Conditioning) of an electric vehicle is generally coupled to the cooling system of the battery and/or the electric motor. This means

models describing a significant portion of a vehicle, i.e., large models, potentially requiring huge amounts of computational power (system simulation could also be used).

Implications for R&D Companies

For R&D departments at car manufacturers or other related businesses, the software selection is one problem among others resulting from the lack of understanding of electric technology and the absence of experience of the development process. The opposite approach of starting from technology is not much easier either as it is also very hard to find people skilled in batteries and electric motors that also have significant experience in the automotive industry.

One option for companies is to train their employees on these new technologies. This requires a clear strategy, a good understanding of key aspects to learn, and a strong will by engineers to move on. Software could be a helping hand for learning and capturing the general trends from this all-new technological world.

Knowledge in electric vehicles, batteries and other electric technologies could bring real opportunities for the engineers who are willing to go the extra educational mile. Combining knowledge of the automotive industry and its constraints with a technical background in electric technologies would create very strong profiles, highly in demand in the industry. In terms of simulation, similar skills are still required but new methods, processes and modelling approaches have to be developed. Most new software suites for electric simulation (stand-alone or coupling with CFD / FEM) offer webinars (direct or replay on YouTube) to learn about such new simulation approaches.

Conclusion

The quick transition from thermal engines to electrification can look scary but is rather exciting and full of opportunities for car manufacturers, suppliers, engineers and software companies. There are so many things to be developed and invented, so many problems to be solved and strategies to be optimised. System complexity and device interconnection and interdependence means that simulation will be one of the main pillars of this journey.

The complexity and the large number of options to be combined offer to simulation a fun playground and will require combination with strong optimisation tools. Companies and engineers will have to develop new tools, new methods and new understanding around this new business...whilst bearing in mind that, unlike for thermal engines, western companies are now not alone or even at the forefront in this competition.

Dr Cecile Pera is Founder and Director of *OROVEL Ltd* After gaining her PhD in Combustion in the CORIA laboratory at INSA / University of Rouen in France, Dr Pera joined *IFP Energies nouvelles* in Paris where she worked from upstream research on combustion to industrial engine development. Most of her activity was dedicated to novel combustion concepts and Fuel/Engine matching (including commercial, racing, and renewable Fuels). Her research led to a methodology to take into account real fuel complex chemistry in CFD software by tabulation approaches. In 2015, she joined *Infineum* in England, a Joint Venture between ExxonMobil and Shell, as Performance Testing Leader. She developed several Engine tests and worked on a large spectrum of Engine issues such as cleanliness (turbocharger and piston deposits, sludge); wear; scuffing; superknock and LSPI; after-treatment (SCR, GPF, DPF).

In 2018, Cecile joined *Convergent Science*, managing key accounts, and in 2020, she founded *OROVEL Ltd*. In her career, Cecile has managed multi-million portfolio projects with numerous customers and partners: OEMs (Daimler, BMW, Volkswagen, PSA, GM, Maruti, MAN, etc.), Tier One Suppliers (Continental, MAHLE, etc.), Engine Labs (AVL, FEV, APL, SwRI, CERTAM, BOSMAL, etc.) and Petroleum companies (Shell, Exxon, Total, etc.) as well as Universities all over the world. She dealt with complex research programs from the technical design to the responsibility of delivery including quotation, cost, stewardship, customer interface and communication. These research programs involved advanced CFD and modelling as well as advanced diagnostics (Telemetry techniques supported by 3D printing, radio-activity tracer, optical diagnostics).



Effective and Efficient Simulation for AD and ADAS Systems

David Felhos, Bay Zoltan Nonprofit Research Ltd.
NAFEMS Eastern Europe Representative

The simulation and overall testing of AD (Autonomous Driving) and ADAS (Advanced Driver-Assistance Systems) systems is probably one of the most complex tasks today. We cannot talk about a specific class of simulation in this case, it is about the management of *many* parallel simulations describing the behaviour of a highly complex autonomous or ADAS-equipped vehicle. Even the nuances can be considered in the models; the aerodynamics, the suspension and powertrain system, the electronic subsystems and the ADAS sensors as well as the AI-based perception and control systems. This is all embedded in a virtual environment where the road, the weather, visual conditions, pedestrians and similar vehicles are modelled and simulated. It sounds like a very difficult environment to simulate! So why do all the OEMs bother? There is a good reason; it is *impossible* to effectively validate AD and ADAS systems without simulation.

There is an excellent example to demonstrate the inevitability of simulations for validation of AD or ADAS systems. If one has the intention to statistically validate the safe function of a relatively simple emergency brake assist system, then an approximately 2.4×10^8 km long test-driving series would be necessary to achieve the goal. When assuming 100 km/h average speed during these tests, 274 years of driving would be needed to carry out the test series [1][2]. This amount of driving need is very frustrating, not to mention the possibility of

injuries and accidental death cases during the tests. It seems unrealistic to perform these tests. So, when testing is not possible and we fail to solve the problem in analytical ways, simulation is the only hope, as a third way of engineering. Of course, the markets have recognized this need, the large simulation software developers have extended their portfolio promptly with AD and ADAS related simulation tools and new software companies have also been established to fulfil consumer needs.

SAE J3016™ LEVELS OF DRIVING AUTOMATION

	SAE LEVEL 0	SAE LEVEL 1	SAE LEVEL 2	SAE LEVEL 3	SAE LEVEL 4	SAE LEVEL 5
What does the human in the driver's seat have to do?	You are driving whenever these driver support features are engaged – even if your feet are off the pedals and you are not steering			You are not driving when these automated driving features are engaged – even if you are seated in “the driver’s seat”		
	You must constantly supervise these support features; you must steer, brake or accelerate as needed to maintain safety			When the feature requests, you must drive	These automated driving features will not require you to take over driving	
What do these features do?	These are driver support features			These are automated driving features		
	These features are limited to providing warnings and momentary assistance	These features provide steering OR brake/acceleration support to the driver	These features provide steering AND brake/acceleration support to the driver	These features can drive the vehicle under limited conditions and will not operate unless all required conditions are met	This feature can drive the vehicle under all conditions	
	<ul style="list-style-type: none"> • automatic emergency braking • blind spot warning • lane departure warning 	<ul style="list-style-type: none"> • lane centering OR • adaptive cruise control 	<ul style="list-style-type: none"> • lane centering AND • adaptive cruise control at the same time 	<ul style="list-style-type: none"> • traffic jam chauffeur 	<ul style="list-style-type: none"> • local driverless taxi • pedals/steering wheel may or may not be installed 	<ul style="list-style-type: none"> • same as level 4, but feature can drive everywhere in all conditions
Example Features						

Figure 1: Levels of Driving Automation (courtesy of SAE International).

‘Based on current standards, today, only real-world tests with real cars and human drivers are accepted in the validation of any automotive system. This is about to change in the near future; we are heavily working on getting simulation results accepted as a part of the validation process. This not only involves many industry-wide discussions but, from a technical perspective, requires an evolution of environment simulation methods to bring high physical fidelity to model ADAS / AD sensor behaviours. Making these simulations accurate enough for sensor simulation and opening up their real-time engines for sensor producers through APIs is one of the critical challenges of automotive simulation. Since efficiency remains a significant factor, we need to create an integrated simulation platform where high-level scenario simulations and CPU & GPU consuming sensor- simulations can co-exist in an integrated and automated process.’

- Mr. Szabolcs Janky, aiSim product manager, AIMotive

‘Beneath the steady improvement of environment and physics modelling methods, efficiency remains the key, applying parallelisation cloud technology and automation. During the verification and validation tests an enormous amount of data is generated, that has to be assessed and returned in the form of Coverage and KPIs. The world is going to scenario-based V&V where a massive number of scenario variants has to be generated, executed and assessed automatically.’

- Roy Fridman Business Development, Sales & Marketing Executive, Foretellix’

In this special field there are more stages of the V&V process where the virtual simulation and physical tests are coupled with each other. The next example to illustrate this relates to special, so-called Driver in the Loop (DiL) simulations. According to new EU regulations for new vehicle types, driver awareness has to be

monitored, which is especially important at L3 level automation (Figure 1) where vehicle control is transmittable between the driver and the automated vehicle itself.

At this level of automation, the driver’s sense of security might be misleading and can lead to dangerous situations when the driver’s attention is distracted. It means that not only does the system have to be tested out, but many of the dangerous scenarios need to be simulated with human drivers too. This can be realized in the DiL simulator where realistic circumstances can be imitated. Of course, the DiL system has to be equipped with all the interfaces to connect the whole Human Machine Interface system, driver monitoring sensors and a head-up display for example. It means that the most integration- ready systems will be the tools of future simulations. In optimal cases these simulators will be settled directly at a test track where the developments can be immediately tested, or even synched with the digital or semi digital twins.

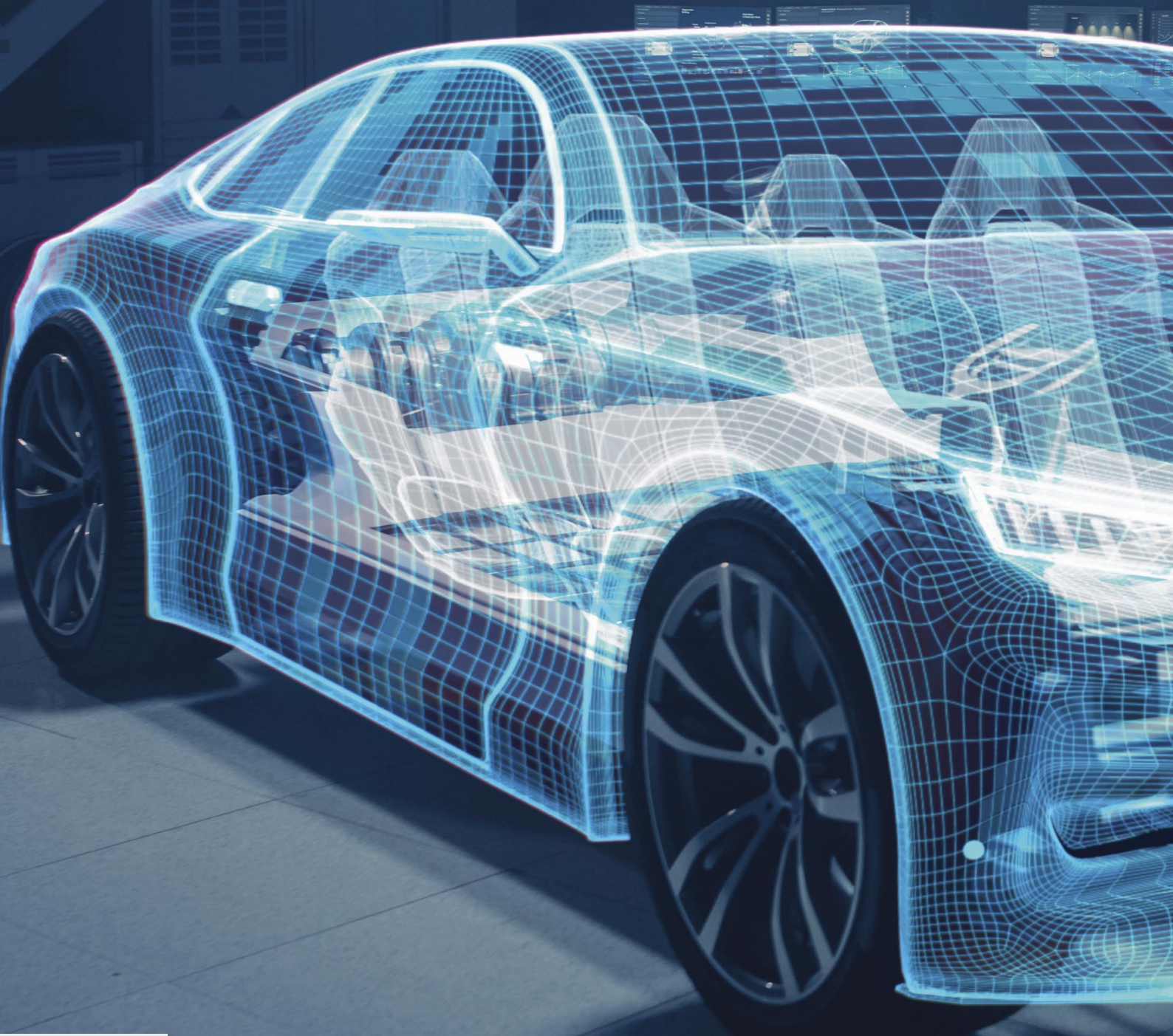
It is not possible to pick one or even a few specific trends and call it the future of AD and ADAS simulations. One thing is for sure; for the V&V of AD and ADAS systems a simulation-based approach is the key. The improvement of simulation methods and management is needed to achieve even more realistic simulation results, and to become even more effective.

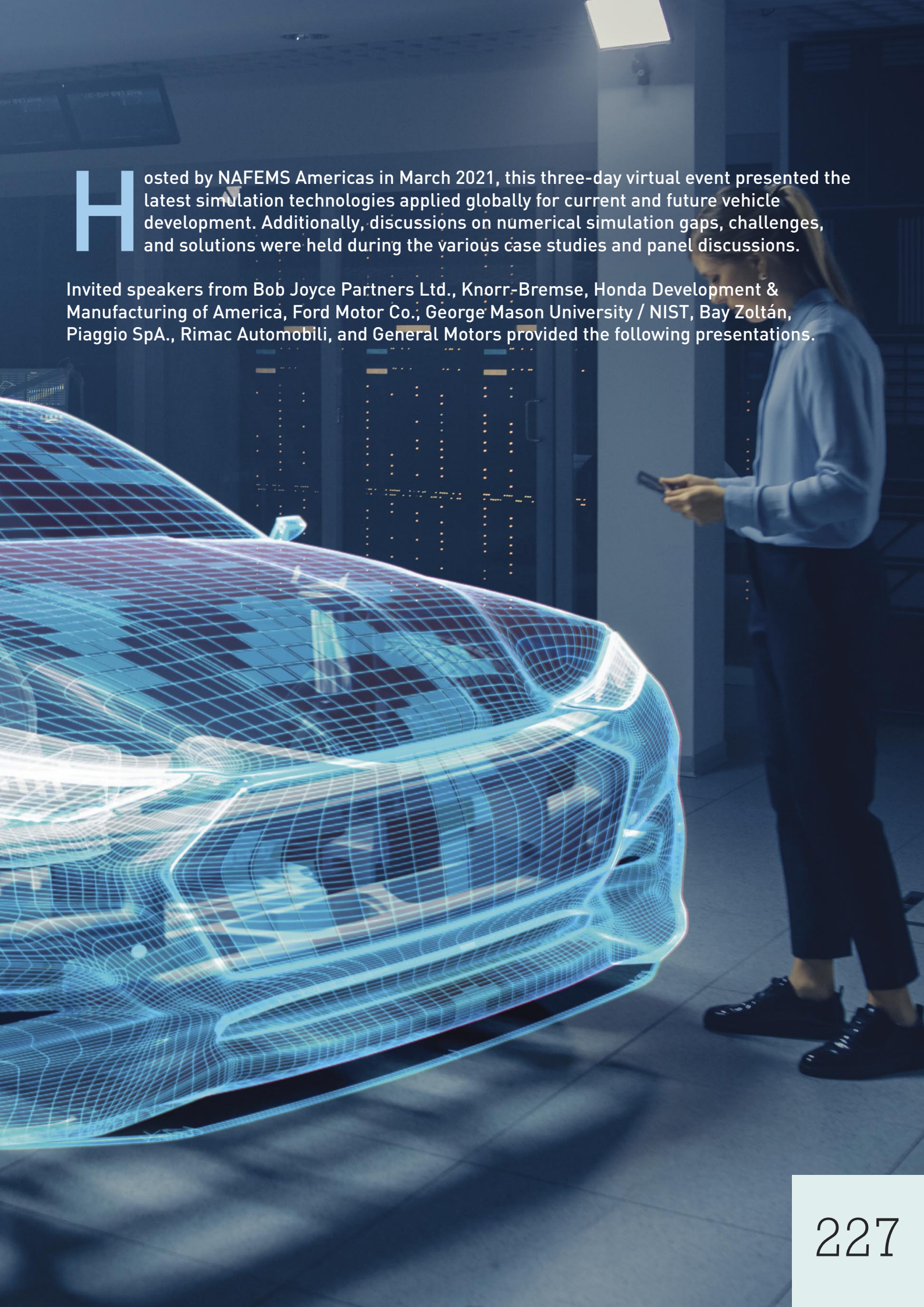
- [1] Feilhauer M., Häring J. (2017) A real-time capable multi-sensor model to validate ADAS in a virtual environment. In: Isermann R. (eds) Fahrerassistenzsysteme 2017. Proceedings. Springer Vieweg, Wiesbaden.
- [2] H. Winner, “Quo vadis, FAS?,” in ATZ/MTZ-Fachbuch, Handbuch Fahrerassistenzsysteme: Grundlagen, Komponenten und Systeme für aktive Sicherheit und Komfort, H. Winner, S. Hakuli, F. Lotz, and C. Singer, Eds., Wiesbaden: Springer Vieweg, 2015, pp. 1167–1186.

Simulation in the Automotive Industry: *Creating the Next Generation Vehicle*

A Summary of the NAFEMS Americas Event

Mario J Felice | NAFEMS Council & Americas Steering Committee Member





Hosted by NAFEMS Americas in March 2021, this three-day virtual event presented the latest simulation technologies applied globally for current and future vehicle development. Additionally, discussions on numerical simulation gaps, challenges, and solutions were held during the various case studies and panel discussions.

Invited speakers from Bob Joyce Partners Ltd., Knorr-Bremse, Honda Development & Manufacturing of America, Ford Motor Co., George Mason University / NIST, Bay Zoltán, Piaggio SpA., Rimac Automobili, and General Motors provided the following presentations.

Multi Level/Multi Physics Battery Strategy

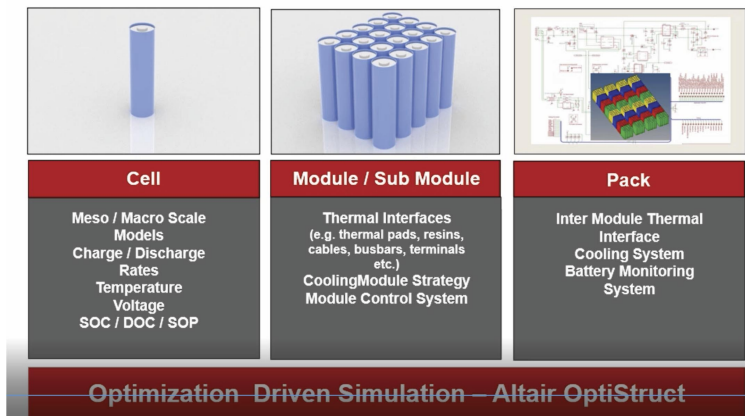


Figure 1: Multi Physics Batter Strategy, presented by Bob Joyce.

Dr. Bob Joyce from Bob Joyce Partners Ltd. was the first keynote speaker. He presented his perspective on the Progression of CAE from the '70s to the present. He cited several cases early in his career demonstrating the importance of simulation. Starting during his time at Ricardo, early in his career, CAE was used very effectively to drive the design of large engines as opposed to using expensive test beds. Later at Jaguar, he drove the decision to invest in CFD simulation at a fraction of the money originally slated for building and running a very expensive large Wind Tunnel Facility. Since then, Jaguar CFD simulation has been effectively used to evaluate the aero dynamics and acoustic performance of vehicles. Additionally, he gave other examples of the effectiveness of simulation and stated, "Analysis always wins over extensive testing".

Over the '70s / '80s simulation grew massively and became very robust. Whereas, over the '80s/'90s, it was Systems & Controls methodologies and their applications that saw extensive growth, facilitating cleaner and efficient engines and vehicles. Software/Complexity technologies are now continuously growing with the

introduction of AI/ML. He stated that the combination of Simulate (optimize the physicals), Systems/Control (create algorithms) and Software/Complexity (control the physicals) provide a multiplying effect on innovation. Dr. Joyce continued discussing the three different elements (Electrification, Autonomy and Connectivity) that are now transforming the industry. Electrification is simply a different powertrain with less parts requiring less servicing and continuous cost efficiencies gains.

The role of CAE in Electrification is to drive Battery Optimization and Electromagnetics, the Controls Systems drive the Battery Management Systems, HVACs, etc. and, finally, the Software drives the Autocode that goes into the ECU driving the vehicle. Dr. Joyce also stated the criticality of multi-level / multi-physics battery simulation from Cell to Module to Pack and how key it is to drive optimization. In the early days BIW analysis was done with extensive testing over a long period of time and now it can all be done in one day through CAE. This has been very transformational. He concluded that there are "no boundaries to the potential of simulation" and noted the importance of working across boundaries.

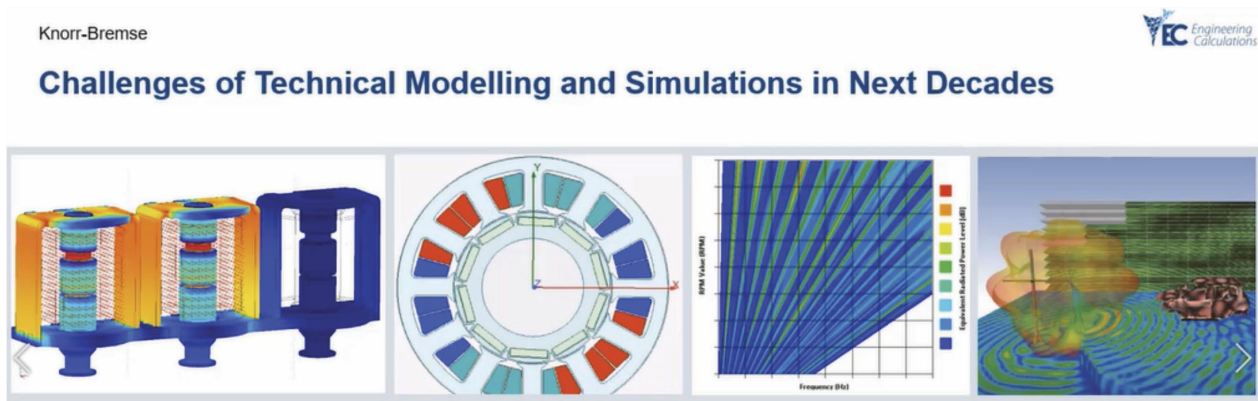


Figure 2: Challenges of Technical Modelling and Simulations in Next Decades, presented by Árpád Veress from Knorr-Bremse CVS. [Source of the right-side figure: nafe.ms/ansys-auto]

Network Synchronization of Count & Speed

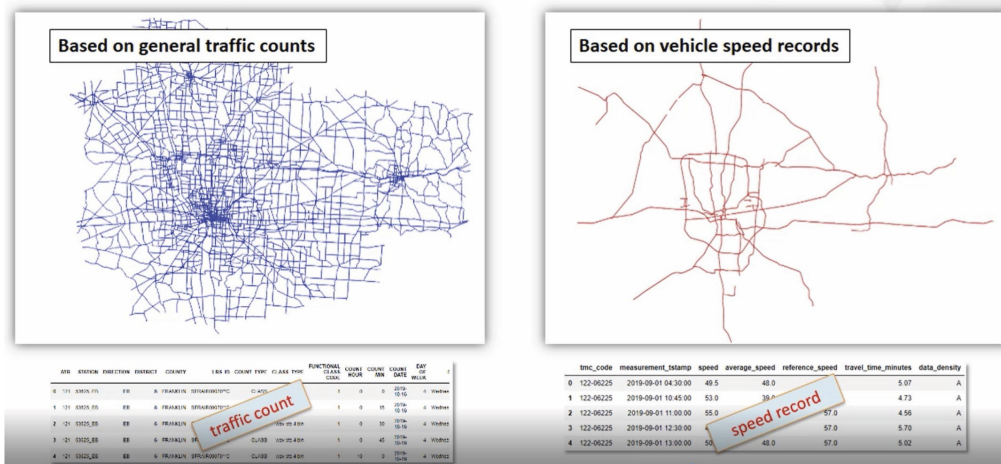


Figure 3: Ohio Roadways Network Model, as presented by Duane Detwiler, Honda.

Dr. Árpád Veress from Knorr-Bremse CVS, provided a detailed introduction of his company indicating he's part of the Commercial Vehicles unit in Budapest. He presented their current simulation capabilities including an automated process for crankshaft fatigue analysis; vibration simulation for exhaust brakes; simulation of brake rubber below; study for evaluating oil fluid effects and impact on crank forces; thermal simulation model development/correlation for microelectronics on PCBs and finally the simulation and optimization of wheel speed sensors indicating great correlation to measurement.

His presentation also covered the challenges of technical modeling and simulations for the next decade. These include the increase in simulation coverage for compressors requiring full FSI integration of thermal dynamics, heat transfer, fluid dynamics, and structural mechanics to improve the accuracy of results. Furthermore, Dr. Veress discussed the need for better adaptability of new technologies in the areas of electronic systems including electromagnetic field simulation coupled with thermal and vibro-acoustics behavior. He concluded by stressing the importance of standardization of CAE tools among software suppliers so that they can easily be used together for total system level analysis.

Mr. Duane Detwiler of Honda Development & Manufacturing of America's presentation was titled "Smarter Mobility by Data Driven Simulation of Transportation Networks". He started by presenting urban mobility data with respect to the behavior and effects of traffic congestion, road accident fatalities, energy consumption, emissions, lack of green space and air pollution pre- and post-COVID-19. He showed

that the impact of COVID-19 was a significant reduction in these effects, and raised the question of whether this might result in continued change in driving behavior into the future.

Mr. Detwiler continued by presenting a future mobility system concept consisting of four technology areas: Connected, Automated, Smart and Electric, all currently being established and growing significantly in application across OEMs. Consumers continue to want mobility systems that are customer centric, accessible, secure and environmentally friendly. This requires an integrated sustainable mobility system approach which can be achieved by using the digital twin to model urban communities and providing a virtual representation of physical assets that are connected to all data and information through use of AI/ML algorithms.

Honda just initiated a research partnership with Carnegie Mellon University to build a data-driven network model for analyzing multi-modal transportation systems. The model provides a method for dynamic traffic demand estimation using real-world data including traffic volume count and traffic flow speed that is coded into a computational graph. It can simulate vehicle trajectories to estimate fuel use, emissions, and various metrics for mobility and energy measures, hence allowing for future planning of mobility, management, and operations traffic strategies.

A network model was constructed for selected Ohio roadways and synchronized based on count and speed of the measured traffic producing a valid representation of the traffic observed. With this a key metric is being developed; "Mobility Energy Productivity" (MEP) to measure a transportation system's ability to connect travelers with destinations relative to convenience, cost, and energy required. Once this project is completed, Mr. Detwiler will present the outcome at a future conference event.

Mr. John Nalevanko of Ford Motor Company talked about building Networks for Modeling and Simulation. As part of his background presentation, he expressed three points: (1) model value and lifespan, (2) the concept of Metcalfe's Law or "The network effect", and (3) the rise and importance of Real-world connectivity. These three points provide the mechanism by which to properly develop and maintain models over time ensuring continuous update through the entire vehicle development cycle, by establishing a network system with the ability to link to real-world data objects and sources.

For this, Mr. Nalevanko presented a process consisting of five bins connecting:

1. Models to data and other models,
2. Models to physical test facilities,
3. Models to manufacturing facilities,
4. Models to vehicles, and
5. Models to third-party data.

However, these would create large sources of data, presenting potential data management challenges. He referred to a study recently done by a data analytics company IDC where they projected the "Internet of Things" with real-world objects is expected to generate 90 Zettabytes (or 90 billion terabytes) of data by 2025. The growth rate of this data for industrial and automotive sector being approximately 60% per year. The challenge is to develop the ability to manage, maintain and connect to this data.

He concluded his presentation by taking a historical perspective of the telephone industry, citing how over the last 110+ years the telephone communication network has grown from limited point-to-point voice connections to an automated network of millions of people and devices; Connecting our analytical models with new sources of data, at scale, will require similar innovations and automation to enable the same network effect.

Professor Duminda Wijesekera from George Mason University presented "Data & Intelligence Requirements for Autonomy and Connectivity". He began by presenting the multiple levels of Autonomy labeled from 0 to 5. With 0 being No Automation, 1- Driver Assistance, 2- Partial Automation, 3- Conditional Automation, 4- High Automation and, 5- Full Automation. The current levels are about 2-3! Any level of autonomous driving requires lots of data!

The car is like a human being in automation, designed by human beings to carry human beings with a simple rule called "Observe, Orient, Decide, and Act". He offered the following true statement "Cars in the future will run on DATA, not Gasoline/Electricity". He continued by presenting a loop diagram for "Conceptual Architectures of Driving Automations", consisting of Acquisition, Perception and Communication feeding to a Decision algorithm sending a signal to Control for vehicle lateral, longitudinal and reactive motion and in turn feeding the Actuation of steering wheel, throttle and brakes.

Professor Wijesekera explained the different messages being provided for situational awareness, accident avoidance, and real time updates from the "seen" and "unseen". Furthermore, he presented the various internal data and intelligence consisting of the data information collected inside the car which is communicated using internal can buses or vehicular ethernet. He then presented the external data and intelligence consisting of vehicle mounted sensors that provide immediate world surroundings of the vehicle, permanent and temporary traffic signals information, emergency vehicles, and buses surrounding and including temporary lane changes.

The presentation then covered Basic Safety Messages, Pedestrian Safety Messages, Collective Perception Messages and Corporate Awareness Messages before going on to look at law enforcement interaction with autonomous vehicles along with Cyber Security and Privacy.

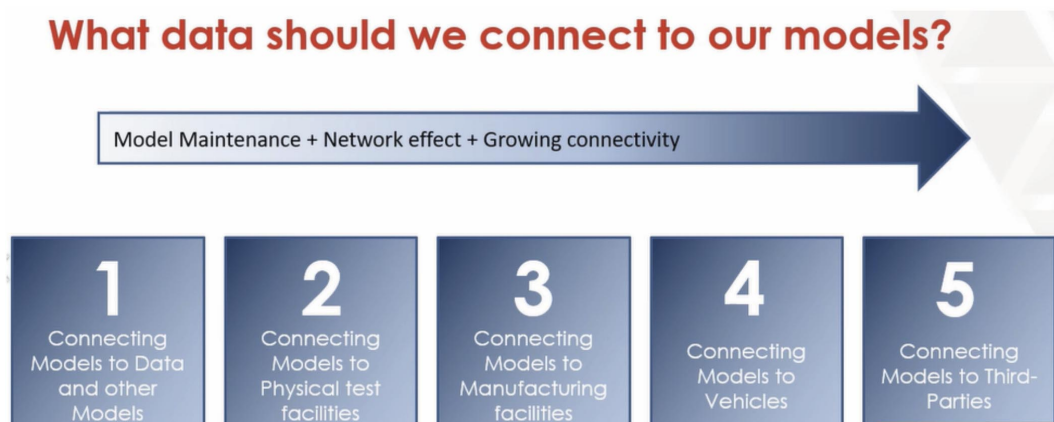


Figure 4: What data should we connect to our models? Presented by John Nalevanko of Ford Motor Company.

A Compendium of Connectivity

- Provides Situational awareness
- Facilitates accident avoidance
- Real time updates from seen and unseen

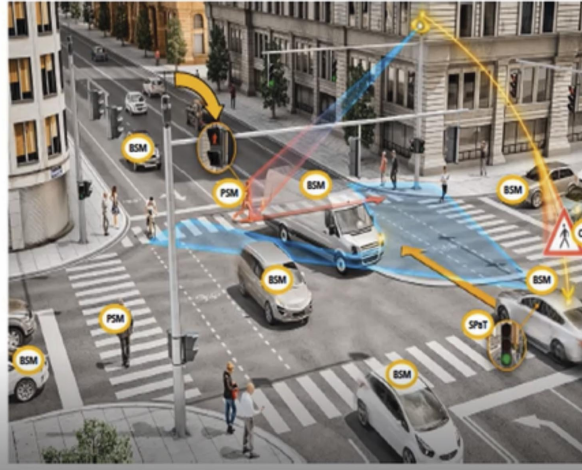


Figure 5: A Compendium of Connectivity, presented by Duminda Wijesekera, George Mason University.

Finally, Professor Wijesekera concluded by talking about how Simulation Matters. He pointed out the need to simulate many different driving conditions, sensory information, and gathering/fusing scenarios. And the need for the capability to run simulations in order to discover questionable or incomplete automations in scenarios, test against misbehavior attacks using AVs, evaluate scenarios in mixed traffic, and learn scalability and performance limitations.

Professor Wijesekera's second presentation was on the "Effects of Failures, Weaknesses & Insensitivities in ADAS". He explained the various ADAS applications and sensing devices that are used. These consist of Advanced Cruise Control (sonar and radar), Lane Departure Warning and Lane Keeping Assist (camera), Adaptive Lighting (camera and IR camera), Driver Monitoring System (camera, IR camera, electric), Automatic Emergency Braking (camera, radar), Pedestrian Detection System (camera, IR Camera, sonar), Road/Traffic Sign Recognition (camera, and IR camera), Night Vision System (IR camera), Blind Spot Detection (radar, Parking Assistance (camera, sonar).

Most of the ADAS applications depend on sensors and intelligence including cameras, infrared sensors (for near and long range), Radars, Lidars, and Ultrasound / Sonar sensors around the vehicle to observe the vehicle's surroundings and get an accurate and timely situation and awareness such that the vehicle can navigate impermissible and free space either with a driver or a fully automated system. Sensor technology increases capability daily and is of essence to making the driving system more efficient. Accuracy and timeliness of sensors contributes to creating an accurate picture of what happens around the car. Software systems use image recognition systems requiring lots of training data

in every conceivable scenario of usage. Hence, simulation is required to reproduce all conceivable scenarios that are impossible to attain with testing.

Professor Wijesekera explained the pros and cons of Vision Based Systems, Thermal Imaging, Radar, Lidar, and Sonar sensors. He concluded by presenting emerging standards such as CAM (corporate awareness messages) and CPMS (corporate perception messages) and the requirement for timely fusion of sensory information with accurate estimation of probabilities and uncertainties.

Dr. Dávid Felhős (Chairman of the NAFEMS East European Steering Committee) and **Krisztián Pintér (Bay Zoltan Nonprofit Ltd for Applied Research)** presented "Simulation of the Human Factor in Autonomous Driving". Dr. Felhos started his presentation by looking at the role of humans "inside the vehicle" and "outside on the road". For these two conditions simulators have been developed —Driver-in-the-Loop (DiL) and Pedestrian-in-the-Loop (PiL) respectively— to study the interaction between humans and machines. These enhance human behavior prediction models which are applied to make much more reliable simulations thereby increasing the development process speed while decreasing testing.

He explained the 3 systems comprising the HMI (Human Machine Interface). These are: (1) Driver Monitoring System (DMS); (2) The internal communication within the cockpit, touch screens and Head Up Displays (HUDs) and, (3) The external communication, which is extremely important for the interaction of the vehicle with pedestrians in urban drive conditions. Vehicle signals are through LED lighting which is used to alert the pedestrian to the vehicle's presence.

ADAS Systems Overview

- Multiple sensors are used in ADAS Systems
- Cameras
- Infrared
 - Near and long range
- RADRS
 - Near and Long range
- LIDARS
- Ultrasound / Sonar

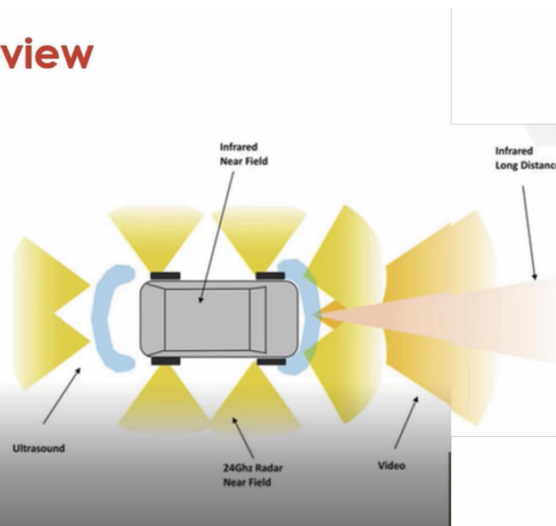


Figure 6: ADAS Systems Overview, presented by Duminda Wijesekera, George Mason University.

The first system described was the DMS which is used to detect the driver's condition. It can detect drowsiness, fatigue, awareness, distraction, health issues, emotions, stress levels, and check driver identification for safety conditions. DMS will soon become a EU regulation! DMS contains a combination of regular cameras as well as near-infra-red cameras, along with contact and non-contact sensors to measure physiological data of the driver and passenger. The DiL simulator is used for safe testing of ADAS functions and HMI (Human Machine Interface) development for driver training. DiL has the ability to check how the driver reacts in different conditions with data collected for HMI modeling.

The human is researched at different automation levels. Level 3 includes Driver awareness monitoring, driver behavior models, control transmission scenarios, ergonomic developments, and stress level measurements in scenarios. The upcoming levels 4-5 will include the PiL, driver/passenger health monitoring and passenger emotion recognition. Dr. Pinter

explained the new-wave testing frameworks including correlation between simulation and real environment and communication from vehicle to pedestrian. He also explained the concept of adaptive obstacle trigger, providing animation of the simulation results.

In conclusion he explained that Human behavior must be investigated with DiL and PiL simulators with the objective to have reliable Human Behavior models for massive simulations.

Professor Steve Kan from George Mason University presented the "Challenges of Future Vehicle Safety". He started the presentation by introducing the university's Center for Collision Safety and Analysis (CCSA) and providing a background for Vehicle Safety consisting of Federal safety regulations (FMVSS), consumer safety rating tests (DOT / NHTSA, NCAP and IIHS) and discussing how safety is affected by driver behavior and external conditions. Key safety components are vehicle structure, occupant protection system and highway protection devices.

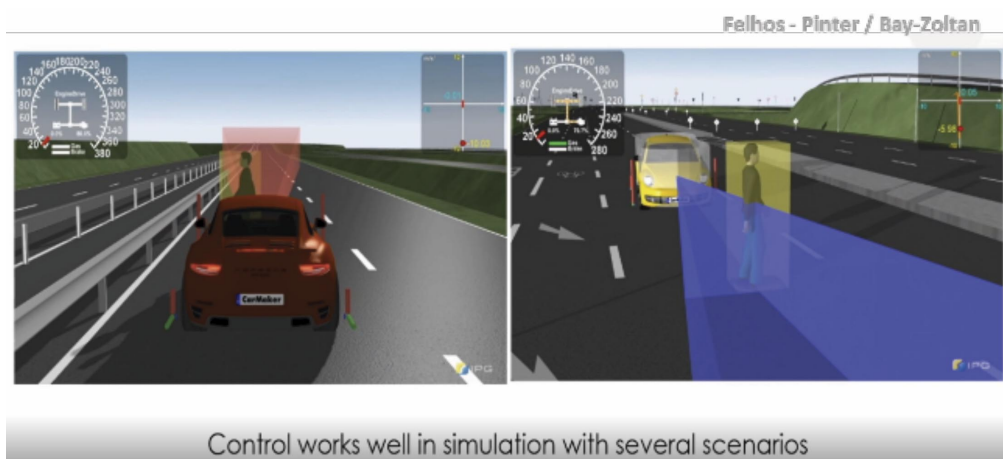


Figure 7: Simulator Examples, presented by Dávid Felhős, Bay Zoltan.

Occupant with Different Seating Positions

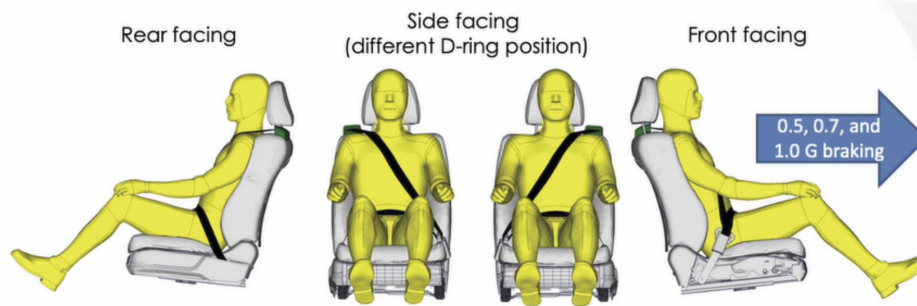


Figure 8: Seating Positions, presented by Steve Kan, George Mason University.

Professor Kan provided historical data on US vehicle road safety indicating 9 of 10 accidents are related to human factors, hence ADS (Automated Driving System) will provide great opportunities to improve road safety in the future. The challenges for vehicle safety are vehicle interaction with roadside infrastructure, mixed vehicle fleet coexisting on highways before full autonomy, and safety for occupant protection. ADS should evaluate a wide range of parameters affecting the outcome of impact with different roadside devices. Roadside hardware devices include street curbs, highway guardrails and different signs and poles on the road.

A government published manual is available for assessing safety hardware (MASH) and the evaluation and certification of roadside devices based on test levels, vehicle classes, and impact configurations. A wide range of impact parameters (mass, impact angle, vehicle speed) are used for the evaluation.

Professor Kan presented simulation on vehicle impact and human injury for condition such as roadside safety barrier and utility pole impact. The knowledge of how impact parameters affect the outcome of an unavoidable collision will be essential for future ADS vehicles. Vehicle Fleet Safety Consideration for ADS and

UADS (un-manned ADS) must be made. UADS could be utility delivery vehicles or shuttle buses. Safety requirements for UADS would only consist in protecting pedestrians and/or incoming vehicles, since there are no humans inside the vehicle.

Also presented were simulations of different impact scenarios and effects on occupant safety for various seating positions using several human body models including GHBM and THUMs. In conclusion, Professor Kan noted that future vehicle safety should include evaluation of new vehicle structures for EV and Fuel-cell vehicle platforms, the evaluation of new occupant protection requirements for the different seating orientations, the integration of vehicle safety technology for passive/active safety, as well as ADS and 5G communication/connectivity.

Mr. Riccardo Testi from Piaggio presented "CAE Simulation of a Driving Mechanism for a Three-Wheeler to Enhance Maneuverability and Ride Comfort". Simulation was used to develop a mechanism to ease the backward parking of a new 3-wheeler Piaggio motorcycle. A simulation model was developed to drive the design which includes a rear axle mechanism driven by an electric motor that will facilitate moving the 3-wheeler backwards for parking.



Figure 9: Three-wheeled motorcycle from Piaggio, presented by Riccardo Testi, Piaggio.



Figure 10: Rimac C_Two Electric Hypercar, presented by Ivan Krajinović, Rimac Automotive.

MBS was used to model the system ensuring the electric motor can move the vehicle backwards and to analyze the interaction of the various gear sets with lubrication assessment. Animation of the gear mechanism system was presented. Stress distribution due to transient analysis was evaluated from the MBS application using a modal superposition approach. Impact velocities from the MBS were later imported into an FEM model for accurate stress distribution. The simulation was used to drive material selection. Additionally, all simulation analyses were validated, thereby driving the build and validation of a prototype design.

Dr. Ivan Krajinović of Rimac Automobili presented the development efforts for the Rimac C_Two fully electric hypercar able to reach 0-100km/h in 1.85secs with 1914hp and max speed of 412km/h. Simulation was heavily used to design the vehicle for safety crash evaluation, aerodynamics for drag and performance as well as cooling for motor and battery pack. All simulations were well correlated once the prototype vehicles were tested for validation. Additionally, simulation was used to model the battery cells as well as vibration and shocks.

Topology optimization was used to design the battery pack holders saving mass and cost. Transient electro-thermal analysis was performed for the battery pack PDU. CFD was also used for battery development, electronic development, gear box lubrication and the overall powertrain development resulting in reduced cost and increased development speeds. The C_Two is equipped with an M2M (machine to machine) system, providing real-time telemetry from the connected vehicle, and displaying various data analytics. Rimac is now developing a Driver Coach system involving autonomous driving to teach driving at extremely high speeds on racetracks up to 400 km/h. This will soon be available in the C2 hypercars. A simulation of Driver Coach was presented.

Dr. Taylor Garrick from GM presented "Electrification in CAE" and initiated his talk by quoting Mark Reuss, GM's president, who stated that "GM believes in an all-electric future". Dr Garrick then announced GM's commitment to at least 30 new electric vehicles by 2025 and GM's vision for a world with "Zero Crashes, Zero Emissions and Zero Congestion". GM aspires to eliminate tailpipe emissions by 2035 and become carbon neutral by 2040.

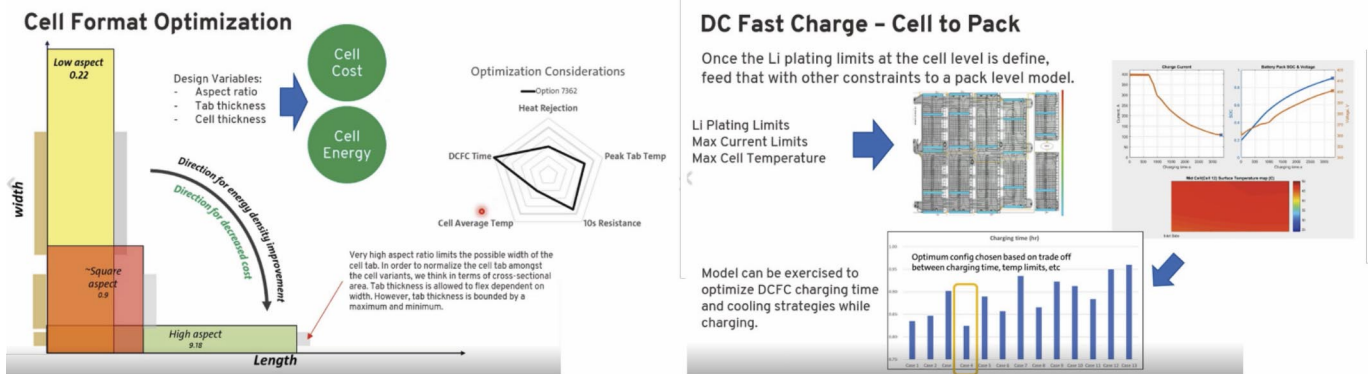


Figure 11: Battery Cell Optimization, presented by Taylor Garrick, GM.

A number of new electric products were shown, highlighting the new “Ultium” platform which offers the ability to repackage battery cells in different configurations to meet different program requirements for range and performance. Dr. Garrick is part of the VDDV (Virtual Design Development and Validation) organization within GM and defined Virtual as “the means to use physics-based models to predict performance”.

He presented some of the simulation performed within VDDV consisting of Structural analysis for body modes and engine stresses; CFD for aerodynamics; Safety for crash; Human Body Modeling for crash impact evaluation; Fuel Spray & Combustion simulation; Electromagnetics flux for rotor and stator including thermal effects; and finally Electrochemistry simulation use for evaluating the transport processes within the battery cell electrodes to understand how lithium transports within the solid and liquid phase and how this affects system considerations like heat generation, structural and electrical outputs.

Dr Garrick also presented how GM’s virtual process is used to select the right propulsion technology for EV range, 0-60mph timing, and top speed requirements. He then continued presenting the battery thermal simulation, which uses CFD, to maintain the optimal operation window for the cell between 20°C to 35°C, as well as maintaining uniform temperature in the battery pack typically within 5°C to 10°C. This same simulation is used to evaluate cabin comfort, since cabin heating can reduce range by up to 50%. He explained one of the

challenges that need to be overcome for EVs full acceptance is the charging time. For example, a typical vehicle takes 3-5mins to fuel a 15-gallon tank which is equivalent to a charge rate of ~10.1 MW. Current max charge rate are ~ 500 KW! Dr. Garrick explained that the energy transfer process between lithium and anode needs to be charged at the appropriate rate to prevent thermal runaway.

He went on to explain the Porous Electrode theory and how cell format is optimized using thousands of different battery designs looking at trade-offs such as heat rejection, resistance, charge time and temperature. He then presented the evaluation of DC Fast Charge (DCFC) limits looking at electrochemistry/material, cell hardware and system/vehicle hardware limits. Simulation models are run to optimize DCFC charging time and cooling strategies during the charging process. Thermal Runway and Propagation is evaluated as part of the pack level CFD. Thermal runaway is the uncontrolled rapid temperature rise in a cell resulting from an exothermic reaction. The simulation focuses on preventing propagation by predicting the impact of cooling, venting and thermal insulating materials.

One of the benefits of this simulation is that lots of evaluations can be done virtually without burning off battery packs or battery modulus repeatedly during tests at different load cases. Electrochemical simulation also offers the ability to predict not only thermal and electrical output, but also material properties for input to the battery pack.

On the third day, a panel discussion was held examining the role of simulation, challenges, and solutions as it relates to delivering cleaner, safer and smarter vehicles in a fast-transforming automotive industry. Mario Felice led the session, along with Dr. Karim Zouani (Ford), Dr. Song He (GM), Dr. Árpád Veress (Knorr-Bremse), Professor Duminda Wijesekera (George Mason University / NIST), Dr. Ivan Krajinović (Rimac Automobili) and Riccardo Testi (Piaggio). Mario summarized key take away points from each of the keynote speakers over the 3-day period and then immediately started a discussion on the simulation requirements for fully supporting the industry's development needs for electrification including motor efficiency prediction, EM force computation and battery technology design.

Additionally, a lot of time was spent by panel members and the audience discussing the challenges of a very fast evolving ADAS and AV technology segment with vast needs for simulation technologies covering the different types of sensor detections and safety modeling.

As part of this event Dr. Rodney Dreisbach (NAFEMS Council Member, Americas Steering Committee Chairman and Technical Fellow) presented Dr. Keith Meintjes with the title of NAFEMS Technical Fellow for his numerous technical contributions in the field of simulation and his active leadership in the various NAFEMS technical groups. Congratulations to Keith!

There were 144 participants at this virtual event with live Q&A, breakout discussions and networking accumulating 87,313 minutes of engagement time with an average of 10.25 hours per person. Ten CAE vendors sponsored the event. These include: Wolf Star Technologies, Hexagon-MSC, SIMULIA, ESTECO, AVL, Gamma Technologies, Nextflow Software, Endurica, Aras and TotalCAE delivering the following Case Studies:

- **“From Baja to EV – Using Load Reconstruction in Real Time”** (Wolf Star Technologies)
- **“Crossing the RUBICON to a Sustainable Future”** (Hexagon | Romax Technology)
- **“Integrated Modeling & Simulation for Battery Module & Pack Design and Optimization”** (Dassault Systèmes SIMULIA)
- **“Assessing ADAS/AD System’s Real-Life Performance: Uniting Real Data, AI and Optimization for Scenario-Driven Design Validation and Optimization”** (ESTECO SPA)
- **“Keeping it Cool - A Thermal Simulation Study of the TESLA Model 3 Cell”** (AVL List GmbH & Batemo)
- **“Integrating Simulation into the Digital Transformation Initiative for Complex Multidisciplinary Systems at MIT Lincoln Laboratory”** (MIT Lincoln Lab & Aras)
- **“Rain Management Applications with SPH Method for Vehicle Sensor’s Location Optimization”** (Nextflow Software)
- **“Block Cycle Durability Schedule Generation for an Elastomeric Control Arm Bushing from 3 Channel Road Load Signals”** (Endurica)
- **“Optimal Electrified Powertrain Controls along a Real-Time Route in a Multi-Physics Simulation Platform”** (Gamma Technologies)

Finally, BIG THANKS to **Andrew Wood** and **Matthew Ladzinski** for their immense work in all the logistics and efforts for putting this world class event together! Also, many thanks to Rod Dreisbach, Duane Detwiler, Karim Zouani, Frank Popielas, Ed Ladzinski, Mahmood Tabaddor, Joshua Huang, along with all presenters and participants.

Mario J. Felice is Principal and Founder of virsolTech Engineering Consulting providing automotive engineering experience to Software Tech Companies helping create “Simple & Practical” integrated automotive simulation technologies.

He serves as a member of the NAFEMS Council (Board of Directors) and the NAFEMS America’s Steering Committee.

Mr. Felice recently retired (Jan 1, 2021) as Global Manager for Powertrain Calibration, Controls and NVH CAE at Ford Motor Company. While at Ford, headed a large team of CAE engineers located in North America, Europe and India, leading all analytical efforts to deliver Ford’s global powertrains for best performance, fuel economy, drivability and sound quality.

Mr. Felice has published and presented at many international symposiums & conferences and been invited numerous times as a visiting professor at the Universities of Rome, Naples and Salerno in Italy.



Raptor Titanium

Sharpening their Claws through Reverse Engineering

Steff Evans | Evotech CAE

Motocross, enduro racing, and FMX (the freestyle version of motocross) are some of the most dynamic wheeled action sports around today. They place the motorcycle in situations that far exceed the performance capabilities of its road-going counterparts. Modern-day 'Evel Knievels', such as the legendary stuntman, Travis Pastrana, and his Nitro Circus counterparts, regularly amaze their audiences, defying death with their feats. When replicating Knievel's iconic jumps over multiple cars and buses, and the odd Caesar's palace fountain or two, failure is not an option, be it the rider's nerve or the bike structure on impact.

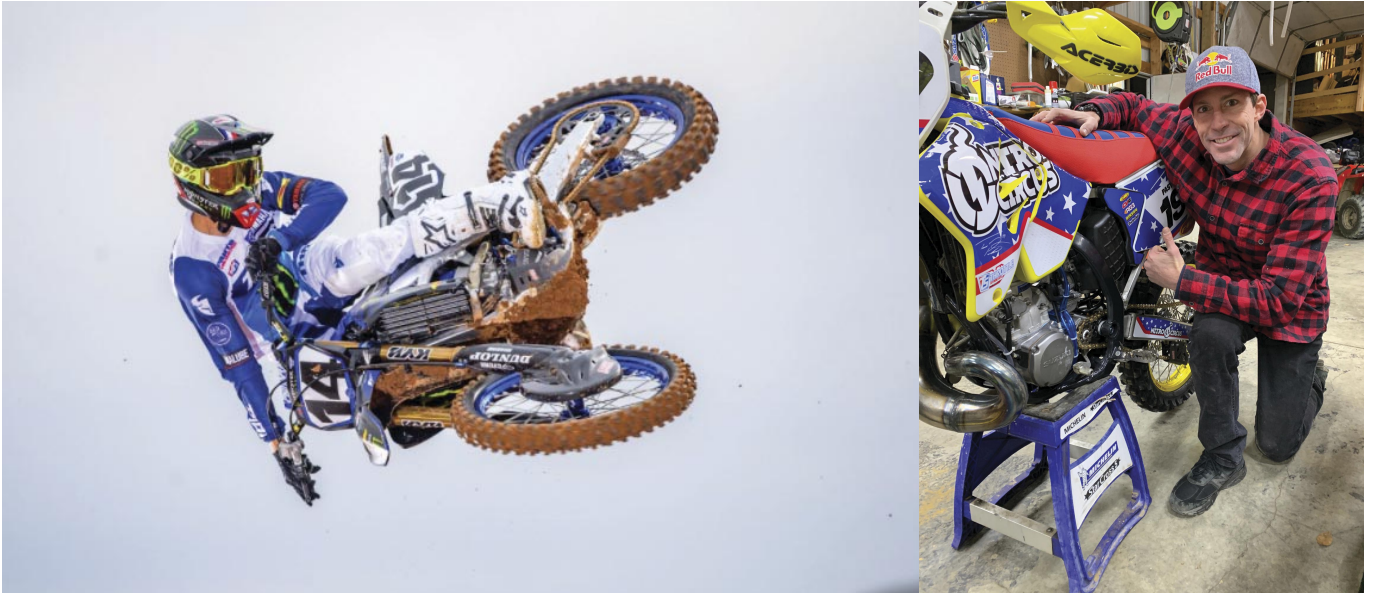


Figure 1: Raptor Pegs in Action

One company crucial to all of this, Raptor Titanium, is based out of Lancashire, in the UK. Their titanium foot-pegs have gained a worldwide reputation through the performance that Pastrana and fellow extreme athletes demonstrate. Raptor had their beginnings in the aerospace industry, supporting the welded manufacture of titanium fan blades used in some of the world's most powerful jet engines. They moved over to foot-peg manufacture through a general love of all things motorcycle, and some pretty fancy-schmanshy welding technology (all top secret by the way).

Now with over 20 years of top-notch manufacturing, they support numerous elite professional teams (think KTM Red Bull, Kawasaki RT, and Rockstar Husqvarna, to name a few) along with title-winning riders, such as Pastrana, Clement Desalle, and Tony Cairoli (all multiple X-games, GP, and world title holders in their own right).

Project Motivation

Historically, Raptor have used significant 'in-field' testing to develop their aggressive designs. This has been based around rider feedback, coupled with a smattering of practical lab testing involving dropped masses to replicate the impact loads seen during riding. Confident in their design, Raptor offer a multi-year warranty with every pair of foot-pegs. That said, breakage is painful at the very least, and catastrophic at worst.

Over the years, development has been a slow, incremental process, based on subtle changes to design, manufacture, and material choice. With a growing customer base, you get market competition firmly biting at your heels, whether it be plain design infringement, or lower cost, inferior manufacture.



Figure 2: Raptor Titanium Foot-Pegs



Figure 3: GOM UK Scanning Technology

We at Evotech CAE were introduced to Raptor through an industry-focused development initiative to upskill companies in the light of the new normal for UK manufacturing that Brexit, COVID-19, and other market factors (such as raw material usage and supplier lead times) have brought. Initial conversations were based on a desire to reduce development time and improve product performance through digital technologies.

With our background in advanced FEA, this was a perfect fit for our skill set. Many readers will see this as an obvious step, but a carefully considered simulation strategy could make a massive difference to Raptor, both in simply better understanding their product (and warranty) and allowing future optimisation.

Optical Scanning

The first stage of this strategy was to obtain reliable 3D geometry of the foot-peg form. The peg assembly was made up of a series of CNC'd titanium parts, with press formed Ti plate, all welded together using Raptor's 'secret sauce'. Sure, CAD data existed for each of the component parts, but a fully welded CAD model (with the organic intricacies of the smoothed weld geometry) simply didn't. This was when scanning and reverse engineering came in.

Through an existing Raptor relationship with GOM UK, we were able to generate the necessary STL data to give us a starting point for reverse engineering. It's at this point that I have to say I learnt a huge amount about the scanning process, and the ability to generate usable CAD for downstream processing. I would say I was naïve in thinking that you just point the scanner, generate the point cloud, then hey-presto, there's your CAD. It's not quite as simple as that, so let me explain...

GOM UK utilised their latest ATOS Q 12M digitizing system, which utilises blue light technology fringe projection and two stereo cameras, to capture high-quality point cloud data of the part. An automated rotation table was used to assist the positioning of the part in different orientations for the cameras – like how you might orientate the part to your eyes to observe the different surfaces. The supporting software, GOM Inspect Suite, brought the data together, with feedback to the user on the data captured.

There were a few issues with 'line of sight' where the cameras simply couldn't reach some of the undercuts where parts came together. Sure, existing 3D geometry would have given us a 'heads up' here, but instead we used the geometry processing capabilities of the GOM Inspect Suite software to fill in the gaps, and generate planar sections required to rebuild the clean geometry.

Side notes on Geometry Manipulation...

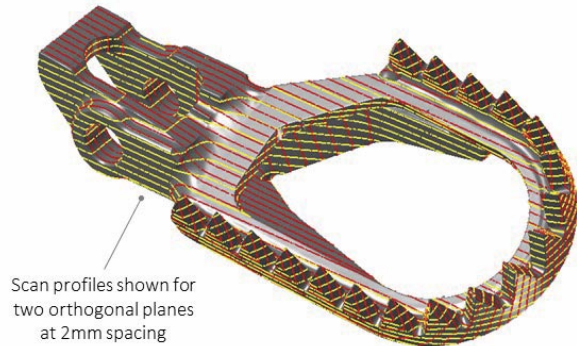
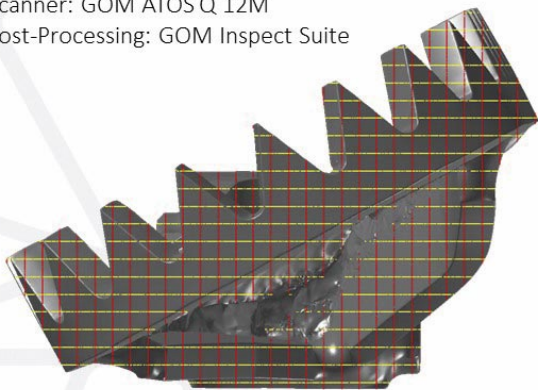
The STL output from a scan (and the post-processed data) is made up of thousands or millions of points, all connected through a huge set of flat triangular faces which enclose a water-tight volume. If you're looking at something fairly regular, with lots of flat faces, then the 'facet body' (as it's known colloquially) will do. However, if you've got lots of features (radii, double-curved surfaces etc.) then a better definition is required.

Non-Uniform Rational B-Spline (NURBS) is a powerful mathematical description of geometry, to yield a far cleaner form than its STL facet body 'little brother'. If you want any kind of smooth geometry that can be easily manipulated (add/removing features, extending solid faces), not to mention FEA-meshed, then NURBS geometry is a must-have. Fortunately, there have been many advances in this kind of geometry definition which make this 1) a reality and 2) accessible in a form that doesn't take forever and break the bank at the same time.

Drum roll for MSC Apex please, which, if you happen to follow my LinkedIn activity (yes, cringe, I am 'The Apex Guy'!), will come as no surprise!

Part Scanning

Scanner: GOM ATOS Q 12M
Post-Processing: GOM Inspect Suite

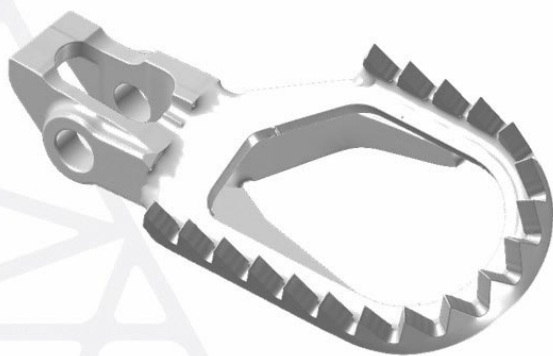


Scan profiles shown for
two orthogonal planes
at 2mm spacing

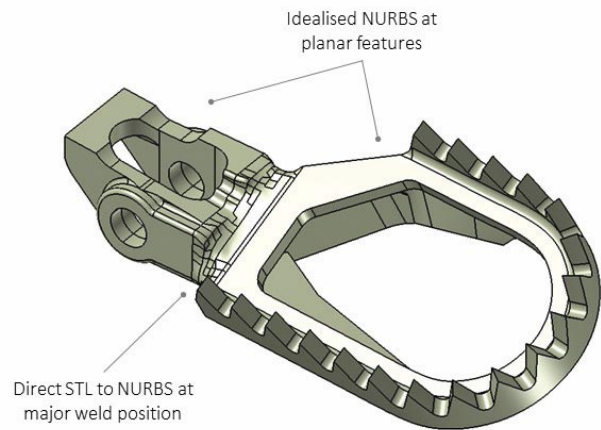
3

Figure 4: Part Scanning

Reverse Engineering



STL Scan (Leftpeg-closedholes.stl)

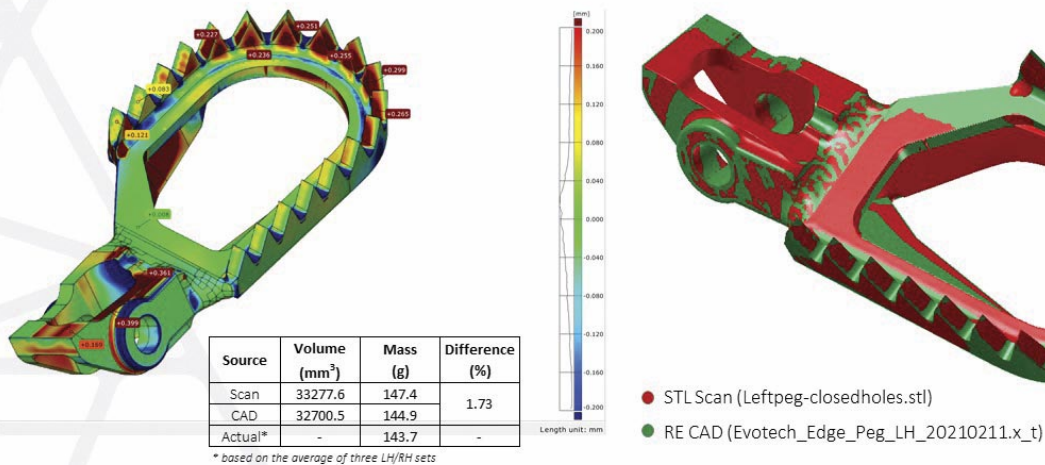


RE CAD (Evotech_Edge_Peg_LH_20210211.x_t)

4

Figure 5: Reverse Engineering

Scan to CAD Comparison



5

Figure 6: Scan to CAD Comparison

Reverse Engineering

MSC Apex uses a state-of-the-art Parasolid geometry kernel for FEA model development. Fundamental to this is the ability to create and manipulate geometry in many forms. There are tools in Apex that easily match or surpass the most powerful CAD software on the market today, and all within a CAE/FEA platform. One of these workflows is the ability to reverse engineer legacy FEA mesh data into a form that can be redefined for a new model, whether that's to include additional structure or to look at different analysis strategies, such as sub-modeling. A by-product of this 'mesh to CAD' workflow, is the ability to reverse engineer imported STL scan data into NURBS geometry.

We used these tools to re-build the geometry from the STL point cloud and the section curves that GOM Inspect Suite generated. The section curves were used as construction geometry for the standard NURBS primitives (planes, cylinders, spheres) for the machined

regions, where it was easier to understand the design intent or shape in the structure. The more organic regions (historically more difficult to handle, especially at the weld interfaces), were represented with double-curved patches which were lofted using shape constraints into the machined region interfaces. Once the geometry had been recreated, we were able to use GOM Inspect Suite to compare with the original STL definition, both in terms of visual overlay and enclosed volume. The overlay showed a high degree of accuracy, especially at previously critical structural features. The calculated volume of the NURBS CAD was within 1.7% of the original STL form. We also checked the left/right comparison for a pair of pegs to understand any manufacturing variance and its impact on the downstream analysis. Any differences were shown to be tiny, and well within the 'noise' of the resultant FEA. A side benefit of the CAD geometry creation meant that Raptor also had reliable assembly CAD for their CAM and inspection processes.

Side notes on 'Mesh to CAD' for Generative Design/Topology Optimisation...

One area where this STL/facet body to NURBS workflow is gaining traction is in the development of 'clean' geometry following a Generative Design/Topology Optimisation run. Historically, this optimisation workflow would have meant lots of semi-manual post-processing (and potential inaccuracy) in developing geometry from a mesh (I've suffered this pain many times – it's not pretty!). These newer Parasolid-based 'Mesh to CAD' techniques mean that the smooth output from 'level set'-type optimisation runs can be converted to NURBS CAD in a fraction of the time taken in the past.

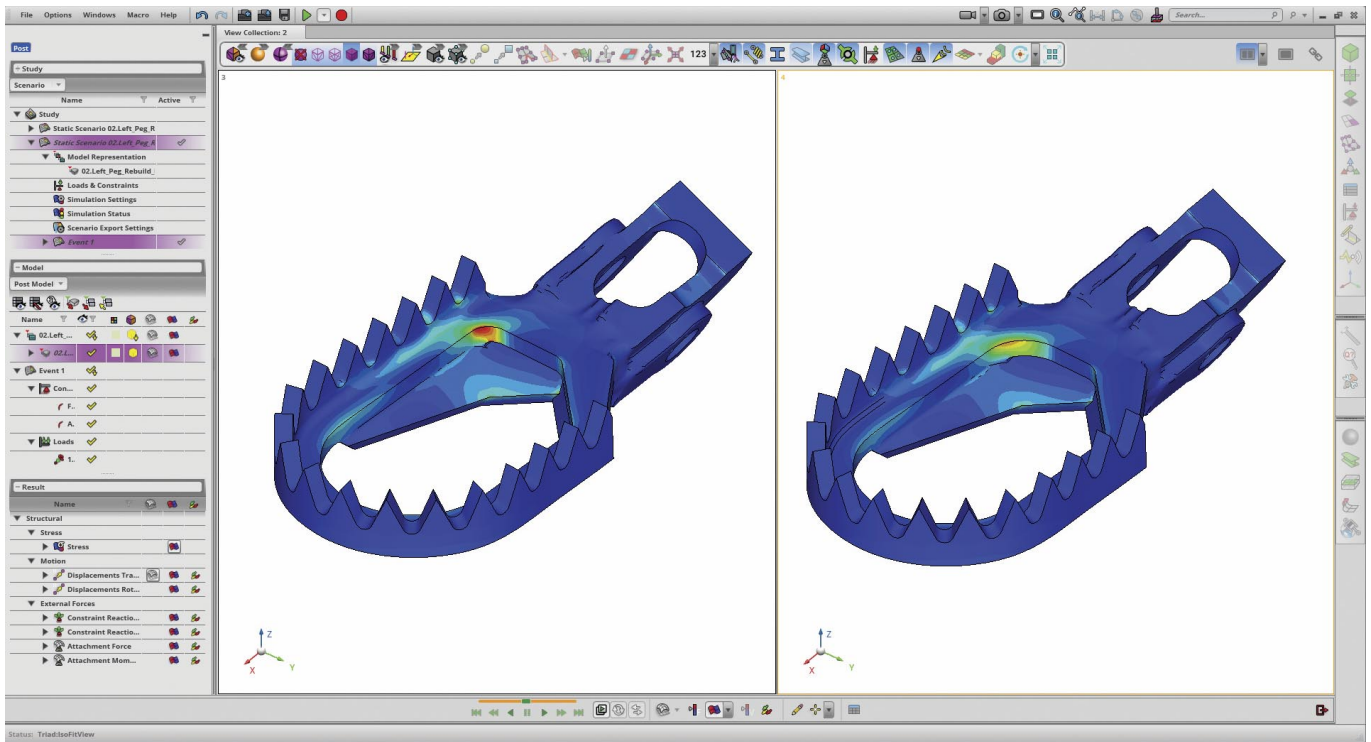


Figure 7: MSC Apex Output Showing Impact of Design Change

FE Analysis

Once generated, the NURBS geometry could be 3D meshed (using 10-noded Tet elements), with the appropriate automatic feature controls on fillets, faces, hole washers, and cylinders. An iterative mesh convergence study was performed using the embedded

Apex 'generative update' tools to give the appropriate balance between converged feature-based stresses and model size. Had the resulting model been too cumbersome, then we could have adopted a hybrid solid meshing approach using hex elements, but this was not the case.

We applied unit static and fatigue loading to determine the load to failure in key directions from the material allowable strength. Once determined, this was assessed both in terms of non-linearity and sensitivity to load direction. Given that we had access to NURBS geometry, we were able to show the impact of design changes (such as thinning the discrete plates or changing weld sizes) from a mass and strength perspective.

The Future

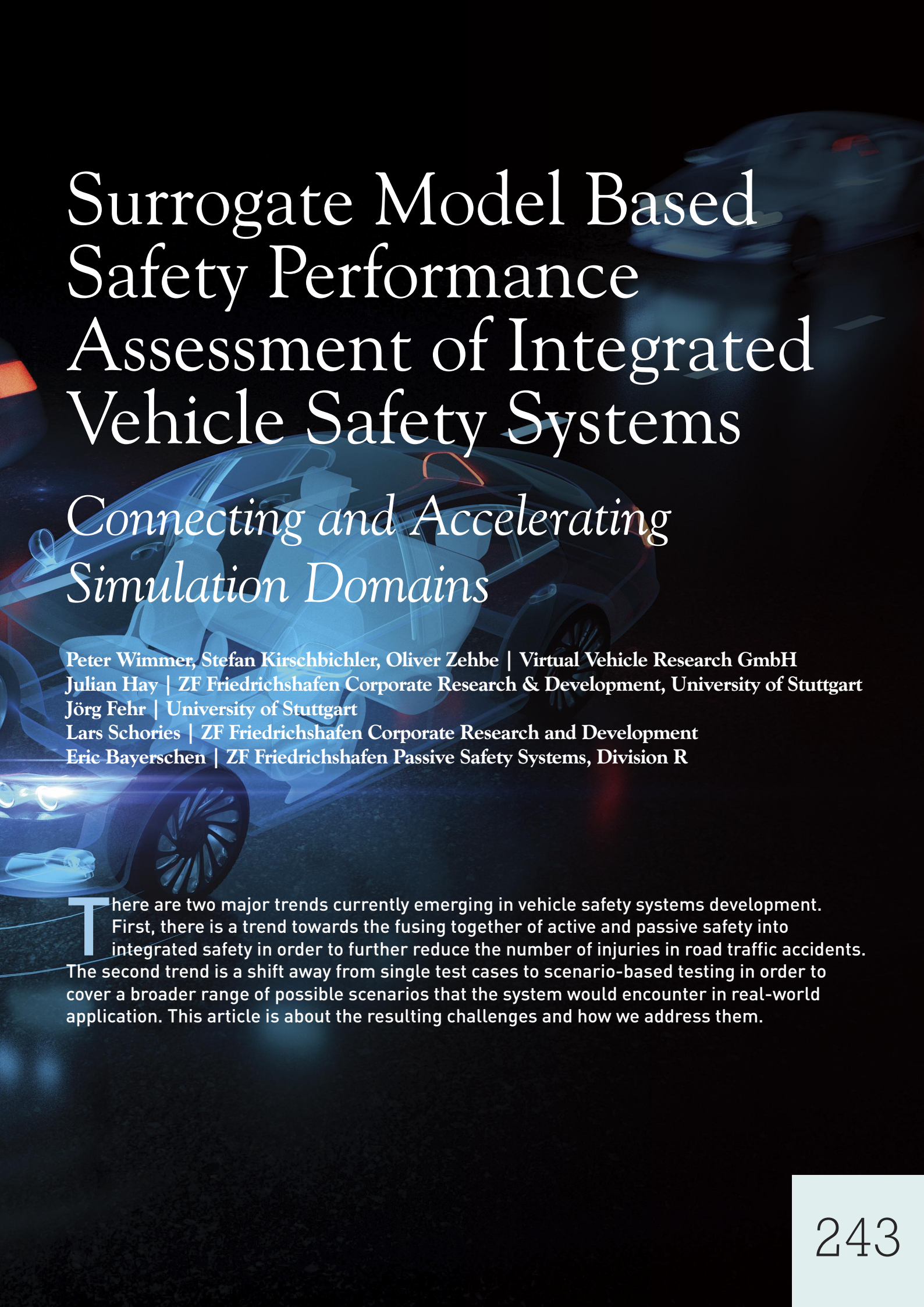
While the FEA aspects of this project were not particularly ground-breaking, the 'part to CAD to FEA' workflow was something pretty new to us. The ability to generate clean geometry in a timely manner, then witness the response, gives at least an order of magnitude of improvement in Raptor's development process. And all using contemporary software that eased the whole process and made it commercially viable.

So, what does this mean for Raptor? Well, they have a much better idea of their product's performance, where the manufacturing and performance sensitivities lie, and what they can do with their next generation of foot-pegs, whether it's looking at new bespoke geometries, manufacturing methods (including AM), or new markets. Reverse engineering has been around for a while, but the ability to use the latest optical scanning techniques, coupled with state of the art 'mesh to CAD' and FEA model generation, gives companies both large and small the edge in designing the products of tomorrow.

As I conclude this, I've noticed that 19 buses have parked up outside my house, blocked the road, and I need to get out to pick up my son, Sol, from school. Where's Travis Pastrana's bike when you need it!

Dr. Steffan Evans is a Doctor of Engineering, specialising in Multi-Parameter Structural Optimisation. A Chartered Mechanical Engineer and NAFEMS Professional Simulation Engineer (Advanced), he spent 20 Years in the Airbus/BAE Systems Supply Chain involved in Strategic FEA Development, Analysis and Verification.

Since 2016, he has been running Evotech CAE Ltd, an engineered product consultancy supporting SMEs with many aspects of CAE, FEA and Design Optimisation, partnered with MSC Software for training and technical resales. Steffan also produces and hosts online training focussed on FEA with MSC Apex.



Surrogate Model Based Safety Performance Assessment of Integrated Vehicle Safety Systems

Connecting and Accelerating Simulation Domains

Peter Wimmer, Stefan Kirschbichler, Oliver Zehbe | Virtual Vehicle Research GmbH

Julian Hay | ZF Friedrichshafen Corporate Research & Development, University of Stuttgart

Jörg Fehr | University of Stuttgart

Lars Schories | ZF Friedrichshafen Corporate Research and Development

Eric Bayerschen | ZF Friedrichshafen Passive Safety Systems, Division R

There are two major trends currently emerging in vehicle safety systems development. First, there is a trend towards the fusing together of active and passive safety into integrated safety in order to further reduce the number of injuries in road traffic accidents. The second trend is a shift away from single test cases to scenario-based testing in order to cover a broader range of possible scenarios that the system would encounter in real-world application. This article is about the resulting challenges and how we address them.

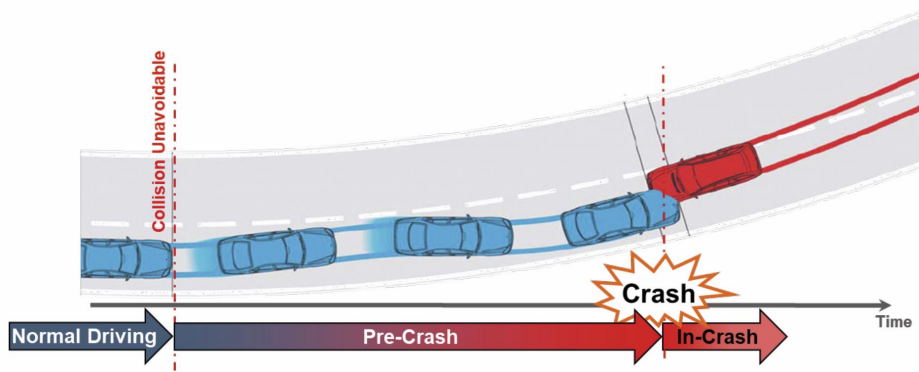


Figure 1: Phases of an accident.

Challenges

The previously described developments result in two challenges:

1. A demand for closer interaction between different, currently separate, simulation domains. This in turn requires that new methods and processes be established so that integrated safety systems can be developed and assessed accordingly. These methods and processes must cover all relevant aspects from normal driving to in-crash (Figure 1), e.g., driving dynamics, sensors, active-safety algorithms, vehicle structure deformations, restraint systems, and occupant behaviour.
2. The requirement for scenario-based assessment instead of evaluating a limited number of test cases. Scenario-based approaches are used to gain more insight in the system's performance by covering a broader area of the assumed field of application. As a safety system has to act properly in many different situations, this results in a very large number of simulation runs. Classical finite element crash simulations require considerable simulation effort to deliver precise results and are therefore not suited for such types of multiparameter analysis. Consequently, new, time-efficient methods need to be developed, which significantly reduce calculation time while still providing acceptable result prediction quality for these parts of the overall simulation method.

How we address both challenges is described in the following. Afterwards, an example shows the application of our solution.

Approaching the Challenges

Closer Interaction of Different Simulation Domains

Typically, the development of safety systems that act once a crash has occurred and systems aimed at avoiding or mitigating a crash is separate with respect to involved simulation domains and development departments. In-crash simulations usually involve high-fidelity finite element methods and models, while pre-crash simulations are more diverse with respect to the simulation methods used, as different aspects need to be considered (mechanics, electronics, software, human behaviour, ...). The first task is therefore to bring together the different domains and establish a smooth transformation from each phase to the next. To do so, we set up a framework which is shown in Figure 2. The framework interfaces are set up in a way so that the outputs of the preceding model are automatically used as initial or boundary conditions. The framework's elements are described in the following.

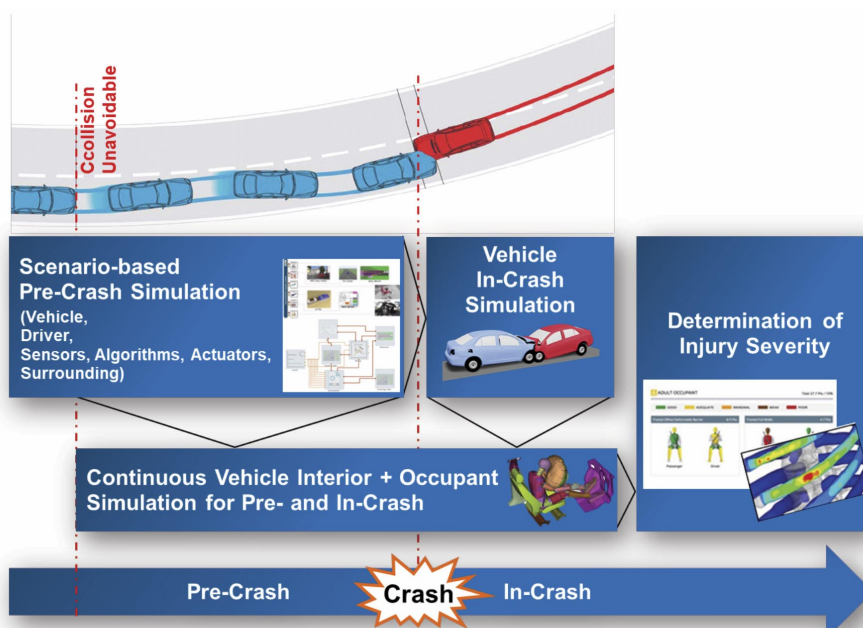


Figure 2: The simulation framework combining all relevant simulation domains for integrated safety covering a complete scenario from normal driving to in-crash.

Scenario-Based Pre-Crash Simulation

The pre-crash simulation model covers the interaction of the vehicle under test with its surroundings, from normal driving state up to the time of crash. This simulation model is set up using a co-simulation platform and it consists of several models:

- A vehicle dynamics model of the vehicle under test. This could be anything from a point-mass model to a complex multi-body system, depending on the use case and required level of detail
- A driver model controlling the motion of the vehicle under test
- A safety system model consisting of sensor, algorithm and actuator models
- A vehicle surrounding model consisting of surrounding traffic and infrastructure

This model with relatively low computational effort is subjected to various scenarios that are well distributed in the field of interest. In each simulation run, this model runs until either the critical situation is resolved by intervention of the active safety system (i.e., crash avoided), or a crash occurs. In that case, the following outputs of this model are used by the other models of the framework:

- The vehicle under test's translational and rotational accelerations as input to the vehicle interior / occupant model
- The crash configuration (vehicle positions and velocities) as input to the in-crash simulation model

Vehicle In-Crash Simulation (Structural Deformation)

The crash simulation model gets into action once a crash occurs. In that case, the crash configuration parameters (vehicle positions and velocities) are used to automatically initialise the model and start the simulation. Classical finite element explicit code is typically used for such applications. The output of this model is the translational and rotational accelerations over time during the crash. These are used as input for the vehicle interior /occupant model.

Continuous Vehicle Interior & Occupant Simulation (Pre- and In-Crash) and Determination of Injury Severity

This is the final element of the simulation framework. It consists of the vehicle interior including the restraint system(s) and a reactive occupant. The reactive occupant mimics human behaviour under low-g accelerations by, e.g., stiffening and actively trying to get back to the initial position. The occupant is loaded with the combined accelerations from pre- and in-crash. Why use the pre-crash accelerations? These determine the position of the occupant at the time of crash, and this position has an influence on resulting injury, e.g., a lateral offset of the head might result in slipping off or even missing the airbag and thus in high levels of head injury. The outputs of this model are injury criteria values (head injury criterion (HIC) and chest deflection) which then can be used to determine the resulting injury severity and injury risk.

Time Efficient Methods (Surrogate Models)

With a simulation framework that connects the different simulation domains set up, only half of the distance to the finishing line is covered: When applying this simulation framework in scenario-based assessments, a huge number of simulation runs is required. As some of the considered simulation methods are known to have long simulation times due to their high level of detail, the resulting overall simulation time is not feasible for a typical system development process. Therefore, these time-consuming simulation elements have to be replaced by faster methods which still provide a good approximation of the high-fidelity models. As a possible solution to this challenge, we used mathematical (i.e., black box) and physical (i.e., white box) surrogate models. These models enable a time-efficient safety performance assessment of combined active and passive safety systems. While these models are fast during the actual simulation, they need a prior training phase to fit the initially unknown internal parameters to the actual problem that should be approximated.

The models in our framework that need acceleration are:

- Vehicle in-crash simulation
- Interior / Occupant simulation (pre- and in-crash)

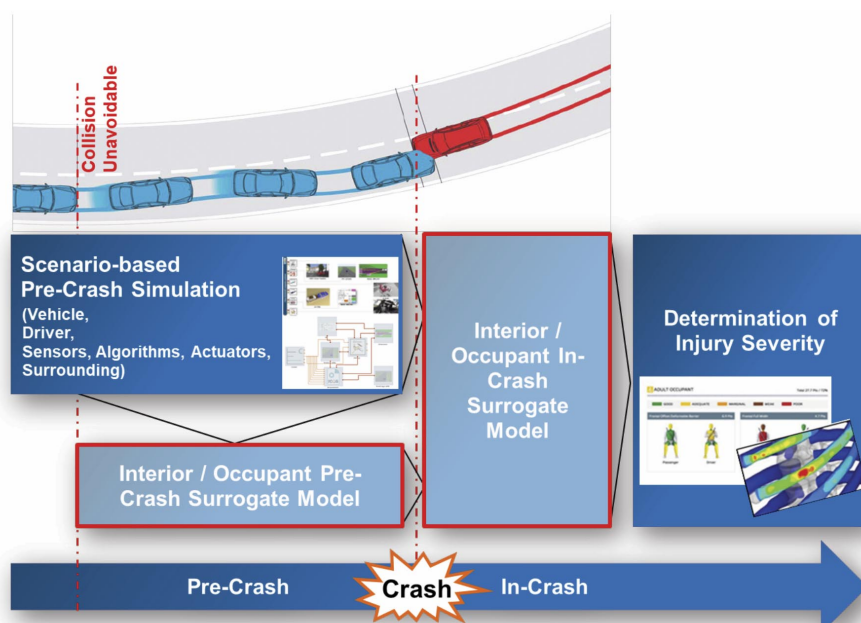


Figure 3: The modified simulation framework with surrogate models (marked red) replacing the time-consuming high-fidelity models.



Figure 4: Crash configuration parameters and their ranges.

Figure 3 shows the modified simulation framework with the surrogate models in place: The interior / occupant pre- and in-crash simulation model is split up into a surrogate model for pre-crash and a surrogate model for in-crash which also includes a crash pulse estimation replacing the vehicle in-crash simulation model.

Occupant Pre-Crash – Prediction of Occupant Pre-Crash Motion

The occupant model is split into two parts: the pre-crash part, described here and the in-crash part, described afterwards. For the pre-crash, we went for a rather simple physical model, a two-mass pendulum whose motion is restricted by the seat and the shoulder belt. This model is not capable of describing the detailed, overall posture of the occupant, it can only predict the torso and head motion under low-g loads typical for braking or steering manoeuvres. We fitted the unknown parameters of this model in a training phase using 10 typical driving manoeuvres. The output of this model is the head and the torso movement relative to the seat over time. The simulation effort of a precrash phase that would take 2 hours using a high-fidelity occupant simulation can be reduced to 5 seconds by using this surrogate model instead.

Occupant In-Crash – Prediction of Occupant Injury

For the in-crash part of the occupant a gaussian process model is used. Its inputs can be categorised into three groups:

- the crash configuration. It is described by angle, offset, and initial velocity of both vehicles, see Figure 4. By these parameters, the in-crash loading of the occupant is described.
- the occupant's head position. The respective longitudinal and lateral position at time of crash relative to the initial position are the result of the occupant's loading during the pre-crash phase.
- The restraint system configuration. 4 parameters of the restraint system were varied for a simplified demonstration of the surrogate method: Airbag time to fire, airbag vent hole diameter, belt retractor time to fire and belt retractor load limiter force.

We trained this model using 100 samples drawn from the whole parameter space. Its outputs are the same as for the high-fidelity vehicle interior & occupant (pre- and in-crash) model. The effort for the in-crash simulation can be reduced from about 21 hours when using high-fidelity vehicle and occupant models to the range of a few milliseconds by using this surrogate model instead.

Application

As a proof-of-concept, we performed an assessment of two integrated safety system variants consisting of an autonomous emergency braking (AEB) system and a standard restraint system. The simulation set consisted of 807 virtually generated accidents involving the vehicle under test and another vehicle, resulting in a head-on collision if no countermeasures were taken. We ran these 807 simulations first without any AEB system (baseline) and then with the two variants of the system. The included AEB system performs a full braking once a certain time-to-collision (TTC) threshold is reached. The TTC thresholds for the two variants are 0.9s and 0.6s.

Out of these $3 \times 807 = 2421$ pre-crash simulations, 285 resulted in crashes in all three variants (i.e., baseline, AEB0.6s and AEB0.9s). AEB0.6s was able to reduce the mean impact velocity by 11% whereas with AEB0.9s, a reduction by 24% was obtained.

As we were mainly interested in the potential to reduce injury severity, we investigated these $285 \times 3 = 855$ simulation runs further by using the pre- and in-crash surrogate occupant models. Here, we obtained a mean AIS2+ injury risk reduction by 6% for AEB0.6s and by 16% for AEB0.9s compared to the baseline (standard restraint system without any AEB pre-crash intervention). The distributions of the respective injury risks are shown in Figure 5.

As an additional benefit, the fast-calculating in-crash surrogate model developed also allows for a case-specific optimisation of the restraint system. This means that the potential for reducing the occupant injury risk can be increased even more. We did an optimisation of the restraint system parameters for each of the AEB0.9s cases. As a result, we were able to reduce the mean AIS2+ injury risk even further from originally -16% to -20%.

Wrap-up

We see a high potential in time-efficient surrogate models as part of an overall framework to enable scenario-based simulation of integrated safety systems as they are a good and efficient approximation to high-fidelity models. Prior to using them, a training phase is required, but this effort is still smaller than using the high-fidelity models instead. However, experience is required to set up the training process properly and efficiently. Here, the kind of sampling strategy and the selection of a good modelling approach is key. This is

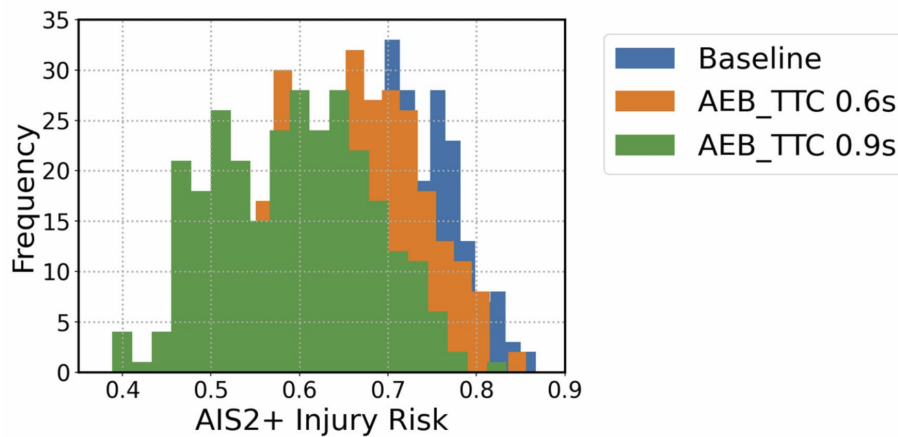


Figure 5: Distributions of the resulting injury risk probabilities for baseline and the two AEB variants.

also where we think that more research is needed, especially in the application field of vehicle safety.

Although some work still needs to be done: with this method, we can increase the prediction capability of simulation in integrated safety system development and thus make road traffic safer in the future! ■

Acknowledgements

The authors would like to acknowledge the financial support within the COMET K2 Competence Centres for Excellent Technologies from the Austrian Federal Ministry for Climate Action (BMK), the Austrian Federal

Ministry for Digital and Economic Affairs (BMDW), the Province of Styria (Dept. 12) and the Styrian Business Promotion Agency (SFG). The Austrian Research Promotion Agency (FFG) has been authorised for the programme management. They would furthermore like to express their thanks to their supporting industrial and scientific project partners.

The authors are delighted to be presenting at the NAFEMS World Congress 2021 on this topic. Their presentation will expand on some of the issues covered here, provide further insights, and give attendees the opportunity to have any of their questions answered. Find out more at nafems.org/congress

Peter Wimmer is lead researcher at Virtual Vehicle Research in Graz, Austria. He is responsible for development of numerical simulation and effectiveness assessment methods for integrated vehicle safety systems. He holds a degree in mechanical engineering and is working with numerical simulation methods since more than 20 years, both in industrial application and research context.

Julian Hay is a doctoral student at ZF Friedrichshafen AG within the Corporate Research & Development in Friedrichshafen and the Institute of Engineering and Computational Mechanics at the University of Stuttgart, Germany. He works on the development and validation of physics-based and data-driven surrogate models to accelerate vehicle safety simulations.

Stefan Kirschbichler has a degree in Mechanical Engineering and Economics of Graz University of Technology since 2008 and is the Head of Occupant and VRS Safety team at Virtual Vehicle Research in Graz, Austria. He is working in the field of biomechanics, accident research and integrated safety. He has experience in project management of several funded projects with international and national projects.

Oliver Zehbe is a senior researcher at Virtual Vehicle Research in Graz, Austria. He works in the field of occupant safety systems and human body models. He holds a degree in Automotive Systems at Technical University Berlin and also has a broad experience in the development of restraint systems for automotive OEMs.

Jörg Fehr is Professor at the Institute for Engineering and Computational Mechanics (ITM) and Cluster of Excellence Simulation Technology (SRC SimTech) at the University of Stuttgart, Germany. One goal of his current research is the development of optimal human body models for the simulation of vehicle safety systems and in the man-machine interaction as well as the speedup of the simulations using physic and data-based model reduction methods.

Lars Schories is researcher & project leader at ZF Friedrichshafen AG within the Corporate Research & Development in Friedrichshafen, Germany. He has been with ZF R&D for almost nine years and is currently working on advanced simulation methods and tools to assess and develop Integrated Safety and Vehicle Safety Functions.

Eric Bayerschen is a simulation engineer at ZF Automotive Germany GmbH, Passive Safety Systems, Division R, based in Alfdorf, Germany. He holds a Dr.-Ing. in Mechanical Engineering and works in the fields of occupant passive safety systems - & human body models simulations.



Graph and Heuristic-based Topology Optimisation of Crash-Loaded Structures: *A Successful Example of Joint Pre-Competitive Industrial Research*

Thorsten Pohl | Stellantis

Two macro trends have influenced the automotive industry in the last few years: On the one hand, there is the imperative to reduce emissions – above all, CO₂. Electrification is a key element of achieving this goal. In addition, the use of fuel cells can also help reduce the environmental footprint. Both these propulsion systems require energy storage systems – a high voltage battery or a hydrogen pressurised tank – that must be kept safe in all circumstances. Additionally, the electric motors do not necessarily have to be located in the front compartment any more as they have been in almost all standard vehicles in the case of internal combustion engines. All this has obvious implications for vehicle layouts. On the other hand, we have an increasing number of assistance systems. These are likely to have an effect on not only how occupants are arranged in the vehicle – just imagine driverless cars – but also on accident scenarios. Hence, vehicle design is currently changing more within a few years than it has changed in several decades.

The change of vehicle layouts means that the traditional layout of the structure may well not be the optimum any more, previous constraints may be gone, new constraints may be set, there is the freedom to design in different ways. Hence the concept phase of the vehicle development process becomes even more important than ever, since the biggest impact on mass and cost reduction can be achieved in these early phases. This in turn means that it is beneficial to start the utilisation of numerical optimisation procedures as early as possible.

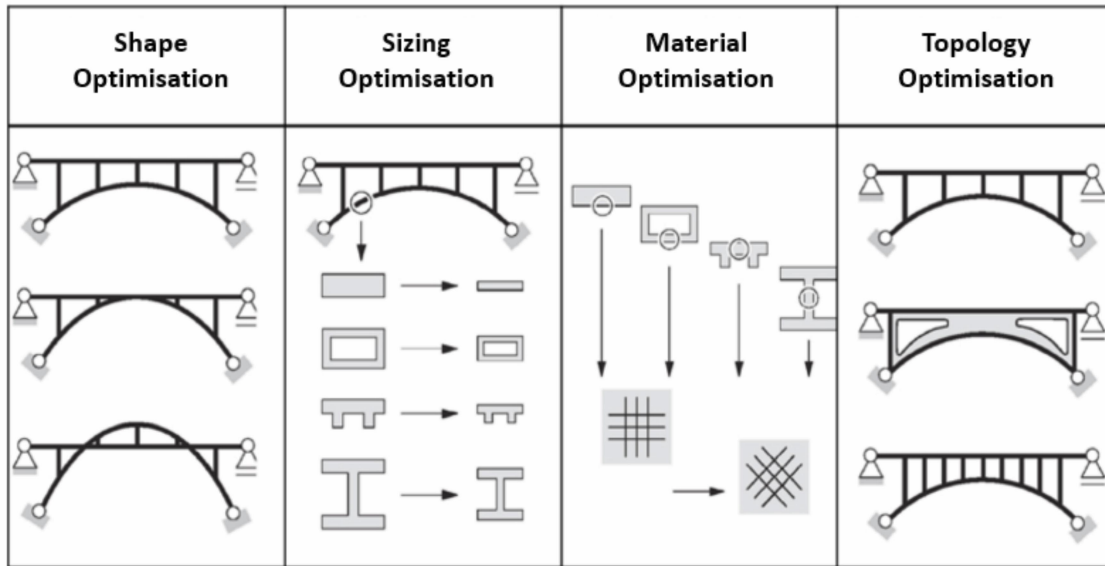


Figure 1: Types of optimisation [1].

Structural Optimisation

There are different methods for structural optimisation, starting with the optimisation of parameters such as the sheet metal thickness. Secondly, there is the shape optimisation. This may modify local and potentially small geometric features such as a radius or a hole, but also large changes such as the cross-section of a profile or the position of a structural member. Third, it is possible to optimise the material, such as fibre direction. Finally, there is the optimisation of the topology of the structure. This will determine the layout of the structure in the design space. The latter is the method that will have the biggest impact in the development of a structural concept [1].

Topology optimisation is a well-established method for linear loadcases. The design space is filled with material, and this initial structure is optimised for minimum compliance, internal elastic energy, with a given

restriction on e.g., the stiffness at a given point and volume fraction of the design space. The density of the elements filling the design space are the design variables, and so the material is distributed in this space in the optimum way.

But in the case of crash loadcases this procedure cannot be applied in the same way. Non-linearities need to be accounted for, such as non-linear material behaviour, components coming into contact in the course of the crash, buckling of structures, or the fracture of material. Hence, the use of gradient-based mathematical optimisation procedures is problematic.

Nevertheless, vehicle safety is still a very important factor, and the corresponding load cases determine the layout of the structure to a large extent. Therefore, from the point of view of the automotive industry, there is a need to have methods available to help to determine optimal structures for these non-linear load cases.



Figure 2: Linear topology optimisation: design space and remaining loadpaths [2].

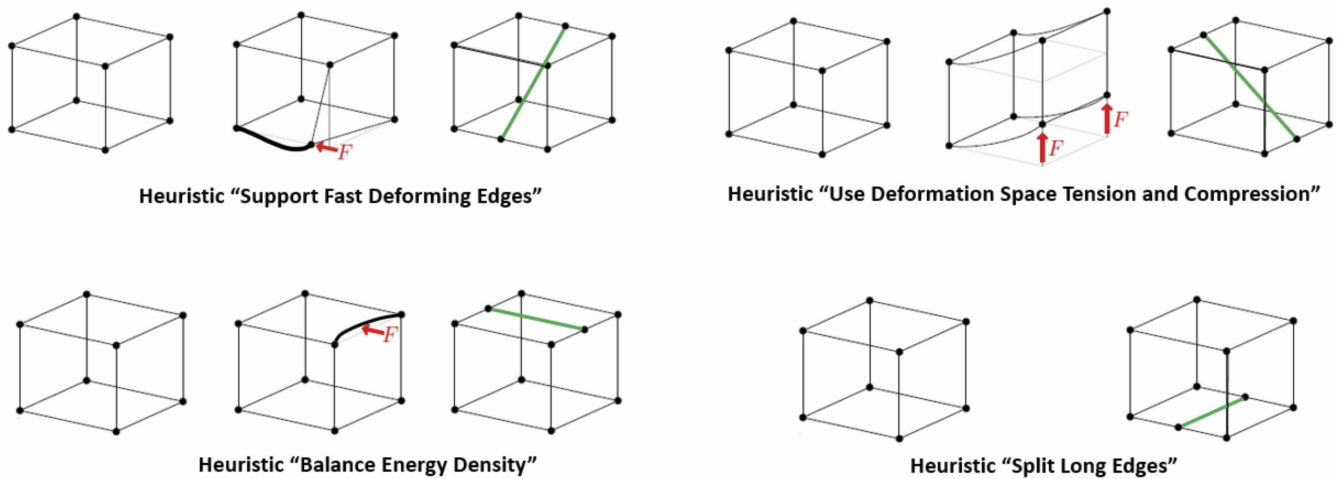


Figure 3: Heuristics for modification of the topology of the structure.

Graph- and Heuristic-based Topology Optimisation

Both the Equivalent Static Load method (ESL) [3, 4] and Hybrid Cellular Automata (HCA) [5] try to address this problem. Another approach to finding the topology of a 2D profile cross-section has been the use of heuristics, i.e., design rules [6]. The idea was born to see whether this approach would also work for 3D structures. The project group “CAE for Concept Definition” from the Research Association of Automotive Technology (FAT), which is part of the German Association of the Automotive Industry (VDA) supports and funds such joint pre-competitive research, hence a project was launched to study the feasibility of the extension of the 2D method into the 3D space. The work has been carried out by Prof. Axel Schumacher’s group at the University of Wuppertal, with participation of Ford, Porsche, Volkswagen, Opel, ZF, Benteler, and Altair [7,8].

What actually is a “heuristic”? As mentioned before, it is a design rule, based on experience and expert knowledge. Already for the development of the 2D method, vehicle safety engineers have been involved in giving their input to come up with a set of typical strategies to counteract undesirable structural behaviour in a crash event.

Several heuristics have been developed, and there are two types: on the one hand, there are competing heuristics, suggesting different ideas for how to improve the structure, as shown in figure 3. On the other, there are non-competing complementary heuristics, e.g., the scaling of part thickness, to make up for the mass of added structures, or to straighten the structure in case of unnecessary angles between edges.

The optimisation procedure is an iterative process. First, there needs to be a starting design that will be simulated in a given loadcase, e.g., a frame crashing into a rigid wall. Next, the result is examined to detect an undesirable structural response. This may be a buckling of a load-bearing member. This is a typical behaviour of slender structures under axial load but energy absorption is low. It is better to keep the structure in position in order to achieve progressive crushing, resulting in high energy absorption. This detection needs to be performed automatically. Several of the competing heuristics will be activated, as there is usually a combination of different deformation patterns. The most promising new structure will be the basis for the next iteration. Since the original and each new design may still have a potential to improve the objective without modifying the topology, a shape optimisation is performed initially and after each step. This results in a nested optimisation procedure, with an outer and an inner loop.

Since it is difficult to implement the changes of the topology – as proposed by the heuristics – directly on a finite element model, the structure is described by a graph.

What is a “graph” description? The graph contains information about the position of end points (vertex) of structural members, how they are connected (edges), and the properties of the structural members, i.e., the cross section and its orientation.

This graph description can be modified easily and is transformed into a corresponding finite element model by an internal model builder. The structure itself is represented by shell elements, the joints by rigid elements with a central node at the position of the graph

```

GRAPH; 1; TYPE (3 DGrid ); SOURCE (profilegraph); NAME (box_3D)
VERTEX; 1; TYPE ( LINK ); COORDINATES ( -100.0 , 100.0 , -100.0)
VERTEX; 2; TYPE ( LINK ); COORDINATES ( -100.0 , -100.0 , -100.0)
EDGE; 1; VERTICES (1, 2); TYPE (ExtrudedProfile, square1); LENGTH(10.0, 10.0) ; ORIENTATIONVECTOR(1.0 , 1.0 , 0.0)

```

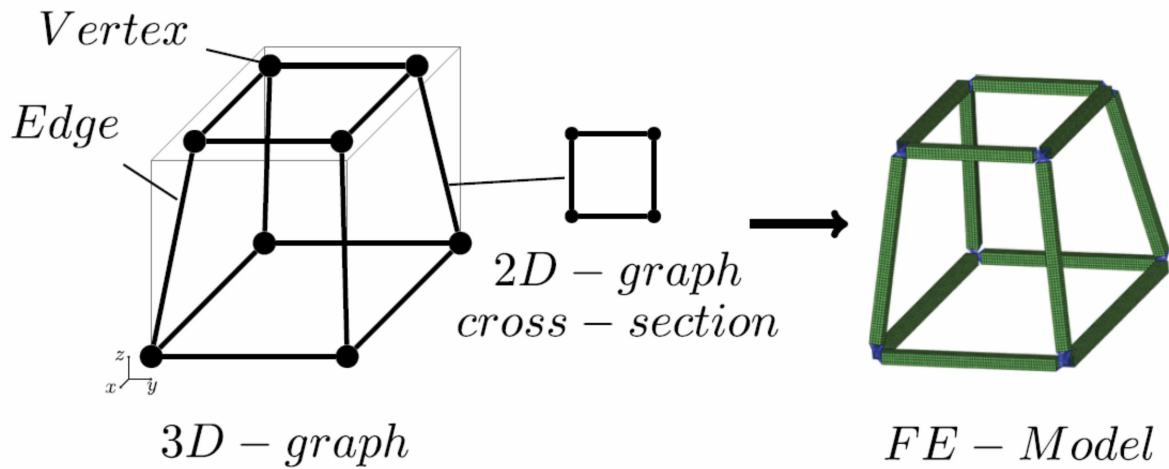


Figure 4: Graph Syntax, Graph Representation and derived Finite Element Model.

vertex (Figure 4). Geometric constraints, representing manufacturing constraints, can be checked as well based on the graph. If the angle between members is too small, the design is marked as invalid. Symmetry can be imposed as well. The crash simulation itself is performed using the LS-Dyna code.

In parallel, Altair showed that it is possible to use Radioss crushable frame spring elements to represent the structure. These are a more simplified representation of the geometry given by the graph, but with the advantage of faster simulation times – an important factor for optimisation procedures.

Applications

This new method has been applied to two loadcases, to validate that the new method works as expected.

The first example was the optimisation of a cubic frame with members at the edges and one fixed side impacted by a pole from below. The optimisation objective was to minimise the intrusion, with the mass of the structure remaining constant. The area inside the initial frame is the design space where additional structures can be created. Initially, there was a large parallelogram type deformation, with an intrusion of 174mm. From the outset the shape optimisation was able to reduce this to 30.5mm. The subsequent application of heuristics resulted in a further reduction, such that the final value was 19.7mm. The subsequent shape optimisation resulted in an additional 5.1mm reduction of the deformation, such that the optimised structure showed 15.6mm of intrusion at the same mass as the original design (Figure 5). The models with the crushable frame springs were giving a similar topology, with one member less near the fixation of the structure, and slightly higher overall intrusions (24.6mm).

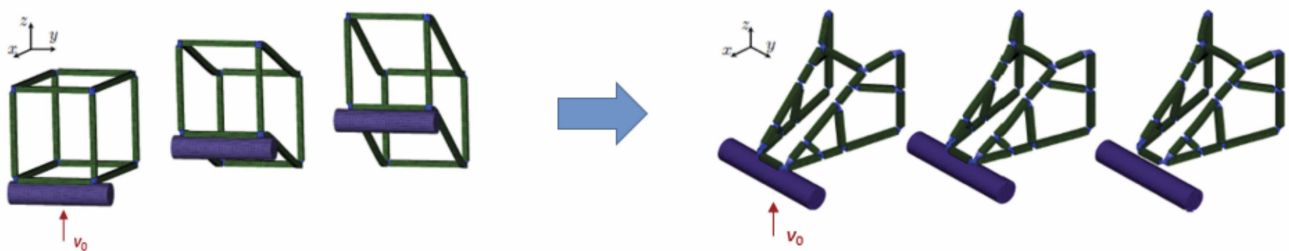


Figure 5: Deformation of initial and optimised structure, at $t_0 = 0\text{ms}$, $T = 15\text{ms}$ and $t = 30\text{ms}$ [7].

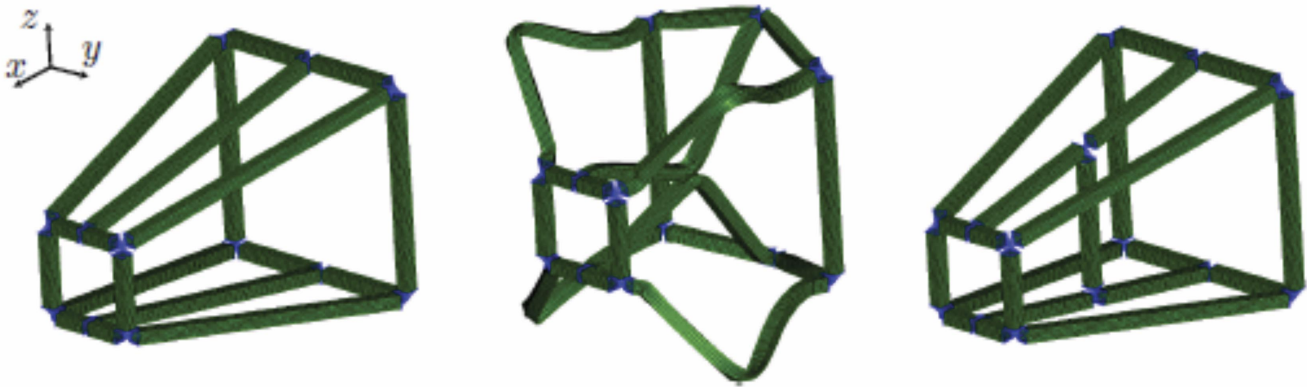


Figure 6: Impact of rigid wall, step from iteration 1 (undeformed and deformed state left and centre) to iteration 2, heuristic “support fast deforming edges” to remediate the buckling of the two middle beams [7].

The same loadcase was optimised but with a different objective – to minimise the contact force between the structure and the cylinder, with a restriction of the maximum intrusion. The force of the initial design was 10kN, and after seven heuristic and the initial and final shape optimisation this was reduced to 5.4kN.

In a second loadcase, the same initial structure was impacted by a rigid wall of 65kg and a velocity of 32 km/h. The first optimisation target was again to minimise the intrusion. The initial shape optimisation reduced the intrusion from 210mm to 116.5mm. The application of heuristics resulted in a further reduction to 45.7mm. The effect of the heuristics was even larger than in the first example. The final shape optimisation resulted in a further reduction by only 1.6mm. Figure 6 shows an intermediate step to indicate how the heuristics are applied in the process.

As before, the reduction of contact force was a second optimisation objective. The maximum allowed intrusion was again 150mm. After the initial shape optimisation,

the contact force was reduced from 89.8kN to 76.4kN. The application of heuristics brought this value down to 53kN, with a final shape optimisation giving a contact force of 30.8kN.

Conclusions

The successful optimisation of the structure in the above loadcases shows that this new method – the utilisation of heuristics in an optimisation procedure – has the potential to help to find better structural layouts for new vehicle concepts for the highly non-linear crash loadcases. A second project has been started, supported by FAT and funded by the German Ministry of Economy via the ‘Arbeitsgemeinschaft industrieller Forschungseinrichtungen’ (AiF), to turn this feasibility study into a process that can be applied in industrial contexts. It will seek to find additional heuristics especially for the three-dimensional case, to include additional constraints and features in the graph description, and to produce improved finite element representations. ■

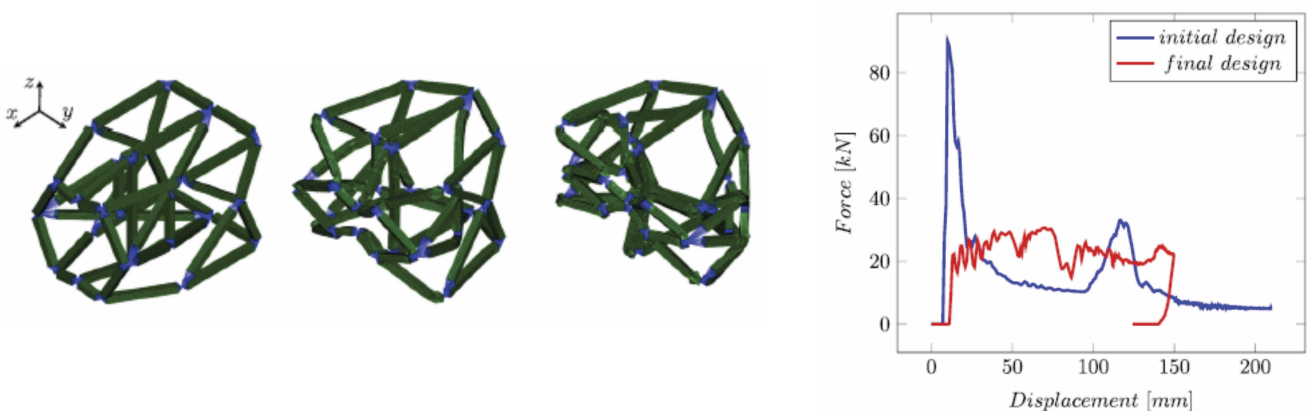


Figure 7: Structure optimised for minimum contact force at $t_0 = 0$ ms, $t = 10$ ms and $t = 40$ ms, and contact force vs. time for initial and final design [7].

Acknowledgements

On behalf of the project group, thanks go to Prof. Dr Axel Schumacher, Florian Beyer, Dominik Schneider and Miriam Kick of the Bergische Universität Wuppertal for performing this work. A thank you is also directed to the research organisation, FAT, of the German Association of the Automotive Industry (VDA) for funding the work, and in particular to the working group AK27 "Simulation Methods and Virtual Validation" as well as to the other members of the project advisory board for fruitful discussions and support:

- Dr. Axel Hänschke (ehem. Ford Werke GmbH, jetzt CPS-Consulting),
- Jens Menzen (Ford Werke GmbH),
- Tobias Duffe (Ford Werke GmbH),
- Dr. Stefan Schwarz (Porsche AG),
- Prof. Lothar Harzheim (Opel Automobile GmbH),
- Dr. Andreas Hillebrand (Volkswagen AG),
- Mathias Brass (Volkswagen Osnabrück),
- Bernd Scholz (ZF Group),
- Dr. Christian Buse (Benteler International AG) und
- Dr. Lars Fredriksson (Altair Engineering GmbH).

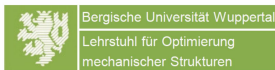


Figure 8: Participating Organisations

References

- [1] A. Schumacher, *Optimization of mechanical structures*, 3rd edition, Berlin Heidelberg New York: Springer (In German), 2020.
- [2] J. Siegmann, "Lightweight Body Design by Consequent Use of Optimization Techniques," 9th European Altair Technology Conference, Frankenthal, Germany, June 26-28, 2017.
- [3] W.S. Choi and G.J. Park, "Structural Optimization using Equivalent Static Loads at all the Time Intervals," *Comput. Methods Appl. Mech. Eng.*, Vol 191, no.19-20, pp. 2105-2122, 2002.
- [4] J. Triller, R. Immel, A. Timmer, and L. Harzheim, "The difference-based equivalent static load method: an improvement of the ESL method's nonlinear approximation quality," *Struct. Multidiscip. Optim.*, Vol. 63, pp. 2705-2720, 2021.
- [5] N.M. Patel, J.E. Renaud, and A. Tovar, "Crashworthiness Design Using Topology Optimization," *ASME. J. of Mech. Design.*, Vol. 132, No.6, 2009.
- [6] C. Ortmann and A. Schumacher, "Mathematical Description and Algorithmization of Expert Knowledge for the Support of the Topology Optimization of Crashworthiness Structures," *PAMM Proc. Appl. Math. Mech.* Vol.14, no.1, pp 1023-1026, 2014.
- [7] F. Beyer and A. Schumacher, "Investigation of the possible uses of graph- and heuristic-based topology optimization for the development of 3D frame structures in crash load cases" (In German) FAT-Series 329, 2020.
- [8] F. Beyer, D. Schneider, and A. Schumacher, "Finding three-dimensional layouts for crashworthiness load cases using the graph and heuristic based topology optimization," *Struct. Multidisc. Optim.* Vol. 63, pp. 59-73, 2021.

Thorsten Pohl holds a Master of Engineering degree in Aeronautics of Imperial College London, and has been working in vehicle CAE at Opel for almost 24 years, initially as part of GM, then of Groupe PSA and now within Stellantis. After being responsible for generation and management of the finite element full vehicle models for safety, structures and NVH, he currently is responsible for CAE strategies and the integration of CAE activities into the overall development process. He is speaker of the project group "CAE for Concept Definition" in the FAT working group AK27 "Simulation Methods and Virtual Validation", and is also involved in Simulation Data Management.

Integration of Driving Physical Properties into the Development of a Virtual Test Field for Highly Automated Vehicle Systems

René Degen, Harry Ott | Cologne University of Applied Sciences & Uppsala University
Fabian Overath, Margot Ruschitzka | Cologne University of Applied Sciences
Florian Klein | Hoersch und Hennrich Architekten GbR
Christian Schyr | AVL Deutschland GmbH
Mats Leijon | Uppsala University

Winner of 'Best Academic Paper' at the NAFEMS World Congress 2021

Advanced Driver Assistance Systems/Autonomous Driving (ADAS/AD) are becoming more and more important in the automotive industry. It is expected, that automated vehicles will provide promising advantages in transportation and mobility [1]. In 2019, 48% of all new cars sold in Germany were equipped with a lane keeping assistant, 39% had an autonomous emergency brake and 38% were delivered with an adaptive cruise control [2]. In 2020 90% of German car drivers were of the opinion that ADAS increased vehicle safety and 89% thought assistance systems make driving more pleasant [3]. Although the data refers to the German market, a similar result can be expected internationally. This leads to the expectation that the market for ADAS will continue to grow in the future. Besides the opportunities ADAS offer for vehicle safety, they also increase vehicle complexity and the testing effort.

In Germany, the Federal Ministry of Transport and Digital Infrastructure (BMVI) creates the legal framework for automated driving functionalities on public roads. On 28th July 2021, a new law was published, which legalizes level 4 functionalities on defined public roads in regular traffic [4].

This article presents a novel approach for combining a highly realistic virtual urban environment with traffic participants, including motion realistic persons, and physically correct models of the vehicle and its sensors.

In Figure 1 the model-structure is shown.

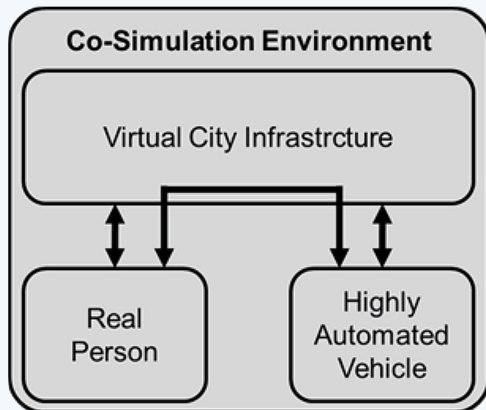


Figure 1: Schematic illustration of the overall model structure.

Virtual Testbed

The accurate simulation of complex inner-city scenarios is an important issue in current automotive research activities. Hence, the following section will introduce an innovative virtual urban traffic environment. The goal is the realistic simulation of complex urban traffic scenarios, taking into account the interactions of automated vehicles, pedestrians, and other road participants. Figure 2 shows the general structure of the used and implemented model network. The core of the research environment is a highly authentic and visually realistic, georeferenced virtual reality city scene. To enable the mentioned interactions, the model is augmented by two sub models; a dynamic pedestrian avatar model steered by real-time network motion capturing, and a vehicle model which includes a physically correct dynamic model and three sensor models. The vehicle avatar serves as an interface to implement real vehicle functions into the scene. Its implementation is done in a closed loop communication between MATLAB and the Virtual Reality engine via network communication. Finally, three sensor models, implemented in the virtual City Model, aim to simulate the surrounding data recognized by the vehicle's sensors.

The visualization and potential further processing of the Radar and Lidar datasets takes place in MATLAB. The camera data is evaluated by an Artificial-Intelligent based object detection algorithm. The data transmission is done by network protocol again. The aim is not only to simulate

the data in a highly realistic way, but also to create a decentralized structure that makes it possible to test complex scenarios independent of the location.

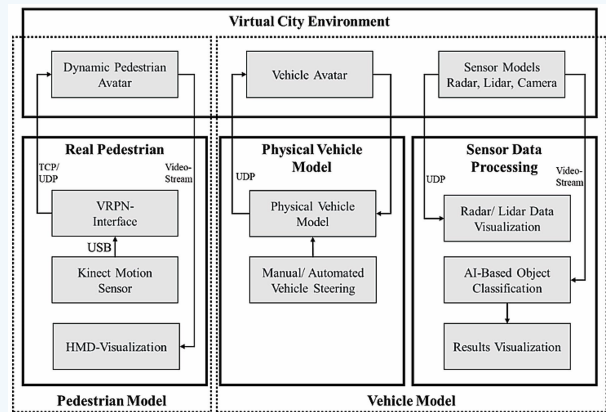


Figure 2: Scheme of the urban traffic model network.

a. Virtual City Environment

The first segment of the virtual testbed is the virtual city environment. The environment is not only characterized as the geometric representation of the virtual inner-city scene, it also serves as an interface for the model network to be implemented, as shown in Figure 2. Due to that, there are some important requirements for the implementation of the city environment. On the one hand, it needs to be optically as realistic as possible, to enable an authentic simulation on the vision-based sensors. On the other hand, it needs to be augmented by further metadata for other environmental sensors like radar and lidar. Furthermore, it needs to enable the implementation of avatars for the test vehicle and the real pedestrian subject, including the necessary network interfaces. Since the implementation of the city model is relatively complex, the development environment must be versatile and universally linkable.

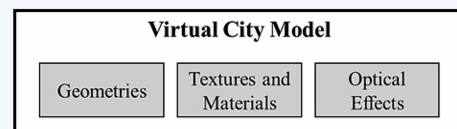


Figure 3: Structure of the virtual city environment.

As shown in Figure 3 the virtual city model can be divided into three sub categories. The geometries provide all necessary physical structures of the buildings, streets, and street furniture. Since these models are colourless, the textures and materials enable a realistic optical representation by applying colours, textures and further surface data to the objects' shells. Finally, additional optical effects provide an accurate overall impression for the virtual interurban scene. The geometric virtual city model is based on so-called GIS Data. These are data used by geo information systems, containing rasterized information like infrastructures, land usages, administrative areas, terrain topography, building data or imagery. It is obvious that not all information provided by

GIS datasets is essential. Due to this, the first processing step is the analysis and filtering of these datasets. The result of this first step is a geo referred geometric representation of the city environment. In the next step, these results are reconditioned to be usable within the gaming engine, using third party tools. An example of a processed building with simplified geometries is provided in Figure 4.

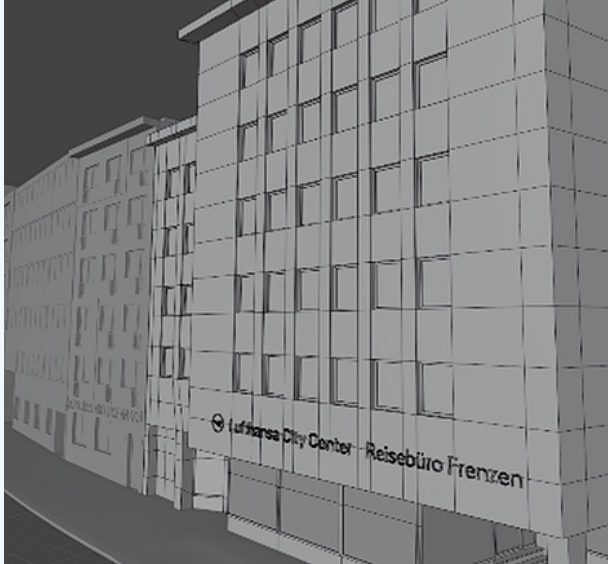


Figure 4: Reconditioned building within 3DSMax.

Besides the city itself, the street furniture is an important part in the urban appearance. Objects like post-boxes, bins, newspaper vending machines, and advertising columns shape the image of the cities. The creation of these objects is done by hand, according to the original objects. Within the Unreal Engine, all street furniture and additional objects are multiplied as often as necessary and placed to fit the appearance of the real environment. The result is an accurate but still uncoloured representation of the real environment, as visualized in Figure 5.



Figure 5: Uncoloured city scene.

To enable the optically realistic representation of the scenario, the next step is the texturing of the imported geometries. Depending on the respective object's appearance, two general texturing methods are distinguished. For surfaces with simple repeating textures, materials are applied to the whole surface. These are either taken from pre-defined material libraries, or

created by hand. For objects with more complex appearances, pictures of the real role model serve as a reference. These images are edited, rectified and then applied to the virtual surfaces.



Figure 6: Comparison of textured objects, real and virtual.

An example of that is provided in Figure 6. The left-hand side provides a picture of the real object that serves as a reference; the right-hand side shows the virtual object for this reference. Hence, it is now possible to visualize the virtual city scene corresponding to the real environment. However, the implementation of the static pedestrian dummies that are used within the scene is different. These dummies are created using a 3D scanning process. This process directly creates the textures, so that the objects can be imported including the associated appearance.

Finally, optical effects are used to illuminate the virtual environment in a realistic way. Different light sources are used, depending on the lighting situation. For example, on a bright day the light from the sun serves as the main light source, at night, the vehicles headlights, the street lights and even illuminated billboards serve as light sources. Additionally, influences like dust, fog or rain can be simulated. This makes it possible to recreate critical lighting situations for the detection of objects with camera-based sensors. An example of that is provided in Figure 7.



Figure 7: Critical lighting situation with low sun and dust.

b. Dynamic Pedestrian Model

As shown in Figure 2, the real human vehicle participant is integrated bidirectionally into the virtual testing environment. Its biomechanical behaviour is detected by motion capturing hardware and integrated into the scene in real-time. Additionally, the participant is able to interact with the virtual scene by using a head mounted display. This way a bidirectional interaction is possible.

For the first methodical approach, the Microsoft Kinect for Windows is used. It uses an optical tracking system with an infrared laser emitting a pattern of dots, a monochrome CMOS infrared sensor to capture the dot pattern and an RGB camera to capture the environment. Based on the deformation of the infrared dots in the environment a depth image is created from the environment 30 times per second by the sensor. Next the Kinect focusses on moving objects and evaluates these pixel-by-pixel to identify parts of the human body [5]. Finally, a skeleton is fitted into the recognized human body, which consists of 20 body joints as shown in Figure 8. Per body joint the position and rotation in quaternions are determined.

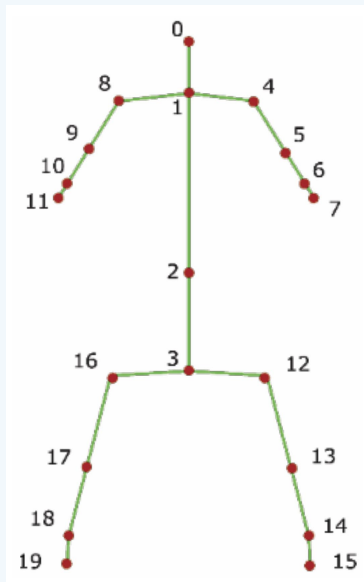


Figure 8: Kinect for Windows skeleton.

To forward the data of the Kinect in real-time, the virtual reality peripheral network (VRPN) is used [6]. Therefore, a VRPN Server connects directly with the Kinect via USB. The VRPN standardizes the data received as one person is called a tracker and all 20 body joints are called sensors within this tracker with their respective sensor number and data. The data is then received by the VRPN-Client and directly forwarded further to the Unreal Engine to be used in the dynamic pedestrian avatar.

As motion capturing data is received multiple times per second and data packages are latency critical, an unreliable UDP connection is used for sending motion capturing data. For establishing a reliable connection and

sending status messages between the instances where latency is not that critical, a separate TCP connection is used.

To realize the dynamic pedestrian avatar inside the virtual city environment mesh models with an inherited skeleton are used to display the movements of the tracked pedestrian in real life. Depending on the avatar's skeleton, the Kinect skeleton can be directly applied or an additional assignment of the body joints has to be done. In order to keep the proportions of the character independent from the tracked subject only rotations are applied to the avatar's skeleton. The position is realized via the hip-centre bone (index 3). Additionally, the avatar's feet are automatically calibrated to the ground of the digital environment respecting its topology. As shown in Figure 9, for the first methodical approach and testing, the default Unreal mannequin is used to display the movement of the real pedestrian.

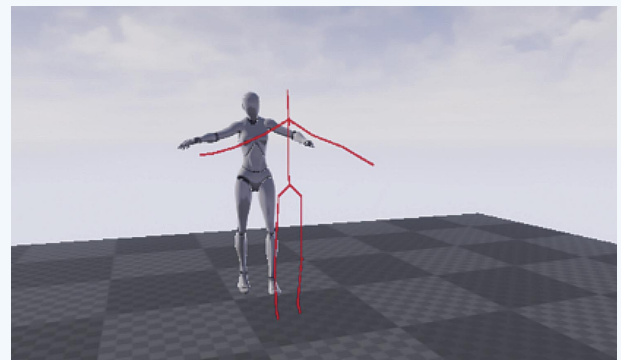


Figure 9: Dynamic pedestrian avatar.

c. Vehicle Model

The vehicle model serves as an interface for the implementation of real vehicles and driving functions into the virtual reality. At this point of development, it consists of four sub models. A physical vehicle dynamics and driver model executed in Matlab enables the accurate steering of the artificial vehicle within the virtual reality either manual or automated. Additionally, three sensor models simulate the data of a Lidar, a Radar and a camera based environmental within the virtual scene.

These sub models are introduced in the following sections.

i. Physical vehicle dynamics and driver model

To implement a vehicle in the virtual environment accurately, it is necessary to simulate the influences of the vehicle dynamics depending on the scene's environmental influences in a realistic way. Since the model needs to run in real-time, it is important to find a complexity level that represents the car's movements to a sufficient accuracy, without taking too much computation resources. Most Virtual Reality development engines do not aim to implement physical simulation models. Therefore, the model is built in MATLAB Simulink. It is composed of different sub models, as shown in Figure 10.

The vehicle's vertical dynamics are simulated using a multibody system. Five bodies represent the vehicle's main masses, consisting of the bodywork and the four wheels. The stimulation of the system is done at the wheels' foot points. This allows the interaction of the model and the virtual city environment, depending on the topography of the scenery. A double track model simulates the lateral dynamics of the vehicle. Additional models represent the drivetrain and the slip angle dependency of the tires as well as environmental influences like rolling, air and gradient resistances.

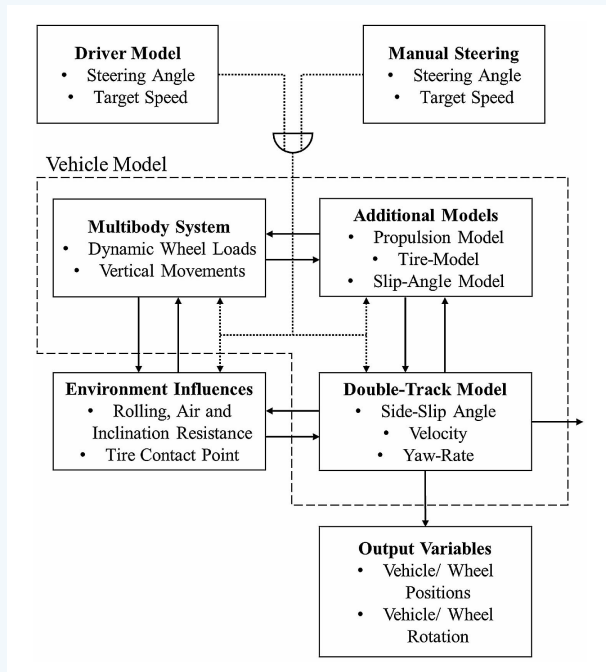


Figure 10: Vehicle model with sub models and steering input.

The steering of the model can either be done manually by a user input or automated by a driver model. The automated model uses pre-defined spline paths, created in the virtual city environment and exported to MATLAB. The implemented path following algorithm bases on a pure pursuit controller, as described by Samuel et al. [7]. It controls the vehicle's steering input by following look ahead points in front of the car lying on the defined spline path.

As already mentioned, the implementation of the vehicle model takes place in MATLAB. Corresponding to Figure 2, a representation of the car in the virtual city environment is needed. Hence, a vehicle avatar is implemented in the Unreal Engine. As the physical model, it consists of five bodies. The UDP protocol is used for communication between the two models. To set the vehicle's transformation at the beginning of each computation frame in the Unreal Engine, the positions of the five bodies, received from MATLAB, are used. After that, a so-called line trace is done, to get the height coordinates of the wheel contact patches. This data is sent back to the vehicle model frequently. Thus, a closed control loop is implemented.

ii. 2.3.2. Lidar Model

An environmental sensor that is often used in modern vehicles with ADAS systems is the Lidar. The technology uses laser beams to scan the surroundings. Multiple beams are sent either one after another or at the same time. Since the following model aims to simulate the physical properties of a Lidar, the scanning principle is not relevant for further considerations. It is only important that a possibility be provided to control the shape and resolution of the Lidar field. For each sent Laser beam the time the light takes to travel to the target object and back to the sensor is determined. According to Winner et al. [8], this can be used to compute the distance as described in Equation 1.

$$d = \frac{c_0 \cdot t_{of}}{2} \quad (1)$$

In this equation, c_0 represents the speed of light, t_{of} is the duration of light travel and d is the distance to the target object. Since it is not possible to simulate the speed of light in a virtual environment, a substitution model is needed. For that, linetraces or raytraces offer an opportunity to model the laser beams. If a ray hits an object within the scene, the impact location and additional data are returned in a structure. To enable the coverage of the field in front of a car corresponding to a real sensor, the field in front of the virtual car is scanned at every simulation step. The azimuth and the elevation angle define the area of interest. For the discretization of the field, the angular resolution of the sensor in the respective direction is used. With that, the complete azimuth range gets scanned, as shown in Figure 11. Then the elevation angle is incremented and the azimuth angle is scanned again, until the whole field is covered.

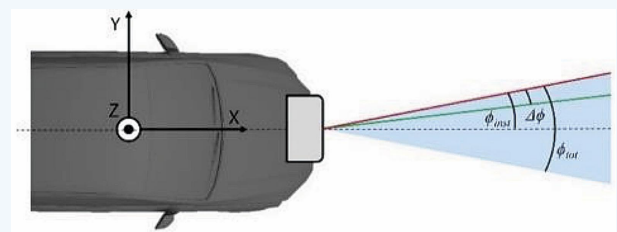


Figure 11: Discret scanning of the Lidar field.

If a ray hits an object, an algorithm is executed, computing the relevant data of the Lidar recognition. The aim is to determine whether a point is detected by the Lidar. An important value for this decision is the signal to noise ratio (SNR), as defined in Equation 2.

$$SNR = \frac{P_r}{P_n} \quad (2)$$

Here P_r represents the power received from the Lidar and P_n is the sum of the induced noise powers. The higher the SNR value, the greater the probability of detection. In accordance with Winner et al. [8], Kim et al. [9], and

Kernhof *et al.* [10] and through additional adaptations and assumptions the fraction of the received power can be expressed by Equation 3.

$$P_r = \frac{\rho_t \cdot A_r \cdot \tau^2 \cdot P_t \cdot \eta_{sys} \cdot \cos(\theta_i)}{Q_V \cdot \pi \cdot d^3} \quad (3)$$

In this equation, ρ_t is the reflectance coefficient of the target object; A_r represents the receiving lens area; τ stands for the atmospheric transmission coefficient; η_{sys} are the summarized system losses; θ_i is the incidence angle of the light beam on the objects surface and Q_V stands for the divergence of the shot beam. For the implementation of this equation into the virtual reality, most of the parameters can be passed as variables. Only the incidence angle and the targets distance are dependent on the linetraces. The distance can directly be read out of the linetrace results, the incidence angle can be computed by equation 4 using the incidence vector \underline{i} and the surface normal \underline{n} at the impact point.

$$\theta_i = \cos^{-1} \left(\frac{|\underline{i} \circ \underline{n}|}{|\underline{i}| \cdot |\underline{n}|} \right) \quad (4)$$

Besides the received power, the noise powers acting on the Lidars receiving systems need to be determined. They are mainly composed of the sun induced noise and the dark current noise. The sun induced noise is generated by sunlight illuminating the target's surface and impinging the sensor. Equation 5, according to Kim *et al.* [9], can compute the power of this noise source.

$$P_{sun} = E_{Si} \cdot B_\lambda \cdot \rho_t \cdot A_r \cdot \tau \cdot IFOV^2 \cdot \eta_{sys} \quad (5)$$

E_{Si} represents the illumination intensity of the sunlight, B_λ is the electromagnetic bandwidth of the receiving unit and $IFOV$ is the instantaneous field of view. Thermal effects of the photo element generate the dark current noise. For the computations of this noise, Equation 6 is used.

$$P_{DK} = \frac{I_D}{\mathfrak{R}_{max}} \quad (6)$$

Here, I_D stands for the dark current and \mathfrak{R}_{max} represents the maximum sensitivity of the photo element. Both parameters can usually be found in the datasheets of photo elements. With that, it is now possible to compute the signal to noise ratio and make a decision whether a point gets recognized or not. Hence, on every simulation step a point cloud with metadata like the SNR-value and the determined powers is generated. However, it is problematic that the coordinates of captured points are shown as perfectly accurate values. Real Lidar sensors have a limited resolution due to the time- capturing system, amplifications, and analog to digital conversions [10]. Since commercial sensors differ in capturing

technologies and used hardware, it is not feasible to model these inadequacies accurately. Instead, the influence of the acting inadequacies is displayed. In the given case, this is done by multiplying the resolution, provided by most sensor manufacturers, with a white Gaussian noise and adding the result to the distance value.

Therefore, all relevant data is known and ready for further processing. To enable this, the values are stored in arrays and sent to MATLAB by an UDP communication. To generate a practical reference, the sensor is parametrized according to the *Valeo SCALA 3D Laser Scanner*, a commercial serial product. The determined values are mainly taken from the sensor's datasheet [11]. All missing values are adopted from the datasheet of a typical photodiode [12] and the works of Weber, [13] and Kim, *et al.* [9]. The environmental parameters like the atmospheric transmission coefficient or the irradiance of the sun are set dynamically within the virtual scene, depending on the particular study.

iii. 2.3.3. Probabilistic Radar Model

Radar sensors are commonly used in applications for autonomous driver assistance Systems, since they are comparatively cheap, they provide a large detection distance and are resistant against environmental influences. The literature provides different approaches for the modelling of Radar sensors. The virtual testbed aims to simulate all necessary environmental data for the interaction of autonomous vehicles and driving functions with pedestrians in real time. Hence, a probabilistic radar model is used. It provides all relevant data in an object list and simulates the phenomena of the radar technology, without performing a full physical simulation.

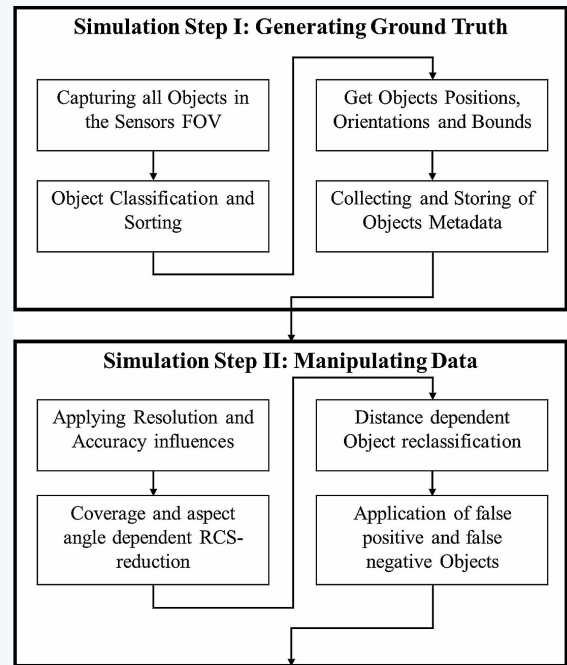


Figure 12: Overview of the probabilistic radar model execution.

The implemented model is largely based on the probabilistic radar model presented by Muckenhuber et al. [14] and is extended by several assumptions. To represent the model as realistically as possible, the real commercially used radar sensor Continental ARS 408 serves as a reference [15]. The execution of the model takes place in two steps, as shown in Figure 12. In a first step, the so-called Ground Truth Data needs to be generated. This is a dataset, containing all possibly detectable Objects in the sensor's field of view and the corresponding metadata without any errors or inaccuracies. After the perfect data is generated, the second execution step manipulates the dataset with respect to measurement errors, resolutions and inaccuracies. Hence, the phenomena of the sensor are mapped.

To generate the Ground Truth all relevant objects lying in the detection area of the sensor need to be captured. The datasheet of the sensor provides the sensing areas displayed in Figure 13.

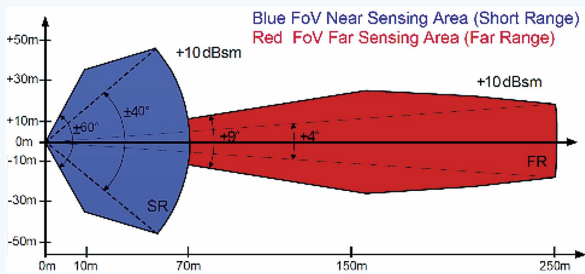


Figure 13: Sensing areas of the Continental ARS 408 [15].

Since the current research illustrates the interaction of traffic participants in inner-city environments, only the displayed near sensing area needs to be modeled. As with the previous described Lidar model, Linetraces will be used to get the relevant objects, similar to Figure 11. However, at this point, it is not important to get the data of the trace itself, instead, the objects are passed to an array if they are hit the first time. The angular resolution of the Linetracing needs to be much higher than at the Lidar model to avoid omitting any objects. Moreover, the detection range of the Sensor is not constant over the azimuth angle. Hence, a case distinction is implemented. In the azimuth range of $\pm 40^\circ$, the tracing length is set to a distance of 70 m. For the range between 40° and 60° a simple approach based on linear equations is used to get the tracing length depending on the azimuth angle. Since not all objects are relevant for the virtual sensor, the next step is the classification and sorting of the objects. Table 1 provides the types of objects for the classification.

Table 1: Object classifications for the probabilistic radar model

Type	Index	Color
Car	1	Cyan
Truck	2	Blue
Pedestrian	3	Red
Motorcycle	4	Yellow
Bicycle	5	Green
Unknown	6	Magenta

Based on that, all relevant actors within the virtual scene are augmented by a tag. These tags are detected if the actor is hit. Additionally, a color is assigned to each class for visualization purposes. The positions and the orientations are provided in global coordinates and thus need to be converted into the local sensor's coordinate system. Besides the positions and orientations, the bounds or bounding boxes of the recognized actors are relevant for further processing. If an actor only consists of one geometry, like a pillar, or a bin, the bounds can directly be read out. If the actor contains more geometries, like a car, consisting of a body and tires, or a bicycle, the bounds need to be computed.

Finally, only the ideal maximum radar cross sections (RCS) are missing for the recognized objects. This value gives an indication of how large the proportion of the reflected radiation energy is, that impinges on an object. In further processing steps the RCS value can be used to make a decision if an object is recognized. As the objects index, the value is predefined in tags for each relevant actor within the scene. Since the value fluctuates depending on the aspect angle, the predefined value provides the maximum possible radar cross section. Previous works such as Degen, et al. [16] show the general possibility to simulate a radar cross-section within a virtual reality engine. However, the paper also offers issues in real-time performance. Due to that, the current probabilistic model uses a predefined RCS for every object and manipulates it to get a realistic value.

If a probabilistic model is to be created from the data, the executions visualized in step II of Figure 12 need to be done. The physical phenomena of the sensor are replicated without simulating its full physics. At first, the influences of the sensor's resolution and accuracy are applied to the ground truth signal as displayed in Figure 14.

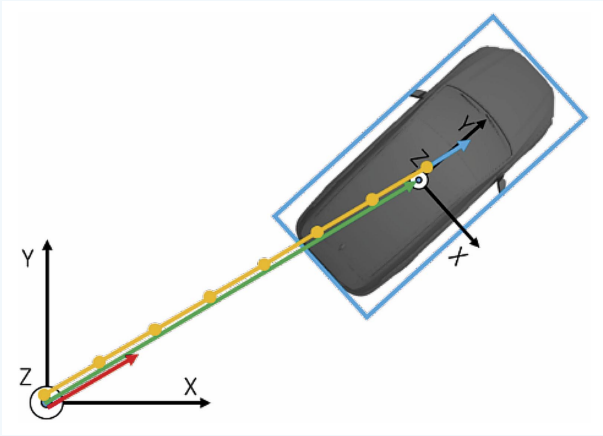


Figure 14: Visualization of the data manipulation to simulate the sensors resolution and accuracy.

The vehicle coordinate system and a theoretical target object are shown. The green vector represents the ideal and error-free position of the target. To implement the resolution influences range gates are formed, corresponding to the sensor's resolution. To sort the distance into the range gates, the length of the vector is divided by the resolution and rounded to an integer value. This results in the number of range gates. Subsequently the resulting integer value is multiplied with the resolution again. This leads to the yellow vector. The effect of the measurement accuracy is implemented next. This value fluctuates randomly in positive and negative direction. Thus, the value of the measurement accuracy, taken from the datasheet [15], is multiplied with a white Gaussian noise with a standard deviation of one. The resulting vector, visualized in blue, is added to the yellow in-range gates sorted vector.

After the range manipulation, the next step is the implementation of aspect angle and coverage effects to the RCS value. The method for that is visualized in Figure 15. The manipulation is based on the assumption that the maximum RCS of an object is given at its longest side. In Figure 15 this is represented by the yellow line. To simulate coverage and aspect angle influences, the recognized length of the target is computed. The result is the line visualized in red. In a next step, this line is projected onto the Y-axis of the local sensor coordinate system. To artificially reduce the ground truth RCS, it gets multiplied with the quotient of the length of the yellow line, representing the objects longest side and the length of the purple line, representing the visible fraction of the object. This completes the reduction of the RCS.

According to Figure 12 the next step of the probabilistic model is the object reclassification. Real radar sensors classify objects on their radar signature. This is only possible in certain distances, depending on the objects type. So far, all objects are recognized and classified correctly. To simulate the real radar's detection behavior, two thresholds are implemented. It is assumed, that cars, trucks and motorcycles are correctly classified up to a distance of 50 m. For pedestrians and bicycles the

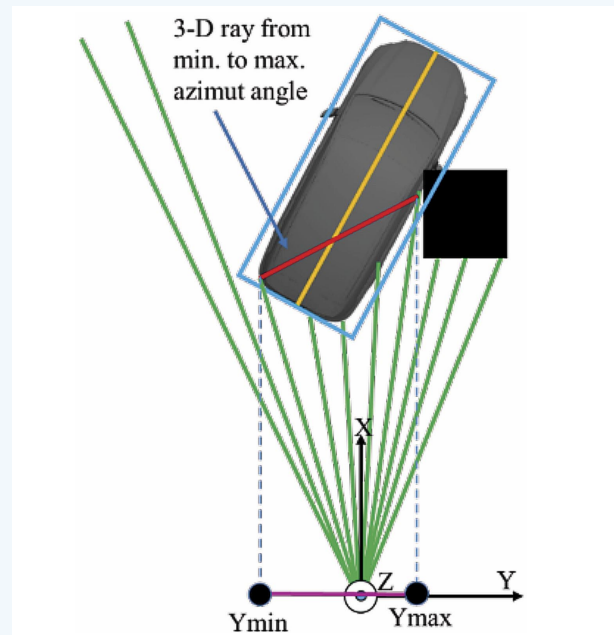


Figure 15: Method for the manipulation of the RCS value.

assumed threshold is 30m. If the distance of any object exceeds the threshold defined for its class, then it gets reclassified to the "unknown" class.

The last manipulation step visualized in Figure 12 is the implementation of false positive (FP) and false negative (FN) objects. This means objects can appear that are not physically part of the real surrounding (FP) and objects that are physically part of the sensing area (FN) can stay undetected for a certain time. Both phenomena are implemented in the following, starting with the FN objects: A detection probability with a value between zero and one is pre-defined for every Object class. On every execution step and for every actor a pseudo random value is generated. If the generated value is smaller than the detection probability, the object is added to the object list. If it is larger, the object is neglected. With this, it is possible to adjust the average false negative rate for every object class.

The implementation of false positive objects is more complex, as the objects are not only to be implemented, but also random positions have to be found for them. At a first step, a value for the average number of recognized FP objects at every frame is defined depending on the object classes. Additionally, typically bounding box sizes are defined. The FP objects are added after the execution of the complete probabilistic radar model. The generation of the FP objects is done for every object class separately, through a loop that iterates the object types. In that loop the class individual average number of FP objects is used to compute the actual number of FP objects for the respective simulation step, by applying a white Gaussian noise to the value and converting it to an integer. After that, a second loop is initiated for the generated integer value, where the respective FP object is generated. The first value that is generated for each FP

object is the extend. For that, the pre-defined average size of the class dependent bounding box is manipulated by a Gaussian noise. The same procedure is also used to generate an artificial RCS value for the respective object. After all metadata is created, the respective object is positioned at a random position with a random orientation within the sensor's field of view. This is repeated until the computed number of false positive objects for the object class is reached. After that, the object class is incremented and the algorithm is executed again.

iv. 2.3.3. Camera Model

The last environmental sensor model implemented in the virtual urban environment is a camera model. Since the camera itself only provides video data, it is augmented by an exemplary application. The resulting video is used in a detection algorithm. The structure of the implemented model, including the detection algorithm and necessary interfaces is visualized in Figure 16.

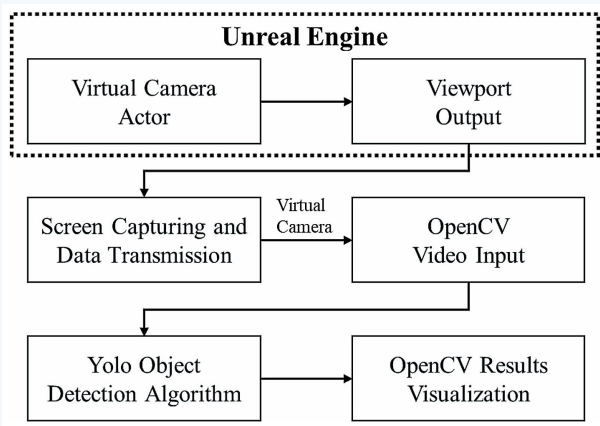


Figure 16: Structure of the implemented camera model, including an object detection algorithm.

To generate video data in a realistic way, the Unreal Engine used provides pre-defined camera actors. These cameras enable the simulation of different camera parameters and inadequacies. These camera actors provide the opportunity to simulate almost any camera in a realistic way (Figure 17). For the generation of the upper image a cheap webcam with many inadequacies is used. The lower image shows the attempt to simulate these inadequacies within the Unreal Engine using a virtual camera actor. It turns out that it is not possible to create an optically identical image, however, it is possible to lower the content of information to the same level. Since the information that can be generated from an image is especially important for ADAS applications, the virtual camera actor of the Unreal Engine provides a valid method for the generation of image data in further considerations.

The output of the generated video data is done in the so-called viewport and thus directly onto the screen of the user. The resolution is dependent on the resolution of the viewport. If the resolution of a physical existing monitor

does not fit the demands, it is also possible to use virtual screens. To enable the object detection based on the video output, it is necessary to capture the screen. The interface for the next processing step is a virtual camera. This virtual camera is used as an input by the open computer vision library (OpenCV) in Python. The Python script separates the single frames of the captured video and passes them to the object detection algorithm.

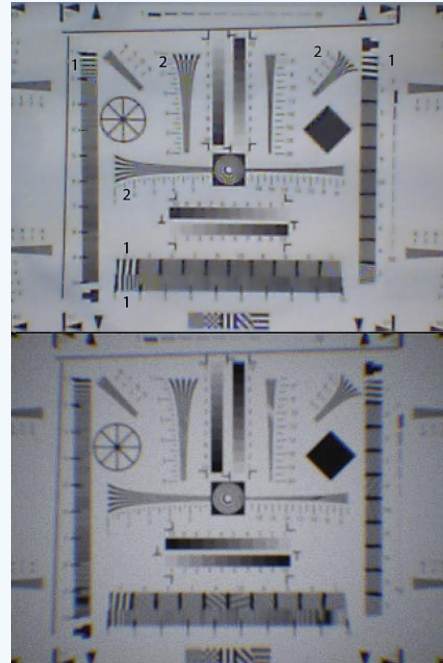


Figure 17: Comparison of real (top) and artificial (bottom) image errors.

The algorithm used is the so-called Yolo algorithm that was developed by Redmon, et al. [17]. Yolo stands for "You Only Look Once" and describes how it works. It recognizes all objects in the respective frame, by looking at the picture only one time, unlike other algorithms that process the picture multiple times.

As mentioned above, the object classification is implemented in a Python script via OpenCV. Since the Algorithm is based on a neural network, training data is needed. In this study, it is not feasible to train the network with individual datasets. Hence, pre-trained files are used. AlexeyAB [18] provides these in the "model zoo". This model enables the detection of 80 different objects, like bicycles, cars, motorcycle, persons or even objects like animals, fruit, bags, and cups. It is not specially designed for traffic scenarios, but contains all relevant object classes. After the execution, the outputs of the model are the object classes, their bounding boxes and the position in the respective image. To visualize the data, OpenCV is used again. The video stream serves as an input and is augmented by the bounding boxes of the recognized objects, labelled with the object types. Furthermore, the positions, the sizes and the object classes are written into a text file and stored for each analysed image.

Virtual Test Field Verification

We now move on to the verification of the previously described and implemented virtual inner-city test field. This is done by testing the implemented vehicle model, including the sensor simulations, and the dynamic pedestrian avatar in a typical urban setup, including further urban furniture and other static traffic participants. The functionality of the virtual test field is assessed based on the general functionality and efficiency of the model as well as the output of the virtual sensors. The aim is to evaluate inadequacies and strengths of the test field.

a. Test Setup

To verify the functionality of all sensor models, it is necessary to implement test objects for all relevant object classes that are described in Table 1, except for the “unknown” class. The scenario used is shown in Figure 18.



Figure 18: Test scene for the virtual testbed assessment.

The vehicle marked in red is the vehicle avatar that enables the interaction of the vehicle model with the virtual scene. It also carries the sensor models. Next to it, a blue car represents the objects class for “cars”. It is to be expected that the vehicle is not completely visible.



Figure 19: Test object for the “Car” class.

The vehicle avatar is positioned in front of a pedestrian crossing with traffic lights. Different traffic participants are crossing the road. Figure 20 represents the two pedestrian dummies crossing the road. The left robotic-

looking object is the dynamic pedestrian avatar, steered by a test person in real-time. The right object is a static pedestrian avatar that is not able to change its pose. Both objects are assigned to the “Pedestrian class”.

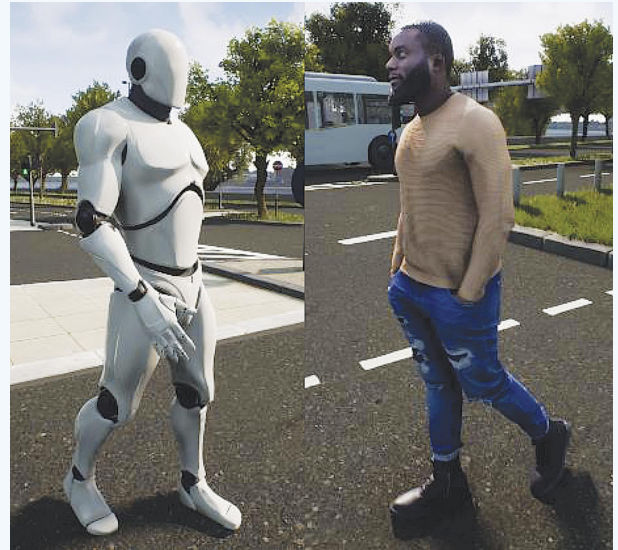


Figure 20: Pedestrian Objects, left dynamic, right static.

In addition to the pedestrians, a cyclist crosses the road. The corresponding model is visualized in Figure 21. It consists of two sub models, the bicycle itself and the rider. The bike is assigned to the bicycle class; the rider is defined as pedestrian. How the sensor outputs are affected by this needs to be investigated.



Figure 21: Test object for the bicycle class.

A four-lane road runs behind the pedestrian crossing. To represents the motorcycle class, a woman riding a scooter is placed on the closer track of that road. As with the bicyclist, the model consists of two submodels. The scooter is tagged as “Motorcycle”, since scooters do not

have their own class. The rider is assigned to the "Pedestrian" class.



Figure 22: Test object for the motorcycle class.

The last test object, placed on the more distant lane, is a typical inner-city public bus. The object is assigned to the "Truck" class, since busses do not have their own class.



Figure 23: Test object for the truck class.

b. Test Execution

As mentioned in the beginning, the aim of this work is to describe the development and implementation of the urban test field. We now move on to look at the testing of the basic functionality of the models. This is done by a static test in the previously described scenario. Further studies, based on the results of this work, could investigate complex and highly dynamic inner-city scenarios. In order to test the model's functionality, a simple static structure is sufficient.

After the scenario is set up corresponding to the last chapter and all relevant metadata are defined for the test objects, the test execution can be done. Since the scenario is static, it is sufficient to capture one simulation step and analyze the results. As described earlier, the radar and the lidar models are parametrized

corresponding to its real equivalents. For the radar model the generation of false positive and false negative objects is activated. The camera is parametrized to a sensor size of 23.76 mm x 13.365 mm, with an aperture of 2.8 and a focal length of 12 mm. This corresponds to a field of view of approximately 90°. The results of all sensor models are displayed on the user's screen. For the representation of the radar and lidar data, Matlab is used. For showing the camera model outputs, an OpenCV video stream augmented by the recognized object is shown to the user. To get the corresponding results for a specific time step, the model is executed stepwise, so that it can be paused and the results for a specific frame can be captured.

i. Results of the Lidar Model

The results of the Lidar Model are shown in Figure 24. The scale of the plot is limited to a lateral distance of 40 m and a longitudinal distance of +/- 20 m, so that the region of interest lies within the captured field. All received points, with a Signal-to-Noise ratio smaller than five are neglected. It is assumed, that this value does not enable a correct recognition. The colored boxes visualized in the plot are added manually, for further explanations. All relevant objects within the scene are recognizable. The points in the purple box near to the test vehicle are generated by the car. The yellow boxes represent both pedestrians. It shows that the static dummy is recognized as well as the dynamic object. The Lidar plot also detects the step-range of the pedestrian. On closer inspection, the plot shows the front leg and the back leg position of the step. Next to that, the points in the red box are generated by the cyclist and the corresponding bike. The points on the left side, lying in the gray box are reflected by trees and signs. The blue box represents the woman on the scooter. It can be seen, that the density of the points is lower, caused by the growing distance. The contour of the bus is also recognizable. It is represented by the green rectangle.

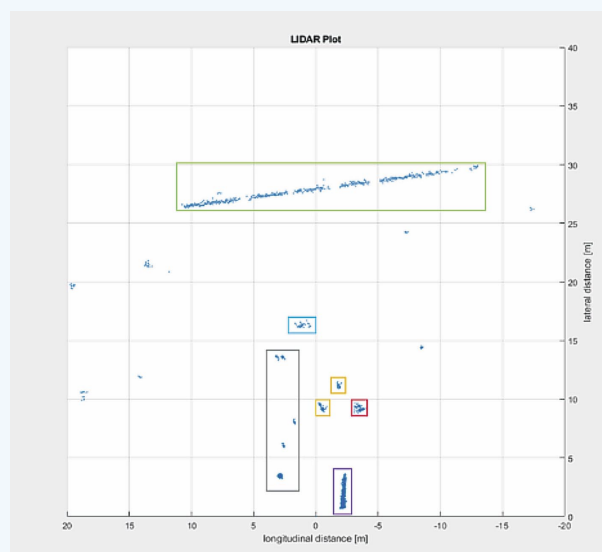


Figure 24: Resulting sensor data of the lidar model.

The lidar model shows valid behavior. All results are plausible and the execution of the model works fluently. Further research and a validation more in depth based on the measured data of real lidar sensors could improve the quality of the model. However, the current implementation shows an adequate possibility for the real-time generation of Lidar raw data.

ii. Results of the Probabilistic Radar Model

The plot in Figure 25 is scaled equivalent to the lidar plot.

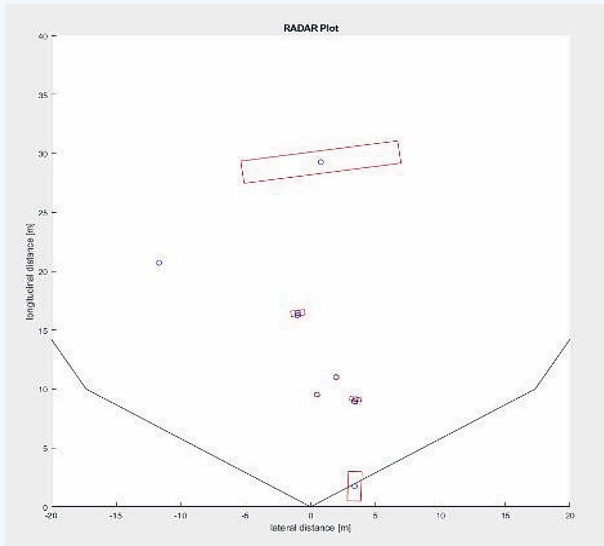


Figure 25: Resulting sensor data of the radar model.

The data also shows plausible results. All relevant objects lying in the scene that have been tagged are recognized. This shows that no false negative object was generated within the frame under investigation. However, a false positive object can be found at a distance of 20 m on the left side. The object is from the “unknown” class. It can also be seen, that neither the cyclist nor the rider of the scooter is centrally placed on the respective vehicle. This is caused by the implemented inaccuracy of the sensor and the fact that the riders and the vehicles are treated as separate objects. At this point further investigations could help to find out if it is better to treat the riders and the vehicles as one object or leave them separate. Nonetheless, the results of the sensor are plausible and the performance of the model execution is sufficient. Here a comparison with real sensor data of the described radar system in a real environment could also help to improve the model quality.

iii. Results of the Camera Model

The upper image in Figure 26 shows the raw camera output of the Unreal Engine that is used as an input for the object recognition algorithm. The lower image shows the same augmented by the output of the algorithm.



Figure 26: Results of the AI-based camera model, without and with recognized objects.

It shows that all relevant objects implemented for testing are recognized. The pedestrians, both static and dynamic, and the cyclist are recognized as “person” with a certainty of 97% or higher, whereas the driver of the scooter is recognized with a certainty of 57%. The bicycle has a certainty of 96% and the scooter 73% to be a motorbike. Additionally, all traffic lights get recognized. The bus lying in the background is also detected, but only with a certainty of 25%. It is conspicuous that not only the car next to vehicle avatars is detected, but also the avatar itself, only by a fraction of its bonnet. Lastly, one false detection is made by the algorithm. A backpack that is not part of the scene is recognized. Nevertheless, the sensor model and algorithm proved to be a good example of camera-based object recognition. Further investigations could analyze the influence of different environmental parameters like fog, rain, snow or dirty optics on the detection behavior. It would also be interesting to examine the influence on camera inadequacies like chromatic aberrations or blur on the results.

Conclusion

The present work shows a novel holistic approach for the accurate testing of autonomous driver assistance systems. It provides a new methodology for the linking of real pedestrians, vehicles, and their functions in a highly realistic urban environment. Hence, inaccuracies in real testing procedures, caused by accident hazards, static test environments or just an inadequate number of test executions are circumvented.

The interaction of the vehicle and its environment is enabled by three different sensor models. These respective models provide an example for the commonly used camera, Lidar and Radar surrounding sensors. Not only is the typical data from these sensors provided, but also typical phenomena and shortcomings are implemented. Furthermore, an accurate vehicle dynamics simulation is used to map the movements of a real vehicle in the virtual environment. To interact with the virtual vehicle directly, this approach enables test subjects to dive into the scenery through motion capturing and a head mounted display. The person sees the virtual surrounding and their movements are presented by an avatar in the city scene. With that, the model provides a new opportunity for the situational real-time testing of autonomous vehicles and their functions. Due to the already large amount of content, it is not possible to do a complete validation of the implemented models within this work. However, a simple verification approach shows plausible results and confirms the real-time capability of the model. Further research could analyze the implemented contents in depth, by investigating various scenarios in the virtual environment as well as on real testing grounds. Additionally, it would be interesting to test the reaction of real vehicles and their functions based on the virtual data provided. ■

Acknowledgement

The Project is funded by the Ministry of Economic Affairs, Innovation, Digitization and Energy of North Rhine-Westphalia in the Leitmarkt Wettbewerb IKT.NRW program.

References

- [1] Bundesministerium für Verkehr und digitale Infrastruktur (BMVI), *Strategy for automated and connected driving: Remain the lead provider, become the lead market, initiate regular operations*, (in German), Berlin: Bundesministerium für Verkehr und digitale Infrastruktur (BMVI), 2015.
- [2] Statista, "Share of cars equipped with selected driver assistance systems in Germany in 2019," (in German), January 2020. [Online]. Available: <https://de.statista.com/statistik/daten/studie/1083873/umfrage/anteil-der-pkw-mit-fahrassistenzsystemen-in-deutschland/>. [Accessed 01 December 2021].
- [3] Statista, "Which of the following statements about assistance systems would you agree with?," (in German), 2020. [Online]. Available: <https://de.statista.com/statistik/daten/studie/1108736/umfrage/meinungsumfrage-zu-assistenzsystemen-in-autos-in-deutschland/>. [Accessed 01 December 2021].
- [4] Bundesministerium für Verkehr und digitale Infrastruktur (BMVI), *Autonomous Driving Act comes into force*, (in German), Berlin: Bundesministerium für Verkehr und digitale Infrastruktur (BMVI), 2021.
- [5] Z. Zhang, "Microsoft Kinect Sensor and its Effect," *IEEE MultiMedia*, vol. 19, no. 2, pp. 4-12, 2012.
- [6] R. Taylor, <https://github.com/vrpn/vrpn>, 2020.
- [7] M. Samuel, M. Hussein and M. B. Mohamad, "A Review of some Pure-Pursuit based Path Tracking Techniques for Control of Autonomous Vehicle," *International Journal of Computer Applications*, vol. 135, no. 1, 2016.
- [8] SpringerLink (Online service), *Handbook of Driver Assistance Systems Basic Information, Components and Systems for Active Safety and Comfort*, H. Winner, S. Hakuli, F. Lotz and C. Singer, Eds., <http://lib.ugent.be/catalog/ebk01:3710000000541992>, 1st ed., 2016.
- [9] S. Kim, I. Lee and Y. J. Kwon, "Simulation of a Geiger-Mode Imaging LADAR System for Performance Assessment.," *Sensors*, vol. 13, no. 7, pp. 8460-8489, 2013.
- [10] J. Kernhof, J. Leuckfeld and G. Tavano, "LiDAR sensor system for automated and autonomous driving (in German)," in *Automobil-Sensorik 2*, Springer Berlin Heidelberg, 2018.
- [11] Hexagon | AutonomousStuff, "Valeo SCALA 3D Laser Scanner (Gen 1)," 2021. [Online]. Available: <https://autonomoustuff.com/products/valeo-scala>. [Accessed 01 December 2021].
- [12] Hamamatsu Photonics K.K., "Si APD, S12021 series, etc.: Low bias operation for 800nm band," December 2020. [Online]. Available: https://www.hamamatsu.com/resources/pdf/ssd/s12023-02_etc_kapd1007e.pdf. [Accessed 01 December 2021].
- [13] H. Weber, "SICK AG Whitepaper : LiDAR sensor functionality and variants," (in German), July 2018. [Online]. Available: https://cdn.sick.com/media/docs/5/25/425/whitepaper_lidar_de_im0079425.pdf. [Accessed 01 December 2021].
- [14] S. Muckenhuber, H. Holzer, J. Rübsam and G. Stettinger, "Object-based sensor model for virtual testing of ADAS/AD functions.," in *2019 IEEE International Conference on Connected Vehicles and Expo (ICCVE)*, Graz, 2019.
- [15] R. Liebske, "ARS 408-21 Premium Long Range Radar Sensor 77 GHz," 31 October 2015. [Online]. Available: https://www.continental-automotive.com/getattachment/5430d956-1ed7-464b-afa3-cd9cdc98ad63/ARS408-21_datasheet_en_170707_V07.pdf.pdf. [Accessed 01 December 2021].
- [16] R. Degen, H. Ott, F. Overath, C. Schyr, M. Leijon and M. Ruschitzka, "Methodical approach to the development of a Radar Sensor model for the Detection of Urban Traffic Participants Using a Virtual Reality Engine.," *Journal of Transportation Technologies*, vol. 11, no. 2, pp. 175-195, 2021.
- [17] J. Redmon, S. Diwala, R. Girshick and A. Farhadi, "You Only Look Once: Unified, Real-Time Object Detection.," in *29th IEEE Conference on Computer Vision and Pattern Recognition.*, Las Vegas, Nevada, 2016.
- [18] AlexeyAB, "YOLOv4 model zoo," GitHub, Inc., 14 July 2020. [Online]. Available: <https://github.com/AlexeyAB/darknet/wiki/YOLOv4-model-zoo>. [Accessed 01 December 2021].

René Degen, M. Sc., is Chief Engineer at CAD CAM Center Cologne (Laboratory of Cologne University of Applied Sciences). He is currently on a cooperative PhD program at Uppsala University, Sweden + Cologne University of Applied Sciences, Germany.

René's research fields include highly automated driving, control systems, and mechatronics.